PATHOGENIC MECHANISMS IN CARDIAC AND SKELETAL MUSCLE DISEASES

EDITED BY: Marcella Canton, Martina Calore and Libero Vitiello
PUBLISHED IN: Frontiers in Physiology

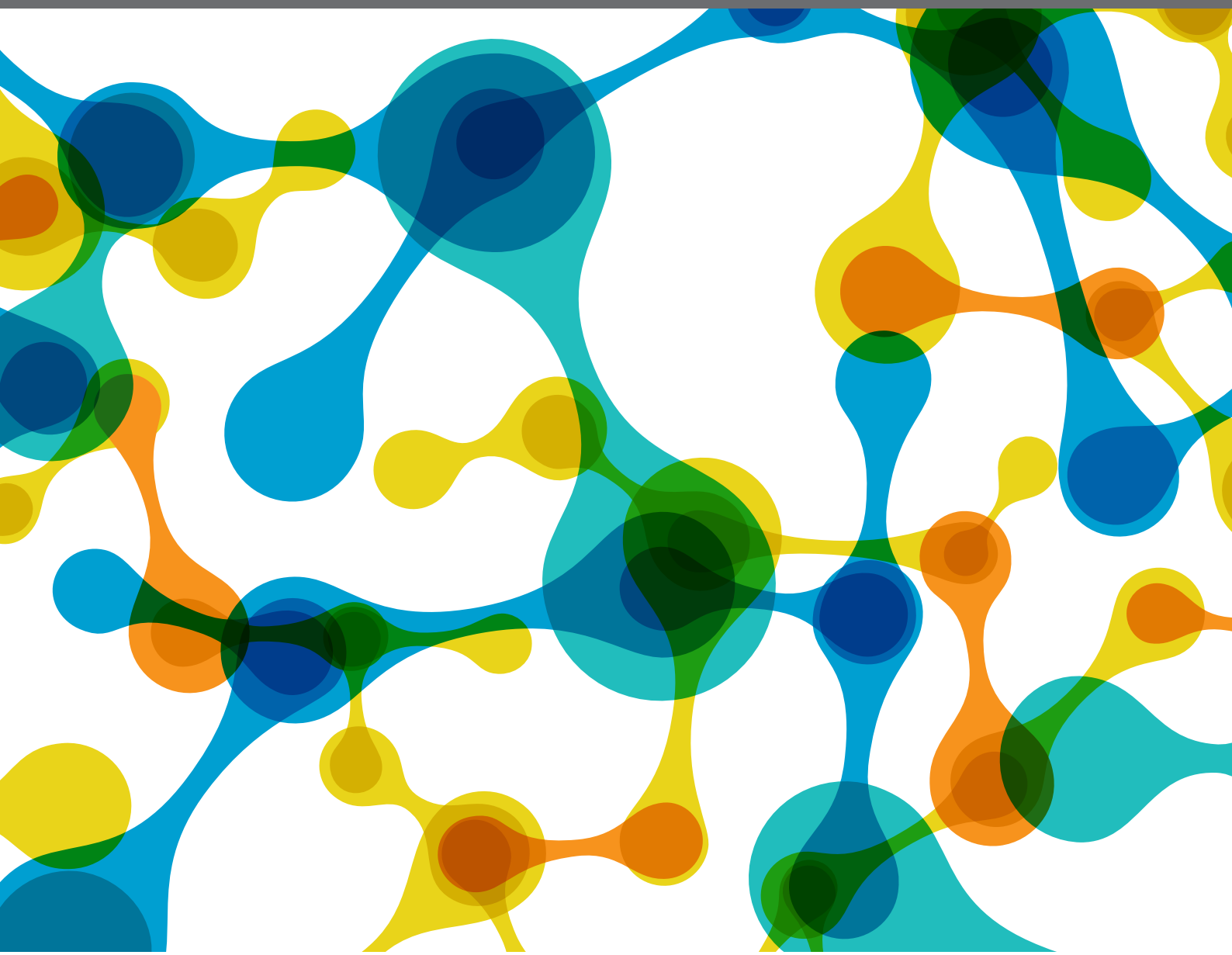

frontiers Research Topics

frontiers

ISSN 1664-8714
ISBN 978-2-88971-726-2
DOI 10.3389/978-2-88971-726-2

About Frontiers

Frontiers is more than just an open-access publisher of scholarly articles: it is a pioneering approach to the world of academia, radically improving the way scholarly research is managed. The grand vision of Frontiers is a world where all people have an equal opportunity to seek, share and generate knowledge. Frontiers provides immediate and permanent online open access to all its publications, but this alone is not enough to realize our grand goals.

Frontiers Journal Series

The Frontiers Journal Series is a multi-tier and interdisciplinary set of open-access, online journals, promising a paradigm shift from the current review, selection and dissemination processes in academic publishing. All Frontiers journals are driven by researchers for researchers; therefore, they constitute a service to the scholarly community. At the same time, the Frontiers Journal Series operates on a revolutionary invention, the tiered publishing system, initially addressing specific communities of scholars, and gradually climbing up to broader public understanding, thus serving the interests of the lay society, too.

Dedication to Quality

Each Frontiers article is a landmark of the highest quality, thanks to genuinely collaborative interactions between authors and review editors, who include some of the world's best academicians. Research must be certified by peers before entering a stream of knowledge that may eventually reach the public - and shape society; therefore, Frontiers only applies the most rigorous and unbiased reviews.
Frontiers revolutionizes research publishing by freely delivering the most outstanding research, evaluated with no bias from both the academic and social point of view. By applying the most advanced information technologies, Frontiers is catapulting scholarly publishing into a new generation.

What are Frontiers Research Topics?

Frontiers Research Topics are very popular trademarks of the Frontiers Journals Series: they are collections of at least ten articles, all centered on a particular subject. With their unique mix of varied contributions from Original Research to Review Articles, Frontiers Research Topics unify the most influential researchers, the latest key findings and historical advances in a hot research area! Find out more on how to host your own Frontiers Research Topic or contribute to one as an author by contacting the Frontiers Editorial Office: frontiersin.org/about/contact

PATHOGENIC MECHANISMS IN CARDIAC AND SKELETAL MUSCLE DISEASES

Topic Editors:
Marcella Canton, University of Padua, Italy
Martina Calore, Maastricht University, Netherlands
Libero Vitiello, University of Padua, Italy

Citation: Canton, M., Calore, M., Vitiello, L., eds. (2021). Pathogenic Mechanisms in Cardiac and Skeletal Muscle Diseases. Lausanne: Frontiers Media SA.
doi: 10.3389/978-2-88971-726-2

Table of Contents

frontiers in Physiology

BRIEF RESEARCH REPORT
published: 05 March 2020
doi: 10.3389/fphys.2020.00184

Inhibition of Myostatin Reduces Collagen Deposition in a Mouse Model of Oculopharyngeal Muscular Dystrophy (OPMD) With Established Disease

Pradeep Harish, Leysa Forrest, Shanti Herath, George Dickson, Alberto Malerba† and Linda Popplewell†*

Department of Biological Sciences, Centre of Gene and Cell Therapy and Biomedical Sciences, Royal Holloway, University of London, Egham, United Kingdom

OPEN ACCESS

Edited by:
Libero Vitiello,
University of Padua, Italy

Reviewed by:
Paola Braghetta,
University of Padua, Italy
Xu Yan,
Victoria University, Australia

***Correspondence:**
Linda Popplewell
linda.popplewell@rhul.ac.uk

†These authors have contributed equally to this work

Specialty section:
This article was submitted to Clinical and Translational Physiology, a section of the journal Frontiers in Physiology

Received: *19 December 2019*
Accepted: *17 February 2020*
Published: *05 March 2020*

Citation:
Harish P, Forrest L, Herath S, Dickson G, Malerba A and Popplewell L (2020) Inhibition of Myostatin Reduces Collagen Deposition in a Mouse Model of Oculopharyngeal Muscular Dystrophy (OPMD) With Established Disease. Front. Physiol. 11:184. doi: 10.3389/fphys.2020.00184

Background: Oculopharyngeal muscular dystrophy (OPMD) is a late-onset muscle disease presented by ptosis, dysphagia, and limb weakness. Affected muscles display increased fibrosis and atrophy, with characteristic inclusion bodies in the nucleus. Myostatin is a negative regulator of muscle mass, and inhibition of myostatin has been demonstrated to improve symptoms in models of muscular dystrophy.

Methods: We systemically administered a monoclonal antibody to block myostatin in the A17 mouse model of OPMD at 42 weeks of age. The mice were administered a weekly dose of 10 mg/kg RK35 intraperitonially for 10 weeks, following which serum and histological analyses were performed on muscle samples.

Results: The administration of the antibody resulted in a significant decrease in serum myostatin and collagen deposition in muscles. However, minimal effects on body mass, muscle mass and myofiber diameter, or the density of intranuclear inclusions (INIs) (a hallmark of disease progression of OPMD) were observed.

Conclusion: This study demonstrates that inhibition of myostatin does not revert muscle atrophy in a mouse model with established OPMD disease, but is effective at reducing observed histological markers of fibrosis in the treated muscles.

Keywords: OPMD, myostatin, antibody, RK35, muscular dystrophy

INTRODUCTION

Oculopharyngeal muscular dystrophy (OPMD) is a late onset muscle wasting disease, whose clinical diagnosis is often compounded by the onset of sarcopenia associated muscle loss (Tome et al., 1997; Blumen et al., 2000; Trollet et al., 2010). The primary clinical indications for the disease involves ptosis, dysphagia, and proximal limb weakness. The genetic basis of the disease revolves around a mutation in the *PABPN1* gene whose product regulates poly (A) tail length on mRNAs, controls the use of alternative polyadenylation (APA) sites, and influences pre-mRNA splicing among other roles (Harish et al., 2015). In OPMD, mutated PABPN1 has a poly-alanine

expansion at the N terminus of the protein, resulting in 11–18 repeats instead of the normal 10 present in unaffected individuals (Brais et al., 1998; Blumen et al., 2000). The alanine expansion results in protein misfolding and consequent accumulation in the nuclei as intranuclear inclusion bodies (INI) (Harish et al., 2018). These INI bodies also sequester other molecules such as poly(A)-containing RNA, various transcription factors of the proteasome ubiquitin pathway (ubiquitin and 20S catalytic proteasomal subunit), molecular chaperones (HDJ-1, HSP70), heterogeneous nuclear ribonucleoprotein A1 (HNRPA1) and arginine methyltransferares (Harish et al., 2018). The sequestration of these proteins may induce defects in transcriptomic or protein folding pathways (Tavanez et al., 2009; Malerba et al., 2017). Current methods to ameliorate disease symptoms are surgical in nature, however, various small molecule and gene therapy strategies have been proposed that directly or indirectly target the INI bodies (Harish et al., 2018). Concordant with other muscular dystrophies, moderate muscle atrophy (especially in non-somitically derived muscles) has also been described in patients with OPMD (Schmitt and Krause, 1981; Little and Perl, 1982), and hence therapeutic agents that target muscle mass may ameliorate symptoms in this disease state.

Myostatin is a known regulator of muscle mass and has been examined as a therapeutic target to ameliorate symptoms of dystrophy, cachexia, and sarcopenia (Rodgers and Garikipati, 2008; Sartori et al., 2013; Mouisel et al., 2014). While primary myostatin signaling is effected as a balance between the bone morphogenetic protein (BMP) and activing receptor IIB (ACTRIIB) signaling pathways, secondary signaling mechanisms also influence cell growth via interactions with the IGF-1, p21/Cdk, Wnt signaling pathways (Rodgers and Garikipati, 2008; McPherron, 2010; Sartori et al., 2013). Studies in myostatin null mice report an increased bone mineral density (as compared to wild-type controls) and ejection fraction, resistance to diet induced obesity, dyslipidemia, atherogenesis, hepatic steatosis and macrophage infiltration, besides a substantial improvement in muscle mass (White and LeBrasseur, 2014). Inhibition of myostatin on disease progression has been studied in aged *mdx* mice (modeling Duchenne muscular dystrophy) and C57 (wildtype) model systems utilizing various strategies, and report variable levels of efficacy (LeBrasseur et al., 2009; Murphy et al., 2010; Arounleut et al., 2013). Unsurprisingly, a variety of strategies to disrupt myostatin signaling are in pre-clinical and clinical development, including but not limited to propeptide, gene therapy, gene editing, ligand traps, and monoclonal antibodies (Wagner et al., 2002, 2008; Bogdanovich et al., 2005; Mendell et al., 2015; Bhattacharya et al., 2017; Campbell et al., 2017).

We recently published that immunological blockade of myostatin in young (12 week old) A17 mice improved muscle mass, muscle force, and reduced collagen deposition (Harish et al., 2019). The A17 model mouse, which expresses a bovine exp*PABPN1* transgene (17 expanded alanine residues driven by a human alpha actin promoter), has been used routinely in various studies as it models OPMD disease progression on a cellular level (Trollet et al., 2010).

In this current study, we utilize the same treatment regimen in relatively older OPMD mice to assess the impact of myostatin inhibition in models with pre-existing muscle atrophy. Here, we show that administration of the anti-myostatin monoclonal antibody RK35 to 42 week old A17 mice for a period of 10 weeks, while not affecting accumulation of intranuclear aggregates, or loss of body mass, muscle atrophy, or muscle strength, does, however, reduce deposition of fibrotic collagen proteins. This would suggest the proposed anti-myostatin therapy may have a role as an adjuvant treatment option in established disease states in addition to gene therapy or small molecule strategies to ameliorate disease symptoms and presents future avenues to be investigated (Malerba et al., 2017, 2019a).

MATERIALS AND METHODS

Animal Handling

A17 and FvB mice were bred in-house and all mice were housed individually with food and water *ad libitum* in a minimal disease facility at Royal Holloway, University of London (Davies et al., 2005). Individual mice were identified by ear-notching at about 4 weeks of age. Due to the heterozygous nature of the disease model, the OPMD mice were analyzed to confirm the genotype by PCR as described previously (Trollet et al., 2010). 42 week old male mice were weighed prior to each injection, at the same time of day. Initial body weights were used to evenly distribute animals among cohorts to ensure equivalent average body weights prior to the commencement of experimental protocols. In this experiment, we administered the anti-myostatin blocking antibody RK35 (Pfizer, United States) diluted in sterile saline (Sigma-Aldrich, United Kingdom) for a final volume of 200 μl. The antibody was injected weekly at 10 mg/kg i.p. for 10 weeks into A17 and FvB mice [9 A17 mice treated with the anti-myostatin antibody RK35 (A17 + RK35), 8 A17 mice treated with saline as vehicle control (A17 + saline), 10 FvB mice treated with the antibody RK35 (FvB + RK35), and 10 FvB mice treated with saline as a strain control (FvB + saline)]. *In vivo* experiments were conducted under statutory Home Office recommendation; regulatory, ethics, and licensing procedures and the Animals (Scientific Procedures) Act 1986 (Project License 36A9994E).

Sample Collection, Processing and Immunological Detection of Serum Myostatin

Mice were euthanized 1 week after the last injection of RK35 at the 53rd week of age, and the Tibialis Anterior (TA) muscle was harvested, weighed and mounted in O.C.T. compound (Thermo Fisher Scientific, United Kingdom), frozen in 2-methylbutane (isopentane) chilled with liquid nitrogen, and stored at −80°C. Blood was extracted by cardiac puncture, allowed to clot overnight at 4°C, serum extracted and spun down successively with increasing speeds at 1000 g, 2000 g, and 3500 g to remove residual cells. The serum sample thus collected was stored at −80°C. Serum samples were then subject to activation (R&D Systems, United States, DY010) and sandwich ELISA (R&D

Systems, United States, DGDF80) to detect serum myostatin as per manufacturer's recommended protocol. Additional samples from mice subject to the same treatment regimen from 12 weeks of age obtained via a previously conducted experiment were also used in this study (Harish et al., 2019).

Histological and Immunohistochemical Analysis

Transverse sections of the tissue were sectioned at 10–12 different intervals at a thickness of 10 μm, along the length of the muscle, allowing the maximal cross-sectional area (CSA) to be determined, the sections were mounted on coated slides (VWR International, United Kingdom), and stored at −80°C. Sections were then air-dried, fixed, stained with anti-PABPN1 (rabbit monoclonal, diluted 1:100, Abcam ab75855, overnight at 4°C), anti-laminin (rat monoclonal, diluted 1:800, Sigma-Aldrich L0663, 1 h at room temperature) and anti- collagen VI (rabbit polyclonal, Abcam ab6588, 1:200, 1 h room temperature) antibodies using previously established protocols (Malerba et al., 2017). Slides were stained with DAPI to visualize nuclei and coverslips were mounted using mounting medium (Vector Labs, United States). Whole muscle images (for laminin based fiber morphometry) or random fields (for PABPN1 and collagen immunostaining) were captured using a microscope (Zeiss, United Kingdom). For analysis of fiber morphometry, the median minimal feret's diameter from 1000 randomly selected fibers were determined for TA muscles for each individual animal analyzed (Harish et al., 2019; Malerba et al., 2019a). For picrosirius red staining, sections were air dried, fixed in PFA 4%, and stained in a 0.3% solution of Sirius red in saturated aqueous picric acid, followed by a treatment with 0.5% acetic acid. Imaging of sirius red staining was performed under white light to analyze collagen deposition.

Statistical Analyses

After checking for the conditions of normality and homoscedasticity, a one way ANOVA was performed to compare multiple groups. Multiple comparison were performed with Bonferroni correction to correct for multiple testing used. All statistical techniques were performed using GraphPad Prism v7.00 (GraphPad Software, California, United States).

RESULTS

Treatment With Anti-myostatin Antibody Has Minimal Effect on Body Mass in 52-Week Old OPMD Mice

To monitor the effects of inhibiting myostatin in a mouse model of OPMD, where the disease is already established, 8–10 male A17 and FvB mice at 42 weeks of age were weighed and the anti-myostatin antibody RK35 (10 mg/kg IP) or an equivalent volume of saline was administered weekly for 10 weeks (**Figure 1A**).

At the beginning of the study a 10% ($p < 0.05$) difference in the initial body mass existed between A17 mice and FvB mice (**Figure 1B**). This difference was maintained throughout the study. The treatment of A17 mice with the antibody caused a non-significant increase in final body mass of 5% ($p > 0.05$) when compared to the saline treated A17 mice (**Figure 1C**). The treatment of FvB control mice resulted in no significant changes in body mass observed.

Treatment With Anti-myostatin Antibody Has Minimal Effect on Muscle Mass and Muscle Fiber Diameter, and Intranuclear Inclusion Density in 52-Week Old OPMD Mice

When examining the change in muscle mass, we detected a significant increase of 20% ($p < 0.01$) in raw muscle masses of A17 and FvB muscles treated with saline (**Figure 2A**). No difference in the mass of the TA (normalized to the initial body mass) was found between the untreated A17 and FvB mice (**Figure 2B**). It should be noted that the administration of the antibody RK35 resulted in no changes to either the normalized

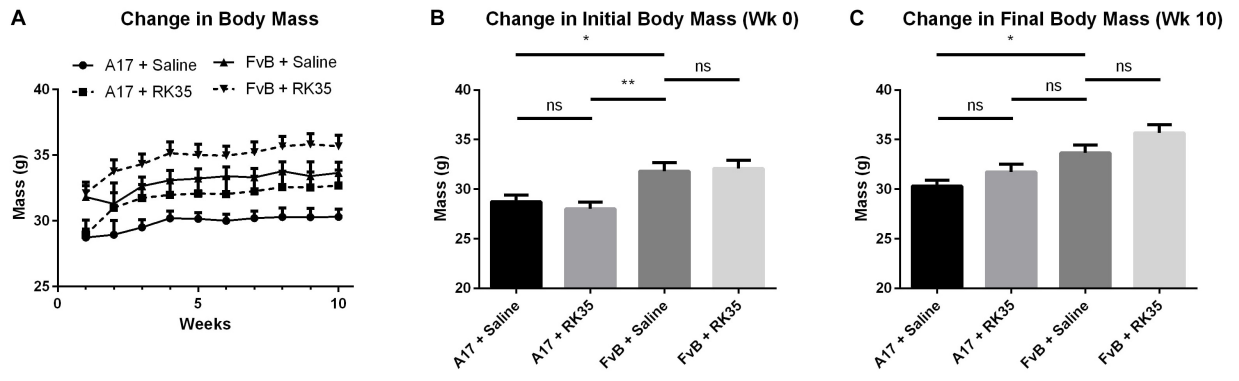

FIGURE 1 | Treatment with RK35 antibody does not affect body mass in 52 week old A17 mice: Mice (n = 8–10) were weighed and administered a weekly regimen of either saline or the RK35 antibody (10 mg/kg i.p.) for 10 weeks from the 42nd week of age. **(A)** The average body mass per group plotted against weeks shows that body masses **(B)** are significantly different at the beginning of the experiment and **(C)** the difference is maintained after 10 weeks of treatment. Data presented as mean with SEM, with p-values obtained by ANOVA after a Bonferroni correction (*$p < 0.05$; **$p < 0.01$).

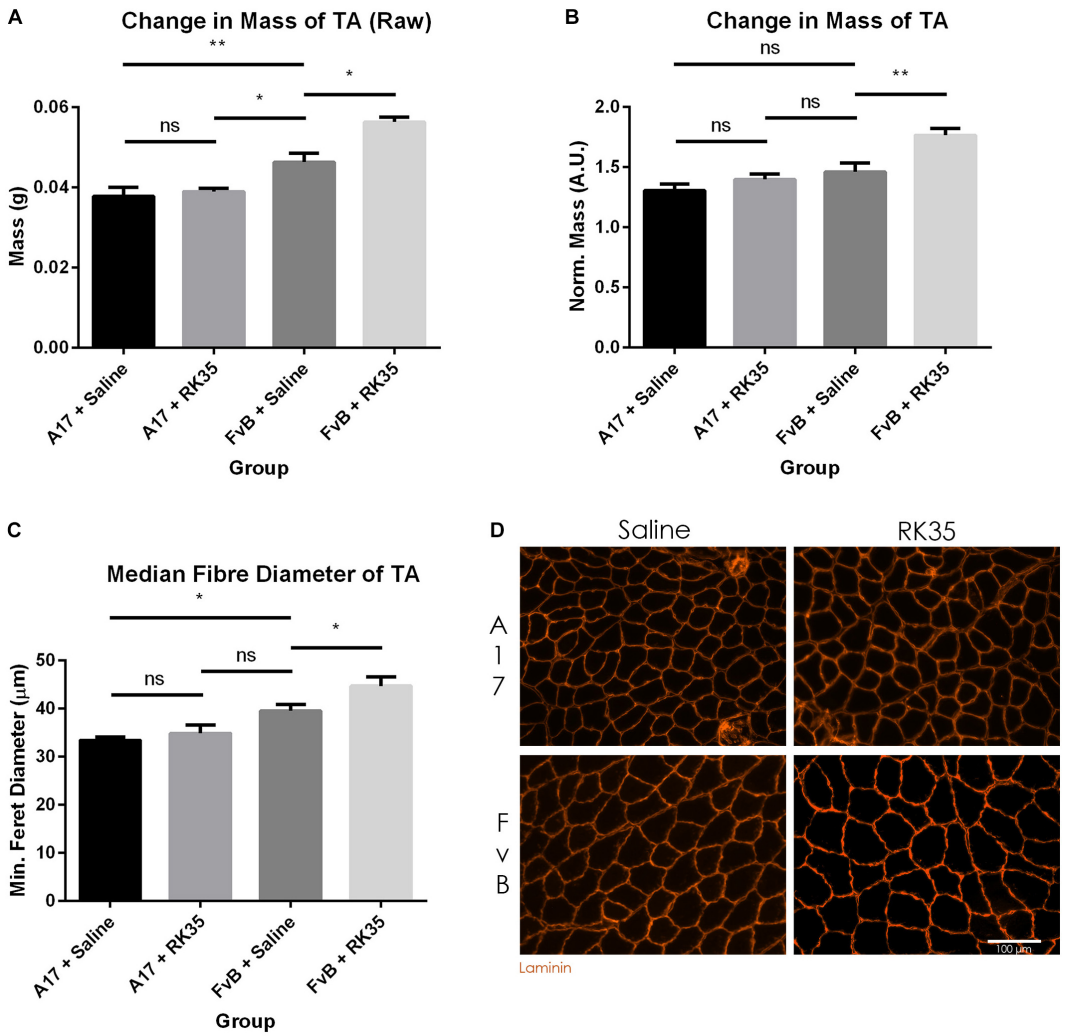

FIGURE 2 | Treatment with RK35 antibody has does not affect muscle mass and myofiber diameter in OPMD mice: Mice were administered with a weekly regimen of either saline or the RK35 antibody (10 mg/kg i.p.) for 10 weeks from 42-weeks of age. The TA was sampled and **(A)** raw muscle mass or **(B)** muscle mass normalized to the initial body mass is presented. Next, muscle samples from five randomly selected mice per group were sectioned and immunostained for laminin. **(C)** 1000 fibers were randomly selected for the TA, and the median minimum feret diameter was analyzed. **(D)** Representative images used to generate myofiber diameter data are shown on the bottom right panel with the scale bar representing 100 μm. The FvB mice treated with the antibody consistently displayed an increased muscle mass and myofiber diameter, with no changes observed in the A17 mice. The average of median minimum feret diameter per group was plotted, Data presented as mean with SEM, with *p*-values obtained by ANOVA after a Bonferroni correction (*$p < 0.05$; **$p < 0.01$).

or raw muscle mass of the TA in the A17 mice when compared to saline controls. However, a significant increase in muscle mass in the treated FvB controls [19% ($p < 0.05$) increase in normalized and raw muscle masses] was observed when compared to the untreated FvB mice, demonstrating the functionality of the administered antibody and suggesting that this treatment was not able to reverse established muscle atrophy (**Figures 2A,B**).

To better characterize the muscle atrophy in aged A17 mice, we analyzed the myofiber size. The decrease in muscle mass in the A17 mice was accompanied by a reduction of myofiber diameter in the TA by 18% ($p < 0.05$) when compared to FvB mice (**Figures 2C,D**). The administration of RK35 to A17 mice resulted in a minimal increase in myofiber diameter of the TA (**Figure 2C**). In accordance with the increase in muscle mass observed in FvB mice, the myofiber diameter in TA muscles of age-matched FvB controls increased by 13% ($p < 0.05$) compared to those of saline-treated FvB mice (**Figure 2C**). Finally, the administration of the RK35 antibody did not affect the levels of INIs in the TA in this study (**Supplementary Figure S1**).

Anti-myostatin Antibody Significantly Reduces Collagen Deposition in A17 Mice

We next examined the effect of inhibition of myostatin on the deposition of collagen proteins as histopathological markers of fibrotic tissue deposition in the muscles. Untreated A17 mice displayed a significantly increased collagen deposition when

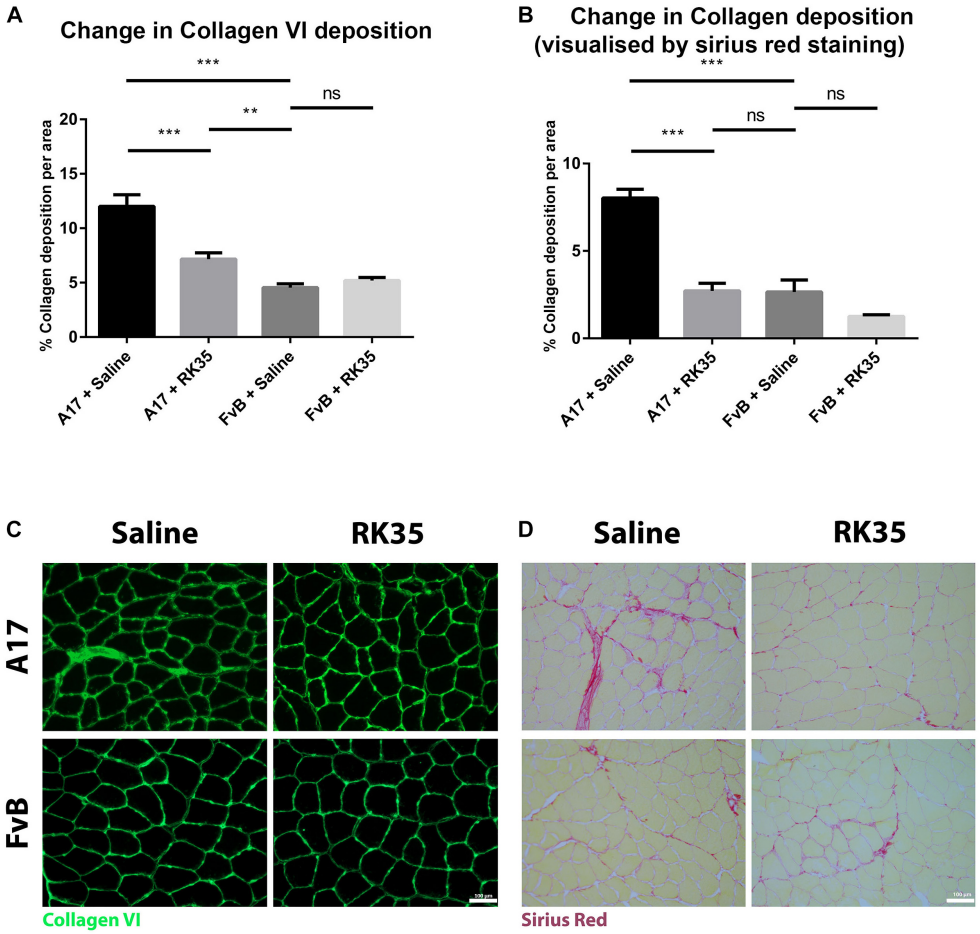

FIGURE 3 | Treatment with RK35 antibody reduces collagen deposition in OPMD mice: Mice were administered with a weekly regimen of either saline or the RK35 antibody (10 mg/kg i.p.) for 10 weeks from 42-weeks of age. Five randomly selected whole TA muscle sections from all groups were stained for **(A)** collagen VI and **(B)** picrosirius red, and five random fields were imaged and analyzed for the percentage area of collagen staining. **(C,D)** Representative images used to generate data are shown below the respective graphs, with the scale bar representing 100 μm. The mice treated with the antibody consistently displayed a reduced collagen deposition, with the area of collagen in the disease model normalized to wild-type levels. The average area per group is plotted, bars representing SEM, with *p*-values obtained by ANOVA after a Bonferroni correction (**$p < 0.01$; ***$p < 0.001$).

compared to control FvB mice [with the control mice displaying 60% ($p < 0.05$) less collagen deposition than the A17 mice] (**Figures 3A,C**). Inhibition of myostatin by administered RK35 antibody reduced deposition of collagen VI in the TA muscle of A17 mice by 40% ($p < 0.001$) and general collagen deposition as visualized by Sirius red staining by 29% ($p < 0.01$) when compared to untreated A17 mice (**Figures 3B,D**). This reduction in collagen deposition (as determined by Sirius red staining) in treated A17 mice was particularly marked since they were ameliorated to the levels seen in the FvB controls (4% difference, $p > 0.05$) (**Figure 3B**).

Treatment With Anti-myostatin Antibody Significantly Reduces Serum Myostatin 52-Week Old OPMD Mice

We next performed a sandwich ELISA in order to quantify the efficacy of the anti-myostatin antibody RK35 used in this study to reduce the levels of serum myostatin. To establish any age-dependency of response, we utilized serum samples from 52 week old or 12 week old A17 and FvB mice treated systemically with either saline or RK35 for 10 weeks, at 10 mg/kg i.p. ($n = 5$ per group) obtained from a previous study (Harish et al., 2019).

When considering the control samples from the 22 week old mice, the levels of serum myostatin are 40% higher ($p < 0.01$) in the FvB mice than the A17 mice (**Figure 4A**). Effective reduction of myostatin using the RK35 antibody levels below the detectable limits of the ELISA is evident for both A17 and FvB young mice (**Figure 4B**). For the older mice, while no significant difference was observed in serum myostatin levels between 52 week old A17 and FvB mice, the treatment with the anti-myostatin antibody RK35 again resulted in reduction of serum myostatin to below detectable levels for both strains of mice (**Figure 4A**). When comparing the levels of serum myostatin between the two age groups, no significant difference was observed between untreated A17 mice at 22 weeks of age or 52 weeks of age. Similarly, no

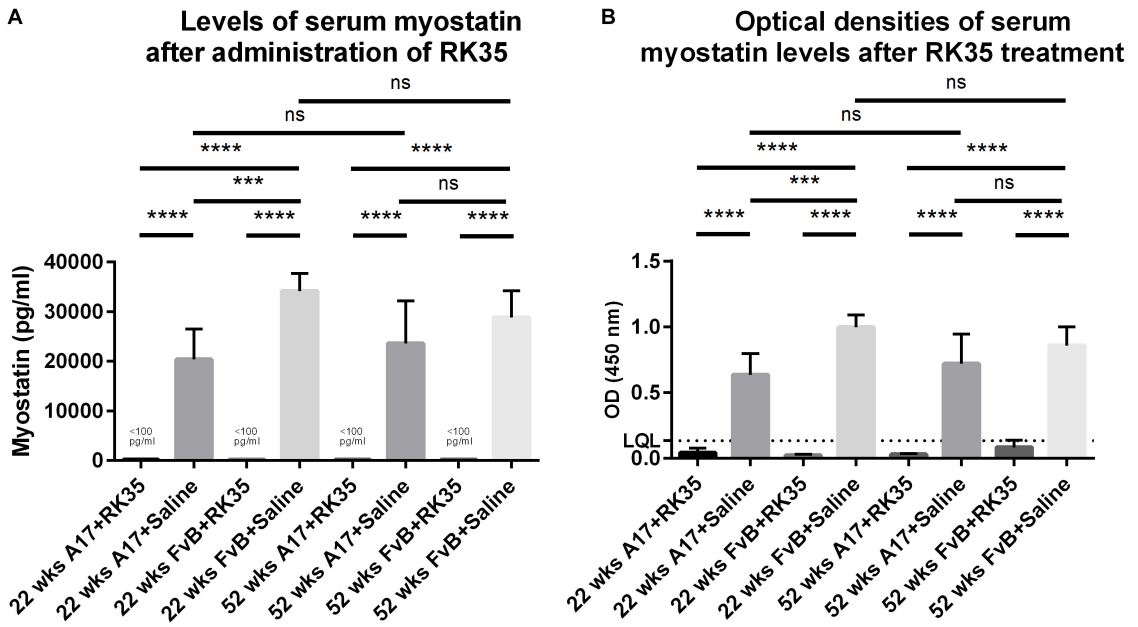

FIGURE 4 | Treatment with RK35 significantly reduces levels of serum myostatin: Serum samples from mice (n = 5) were subject to a weekly regimen of either saline or the anti-myostatin RK35 antibody i.p. for 10 weeks from 42 weeks of age, or samples were utilized from a previously published study (Harish et al., 2019) were subject to a sandwich ELISA to detect myostatin. **(A)** The administration of the antibody resulted in the reduction of serum myostatin below the lower quantitation limit (LQL) of 100 pg/ml. **(B)** Optical densities corrected for background readings are plotted for each group analyzed. Data presented as mean with SEM, with p-values obtained by ANOVA after a Bonferroni correction (***$p < 0.001$, ****$p < 0.0001$).

significant difference was observed between untreated FvB mice at 22 weeks of age or 52 weeks of age (**Figure 4A**).

DISCUSSION

Myostatin is a negative regulator of muscle mass (Rodgers and Garikipati, 2008). Subsequently, the most striking result of inhibition of myostatin involves significant increases in muscle mass and muscle fiber diameter (McPherron et al., 1997). Hence, agents that either directly or indirectly disrupt myostatin signaling are being investigated by various pharmaceutical industries as a generic broad-spectrum therapeutic strategy to alleviate muscle loss arising from cachexia, sarcopenia, or muscular dystrophy (Rodgers and Garikipati, 2008; Lu-Nguyen et al., 2015, 2017; Camporez et al., 2016; Andre et al., 2017; Tinklenberg et al., 2017). OPMD is a rare poly-alanine expansion induced protein aggregopathy, and has been modeled in the A17 mouse strain (Davies et al., 2005). It is reported that the disease progression manifests as visible changes in muscle mass at 18 weeks of age in the model mice (Trollet et al., 2010). Recent efforts to ameliorate symptoms have focused on small molecule approaches to target protein aggregation and gene therapy approaches to correct the mutation (Malerba et al., 2017, 2019a,b). In our previous study we showed that the administration of the RK35 antibody counteracted the muscle atrophy and improved histopathological features of the disease (Harish et al., 2019). Screening of therapeutic reagents in relatively younger murine models of late-onset diseases, such as OPMD, presents challenges in translating into clinical trials (Harish et al., 2015). Furthermore, pathogenesis of disease in OPMD mice is markedly different from disease progression in human patients. While the disease profile in the A17 mouse model is present in all skeletal muscles, the etiological profile in humans is localized to the extraocular and pharyngeal muscles, with proximal limb muscle involvement depending on disease progression and severity (Davies et al., 2005; Trollet et al., 2010). Therefore, the rationale behind this study was to assess the efficacy of myostatin inhibition in an OPMD disease model with an established disease state.

The A17 mouse model at 52-weeks of age possesses a lower body and muscle mass than the FvB controls, along with a significantly reduced myofiber diameter and increased collagen deposition. The inhibition of myostatin produced no increase in muscle mass in the A17 model mice, which is in contrast to what we observed in younger A17 mice (Harish et al., 2019). Interestingly, the functionality of the antibody was evident in the healthy 52-week old FvB control mice, with significantly increased muscle mass and myofiber diameters observed in this study. We originally hypothesized that different levels of serum myostatin between A17 and FvB mice could be implicated in the differing efficacy of myostatin inhibition observed between the two age groups. Indeed, Mariot et al. (2017) have reported that levels of serum myostatin might be directly dependant on type of disease and state of disease progression. We report here that the levels of serum myostatin are significantly lower in 22-week old A17 mice when compared to the FvB controls and this correlates

well with the results obtained in younger mice (Harish et al., 2019). However, no such difference exists in the 52-weeks cohort.

The mechanistic reason behind this differing effect will need to be investigated further in a future study. We speculate a combined sarcopenic and dystrophic phenotype may irreversibly alter muscle structure and attenuate the efficacy of the therapeutic regimen as compared to models in earlier stages of the disease, thereby preventing regrowth of the muscle mass with myostatin inhibition. For example, we speculate crucial molecules involved in the myostatin pathway (e.g., the activin receptor IIb) or molecular pathways affecting the muscle growth (e.g., Insulin like growth factors) may be dysregulated as result of the OPMD pathology significantly reducing the impact of myostatin inhibition. Alternatively, other molecules which negatively regulate muscle mass (such as activin A), might reduce the efficacy of myostatin knockdown in this older cohort (Latres et al., 2017).

Promisingly, while the untreated A17 mice displayed a marked increased collagen deposition when compared to the untreated FvB controls in the TA, the administration of the treatment regimen reduced the collagen deposition. Pathophysiological fibrosis associated with aging/dystrophy results in sarcolemmal fragility, disturbances in calcium ion homeostasis, inflammation, reduction of motile and contractile functions, and reduction of available tissue for therapeutic intervention (Desguerre et al., 2009; Mann et al., 2011). Attenuation of muscle fibrotic processes may have long term benefits to a dystrophic muscle in terms of promoting regeneration, muscle force transfer, and maintaining structural integrity. Myostatin is a known regulator of fibroblast activation and apoptosis (Li et al., 2008), with anti-myostatin agents shown to have an anti-fibrotic effect in other models of muscular dystrophy (Wagner et al., 2002; Li et al., 2012).

It is interesting to note in our studies that while inhibiting myostatin in younger mice improved muscle atrophy and reduced collagen deposition (Harish et al., 2019), the inhibition of myostatin in older mice had only a significant effect on reducing collagen deposition. This underlines the importance of elucidating the mechanism of myostatin inhibition on pre-existing muscle atrophy, as this may have an impact on translating anti-myostatin treatment regimens to the clinic. Indeed, most direct immunological blockers of myostatin activity have had limited success in clinical trials (Wagner et al., 2008; Campbell et al., 2017), with primary endpoints being a readout of lean mass, muscle volume, inflammatory responses or muscle regeneration. It may be informative to verify the therapeutic benefit of the anti-fibrotic action of myostatin inhibition in late-onset muscle diseases.

DATA AVAILABILITY STATEMENT

All datasets generated for this study are included in the article/**Supplementary Material**.

ETHICS STATEMENT

The animal study was reviewed, approved, and performed under regulations and recommendations laid down by the UK Home Office (ASPA 1986).

AUTHOR CONTRIBUTIONS

PH, AM, LP, and GD contributed to the study design. PH, AM, SH, and LF participated in the data collection and interpretation. PH and AM prepared the manuscript. All authors provided the manuscript review and revisions.

ACKNOWLEDGMENTS

The authors wish to thank Jane Owens, Michael St-Andre, Carl Morris, and other colleagues at Pfizer for providing the antibody RK35, and for support designing the study.

SUPPLEMENTARY MATERIAL

The Supplementary Material for this article can be found online at: https://www.frontiersin.org/articles/10.3389/fphys.2020.00184/full#supplementary-material

FIGURE S1 | Treatment with RK35 does not affect the amount of intranuclear aggregates: Mice were subject to a weekly regimen of either saline or the anti-myostatin RK35 antibody i.p. for 10 weeks from 42 weeks of age. **(A)** Five muscle samples from all groups were stained for endogenous PABPN1 after a 1M KCl treatment with the scale bar representing 50 μm, and five random fields were imaged and analyzed for the percentage number of positive PABPN1 stains to all myonuclei. **(B)** The administration of the treatment regimen did not change the number of intranuclear aggregates observed. The average density is plotted, bars representing SEM, with p-values obtained by ANOVA after a Bonferroni correction (***$P < 0.001$).

REFERENCES

Andre, M. S., Johnson, M., Bansal, P. N., Wellen, J., Robertson, A., Opsahl, A., et al. (2017). A mouse anti-myostatin antibody increases muscle mass and improves muscle strength and contractility in the mdx mouse model of Duchenne muscular dystrophy and its humanized equivalent, domagrozumab (PF-06252616), increases muscle volume in cynomolgus monkeys. *Skelet. Muscle* 7:25. doi: 10.1186/s13395-017-0141-y

Arounleut, P., Bialek, P., Liang, L. F., Upadhyay, S., Fulzele, S., Johnson, M., et al. (2013). A myostatin inhibitor (propeptide-Fc) increases muscle mass and muscle fiber size in aged mice but does not increase bone density or bone strength. *Exp. Gerontol.* 48, 898–904. doi: 10.1016/j.exger.2013.06.004

Bhattacharya, I., Pawlak, S., Marraffino, S., Christensen, J., Sherlock, S. P., Alvey, C., et al. (2017). Safety, tolerability, pharmacokinetics, and pharmacodynamics of domagrozumab (PF-06252616), an antimyostatin monoclonal antibody, in healthy subjects. *Clin. Pharmacol. Drug Dev.* 7, 484–497. doi: 10.1002/cpdd.386

Blumen, S. C., Korczyn, A. D., Lavoie, H., Medynski, S., Chapman, J., Asherov, A., et al. (2000). Oculopharyngeal MD among bukhara jews is due to a founder (GCG)9 mutation in the PABP2 gene. *Neurology* 55, 1267–1270. doi: 10.1212/wnl.55.9.1267

Bogdanovich, S., Perkins, K. J., Krag, T. O. B., Whittemore, A. L., and Khurana, T. S. (2005). Myostatin propeptide-mediated amelioration of dystrophic pathophysiology. *FASEB J.* 19, 543–549. doi: 10.1096/fj.04-2796com

Brais, B., Bouchard, J. P., Xie, Y. G., Rochefort, D. L., and Chrtien, N. (1998). Short GCG expansions in the PABP2 gene cause oculopharyngeal muscular dystrophy. *Nat. Genet.* 18, 164–167. doi: 10.1038/ng0298-164

Campbell, C., McMillan, H. J., Mah, J. K., Tarnopolsky, M., Selby, K., McClure, T., et al. (2017). Myostatin inhibitor ACE-031 treatment of ambulatory boys with Duchenne muscular dystrophy: Results of a randomized, placebo-controlled clinical trial. *Muscle Nerve* 55, 458–464. doi: 10.1002/mus.25268

Camporez, J. P., Petersen, M. C., Abudukadier, A., Moreira, G. V., Jurczak, M. J., Friedman, G., et al. (2016). Anti-myostatin antibody increases muscle mass and strength and improves insulin sensitivity in old mice. *Proc. Natl. Acad. Sci. U.S.A.* 113, 2212–2217. doi: 10.1073/pnas.1525795113

Davies, J. E., Wang, L., Garcia-Oroz, L., Cook, L. J., Vacher, C., O'Donovan, D. G., et al. (2005). Doxycycline attenuates and delays toxicity of the oculopharyngeal muscular dystrophy mutation in transgenic mice. *Nat. Med.* 11, 672–677. doi: 10.1038/nm1242

Desguerre, I., Mayer, M., Leturcq, F., Barbet, P. J., Gherardi, R. K., and Christov, C. (2009). Endomysial fibrosis in duchenne muscular dystrophy: a marker of poor outcome associated with macrophage alternative activation. *J. Neuropathol. Exp. Neurol.* 68, 762–773. doi: 10.1097/NEN.0b013e3181aa31c2

Harish, P., Dickson, G., and Malerba, A. (2018). Advances in emerging therapeutics for oculopharyngeal muscular dystrophy. *Exp. Opin. Orphan Drugs* 6, 693–701. doi: 10.1080/21678707.2018.1536542

Harish, P., Malerba, A., Dickson, G., and Bachtarzi, H. (2015). Progress on gene therapy, cell therapy, and pharmacological strategies toward the treatment of oculopharyngeal muscular dystrophy. *Hum. Gene Ther.* 26, 286–292. doi: 10.1089/hum.2015.014

Harish, P., Malerba, A., Lu-Nguyen, N., Forrest, L., Cappellari, O., Roth, F., et al. (2019). Inhibition of myostatin improves muscle atrophy in oculopharyngeal muscular dystrophy (OPMD). *J. Cachexia Sarcopenia Muscle* 10, 1016–1026. doi: 10.1002/jcsm.12438

Latres, E., Mastaitis, J., Fury, W., Miloscio, L., Trejos, J., Pangilinan, J., et al. (2017). Activin a more prominently regulates muscle mass in primates than does GDF8. *Nat. Commun.* 8:15153. doi: 10.1038/ncomms15153

LeBrasseur, N. K., Schelhorn, T. M., Bernardo, B. L., Cosgrove, P. G., Loria, P. M., and Brown, T. A. (2009). Myostatin inhibition enhances the effects of exercise on performance and metabolic outcomes in aged mice. *J. Gerontol. Ser. A* 64, 940–948. doi: 10.1093/gerona/glp068

Li, Z. B., Kollias, H. D., and Wagner, K. R. (2008). Myostatin directly regulates skeletal muscle fibrosis. *J. Biol. Chem.* 283, 19371–19378. doi: 10.1074/jbc.M802585200

Li, Z. B., Zhang, J., and Wagner, K. R. (2012). Inhibition of myostatin reverses muscle fibrosis through apoptosis. *J. Cell Sci.* 125, 3957–3965. doi: 10.1242/jcs.090365

Little, B. W., and Perl, D. P. (1982). Oculopharyngeal muscular dystrophy: an autopsied case from the french-canadian kindred. *J. Neurol. Sci.* 53, 145–158.

Lu-Nguyen, N., Malerba, A., Popplewell, L., Schnell, F., Hanson, G., and Dickson, G. (2017). Systemic antisense therapeutics for dystrophin and myostatin exon splice modulation improve muscle pathology of adult mdx mice. *Mol. Ther. Nucleic Acids* 6, 15–28. doi: 10.1016/j.omtn.2016.11.009

Lu-Nguyen, N. B., Jarmin, S. A., Saleh, A. F., Popplewell, L., Gait, M. J., and Dickson, G. (2015). Combination antisense treatment for destructive exon skipping of myostatin and open reading frame rescue of dystrophin in neonatal mdx mice. *Mol. Ther.* 23, 1341–1348. doi: 10.1038/mt.2015.88

Malerba, A., Klein, P., Bachtarzi, H., Jarmin, S. A., Cordova, G., Ferry, A., et al. (2017). PABPN1 gene therapy for oculopharyngeal muscular dystrophy. *Nat. Commun.* 8:14848. doi: 10.1038/ncomms14848

Malerba, A., Roth, F., Harish, P., Dhiab, J., Lu-Nguyen, N., Cappellari, O., et al. (2019a). Pharmacological modulation of the ER stress response ameliorates oculopharyngeal muscular dystrophy. *Hum. Mol. Genet.* 28, 1694–1708. doi: 10.1093/hmg/ddz007

Malerba, A., Roth, F., Strings, V., Harish, P., Suhy, D., Trollet, C., et al. (2019b). Gene therapy for oculopharyngeal muscular dystrophy. *Muscle Gene Ther.* 2019, 549–564. doi: 10.1007/978-3-030-03095-7_31

Mann, C. J., Perdiguero, E., Kharraz, Y., Aguilar, S., Pessina, P., Serrano, A. L., et al. (2011). Aberrant repair and fibrosis development in skeletal muscle. *Skelet. Muscle* 1:21. doi: 10.1186/2044-5040-1-21

Mariot, V., Joubert, R., and Hourd, C. (2017). Downregulation of myostatin pathway in neuromuscular diseases may explain challenges of anti-myostatin therapeutic approaches. *Nat. Commun.* 8:1859. doi: 10.1038/s41467-017-01486-4

McPherron, A. C. (2010). Metabolic functions of myostatin and GDF11. *Immunol. Endocr. Metab. Agents Med. Chem.* 10, 217–231. doi: 10.2174/187152210793663810

McPherron, A. C., Lawler, A. M., and Lee, S. J. (1997). Regulation of skeletal muscle mass in mice by a new TGF-beta superfamily member. *Nature* 387, 83–90. doi: 10.1038/387083a0

Mendell, J. R., Sahenk, Z., Malik, V., Gomez, A. M., Flanigan, K. M., Lowes, L. P., et al. (2015). A phase 1/2a follistatin gene therapy trial for becker muscular dystrophy. *Mol. Ther.* 23, 192–201. doi: 10.1038/mt.2014.200

Mouisel, E., Relizani, K., Mille-Hamard, L., Denis, R., and Hourd, C. (2014). Myostatin is a key mediator between energy metabolism and endurance capacity of skeletal muscle. *Am. J. Physiol. Regul. Integr. Comp. Physiol.* 307, R444–R454. doi: 10.1152/ajpregu.00377.2013

Murphy, K. T., Koopman, R., Naim, T., Lger, B., Trieu, J., Ibebunjo, C., et al. (2010). Antibody-directed myostatin inhibition in 21-mo-old mice reveals novel roles for myostatin signaling in skeletal muscle structure and function. *FASEB J.* 24, 4433–4442. doi: 10.1096/fj.10-159608

Rodgers, B. D., and Garikipati, D. K. (2008). Clinical, agricultural, and evolutionary biology of myostatin: a comparative review. *Endocr. Rev.* 29, 513–534. doi: 10.1210/er.2008-0003

Sartori, R., Schirwis, E., Blaauw, B., Bortolanza, S., Zhao, J., Enzo, E., et al. (2013). BMP signaling controls muscle mass. *Nat. Genet.* 45, 1309–1318. doi: 10.1038/ng.2772

Schmitt, H. P., and Krause, K. H. (1981). An autopsy study of a familial oculopharyngeal muscular dystrophy (OPMD) with distal spread and neurogenic involvement. *Muscle Nerve* 4, 296–305. doi: 10.1002/mus.880040406

Tavanez, J. P., Bengoechea, R., Berciano, M. T., Lafarga, M., Carmo-Fonseca, M., and Enguita, F. J. (2009). Hsp70 chaperones and type I PRMTs are sequestered at intranuclear inclusions caused by polyalanine expansions in PABPN1. *PLoS One* 4:e6418. doi: 10.1371/journal.pone.0006418

Tinklenberg, J. A., Siebers, E. M., Beatka, M. J., Meng, H., Yang, L., Zhang, Z., et al. (2017). Myostatin inhibition using mRK35 produces skeletal muscle growth and tubular aggregate formation in wild type and TgACTA1D286G nemaline myopathy mice. *Hum. Mol. Genet.* 27, 638–648. doi: 10.1093/hmg/ddx431

Tome, F. M., Chateau, D., Helbling-Leclerc, A., and Fardeau, M. (1997). Morphological changes in muscle fibers in oculopharyngeal muscular dystrophy. *Neuromuscul. Disord.* 7(Suppl. 1), S63–S69.

Trollet, C., Anvar, S. Y., Venema, A., Hargreaves, I. P., Foster, K., Vignaud, A., et al. (2010). Molecular and phenotypic characterization of a mouse model of oculopharyngeal muscular dystrophy reveals severe muscular atrophy restricted to fast glycolytic fibres. *Hum. Mol. Genet.* 19, 2191–2207. doi: 10.1093/hmg/ddq098

Wagner, K. R., Fleckenstein, J. L., Amato, A. A., Barohn, R. J., Bushby, K., Escolar, D. M., et al. (2008). A phase I/IItrial of MYO-029 in adult subjects with muscular dystrophy. *Ann. Neurol.* 63, 561–571. doi: 10.1002/ana.21338

Wagner, K. R., McPherron, A. C., Winik, N., and Lee, S. J. (2002). Loss of myostatin attenuates severity of muscular dystrophy in mdx mice. *Ann. Neurol.* 52, 832–836. doi: 10.1002/ana.10385

White, T. A., and LeBrasseur, N. K. (2014). Myostatin and sarcopenia: opportunities and challenges-a mini-review. *Gerontology* 60, 289–293. doi: 10.1159/000356740

Conflict of Interest: The authors declare that the research was conducted in the absence of any commercial or financial relationships that could be construed as a potential conflict of interest.

frontiers in Physiology

REVIEW
published: 03 April 2020
doi: 10.3389/fphys.2020.00279

Fibrosis in Arrhythmogenic Cardiomyopathy: The Phantom Thread in the Fibro-Adipose Tissue

Angela Serena Maione[1], Chiara Assunta Pilato[1], Michela Casella[2], Alessio Gasperetti[2,3], Ilaria Stadiotti[1], Giulio Pompilio[1,4] and Elena Sommariva[1]*

[1] Vascular Biology and Regenerative Medicine Unit, Centro Cardiologico Monzino IRCCS, Milan, Italy, [2] Heart Rhythm Center, Centro Cardiologico Monzino IRCCS, Milan, Italy, [3] University Heart Center, Zurich University Hospital, Zurich, Switzerland, [4] Department of Clinical Sciences and Community Health, University of Milan, Milan, Italy

Arrhythmogenic cardiomyopathy (ACM) is an inherited heart disorder, predisposing to malignant ventricular arrhythmias leading to sudden cardiac death, particularly in young and athletic patients. Pathological features include a progressive loss of myocardium with fibrous or fibro-fatty substitution. During the last few decades, different clinical aspects of ACM have been well investigated but still little is known about the molecular mechanisms that underlie ACM pathogenesis, leading to these phenotypes. In about 50% of ACM patients, a genetic mutation, predominantly in genes that encode for desmosomal proteins, has been identified. However, the mutation-associated mechanisms, causing the observed cardiac phenotype are not always clear. Until now, the attention has been principally focused on the study of molecular mechanisms that lead to a prominent myocardium adipose substitution, an uncommon marker for a cardiac disease, thus often recognized as hallmark of ACM. Nonetheless, based on Task Force Criteria for the diagnosis of ACM, cardiomyocytes death associated with fibrous replacement of the ventricular free wall must be considered the main tissue feature in ACM patients. For this reason, it urges to investigate ACM cardiac fibrosis. In this review, we give an overview on the cellular effectors, possible triggers, and molecular mechanisms that could be responsible for the ventricular fibrotic remodeling in ACM patients.

Keywords: arrhythmogenic cardiomyopathy, cardiac fibrosis, cardiac extracellular matrix, scar formation, cellular effectors

OPEN ACCESS

Edited by:
Martina Calore,
Maastricht University, Netherlands

Reviewed by:
Michelle S. Parvatiyar,
Florida State University, United States
Raffaella Lombardi,
University of Naples Federico II, Italy

****Correspondence:***
Angela Serena Maione
angela.maione@ccfm.it

Specialty section:
This article was submitted to Striated Muscle Physiology, a section of the journal Frontiers in Physiology

Received: *02 January 2020*
Accepted: *12 March 2020*
Published: *03 April 2020*

Citation:
Maione AS, Pilato CA, Casella M, Gasperetti A, Stadiotti I, Pompilio G and Sommariva E (2020) Fibrosis in Arrhythmogenic Cardiomyopathy: The Phantom Thread in the Fibro-Adipose Tissue. Front. Physiol. 11:279. doi: 10.3389/fphys.2020.00279

INTRODUCTION

Arrhythmogenic cardiomyopathy (ACM) is a rare genetic cardiac disease, with an incidence estimated in 1:5000 (Corrado et al., 2017), which affects predominantly the right ventricle (RV), although left or biventricular forms have been also described. In about 50% of ACM patients, a genetic mutation can be identified, mostly in genes coding for cardiac desmosomes. Non-desmosomal forms of ACM also exist. The mode of inheritance is generally autosomic dominant, even if recessive syndromic forms are also described (Stadiotti et al., 2019). However, these different genetic determinants lead to a similar disease phenotype. All forms of ACM are characterized by incomplete penetrance and variable expressivity even in carriers of the same causative mutation.

This characteristic likely means that different factors, such as genetic background, or environmental determinants, contribute to define the clinical phenotype. From an anatomo-pathological point of view, ACM hearts show a progressive loss of myocardium, inflammatory infiltrates, and fibrous or fibro-fatty replacement. Such tissue heterogeneity predisposes to re-entrant electrical activity that is known to support ventricular arrhythmias, cause, in the worst-case scenario, of sudden cardiac death. Specifically, cardiac fibrosis is originally a protective mechanism against injury, but its uncontrolled progression may lead to excessive collagen deposition and myocardial scar formation. The fibrotic molecular mechanisms are known for cardiac diseases but those specific for ACM still need to be investigated in order to uncover therapeutic targets to improve ACM clinical management.

CLINICAL ASPECTS OF FIBROSIS IN ACM PATIENTS

Arrhythmogenic cardiomyopathy is a rare cardiac pathology characterized by cardiomyocytes (CM) death and replacement of myocardium with fibrotic or fibro-fatty tissue. The fibrotic and fibro-fatty substitution, regardless of the ventricular district, progresses from epicardium to endocardium provoking structural and functional myocardial alterations (Lin et al., 2018). Generally, segmental or irregular fibro-fatty tissue distribution can be observed among patches of CM (Hoorntje et al., 2017). In most cases, the region of the heart typically interested by pathological changes is the RV where abnormal myocardium remodeling is localized in the so-called "triangle of dysplasia," composed by RV inflow tract, RV outflow tract, and RV apex. In particular, during the first stages of the disease, the basal inferior RV region is usually compromised, while RV apex involvement occurs in advanced phases of ACM progression (Te Riele et al., 2013). Fibrosis in the ventricular septum is rare (Hoorntje et al., 2017).

Although ACM has long been defined as a pathology of the RV, left ventricle (LV) involvement has also been reported either in advanced stages of the RV disease or in peculiar LV-dominant forms. Particularly, in the LV, myocardial remodeling mainly affects the posterolateral area and the original concept of "triangle of dysplasia," has evolved to a new scenery of a "quadrangle of ACM" (Te Riele et al., 2013). It has been shown that the LV involvement is different based on the genetic defect. Specifically, more fibrosis is located in the LV free wall of the ACM hearts mutated for phospholamban (*PLN*) than those mutated in desmosomes (Sepehrkhouy et al., 2017). Among desmosomal gene mutations, desmoplakin (*DSP*) or desmoglein 2 (*DSG2*) are often associated with LV-forms (Norman et al., 2005; Pilichou et al., 2006; Sen-Chowdhry et al., 2008). Mechanisms of regional-differences are still to be investigated.

The presence of fibro-fatty substitution in ACM hearts could be evidenced through different diagnostic tools. Echocardiography is the standard imaging technique used to evaluate structural and functional abnormalities of the RV chamber, although it provides limited information on the presence and extent of fibrotic replacement. For these reasons, magnetic resonance imaging (MRI) is currently increasingly recommended for a definitive diagnosis (de Boer et al., 2019). MRI allows to asses ventricular volumes, systolic function, and regional wall motion that are included in diagnostic criteria (Marcus et al., 1982, 2010). Moreover, MRI can detect adipose tissue, and, thanks to gadolinium delayed contrast enhancement acquisition, MRI is the gold-standard exam to characterize myocardial tissue in terms of fibrosis, fatty infiltration, and fibrofatty scar (Kim et al., 1999, 2000; Tandri et al., 2002, 2005).

Invasive tissue characterization to confirm ACM diagnosis can be obtained by an endomyocardial biopsy (EMB). In this setting, an extensive application of EMB has been limited by the low sensitivity of biopsies usually obtained from the interventricular septum, not frequently involved by the disease. In the last few years, EMB is performed after a complete and detailed 3D electroanatomic mapping (EAM) of the ventricular chamber. EAM is used to detect bipolar and/or unipolar low potential areas, which, in ACM, mostly correspond to fibrotic or fibro-adipogenic scar tissue (Santangeli et al., 2012; Casella et al., 2015). Thus, a preliminary EAM allows to directly identify fibrotic substitution areas and perform EMB in the portion of RV wall in the immediate adjacency of the scar (Casella et al., 2017). However, EAM and EAM-guided EMB are not yet recognized in task force guidelines (Santangeli et al., 2011).

PRO-FIBROTIC TRIGGERS

The compromised heart of ACM patients undergoes a functional worsening when subject to intense physical exercise. The practice of physical activity at a competitive level represents one of the major triggers for life-threatening arrhythmias and sudden death in the ACM setting and therefore it is highly discouraged for ACM patients (Cerrone, 2018). Endurance athletes become symptomatic at an earlier age, more likely develop an overt phenotype, and show more frequently ventricular arrhythmias and heart failure (James et al., 2013). Therefore, an athletic lifestyle affects disease penetrance. Furthermore, it is associated with the activation of the sympathetic nervous system, mechanical and oxidative stress, which may prime ACM pathogenesis.

It has been reported that sympathetic dysinnervation characterize both the left (Wichter et al., 1994; Paul et al., 2011) and the RVs (Todica et al., 2018) of ACM patients: the areas affected by myocardial replacement show reduced reuptake of norepinephrine leading to chronic stimulation of adrenergic receptors, which in turn has been related to cardiac fibrosis. The norepinephrine treatment induces cardiac fibrosis promoting a series of events, such as CM death and collagen and transforming growth factor beta 1 (TGFβ1) gene expression in rats' ventricular endocardium (Bhambi and Eghbali, 1991; Castaldi et al., 2014). TGFβ1 overexpression, in turn, could promote an increase of β-adrenergic expression, further enhancing interstitial fibrosis (Iizuka et al., 1994; Mak et al., 2000; Rosenkranz et al., 2002).

Moreover, the β-adrenergic system could regulate the extracellular matrix (ECM) protein turnover: norepinephrine

could increase the expression of metalloproteinase-2 (MMP-2) and decrease the expression of tissue inhibitors of metalloproteinases 1 and 2 (TIMP-1/2) during cardiac remodeling (Briest et al., 2001; Meier et al., 2007).

High-level sport activity also implies an excessive effort of the heart muscle.

Excessive heart stimulation can cause mechanical stretch of fibers. It has been reported that athletes with a history of endurance sport have increased levels of plasmatic TGFβ1 and develop myocardial fibrosis in contrast to novice athletes (Heinemeier et al., 2003; Czarkowska-Paczek et al., 2006). While the physiological adaptation to strength training causes a pressure load and resulting eccentric hypertrophy, endurance exercise causes a volume load and ventricular dilation mostly affecting the RV (Morganroth et al., 1975; Wilson et al., 1985; La Gerche et al., 2012). Interestingly, a positive loop promoting fibrosis is described: changes in ECM composition during cardiac fibrosis alter the mechanical tissue properties increasing its rigidity. Tissue stiffness further promotes the differentiation of myofibroblasts that produce and release collagen. Collagen deposition, in turn, increases stiffness of the tissue (Hinz, 2009). Independently of ACM, exercise training is a known source of fibrotic cardiac remodeling. A rat model of intensive training is characterized by increased cardiac mass, diffuse interstitial collagen deposition, and increased levels of TGFβ1, fibronectin-1, and MMP-2. Intriguingly, detraining can revert the cardiac remodeling observed to control levels (Benito et al., 2011).

In ACM patients, due to (Wang et al., 2018) the genetically determined fragility of desmosomes, the mechanical stretch of CM during endurance exercise may favor cell injury and accentuate the development of the disease. Moreover, a mechanotransduction mechanism (the Hippo pathway), translating mechanical stimuli into activation of fibro-adipogenic signals, is known to participate in ACM pathogenesis (Dupont et al., 2011; Chen et al., 2014). Cardiac overload reduction therapies have been proposed based on ACM animal model findings (Fabritz et al., 2011). Detraining has only a limited effect on arrhythmias reduction (Wang et al., 2018).

Excessive training is also associated with oxidative stress increase (Fabritz et al., 2011; Wang et al., 2018). Uncontrolled reactive oxygen species (ROS) balance causes cell necrosis and apoptosis due to ROS oxidizing effects on proteins, lipids, and DNA, and prompting of pathway modifications (Moris et al., 2017). ROS are involved in the development and progression of cardiovascular diseases, such as cardiac hypertrophy, heart failure, and hypertension (Rani et al., 2016; Siasos et al., 2018). Moreover, oxidative stress is linked to cardiac fibrotic remodeling by regulating fibroblast function and ECM composition. TGFβ1 and ROS positively affect each other during myofibroblast differentiation. Particularly, TGFβ increases oxidative stress by inducing ROS production by mitochondria and decreasing the activity of antioxidant enzymes (Purnomo et al., 2013; Liu and Desai, 2015). In particular, TGFβ1 acts: (1) on mitochondrial ROS production by inducing the expression of NAD(P)H Oxidases4; (2) reducing the concentration of glutathione. Both these events typically occur in fibrotic disease (Cucoranu et al., 2005; Liu and Gaston Pravia, 2010). On the other hand, ROS promote the generation of active TGFβ and regulate ECM protein expression and degradation acting on synthesis and activity of MMPs (Barcellos-Hoff and Dix, 1996; Siwik et al., 2001; Jacob-Ferreira and Schulz, 2013).

Although numerous pieces of evidence concur to a role of oxidative stress in fibrosis, its implication in ACM fibrotic remodeling still to be investigated. Indeed, only one report described increased ROS levels in an ACM cell model (Kim et al., 2013).

An important independent fibrosis cofactor in ACM hearts is inflammation. ACM hearts are characterized by progressive CM death that is replaced by non-contractile fibrotic tissue according to a reparative mechanism against myocardial loss (Valente et al., 1998; Rusciano et al., 2019).

Cardiac fibroblasts and CM are in contact through soluble factors and cell–cell interactions. CM death may represent the initial phase in the remodeling process, by initiating an inflammatory response, myofibroblast activation, and myocardial scar formation (Frangogiannis, 2008; Kakkar and Lee, 2010; Suthahar et al., 2017). Moreover, during inflammation, inflammatory cytokines IL-6, TNFα, and IL-1β are upregulated and involved in promoting cardiac fibroblast proliferation and activation (Plenz et al., 1998; Ferrari, 1999; Turner et al., 2007; Bujak and Frangogiannis, 2009).

Transgenic mice with cardiac restricted overexpression of TNFα exhibit increased collagen synthesis and deposition, MMP-2 and MMP-9 activity and TGFβ expression (Sivasubramanian et al., 2001). Furthermore, it has been demonstrated that the suppression of the IL-1 signaling ameliorates the adverse fibrotic remodeling in association with a reduced inflammation (Bujak et al., 2008). The presence of inflammatory cell patches, mostly macrophages, neutrophils, and T-lymphocytes, in the ventricular wall affected by CM death, has been reported in ACM heart along with a high plasmatic level of pro-inflammatory cytokines (Campian et al., 2010; Asimaki et al., 2011; Campuzano et al., 2012). It has been observed that NFκB signaling is activated in ACM mouse and cell models characterized by different causative desmosomal gene variants. The inhibition of NFκB signaling is able to rescue, *in vitro*, different ACM phenotypic features as distribution of plakoglobin (PG), Cx43, and GSK3β, apoptotic rate, and inflammatory cytokines production. *In vivo*, the pharmacological inhibition of NFκB signaling improves contractile function, reduces the amount of ventricular myocardial necrosis and fibrosis and the number of apoptotic cells, and normalizes the ECG abnormalities (Chelko et al., 2019). This evidence hints to a primary role of inflammation in ACM. In a translational prospect, targeting inflammation could improve different aspects of ACM pathogenesis.

Arrhythmogenic cardiomyopathy most frequently occurs in men, with more severe clinical complications compared to women (Bauce et al., 2008). ACM affected women are characterized by low serum levels of estradiol and raised cardiovascular events underling the cardioprotective role of this hormone. In contrast, a high level of testosterone has been found in the ACM male serum, in line with previous data describing the involvement of testosterone in arrhythmia induction (Ayaz and Howlett, 2015; Akdis et al., 2017; Stadiotti et al., 2019).

Interestingly, the development of cardiac fibrosis has also been linked to gender-associated differences. During cardiac fibrosis collagen type I and III deposition is higher in men compared to women (Kararigas et al., 2014; Regitz-Zagrosek and Kararigas, 2017).

The molecular mechanisms underlying the cardioprotective role of estrogens have not been fully clarified (Piro et al., 2010). It is known that female hormones inhibit cardiac fibroblast proliferation and their capability to synthesize and deposit collagen (Dubey et al., 1998).

Notably, the estradiol differentially acts on collagen expression in cardiac fibroblasts in a gender-dependent manner. Indeed, an estradiol treatment decreases collagen I and III expression in female derived cardiac fibroblasts *via* estradiol receptor α, while in men cardiac fibroblasts, the activation of estradiol receptor β induces the upregulation of collagen synthesis (Mahmoodzadeh et al., 2010).

Moreover, the estradiol could regulate ECM turnover by affecting the expression of MMP-2, which in turn is associated with altered ventricular remodeling in different cardiovascular pathologies (Dworatzek et al., 2019).

The anti-fibrotic effects of estradiol have also been reported in a mouse model of heart failure where the treatment reduces the expression of TGFβ1 and profibrotic genes, like collagen I, and therefore suppresses cardiac fibrosis (Iorga et al., 2016). One report demonstrated the role of sex hormones on different ACM phenotypes in an ACM CM model (Akdis et al., 2017). Nevertheless, further investigations are needed in order to link the sex hormones involvement to ACM associated fibrosis.

CARDIAC EXTRACELLULAR MATRIX REGULATION

The excessive deposition of fibrous connective tissue leads to the formation of a myocardial scar which contributes to the dysregulation of cardiac electrical properties and thus to arrhythmic events.

Cardiac ECM is a well-organized network composed of support proteins that create a solid substrate in which myocytes and non-contractile cells such as fibroblasts, leukocytes, and endothelial cells are placed (Aggeli et al., 2012).

The cardiac ECM supporting fibers are predominantly composed of collagen type I (which forms thick fibers that ensure tensile strength), collagen type III (which forms thin fibers that ensure elasticity) and in a minor fraction by collagen type IV, V, and VI. Moreover, cardiac ECM contains glycosaminoglycans, glycoproteins, and proteoglycans (Frangogiannis, 2012). The ECM also plays a non-structural function supplying growth factors, cytokines, and proteases necessary for cardiac function, cardiac cell destiny, and homeostatic regulation (Rienks et al., 2014).

Extracellular matrix deposition is mostly associated with fibroblasts activation. Different proteinases such as matrix MMPs and TIMPs overall act to a fine regulated homeostatic balance between synthesis and degradation (Kassiri and Khokha, 2005; Spinale et al., 2016).

Following cardiac injury, ECM degradation occurs and promotes inflammatory cell infiltration and fibroblast proliferation. The following fibroblasts to myofibroblasts differentiation represents the event responsible for consistent novel ECM deposition during scar formation.

Alterations in ECM composition and turnover are involved in different cardiac diseases characterized by adverse remodeling with loss of myocardium integrity (Swynghedauw, 1999; Aggeli et al., 2012; Santulli et al., 2012; Cipolletta et al., 2015). Patients affected by idiopathic dilated cardiomyopathy are characterized by an excessive deposition of collagen type III fibers that are poorly cross-linked and lead to cell slippage, ventricular dilatation, and altered diastolic compliance (Gunja-Smith et al., 1996). Furthermore, altered expression of TIMP and MMP levels have been found in the explanted hearts of these patients while increased plasma concentrations have been associated with systolic dysfunction during hypertrophic cardiomyopathy (Brilla et al., 1994; Tyagi et al., 1996; Thomas et al., 1998; Noji et al., 2004).

The molecular basis of ECM organization and remodeling in ACM is still under-investigated. Recently few papers identified a signature of ACM cardiac cell microRNAs, known to be involved in ECM turnover and mechanosensing (Rainer et al., 2018; Puzzi et al., 2019).

CELLULAR EFFECTORS

Cardiac injury represents a trigger for the activation of immune cells that in turn stimulate fibroblasts proliferation and differentiation in myofibroblasts. During physiological cardiac repair, after the wound closure, myofibroblasts apoptosis occurs with consequent resolution of the process. On the contrary, during pathological conditions, myofibroblast secretory activity results extended, inducing the switch from reparative process to fibrotic scar formation (Tomasek et al., 2002; Santiago et al., 2010; Stempien-Otero et al., 2016; Murtha et al., 2017).

To date, the cellular source of myofibroblasts is still not fully defined. The most reliable hypothesis is that resident cardiac fibroblasts are activated during damage, as following pressure overload, with consequent differentiation into myofibroblasts. Notably, it has been reported that ventricular resident Tcf21 positive fibroblasts are a source of myofibroblasts involved in cardiac fibrosis after myocardial infarction (Moore-Morris et al., 2014; Furtado et al., 2016; Kanisicak et al., 2016).

In this context, it is known that epicardial cells undergo epithelial-to-mesenchymal transition (EMT) to generated fibroblasts that could populate the cardiac injury area promoting fibrotic remodeling (Russell et al., 2011; Ruiz-Villalba et al., 2013). Notably, typical pro-fibrotic factors such as TGFβ can induce the EMT of the epicardial cells after cardiac injury (Zeisberg et al., 2007).

Recently, a subset of resident adult cardiac stem cells characterized by the expression of PW1 has been identified as responsible for fibrosis after myocardial infarction. The amount of PW1 positive cells is increased in the ischemic damaged area. PW1 cells are characterized by the high expression of

profibrotic genes and the ability to differentiate into fibroblasts (Yaniz-Galende et al., 2017).

However, other studies indicate that cardiac fibroblasts could derive from resident cardiac mesenchymal cells (C-MSC). In the injured mouse heart, as during myocardial infarction, C-MSC resident population (not recruited from the bone marrow) express stem cell and fibroblast markers like collagen type I and DDR2, suggesting their involvement in scar formation (Carlson et al., 2011). C-MSC have been involved as major player of ACM adipogenesis (Sommariva et al., 2016; Pilato et al., 2018). A C-MSC population isolated based on PDGFRα and Sca1 could be responsible for fibrofatty scar formation in ACM patients. In human and mouse hearts, the fibro-adipogenic progenitors (FAP) population have been implicated in the fibro-fatty substitution in ACM. Indeed, they were characterized as bi-potential cells, most with fibrous commitment, and a small percentage with fat genes expression. In particular, the cardiac FAP limited deletion of DSP leads to an increase interstitial fibrosis with a high TGFβ1 level in mice ventricular myocardium (Lombardi et al., 2016; Sommariva et al., 2017).

Moreover, the possible origin of cardiac fibroblasts from non-cardiac departments is still a matter of debate. It has been reported that bone marrow-derived cells could generate fibroblasts that are in turn involved in cardiac scar formation after myocardial infarction (van Amerongen et al., 2008). Indeed, EGFP positive cells, that are able to produce collagen I contributing to scar formation, have been found in the infarcted cardiac area of EGFP bone marrow chimeric mice. Bone marrow cells may represent the fibroblast population in the initial phase of the remodeling process but are not involved in the persistent fibrotic deposition (van Amerongen et al., 2008).

In addition, fibrocytes could be a further circulating source of cardiac fibroblasts as CD34/CD45 positive cells that expressed fibroblast markers and have been identified in a model of fibrotic ischemia/reperfusion cardiomyopathy (Abe et al., 2001; Haudek et al., 2006; Mollmann et al., 2006; Krenning et al., 2010).

MOLECULAR MECHANISMS

The most well-known pro-fibrotic cytokine involved in cardiac fibrosis is TGFβ (Lloyd-Jones et al., 2009; Borthwick et al., 2013). It participates to tissue remodeling by: (1) promoting fibroblasts expansion and conversion into myofibroblasts; (2) inducing the production and deposition of ECM; and (3) preventing matrix degradation by increasing the expression of TIMP (Bujak and Frangogiannis, 2007).

Specifically, binding of TGFβ to its receptors is the starting point for the activation of downstream signaling cascade that involves different mediators of the canonical (SMADs proteins) or non-canonical (ERK, JNK, and p38 MAPK) pathways.

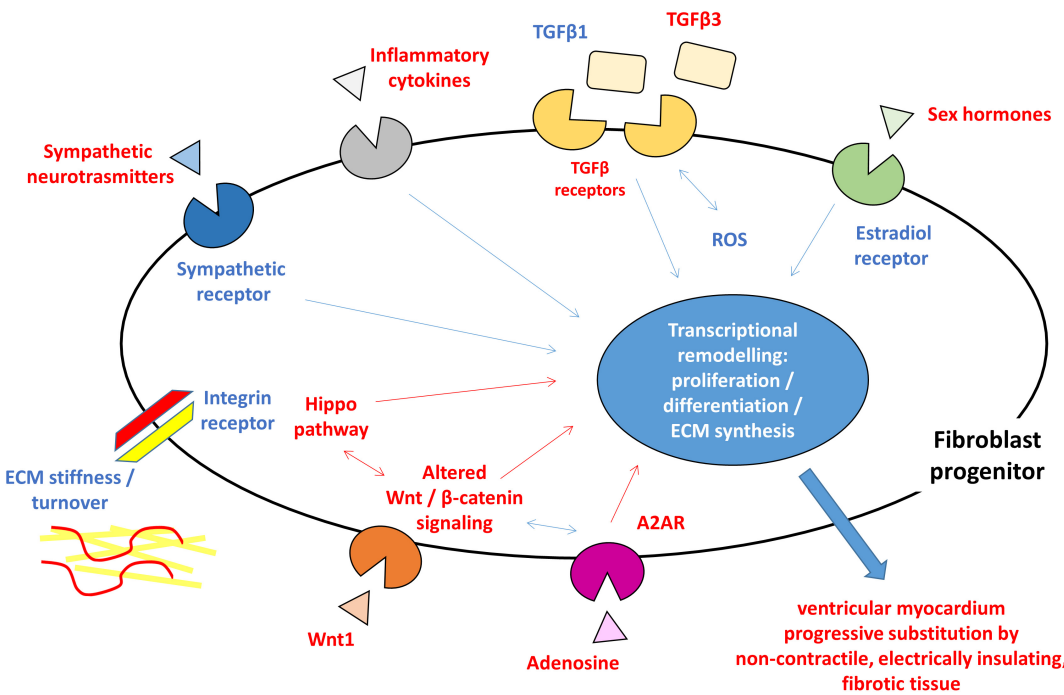

FIGURE 1 | Schematic figure highlighting the hypothesized pro-fibrotic process in ACM. The presence of different triggers (sympathetic nervous system activity, extracellular matrix ECM component, reactive oxygen species ROS, inflammatory cytokines, and sex hormones) and the activation of molecular pathways (Hippo, Wnt/β-catenin, and TGFβ) lead to transcriptional rearrangement for excessive proliferation and myofibroblasts differentiation of fibroblast progenitors. These changes ultimately result in ventricular myocardium progressive substitution by non-contractile, electrically insulating, fibrotic tissue. In blue, what is known about pro-fibrotic mechanisms in general and hypothesized in ACM, in red what is reported for ACM pathogenesis. ACM: arrhythmogenic cardiomyopathy; A2AR: adenosine 2A receptor; ECM: extracellular matrix; ROS: reactive oxygen species; TGFβ: transforming growth factor β.

Although ACM is commonly defined as a "desmosomal disease" being the majority of the patients mutated in desmosomal genes, additional mutations have been identified in genes that encode for non-desmosomal proteins (Moccia et al., 2019). One of those in *TGFB3*, responsible for the ARVD1 form (Beffagna et al., 2005). In ACM patients, mutations in *TGFB3* are linked both to an increase in cardiac fibrotic remodeling and to the regulation of desmosomal gene expression (Beffagna et al., 2005; Tamargo, 2012). Interestingly, also the existence of a possible desmosomal protein-dependent TGFβ expression has been reported. Particularly, it has been demonstrated that plakophilin 2 (PKP2) and DSP control the activity of TGFβ1/p38 MAPK pathway both *in vitro* and *in vivo*. Indeed, in CM with a loss of PKP2, an increase in TGFβ1 signaling is observed with consequent fibrotic genes expression, like collagen and fibronectin (Li et al., 2011). Moreover, DSP expression is lost following *PKP2* knockdown. Since the restoration of DSP expression rescues the activation of TGFβ1/p38 signaling, DSP acts upstream TGFβ1/p38 and downstream PKP2 (Dubash et al., 2016).

Conversely, TGFβ1 treatment induces both an increase of DSP I and II expression and a reduction of DSP degradation in bronchial epithelia (Yoshida et al., 1992).

Overall, these observations demonstrate that TGFβ could modulate the expression of junctional proteins leading to the modification of cellular phenotype and promoting the formation of fibroblasts. In this context, it is important to underline that TGFβ promotes EMT, which is a process characterized by cell–cell contact changes (Zeisberg et al., 2007).

It has been hypothesized that, in ACM, desmosome mutations cause PG translocation from intercalated discs to the nucleus where it competes with β-catenin for the binding to TCF/LEF transcription factors based on the high structural homology (Garcia-Gras et al., 2006; Miravet et al., 2016). The abnormal PG translocation causes the altered canonical activation of Wnt/β-catenin signaling pathway promoting the pathological fibro-adipose myocardial tissue substitution (Garcia-Gras et al., 2006; Moccia et al., 2019).

Intriguingly, it has been reported that TGFβ influences Wnt/β-catenin signaling in a positive manner (Dzialo et al., 2018). TGFβ acts on canonical Wnt pathway in cardiac fibroblasts by: (1) inducing Wnt proteins release; (2) decreasing the expression of Wnt pathway inhibitors; and (3) inhibiting GSK-3β leading to the translocation of active β-catenin from the cytosol to the nucleus (Akhmetshina et al., 2012; Lal et al., 2014; Blyszczuk et al., 2017).

On the other hand, the action of Wnt1 ligand, overexpressed in ventricular epicardium after cardiac damage, causes the activation of Wnt pathway, with consequent differentiation of epicardial fibroblasts into myofibroblasts with collagen synthesis (Duan et al., 2012). The presence of Wnt ligands, in combination with decreased expression of Wnt pathway inhibitors, contributes to nuclear β-catenin localization in human fibroblasts during the fibrotic process while loss of β-catenin in cardiac fibroblasts reduced ECM gene expression and collagen deposition (Xiang et al., 2017).

It is important to emphasize that adipogenesis and fibrogenesis are differentiation programs well regulated by independent pathways. TGFβ1 induces myofibroblast differentiation reducing in parallel the expression of PPARγ, the mast regulator of adipogenic differentiation (Vallee et al., 2017). On the contrary, PPARγ acts preventing myofibroblasts differentiation and collagen deposition.

One further molecular mechanism involved in ACM pathogenesis as well as in myofibroblast differentiation is the Hippo pathway that acts by regulating YAP/TAZ shuttling between nucleus and cytoplasm. Specifically, in the ACM context, the altered PG distribution induces the retention of YAP into the cytoplasm with activation of Hippo pathway and suppression of canonical Wnt-related gene expression (Wada et al., 2011; Zhou and Zhao, 2018). Furthermore, during myofibroblasts differentiation, the YAP/TAZ nuclear localization is associated with Wnt activation and TGFβ1 increase level with consequent SMAD phosphorylation in fibrotic tissues (Liu et al., 2015, 2018; Piersma et al., 2015).

Recently, the activation of the adenosine 2A receptor (A2AR) has been reported to contribute to the progression of fibrosis in an ACM animal model (Cerrone et al., 2018). The binding of adenosine to A2AR stimulates expression of TGFβ, CTGF, and matrix production (Shaikh et al., 2016). Moreover, A2AR activation interacts with the Wnt pathway (Shaikh et al., 2016; Zhang et al., 2017).

CONCLUSION

The ACM specific cardiac remodeling is characterized by the progressive substitution of ventricular myocardium of patients by non-contractile fibrotic or adipose tissue. While adipogenesis has been extensively studied in this pathological context, fibrosis, a cardiac phenotype common to most cardiac diseases, remains under-investigated.

Myocardial fibrosis is a clinical feature shared by several heart diseases such as ischemic cardiomyopathy, dilated cardiomyopathy, hypertrophic cardiomyopathy, hypertensive heart disease, and heart failure. Ventricular fibrosis may develop different modality depending on disease progression and typically result in the formation of substrate vulnerable to arrhythmic events. The cardiac fibroblast activation and differentiation into myofibroblasts and the resulting scar formation commonly occur following a cardiac injury. This event represents a reparative process but during a pathological cardiac condition, it becomes a persistent status that leads to altered myocardial structure and function. As described in other cardiac diseases, the presence of fibroblasts and fibroblast progenitors, the excessive collagen deposition, and the following modification of mechanical stiffness may improve the tissue discontinuity occurring in the ACM hearts. Therefore, most of what is known about fibrotic processes and is summarized in this review is iterated from studies in other settings. However, it is expected that triggering agents, cellular effectors, and mechanisms are comparable to what previously described. Responsible cells are likely cardiac fibroblasts, either from

FAP progenitors or C-MSC. ACM key pathogenic mechanisms such as Wnt and Hippo are playing direct roles, with the support of TGFβ-mediated mechanisms, which prompts fibrosis as an alternative to adipogenesis. The whole process is possibly triggered by genetically driven myocardial damage, and inflammation, oxidative stress, mechanical and neuro-hormonal signaling are magnifying factors (**Figure 1**), thus representing possible targets for therapies.

Nevertheless, ACM specific fibrosis remains a scientific gap of knowledge to be filled with further studies, in order to clarify specific pathways as target for novel specific therapeutic actions.

AUTHOR CONTRIBUTIONS

All authors contributed to the writing of the paragraphs and to the critical review of them.

FUNDING

This study was supported by the Transnational Research Projects on Cardiovascular Diseases (ACM-HFJTC2016_FP-40-021) and the Italian Ministry of Health (RC 2019 – ID 2754330 to Centro Cardiologico Monzino-IRCCS).

REFERENCES

Abe, R., Donnelly, S. C., Peng, T., Bucala, R., and Metz, C. N. (2001). Peripheral blood fibrocytes: differentiation pathway and migration to wound sites. *J. Immunol.* 166, 7556–7562. doi: 10.4049/jimmunol.166.12.7556

Aggeli, C., Pietri, P., Felekos, I., Rautopoulos, L., Toutouzas, K., Tsiamis, E., et al. (2012). Myocardial structure and matrix metalloproteinases. *Curr. Top. Med. Chem.* 12, 1113–1131. doi: 10.2174/1568026611208011113

Akdis, D., Saguner, A. M., Shah, K., Wei, C., Medeiros-Domingo, A., von Eckardstein, A., et al. (2017). Sex hormones affect outcome in arrhythmogenic right ventricular cardiomyopathy/dysplasia: from a stem cell derived cardiomyocyte-based model to clinical biomarkers of disease outcome. *Eur. Heart J.* 38, 1498–1508. doi: 10.1093/eurheartj/ehx011

Akhmetshina, A., Palumbo, K., Dees, C., Bergmann, C., Venalis, P., Zerr, P., et al. (2012). Activation of canonical Wnt signalling is required for TGF-beta-mediated fibrosis. *Nat. Commun.* 3:735. doi: 10.1038/ncomms1734

Asimaki, A., Tandri, H., Duffy, E. R., Winterfield, J. R., Mackey-Bojack, S., Picken, M. M., et al. (2011). Altered desmosomal proteins in granulomatous myocarditis and potential pathogenic links to arrhythmogenic right ventricular cardiomyopathy. *Circ. Arrhythm Electrophysiol.* 4, 743–752. doi: 10.1161/CIRCEP.111.964890

Ayaz, O., and Howlett, S. E. (2015). Testosterone modulates cardiac contraction and calcium homeostasis: cellular and molecular mechanisms. *Biol. Sex Differ.* 6:9. doi: 10.1186/s13293-015-0027-9

Barcellos-Hoff, M. H., and Dix, T. A. (1996). Redox-mediated activation of latent transforming growth factor-beta 1. *Mol. Endocrinol.* 10, 1077–1083. doi: 10.1210/me.10.9.1077

Bauce, B., Frigo, G., Marcus, F. I., Basso, C., Rampazzo, A., Maddalena, F., et al. (2008). Comparison of clinical features of arrhythmogenic right ventricular cardiomyopathy in men versus women. *Am. J. Cardiol.* 102, 1252–1257. doi: 10.1016/j.amjcard.2008.06.054

Beffagna, G., Occhi, G., Nava, A., Vitiello, L., Ditadi, A., Basso, C., et al. (2005). Regulatory mutations in transforming growth factor-beta3 gene cause arrhythmogenic right ventricular cardiomyopathy type 1. *Cardiovasc. Res.* 65, 366–373. doi: 10.1016/j.cardiores.2004.10.005

Benito, B., Gay-Jordi, G., Serrano-Mollar, A., Guasch, E., Shi, Y., Tardif, J. C., et al. (2011). Cardiac arrhythmogenic remodeling in a rat model of long-term intensive exercise training. *Circulation* 123, 13–22. doi: 10.1161/circulationaha.110.938282

Bhambi, B., and Eghbali, M. (1991). Effect of norepinephrine on myocardial collagen gene expression and response of cardiac fibroblasts after norepinephrine treatment. *Am. J. Pathol.* 139, 1131–1142.

Blyszczuk, P., Muller-Edenborn, B., Valenta, T., Osto, E., Stellato, M., Behnke, S., et al. (2017). Transforming growth factor-beta-dependent Wnt secretion controls myofibroblast formation and myocardial fibrosis progression in experimental autoimmune myocarditis. *Eur. Heart J.* 38, 1413–1425.

Borthwick, L. A., Wynn, T. A., and Fisher, A. J. (2013). Cytokine mediated tissue fibrosis. *Biochim. Biophys. Acta* 1832, 1049–1060. doi: 10.1016/j.bbadis.2012.09.014

Briest, W., Holzl, A., Rassler, B., Deten, A., Leicht, M., Baba, H. A., et al. (2001). Cardiac remodeling after long term norepinephrine treatment in rats. *Cardiovasc. Res.* 52, 265–273. doi: 10.1016/s0008-6363(01)00398-4

Brilla, C. G., Zhou, G., Matsubara, L., and Weber, K. T. (1994). Collagen metabolism in cultured adult rat cardiac fibroblasts: response to angiotensin II and aldosterone. *J. Mol. Cell Cardiol.* 26, 809–820. doi: 10.1006/jmcc.1994.1098

Bujak, M., Dobaczewski, M., Chatila, K., Mendoza, L. H., Li, N., Reddy, A., et al. (2008). Interleukin-1 receptor type I signaling critically regulates infarct healing and cardiac remodeling. *Am. J. Pathol.* 173, 57–67. doi: 10.2353/ajpath.2008.070974

Bujak, M., and Frangogiannis, N. G. (2007). The role of TGF-beta signaling in myocardial infarction and cardiac remodeling. *Cardiovasc. Res.* 74, 184–195. doi: 10.1016/j.cardiores.2006.10.002

Bujak, M., and Frangogiannis, N. G. (2009). The role of IL-1 in the pathogenesis of heart disease. *Arch. Immunol. Ther. Exp. (Warsz)* 57, 165–176. doi: 10.1007/s00005-009-0024-y

Campian, M. E., Verberne, H. J., Hardziyenka, M., de Groot, E. A., van Moerkerken, A. F., van Eck-Smit, B. L., et al. (2010). Assessment of inflammation in patients with arrhythmogenic right ventricular cardiomyopathy/dysplasia. *Eur. J. Nucl. Med. Mol. Imaging* 37, 2079–2085. doi: 10.1007/s00259-010-1525-y

Campuzano, O., Alcalde, M., Iglesias, A., Barahona-Dussault, C., Sarquella-Brugada, G., Benito, B., et al. (2012). Arrhythmogenic right ventricular cardiomyopathy: severe structural alterations are associated with inflammation. *J. Clin. Pathol.* 65, 1077–1083. doi: 10.1136/jclinpath-2012-201022

Carlson, S., Trial, J., Soeller, C., and Entman, M. L. (2011). Cardiac mesenchymal stem cells contribute to scar formation after myocardial infarction. *Cardiovasc. Res.* 2011, 99–107. doi: 10.1093/cvr/cvr061

Casella, M., Dello Russo, A., Vettor, G., Lumia, G., Catto, V., Sommariva, E., et al. (2017). Electroanatomical mapping systems and intracardiac echo integration for guided endomyocardial biopsy. *Expert Rev. Med. Dev.* 14, 609–619. doi: 10.1080/17434440.2017.1351875

Casella, M., Pizzamiglio, F., Dello Russo, A., Carbucicchio, C., Al-Mohani, G., Russo, E., et al. (2015). Feasibility of combined unipolar and bipolar voltage maps to improve sensitivity of endomyocardial biopsy. *Circ. Arrhythm Electrophysiol.* 8, 625–632. doi: 10.1161/CIRCEP.114.002216

Castaldi, A., Zaglia, T., Di Mauro, V., Carullo, P., Viggiani, G., Borile, G., et al. (2014). MicroRNA-133 modulates the beta1-adrenergic receptor transduction cascade. *Circ Res.* 115, 273–283. doi: 10.1161/CIRCRESAHA.115.303252

Cerrone, M. (2018). Exercise: a risky subject in arrhythmogenic cardiomyopathy. *J. Am. Heart Assoc.* 7:e009611.

Cerrone, M., van Opbergen, C. J. M., Malkani, K., Irrera, N., Zhang, M., Van Veen, T. A. B., et al. (2018). Blockade of the adenosine 2A receptor mitigates the cardiomyopathy induced by loss of plakophilin-2 expression. *Front. Physiol.* 9:1750. doi: 10.3389/fphys.2018.01750

Chelko, S. P., Asimaki, A., Lowenthal, J., Bueno-Beti, C., Bedja, D., Scalco, A., et al. (2019). Therapeutic modulation of the immune response in arrhythmogenic cardiomyopathy. *Circulation* 140, 1491–1505. doi: 10.1161/CIRCULATIONAHA.119.040676

Chen, S. N., Gurha, P., Lombardi, R., Ruggiero, A., Willerson, J. T., and Marian, A. J. (2014). The hippo pathway is activated and is a causal mechanism for

adipogenesis in arrhythmogenic cardiomyopathy. *Circ. Res.* 114, 454–468. doi: 10.1161/CIRCRESAHA.114.302810

Cipolletta, E., Rusciano, M. R., Maione, A. S., Santulli, G., Sorriento, D., Del Giudice, C., et al. (2015). Targeting the CaMKII/ERK interaction in the heart prevents cardiac hypertrophy. *PLoS ONE* 10:e0130477. doi: 10.1371/journal.pone.0130477

Corrado, D., Link, M. S., and Calkins, H. (2017). Arrhythmogenic right ventricular cardiomyopathy. *N. Engl. J. Med.* 376, 61–72.

Cucoranu, I., Clempus, R., Dikalova, A., Phelan, P. J., Ariyan, S., Dikalov, S., et al. (2005). NAD(P)H oxidase 4 mediates transforming growth factor-beta1-induced differentiation of cardiac fibroblasts into myofibroblasts. *Circ Res.* 97, 900–907. doi: 10.1161/01.res.0000187457.24338.3d

Czarkowska-Paczek, B., Bartlomiejczyk, I., and Przybylski, J. (2006). The serum levels of growth factors: PDGF, TGF-beta and VEGF are increased after strenuous physical exercise. *J. Physiol. Pharmacol.* 57, 189–197.

de Boer, R. A., De Keulenaer, G., Bauersachs, J., Brutsaert, D., Cleland, J. G., Diez, J., et al. (2019). Towards better definition, quantification and treatment of fibrosis in heart failure. A scientific roadmap by the committee of translational research of the heart failure association (HFA) of the european society of cardiology. *Eur. J. Heart Fail* 21, 272–285. doi: 10.1002/ejhf.1406

Duan, J., Gherghe, C., Liu, D., Hamlett, E., Srikantha, L., Rodgers, L., et al. (2012). Wnt1/betacatenin injury response activates the epicardium and cardiac fibroblasts to promote cardiac repair. *EMBO J.* 31, 429–442. doi: 10.1038/emboj.2011.418

Dubash, A. D., Kam, C. Y., Aguado, B. A., Patel, D. M., Delmar, M., Shea, L. D., et al. (2016). Plakophilin-2 loss promotes TGF-beta1/p38 MAPK-dependent fibrotic gene expression in cardiomyocytes. *J. Cell Biol.* 212, 425–438. doi: 10.1083/jcb.201507018

Dubey, R. K., Gillespie, D. G., Jackson, E. K., and Keller, P. J. (1998). 17Beta-estradiol, its metabolites, and progesterone inhibit cardiac fibroblast growth. *Hypertension* 31(1 Pt 2), 522–528. doi: 10.1161/01.hyp.31.1.522

Dupont, S., Morsut, L., Aragona, M., Enzo, E., Giulitti, S., Cordenonsi, M., et al. (2011). Role of YAP/TAZ in mechanotransduction. *Nature* 474, 179–183. doi: 10.1038/nature10137

Dworatzek, E., Mahmoodzadeh, S., Schriever, C., Kusumoto, K., Kramer, L., Santos, G., et al. (2019). Sex-specific regulation of collagen I and III expression by 17beta-Estradiol in cardiac fibroblasts: role of estrogen receptors. *Cardiovasc. Res.* 115, 315–327. doi: 10.1093/cvr/cvy185

Dzialo, E., Tkacz, K., and Blyszczuk, P. (2018). Crosstalk between the TGF-beta and WNT signalling pathways during cardiac fibrogenesis. *Acta Biochim. Pol.* 65, 341–349. doi: 10.18388/abp.2018_2635

Fabritz, L., Hoogendijk, M. G., Scicluna, B. P., van Amersfoorth, S. C., Fortmueller, L., Wolf, S., et al. (2011). Load-reducing therapy prevents development of arrhythmogenic right ventricular cardiomyopathy in plakoglobin-deficient mice. *J. Am. Coll. Cardiol.* 57, 740–750. doi: 10.1016/j.jacc.2010.09.046

Ferrari, R. (1999). The role of TNF in cardiovascular disease. *Pharmacol. Res.* 40, 97–105. doi: 10.1006/phrs.1998.0463

Frangogiannis, N. G. (2008). The immune system and cardiac repair. *Pharmacol. Res.* 58, 88–111. doi: 10.1016/j.phrs.2008.06.007

Frangogiannis, N. G. (2012). Matricellular proteins in cardiac adaptation and disease. *Physiol. Rev.* 92, 635–688. doi: 10.1152/physrev.00008.2011

Furtado, M. B., Costa, M. W., and Rosenthal, N. A. (2016). The cardiac fibroblast: origin, identity and role in homeostasis and disease. *Differentiation* 92, 93–101. doi: 10.1016/j.diff.2016.06.004

Garcia-Gras, E., Lombardi, R., Giocondo, M. J., Willerson, J. T., Schneider, M. D., Khoury, D. S., et al. (2006). Suppression of canonical Wnt/beta-catenin signaling by nuclear plakoglobin recapitulates phenotype of arrhythmogenic right ventricular cardiomyopathy. *J. Clin. Invest.* 116, 2012–2021. doi: 10.1172/jci27751

Gunja-Smith, Z., Morales, A. R., Romanelli, R., and Woessner, J. F. Jr. (1996). Remodeling of human myocardial collagen in idiopathic dilated cardiomyopathy. Role of metalloproteinases and pyridinoline cross-links. *Am. J. Pathol.* 148, 1639–1648.

Haudek, S. B., Xia, Y., Huebener, P., Lee, J. M., Carlson, S., Crawford, J. R., et al. (2006). Bone marrow-derived fibroblast precursors mediate ischemic cardiomyopathy in mice. *Proc. Natl. Acad. Sci. U.S.A.* 103, 18284–18289. doi: 10.1073/pnas.0608799103

Heinemeier, K., Langberg, H., and Kjaer, M. (2003). Exercise-induced changes in circulating levels of transforming growth factor-beta-1 in humans: methodological considerations. *Eur. J. Appl. Physiol.* 90, 171–177. doi: 10.1007/s00421-003-0881-8

Hinz, B. (2009). Tissue stiffness, latent TGF-beta1 activation, and mechanical signal transduction: implications for the pathogenesis and treatment of fibrosis. *Curr. Rheumatol. Rep.* 11, 120–126. doi: 10.1007/s11926-009-0017-1

Hoorntje, E. T., Te Rijdt, W. P., James, C. A., Pilichou, K., Basso, C., Judge, D. P., et al. (2017). Arrhythmogenic cardiomyopathy: pathology, genetics, and concepts in pathogenesis. *Cardiovasc. Res.* 113, 1521–1531. doi: 10.1093/cvr/cvx150

Iizuka, K., Sano, H., Kawaguchi, H., and Kitabatake, A. (1994). Transforming growth factor beta-1 modulates the number of beta-adrenergic receptors in cardiac fibroblasts. *J. Mol. Cell Cardiol.* 26, 435–440.

Iorga, A., Li, J., Sharma, S., Umar, S., Bopassa, J. C., Nadadur, R. D., et al. (2016). Rescue of pressure overload-induced heart failure by estrogen therapy. *J. Am. Heart Assoc.* 5:e002482.

Jacob-Ferreira, A. L., and Schulz, R. (2013). Activation of intracellular matrix metalloproteinase-2 by reactive oxygen-nitrogen species: consequences and therapeutic strategies in the heart. *Arch. Biochem. Biophys.* 540, 82–93. doi: 10.1016/j.abb.2013.09.019

James, C. A., Bhonsale, A., Tichnell, C., Murray, B., Russell, S. D., Tandri, H., et al. (2013). Exercise increases age-related penetrance and arrhythmic risk in arrhythmogenic right ventricular dysplasia/cardiomyopathy-associated desmosomal mutation carriers. *J. Am. Coll. Cardiol.* 62, 1290–1297. doi: 10.1016/j.jacc.2013.06.033

Kakkar, R., and Lee, R. T. (2010). Intramyocardial fibroblast myocyte communication. *Circ. Res.* 106, 47–57. doi: 10.1161/CIRCRESAHA.109.207456

Kanisicak, O., Khalil, H., Ivey, M. J., Karch, J., Maliken, B. D., Correll, R. N., et al. (2016). Genetic lineage tracing defines myofibroblast origin and function in the injured heart. *Nat. Commun.* 7:12260. doi: 10.1038/ncomms12260

Kararigas, G., Dworatzek, E., Petrov, G., Summer, H., Schulze, T. M., Baczko, I., et al. (2014). Sex-dependent regulation of fibrosis and inflammation in human left ventricular remodelling under pressure overload. *Eur. J. Heart Fail* 2014, 1160–1167. doi: 10.1002/ejhf.171

Kassiri, Z., and Khokha, R. (2005). Myocardial extra-cellular matrix and its regulation by metalloproteinases and their inhibitors. *Thromb. Haemost* 93, 212–219. doi: 10.1160/th04-08-0522

Kim, C., Wong, J., Wen, J., Wang, S., Wang, C., Spiering, S., et al. (2013). Studying arrhythmogenic right ventricular dysplasia with patient-specific iPSCs. *Nature* 494, 105–110. doi: 10.1038/nature11799

Kim, R. J., Fieno, D. S., Parrish, T. B., Harris, K., Chen, E. L., Simonetti, O., et al. (1999). Relationship of MRI delayed contrast enhancement to irreversible injury, infarct age, and contractile function. *Circulation* 100, 1992–2002. doi: 10.1161/01.cir.100.19.1992

Kim, R. J., Wu, E., Rafael, A., Chen, E. L., Parker, M. A., Simonetti, O., et al. (2000). The use of contrast-enhanced magnetic resonance imaging to identify reversible myocardial dysfunction. *N. Engl. J. Med.* 343, 1445–1453. doi: 10.1056/nejm200011163432003

Krenning, G., Zeisberg, E. M., and Kalluri, R. (2010). The origin of fibroblasts and mechanism of cardiac fibrosis. *J. Cell Physiol.* 2010, 631–637. doi: 10.1002/jcp.22322

La Gerche, A., Burns, A. T., Mooney, D. J., Inder, W. J., Taylor, A. J., Bogaert, J., et al. (2012). Exercise-induced right ventricular dysfunction and structural remodelling in endurance athletes. *Eur. Heart J.* 33, 998–1006. doi: 10.1093/eurheartj/ehr397

Lal, H., Ahmad, F., Zhou, J., Yu, J. E., Vagnozzi, R. J., Guo, Y., et al. (2014). Cardiac fibroblast glycogen synthase kinase-3beta regulates ventricular remodeling and dysfunction in ischemic heart. *Circulation* 130, 419–430. doi: 10.1161/CIRCULATIONAHA.113.008364

Li, D., Liu, Y., Maruyama, M., Zhu, W., Chen, H., Zhang, W., et al. (2011). Restrictive loss of plakoglobin in cardiomyocytes leads to arrhythmogenic cardiomyopathy. *Hum. Mol. Genet.* 20, 4582–4596. doi: 10.1093/hmg/ddr392

Lin, C. Y., Lin, Y. J., Li, C. H., Chung, F. P., Lo, M. T., Lin, C., et al. (2018). Heterogeneous distribution of substrates between the endocardium and epicardium promotes ventricular fibrillation in arrhythmogenic right

ventricular dysplasia/cardiomyopathy. *Europace* 20, 501–511. doi: 10.1093/europace/euw393

Liu, F., Lagares, D., Choi, K. M., Stopfer, L., Marinkovic, A., Vrbanac, V., et al. (2015). Mechanosignaling through YAP and TAZ drives fibroblast activation and fibrosis. *Am. J. Physiol. Lung Cell Mol. Physiol.* 308, L344–L357. doi: 10.1152/ajplung.00300.2014

Liu, R. M., and Desai, L. P. (2015). Reciprocal regulation of TGF-beta and reactive oxygen species: a perverse cycle for fibrosis. *Redox Biol.* 6, 565–577. doi: 10.1016/j.redox.2015.09.009

Liu, R. M., and Gaston Pravia, K. A. (2010). Oxidative stress and glutathione in TGF-beta-mediated fibrogenesis. *Free Radic. Biol. Med.* 48, 1–15. doi: 10.1016/j.freeradbiomed.2009.09.026

Liu, X., Long, X., Liu, W., Zhao, Y., Hayashi, T., Yamato, M., et al. (2018). Type I collagen induces mesenchymal cell differentiation into myofibroblasts through YAP-induced TGF-beta1 activation. *Biochimie* 150, 110–130. doi: 10.1016/j.biochi.2018.05.005

Lloyd-Jones, D., Adams, R., Carnethon, M., De Simone, G., Ferguson, T. B., Flegal, K., et al. (2009). Heart disease and stroke statistics–2009 update: a report from the American Heart Association Statistics Committee and Stroke Statistics Subcommittee. *Circulation* 119, e21–e181.

Lombardi, R., Chen, S. N., Ruggiero, A., Gurha, P., Czernuszewicz, G. Z., Willerson, J. T., et al. (2016). Cardiac fibro-adipocyte progenitors express desmosome proteins and preferentially differentiate to adipocytes upon deletion of the desmoplakin gene. *Circ. Res.* 119, 41–54. doi: 10.1161/CIRCRESAHA.115.308136

Mahmoodzadeh, S., Dworatzek, E., Fritschka, S., Pham, T. H., and Regitz-Zagrosek, V. (2010). 17beta-Estradiol inhibits matrix metalloproteinase-2 transcription via MAP kinase in fibroblasts. *Cardiovasc. Res.* 85, 719–728. doi: 10.1093/cvr/cvp350

Mak, J. C., Rousell, J., Haddad, E. B., and Barnes, P. J. (2000). Transforming growth factor-beta1 inhibits beta2-adrenoceptor gene transcription. *Naunyn Schmiedebergs Arch. Pharmacol.* 362, 520–525. doi: 10.1007/s002100000321

Marcus, F. I., Fontaine, G. H., Guiraudon, G., Frank, R., Laurenceau, J. L., Malergue, C., et al. (1982). Right ventricular dysplasia: a report of 24 adult cases. *Circulation* 65, 384–398. doi: 10.1161/01.cir.65.2.384

Marcus, F. I., McKenna, W. J., Sherrill, D., Basso, C., Bauce, B., Bluemke, D. A., et al. (2010). Diagnosis of arrhythmogenic right ventricular cardiomyopathy/dysplasia: proposed modification of the Task Force Criteria. *Eur. Heart J.* 31, 806–814. doi: 10.1093/eurheartj/ehq025

Meier, H., Bullinger, J., Deten, A., Marx, G., Rabald, S., Zimmer, H. G., et al. (2007). Tissue inhibitor of matrix metalloproteinase-1 in norepinephrine-induced remodeling of the mouse heart. *Cell Physiol. Biochem.* 20, 825–836. doi: 10.1159/000110442

Miravet, S., Piedra, J., Miro, F., Itarte, E., Garcia, de Herreros, A., et al. (2016). The transcriptional factor Tcf-4 contains different binding sites for beta-catenin and plakoglobin. *J. Biol. Chem.* 291:18854. doi: 10.1074/jbc.a116.110248

Moccia, F., Lodola, F., Stadiotti, I., Pilato, C. A., Bellin, M., Carugo, S., et al. (2019). Calcium as a key player in arrhythmogenic cardiomyopathy: adhesion disorder or intracellular alteration? *Int. J. Mol. Sci.* 20:3986. doi: 10.3390/ijms20163986

Mollmann, H., Nef, H. M., Kostin, S., von Kalle, C., Pilz, I., Weber, M., et al. (2006). Bone marrow-derived cells contribute to infarct remodelling. *Cardiovasc. Res.* 71, 661–671. doi: 10.1016/j.cardiores.2006.06.013

Moore-Morris, T., Guimaraes-Camboa, N., Banerjee, I., Zambon, A. C., Kisseleva, T., Velayoudon, A., et al. (2014). Resident fibroblast lineages mediate pressure overload-induced cardiac fibrosis. *J. Clin. Invest.* 124, 2921–2934. doi: 10.1172/JCI74783

Morganroth, J., Maron, B. J., Henry, W. L., and Epstein, S. E. (1975). Comparative left ventricular dimensions in trained athletes. *Ann. Intern. Med.* 82, 521–524.

Moris, D., Spartalis, M., Spartalis, E., Karachaliou, G. S., Karaolanis, G. I., Tsourouflis, G., et al. (2017). The role of reactive oxygen species in the pathophysiology of cardiovascular diseases and the clinical significance of myocardial redox. *Ann. Transl. Med.* 5:326. doi: 10.21037/atm.2017.06.27

Murtha, L. A., Schuliga, M. J., Mabotuwana, N. S., Hardy, S. A., Waters, D. W., Burgess, J. K., et al. (2017). The processes and mechanisms of cardiac and pulmonary fibrosis. *Front. Physiol.* 8:777. doi: 10.3389/fphys.2017.00777

Noji, Y., Shimizu, M., Ino, H., Higashikata, T., Yamaguchi, M., Nohara, A., et al. (2004). Increased circulating matrix metalloproteinase-2 in patients with hypertrophic cardiomyopathy with systolic dysfunction. *Circ. J.* 68, 355–360. doi: 10.1253/circj.68.355

Norman, M., Simpson, M., Mogensen, J., Shaw, A., Hughes, S., Syrris, P., et al. (2005). Novel mutation in desmoplakin causes arrhythmogenic left ventricular cardiomyopathy. *Circulation* 112, 636–642. doi: 10.1161/circulationaha.104.532234

Paul, M., Wichter, T., Kies, P., Gerss, J., Wollmann, C., Rahbar, K., et al. (2011). Cardiac sympathetic dysfunction in genotyped patients with arrhythmogenic right ventricular cardiomyopathy and risk of recurrent ventricular tachyarrhythmias. *J. Nucl. Med.* 52, 1559–1565. doi: 10.2967/jnumed.111.088997

Piersma, B., Bank, R. A., and Boersema, M. (2015). Signaling in fibrosis: TGF-beta, WNT, and YAP/TAZ converge. *Front. Med. (Lausanne)* 2:59. doi: 10.3389/fmed.2015.00059

Pilato, C. A., Stadiotti, I., Maione, A. S., Saverio, V., Catto, V., Tundo, F., et al. (2018). Isolation and characterization of cardiac mesenchymal stromal cells from endomyocardial bioptic samples of arrhythmogenic cardiomyopathy patients. *J. Vis. Exp.* 28:57263.

Pilichou, K., Nava, A., Basso, C., Beffagna, G., Bauce, B., Lorenzon, A., et al. (2006). Mutations in desmoglein-2 gene are associated with arrhythmogenic right ventricular cardiomyopathy. *Circulation* 113, 1171–1179.

Piro, M., Della Bona, R., Abbate, A., Biasucci, L. M., and Crea, F. (2010). Sex-related differences in myocardial remodeling. *J. Am. Coll. Cardiol.* 55, 1057–1065. doi: 10.1016/j.jacc.2009.09.065

Plenz, G., Song, Z. F., Reichenberg, S., Tjan, T. D., Robenek, H., and Deng, M. C. (1998). Left-ventricular expression of interleukin-6 messenger-RNA higher in idiopathic dilated than in ischemic cardiomyopathy. *Thorac. Cardiovasc. Surg.* 46, 213–216. doi: 10.1055/s-2007-1010227

Purnomo, Y., Piccart, Y., Coenen, T., Prihadi, J. S., and Lijnen, P. J. (2013). Oxidative stress and transforming growth factor-beta1-induced cardiac fibrosis. *Cardiovasc. Hematol. Disord. Drug Targets* 13, 165–172. doi: 10.2174/1871529x11313020010

Puzzi, L., Borin, D., Gurha, P., Lombardi, R., Martinelli, V., Weiss, M., et al. (2019). Knock down of plakophillin 2 dysregulates adhesion pathway through upregulation of mir200b and alters the mechanical properties in cardiac cells. *Cells* 8:E1639.

Rainer, J., Meraviglia, V., Blankenburg, H., Piubelli, C., Pramstaller, P. P., Paolin, A., et al. (2018). The arrhythmogenic cardiomyopathy-specific coding and non-coding transcriptome in human cardiac stromal cells. *BMC Genomics* 19:491. doi: 10.1186/s12864-018-4876-6

Rani, V., Deep, G., Singh, R. K., Palle, K., and Yadav, U. C. (2016). Oxidative stress and metabolic disorders: pathogenesis and therapeutic strategies. *Life Sci.* 148, 183–193. doi: 10.1016/j.lfs.2016.02.002

Regitz-Zagrosek, V., and Kararigas, G. (2017). Mechanistic pathways of sex differences in cardiovascular disease. *Physiol. Rev.* 97, 1–37. doi: 10.1152/physrev.00021.2015

Rienks, M., Papageorgiou, A. P., Frangogiannis, N. G., and Heymans, S. (2014). Myocardial extracellular matrix: an ever-changing and diverse entity. *Circ. Res.* 114, 872–888. doi: 10.1161/CIRCRESAHA.114.302533

Rosenkranz, S., Flesch, M., Amann, K., Haeuseler, C., Kilter, H., Seeland, U., et al. (2002). Alterations of beta-adrenergic signaling and cardiac hypertrophy in transgenic mice overexpressing TGF-beta(1). *Am. J. Physiol. Heart Circ. Physiol.* 283, H1253–H1262.

Ruiz-Villalba, A., Ziogas, A., Ehrbar, M., and Perez-Pomares, J. M. (2013). Characterization of epicardial-derived cardiac interstitial cells: differentiation and mobilization of heart fibroblast progenitors. *PLoS ONE* 8:e53694. doi: 10.1371/journal.pone.0053694

Rusciano, M. R., Sommariva, E., Douin-Echinard, V., Ciccarelli, M., Poggio, P., and Maione, A. S. (2019). CaMKII activity in the inflammatory response of cardiac diseases. *Int. J. Mol. Sci.* 20:E4374.

Russell, J. L., Goetsch, S. C., Gaiano, N. R., Hill, J. A., Olson, E. N., and Schneider, J. W. (2011). A dynamic notch injury response activates epicardium and contributes to fibrosis repair. *Circ. Res.* 108, 51–59. doi: 10.1161/CIRCRESAHA.110.233262

Santangeli, P., Dello Russo, A., Pieroni, M., Casella, M., Di Biase, L., Burkhardt, J. D., et al. (2012). Fragmented and delayed electrograms within fibrofatty scar predict arrhythmic events in arrhythmogenic right ventricular cardiomyopathy: results from a prospective risk stratification study. *Heart Rhythm* 9, 1200–1206. doi: 10.1016/j.hrthm.2012.03.057

Santangeli, P., Hamilton-Craig, C., Dello Russo, A., Pieroni, M., Casella, M., Pelargonio, G., et al. (2011). Imaging of scar in patients with ventricular arrhythmias of right ventricular origin: cardiac magnetic resonance versus electroanatomic mapping. *J. Cardiovasc. Electrophysiol.* 22, 1359–1366. doi: 10.1111/j.1540-8167.2011.02127.x

Santiago, J. J., Dangerfield, A. L., Rattan, S. G., Bathe, K. L., Cunnington, R. H., Raizman, J. E., et al. (2010). Cardiac fibroblast to myofibroblast differentiation in vivo and in vitro: expression of focal adhesion components in neonatal and adult rat ventricular myofibroblasts. *Dev. Dyn.* 239, 1573–1584. doi: 10.1002/dvdy.22280

Santulli, G., Cipolletta, E., Sorriento, D., Del Giudice, C., Anastasio, A., Monaco, S., et al. (2012). CaMK4 gene deletion induces hypertension. *J. Am. Heart Assoc.* 1:e001081. doi: 10.1161/JAHA.112.001081

Sen-Chowdhry, S., Syrris, P., Prasad, S. K., Hughes, S. E., Merrifield, R., Ward, D., et al. (2008). Left-dominant arrhythmogenic cardiomyopathy: an under-recognized clinical entity. *J. Am. Coll. Cardiol.* 52, 2175–2187. doi: 10.1016/j.jacc.2008.09.019

Sepehrkhouy, S., Gho, J., van Es, R., Harakalova, M., de Jonge, N., Dooijes, D., et al. (2017). Distinct fibrosis pattern in desmosomal and phospholamban mutation carriers in hereditary cardiomyopathies. *Heart Rhythm* 14, 1024–1032. doi: 10.1016/j.hrthm.2017.03.034

Shaikh, G., Zhang, J., Perez-Aso, M., Mediero, A., and Cronstein, B. (2016). Adenosine A2A receptor promotes collagen type III synthesis via beta-catenin activation in human dermal fibroblasts. *Br. J. Pharmacol.* 173, 3279–3291. doi: 10.1111/bph.13615

Siasos, G., Tsigkou, V., Kosmopoulos, M., Theodosiadis, D., Simantiris, S., Tagkou, N. M., et al. (2018). Mitochondria and cardiovascular diseases-from pathophysiology to treatment. *Ann. Transl. Med.* 6:256. doi: 10.21037/atm.2018.06.21

Sivasubramanian, N., Coker, M. L., Kurrelmeyer, K. M., MacLellan, W. R., DeMayo, F. J., Spinale, F. G., et al. (2001). Left ventricular remodeling in transgenic mice with cardiac restricted overexpression of tumor necrosis factor. *Circulation* 104, 826–831. doi: 10.1161/hc3401.093154

Siwik, D. A., Pagano, P. J., and Colucci, W. S. (2001). Oxidative stress regulates collagen synthesis and matrix metalloproteinase activity in cardiac fibroblasts. *Am. J. Physiol. Cell Physiol.* 280, C53–C60.

Sommariva, E., Brambilla, S., Carbucicchio, C., Gambini, E., Meraviglia, V., Dello Russo, A., et al. (2016). Cardiac mesenchymal stromal cells are a source of adipocytes in arrhythmogenic cardiomyopathy. *Eur. Heart J.* 37, 1835–1846. doi: 10.1093/eurheartj/ehv579

Sommariva, E., Stadiotti, I., Perrucci, G. L., Tondo, C., and Pompilio, G. (2017). Cell models of arrhythmogenic cardiomyopathy: advances and opportunities. *Dis. Model Mech.* 10, 823–835. doi: 10.1242/dmm.029363

Spinale, F. G., Frangogiannis, N. G., Hinz, B., Holmes, J. W., Kassiri, Z., and Lindsey, M. L. (2016). Crossing into the next frontier of cardiac extracellular matrix research. *Circ. Res.* 119, 1040–1045.

Stadiotti, I., Pompilio, G., Maione, A. S., Pilato, C. A., D'Alessandra, Y., and Sommariva, E. (2019). Arrhythmogenic cardiomyopathy: what blood can reveal? *Heart Rhythm* 16, 470–477. doi: 10.1016/j.hrthm.2018.09.023

Stempien-Otero, A., Kim, D. H., and Davis, J. (2016). Molecular networks underlying myofibroblast fate and fibrosis. *J. Mol. Cell Cardiol.* 2016, 153–161. doi: 10.1016/j.yjmcc.2016.05.002

Suthahar, N., Meijers, W. C., Sillje, H. H. W., and de Boer, R. A. (2017). From inflammation to fibrosis-molecular and cellular mechanisms of myocardial tissue remodelling and perspectives on differential treatment opportunities. *Curr. Heart Fail Rep.* 14, 235–250. doi: 10.1007/s11897-017-0343-y

Swynghedauw, B. (1999). Molecular mechanisms of myocardial remodeling. *Physiol. Rev.* 1999, 215–262.

Tamargo, J. (2012). TGFbeta3 mutations cause arrhythmogenic right ventricular dysplasia type 1 and open the door to understanding the biological role of TGFbeta3 (where there's a will, there's a way). *Cardiovasc. Res.* 96, 188–190; discussion 191–194.

Tandri, H., Rutberg, J., Bluemke, D. A., and Calkins, H. (2002). Magnetic resonance imaging of arrhythmogenic right ventricular dysplasia. *J. Cardiovasc. Electrophysiol.* 13:1180.

Tandri, H., Saranathan, M., Rodriguez, E. R., Martinez, C., Bomma, C., Nasir, K., et al. (2005). Noninvasive detection of myocardial fibrosis in arrhythmogenic right ventricular cardiomyopathy using delayed-enhancement magnetic resonance imaging. *J. Am. Coll. Cardiol.* 45, 98–103. doi: 10.1016/j.jacc.2004.09.053

Te Riele, A. S., James, C. A., Philips, B., Rastegar, N., Bhonsale, A., Groeneweg, J. A., et al. (2013). Mutation-positive arrhythmogenic right ventricular dysplasia/cardiomyopathy: the triangle of dysplasia displaced. *J. Cardiovasc. Electrophysiol.* 24, 1311–1320. doi: 10.1111/jce.12222

Thomas, C. V., Coker, M. L., Zellner, J. L., Handy, J. R., Crumbley, A. J. III, and Spinale, F. G. (1998). Increased matrix metalloproteinase activity and selective upregulation in LV myocardium from patients with end-stage dilated cardiomyopathy. *Circulation* 97, 1708–1715. doi: 10.1161/01.cir.97.17.1708

Todica, A., Siebermair, J., Schiller, J., Zacherl, M. J., Fendler, W. P., Massberg, S., et al. (2018). Assessment of right ventricular sympathetic dysfunction in patients with arrhythmogenic right ventricular cardiomyopathy: an (123)I-metaiodobenzylguanidine SPECT/CT study. *J. Nucl. Cardiol.* [Epub ahead of print].

Tomasek, J. J., Gabbiani, G., Hinz, B., Chaponnier, C., and Brown, R. A. (2002). Myofibroblasts and mechano-regulation of connective tissue remodelling. *Nat. Rev. Mol. Cell Biol.* 3, 349–363. doi: 10.1038/nrm809

Turner, N. A., Mughal, R. S., Warburton, P., O'Regan, D. J., Ball, S. G., and Porter, K. E. (2007). Mechanism of TNFalpha-induced IL-1alpha, IL-1beta and IL-6 expression in human cardiac fibroblasts: effects of statins and thiazolidinediones. *Cardiovasc. Res.* 76, 81–90. doi: 10.1016/j.cardiores.2007.06.003

Tyagi, S. C., Kumar, S., Voelker, D. J., Reddy, H. K., Janicki, J. S., and Curtis, J. J. (1996). Differential gene expression of extracellular matrix components in dilated cardiomyopathy. *J. Cell Biochem.* 63, 185–198. doi: 10.1002/(sici)1097-4644(19961101)63:2<185::aid-jcb6>3.0.co;2-u

Valente, M., Calabrese, F., Thiene, G., Angelini, A., Basso, C., Nava, A., et al. (1998). In vivo evidence of apoptosis in arrhythmogenic right ventricular cardiomyopathy. *Am. J. Pathol.* 152, 479–484.

Vallee, A., Lecarpentier, Y., Guillevin, R., and Vallee, J. N. (2017). Interactions between TGF-beta1, canonical WNT/beta-catenin pathway and PPAR gamma in radiation-induced fibrosis. *Oncotarget* 8, 90579–90604. doi: 10.18632/oncotarget.21234

van Amerongen, M. J., Bou-Gharios, G., Popa, E., van Ark, J., Petersen, A. H., van Dam, G. M., et al. (2008). Bone marrow-derived myofibroblasts contribute functionally to scar formation after myocardial infarction. *J. Pathol.* 214, 377–386. doi: 10.1002/path.2281

Wada, K., Itoga, K., Okano, T., Yonemura, S., and Sasaki, H. (2011). Hippo pathway regulation by cell morphology and stress fibers. *Development* 138, 3907–3914. doi: 10.1242/dev.070987

Wang, W., Orgeron, G., Tichnell, C., Murray, B., Crosson, J., Monfredi, O., et al. (2018). Impact of exercise restriction on arrhythmic risk among patients with arrhythmogenic right ventricular cardiomyopathy. *J. Am. Heart Assoc.* 7:e008843.

Wichter, T., Hindricks, G., Lerch, H., Bartenstein, P., Borggrefe, M., Schober, O., et al. (1994). Regional myocardial sympathetic dysinnervation in arrhythmogenic right ventricular cardiomyopathy. An analysis using 123I-meta-iodobenzylguanidine scintigraphy. *Circulation* 89, 667–683. doi: 10.1161/01.cir.89.2.667

Wilson, M., O'Hanlon, R., Prasad, S., Deighan, A., Macmillan, P., Oxborough, D., et al. (1985). Diverse patterns of myocardial fibrosis in lifelong, veteran endurance athletes. *J. Appl. Physiol.* 2011, 1622–1626. doi: 10.1152/japplphysiol.01280.2010

Xiang, F. L., Fang, M., and Yutzey, K. E. (2017). Loss of beta-catenin in resident cardiac fibroblasts attenuates fibrosis induced by pressure overload in mice. *Nat. Commun.* 8:712. doi: 10.1038/s41467-017-00840-w

Yaniz-Galende, E., Roux, M., Nadaud, S., Mougenot, N., Bouvet, M., Claude, O., et al. (2017). Fibrogenic potential of PW1/Peg3 expressing cardiac stem cells. *J. Am. Coll. Cardiol.* 70, 728–741. doi: 10.1016/j.jacc.2017.06.010

Yoshida, M., Romberger, D. J., Illig, M. G., Takizawa, H., Sacco, O., Spurzem, J. R., et al. (1992). Transforming growth factor-beta stimulates the expression of desmosomal proteins in bronchial epithelial cells. *Am. J. Respir. Cell Mol. Biol.* 6, 439–445. doi: 10.1165/ajrcmb/6.4.439

Zeisberg, E. M., Tarnavski, O., Zeisberg, M., Dorfman, A. L., McMullen, J. R., Gustafsson, E., et al. (2007). Endothelial-to-mesenchymal transition contributes to cardiac fibrosis. *Nat. Med.* 13, 952–961.

Zhang, J., Corciulo, C., Liu, H., Wilder, T., Ito, M., and Cronstein, B. (2017). Adenosine A2a receptor blockade diminishes wnt/beta-catenin signaling in a murine model of bleomycin-induced dermal fibrosis. *Am. J. Pathol.* 187, 1935–1944. doi: 10.1016/j.ajpath.2017.05.005

Zhou, W., and Zhao, M. (2018). How hippo signaling pathway modulates cardiovascular development and diseases. *J. Immunol. Res.* 2018:3696914. doi: 10.1155/2018/3696914

Conflict of Interest: The authors declare that the research was conducted in the absence of any commercial or financial relationships that could be construed as a potential conflict of interest.

frontiers in Physiology

MINI REVIEW
published: 22 April 2020
doi: 10.3389/fphys.2020.00384

Beyond Family: Modeling Non-hereditary Heart Diseases With Human Pluripotent Stem Cell-Derived Cardiomyocytes

Sebastian Martewicz[1], Michael Magnussen[2] and Nicola Elvassore[1,2,3,4]**

[1] Shanghai Institute for Advanced Immunochemical Studies (SIAIS), ShanghaiTech University, Shanghai, China, [2] Stem Cells & Regenerative Medicine Section, UCL Great Ormond Street Institute of Child Health, London, United Kingdom, [3] Venetian Institute of Molecular Medicine, Padua, Italy, [4] Department of Industrial Engineering, University of Padova, Padua, Italy

Non-genetic cardiac pathologies develop as an aftermath of extracellular stress-conditions. Nevertheless, the response to pathological stimuli depends deeply on intracellular factors such as physiological state and complex genetic backgrounds. Without a thorough characterization of their *in vitro* phenotype, modeling of maladaptive hypertrophy, ischemia and reperfusion injury or diabetes in human pluripotent stem cell-derived cardiomyocytes (hPSC-CMs) has been more challenging than hereditary diseases with defined molecular causes. In past years, greater insights into hPSC-CM *in vitro* physiology and advancements in technological solutions and culture protocols have generated cell types displaying stress-responsive phenotypes reminiscent of *in vivo* pathological events, unlocking their application as a reductionist model of human cardiomyocytes, if not the adult human myocardium. Here, we provide an overview of the available literature of pathology models for cardiac non-genetic conditions employing healthy (or asymptomatic) hPSC-CMs. In terms of numbers of published articles, these models are significantly lagging behind monogenic diseases, which misrepresents the incidence of heart disease causes in the human population.

Keywords: ischemia – reperfusion, diabetes, non-genetic diseases, HPSC-cardiomyocytes, hPSC-CM, maladaptive hypertrophy

OPEN ACCESS

Edited by:
Martina Calore,
Maastricht University, Netherlands

Reviewed by:
Elisa Di Pasquale,
Italian National Research Council, Italy
Jonathan Satin,
University of Kentucky, United States

****Correspondence:***
Sebastian Martewicz
smartewicz@shanghaitech.edu.cn
Nicola Elvassore
nicola.elvassore@unipd.it

Specialty section:
This article was submitted to Striated Muscle Physiology, a section of the journal Frontiers in Physiology

Received: *06 January 2020*
Accepted: *30 March 2020*
Published: *22 April 2020*

Citation:
Martewicz S, Magnussen M and Elvassore N (2020) Beyond Family: Modeling Non-hereditary Heart Diseases With Human Pluripotent Stem Cell-Derived Cardiomyocytes. Front. Physiol. 11:384. doi: 10.3389/fphys.2020.00384

INTRODUCTION ON HPSC-CMS

Nearly two decades since their first description (Kehat et al., 2001), hPSC-CMs are beginning to fulfill their potential as a reductionist model of the human cardiac muscle. Thanks to constant improvements in differentiation protocols (Mummery et al., 2003; Laflamme et al., 2007; Yang et al., 2008; Kattman et al., 2011; Lian et al., 2012; Burridge et al., 2014) and increasing understanding of their *in vitro* cardiac phenotype, hPSC-CMs are now an integral part of proposed high-throughput drug screening (Kirby et al., 2018; Fiedler et al., 2019) and drug risk-assessment platforms (Yang and Papoian, 2018; Lu H.R. et al., 2019; Li et al., 2020). Furthermore, there is evidence for their increasing reliability in predicting adverse drug effects (Blinova et al., 2018).

The successful induction of pluripotency in human somatic cells (Takahashi et al., 2007; Yu et al., 2007; Lowry et al., 2008; Park et al., 2008) opened the cardiac field to patient-specific disease modeling (Carvajal-Vergara et al., 2010; Moretti et al., 2010), although patient-specific

treatment modeling still remains an open challenge (Blinova et al., 2019). The race toward generating mutation-specific *in vitro* models produced >150 independent hiPSC lines over the past 10 years and hundreds of scientific papers frequently and comprehensively reviewed (Ross et al., 2018; van Mil et al., 2018; van den Brink et al., 2019). Consequently, there is a clear literature unbalance against non-genetic cardiac pathology models, often coming with additional challenges in recreating *in vitro* either the pathological phenotype, the pathological environment or both (**Figure 1**).

Here, we discuss modeling of non-genetic heart conditions, focusing exclusively on results obtained on human cells when the referenced study makes only sparing use of hPSC-CMs

ADVANTAGES AND LIMITATIONS

Inter-species differences are a major concern in translational research. Therefore, the human origin paired with virtually unlimited low-cost supply constitute the most valuable advantages of hPSC-CMs. Beyond the most often quoted heart size, beating rate, electrophysiology and protein function (Nerbonne et al., 2001; Haghighi et al., 2003), more subtle differences are apparent also in stress-responses. For instance, an *in vitro* angiotensin-II-induced heart failure model reproduces the appearance observed in failing myocardia of two loss-of-function $Na_V1.5$ channel isoforms produced by abnormal *SCN5A* splicing through a mechanism absent in species other than primates (Gao et al., 2011, 2013). Such response contributes to the sodium current reduction in angiotensin-II-treated hPSC-CMs, mimicking pro-arrhythmic conditions in failing ventricles (Mathieu et al., 2016). Similarly, evolutionarily closer species display divergent transcriptomic responses to ischemia-mimetic environments, with rhesus macaque monkey PSC-CMs failing to overlap results with hPSC-CMs at gene regulation level (Zhao et al., 2018), and chimpanzee PSC-CMs still diverging in regulation of critical genes tightly related to human ischemia/reperfusion pathogenesis (Ward and Gilad, 2019).

Although hPSC-CMs can develop full adult phenotypes, these have been achieved so far only by integration within healthy animal myocardia (Cho et al., 2017; Kadota et al., 2017), and hPSC-CM developmental immaturity is seen as their major drawback. We (Martewicz et al., 2019) and others (van den Berg et al., 2015) have shown that transcriptomic profiling places hPSC-CMs within the first trimester of fetal development, with structural, functional and metabolic features further supporting such characterization (Machiraju and Greenway, 2019).

Nevertheless, unprimed hPSC-CMs (no maturation protocol applied) still represent a valid reductionist model in dissecting molecular mechanisms within human and cardiac cell backgrounds. For instance, a recent study successfully identified direct inactivation mechanisms of human voltage-sensitive L-type calcium channels by molecular O_2 and acidosis (Fernandez-Morales et al., 2019), complementing our findings in murine models (Martewicz et al., 2012). Simultaneously, the authors clearly show how studying more complex functional features requires careful evaluation of cardiac structural maturation, with whole-cell ion dynamics changing following substrate interaction, which our group showed to be mediated by mechanotransduction signaling (Martewicz et al., 2017).

Additionally, taking advantage of developmentally early phenotypes of hPSC-CM and hijacking the differentiation process from hPSCs allows modeling developmental defects leading to postnatal pathological conditions. Such is the case of hypoplastic left heart syndrome in a chronic-hypoxia model (Gaber et al., 2013), which preceded patient-specific hPSC-CMs models ultimately identifying the underlying genetic-driven molecular mechanisms (Jiang et al., 2014; Kobayashi et al., 2014; Tomita-Mitchell et al., 2016; Hrstka et al., 2017; Yang et al., 2017). Similarly, hPSC-CMs were used to model the role of the mitochondrial calcium uniporter in cardiac fetal development and maturation (Shanmughapriya et al., 2018). Finally, although chemically induced cardiotoxicity will not be a subject of this review [see (Magdy et al., 2018)], one recent study considered the impact of ethanol on hPSC-CM functionality as a model of prenatal exposure during maternal alcohol intoxication (Rampoldi et al., 2019).

MALADAPTIVE HYPERTROPHY MODELING

The developmentally early phenotype of hPSC-CMs provides additional complexity in modeling hypertrophy *in vitro*, with differentiation/maturation phenomena blurring distinctions between physiological and pathological hypertrophy. Physiological hypertrophic growth is a cardiac perinatal maturation process, reactivated in adulthood upon regular physical activity, and differs substantially from pathological (or maladaptive) hypertrophy in activation mechanisms and elicited functional responses (McMullen and Jennings, 2007). For instance, the evaluation of cell-size increase must be performed carefully, being an ambivalent hallmark for both processes (Rupert et al., 2017), and appears to be absent in advanced maturation stages (Ronaldson-Bouchard et al., 2018). Similarly ambivalent is the application of mechanical stretch, which simultaneously induces hypertrophic responses and promotes hPSC-CM maturation (LaBarge et al., 2019), generating phenotypes divergent from pathological neurohormonal stimulation relative to αMHC/βMHC transcription activation ratios (Foldes et al., 2011) or CathepsinD/TroponinT release (Hoes et al., 2019).

Chronic adrenergic activation is one of the pathogenic triggers of maladaptive hypertrophy, and the effects of prolonged exposure to isoproterenol or phenylephrine have been studied in hPSC-CMs in regard to hypertrophy-inhibiting effects of several active compounds (Foldes et al., 2011; Martin et al., 2014; Gesmundo et al., 2017). Nevertheless, the reliability of this approach is hindered by hPSC-CM immature adrenergic signaling (Jung et al., 2016; Uzun et al., 2016; Trieschmann et al., 2019), which generates highly variable and aberrant stress-responses (Foldes et al., 2014) often failing to produce representative pathological phenotypes *in vitro* (Tanaka et al., 2014; Cui et al., 2016; Naftali-Shani et al., 2018).

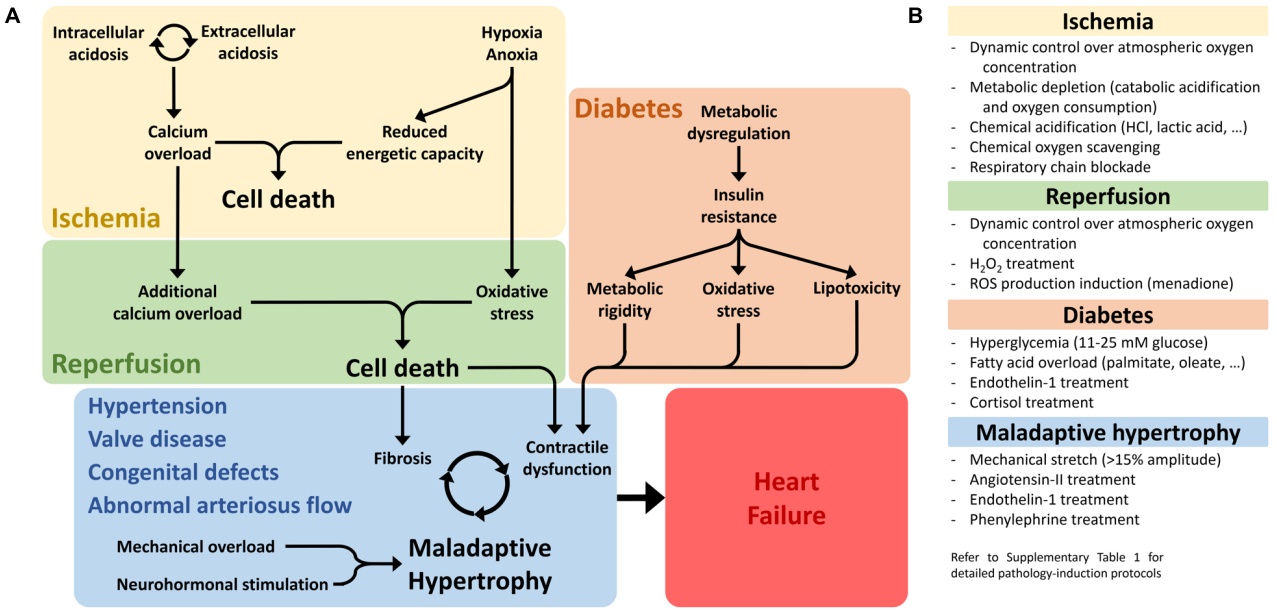

FIGURE 1 | Non-genetic pathological conditions leading to heart failure. **(A)** The three main pathological conditions discussed in this review are schematically represented, highlighting the major molecular drivers and pathological phenotypes that need to be reproduced *in vitro* in order to generate a representative and reliable pathology model. **(B)** Main experimental strategies employed to generate pathological phenotypes in non-genetic cardiac disease models *in vitro*. For detailed experimental protocols employed in the reviewed studies, see **Supplementary Materials**.

Hormonal stimulation has been shown to be more effective for maladaptive hypertrophy modeling purposes, with angiotensin-II and especially endothelin-1 treatments successfully recapitulating hypertrophic phenotypes in terms of expression/secretion of natriuretic peptides A and B (Carlson et al., 2013), myofibrillar disarray (Tanaka et al., 2014) and mRNA/miRNA profiling (Aggarwal et al., 2014). Such a model has been dually employed thus far to study the molecular mechanisms of maladaptation *in vitro* (Cui et al., 2016; Rosales and Lizcano, 2018), and evaluate anti-hypertrophic effects of miRNAs (Scrimgeour et al., 2019), herbal extracts (Zhang et al., 2017) and antiparasitic compounds (Qin et al., 2017), for which hPSC-CMs are superior to murine cardiac cell lines lacking in expression of several key target proteins (Nagai et al., 2017).

Alternatively to being employed as *in vitro* hypertrophy modeling platform, hPSC-CMs have proven useful in experimentally confirming observations made in human and murine hypertrophic heart biopsies of the involvement of non-coding RNAs in maladaptive pathogenesis (Wang et al., 2016; Mirtschink et al., 2019).

ISCHEMIA/REPERFUSION INJURY MODELING

Ischemia is the most dramatic of cardiac insults, leading to or aggravating pre-existing stages of heart failure. The nature of the pathological stressors (a composite of fast dynamic changes in nutrients, waste products, O_2 and ROS) makes cellular responses and pathological fallouts tightly connected to adult cardiomyocyte metabolic processes, elevating hPSC-CM maturation to a necessity for modeling purposes.

Indeed, several studies describe little or no response to I/R-mimetic conditions in unprimed hPSC-CMs, although showing minimal but relatively significant cardioprotection by the individual molecules of interest (Hsieh et al., 2015; Wei et al., 2017; Mo et al., 2019). Our own experiments with oxygen/glucose deprivation in microfluidic devices show clearly divergent responses of postnatal murine cardiomyocytes and unprimed hPSC-CMs characterized by abnormal intracellular glycogen stores (Martewicz et al., 2018). Similar experimental setups have been used to study the mechanistic action of anesthetics (Lu Y. et al., 2019) and miRNA-based regulation of metalloproteases (Scrimgeour et al., 2019).

Recent studies demonstrate how developing a stress-responsive phenotype must be set as an essential element in a feasible hPSC-CM model for I/R studies. Priming hPSC-CMs through simple maturation steps generates cells responsive to I/R with mortality rates unseen in their unprimed counterparts, ultimately providing the biological model needed to test clinically effective small molecules (Hidalgo et al., 2018) or investigate the cardioprotective mechanism of cardiac progenitors (Sebastiao et al., 2019). The most intriguing example of *in vitro* I/R modeling to date fully embraces hPSC-CMs as platform for both drug screening and development (Fiedler et al., 2019). The researchers identify MAP4K4 as a druggable target, activity of which is altered across several clinically relevant heart failure models, and employ an I/R setup with primed hPSC-CMs to screen for suitable small-molecule inhibitors. After using the identified lead-compound to develop a *novel* inhibitor, they ultimately

translate the cardioprotective properties of a small-molecule newly developed in hPSC-CMs to an *in vivo* murine model of ischemic insult.

DIABETES MODELING

Similar to ischemia models, replicating diabetic pathophysiology *in vitro* requires primed hPSC-CMs as starting point. While underlying genetic factors might further its severity, prolonged exposure to altered metabolic stimuli is the leading trigger and driving force of the clinical manifestations of diabetic cardiomyopathy (Graneli et al., 2019). Indeed, an I/R model that linked anesthetic-conferred cardioprotection to pharmacological tuning of mitochondrial function in hPSC-CMs (Sepac et al., 2010; Canfield et al., 2016) produced no differences between diabetic patient-specific cells and healthy controls. Both showed equal abrogation of protection under acute hyperglycemic conditions, thus failing to replicate the clinical differences between healthy and diabetic surgery patients (Canfield et al., 2012).

On the other hand, when allowed to adapt to prolonged exposure to hyperglycemic stress, hPSC-CMs develop pathological hypertrophy characterized by contractile and calcium cycling dysfunctions (Ng et al., 2018). Capitalizing on this phenotype has enabled investigations into mechanisms behind unexpected clinical trial evidence of empagliflozin-driven reduction of deadly cardiovascular complications in diabetic patients. Similar approaches of metabolic overload with fatty acids allow the induction of insulin-resistance and dissection of its mechanism in hPSC-CMs (Chanda et al., 2017; Liu et al., 2017; Graneli et al., 2019).

Primed hPSC-CMs develop a complete panel of diabetic cardiomyopathy phenotypes by integrating metabolic overload conditions with additional hormonal stimulation abnormally present in the diabetic milieu (Idris-Khodja et al., 2016; Joseph and Golden, 2017), proven by aggravated contractile dysfunction following endothelin-1 stimulation (Wu et al., 2018). A complete set of stressors (metabolic overload, endothelin-1 and cortisol treatment) recapitulates *in vitro* hypertrophic-like transcriptomic changes, increased BNP secretion, compromised calcium cycling and contraction, lipid accumulation and oxidation, sarcomeric disorganization (Drawnel et al., 2014), insulin-resistance and reduced respiratory capacity (Graneli et al., 2019), and deregulated non-coding RNAs expression (Pant et al., 2019). Satisfying all of these conditions in such a multifactorial pathological setting provides the necessary platform for drug-screening experiments and is instrumental in revealing underlying differences between healthy and patient-derived hPSC-CMs (Drawnel et al., 2014).

OTHER PATHOLOGY MODELS

Hypertrophy, ischemia/reperfusion and diabetes are conditions with major economic and social impacts. Nevertheless, hPSC-CMs have been also employed in modeling less common pathological settings, such as systemic pathogen infections leading to myocarditis and heart failure. Modeling septic shock by exposure to bacterial lipopolysaccharides affects hPSC-CM survival, electrophysiology and demonstrates their competence in activating innate immune inflammatory responses (Yucel et al., 2017). Indeed, hPSC-CM display stronger macrophage chemo-attractant properties than purified chemokines (Pallotta et al., 2015) and significant stress-responsive paracrine pro-inflammatory signaling (Sebastiao et al., 2020) mediating fibrosis *in vivo* and *in vitro* (Kumar et al., 2019; Zhang et al., 2019). Furthermore, functional expression of coxsackievirus and adenovirus receptor (Scassa et al., 2011) makes hPSC-CMs a better predictive model than murine cardiac cell lines for therapeutic approaches against viral myocarditis (Sharma et al., 2014). Similarly, hPSC-CMs are a viable host for parasites causing Chagas disease (da Silva Lara et al., 2018; Bozzi et al., 2019) and, consequently, a good screening platform for novel drugs preventing infection and major cardiac fallouts of the pathology (Sass et al., 2019a,b).

Spaceflight-associated stressors such as radiation and microgravity induce cardiac atrophy and arrhythmias, increasing cardiovascular complication rates in astronauts (Acharya et al., 2019). Thus far, the intrinsic challenges of hPSC-CM aerospace applications limit *in vitro* models to phenotypic descriptions, orphan of underlying molecular mechanisms. Microgravity modeling, for instance, has been performed only twice on human PSC-CMs, observing increases in beating rate under acute conditions during parabolic flight (Acharya et al., 2019) and mainly transcriptomic changes during chronic exposure onboard the International Space Station (Wnorowski et al., 2019). Although studied relative to anti-cancer treatment, radiation-induced heart disease is another astronaut concern, and hPSC-CMs respond to ionizing radiations in dose-dependent manner with electrophysiological (Becker et al., 2018b) and transcriptomic (Becker et al., 2018a) alterations.

DISEASE MODELING WITH 3D CONSTRUCTS

hPSC-CM maturation *in vitro* is relatively fast in comparison with *in vivo* development, supporting the idea that these mechanisms differ substantially. Thus, modeling non-genetic pathologies mostly originating from insults to the adult heart in the late stages of cardiac development is within reach of 1,2 month-long cultures. While originally proposed as a maturation mechanism (Sartiani et al., 2007; Otsuji et al., 2010; Kamakura et al., 2013; Lundy et al., 2013), extended time in culture was recently extensively characterized over a 4-month period showing expression of aging markers in unprimed hPSC-CMs and increased sensitivity to I/R in disorganized 3D aggregates (Acun et al., 2019). To date, human engineered heart tissues (hEHTs) provide the closest match to an adult cardiomyocyte phenotype *in vitro* (Tiburcy et al., 2017; Ronaldson-Bouchard et al., 2018).

hEHTs assemble hPSC-CMs into 3D constructs integrating multifactorial stimuli such as electrophysiological pacing (Lemme et al., 2019; Zhao et al., 2019), mechanical loading

(Leonard et al., 2018), ECM structure (Goldfracht et al., 2019) and non-myocyte cell interactions (Varzideh et al., 2019). Such constructs, in their immature state, have been proposed as models to study human cardiac self-regenerative potential after localized injury (Voges et al., 2017), and produce structurally and metabolically primed hPSC-CMs when allowed to develop further, even in absence of additional stimuli (Ulmer et al., 2018).

A recent hEHT I/R model showed for the first time in human cells the cardioprotective effect of ischemic preconditioning and efficacy of one out of three proposed cardioprotection treatments for reperfusion injury (Chen and Vunjak-Novakovic, 2019). Nevertheless, similar hEHTs generated by pure hPSC-CM populations are limited in their maturation potential (Park et al., 2019) and limit the study of the complex bidirectional crosstalk of multiple cell types, important during ischemic stress *via* paracrine signaling (Sandstedt et al., 2018; Sebastiao et al., 2019, 2020) and neurohormonal stimulation. The latter can be effectively modeled solely with hEHTs, as 2D cultures lack or display functionally impaired a β-adrenergic signaling cascades (Jung et al., 2016; Uzun et al., 2016; Trieschmann et al., 2019),

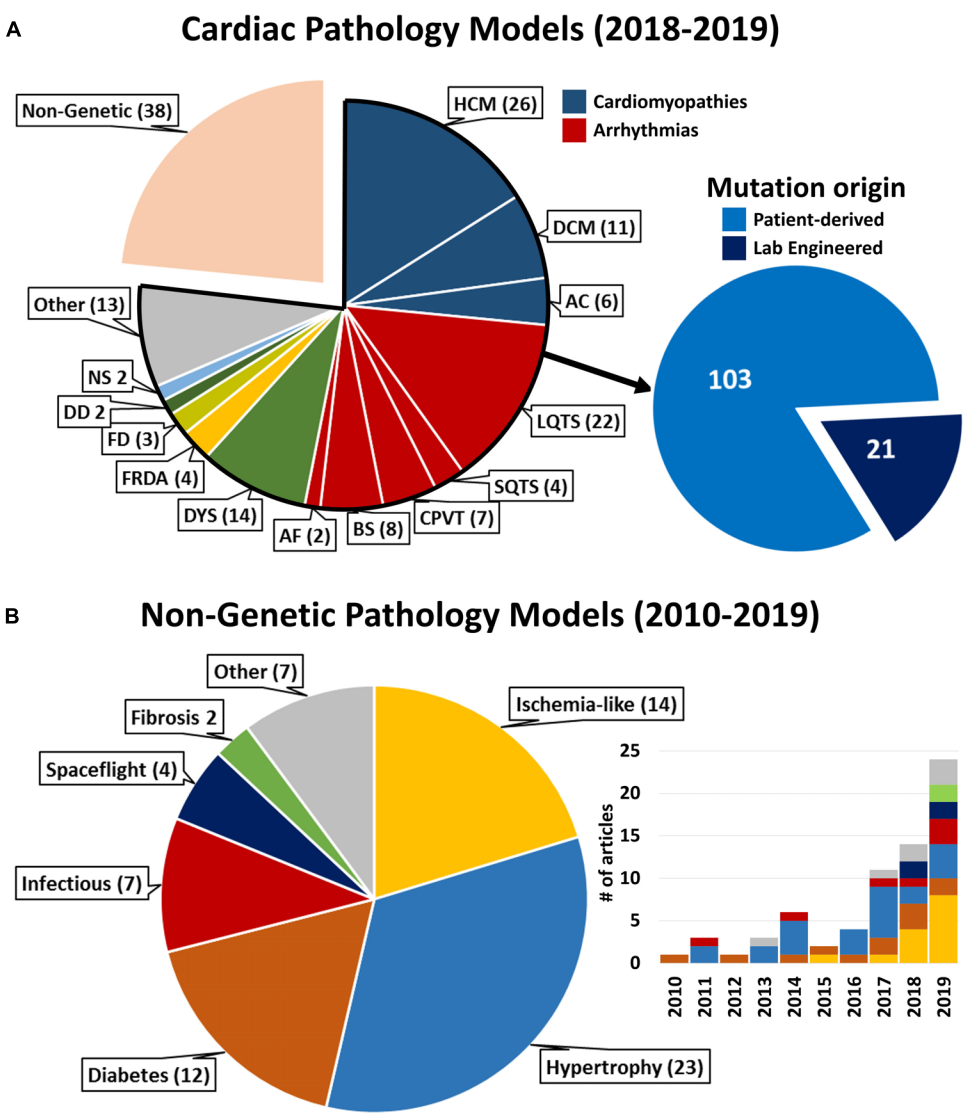

FIGURE 2 | Literature statistics on cardiac pathology models and cited references. **(A)** Complete representation of pathological models for cardiac diseases available on PubMed between January 1st 2018 and January 2nd 2020. HCM, Hypertrophic Cardiomyopathy; DCM, Dilated Cardiomyopathy; AC, Arrhythmogenic Cardiomyopathy; L/SQTS, Long/Short QT Syndrome; CPVT, Catecholaminergic Polymorphic Ventricular Tachycardia; BS, Brugada Syndrome; AF, Atrial Fibrillation; DYS, Muscular Dystrophies [Duchenne (9), Myotonic (4), Limb-Girdle (1)]; FRDA, Friedriech's Ataxia; FD, Fabry Disease; DD, Danon Disease; NS, Noonan Syndrome; Other, different genetic diseases represented by (1) article. *Inset*: all cardiac genetic pathology models reported in 2018–2019 relative to cell model derivation. "Lab engineered": healthy hPSC genetically edited to carry the mutation under consideration. **(B)** Representation of non-genetic conditions referenced in this review according to the pathological condition modeled. *Inset*: distribution *per* year of publication of the referenced articles (same color coding). For bibliographical research methods and full list of references reported in this figure, see **Supplementary Material**.

despite being able to form functional sympathetic neuro-junctions (Sakai et al., 2017). Indeed, chronic exposure of hEHTs to norepinephrine induces contractile dysfunction and β-adrenergic desensitization, which with additional endothelin-1-driven hypertrophic stimulation, generates an advanced model of heart failure (Tiburcy et al., 2017). Notably, endothelin -1 treatment does not produce additional hypertrophic growth in hPSC-CM at such late stages of maturation, but induces more clinically relevant hypertrophic features, such as contractile dysfunction (Ronaldson-Bouchard et al., 2018). Additionally, porcine scaffold-based hEHTs have been employed recently to highlight the vicious cycle of maladaptive hypertrophy, with healthy hPSC-CMs responding to hypertrophic ECMs with impaired function, which *in vivo* would feed-back to the cardiac microenvironment triggering additional maladaptation preventing recovery under pharmacological treatment (Sewanan et al., 2019).

CONCLUSION AND FUTURE PERSPECTIVES

Animal-derived models often incorrectly represent human cardiac features and diverge in stress-responses (Olson et al., 2000; Davis et al., 2011). hPSC-CMs offer an invaluable tool to study the human heart *in vitro*, provided that stress-responsive phenotypes are apparent and representative of *in vivo* conditions. The necessity of hPSC-CM priming for pathology modeling is apparent in some hereditary monogenic pathologies (Kim et al., 2013), but becomes essential for most non-genetic diseases described here, given their incidence later in adult life. Optimization of cardiac maturation and metabolic priming protocols generated better insight into the crosstalk between structural, functional and metabolic states of hPSC-CMs. These advances now allow more representative modeling of non-genetic diseases, still lagging behind the highly penetrant genetic conditions with clear analytical read-outs that dominate hPSC-CM literature (**Figure 2A**).

Currently, advanced modeling of the adult myocardium requires hEHTs. These multiparametric setups integrating stimulation and data acquisition systems, act as human preclinical models refining the predictive efficacy of less throughput-limited 2D hPSC-CM models (Fiedler et al., 2019). Nevertheless, while closely resembling adult tissue transcriptomic and functional features, hEHTs fall short of gaining the status of full-fledged *organoids*, not fully mimicking adult myocardial macroscopic ultrastructure (Tiburcy et al., 2017; Ronaldson-Bouchard et al., 2018), thus requiring additional bioengineering efforts to scale up the systems from tissue- to organ-models, as the recently proposed atrioventricular composite (Zhao et al., 2019).

Importantly, the widespread use of commercially available cell products in the studies reported here (**Supplementary Table S1**) highlights the necessity of increasing robustness and reproducibility of the results through differentiation and culture protocols standardization. Indeed, whenever patient-specificity is not essential, employment of standardized experimental platforms is desirable to study a plethora of environmental cardiac insults (Turnbull et al., 2018; **Figure 2B**), remaining mindful of the pitfalls of broadening the results of few cell lines to the general population and of the aspirations toward personalized medicine approaches.

Finally, combining hPSC-CM-based models with high precision genome-editing technologies will be instrumental in not only supporting modeling of hereditary diseases by screening artificially introduced genetic variants of unknown significance (VUSs) (**Figure 2A**), but also in dissecting complex dynamics between non-genetic pathological stimuli and genetic backgrounds characterized by polygenic interactions.

AUTHOR CONTRIBUTIONS

All authors reviewed the literature, wrote, edited, and approved the final version of the manuscript.

ACKNOWLEDGMENTS

This work was supported by ShanghaiTech University (SM, NE, Grant F-0301-15-009); Oak Foundation Award (NE, Grant W1095/OCAY-14-191); British Heart Foundation (MM, Grant FS/17/70/33482).

SUPPLEMENTARY MATERIAL

The Supplementary Material for this article can be found online at: https://www.frontiersin.org/articles/10.3389/fphys.2020.00384/full#supplementary-material

REFERENCES

Acharya, A., Brungs, S., Lichterfeld, Y., Hescheler, J., Hemmersbach, R., Boeuf, H., et al. (2019). Parabolic, flight-induced, acute hypergravity and microgravity effects on the beating rate of human cardiomyocytes. *Cells* 8:352. doi: 10.3390/cells8040352

Acun, A., Nguyen, T. D., and Zorlutuna, P. (2019). In vitro aged, hiPSC-origin engineered heart tissue models with age-dependent functional deterioration to study myocardial infarction. *Acta Biomater.* 94, 372–391. doi: 10.1016/j.actbio.2019.05.064

Aggarwal, P., Turner, A., Matter, A., Kattman, S. J., Stoddard, A., Lorier, R., et al. (2014). RNA expression profiling of human iPSC-derived cardiomyocytes in a cardiac hypertrophy model. *PLoS One* 9:e108051. doi: 10.1371/journal.pone.0108051

Becker, B. V., Majewski, M., Abend, M., Palnek, A., Nestler, K., Port, M., et al. (2018a). Gene expression changes in human iPSC-derived cardiomyocytes after X-ray irradiation. *Int. J. Radiat. Biol.* 94, 1095–1103. doi: 10.1080/09553002.2018.1516908

Becker, B. V., Seeger, T., Beiert, T., Antwerpen, M., Palnek, A., Port, M., et al. (2018b). Impact of Ionizing radiation on electrophysiological behavior of human-induced ipsc-derived cardiomyocytes on multielectrode arrays. *Health Phys.* 115, 21–28. doi: 10.1097/hp.0000000000000817

Blinova, K., Dang, Q., Millard, D., Smith, G., Pierson, J., Guo, L., et al. (2018). International multisite study of human-induced pluripotent stem cell-derived

cardiomyocytes for drug proarrhythmic potential assessment. *Cell Rep.* 24, 3582–3592. doi: 10.1016/j.celrep.2018.08.079

Blinova, K., Schocken, D., Patel, D., Daluwatte, C., Vicente, J., Wu, J. C., et al. (2019). Clinical trial in a dish: personalized stem cell-derived cardiomyocyte assay compared with clinical trial results for two qt-prolonging drugs. *Clin. Transl. Sci.* 12, 687–697. doi: 10.1111/cts.12674

Bozzi, A., Sayed, N., Matsa, E., Sass, G., Neofytou, E., Clemons, K. V., et al. (2019). Using human induced pluripotent stem cell-derived cardiomyocytes as a model to study trypanosoma cruzi infection. *Stem Cell Rep.* 12, 1232–1241. doi: 10.1016/j.stemcr.2019.04.017

Burridge, P. W., Matsa, E., Shukla, P., Lin, Z. C., Churko, J. M., Ebert, A. D., et al. (2014). Chemically defined generation of human cardiomyocytes. *Nat. Methods* 11, 855–860. doi: 10.1038/nmeth.2999

Canfield, S. G., Sepac, A., Sedlic, F., Muravyeva, M. Y., Bai, X., and Bosnjak, Z. J. (2012). Marked hyperglycemia attenuates anesthetic preconditioning in human-induced pluripotent stem cell-derived cardiomyocytes. *Anesthesiology* 117, 735–744. doi: 10.1097/ALN.0b013e3182655e96

Canfield, S. G., Zaja, I., Godshaw, B., Twaroski, D., Bai, X., and Bosnjak, Z. J. (2016). High glucose attenuates anesthetic cardioprotection in stem-cell-derived cardiomyocytes: the role of reactive oxygen species and mitochondrial fission. *Anesth Analg.* 122, 1269–1279. doi: 10.1213/ane.0000000000001254

Carlson, C., Koonce, C., Aoyama, N., Einhorn, S., Fiene, S., Thompson, A., et al. (2013). Phenotypic screening with human iPS cell-derived cardiomyocytes: HTS-compatible assays for interrogating cardiac hypertrophy. *J. Biomol. Screen* 18, 1203–1211. doi: 10.1177/1087057113500812

Carvajal-Vergara, X., Sevilla, A., D'Souza, S. L., Ang, Y. S., Schaniel, C., Lee, D. F., et al. (2010). Patient-specific induced pluripotent stem-cell-derived models of LEOPARD syndrome. *Nature* 465, 808–812. doi: 10.1038/nature09005

Chanda, D., Oligschlaeger, Y., Geraets, I., Liu, Y., Zhu, X., Li, J., et al. (2017). 2-Arachidonoylglycerol ameliorates inflammatory stress-induced insulin resistance in cardiomyocytes. *J. Biol. Chem.* 292, 7105–7114. doi: 10.1074/jbc.M116.767384

Chen, T., and Vunjak-Novakovic, G. (2019). Human tissue-engineered model of myocardial ischemia-reperfusion injury. *Tissue Eng. Part A* 25, 711–724. doi: 10.1089/ten.TEA.2018.0212

Cho, G.-S., Lee, D. I., Tampakakis, E., Murphy, S., Andersen, P., Uosaki, H., et al. (2017). Neonatal transplantation confers maturation of PSC-Derived cardiomyocytes conducive to modeling cardiomyopathy. *Cell Rep.* 18, 571–582. doi: 10.1016/j.celrep.2016.12.040

Cui, H., Schlesinger, J., Schoenhals, S., Tonjes, M., Dunkel, I., Meierhofer, D., et al. (2016). Phosphorylation of the chromatin remodeling factor DPF3a induces cardiac hypertrophy through releasing HEY repressors from DNA. *Nucleic Acids Res.* 44, 2538–2553. doi: 10.1093/nar/gkv1244

da Silva Lara, L., Andrade-Lima, L., Magalhaes Calvet, C., Borsoi, J., Lopes Alberto, et al. (2018). Trypanosoma cruzi infection of human induced pluripotent stem cell-derived cardiomyocytes: an in vitro model for drug screening for Chagas disease. *Microbes Infect.* 20, 312–316. doi: 10.1016/j.micinf.2018.03.002

Davis, R. P., van den Berg, C. W., Casini, S., Braam, S. R., and Mummery, C. L. (2011). Pluripotent stem cell models of cardiac disease and their implication for drug discovery and development. *Trends Mol. Med.* 17, 475–484. doi: 10.1016/j.molmed.2011.05.001

Drawnel, F. M., Boccardo, S., Prummer, M., Delobel, F., Graff, A., Weber, M., et al. (2014). Disease modeling and phenotypic drug screening for diabetic cardiomyopathy using human induced pluripotent stem cells. *Cell Rep.* 9, 810–821. doi: 10.1016/j.celrep.2014.09.055

Fernandez-Morales, J. C., Hua, W., Yao, Y., and Morad, M. (2019). Regulation of Ca(2+) signaling by acute hypoxia and acidosis in cardiomyocytes derived from human induced pluripotent stem cells. *Cell Calcium* 78, 1–14. doi: 10.1016/j.ceca.2018.12.006

Fiedler, L. R., Chapman, K., Xie, M., Maifoshie, E., Jenkins, M., Golforoush, P. A., et al. (2019). MAP4K4 inhibition promotes survival of human stem cell-derived cardiomyocytes and reduces infarct size In Vivo. *Cell Stem Cell* 24, 579.e12–591.e12. doi: 10.1016/j.stem.2019.01.013

Foldes, G., Matsa, E., Kriston-Vizi, J., Leja, T., Amisten, S., Kolker, L., et al. (2014). Aberrant alpha-adrenergic hypertrophic response in cardiomyocytes from human induced pluripotent cells. *Stem Cell Rep.* 3, 905–914. doi: 10.1016/j.stemcr.2014.09.002

Foldes, G., Mioulane, M., Wright, J. S., Liu, A. Q., Novak, P., Merkely, B., et al. (2011). Modulation of human embryonic stem cell-derived cardiomyocyte growth: a testbed for studying human cardiac hypertrophy? *J. Mol. Cell Cardiol.* 50, 367–376. doi: 10.1016/j.yjmcc.2010.10.029

Gaber, N., Gagliardi, M., Patel, P., Kinnear, C., Zhang, C., Chitayat, D., et al. (2013). Fetal reprogramming and senescence in hypoplastic left heart syndrome and in human pluripotent stem cells during cardiac differentiation. *Am. J. Pathol.* 183, 720–734. doi: 10.1016/j.ajpath.2013.05.022

Gao, G., Xie, A., Huang, S.-C., Zhou, A., Zhang, J., Herman, A. M., et al. (2011). Role of RBM25/LUC7L3 in abnormal cardiac sodium channel splicing regulation in human heart failure. *Circulation* 124, 1124–1131. doi: 10.1161/CIRCULATIONAHA.111.044495

Gao, G., Xie, A., Zhang, J., Herman, A. M., Jeong, E. M., Gu, L., et al. (2013). Unfolded protein response regulates cardiac sodium current in systolic human heart failure. *Circ. Arrhythm. Electrophysiol.* 6, 1018–1024. doi: 10.1161/circep.113.000274

Gesmundo, I., Miragoli, M., Carullo, P., Trovato, L., Larcher, V., Di Pasquale, E., et al. (2017). Growth hormone-releasing hormone attenuates cardiac hypertrophy and improves heart function in pressure overload-induced heart failure. *Proc. Natl. Acad. Sci. U.S.A.* 114, 12033–12038. doi: 10.1073/pnas.1712612114

Goldfracht, I., Efraim, Y., Shinnawi, R., Kovalev, E., Huber, I., Gepstein, A., et al. (2019). Engineered heart tissue models from hiPSC-derived cardiomyocytes and cardiac ECM for disease modeling and drug testing applications. *Acta Biomater.* 92, 145–159. doi: 10.1016/j.actbio.2019.05.016

Graneli, C., Hicks, R., Brolen, G., Synnergren, J., and Sartipy, P. (2019). Diabetic cardiomyopathy modelling using induced pluripotent stem cell derived cardiomyocytes: recent advances and emerging models. *Stem Cell Rev Rep.* 15, 13–22. doi: 10.1007/s12015-018-9858-1

Haghighi, K., Kolokathis, F., Pater, L., Lynch, R. A., Asahi, M., Gramolini, A. O., et al. (2003). Human phospholamban null results in lethal dilated cardiomyopathy revealing a critical difference between mouse and human. *J. Clin. Investig.* 111, 869–876. doi: 10.1172/JCI17892

Hidalgo, A., Glass, N., Ovchinnikov, D., Yang, S. K., Zhang, X., Mazzone, S., et al. (2018). Modelling ischemia-reperfusion injury (IRI) in vitro using metabolically matured induced pluripotent stem cell-derived cardiomyocytes. *APL Bioeng* 2:026102. doi: 10.1063/1.5000746

Hoes, M. F., Tromp, J., Ouwerkerk, W., Bomer, N., Oberdorf-Maass, S. U., Samani, N. J., et al. (2019). The role of cathepsin D in the pathophysiology of heart failure and its potentially beneficial properties: a translational approach. *Eur. J. Heart Fail* doi: 10.1002/ejhf.1674

Hrstka, S. C., Li, X., and Nelson, T. J. (2017). NOTCH1-dependent nitric oxide signaling deficiency in hypoplastic left heart syndrome revealed through patient-specific phenotypes detected in bioengineered cardiogenesis. *Stem Cells* 35, 1106–1119. doi: 10.1002/stem.2582

Hsieh, A., Feric, N. T., and Radisic, M. (2015). Combined hypoxia and sodium nitrite pretreatment for cardiomyocyte protection in vitro. *Biotechnol. Prog.* 31, 482–492. doi: 10.1002/btpr.2039

Idris-Khodja, N., Ouerd, S., Mian, M. O. R., Gornitsky, J., Barhoumi, T., Paradis, P., et al. (2016). Endothelin-1 overexpression exaggerates diabetes-induced endothelial dysfunction by altering oxidative stress. *Am. J. Hypertens* 29, 1245–1251. doi: 10.1093/ajh/hpw078

Jiang, Y., Habibollah, S., Tilgner, K., Collin, J., Barta, T., Al-Aama, J. Y., et al. (2014). An induced pluripotent stem cell model of hypoplastic left heart syndrome (HLHS) reveals multiple expression and functional differences in HLHS-derived cardiac myocytes. *Stem Cells Transl. Med.* 3, 416–423. doi: 10.5966/sctm.2013-0105

Joseph, J. J., and Golden, S. H. (2017). Cortisol dysregulation: the bidirectional link between stress, depression, and type 2 diabetes mellitus. *Ann. N. Y. Acad. Sci.* 1391, 20–34. doi: 10.1111/nyas.13217

Jung, G., Fajardo, G., Ribeiro, A. J., Kooiker, K. B., Coronado, M., Zhao, M., et al. (2016). Time-dependent evolution of functional vs. remodeling signaling in induced pluripotent stem cell-derived cardiomyocytes and induced maturation with biomechanical stimulation. *Faseb J.* 30, 1464–1479. doi: 10.1096/fj.15-280982

Kadota, S., Pabon, L., Reinecke, H., and Murry, C. E. (2017). In Vivo maturation of human induced pluripotent stem cell-derived cardiomyocytes in neonatal and adult rat hearts. *Stem Cell Rep.* 8, 278–289. doi: 10.1016/j.stemcr.2016.10.009

Kamakura, T., Makiyama, T., Sasaki, K., Yoshida, Y., Wuriyanghai, Y., Chen, J., et al. (2013). Ultrastructural maturation of human-induced pluripotent stem cell-derived cardiomyocytes in a long-term culture. *Circ. J.* 77, 1307–1314. doi: 10.1253/circj.CJ-12-0987

Kattman, S. J., Witty, A. D., Gagliardi, M., Dubois, N. C., Niapour, M., Hotta, A., et al. (2011). Stage-specific optimization of activin/nodal and BMP signaling promotes cardiac differentiation of mouse and human pluripotent stem cell lines. *Cell Stem Cell* 8, 228–240. doi: 10.1016/j.stem.2010.12.008

Kehat, I., Kenyagin-Karsenti, D., Snir, M., Segev, H., Amit, M., Gepstein, A., et al. (2001). Human embryonic stem cells can differentiate into myocytes with structural and functional properties of cardiomyocytes. *J. Clin. Invest* 108, 407–414. doi: 10.1172/jci12131

Kim, C., Wong, J., Wen, J., Wang, S., Wang, C., Spiering, S., et al. (2013). Studying arrhythmogenic right ventricular dysplasia with patient-specific iPSCs. *Nature* 494, 105–110. doi: 10.1038/nature11799

Kirby, R. J., Divlianska, D. B., Whig, K., Bryan, N., Morfa, C. J., Koo, A., et al. (2018). Discovery of novel small-molecule inducers of heme oxygenase-1 that protect human ipsc-derived cardiomyocytes from oxidative stress. *J. Pharmacol. Exp. Ther.* 364, 87–96. doi: 10.1124/jpet.117.243717

Kobayashi, J., Yoshida, M., Tarui, S., Hirata, M., Nagai, Y., Kasahara, S., et al. (2014). Directed differentiation of patient-specific induced pluripotent stem cells identifies the transcriptional repression and epigenetic modification of NKX2-5. HAND1, and NOTCH1 in hypoplastic left heart syndrome. *PLoS One* 9:e102796. doi: 10.1371/journal.pone.0102796

Kumar, A., Thomas, S. K., Wong, K. C., Lo Sardo, V., Cheah, D. S., Hou, Y. H., et al. (2019). Mechanical activation of noncoding-RNA-mediated regulation of disease-associated phenotypes in human cardiomyocytes. *Nat. Biomed. Eng.* 3, 137–146. doi: 10.1038/s41551-018-0344-5

LaBarge, W., Mattappally, S., Kannappan, R., Fast, V. G., Pretorius, D., Berry, J. L., et al. (2019). Maturation of three-dimensional, hiPSC-derived cardiomyocyte spheroids utilizing cyclic, uniaxial stretch and electrical stimulation. *PLoS One* 14:e0219442. doi: 10.1371/journal.pone.0219442

Laflamme, M. A., Chen, K. Y., Naumova, A. V., Muskheli, V., Fugate, J. A., Dupras, S. K., et al. (2007). Cardiomyocytes derived from human embryonic stem cells in pro-survival factors enhance function of infarcted rat hearts. *Nat. Biotechnol.* 25, 1015–1024. doi: 10.1038/nbt1327

Lemme, M., Braren, I., Prondzynski, M., Aksehirlioglu, B., Ulmer, B. M., Schulze, M. L., et al. (2019). Chronic intermittent tachypacing by an optogenetic approach induces arrhythmia vulnerability in human engineered heart tissue. *Cardiovasc. Res.* cvz245. doi: 10.1093/cvr/cvz245

Leonard, A., Bertero, A., Powers, J. D., Beussman, K. M., Bhandari, S., Regnier, M., et al. (2018). Afterload promotes maturation of human induced pluripotent stem cell derived cardiomyocytes in engineered heart tissues. *J. Mol. Cell Cardiol.* 118, 147–158. doi: 10.1016/j.yjmcc.2018.03.016

Li, Z., Mirams, G. R., Yoshinaga, T., Ridder, B. J., Han, X., Chen, J. E., et al. (2020). General principles for the validation of proarrhythmia risk prediction models: an extension of the CiPA in silico strategy. *Clin. Pharmacol. Ther.* 107, 102–111. doi: 10.1002/cpt.1647

Lian, X., Hsiao, C., Wilson, G., Zhu, K., Hazeltine, L. B., Azarin, S. M., et al. (2012). Robust cardiomyocyte differentiation from human pluripotent stem cells via temporal modulation of canonical Wnt signaling. *Proc. Natl. Acad. Sci. U.S.A.* 109, E1848–E1857. doi: 10.1073/pnas.1200250109

Liu, Y., Steinbusch, L. K. M., Nabben, M., Kapsokalyvas, D., van Zandvoort, M., Schönleitner, P., et al. (2017). Palmitate-induced vacuolar-type H^+-ATPase inhibition feeds forward into insulin resistance and contractile dysfunction. *Diabetes* 66, 1521–1534. doi: 10.2337/db16-0727

Lowry, W. E., Richter, L., Yachechko, R., Pyle, A. D., Tchieu, J., Sridharan, R., et al. (2008). Generation of human induced pluripotent stem cells from dermal fibroblasts. *Proc. Natl. Acad. Sci.* 105, 2883–2888. doi: 10.1073/pnas.0711983105

Lu, H. R., Zeng, H., Kettenhofen, R., Guo, L., Kopljar, I., van Ammel, K., et al. (2019). Assessing drug-induced long QT and proarrhythmic risk using human stem-cell-derived cardiomyocytes in a Ca2+ imaging assay: evaluation of 28 CiPA compounds at three test sites. *Toxicol. Sci.* 170, 345–356. doi: 10.1093/toxsci/kfz102

Lu, Y., Bu, M., and Yun, H. (2019). Sevoflurane prevents hypoxia/reoxygenation-induced cardiomyocyte apoptosis by inhibiting PI3KC3-mediated autophagy. *Hum. Cell* 32, 150–159. doi: 10.1007/s13577-018-00230-4

Lundy, S. D., Zhu, W.-Z., Regnier, M., and Laflamme, M. A. (2013). Structural and functional maturation of cardiomyocytes derived from human pluripotent stem cells. *Stem Cells Dev.* 22, 1991–2002. doi: 10.1089/scd.2012.0490

Machiraju, P., and Greenway, S. C. (2019). Current methods for the maturation of induced pluripotent stem cell-derived cardiomyocytes. *World J. Stem Cells* 11, 33–43. doi: 10.4252/wjsc.v11.i1.33

Magdy, T., Schuldt, A. J. T., Wu, J. C., Bernstein, D., and Burridge, P. W. (2018). Human induced pluripotent stem cell (hiPSC)-derived cells to assess drug cardiotoxicity: opportunities and problems. *Annu. Rev. Pharmacol. Toxicol.* 58, 83–103. doi: 10.1146/annurev-pharmtox-010617-053110

Martewicz, S., Gabrel, G., Campesan, M., Canton, M., Di Lisa, F., and Elvassore, N. (2018). Live cell imaging in microfluidic device proves resistance to oxygen/glucose deprivation in human induced pluripotent stem cell-derived cardiomyocytes. *Anal. Chem.* 90, 5687–5695. doi: 10.1021/acs.analchem.7b05347

Martewicz, S., Luni, C., Serena, E., Pavan, P., Chen, H. V., Rampazzo, A., et al. (2019). Transcriptomic characterization of a human in vitro model of arrhythmogenic cardiomyopathy under topological and mechanical stimuli. *Ann. Biomed. Eng.* 47, 852–865. doi: 10.1007/s10439-018-02134-8

Martewicz, S., Michielin, F., Serena, E., Zambon, A., Mongillo, M., and Elvassore, N. (2012). Reversible alteration of calcium dynamics in cardiomyocytes during acute hypoxia transient in a microfluidic platform. *Integr. Biol.* 4, 153–164. doi: 10.1039/c1ib00087j

Martewicz, S., Serena, E., Zatti, S., Keller, G., and Elvassore, N. (2017). Substrate and mechanotransduction influence SERCA2a localization in human pluripotent stem cell-derived cardiomyocytes affecting functional performance. *Stem Cell Res.* 25, 107–114. doi: 10.1016/j.scr.2017.10.011

Martin, T. P., Hortigon-Vinagre, M. P., Findlay, J. E., Elliott, C., Currie, S., and Baillie, G. S. (2014). Targeted disruption of the heat shock protein 20-phosphodiesterase 4D (PDE4D) interaction protects against pathological cardiac remodelling in a mouse model of hypertrophy. *FEBS Open Bio* 4, 923–927. doi: 10.1016/j.fob.2014.10.011

Mathieu, S., El Khoury, N., Rivard, K., Gelinas, R., Goyette, P., Paradis, P., et al. (2016). Reduction in Na(+) current by angiotensin II is mediated by PKCalpha in mouse and human-induced pluripotent stem cell-derived cardiomyocytes. *Heart Rhythm* 13, 1346–1354. doi: 10.1016/j.hrthm.2016.02.015

McMullen, J. R., and Jennings, G. L. (2007). Differences between pathological and physiological cardiac hypertrophy: novel therapeutic strategies to treat heart failure. *Clin. Exp. Pharmacol. Physiol.* 34, 255–262. doi: 10.1111/j.1440-1681.2007.04585.x

Mirtschink, P., Bischof, C., Pham, M. D., Sharma, R., Khadayate, S., Rossi, G., et al. (2019). Inhibition of the hypoxia-inducible factor 1alpha-induced cardiospecific herna1 enhance-templated RNA protects from heart disease. *Circulation* 139, 2778–2792. doi: 10.1161/circulationaha.118.036769

Mo, B., Wu, X., Wang, X., Xie, J., Ye, Z., and Li, L. (2019). miR-30e-5p mitigates hypoxia-induced apoptosis in human stem cell-derived cardiomyocytes by suppressing bim. *Int. J. Biol. Sci.* 15, 1042–1051. doi: 10.7150/ijbs.31099

Moretti, A., Bellin, M., Welling, A., Jung, C. B., Lam, J. T., Bott-Flugel, L., et al. (2010). Patient-specific induced pluripotent stem-cell models for long-QT syndrome. *N. Engl. J. Med.* 363, 1397–1409. doi: 10.1056/NEJMoa0908679

Mummery, C., Ward-van Oostwaard, D., Doevendans, P., Spijker, R., van den Brink, S., Hassink, R., et al. (2003). Differentiation of human embryonic stem cells to cardiomyocytes: role of coculture with visceral endoderm-like cells. *Circulation* 107, 2733–2740. doi: 10.1161/01.Cir.0000068356.38592.68

Naftali-Shani, N., Molotski, N., Nevo-Caspi, Y., Arad, M., Kuperstein, R., Amit, U., et al. (2018). Modeling peripartum cardiomyopathy with human induced pluripotent stem cells reveals distinctive abnormal function of cardiomyocytes. *Circulation* 138, 2721–2723. doi: 10.1161/circulationaha.118.035950

Nagai, H., Satomi, T., Abiru, A., Miyamoto, K., Nagasawa, K., Maruyama, M., et al. (2017). Antihypertrophic effects of small molecules that maintain mitochondrial ATP levels under hypoxia. *EBioMed.* 24, 147–158. doi: 10.1016/j.ebiom.2017.09.022

Nerbonne, J. M., Nichols, C. G., Schwarz, T. L., and Escande, D. (2001). Genetic manipulation of cardiac K(+) channel function in mice: what have we learned, and where do we go from here? *Circ. Res.* 89, 944–956. doi: 10.1161/hh2301.100349

Ng, K. M., Lau, Y. M., Dhandhania, V., Cai, Z. J., Lee, Y. K., Lai, W. H., et al. (2018). Empagliflozin ameliorates high glucose induced-cardiac dysfuntion in

human iPSC-Derived cardiomyocytes. *Sci. Rep.* 8:14872. doi: 10.1038/s41598-018-33293-2

Olson, H., Betton, G., Robinson, D., Thomas, K., Monro, A., Kolaja, G., et al. (2000). Concordance of the toxicity of pharmaceuticals in humans and in animals. *Regul. Toxicol. Pharmacol.* 32, 56–67. doi: 10.1006/rtph.2000.1399

Otsuji, T. G., Minami, I., Kurose, Y., Yamauchi, K., Tada, M., and Nakatsuji, N. (2010). Progressive maturation in contracting cardiomyocytes derived from human embryonic stem cells: qualitative effects on electrophysiological responses to drugs. *Stem Cell Res.* 4, 201–213. doi: 10.1016/j.scr.2010.01.002

Pallotta, I., Sun, B., Wrona, E. A., and Freytes, D. O. (2015). BMP protein-mediated crosstalk between inflammatory cells and human pluripotent stem cell-derived cardiomyocytes. *J. Tissue Eng. Regen. Med.* 11, 1466–1478. doi: 10.1002/term.2045

Pant, T., Mishra, M. K., Bai, X., Ge, Z. D., Bosnjak, Z. J., and Dhanasekaran, A. (2019). Microarray analysis of long non-coding RNA and mRNA expression profiles in diabetic cardiomyopathy using human induced pluripotent stem cell-derived cardiomyocytes. *Diab. Vasc. Dis. Res.* 16, 57–68. doi: 10.1177/1479164118813888

Park, I.-H., Zhao, R., West, J. A., Yabuuchi, A., Huo, H., Ince, T. A., et al. (2008). Reprogramming of human somatic cells to pluripotency with defined factors. *Nature* 451, 141–146. doi: 10.1038/nature06534

Park, J., Anderson, C. W., Sewanan, L. R., Kural, M. H., Huang, Y., Luo, J., et al. (2019). Modular design of a tissue engineered pulsatile conduit using human induced pluripotent stem cell-derived cardiomyocytes. *Acta Biomater* 102, 220–230. doi: 10.1016/j.actbio.2019.10.019

Qin, P., Arabacilar, P., Bernard, R. E., Bao, W., Olzinski, A. R., Guo, Y., et al. (2017). Activation of the amino acid response pathway blunts the effects of cardiac stress. *J. Am. Heart Assoc.* 6:e004453. doi: 10.1161/jaha.116.004453

Rampoldi, A., Singh, M., Wu, Q., Duan, M., Jha, R., Maxwell, J. T., et al. (2019). Cardiac toxicity from ethanol exposure in human-induced pluripotent stem cell-derived cardiomyocytes. *Toxicol. Sci.* 169, 280–292. doi: 10.1093/toxsci/kfz038

Ronaldson-Bouchard, K., Ma, S. P., Yeager, K., Chen, T., Song, L., Sirabella, D., et al. (2018). Advanced maturation of human cardiac tissue grown from pluripotent stem cells. *Nature* 556, 239–243. doi: 10.1038/s41586-018-0016-3

Rosales, W., and Lizcano, F. (2018). The histone demethylase JMJD2A modulates the induction of hypertrophy markers in ipsc-derived cardiomyocytes. *Front. Genet.* 9:14. doi: 10.3389/fgene.2018.00014

Ross, S. B., Fraser, S. T., and Semsarian, C. (2018). Induced pluripotent stem cell technology and inherited arrhythmia syndromes. *Heart Rhythm* 15, 137–144. doi: 10.1016/j.hrthm.2017.08.013

Rupert, C. E., Chang, H. H., and Coulombe, K. L. (2017). Hypertrophy changes 3D shape of hiPSC-cardiomyocytes: implications for cellular maturation in regenerative medicine. *Cell Mol. Bioeng* 10, 54–62. doi: 10.1007/s12195-016-0462-7

Sakai, K., Shimba, K., Ishizuka, K., Yang, Z., Oiwa, K., Takeuchi, A., et al. (2017). Functional innervation of human induced pluripotent stem cell-derived cardiomyocytes by co-culture with sympathetic neurons developed using a microtunnel technique. *Biochem. Biophys. Res. Commun.* 494, 138–143. doi: 10.1016/j.bbrc.2017.10.065

Sandstedt, M., Rotter Sopasakis, V., Lundqvist, A., Vukusic, K., Oldfors, A., Dellgren, G., et al. (2018). Hypoxic cardiac fibroblasts from failing human hearts decrease cardiomyocyte beating frequency in an ALOX15 dependent manner. *PLoS One* 13:e0202693. doi: 10.1371/journal.pone.0202693

Sartiani, L., Bettiol, E., Stillitano, F., Mugelli, A., Cerbai, E., and Jaconi, M. E. (2007). Developmental changes in cardiomyocytes differentiated from human embryonic stem cells: a molecular and electrophysiological approach. *Stem Cells* 25, 1136–1144. doi: 10.1634/stemcells.2006-0466

Sass, G., Madigan, R. T., Joubert, L. M., Bozzi, A., Sayed, N., Wu, J. C., et al. (2019a). A combination of itraconazole and amiodarone is highly effective against trypanosoma cruzi Infection of human stem cell-derived cardiomyocytes. *Am. J. Trop. Med. Hyg.* 101, 383–391. doi: 10.4269/ajtmh.19-0023

Sass, G., Tsamo, A. T., Chounda, G. A. M., Nangmo, P. K., Sayed, N., Bozzi, A., et al. (2019b). Vismione B interferes with trypanosoma cruzi infection of vero cells and human stem cell-derived cardiomyocytes. *Am. J. Trop. Med. Hyg.* 101, 1359–1368. doi: 10.4269/ajtmh.19-0350

Scassa, M. E., Jaquenod, de Giusti, C., Questa, M., Pretre, G., Richardson, G. A., et al. (2011). Human embryonic stem cells and derived contractile embryoid bodies are susceptible to Coxsakievirus B infection and respond to interferon Ibeta treatment. *Stem Cell Res.* 6, 13–22. doi: 10.1016/j.scr.2010.09.002

Scrimgeour, N. R., Wrobel, A., Pinho, M. J., and Hoydal, M. A. (2019). microRNA-451a prevents activation of matrix metalloproteinases 2/9 in human cardiomyocytes during pathological stress stimulation. *Am. J. Physiol. Cell Physiol.* 318, C94–C102. doi: 10.1152/ajpcell.00204.2019

Sebastiao, M. J., Gomes-Alves, P., Reis, I., Sanchez, B., Palacios, I., Serra, M., et al. (2020). Bioreactor-based 3D human myocardial ischemia/reperfusion in vitro model: a novel tool to unveil key paracrine factors upon acute myocardial infarction. *Transl. Res.* 215, 57–74. doi: 10.1016/j.trsl.2019.09.001

Sebastiao, M. J., Serra, M., Pereira, R., Palacios, I., Gomes-Alves, P., and Alves, P. M. (2019). Human cardiac progenitor cell activation and regeneration mechanisms: exploring a novel myocardial ischemia/reperfusion in vitro model. *Stem Cell Res Ther.* 10:77. doi: 10.1186/s13287-019-1174-4

Sepac, A., Sedlic, F., Si-Tayeb, K., Lough, J., Duncan, S. A., Bienengraeber, M., et al. (2010). Isoflurane preconditioning elicits competent endogenous mechanisms of protection from oxidative stress in cardiomyocytes derived from human embryonic stem cells. *Anesthesiology* 113, 906–916. doi: 10.1097/ALN.0b013e3181eff6b7

Sewanan, L. R., Schwan, J., Kluger, J., Park, J., Jacoby, D. L., Qyang, Y., et al. (2019). Extracellular matrix from hypertrophic myocardium provokes impaired twitch dynamics in healthy cardiomyocytes. *JACC Basic Transl. Sci.* 4, 495–505. doi: 10.1016/j.jacbts.2019.03.004

Shanmughapriya, S., Tomar, D., Dong, Z., Slovik, K. J., Nemani, N., Natarajaseenivasan, K., et al. (2018). FOXD1-dependent MICU1 expression regulates mitochondrial activity and cell differentiation. *Nat. Commun.* 9:3449. doi: 10.1038/s41467-018-05856-4

Sharma, A., Marceau, C., Hamaguchi, R., Burridge, P. W., Rajarajan, K., Churko, J. M., et al. (2014). Human induced pluripotent stem cell-derived cardiomyocytes as an in vitro model for coxsackievirus B3-induced myocarditis and antiviral drug screening platform. *Circ. Res.* 115, 556–566. doi: 10.1161/circresaha.115.303810

Takahashi, K., Tanabe, K., Ohnuki, M., Narita, M., Ichisaka, T., Tomoda, K., et al. (2007). Induction of pluripotent stem cells from adult human fibroblasts by defined factors. *Cell* 131, 861–872. doi: 10.1016/j.cell.2007.11.019

Tanaka, A., Yuasa, S., Mearini, G., Egashira, T., Seki, T., Kodaira, M., et al. (2014). Endothelin-1 induces myofibrillar disarray and contractile vector variability in hypertrophic cardiomyopathy-induced pluripotent stem cell-derived cardiomyocytes. *J. Am. Heart Assoc.* 3:e001263. doi: 10.1161/jaha.114.001263

Tiburcy, M., Hudson, J. E., Balfanz, P., Schlick, S., Meyer, T., Chang Liao, M. L., et al. (2017). Defined engineered human myocardium with advanced maturation for applications in heart failure modeling and repair. *Circulation* 135, 1832–1847. doi: 10.1161/circulationaha.116.024145

Tomita-Mitchell, A., Stamm, K. D., Mahnke, D. K., Kim, M. S., Hidestrand, P. M., Liang, H. L., et al. (2016). Impact of MYH6 variants in hypoplastic left heart syndrome. *Physiol. Genomics* 48, 912–921. doi: 10.1152/physiolgenomics.00091.2016

Trieschmann, J., Haustein, M., Koster, A., Hescheler, J., Brockmeier, K., Bennink, G., et al. (2019). Different responses to drug safety screening targets between human neonatal and infantile heart tissue and cardiac bodies derived from human-induced pluripotent stem cells. *Stem Cells Int.* 2019:6096294. doi: 10.1155/2019/6096294

Turnbull, I. C., Mayourian, J., Murphy, J. F., Stillitano, F., Ceholski, D. K., and Costa, K. D. (2018). Cardiac tissue engineering models of inherited and acquired cardiomyopathies. *Methods Mol. Biol.* 1816, 145–159. doi: 10.1007/978-1-4939-8597-5_11

Ulmer, B. M., Stoehr, A., Schulze, M. L., Patel, S., Gucek, M., Mannhardt, I., et al. (2018). Contractile work contributes to maturation of energy metabolism in hiPSC-derived cardiomyocytes. *Stem Cell Rep.* 10, 834–847. doi: 10.1016/j.stemcr.2018.01.039

Uzun, A. U., Mannhardt, I., Breckwoldt, K., Horvath, A., Johannsen, S. S., Hansen, A., et al. (2016). Ca(2+)-currents in human induced pluripotent stem cell-derived cardiomyocytes effects of two different culture conditions. *Front. Pharmacol.* 7:300. doi: 10.3389/fphar.2016.00300

van den Berg, C. W., Okawa, S., Chuva, de Sousa Lopes, S. M., van Iperen, L., Passier, R., et al. (2015). Transcriptome of human foetal heart compared with

cardiomyocytes from pluripotent stem cells. *Development* 142, 3231–3238. doi: 10.1242/dev.123810

van den Brink, L., Grandela, C., Mummery, C. L., and Davis, R. P. (2019). Inherited cardiac diseases, pluripotent stem cells and genome editing combined - the past, present and future. *Stem Cells*. 38, 174–186. doi: 10.1002/stem.3110

van Mil, A., Balk, G. M., Neef, K., Buikema, J. W., Asselbergs, F. W., Wu, S. M., et al. (2018). Modelling inherited cardiac disease using human induced pluripotent stem cell-derived cardiomyocytes: progress, pitfalls, and potential. *Cardiovasc. Res.* 114, 1828–1842. doi: 10.1093/cvr/cvy208

Varzideh, F., Mahmoudi, E., and Pahlavan, S. (2019). Coculture with noncardiac cells promoted maturation of human stem cell-derived cardiomyocyte microtissues. *J. Cell Biochem.* 120, 16681–16691. doi: 10.1002/jcb.28926

Voges, H. K., Mills, R. J., Elliott, D. A., Parton, R. G., Porrello, E. R., and Hudson, J. E. (2017). Development of a human cardiac organoid injury model reveals innate regenerative potential. *Development* 144, 1118–1127. doi: 10.1242/dev.143966

Wang, Z., Zhang, X. J., Ji, Y. X., Zhang, P., Deng, K. Q., Gong, J., et al. (2016). The long noncoding RNA Chaer defines an epigenetic checkpoint in cardiac hypertrophy. *Nat. Med.* 22, 1131–1139. doi: 10.1038/nm.4179

Ward, M. C., and Gilad, Y. (2019). A generally conserved response to hypoxia in iPSC-derived cardiomyocytes from humans and chimpanzees. *eLife* 8:e42374. doi: 10.7554/eLife.42374

Wei, W., Liu, Y., Zhang, Q., Wang, Y., Zhang, X., and Zhang, H. (2017). Danshen-enhanced cardioprotective effect of cardioplegia on ischemia reperfusion injury in a human-induced pluripotent stem cell-derived cardiomyocytes model. *Artif. Organs* 41, 452–460. doi: 10.1111/aor.12801

Wnorowski, A., Sharma, A., Chen, H., Wu, H., Shao, N. Y., Sayed, N., et al. (2019). Effects of spaceflight on human induced pluripotent stem cell-derived cardiomyocyte structure and function. *Stem Cell Rep.* 13, 960–969. doi: 10.1016/j.stemcr.2019.10.006

Wu, D., Zhang, Q., Yu, Y., Zhang, Y., Zhang, M., Liu, Q., et al. (2018). Oleanolic acid, a novel endothelin a receptor antagonist, alleviated high glucose-induced cardiomyocytes injury. *Am. J. Chin. Med.* 46, 1187–1201. doi: 10.1142/s0192415x18500623

Yang, C., Xu, Y., Yu, M., Lee, D., Alharti, S., Hellen, N., et al. (2017). Induced pluripotent stem cell modelling of HLHS underlines the contribution of dysfunctional NOTCH signalling to impaired cardiogenesis. *Hum. Mol. Genet.* 26, 3031–3045. doi: 10.1093/hmg/ddx140

Yang, L., Soonpaa, M. H., Adler, E. D., Roepke, T. K., Kattman, S. J., Kennedy, M., et al. (2008). Human cardiovascular progenitor cells develop from a KDR+ embryonic-stem-cell-derived population. *Nature* 453, 524–528. doi: 10.1038/nature06894

Yang, X., and Papoian, T. (2018). Moving beyond the comprehensive in vitro proarrhythmia assay: use of human-induced pluripotent stem cell-derived cardiomyocytes to assess contractile effects associated with drug-induced structural cardiotoxicity. *J. Appl. Toxicol.* 38, 1166–1176. doi: 10.1002/jat.3611

Yu, J., Vodyanik, M. A., Smuga-Otto, K., Antosiewicz-Bourget, J., Frane, J. L., Tian, S., et al. (2007). Induced pluripotent stem cell lines derived from human somatic cells. *Science* 318, 1917–1920. doi: 10.1126/science.1151526

Yucel, G., Zhao, Z., El-Battrawy, I., Lan, H., Lang, S., Li, X., et al. (2017). Lipopolysaccharides induced inflammatory responses and electrophysiological dysfunctions in human-induced pluripotent stem cell derived cardiomyocytes. *Sci. Rep.* 7:2935. doi: 10.1038/s41598-017-03147-4

Zhang, H., Tian, L., Shen, M., Tu, C., Wu, H., Gu, M., et al. (2019). Generation of quiescent cardiac fibroblasts from human induced pluripotent stem cells for in vitro modeling of cardiac fibrosis. *Circ. Res.* 125, 552–566. doi: 10.1161/circresaha.119.315491

Zhang, M. Y., Guo, F. F., Wu, H. W., Yu, Y. Y., Wei, J. Y., Wang, S. F., et al. (2017). DanHong injection targets endothelin receptor type B and angiotensin II receptor type 1 in protection against cardiac hypertrophy. *Oncotarget* 8:103393–103409. doi: 10.18632/oncotarget.21900

Zhao, X., Chen, H., Xiao, D., Yang, H., Itzhaki, I., Qin, X., et al. (2018). Comparison of Non-human primate versus human induced pluripotent stem cell-derived cardiomyocytes for treatment of myocardial infarction. *Stem Cell Rep.* 10, 422–435. doi: 10.1016/j.stemcr.2018.01.002

Zhao, Y., Rafatian, N., Feric, N. T., Cox, B. J., Aschar-Sobbi, R., Wang, E. Y., et al. (2019). A platform for generation of chamber-specific cardiac tissues and disease modeling. *Cell* 176, 913.e18–927.e18. doi: 10.1016/j.cell.2018.11.042

Conflict of Interest: The authors declare that the research was conducted in the absence of any commercial or financial relationships that could be construed as a potential conflict of interest.

frontiers in Physiology

ORIGINAL RESEARCH
published: 25 May 2020
doi: 10.3389/fphys.2020.00520

Inflammatory Drivers of Cardiovascular Disease: Molecular Characterization of Senescent Coronary Vascular Smooth Muscle Cells

Stevan D. Stojanović[1,2], Maximilian Fuchs[3,4], Meik Kunz[3], Ke Xiao[1], Annette Just[1], Andreas Pich[5], Johann Bauersachs[2,6], Jan Fiedler[1†], Daniel Sedding[7†] and Thomas Thum[1,6*†]*

[1] Institute of Molecular and Translational Therapeutic Strategies, Hannover Medical School, Hanover, Germany, [2] Department of Cardiology and Angiology, Hannover Medical School, Hanover, Germany, [3] Chair of Medical Informatics, Friedrich-Alexander University of Erlangen-Nürnberg, Erlangen, Germany, [4] Functional Genomics and Systems Biology Group, Department of Bioinformatics, University of Würzburg, Würzburg, Germany, [5] Institute of Toxicology and Core Unit Proteomics, Hannover Medical School, Hanover, Germany, [6] REBIRTH Center of Translational Regenerative Medicine, Hannover Medical School, Hanover, Germany, [7] Department of Internal Medicine III, Cardiology, Angiology and Intensive Care Medicine Martin-Luther-University Halle (Saale), Halle (Saale), Germany

OPEN ACCESS

Edited by:
Gaetano Santulli, Columbia University, United States

Reviewed by:
Michael Autieri, Temple University, United States
Francesco Prattichizzo, MultiMedica (IRCCS), Italy
Darren Baker, Mayo Clinic, United States

***Correspondence:**
Daniel Sedding
Daniel.Sedding@uk-halle.de
Thomas Thum
Thum.Thomas@mh-hannover.de

† These authors share last authorship

Specialty section:
This article was submitted to Clinical and Translational Physiology, a section of the journal Frontiers in Physiology

Received: *03 March 2020*
Accepted: *27 April 2020*
Published: *25 May 2020*

Citation:
Stojanović SD, Fuchs M, Kunz M, Xiao K, Just A, Pich A, Bauersachs J, Fiedler J, Sedding D and Thum T (2020) Inflammatory Drivers of Cardiovascular Disease: Molecular Characterization of Senescent Coronary Vascular Smooth Muscle Cells. Front. Physiol. 11:520. doi: 10.3389/fphys.2020.00520

The senescence of vascular smooth muscle cells (VSMCs) has been implicated as a causal pro-inflammatory mechanism for cardiovascular disease development and progression of atherosclerosis, the instigator of ischemic heart disease. Contemporary limitations related to studying this cellular population and senescence-related therapeutics are caused by a lack of specific markers enabling their detection. Therefore, we aimed to profile a phenotypical and molecular signature of senescent VSMCs to allow reliable identification. To achieve this goal, we have compared non-senescent and senescent VSMCs from two *in vitro* models of senescence, replicative senescence (RS) and DNA-damage induced senescence (DS), by analyzing the expressions of established senescence markers: cell cycle inhibitors- p16 INK4a, p14 ARF, p21 and p53; pro-inflammatory factors-Interleukin 1β (IL-1β), IL-6 and high mobility group box-1 (HMGB-1); contractile proteins-smooth muscle heavy chain- (MYH11), smoothelin and transgelin (TAGLN), as well as structural features (nuclear morphology and LMNB1 (Lamin B1) expression). The different senescence-inducing modalities resulted in a lack of the proliferative activity. Nucleomegaly was seen in senescent VSMC as compared to freshly isolated VSMC Phenotypically, senescent VSMC appeared with a significantly larger cell size and polygonal, non-spindle-shaped cell morphology. In line with the supposed switch to a pro-inflammatory phenotype known as the senescence associated secretory phenotype (SASP), we found that both RS and DS upregulated IL-1β and released HMGB-1 from the nucleus, while RS also showed IL-6 upregulation. In regard to cell cycle-regulating molecules, we detected modestly increased p16 levels in both RS and DS, but largely inconsistent p21, p14ARF, and p53 expressions in senescent VSMCs. Since these classical markers of senescence showed insufficient

deregulation to warrant senescent VSMC detection, we have conducted a non-biased proteomics and *in silico* analysis of RS VSMC demonstrating altered RNA biology as the central molecular feature of senescence in this cell type. Therefore, key proteins involved with RNA functionality, HMGB-1 release, LMNB-1 downregulation, in junction with nuclear enlargement, can be used as markers of VSMC senescence, enabling the detection of these pathogenic pro-inflammatory cells in future therapeutic studies in ischemic heart disease and atherosclerosis.

Keywords: inflammation, cardiovascular, aging, senescence, smooth muscle cell

INTRODUCTION

Inflammation is a hallmark and potent promoter of cardiovascular disease, in addition to other well-defined risk factors that contribute to the multifactorial processes of disease progression (hypercholesterolemia, diabetes, hypertension, and smoking) (Dzau et al., 2002). Elevated inflammatory marker levels, such as interleukin-1β (IL-1β), IL-6, and HMGB-1 are associated with an cardiovascular risk (Ridker, 2016). The CANTOS clinical trial demonstrated that an anti-inflammatory approach through IL-1β blockade improves CV (cardiovascular) outcomes (Ridker et al., 2017). While the results of the trial provide proof of concept that the anti-inflammatory approach provides significant CV benefit, a long-term systemic immunosuppressive therapy highlighted serious concerns about infections and sepsis (Hidalgo and Tall, 2019). Targeting the source and cause of inflammation, rather than individual cytokines may be a solution for these issues.

Cellular senescence has been proposed the key source of inflammation in atherosclerosis and cardiovascular disease (CVD) (Stojanović et al., 2020). Senescent cells are irreversibly cell cycle-arrested and characterized with a pro-inflammatory phenotype known as the senescence associated secretory phenotype (SASP) (Bennett and Clarke, 2016). Experimental evidence showed that the SASP includes several pro-inflammatory cytokines (IL-1β, IL-6, HMGB-1), many of which are known cardiovascular risk factors (Ridker, 2014).

Senescence of various cell types has been implicated in CVD development (Stojanović et al., 2020). In particular, senescent vascular smooth muscle cells (VSMCs) were reported to be one of the key pro-inflammatory senescent cell populations, and were found in unstable, rupture-prone atherosclerotic plaques (Bennett et al., 2016; Uryga and Bennett, 2016; Hamczyk et al., 2018; Katsuumi et al., 2018).

Therapeutic options to target these senescent cells have recently emerged (Stojanović et al., 2020). However, the further development of these strategies and their adaptation for the cardiovascular system is limited by a lack of specific markers that would enable the detection of senescent cell populations. Recent research pointed out toward the limitations of classical senescence markers. Cell cycle inhibitors p16 and p21 were not found to be consistently differentially regulated in senescence of various cell types (Hernandez-Segura et al., 2017). Inconsistencies between patterns of gene and protein expression of these markers were also observed (Marthandan et al., 2016). Additionally, p16 and the senescence-associated β-galactosidase staining (SAβG) levels can be reversibly increased in macrophages (Hall et al., 2017). Most SASP factors can be secreted by immune cells (Stojanović et al., 2020). Moreover, specific markers to detect and differentiate senescent VSMCs from other cell populations are lacking.

To test if the deregulation of previously reported senescence markers applies to senescent human coronary VSMCs, we have performed a detailed characterization of the molecular and phenotypical markers that are common in two separate senescence models *in vitro*, replicative senescence (RS) and DNA-damage-induced senescence (DS). We analyzed classical senescence markers: morphology and structural features of senescent VSMCs cells, cell cycle inhibitor and SASP marker expression, as well as contractile protein expression. To find a more specific signature of VSMC senescence, we conducted an unbiased high-throughput proteomics analysis to reveal novel markers of senescence in VSMCs.

MATERIALS AND METHODS

Chemicals and Antibodies

Bleomycin sulfate was purchased from Enzo Life Sciences (BML-AP302). The following antibodies were purchased: α-Tubulin (Cell Signaling, #2144), ACTA2 (Sigma Aldrich, C6198), β-Actin (Cell Signaling, #4967), HMGB1 (Abcam, ab18256), MYH11 (Abcam, ab53219), Phalloidin-TRITC (Sigma Aldrich, P1951), p16 (Proteintech, 10883-1-AP), p21 (Cell Signaling, #2947), p53 (Santa Cruz, sc6243), smoothelin (Santa Cruz, sc 28562), TAGLN (Abcam, ab14106).

Cell Culture

Human coronary smooth muscle cells from a young healthy donor were purchased from Promocell (C-12511) and cultured in growth medium (Promocell, C-22062), supplemented with 10% FBS and 1% penicillin-streptomicin (Sigma Aldrich). To achieve RS, cells were serially passaged (Bielak-Zmijewska et al., 2014). Cells were cultured until 70–80% confluence and re-seeded in T75 Flasks (Thermo Fisher Scientific, Nunc EasYFlask, #156499) at a density of 3.5×10^3 cells/cm^2 until proliferative arrest (passage 6–8). Cumulative population doublings were counted using the formula cPD = X + 3.322*(log Y−log I), X representing the cumulative population doubling of the subculture used to initiate the culture, Y being the viable cell number on harvest, and

I the cell number on inoculation. Low passage VSMCs (passage 2–3) were treated with bleomycin to induce DS, as previously reported (Gardner et al., 2015).

RNA Isolation and RT-qPCR

Gene expressions of p16, p14, p21, IL-1β, IL-6, TNF-α, LMNB-1, and TNFRSF10C were measured through RT-qPCR, and normalized to the mean expression of two housekeeping genes, FBXO7 and GAPDH, as previously suggested (Hernandez-Segura et al., 2019). Total RNA was extracted using the RNeasy Mini Kit (Qiagen, #74104). Reverse transcription was performed using the iScript™ cDNA Synthesis Kit (Biorad, #1708891) and quantitative expression using the iQ™ SYBR® Green Supermix (Biorad, #1708880), utilizing target specific human primers: p16INK4a (Forward 5′-GGGGGCACCAGAGGCAGT-3′; Reverse 5′-GGTTGTGGCG GGGGCAGTT-3′), p14ARF (5′-CCCTCGTGCTGATGCTAC TG-3′; Reverse 5′-CATCATGACCTGGTCTTCTAGGAA-3′), p21 (Forward 5′-TGTCCGTCAGAACCCATGC-3′; Reverse 5′-AAAGTCGAAGTTCCATCGCTC-3′), IL-1β (Forward 5′-GC TGCTCTGGGATTCTCTTC-3′; Reverse 5′-TGCCACTGTA ATAAGCCATCA-3′), IL-6 (Forward 5′-GGCACTGGCAGAA AACAACC -3′; Reverse 5′-GCAAGTCTCCTCATTGAATCC-3′), TNF-α (Forward 5′-GGCGTGGAGCTGAGAGATA-3′, Reverse 5′-CAGCCTTGGCCCTTGAAGA-3′), LMNB-1 (Forward 5′-AAGCAGCTGGAGTGGTTGTT-3′; Reverse 5′-TTG GATGCTCTTGGGGTTC-3′); TNFRSF10C (Forward 5′-CACC AACGCTTCCAACAATGAACC-3′; Reverse 5′- TCCGGAAG GTGCCTTCTTTACACT-3′), GAPDH (Forward 5′- TGCACC ACCAACTGCTTAGC-3′; Reverse 5′-GGCATGGACTGTGG TCATGAG-3′), FBXO7 (Forward 5′-GCTCGCACCTGAGGC AGTCC-3′; Reverse 5′-GTCTCTTCATCTCCAGTGAG GGG-3′).

Protein Isolation and Western Blot

Total protein was obtained from cell pellets, which were previously washed with PBS, via the lysis buffer (Biorad). Samples were loaded on 15% polyacrylamide gels for electrophoresis and transferred to a nitrocellulose membrane (Biorad). After blocking for 1 h in 5% milk-tris buffered saline Tween (TBST), membranes were incubated in 5% milk-TBST solution containing the primary antibody overnight. After washing in TBST, the membranes were incubated with the Secondary IgG-HRP secondary antibody (Santa Cruz) for 2 h, ultimately being rinsed and developed by using the enhanced chemiluminescence (ECL) reagent (Biorad).

Immunofluorescence and Nuclear/Cell Size Measurement

Cells were fixed using the Cytofix Fixation Buffer (BD Biosciences, #554655) for 15 min, washed with Phosphate Buffered Saline (PBS), incubated with blocking buffer for 30 min (Thermo Fisher Scientific, #37515). After adding primary antibodies in blocking buffer, cells were incubated overnight in the dark, washed and stained with secondary antibodies Alexa Flour 488 and 546 (Thermo Fisher Scientific). Cells were then washed with PBS and stained with DAPI (Thermo Fisher Scientific). Images were acquired using the Nikon Ni-E fluorescence microscope, with four fields of view per condition, containing at least 300 cells. Nuclear or cell size measurements and nuclear morphometric analysis were performed in Image J software (version 1.6), as described previously (Filippi-Chiela et al., 2012).

Senescence-Associated β-Galactosidase Staining (SAβG)

The protocol was performed as described by Dimri et al. (1995). Briefly, cells were fixed, washed and incubated in freshly prepared SAβG staining solution (1 mg/ml 5-bromo-4-chloro-3-indolyl-beta-d-galactopyranoside (X-gal), 1 × citric acid/sodium phosphate buffer (pH 6.0), 5 mM potassium ferricyanide, 5 mM potassium ferrocyanide, 150 mM NaCl, and 2 mM $MgCl_2$) at 37°C for 16 h. The enzymatic reaction was stopped by washing with cold PBS and cells were counted via bright-field microscopy.

Liquid Chromatography–Masspectrometry (LC-MS) and Bioinformatical Analysis

LC-MS was performed as described previously (Sonnenschein et al., 2019). Briefly, the whole cell lysate total protein from replicative senescence VSMCs was used for immunoprecipitation and stained via the Coomassie solution for 45min at room temperature. The gel was then de-stained, lanes digested using trypsin and extracted peptides were separated with a LC-MS system (RSLC, Thermo Fisher Scientific, Germany). Raw data was analyzed with MaxQuant software (version 1.5.3.30) and peptides were searched against all human entries of the UniProtKB/Swiss-Prot database via the Andromeda search engine. A false discovery rate of 0.01 on peptide and protein level was used for identification. Data were analyzed using Perseus (version 1.5.2.6) and if applicable two sided one-sample Student's *t*-test was applied for comparison and visualized via Graph Pad Prism 8. *In silico* analysis of differentially expressed proteins (mean difference $>1/<-1$) were analyzed using g:Profiler web tool (Raudvere et al., 2019). Functional profiling results were plotted in R (version 3.6.3) using ggplot2 package (version 3.3.0) (Wickham, 2016).

Statistical Analysis

Results are represented as means ± SEM and were analyzed in Graph Pad Prism 6/8 software. The analysis was performed with the two-sided Student's *t*-test for unpaired samples and two-way ANOVA for multiple group comparisons. Statistical significance was set at $p < 0.05$.

RESULTS

Senescent Coronary VSMCs Have an Enlarged Morphology, but Retain Smooth Muscle Cell Features

To determine if altered morphology can be used to distinguish senescent VSMCs, we induced replicative senescence through

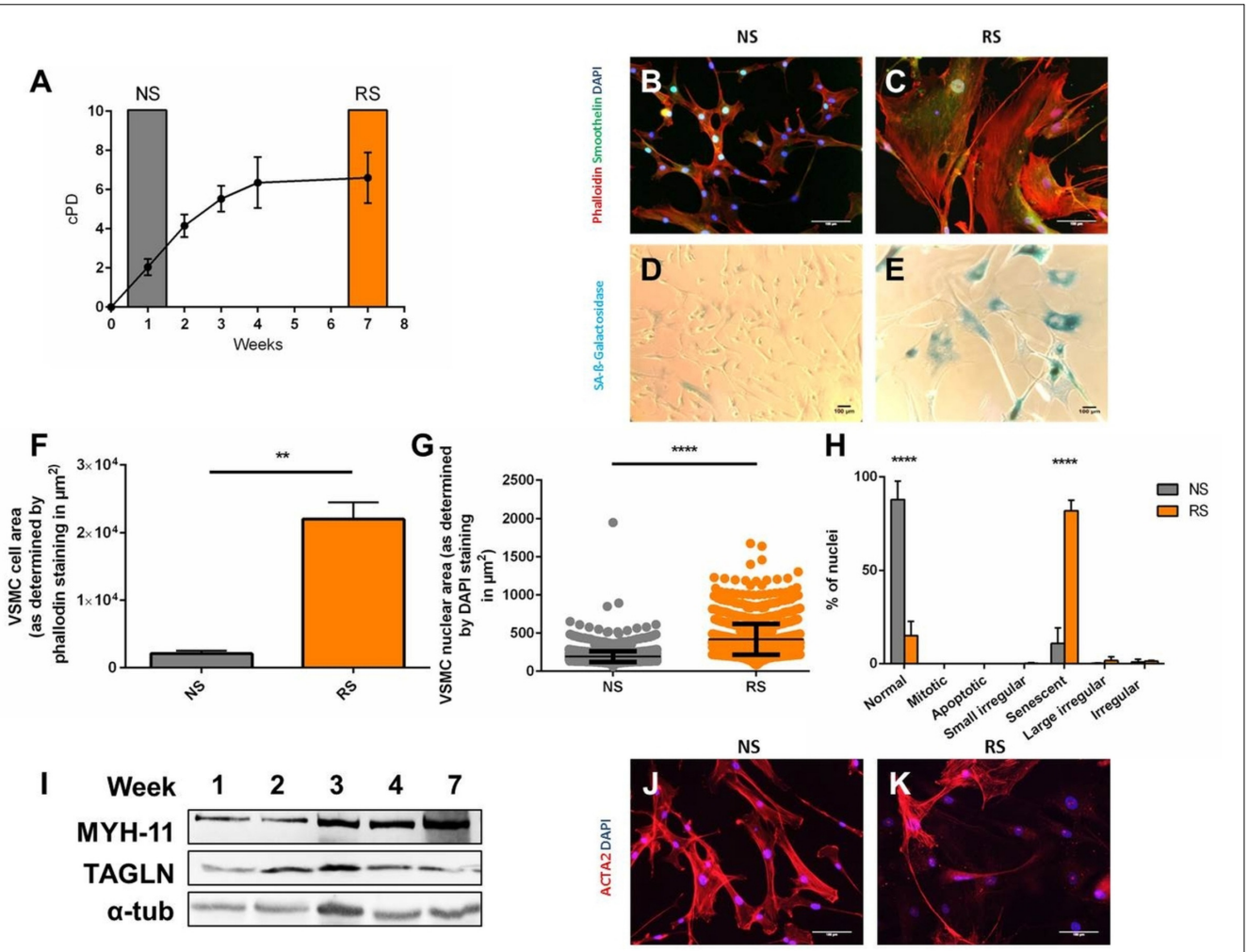

FIGURE 1 | Induction and morphological markers of replicative senescence. Cells were stained DAPI, phalloidin, smoothelin, and α-smooth muscle actin (ACTA2) enabling measurement of cell nuclear size in Image J and characterization. Western blot was per **(A)** Cumulative population doublings (cPD) of serially passaged VSMCs ($n = 3$). **(B,C)** Immunofluorescence microscopy of RS VSMCs, on 20× magnification. **(D,E)** Bright field microscopy of SA-β-galactosidase staining, on 10× magnification. **(F)** Cell size comparison between NS and RS VSMCs, $n = 3$, t-test. **(G)** Nuclear size comparison between NS and RS VSMCs, $n = 3$, t-test. **(H)** Nuclear morphology categorization via NMA; two-way ANOVA with multiple testing corrections, $n = 3$. **(I)** Western blots of Myosin-11 (MYH-11), Transgelin (TAGLN) and α-tubulin (α-tub) of a passaging timeline in RS. **(J,K)** Immunofluorescence microscopy of ACTA2 in NS and RS VSMCs, on 20× magnification. $^{**}p < 0.01$, $^{****}p < 0.0001$.

serial passaging (**Figure 1A**) and analyzed non-senescent low passage (NS, week 1 of culture) and replicatively senescent coronary VSMCs (RS, week 7 of culture). NS VSMCs (**Figure 1B**) showed a spindle-like morphology, typical of contractile VSMCs (Bennett et al., 2016). RS VSMCs (**Figure 1C**) lost these characteristics, having a flat, enlarged, polygonal morphology. Compared to NS cells (**Figure 1D**), the increase of size RS cells coincided with SA-β-galactosidase staining positivity (SAβG) (**Figure 1E**). The quantification of these parameters showed that replicatively senescent cells have an increased cell size (**Figure 1F**) and enlarged nuclei compared to non-senescent VSMCs (**Figure 1G**). To confirm that the nuclear enlargement is a consequence of senescence, further analysis conducted via Nuclear Morphometric Analysis (Filippi-Chiela et al., 2012). This high-throughput analysis tool compares size and irregularity of nuclei, enabling the distinction between the morphology of NS nuclei ("normal") and various other nuclear shapes seen in mitosis, apoptosis and mitotic catastrophe. This analysis confirmed that RS VSMC nuclei are dominantly large and regular, which is a feature of senescent nuclei, excluding other causes of nuclear enlargement (**Figure 1H**). These findings imply that nuclear morphology can be used as a reliable detection method of senescence, and was therefore used in subsequent experiments. To assess if this abnormal morphology is a consequence of de-differentiation, we observed that some common VSMC markers are retained, as seen on immunofluorescence (smoothelin) and Western blot (MYH11, TAGLN) (**Figure 1I**). However, RS VSMCs display variable expression of alpha smooth muscle actin (ACTA2) on immunofluorescence (**Figures 1J,K**).

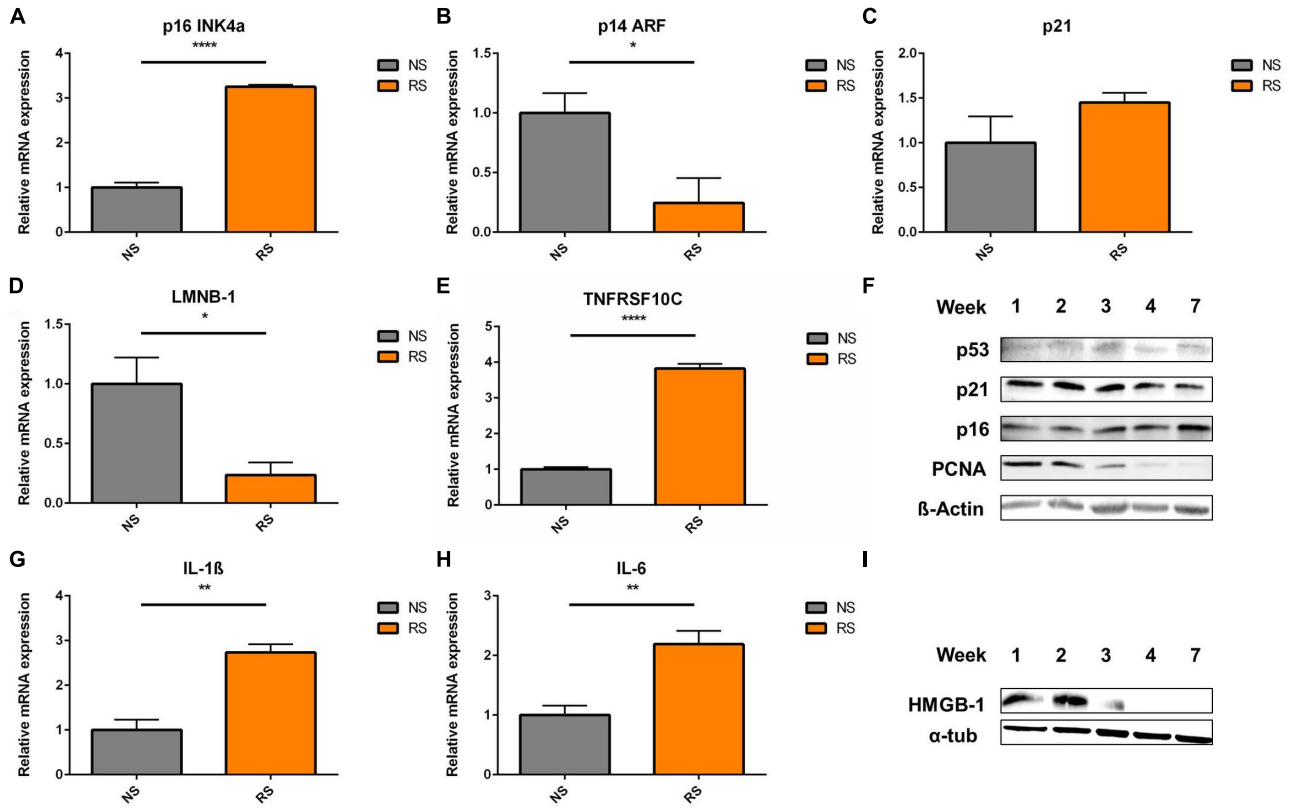

FIGURE 2 | Cell cycle inhibitors and SASP markers in replicative senescence; Expression levels of cell cycle inhibitors **(A)** p16, **(B)** p14, **(C)** p21; **(D)** nuclear envelope protein LMNB-1- Lamin B1 ($n = 4$) and **(E)** TRAIL receptor 3 and tumor necrosis factor receptor superfamily member 10C (TNFRSF10C) interleukins **(G)** IL-1β, **(H)** IL-6- interleukins ($n = 3$), were measured via RT-qPCR, *t*-test; **(F)** shows the Western blots a timeline of p53, p21, p16, and PCNA- Proliferating cell nuclear antigen; α-tub- α-tubulin; **(I)** HMGB-1 (High mobility group box 1) levels in whole cell lysates were analyzed in a passaging timeline until replicative arrest; $^{*}p < 0.05$, $^{**}p < 0.01$, $^{****}p < 0.0001$.

Senescent Coronary VSMCs Modestly Upregulate Cell Cycle Inhibitor p16 and Pro-Inflammatory Markers, but Not p14, p21, and p53

In terms of cell cycle inhibitors, upregulation of p16 mRNA level was seen in RS VSMCs (**Figure 2A**). However, p14 was downregulated (**Figure 2B**) and p21 showed similar expression levels (**Figure 2C**), when comparing NS to RS, while LMNB-1 was downregulated (**Figure 2D**) and TNFRSF10C (also known as Decoy receptor 1) was upregulated (**Figure 2E**), as two additional senescence markers. Analysis at the protein level was conducted on different subsequent passages until cessation of proliferation, as shown by the absence of proliferative cell antigen (PCNA) expression (**Figure 2F**). p16 showed a mild upregulation trend in the passaging timeline, while p21 and p53 seemed not to be differentially expressed on a protein level (**Figure 2F**). Senescent VSMCs display a pro-inflammatory phenotype and SASP markers. IL-1β and IL-6 gene expression was increased (**Figures 2G,H**). HMGB-1 was released from whole cell lysates in the final passages (**Figure 2I**). When released from the cell, HMGB-1 functions as an aggravating factor in inflammation (Davalos et al., 2013). In conclusion, cell cycle inhibitors were not consistently deregulated and senescent VSMCs possess a pro-inflammatory phenotype. To gain insight into their time-dynamic regulation in another model of senescence, we proceeded to measure their expression levels in a timeline of DNA-damage-induced senescence.

Senescence Markers Show a Dynamic Development

The markers were further evaluated in a setting of DNA-damage induced senescence (DS) by bleomycin, which induces double strand breaks (**Figure 3A**; Gardner et al., 2015). An analysis of time and dose-dependent responses in DS revealed a dynamic development of senescence markers. SAβG staining positivity and NMA showed comparable and gradual upward trends, starting at 7.5–25.5% at day 8 and reaching up to 72.9% at day 16, the effect being mostly dose dependant at 0–25 μg/ml bleomycin dose (**Figures 3B,C**). Cell cycle inhibitors and SASP markers showed a gradual dose- and time-dependant development. It appears that the time-dependence of senescence marker development shows a similar trend across all time points (**Figures 3D–G**): p16 levels peaked at day 11 and remain stable;

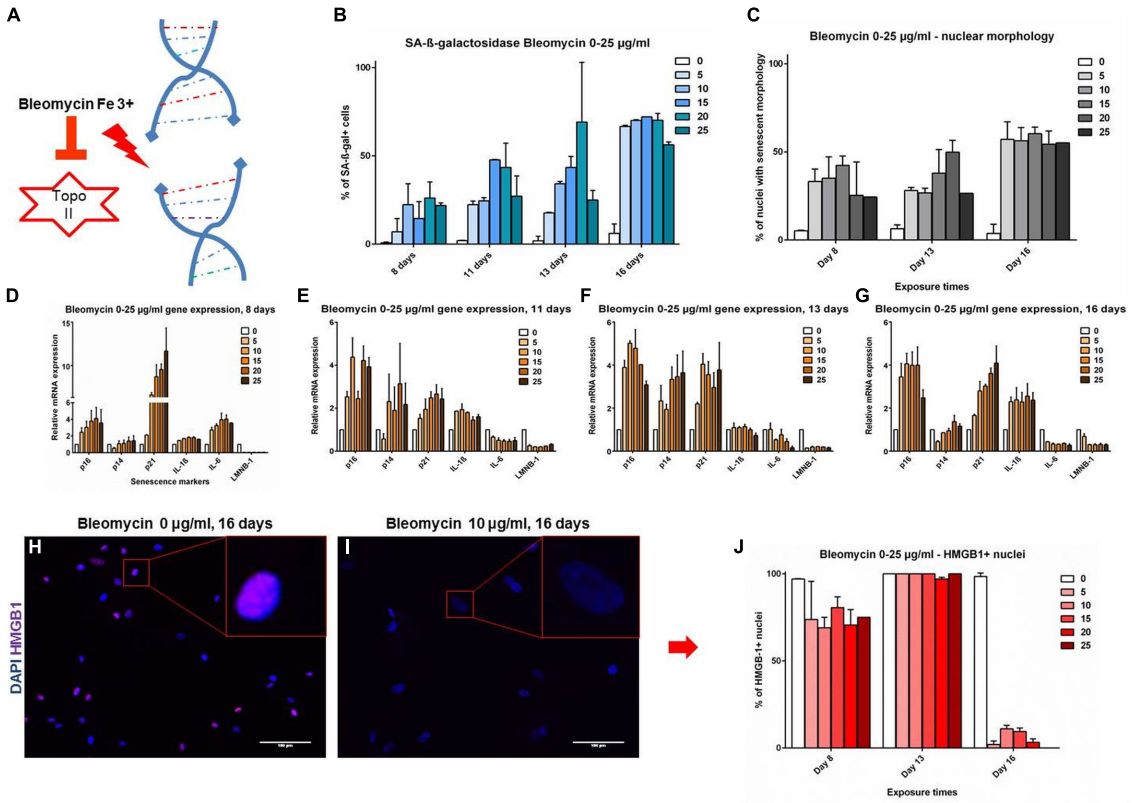

FIGURE 3 | (A–G) Senescence markers in DNA damage-induced senescence. Coronary VSMCs were treated with 0–25 μg/ml with bleomycin for 3 h and incubated for indicated time-points (n = 2). **(H–J)** Immuno-fluorescence of HMGB-1 localization (n = 2). Topo II- Topoisomerase 2; 0-25- bleomycin doses in μg per ml; DAPI- 4',6-diamidino-2-phenylindole; p16, p14, p21- cell cycle inhibitors; IL-1β, IL-6- interleukins; LMNB-1- Lamin B1; HMGB-1- High mobility group box1.

p14 is upregulated at intermediate time points (days 11 and 13), but returned to baseline levels on day 16. p21 was strongly upregulated early on day 8, but showed lesser upregulation at day 16; IL-1β was upregulated on day 16, coinciding with HMGB-1 release (**Figures 3H–J**). IL-6 showed upregulation on day 8, but that evolved into downregulation by day 16; LMNB-1 showed low levels throughout the timeline, with a slight trend of recovery on day 16. The data demonstrates that some senescence markers (p21, p14 and IL-6) can be transiently expressed at different stages of VSMC senescence evolution, without upregulation in late stages. Other markers are more consistently expressed and overlapping with RS (IL-1β, HMGB-1, LMNB-1, nuclear morphology). To find markers that are consistent features of senescent VSMCs in an unbiased, -omics approach, we have analyzed RS VSMCs protein expression with mass spectrometry.

LC-MS Reveals RNA Metabolism Disturbance as a Key Novel Marker of VSMC Senescence

To find reliable markers of senescence, we have compared NS (1 week of passaging) to RS (7 weeks of passaging) VSMC protein content with unbiased LC-MS technology (**Figure 4A**). The expression levels of known markers p16INK4a and p21 were not significantly upregulated, but cyclin dependant kinase 1 (CDK1) and PCNA was low in senescent VSMCs. In terms of other classical markers that were deregulated, IL-1β was upregulated, while LMNB-1 was downregulated. Pro-inflammatory factor HMGB-1, but also of HMGB-2, intracellular protein levels were decreased. We have therefore set out to find potential novel marker candidates among the 1083 significantly differentially regulated proteins in the dataset.

To study the functional changes in senescent cells, we have performed a gene enrichment analysis of the top downregulated (**Figure 4B**) and upregulated proteins (**Figure 4C**). Several processes known to be linked to senescence were found, including nuclear membrane abnormalities and inflammation. RNA-related metabolism appeared amongst the most strongly implicated biological processes to be deregulated in senescence, involving a large group of proteins associated with this process (**Figure 4B**). In addition, RS VSMCs have low glycolytic activity but a high enrichment of secretory processes.

DISCUSSION

Cellular senescence is defined as an irreversible cell cycle arrest, and is associated with the pro-inflammatory SASP (Stojanović et al., 2020). Senescence has been implicated in multiple

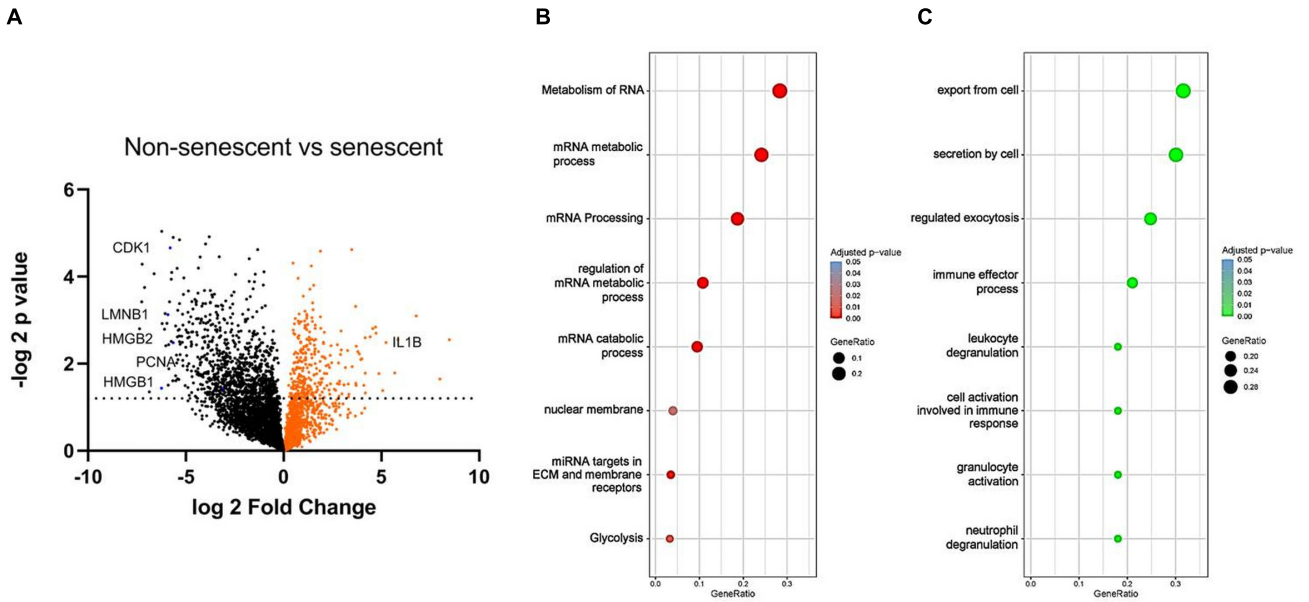

FIGURE 4 | (A) Volcano plot of NS and RS VSMC protein expression measured by LC-MS. False discovery rate was set at 0.01, $n = 3$, *t*-test. Gene ontology analysis via the g:Profiler tool of **(B)** downregulated and **(C)** upregulated processes in RS, *t*-test.

chronic diseases, including atherosclerosis, heart failure and aneurism development (Stojanović et al., 2020). To counter these deleterious effects, multiple experimental and therapeutic strategies are currently under development. Due to the limitation of options to detect cellular senescence *in vivo,* these studies utilize mice with reporter genes inserted into the *CDKN2A* gene, which encodes the p16INK4a cell cycle inhibitor (Childs et al., 2016; Schafer et al., 2017). *In vitro* evaluation of senescence in therapeutic studies is often conducted by counting cells positive for SAβG, p21, p53, nuclear enlargement and negative for nuclear HMGB-1 (Jeon et al., 2017; Schafer et al., 2017; Bussian et al., 2018). Recent efforts to improve senescent cell detection revealed that these markers may not be the best option to detect all senescent cell types. p16 and p21 did not universally belong to the senescence signature of various cell lines (Hernandez-Segura et al., 2017). A single cell qPCR study showed that p16 is not the most reliable features of fibroblast senescence on a cell to cell basis (Wiley et al., 2017). Possible explanations for these issues include cell type specificity of the senescence machinery (Hernandez-Segura et al., 2017), dependency on the causative stimulus (Olivieri et al., 2018), the transient nature of the expression of some markers (Hernandez-Segura et al., 2017), and differences between expression levels on the mRNA and protein level (Marthandan et al., 2016).

In our study, we aimed to characterize the senescence of vascular smooth muscle cells, as these cells have been implicated in promoting atherosclerotic disease through the secretion of pro-inflammatory factors (IL-1β, IL-6, HMGB-1) and are thus an interesting anti-inflammatory therapeutic target (Stojanović et al., 2020).

We could show that senescent VSMCs demonstrate nuclear enlargement and cell morphology abnormalities in both RS and DS, a feature of senescence found in various cell types (Filippi-Chiela et al., 2012; Ogrodnik et al., 2017). In line with the nuclear abnormalities, senescent VSMCs in both RS and DS show low LMNB1 levels, from the earlier time points in DS. However, nucleomegaly takes more time to fully develop and seems to occur at intermediate to late phases of DS development *in vitro*. Whether LMNB1 abundancy is actively regulated (transcriptionally or post-transcriptionally) remains unclear.

VSMCs are known to undergo a phenotypic switch from a contractile to a secretory phenotype (Bennett et al., 2016). Highly passaged VSMCs were reported to lose smooth muscle cell contractile markers (Bennett et al., 2016). We indeed observe decreased and disorganized ACTA2 expression in RS on immunofluorescence, as well as active secretory processes *in silico*. However, some RS cells remain positive for ACTA2. Furthermore, RS VSMCs retain MYH11 and TAGLN expression, which is also consistent with previous studies for TAGLN (Miao et al., 2017). These results are in line with recent research showing heterogeneity of senescent cells (van Deursen, 2014; Olivieri et al., 2018; Tang et al., 2019), and warrant future study on a single-cell level (Olivieri et al., 2018).

Senescent VSMCs show a complex cell cycle footprint, with low PCNA and CDK1 levels, that indicate a lack of proliferation. Cell cycle inhibitor expression includes consistently increased p16 levels on a mRNA, and a time-dependant dynamic p14/p21/p53 regulation. These dynamic trends in DS are schematically represented in **Figure 5**. In addition, p14, p21 and p53 are key regulators of quiescence (Hernandez-Segura et al., 2017), which may make the detection of senescent cells less specific.

Our data at an mRNA (RT-qPCR) and protein level (LC-MS) shows that senescent VSMCs upregulate several

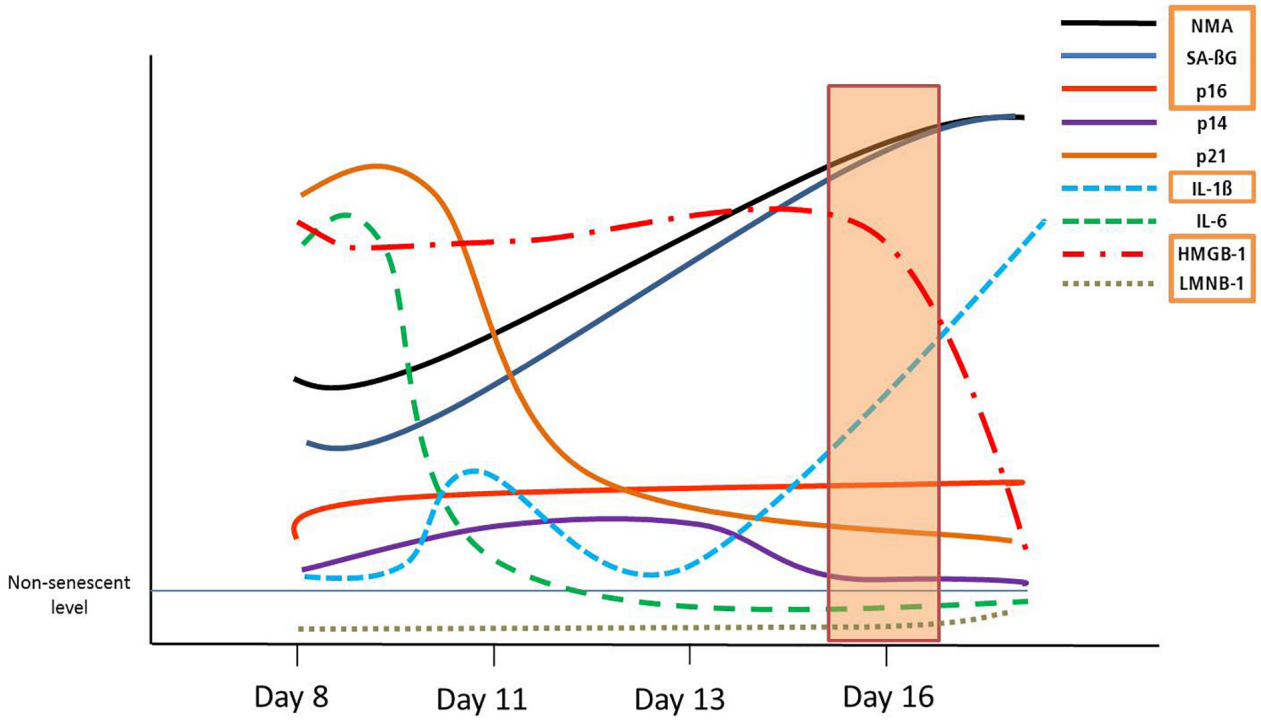

FIGURE 5 | Graphical summary of the dynamic development of senescence markers in DS. Orange rectangles signify markers shared with RS, from day 16.

pro-inflammatory factors. IL-1β is overexpressed in both RS and DS, while IL-6 seems to be upregulated in RS and "early-phase" DS. HMGB-1and HMGB-2 are key regulators of the SASP, and show downregulated intracellular levels in senescence (Davalos et al., 2013; Guerrero and Gil, 2016). HMGB-1 nuclear release to the extracellular space has been implicated as another mechanism of the inflammation activation by senescent cells, where it acts as an alarmin that promotes the response of innate immunity (Davalos et al., 2013; Guerrero and Gil, 2016). In both RS and DS, VSMCs released this factor consistently. Indeed, *in silico* functional analysis confirmed that senescent VSMCs show a pro-inflammatory phenotype that promotes innate immunity activation. Therefore, we could confirm that senescent VSMCs are a source of inflammatory factors. Hypothetically, senescent VSMCs may be able to persistently self-activate inflammation in an autocrine and paracrine manner through an IL-1α – IL-1β – HMGB1 feedback loop. Others have reported that the IL-1α protein acts as a key driver of the SASP in senescent VSMCs (Orjalo et al., 2009; Gardner et al., 2015). IL-1α can aid IL-1β production by promoting IL-1-receptor signaling (Di Paolo and Shayakhmetov, 2016). HMGB-1 also triggers IL-1β release in VSMCs (Kim et al., 2018). Although we could not find IL-1α deregulation in our dataset, it still may be a key intermediary in this process, independently of its expression levels. Such mechanisms may explain the multimodal contribution of senescent VSMCs to chronic systemic and vascular inflammation, and are thus a valid therapeutic entry point (Stojanović et al., 2020).

Based on results above, it appeared that not all classical senescence markers display sufficient consistency and differential regulation to serve as reliable detection tools for senescent VSMCs. To tackle this issue, we have generated a proteomics dataset from RS samples. We could find global RNA metabolism processes highly enriched in our proteomic dataset, with mRNA splicing, transport and catabolism being significantly affected. Indeed, altered RNA splicing has been reported in senescence for specific molecules, such as p53 (Deschenes and Chabot, 2017). This mechanism may explain the discrepancy between expression levels of p16 on an mRNA and protein level, as RNA-binding proteins are known to regulate tumor suppressor expression at a pre-translational level (Wang et al., 2005; Majumder et al., 2016). Additionally, the amino-acid sequence based detection in LC-MS does not allow the detection of post-translational modifications of proteins (Frescas et al., 2017), which may be a limiting factor in detection. These observations need to be studied further, but may be an important point of considerations in studies encountering issues with p16INK4a detection (Marthandan et al., 2016; Hernandez-Segura et al., 2017; Wiley et al., 2017). Nevertheless, altered proteins involved in RNA metabolism appear to be a key feature of VSMC senescence and may be used as markers to detect these cells.

In summary, we found that VSMCs display an atypical molecular signature that only partially adheres to the commonly used senescence markers. Altered RNA metabolism is a consistent feature of senescent VSMCs, potentially facilitating their detection in future mechanistic and therapeutic studies.

DATA AVAILABILITY STATEMENT

All datasets generated for this study are included in the article/**Supplementary Material**, further inquiries can be directed to the corresponding authors.

AUTHOR CONTRIBUTIONS

SS, MF, MK, KX, AJ, AP, JB, JF, DS, and TT contributed to the conception and design of the study. SS performed expression and microscopy experiments and wrote the first draft of the manuscript. AJ and AP performed the mass spectrometry. SS, MF, MK, KX organized the proteomics database. SS, MF, MK, KX, AP, and JF performed the statistical and *in silico* analysis. SS and MF wrote sections of the manuscript. DS and TT equally contributed in the supervision of the process. All authors contributed to manuscript revision, read and approved the submitted version.

FUNDING

This work was funded by the Deutsche Forschungsgemeinschaft (KFO FOR311-2, TH903/20-1 to TT), Cluster of Excellence REBIRTH (from Regenerative Biology to Reconstructive Therapy EXC 62 to SS, JB, and TT), H2020 Project 777111-REPO-TRIAL (to JB), German Academic Exchange Service Graduate School Scholarship Programme (DAAD-GSSP) (57320205, to SS), Federal Ministry of Education and Research (BMBF), Era-Net grant 01KT1801 (to MF and MK), Foundation Leducq (to TT) and the ERA Network grant EXPERT (to TT).

SUPPLEMENTARY MATERIAL

The Supplementary Material for this article can be found online at: https://www.frontiersin.org/articles/10.3389/fphys.2020.00520/full#supplementary-material

TABLE S1 | Proteomics dataset of NS vs RS VSMCs.

REFERENCES

Bennett, M. R., and Clarke, M. C. (2016). Basic research: killing the old: cell senescence in atherosclerosis. *Nat. Rev. Cardiol.* 14, 8–9. doi: 10.1038/nrcardio.2016.195

Bennett, M. R., Sinha, S., and Owens, G. K. (2016). Vascular smooth muscle cells in atherosclerosis. *Circ. Res.* 118, 692–702. doi: 10.1161/CIRCRESAHA.115.306361

Bielak-Zmijewska, A., Wnuk, M., Przybylska, D., Grabowska, W., Lewinska, A., Alster, O., et al. (2014). A comparison of replicative senescence and doxorubicin-induced premature senescence of vascular smooth muscle cells isolated from human aorta. *Biogerontology* 15, 47–64. doi: 10.1007/s10522-013-9477-9

Bussian, T. J., Aziz, A., Meyer, C. F., Swenson, B. L., van Deursen, J. M., and Baker, D. J. (2018). Clearance of senescent glial cells prevents tau-dependent pathology and cognitive decline. *Nature* 562, 578–582. doi: 10.1038/s41586-018-0543-y

Childs, B. G., Baker, D. J., Wijshake, T., Conover, C. A., Campisi, J., and van Deursen, J. M. (2016). Senescent intimal foam cells are deleterious at all stages of atherosclerosis. *Science* 354, 472–477. doi: 10.1126/science.aaf6659

Davalos, A. R., Kawahara, M., Malhotra, G. K., Schaum, N., Huang, J., Ved, U., et al. (2013). p53-dependent release of Alarmin HMGB1 is a central mediator of senescent phenotypes. *J. Cell Biol.* 201, 613–629. doi: 10.1083/jcb.201206006

Deschenes, M., and Chabot, B. (2017). The emerging role of alternative splicing in senescence and aging. *Aging Cell* 16, 918–933. doi: 10.1111/acel.12646

Di Paolo, N. C., and Shayakhmetov, D. M. (2016). Interleukin 1alpha and the inflammatory process. *Nat. Immunol.* 17, 906–913. doi: 10.1038/ni.3503

Dimri, G. P., Lee, X., Basile, G., Acosta, M., Scott, G., Roskelley, C., et al. (1995). A biomarker that identifies senescent human cells in culture and in aging skin in vivo. *Proc. Natl. Acad. Sci. U.S.A.* 92, 9363–9367. doi: 10.1073/pnas.92.20.9363

Dzau, V. J., Braun-Dullaeus, R. C., and Sedding, D. G. (2002). Vascular proliferation and atherosclerosis: new perspectives and therapeutic strategies. *Nat. Med.* 8, 1249–1256. doi: 10.1038/nm1102-1249

Filippi-Chiela, E. C., Oliveira, M. M., Jurkovski, B., Callegari-Jacques, S. M., da Silva, V. D., and Lenz, G. (2012). Nuclear morphometric analysis (NMA): screening of senescence, apoptosis and nuclear irregularities. *PLoS One* 7:e42522. doi: 10.1371/journal.pone.0042522

Frescas, D., Roux, C. M., Aygun-Sunar, S., Gleiberman, A. S., Krasnov, P., Kurnasov, O. V., et al. (2017). Senescent cells expose and secrete an oxidized form of membrane-bound vimentin as revealed by a natural polyreactive antibody. *Proc. Natl. Acad. Sci. U.S.A.* 114, E1668–E1677. doi: 10.1073/pnas.1614661114

Gardner, S. E., Humphry, M., Bennett, M. R., and Clarke, M. C. H. (2015). Senescent vascular smooth muscle cells drive inflammation through an interleukin-1α–dependent senescence-associated secretory phenotype. *Arterioscler. Thromb. Vasc. Biol.* 35, 1963–1974. doi: 10.1161/atvbaha.115.305896

Guerrero, A., and Gil, J. (2016). HMGB2 holds the key to the senescence-associated secretory phenotype. *J. Cell Biol.* 215, 297–299. doi: 10.1083/jcb.201610044

Hall, B. M., Balan, V., Gleiberman, A. S., Strom, E., Krasnov, P., Virtuoso, L. P., et al. (2017). p16(Ink4a) and senescence-associated beta-galactosidase can be induced in macrophages as part of a reversible response to physiological stimuli. *Aging* 9, 1867–1884. doi: 10.18632/aging.101268

Hamczyk, M. R., Villa-Bellosta, R., Gonzalo, P., Andres-Manzano, M. J., Nogales, P., Bentzon, J. F., et al. (2018). Vascular smooth muscle-specific progerin expression accelerates atherosclerosis and death in a mouse model of hutchinson-gilford progeria syndrome. *Circulation* 138, 266–282. doi: 10.1161/CIRCULATIONAHA.117.030856

Hernandez-Segura, A., de Jong, T. V., Melov, S., Guryev, V., Campisi, J., and Demaria, M. (2017). Unmasking transcriptional heterogeneity in senescent cells. *Curr. Biol.* 27, 2652–2660. doi: 10.1016/j.cub.2017.07.033

Hernandez-Segura, A., Rubingh, R., and Demaria, M. (2019). Identification of stable senescence-associated reference genes. *Aging Cell* 18:e12911. doi: 10.1111/acel.12911

Hidalgo, A., and Tall, A. R. (2019). Leducq transatlantic network on clonal hematopoiesis and atherosclerosis. *Circ. Res.* 124, 481–483. doi: 10.1161/circresaha.119.314677

Jeon, O. H., Kim, C., Laberge, R. M., Demaria, M., Rathod, S., Vasserot, A. P., et al. (2017). Local clearance of senescent cells attenuates the development of post-traumatic osteoarthritis and creates a pro-regenerative environment. *Nat. Med.* 23, 775–781. doi: 10.1038/nm.4324

Katsuumi, G., Shimizu, I., Yoshida, Y., and Minamino, T. (2018). Vascular senescence in cardiovascular and metabolic diseases. *Front. Cardiovas. Med.* 5:18. doi: 10.3389/fcvm.2018.00018

Kim, E. J., Park, S. Y., Baek, S. E., Jang, M. A., Lee, W. S., Bae, S. S., et al. (2018). HMGB1 Increases IL-1beta production in vascular smooth muscle cells via NLRP3 inflammasome. *Front. Physiol.* 9:313. doi: 10.3389/fphys.2018.00313

Majumder, M., House, R., Palanisamy, N., Qie, S., Day, T. A., Neskey, D., et al. (2016). RNA-binding protein FXR1 regulates p21 and TERC RNA to bypass p53-mediated cellular senescence in OSCC. *PLoS Genet.* 12:e1006306. doi: 10.1371/journal.pgen.1006306

Marthandan, S., Baumgart, M., Priebe, S., Groth, M., Schaer, J., Kaether, C., et al. (2016). Conserved senescence associated genes and pathways in primary human

fibroblasts detected by RNA-Seq. *PLoS One* 11:e0154531. doi: 10.1371/journal.pone.0154531

Miao, S. B., Xie, X. L., Yin, Y. J., Zhao, L. L., Zhang, F., Shu, Y. N., et al. (2017). Accumulation of smooth muscle 22alpha protein accelerates senescence of vascular smooth muscle cells via stabilization of p53 in vitro and in vivo. *Arterioscler. Thromb. Vasc. Biol.* 37, 1849–1859. doi: 10.1161/atvbaha.117.309378

Ogrodnik, M., Miwa, S., Tchkonia, T., Tiniakos, D., Wilson, C. L., Lahat, A., et al. (2017). Cellular senescence drives age-dependent hepatic steatosis. *Nat. Commun.* 8:15691. doi: 10.1038/ncomms15691

Olivieri, F., Prattichizzo, F., Grillari, J., and Balistreri, C. R. (2018). Cellular senescence and inflammaging in age-related diseases. *Med. Inflamm.* 2018:9076485. doi: 10.1155/2018/9076485

Orjalo, A. V., Bhaumik, D., Gengler, B. K., Scott, G. K., and Campisi, J. (2009). Cell surface-bound IL-1alpha is an upstream regulator of the senescence-associated IL-6/IL-8 cytokine network. *Proc. Natl. Acad. Sci. U.S.A.* 106, 17031–17036. doi: 10.1073/pnas.0905299106

Raudvere, U., Kolberg, L., Kuzmin, I., Arak, T., Adler, P., Peterson, H., et al. (2019). g:Profiler: a web server for functional enrichment analysis and conversions of gene lists (2019 update). *Nucleic Acids Res.* 47, W191–W198. doi: 10.1093/nar/gkz369

Ridker, P. M. (2014). Targeting inflammatory pathways for the treatment of cardiovascular disease. *Eur. Heart J.* 35, 540–543. doi: 10.1093/eurheartj/eht398

Ridker, P. M. (2016). From CRP to IL-6 to IL-1: moving upstream to identify novel targets for atheroprotection. *Circ. Res.* 118, 145–156. doi: 10.1161/circresaha.115.306656

Ridker, P. M., Everett, B. M., Thuren, T., MacFadyen, J. G., Chang, W. H., Ballantyne, C., et al. (2017). Antiinflammatory therapy with canakinumab for atherosclerotic disease. *N. Engl. J. Med.* 377, 1119–1131.

Schafer, M. J., White, T. A., Iijima, K., Haak, A. J., Ligresti, G., Atkinson, E. J., et al. (2017). Cellular senescence mediates fibrotic pulmonary disease. *Nat. Commun.* 8:14532. doi: 10.1038/ncomms14532

Sonnenschein, K., Fiedler, J., Pfanne, A., Just, A., Mitzka, S., Geffers, R., et al. (2019). Therapeutic modulation of RNA-binding protein Rbm38 facilitates re-endothelialization after arterial injury. *Cardiovasc. Res.* 115, 1804–1810. doi: 10.1093/cvr/cvz063

Stojanović, S. D., Fiedler, J., Bauersachs, J., Thum, T., and Sedding, D. G. (2020). Senescence-induced inflammation: an important player and key therapeutic target in atherosclerosis. *Eur. Heart J.* 2020:ehz919. doi: 10.1093/eurheartj/ehz919

Tang, H., Geng, A., Zhang, T., Wang, C., Jiang, Y., and Mao, Z. (2019). Single senescent cell sequencing reveals heterogeneity in senescent cells induced by telomere erosion. *Protein Cell* 10, 370–375. doi: 10.1007/s13238-018-0591-y

Uryga, A. K., and Bennett, M. R. (2016). Ageing induced vascular smooth muscle cell senescence in atherosclerosis. *J. Physiol.* 594, 2115–2124. doi: 10.1113/JP270923

van Deursen, J. M. (2014). The role of senescent cells in ageing. *Nature* 509, 439–446. doi: 10.1038/nature13193

Wang, W., Martindale, J. L., Yang, X., Chrest, F. J., and Gorospe, M. (2005). Increased stability of the p16 mRNA with replicative senescence. *EMBO Rep.* 6, 158–164. doi: 10.1038/sj.embor.7400346

Wickham, H. (2016). *Ggplot2: Elegant Graphics For Data Analysis*. Berlin: Springer.

Wiley, C. D., Flynn, J. M., Morrissey, C., Lebofsky, R., Shuga, J., Dong, X., et al. (2017). Analysis of individual cells identifies cell-to-cell variability following induction of cellular senescence. *Aging Cell* 16, 1043–1050. doi: 10.1111/acel.12632

Conflict of Interest: TT has filed and licensed patents regarding non-coding RNAs in CVD. TT was the founder and shareholder of Cardior Pharmaceuticals GmbH.

The remaining authors declare that the research was conducted in the absence of any commercial or financial relationships that could be construed as a potential conflict of interest.

frontiers in Physiology

ORIGINAL RESEARCH
published: 18 June 2020
doi: 10.3389/fphys.2020.00539

The Histone Demethylase JMJD1C Regulates CAMKK2-AMPK Signaling to Participate in Cardiac Hypertrophy

Shuang Yu[1†], *Yihong Li*[1†], *Hongwei Zhao*[2], *Qingdong Wang*[3] *and Ping Chen*[4*]

[1] Department of Cardiology, First Affiliated Hospital of Jiamusi University, Jiamusi, China, [2] Department of Emergency, First Affiliated Hospital of Jiamusi University, Jiamusi, China, [3] Department of Anesthesiology, First Affiliated Hospital of Jiamusi University, Jiamusi, China, [4] Department of Obstetrics and Gynecology, First Affiliated Hospital of Jiamusi University, Jiamusi, China

The roles of the histone demethylase JMJD1C in cardiac hypertrophy remain unknown. JMJD1C was overexpressed in hypertrophic hearts of humans and mice, whereas the histone methylation was reduced. *Jmjd1c* knockdown repressed the angiotensin II (Ang II)-mediated increase in cardiomyocyte size and overexpression of hypertrophic genes in cardiomyocytes. By contrast, JMJD1C overexpression promoted the hypertrophic response of cardiomyocytes. Our further molecular mechanism study revealed that JMJD1C regulated AMP-dependent kinase (AMPK) in cardiomyocytes. JMJD1C did not influence LKB1 but repressed *Camkk2* expression in cardiomyocytes. Inhibition of CAMKK2 with STO609 blocked the effects of JMJD1C on AMPK. AMPK knockdown blocked the inhibitory functions of JMJD1C knockdown on Ang II-induced hypertrophic response, whereas metformin reduced the functions of JMJD1C and repressed the hypertrophic response in cardiomyocytes.

Keywords: cardiac hypertrophy, histone methylation, JMJD1C, AMPK, CAMKK2

OPEN ACCESS

Edited by:
Xuejun Wang,
University of South Dakota, United States

Reviewed by:
Manish Gupta,
University of Central Florida, United States
Hanming Zhang,
Yale University, United States

***Correspondence:**
Ping Chen
pingchenjmsu@sohu.com;
mhnhua@163.com

[†]*These authors have contributed equally to this work*

Specialty section:
This article was submitted to Striated Muscle Physiology, a section of the journal Frontiers in Physiology

Received: *02 March 2020*
Accepted: *30 April 2020*
Published: *18 June 2020*

Citation:
Yu S, Li Y, Zhao H, Wang Q and Chen P (2020) The Histone Demethylase JMJD1C Regulates CAMKK2-AMPK Signaling to Participate in Cardiac Hypertrophy. Front. Physiol. 11:539. doi: 10.3389/fphys.2020.00539

INTRODUCTION

Currently, cardiovascular disease has become the leading cause of death all around the world. Cardiac hypertrophy is a pathological foundation of diverse cardiovascular diseases, including heart failure and hypertension (Veselka et al., 2017). The heart of mature mammals shows the low potential of cardiomyocyte proliferation. When the heart is injured and cardiomyocyte apoptosis occurs, the number of cardiomyocytes decreases (Nakamura and Sadoshima, 2018). The cardiomyocytes are unable to proliferate to support the increased demand of the heart. Instead, the cardiomyocytes undergo growth or hypertrophy to satisfy the demand. Pathological cardiac hypertrophy is a fundamental mechanism underlying diverse cardiovascular diseases, and sustained hypertrophy leads to arrhythmia and heart failure (Hou and Kang, 2012).

Metabolic dysfunction is a core mechanism underlying cardiac hypertrophy. Under physiological conditions, the cardiomyocytes use fatty acids to support the energy demand of the heart (Noordali et al., 2018). However, when pathological cardiac hypertrophy occurs, the cardiomyocytes undergo a metabolic switch (Riehle and Abel, 2016; Noordali et al., 2018). In hypertrophic cardiomyocytes, the cells prefer to utilize glucose as the energy source (Riehle and Abel, 2016). The metabolism of cardiomyocytes is regulated by several core regulators, including Sirtuins, AMPK, FoxO, and insulin signaling (Doenst et al., 2013; Riehle and Abel, 2016). For example, AMPK signaling is repressed during cardiac hypertrophy, and cardiac-specific

knockout of AMPK promoted stress-induced cardiac hypertrophy (Salt and Hardie, 2017). By contrast, metformin-mediated activation of AMPK prevented metabolic dysfunction and cardiac hypertrophy as well as heart failure (Daskalopoulos et al., 2016). Generally, AMPK activation is induced by the calcium/calmodulin–dependent protein kinase (CAMKK2) or the AMP-dependent liver kinase B1 (LKB1) (Steinberg and Carling, 2019). Inactivation of either LKB1 or CAMKK2 could facilitate the development of metabolic dysfunction and cardiac hypertrophy (Dolinsky et al., 2009; Watanabe et al., 2014). However, the mechanism by which the AMPK signaling is regulated during cardiac hypertrophy is not fully understood.

In general, H3K4 (lysine 4 at histone H3) methylation is correlated with gene activation, whereas the methylation of H3K9 (H3K9me) and H3K27 (H3K27me) is related to the repression of gene transcription (Greer and Shi, 2012). The demethylation of H3K9 is generally controlled by the Jumonji C domain-containing proteins (JMJD), which include the PHF8, JMJD1 family, and JMJD2 family (Jambhekar et al., 2019). The histone demethylase JMJD1C can remove the methylation motif from H3K9me1, H3K9me2, and H3K9me3 (Michalak et al., 2019). JMJD1C and WHISTLE mediate the balance of histone methylation by WHISTLE and demethylation by JMJD1C with WHISTLE acting as a transcriptional repressor during testis development in mice (Kim et al., 2010). During DNA break repair, the histone demethylase JMJD1C targets MDC1 to regulate the response of chromatin to DNA breaks mediated by RNF8 and BRCA1 (Watanabe et al., 2013). JMJD1C also regulates the expression of miR-302 to inhibit the differentiation of human embryonic stem cells to neurons (Wang et al., 2014). In addition, JMJD1C ensures cellular self-renewal and reprogramming by controlling the expression of microRNAs in mouse embryonic stem cells (Xiao et al., 2017). JMJD1C is also required for the maintenance of leukemia. JMJD1C depletion induces a growth defect that is primarily attributed to the increase in apoptosis of leukemia cells from either mouse or human (Sroczynska et al., 2014). JMJD1C is critically involved in the survival of acute myeloid leukemia cells by serving as the coactivator of pivotal transcription factors (Chen et al., 2015). Furthermore, JMJD1C essentially contributes to MLL-AF9/HOXA9-mediated self-renewal of leukemia stem cells (Zhu et al., 2016). Partially, JMJD1C-induced metabolic dysfunction contributes to HOXA9-dependent leukemogenesis (Lynch et al., 2019), which implies that JMJD1C may be a regulator of cellular metabolism. The role of JMJD1C in the cardiovascular system is not known.

Here, we investigate the roles of JMJD1C during cardiac hypertrophy in humans and mice. JMJD1C was significantly overexpressed in hypertrophic hearts of humans and mice, which was coupled with the downregulation of the methylation of H3K9. JMJD1C promoted cardiomyocyte hypertrophy induced by Ang II, which relied on the AMPK signaling in a CAMKK2-dependent manner.

MATERIALS AND METHODS

Heart Samples From Humans

Ten tissue samples of patients with hypertrophic cardiomyopathy and 10 from control donors were enrolled in this study. The hypertrophic heart tissues were obtained from patients who were diagnosed with hypertrophic cardiomyopathy (HCM). The control heart tissues were obtained from vehicle accident victims. The samples were obtained and stored in liquid nitrogen after informed consent was signed by the patients or the families of the donors. The study was approved by the institutional review boards for a clinical study at Jiamusi University.

TABLE 1 | Primers used for quantitative real-time PCR.

Gene name	Forward primer (5′-3′)	Reverse primer (5′-3′)
Human *JMJD1C*	CAGGTCTCGTGCCAATCAAAA	GCTGTTGCTGGTGTGTATTCT
Human *Tubulin*	TGGACTCTGTTCGCTCAGGT	TGCCTCCTTCCGTACCACAT
Human *ANP*	GATGGTGACTTCCTCGCCTC	AAGAAAGCACACCAACGCAG
Human *BNP*	TGGAAACGTCCGGGTTACAG	CTGATCCGGTCCATCTTCCT
Human *MYH7*	AGTGGCAATAAAAGGGGTAGC	CCAAGTTCACTCACATCCATCA
Mouse *JMJD1C*	CACCCGCACCATGATCGTTAT	CTTCGCCGTGATGTAATGCC
Mouse *Tubulin*	CACTTACCACGGAGATAGCGA	ACCTTCTGTGTAGTGCCCCTT
Mouse *ANP*	GCTTCCAGGCCATATTGGAG	GGGGGCATGACCTCATCTT
Mouse *BNP*	GAGGTCACTCCTATCCTCTGG	GCCATTTCCTCCGACTTTTCTC
Mouse *MYH7*	CATGGGATGGTAAGAAACGGG	TCCTCCAGTAAGTCGAAACGG
Rat *JMJD1C*	AGCTAGTGGGAAAGCGGTTC	AATTCCACGTAGACCGCCAG
Rat *Tubulin*	CAACTATGTGGGGGACTCGG	TGGCTCTGGGCACATACTTG
Rat *ANP*	CCTGGACTGGGGAAGTCAAC	ATCTATCGGAGGGGTCCCAG
Rat *BNP*	TGACGGGCTGAGGTTGTTTT	ACACTGTGGCAAGTTTGTGC
Rat *MYH7*	CCCAACCCTAAGGATGCCTG	TGTGTTTCTGCCTAAGGTGCT
Rat *CAMKK2*	AGAACTGCACACTGGTCGAG	CCGGCTACCTTCAAATGGGT

Animal Experiments

Cardiac hypertrophy in 8-week-old male C57BL/6N mice was induced by chronic infusion of angiotensin II (Sigma, 1.5 mg/kg/day) for a continuous 4 weeks as described previously (Tang et al., 2017). In brief, an Ang II-contained minipump (ALZET 2004) was placed into the mouse subcutaneously. Mice and SD rats were purchased from Charles River. The protocol for the animal study was approved by the ethics review boards at Jiamusi University.

Isolation and Treatment of Cardiomyocyte

Cardiomyocytes were isolated from the heart ventricles of 1- to 3-day neonatal SD rats as described previously (Tang et al., 2016). Neonatal rat cardiomyocytes (NRCMs) were then cultured in DMEM medium supplied with 10% fetal bovine serum (FBS, Gibco), 1% antibiotic-antimycotic (ThermoFisher) for 48 h. The NRCMs were cultured in DMEM with 1% fetal bovine serum for 24 h and then the hypertrophy of NRCMs was induced by angiotensin II (1 μM) treatment for 48 h as reffed from previous publications (Luo et al., 2017; Tang et al., 2017). Cardiomyocyte size was measured with Image J software. For each group at each experiment, >100 cardiomyocytes were quantified for average cardiomyocyte size, and the results of three independent experiments were shown.

Preparation of Adenovirus

For gene knockdown or overexpression, the adenovirus system was applied. Adenoviral vectors expressing rat *Jmjd1c* (Ad-*Jmjd1c*), control construct (Ad-Ctrl), sh*Jmjd1c* (Ad-sh*Jmjd1c*, shRNA sequence: GCGCTGACCTTCAAACCATTG),

or sh*Prkaa1* (Ad-sh*Prkaa1*, shRNA sequence: GCACGAGTTGACTGGACATAA) and negative control (Ad-shCtrl) were obtained using the AdEasy Vector kit (Jia et al., 2014).

Quantitative Real-Time PCR (qRT-PCR)

The cultured cells and heart tissues were washed with cold PBS and then subjected to RNA extraction with TRIZOL reagent (ThermoFisher). Next, the SuperScript III first-strand synthesis system kit (Invitrogen) was applied for cDNA synthesis with 1 ug of total RNA. Finally, SYBR green real-time PCR master mixes (Invitrogen) were applied to analyze the expression of target genes with the cDNA. The primers are shown in **Table 1**. The double delta CT method was applied for the quantification of mRNA expression.

Western Blot

The cultured cells and heart tissues were washed with cold PBS and then subjected to protein extraction with RIPA buffer (Millipore) supplemented with a phosphatase inhibitor cocktail (Roche) and a protease inhibitor cocktail (Roche). Protein concentration was measured with a BCA kit (ThermoFisher). SDS-PAGE was applied to separate the proteins in gel with 30 ug of total protein; then the proteins were transferred to PVDF membranes (Beyotime) followed by blockade with 5% fat-free milk in TBST for 1 h. Then, the membranes were washed with TBST three times and incubated with primary antibodies at 4°C overnight. The next day, the membranes were washed and incubated with HRP-conjected secondary antibodies. Finally, the expression of proteins was analyzed with the chemiluminescent Western blot detection kit (Millipore). The following primary antibodies were used: anti-Tubulin antibody (Cell Signaling Technology, #2144), anti-JMJD1C antibody (ThermoFisher, #PA5-20804), anti-Histone H3 antibody (Abcam, #ab1791), anti-H3K9me1 antibody (Active Motif, #39249), anti-H3K9me2 antibody (Active Motif, #39683), anti-H3K9me3 antibody (Active Motif, #61013), anti-AMPK antibody (Proteintech, #66536-1-Ig), anti-pAMPK antibody (Cell Signaling Technology, #2535), anti-ACC antibody (Proteintech, #67373-1-Ig), anti-pACC antibody (Cell Signaling Technology, #11818), anti-LKB1 antibody (Santa Cruz Biotechnology, #sc-32245), anti-pLKB1 antibody (Santa Cruz Biotechnology, #sc-271924), anti-CAMKK2 antibody (ThermoFisher, #PA5-69921), anti-PGC1a antibody (Cell Signaling Technology, #2178), anti-O-GlcNAcylation antibody (Abcam, #ab2739), anti-p-p70S6K1 antibody (Cell Signaling Technology, #9205), anti-p70S6K1 antibody (Cell Signaling Technology, #2708), anti-p-eEF2 antibody (Cell Signaling Technology, #2331), anti-eEF2 antibody (Cell Signaling Technology, #2332),

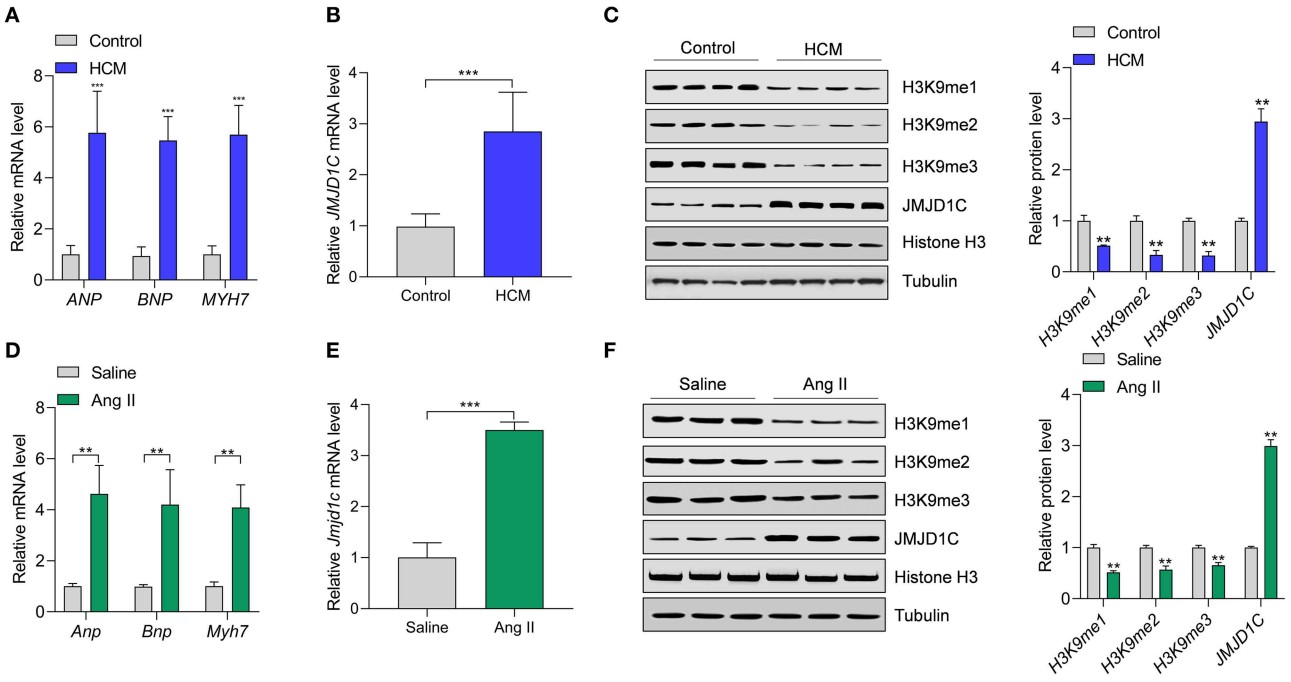

FIGURE 1 | JMJD1C expression is increased in hypertrophic hearts. **(A)** Expression of hypertrophy-related fetal genes (*ANP*, *BNP*, *MYH7*) in hypertrophic hearts (HCM) of human patients ($n = 10$) and in control donors ($n = 10$). ***$p < 0.001$ vs. control. **(B)** JMJD1C mRNA expression in hypertrophic hearts of human patients ($n = 10$) and in control donors ($n = 10$). ***$p < 0.001$ vs. control. **(C)** JMJD1C protein and levels of related histone methylation marks (H3K9me1, H3K9me2, H3K9me3) in hypertrophic hearts of human patients and in control donors. **$p < 0.01$ vs. control. $n = 4$ in each group. **(D)** Hypertrophy-related fetal gene levels in the hearts of mice undergoing saline or Angiotensin II (Ang II) infusion for 4 weeks. **$p < 0.01$ vs. saline. $n = 5$ in each group. **(E)** *Jmjd1c* mRNA expression in control and hypertrophic hearts of mice treated as in **(D)**. ***$p < 0.001$ vs. saline. $n = 5$ in each group. **(F)** Levels of JMJD1C protein and related histone methylation marks (H3K9me1, H3K9me2, H3K9me3) in the control and hypertrophic hearts of mice treated as in **(D)**. In **(C,F)**, a representative tubulin blot is shown as control, and all the loading controls were very similar. **$p < 0.01$ vs. saline. $n = 4$ in each group.

anti-H3K4me1 antibody (Abcam, #ab8895), anti-H3K4me3 antibody (Abcam, #ab8580), anti-H3K9ac antibody (Active Motif, #61663).

Chromatin Immunoprecipitation (ChIP) Assay

A ChIP assay was performed with the chromatin immunoprecipitation (ChIP) assay kit (17-295) with ChIP-grade primary antibodies. Immunoprecipitated chromatin fragments were quantified by SYBR-based qRT-PCR, normalized using the input.

Protein Synthesis Assay

The protein synthesis assay was performed by analyzing the incorporation of [^{14}C]-phenylalanine into proteins of cultured NRVMs as described previously (Sundaresan et al., 2009).

Statistical Analysis

The statistical analysis was performed with SPSS software, and all the values are expressed as mean ± *SD*. Student's *t*-test was applied for the analysis of the difference between the two groups. One-way ANOVA followed by Tukey's *post hoc* test was used when more than two groups exist.

RESULTS

JMJD1C Expression and Histone H3K9 Methylation Levels Were Changed in Hypertrophic Hearts in Human and Mice

To understand the functions of JMJD1C in cardiac hypertrophy, JMJD1C expression was examined in hypertrophic hearts of humans and mice. We collected heart tissues from 10 cases of hypertrophic cardiomyopathy (HCM) and from 10 control donors. We confirmed the upregulation of hypertrophy-related fetal genes (e.g., *ANP*, *BNP*, and *MYH7*) in HCM tissues compared with the control donors (**Figure 1A**). Compared with control tissues, the expression levels of JMJD1C mRNA and protein were significantly increased in HCM tissues (**Figures 1B,C**). Next, we observed that the levels of H3K9me1, H3Kme2, and H3K9me3 were downregulated in HCM tissues, which was associated with the upregulation of JMJD1C (**Figure 1C**). In addition, cardiac hypertrophy was induced in mice by chronic infusion of Ang II for 4 weeks. The overexpression of hypertrophy-related fetal genes was confirmed in hypertrophic hearts (**Figure 1D**). In hypertrophic hearts, the expression of JMJD1C was remarkably increased (**Figures 1E,F**), and the levels of H3K9me1, H3K9me2, and H3K9me3 were decreased (**Figure 1F**). In addition, we

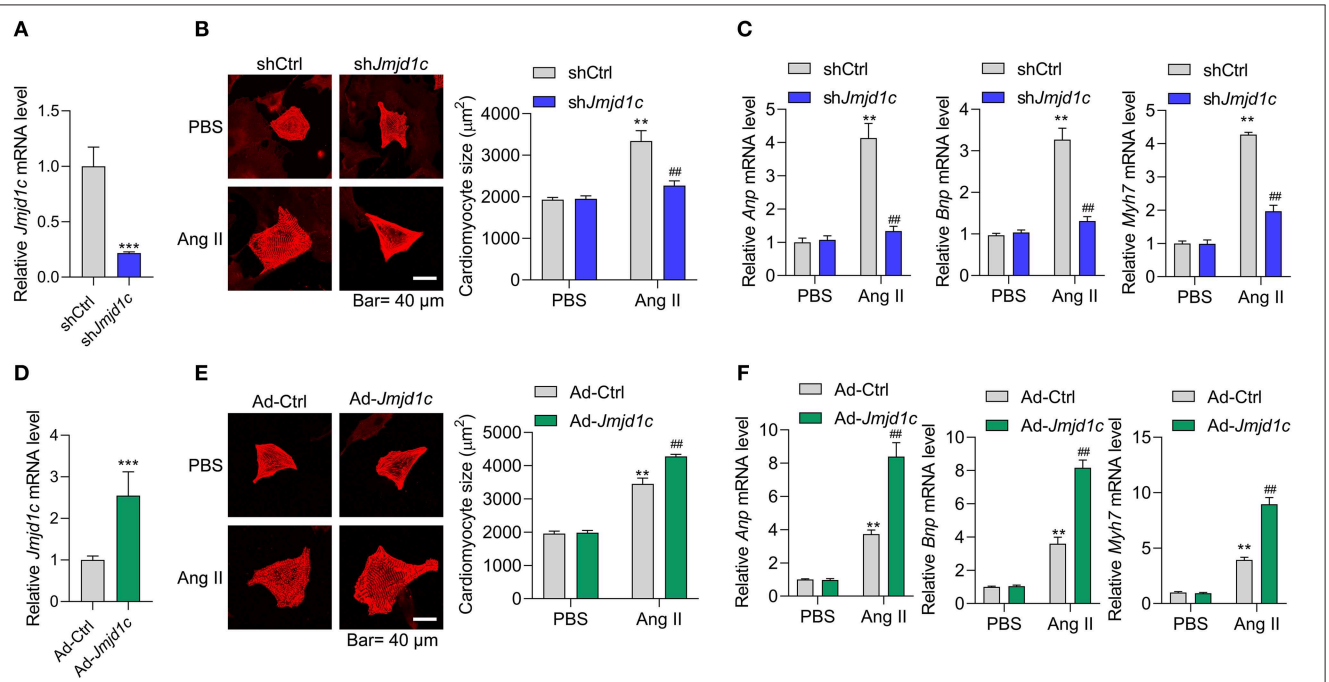

FIGURE 2 | JMJD1C promotes cardiomyocyte hypertrophy. **(A)** *Jmjd1c* knockdown in neonatal rat cardiomyocytes (NRCMs). The cells were infected with adenovirus expressing sh*Jmjd1c* or shCtrl for 48 h. ***$p < 0.001$ vs. shCtrl. **(B,C)** *Jmjd1c* knockdown reduces the Ang II-mediated increase in the size of cardiomyocytes **(B)** and the expression of fetal genes **(C)**. Cardiomyocytes infected with adenovirus expressing sh*Jmjd1c* or shCtrl were treated with Ang II (1 μM) for 48 h to induce hypertrophy. Then α-actinin staining was performed and cardiomyocyte size was analyzed. **$p < 0.01$ vs. shCtrl+PBS, ##$p < 0.01$ vs. shCtrl+Ang II. **(D)** *Exogenous Jmjd1c* overexpression in NRCMs. The cells were infected with adenovirus overexpressing *Jmjd1c* for 48 h. ***$p < 0.001$ vs. Ad-Ctrl. **(E,F)** Exogenous *Jmjd1c* overexpression enhances the increase in cardiomyocyte size **(E)** and hypertrophic fetal gene expression **(F)** induced by Ang II. NRCMs with/without *Jmjd1c* overexpression were treated with Ang II for 48 h to induce hypertrophy. Then cardiomyocyte size was analyzed. **$p < 0.01$ vs. Ad-Ctrl+PBS, ##$p < 0.01$ vs. Ad-Ctrl+Ang II. All results are from three independent experiments.

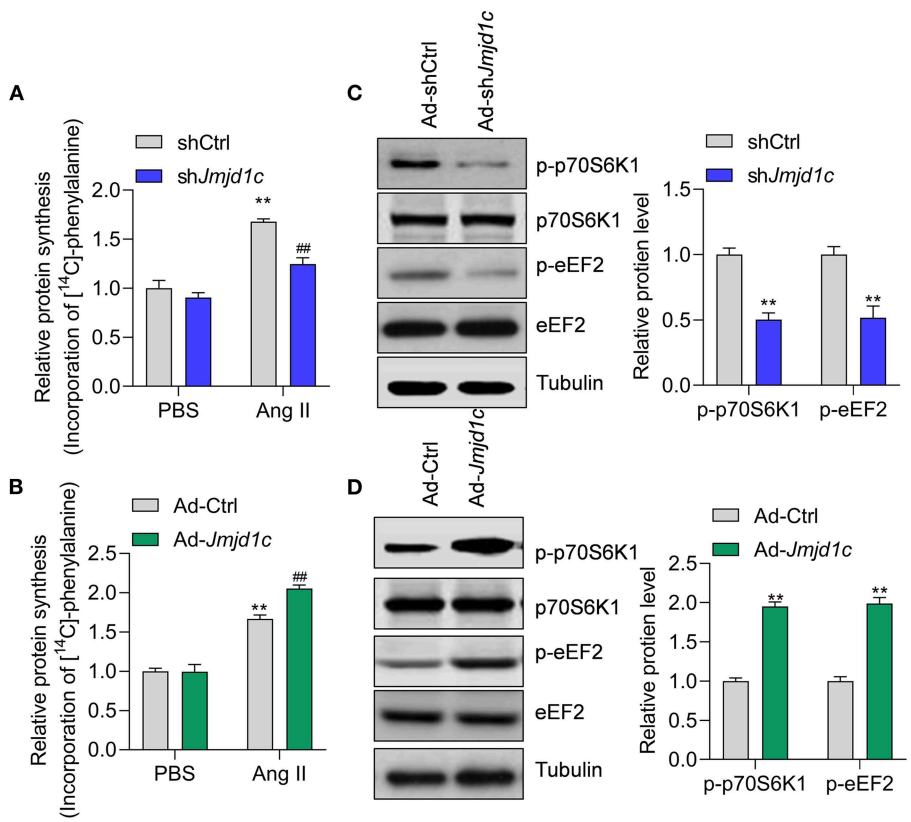

FIGURE 3 | JMJD1C regulates protein synthesis in cardiomyocytes. **(A)** JMJD1C knockdown reduces Ang II-induced protein synthesis. $^{**}p < 0.01$ vs. Ad-shCtrl+PBS; $^{\#\#}p < 0.01$ vs. Ad-shCtrl+Ang II. $n = 3$ in each group. **(B)** JMJD1C overexpression promotes Ang II-induced protein synthesis. $^{**}p < 0.01$ vs. Ad-Ctrl+PBS; $^{\#\#}p < 0.01$ vs. Ad-Ctrl+Ang II. $n = 3$ in each group. **(C)** JMJD1C knockdown reduces phosphorylation of p70S6K1 and eEF2 in Ang II-treated cardiomyocytes. $^{**}p < 0.01$ vs. Ad-shCtrl. $n = 3$ in each group. **(D)** JMJD1C overexpression increases phosphorylation of p70S6K1 and eEF2 in Ang II-treated cardiomyocytes. $^{**}p < 0.01$ vs. Ad-Ctrl. $n = 3$ in each group.

observed the increase in methylation of H3K4 (H3K4me1 and H3K4me3) as well as acetylation of H3K9 in hypertrophic mouse hearts (**Supplementary Figure 1**). Collectively, these findings demonstrated that JMJD1C was overexpressed in cardiac hypertrophy, which was associated with the downregulation of methylation of H3K9.

JMJD1C Controlled Cardiomyocyte Hypertrophy

Next, we investigated the roles of JMJD1C in the regulation of cardiac hypertrophy using neonatal rat cardiomyocyte (NRCMs). We knocked down the expression of *Jmjd1c* in NRCMs with adenovirus-mediated shRNA (**Figure 2A**) and induced cardiomyocyte hypertrophy with Ang II. Treatment with Ang II increased the size of cardiomyocytes and led to overexpression of the hypertrophy-related fetal genes *Anp*, *Bnp*, and *Myh7*. Knockdown of *Jmjd1c* repressed hypertrophy of cardiomyocytes induced by Ang II treatment (**Figures 2B,C**). We also overexpressed Jmjd1c in NRCMs with adenovirus-mediated overexpression (**Figure 2D**). *Jmjd1c* overexpression promoted the Ang II-mediated increase in the size of cardiomyocytes and the overexpression of hypertrophy-related fetal markers (**Figures 2E,F**). Protein synthesis is a hallmark of cardiac hypertrophy (Tang et al., 2020a); thus, we tested the effects of JMJD1C on protein synthesis by performing [^{14}C]-phenylalanine incorporation assay. We observed that JMJD1C knockdown reduced Ang II-induced protein synthesis (**Figure 3A**), whereas JMJD1C overexpression promoted Ang II-induced protein synthesis (**Figure 3B**). In addition, we tested the effects of JMJD1C on proteins that critically participate in protein synthesis. We analyzed the phosphorylations of p70S6K1 and eEF2. The results showed that JMJD1C knockdown inhibited the phosphorylations of p70S6K1 and Eef2, whereas the opposite effects were observed in JMJD1C-overexpressed cardiomyocytes (**Figures 3C,D**). Taken together, these findings revealed that JMJD1C promotes cardiomyocyte hypertrophy partially via regulating protein synthesis.

JMJD1C Regulates the Activation of AMPK

We next explored the mechanism of JMJD1C function in hypertrophy of cardiomyocytes. Metabolism is critically involved in the physiological and pathological progress of the heart (Tang et al., 2020b). The metabolic sensor AMPK serves as one of the key regulators of glucose and fatty acid metabolism

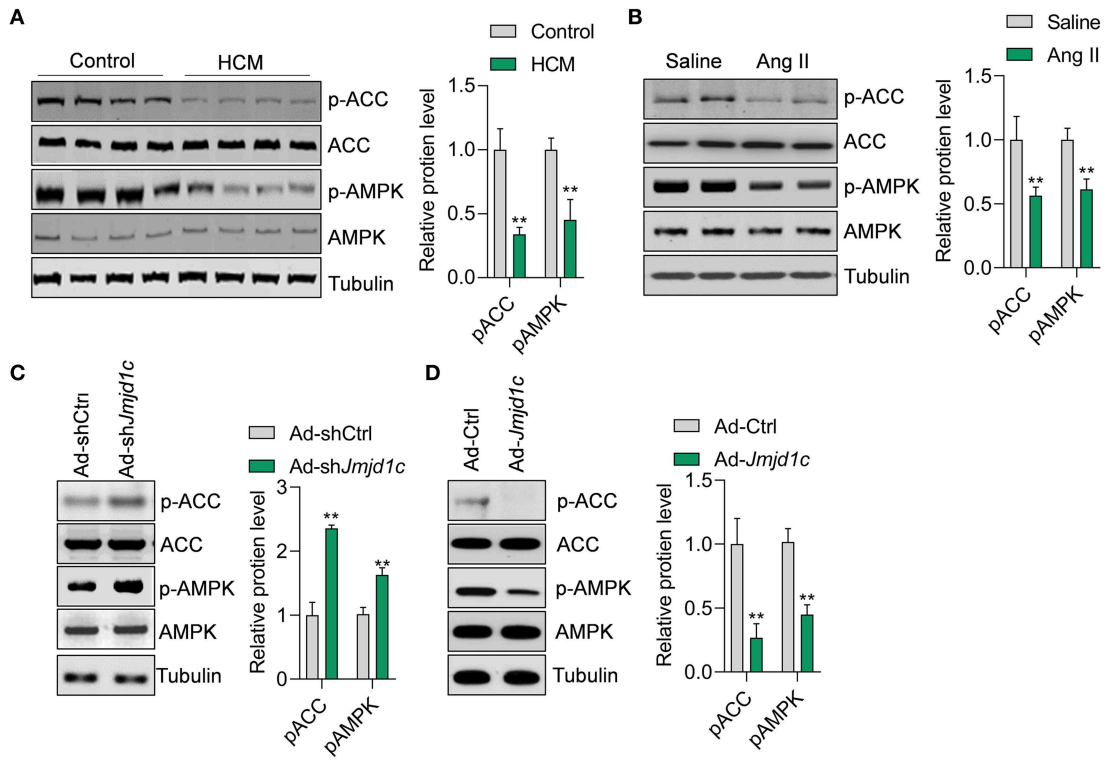

FIGURE 4 | JMJD1C represses AMPK activation in cardiomyocytes. **(A,B)** The AMPK signaling pathway is repressed in hypertrophic hearts in humans and mice. $^{**}p < 0.01$ vs. control or saline. $n = 4$ in each group. **(C)** *Jmjd1c* knockdown activates AMPK signaling. NRCMs were infected with adenovirus expressing sh*Jmjd1c* or shCtrl for 24 h, followed by Ang II treatment for an additional 24 h. $^{**}p < 0.01$ vs. Ad-shCtrl. $n = 3$ in each group. **(D)** JMJD1C overexpression represses AMPK activation. NRCMs were infected with adenovirus expressing *Jmjd1c* for 24 h, followed by Ang II treatment for an additional 24 h. $^{**}p < 0.01$ vs. Ad-Ctrl. $n = 3$ in each group.

of cardiomyocytes, and the deregulation of AMPK signaling participates in hypertrophic cardiomyopathy and other cardiac diseases. In this study, we observed that the phosphorylation levels of the kinase AMPK and its downstream factor ACC were significantly downregulated in hypertrophic hearts in humans and mice (**Figures 4A,B**). Additionally, we observed that *Jmjd1c* knockdown promoted the activation of AMPK signaling, whereas *Jmjd1c* overexpression repressed AMPK signaling activation in Ang II-treated NRCMs (**Figures 4C,D**). AMPK was reported to regulate cardiac hypertrophy by inducing PGC1a (Peroxisome proliferator–activated receptor gamma coactivator 1-alpha) expression and reducing protein O-GlcNAcylation (Watanabe et al., 2014; Gelinas et al., 2018). Indeed, we observed that *Jmjd1c* knockdown increased the PGC1a protein level and reduced total protein O-GlcNAcylation, which was blocked by AMPK knockdown (**Supplementary Figure 2**). Therefore, these findings support the notion that JMJD1C represses AMPK signaling during cardiac hypertrophy.

JMJD1C Regulates the Expression of CAMKK2 to Target AMPK

We attempted to investigate the molecular mechanism underlying JMJD1C-mediated AMPK inactivation. AMPK is generally activated by two kinases, LKB1 and CAMKK2. We observed that LKB1 expression and activation and its interaction partners STRAD and MO25 were not affected by *Jmjd1c* knockdown or overexpression (**Figures 5A,B**). Interestingly, we observed that *Jmjd1c* knockdown increased the protein levels of CAMKK2, whereas *Jmjc1c* overexpression downregulated the protein levels of CAMKK2 in NRCMs (**Figure 5C**). Importantly, we showed that JMJD1C controlled the expression of CAMKK2 at the transcriptional level because JMJD1C overexpression reduced and knockdown increased the levels of CAMKK2 mRNA (**Figure 5E**). Next, we analyzed the mechanism by which JMJD1C regulated CAMKK2 expression. JMJD2A and JMJD3 were reported to regulate cardiac hypertrophy by epigenetically targeting the *FHL1 (four-and-a-half LIM domains 1)* and the *β-MHC* promoter, respectively (Zhang et al., 2011; Guo et al., 2018). Our chromatin immunoprecipitation assay did not reveal the enrichment of JMJD2A and JMJD3 at the CAMKK2 promoter nor of JMJD1C at the FHL1 or MHC promoters. By contrast, JMJD1C selectively bound the CAMKK2 promoter (**Figure 5F**). In addition, overexpression of JMJD1C reduced H3K9me1/2/3 levels at the CAMKK2 promoter (**Figure 5G**, **Supplementary Figure 3**). Finally, we treated NRCMs with the CAMKK2 inhibitor STO-609 and observed that STO-609 treatment blocked the roles of JMJD1C on the activation of the AMPK pathway (**Figure 5H**). These

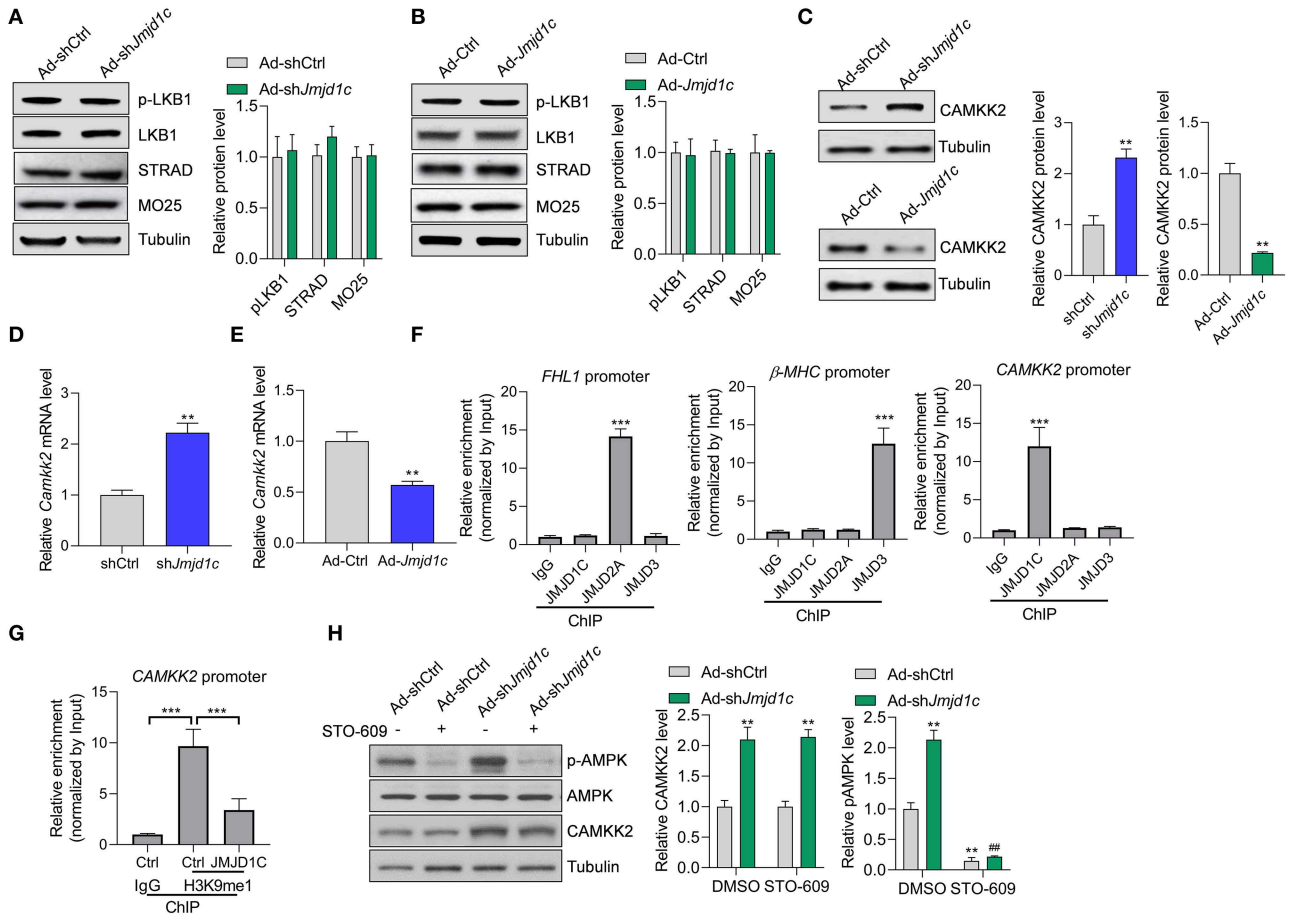

FIGURE 5 | JMJD1C regulates AMPK in a CAMKK2-dependent manner. **(A,B)** JMJD1C does not affect activation of LKB1 or levels of its activation partners STRAD and MO25 in NRCMs. The cells were infected with adenovirus expressing *Jmjd1c*, sh*Jmjd1c*, or the control constructs for 24 h, followed by Ang II treatment for an additional 24 h. $n = 3$ in each group. **(C)** Effects of JMJD1C on CAMKK2 expression. NRCMs were treated as in **(A)**. $^{**}p < 0.01$ vs. Ad-Ctrl or shCtrl. $n = 3$ in each group. **(D,E)** Effects of JMJD1C on CAMKK2 mRNA expression. NRCMs were treated as in **(A)**. $^{**}p < 0.01$ vs. Ad-Ctrl or shCtrl. **(F)** Chromatin immunoprecipitation (ChIP) assay showing the binding of JMJD1C, JMJD2A, and JMJD3 on the FHL1, β-MHC, and CAMKK2 promoters. IgG was used for negative control, and the enrichment was normalized to the input. $^{***}p < 0.001$ vs. IgG. **(G)** ChIP assay showing that JMJD1C overexpression reduced H3K9me1 enrichment at the CAMKK2 promoter in cardiomyocytes. $^{***}p < 0.001$ **(H)**. The inhibition of CAMKK2 blocks the effects of JMJD1C on AMPK activation in NRCMs. The cells were treated with adenovirus expressing sh*Jmjd1c* or shCtrl; then the cells were treated with Ang II and the CAMKK2 inhibitor STO-609 (20 μM) for an additional 24 h. All results are from three independent experiments. $^{**}p < 0.01$ vs. Ad-shCtrl+PBS; $^{\#\#}p < 0.01$ vs. Ad-shCtrl+STO-609. $n = 3$ in each group.

results demonstrated that JMJD1C controls AMPK signaling via a CAMKK2-dependent mechanism.

AMPK Is Essentially Involved in the Function of JMJD1C

Finally, we investigated whether JMJD1C-mediated AMPK inactivation was critically involved in the function of JMJD1C. We knocked down the expression of AMPK (*Prkaa1*) in NRCMs (**Figure 6A**) and induced cardiomyocyte hypertrophy with Ang II. We observed that AMPK knockdown promoted the hypertrophic response induced by Ang II and blocked the prevention of cardiomyocyte hypertrophy mediated by *Jmjd1c* knockdown (**Figures 6B,C**). In addition, we observed that metformin, an AMPK activator, rescued AMPK activation in NRCMs with Jmjd1c overexpression (**Figure 6D**). Significantly, metformin treatment repressed cardiomyocyte hypertrophy and blocked the function of JMJD1C overexpression (**Figures 6E,F**). Finally, we also tested whether JMJD1C promoted cardiomyocyte hypertrophy via CAMKK2. We inhibited CAMKK2 with STO-609 or knocked down Camkk2 expression and observed that either inhibition of CAMKK2 with STO-609 or Camkk2 knockdown blocked the inhibitory effects of Jmjd1c knockdown on cardiomyocyte hypertrophy (**Figures 6G,H**). Therefore, AMPK signaling critically participated in the roles of JMJD1C during the hypertrophic response of cardiomyocytes.

DISCUSSION

Here we demonstrate that JMJD1C serves as an epigenetic regulator that is involved in pathological cardiac hypertrophy.

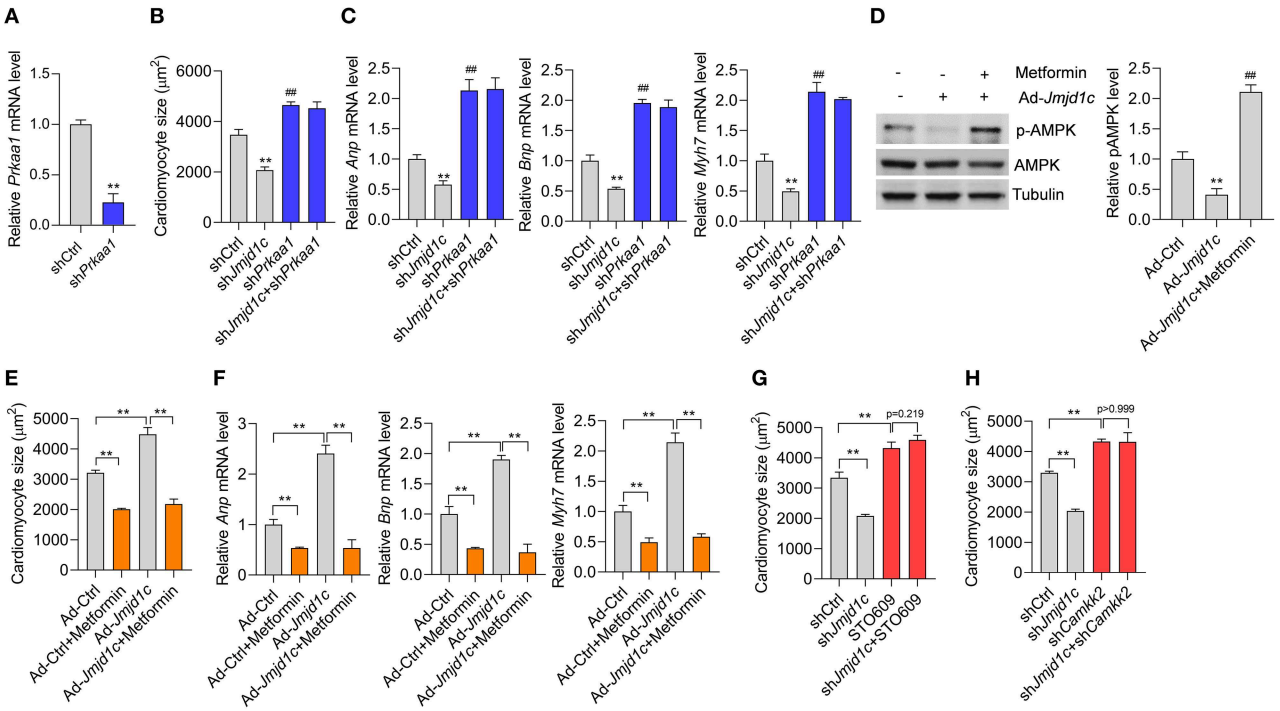

FIGURE 6 | AMPK participates in the role of JMJD1C during cardiomyocyte hypertrophy. **(A)** *Prkaa1* knockdown in cardiomyocytes. The cells were treated with adenovirus expressing sh*Prkaa1* or with a control virus for 48 h **(B,C)**. *Prkaa1* knockdown blocks the influence of *Jmjd1c* knockdown on Ang II-induced increase in cardiomyocytes. The cells with/without *Prkaa1* or *Jmjd1c* knockdown were subjected to hypertrophy induction with Ang II for 48 h. Then cardiomyocyte size **(B)** and gene expression **(C)** were analyzed. $^{**}p < 0.01$ vs. shCtrl. $^{\#\#}p < 0.01$ vs. shCtrl **(D)**. Metformin activates AMPK. The indicated cardiomyocytes were treated with metformin (1 mM) for 24 h. $^{**}p < 0.01$ vs. Ad-Ctrl; $^{\#\#}p < 0.01$ vs. Ad-Jmjd1c. $n = 3$ in each group **(E,F)**. Metformin-mediated activation of AMPK blocks the influence of JMJD1C overexpression on cardiomyocyte hypertrophy induced by Ang II stimuli. NRCMs were infected with/without adenovirus carrying *Jmjd1c* for 24 h; then the cells were treated with Ang II (1 μM) metformin (1 mM) for an additional 48 h. Cardiomyocyte size **(E)** and gene expression **(F)** were analyzed $^{**}p < 0.01$. **(G)** STO-609 blocks the influence of *Jmjd1c* knockdown on the Ang II-induced increase in cardiomyocytes. $^{**}p < 0.01$. **(H)** *Camkk2* knockdown blocks the influence of *Jmjd1c* knockdown on Ang II-induced increase in cardiomyocytes. $^{**}p < 0.01$. All results are from three independent experiments.

The expression of JMJD1C mRNA and protein was increased during cardiac hypertrophy in humans and mice, which was associated with decreased methylation of H3K9. Further experimental evidence demonstrated that JMJD1C promoted the hypertrophic response of cardiomyocytes induced by Ang II. JMJD1C repressed AMPK through transcriptionally repressing the expression of CAMKK2 but not LKB1 in cardiomyocytes, which was involved in the roles of JMJD1C during cardiomyocyte hypertrophy.

Epigenetic regulators have been reported to be essential for the initiation and progress of cardiac hypertrophy. For instance, the histone deacetylase (HDACs) and Sirtuins participated in cardiac hypertrophy by targeting histone and non-histone targets (Li et al., 2019). The histone demethylase family is also critically involved in pathological cardiac hypertrophy. For instance, JMJD2A demethylated H3K9me3 and activated transcription of pro-hypertrophic genes. In animals, JMJD2A promoted cardiac hypertrophy (Zhang et al., 2011). KDM3A promoted pressure overload–induced cardiac hypertrophy and fibrosis. And KDM3A activated *Timp1* expression with pro-fibrotic activity in cardiomyocytes. Interestingly, JIB-04, the pan-KDM inhibitor, repressed pathological cardiac hypertrophy and fibrosis (Zhang et al., 2018).

In this study, JMJD1C expression levels were increased in hypertrophic hearts in mice and humans. The upregulation of JMJD1C was associated with downregulated levels of H3K9me1, H3K9me2, and H3K9me3. We knocked down or overexpressed JMJD1C in cardiomyocytes and found that JMJD1C promoted the increase in the size of cardiomyocytes and expression of hypertrophy-related fetal genes, including *Anp*, *Bnp*, and *Myh7*, during Ang II-induced cardiomyocyte hypertrophy. Therefore, the JMJD family members are generally pro-hypertrophic epigenetic regulators (Zhang et al., 2011, 2018). However, our study was based on cardiomyocytes *in vitro*; further study is needed to explore the *in vivo* function of JMJD1C during cardiac hypertrophy with a cardiomyocyte-specific JMJD1C knockout mouse line.

The metabolic switch is a hallmark of hypertrophic cardiomyocytes. The metabolic sensor AMPK has critical functions in cardiac hypertrophy by diverse metabolism-dependent and independent mechanisms (Daskalopoulos et al., 2016). The previous study implicated the histone deacetylase SIRT2 in the activation of AMPK via LKB1 to repress cardiac

hypertrophy (Tang et al., 2017). However, the negative epigenetic regulator of AMPK during cardiac hypertrophy remains unknown. Here we observed that JMJD1C repressed the activation of AMPK during cardiac hypertrophy. However, JMJD1C-mediated repression of AMPK signaling did not depend on LKB1, but rather on reducing CAMKK2 expression. Finally, our findings showed that AMPK activation with metformin blocked the effects of JMJD1C hyperexpression, whereas AMPK knockdown blockaded the effects of JMJD1C downregulation during cardiac hypertrophy. These findings demonstrated that the AMPK signaling pathway is essentially involved in JMJD1C-mediated function in pathological cardiac hypertrophy.

JMJD2A and JMJD3 were reported to regulate cardiac hypertrophy by epigenetically targeting FHL1 and MHC promoter, respectively (Zhang et al., 2011; Guo et al., 2018). We observed that JMJD2A was enriched at the FHL1 and JMJD3 at the beta-MHC promoter, respectively, but neither bound to the CaMKK2 promoter. In contrast, JMJD1C bound to the CaMKK2 promoter and regulated methylation of H3K9me1, implicating JMJD1C in the regulation of the expression of CaMKK2 via demethylating H3K9. In this study, we observed that JMJD1C bound the CaMKK2 promoter and reduced the H3K9me level, which was associated with CaMKK2 gene silence. This finding was contradictory to previous notions that H3K9me was a mark of gene repression and that JMJD1C was a transcriptional activator (Chen et al., 2015). Thus, the effects of JMJD1C on CaMKK2 expression may also rely on other mechanisms. For instance, the JMJD1C-mediated changes in the local chromatin 3-D structure at the CaMKK2 promoter may also recruit some transcriptional repressor. The transcriptional repressive roles were also observed in JMJD2A (Mallette and Richard, 2012; Li et al., 2014). In leukemia cells, Runx1 (Runt-related transcription factor 1) directly interacts with and recruits JMJD1C to target genes (Chen et al., 2015). In addition, JMJD1C regulates Runx1 target genes by maintaining low H3K9me1/2 levels (Chen et al., 2015). Interestingly, the promoter and 5'UTR region of the human CaMKK2 gene has consensus DNA-binding sequences for Runx1 (Racioppi and Means, 2012). Given that Runx1 also plays a critical role in the cardiovascular system (McCarroll et al., 2018), it will be very interesting to investigate whether Runx1 is also enriched at the CAMKK2 promoter. To this end, JMJD1C regulated CaMKK2 expression via a complex mechanism. In addition, we did not observe the effects of JMJD1C on total H3K27me3 (data not shown). As such, JMJD2A, JMJD3, and JMJD1C may show different enrichment at the genome and regulate the expression of different genes.

Taken together, here we identified JMJD1C as a new epigenetic regulator of cardiac hypertrophy by targeting the metabolic AMPK pathway.

DATA AVAILABILITY STATEMENT

The datasets generated for this study are available on request to the corresponding author.

ETHICS STATEMENT

The studies involving human participants were reviewed and approved by institutional review boards for a clinical study at Jiamusi University. The patients/participants provided their written informed consent to participate in this study. The animal study was reviewed and approved by ethics review boards at Jiamusi University.

AUTHOR CONTRIBUTIONS

SY and PC designed the study. SY and YL performed most of the experiments. PC wrote the manuscript. QW performed cell culture and qPCR experiments. All authors contributed to the article and approved the submitted version.

FUNDING

This work was supported by Health Department of Heilongjiang Province (Grand No. 2018329).

SUPPLEMENTARY MATERIAL

The Supplementary Material for this article can be found online at: https://www.frontiersin.org/articles/10.3389/fphys.2020.00539/full#supplementary-material

REFERENCES

Chen, M., Zhu, N., Liu, X., Laurent, B., Tang, Z., Eng, R., et al. (2015). JMJD1C is required for the survival of acute myeloid leukemia by functioning as a coactivator for key transcription factors. *Genes Dev.* 29, 2123–2139. doi: 10.1101/gad.267278.115

Daskalopoulos, E. P., Dufeys, C., Bertrand, L., Beauloye, C., and Horman, S. (2016). AMPK in cardiac fibrosis and repair: actions beyond metabolic regulation. *J. Mol. Cell. Cardiol.* 91, 188–200. doi: 10.1016/j.yjmcc.2016.01.001

Doenst, T., Nguyen, T. D., and Abel, E. D. (2013). Cardiac metabolism in heart failure: implications beyond ATP production. *Circ. Res.* 113, 709–724. doi: 10.1161/CIRCRESAHA.113.300376

Dolinsky, V. W., Chan, A. Y., Robillard Frayne, I., Light, P. E., Des Rosiers, C., and Dyck, J. R. (2009). Resveratrol prevents the prohypertrophic effects of oxidative stress on LKB1. *Circulation* 119, 1643–1652. doi: 10.1161/CIRCULATIONAHA.108.787440

Gelinas, R., Mailleux, F., Dontaine, J., Bultot, L., Demeulder, B., Ginion, A., et al. (2018). AMPK activation counteracts cardiac hypertrophy by reducing O-GlcNAcylation. *Nat. Commun.* 9:374. doi: 10.1038/s41467-017-02795-4

Greer, E. L., and Shi, Y. (2012). Histone methylation: a dynamic mark in health, disease and inheritance. *Nat. Rev. Genet.* 13, 343–357. doi: 10.1038/nrg3173

Guo, Z., Lu, J., Li, J., Wang, P., Li, Z., Zhong, Y., et al. (2018). JMJD3 inhibition protects against isoproterenol-induced cardiac hypertrophy by suppressing beta-MHC expression. *Mol. Cell. Endocrinol.* 477, 1–14. doi: 10.1016/j.mce.2018.05.009

Hou, J., and Kang, Y. J. (2012). Regression of pathological cardiac hypertrophy: signaling pathways and therapeutic targets. *Pharmacol. Ther.* 135, 337–354. doi: 10.1016/j.pharmthera.2012.06.006

Jambhekar, A., Dhall, A., and Shi, Y. (2019). Roles and regulation of histone methylation in animal development. *Nat. Rev. Mol. Cell Biol.* 20, 625–641. doi: 10.1038/s41580-019-0151-1

Jia, Y.-Y., Lu, J., Huang, Y., Liu, G., Gao, P., Wan, Y.-Z., et al. (2014). The involvement of NFAT transcriptional activity suppression in SIRT1-mediated inhibition of COX-2 expression induced by PMA/Ionomycin. *PLoS ONE* 9:e97999. doi: 10.1371/journal.pone.0097999

Kim, S.-M., Kim, J.-Y., Choe, N.-W., Cho, I.-H., Kim, J.-R., Kim, D.-W., et al. (2010). Regulation of mouse steroidogenesis by WHISTLE and JMJD1C through histone methylation balance. *Nucleic Acids Res.* 38, 6389–6403. doi: 10.1093/nar/gkq491

Li, L.-L., Xue, A.-M., Li, B.-X., Shen, Y.-W., Li, Y.-H., Luo, C.-L., et al. (2014). JMJD2A contributes to breast cancer progression through transcriptional repression of the tumor suppressor ARHI. *Breast Cancer Res.* 16:R56. doi: 10.1186/bcr3667

Li, P., Ge, J., and Li, H. (2019). Lysine acetyltransferases and lysine deacetylases as targets for cardiovascular disease. *Nat. Rev. Cardiol.* 17, 96–115. doi: 10.1038/s41569-019-0235-9

Luo, Y.-X., Tang, X., An, X.-Z., Xie, X.-M., Chen, X.-F., Zhao, X., et al. (2017). Sirt4 accelerates Ang II-induced pathological cardiac hypertrophy by inhibiting manganese superoxide dismutase activity. *Eur. Heart J.* 38:1389–1398. doi: 10.1093/eurheartj/ehw138

Lynch, J. R., Salik, B., Connerty, P., Vick, B., Leung, H., Pijning, A., et al. (2019). JMJD1C-mediated metabolic dysregulation contributes to HOXA9-dependent leukemogenesis. *Leukemia* 33, 1400–1410. doi: 10.1038/s41375-018-0354-z

Mallette, F. A., and Richard, S. (2012). JMJD2A promotes cellular transformation by blocking cellular senescence through transcriptional repression of the tumor suppressor CHD5, Cell *reports* 2, 1233–1243. doi: 10.1016/j.celrep2012.09.033

McCarroll, C. S., He, W., Foote, K., Bradley, A., McGlynn, K., Vidler, F., et al. (2018). Runx1 deficiency protects against adverse cardiac remodeling after myocardial infarction. *Circulation* 137, 57–70. doi: 10.1161/CIRCULATIONAHA.117.028911

Michalak, E. M., Burr, M. L., Bannister, A. J., and Dawson, M. A. (2019). The roles of DNA, RNA and histone methylation in ageing and cancer. *Nat. Rev. Mol. Cell Biol.* 20, 573–589. doi: 10.1038/s41580-019-0143-1

Nakamura, M., and Sadoshima, J. (2018). Mechanisms of physiological and pathological cardiac hypertrophy. *Nat. Rev. Cardiol.* 15, 387–407. doi: 10.1038/s41569-018-0007-y

Noordali, H., Loudon, B. L., Frenneaux, M. P., and Madhani, M. (2018). Cardiac metabolism - A promising therapeutic target for heart failure. *Pharmacol. Ther.* 182, 95–114. doi: 10.1016/j.pharmthera.2017.08.001

Racioppi, L., and Means, A. R. (2012). Calcium/calmodulin-dependent protein kinase kinase 2: roles in signaling and pathophysiology. *J. Biol. Chem.* 287, 31658–31665. doi: 10.1074/jbc.R112.356485

Riehle, C., and Abel, E. D. (2016). Insulin signaling and heart failure. *Circ. Res.* 118, 1151–1169. doi: 10.1161/CIRCRESAHA.116.306206

Salt, I. P., and Hardie, D. G. (2017). AMP-activated protein kinase: an ubiquitous signaling pathway with key roles in the cardiovascular system. *Circ. Res.* 120, 1825–1841. doi: 10.1161/CIRCRESAHA.117.309633

Sroczynska, P., Cruickshank, V. A., Bukowski, J.-P., Miyagi, S., Bagger, F. O., Walfridsson, J., et al. (2014). shRNA screening identifies JMJD1C as being required for leukemia maintenance. *Blood* 123, 1870–1882. doi: 10.1182/blood-2013-08-522094

Steinberg, G. R., and Carling, D. (2019). AMP-activated protein kinase: the current landscape for drug development. *Nat. Rev. Drug Discov.* 18, 527–551. doi: 10.1038/s41573-019-0019-2

Sundaresan, N. R., Gupta, M., Kim, G., Rajamohan, S. B., Isbatan, A., and Gupta, M. P. (2009). Sirt3 blocks the cardiac hypertrophic response by augmenting Foxo3a-dependent antioxidant defense mechanisms in mice. *J. Clin. Invest.* 119, 2758–2771. doi: 10.1172/JCI39162

Tang, X., Chen, X., and Chen, X.-F. (2020b). Short-chain fatty acid, acylation and cardiovascular diseases. *Clin. Sci.* 134, 657–676. doi: 10.1042/CS20200128

Tang, X., Chen, X.-F., Wang, N.-Y., Wang, X.-M., Liang, S.-T., Zheng, W., et al. (2017). SIRT2 acts as a cardioprotective deacetylase in pathological cardiac hypertrophy. *Circulation* 136, 2051–2067. doi: 10.1161/CIRCULATIONAHA.117.028728

Tang, X., Li, P.-H., and Chen, H.-Z. (2020a). Cardiomyocyte senescence and cellular communications within myocardial microenvironment. *Front. Endocrinol. (Lausanne)*. 11:280. doi: 10.3389/fendo.2020.00280

Tang, X., Ma, H., Han, L., Zheng, W., Lu, Y.-B., Chen, X.-F., et al. (2016). SIRT1 deacetylates the cardiac transcription factor Nkx2.5 and inhibits its transcriptional activity. *Sci. Rep.* 6:36576. doi: 10.1038/srep36576

Veselka, J., Anavekar, N. S., and Charron, P. (2017). Hypertrophic obstructive cardiomyopathy. *Lancet* 389, 1253–1267. doi: 10.1016/S0140-6736(16)31321-6

Wang, J., Park, J. W., Drissi, H., Wang, X., and R.-,Xu, H. (2014). Epigenetic regulation of miR-302 by JMJD1C inhibits neural differentiation of human embryonic stem cells. *J. Biol. Chem.* 289, 2384–2395. doi: 10.1074/jbc.M113.535799

Watanabe, S., Horie, T., Nagao, K., Kuwabara, Y., Baba, O., Nishi, H., et al. (2014). Cardiac-specific inhibition of kinase activity in calcium/calmodulin-dependent protein kinase kinase-beta leads to accelerated left ventricular remodeling and heart failure after transverse aortic constriction in mice. *PLoS ONE* 9:e108201. doi: 10.1371/journal.pone.0108201

Watanabe, S., Watanabe, K., Akimov, V., Bartkova, J., Blagoev, B., Lukas, J., et al. (2013). JMJD1C demethylates MDC1 to regulate the RNF8 and BRCA1–mediated chromatin response to DNA breaks. *Nat. Struct. Mol. Biol.* 20, 1425–1433. doi: 10.1038/nsmb.2702

Xiao, F., Liao, B., Hu, J., Li, S., Zhao, H., Sun, M., et al. (2017). JMJD1C ensures mouse embryonic stem cell self-renewal and somatic cell reprogramming through controlling microRNA expression. *Stem Cell Reports* 9, 927–942. doi: 10.1016/j.stemcr.2017.07.013

Zhang, Q.-J., Chen, H.-Z., Wang, L., Liu, D.-P., Hill, J. A., and Liu, Z.-P. (2011). The histone trimethyllysine demethylase JMJD2A promotes cardiac hypertrophy in response to hypertrophic stimuli in mice. *J. Clin. Invest.* 121, 2447–2456. doi: 10.1172/JCI46277

Zhang, Q.-J., Tran, A. T., Wang, M., Ranek, M. J., Kokkonen-Simon, K. M., Gao, J., et al. (2018). Histone lysine dimethyl-demethylase KDM3A controls pathological cardiac hypertrophy and fibrosis. *Nat. Commun.* 9:5230. doi: 10.1038/s41467-018-07173-2

Zhu, N., Chen, M., Eng, R., DeJong, J., Sinha, A. U., Rahnamay, N. F., et al. (2016). MLL-AF9– and HOXA9-mediated acute myeloid leukemia stem cell self-renewal requires JMJD1C. *J. Clin. Investigation* 126, 997–1011. doi: 10.1172/JCI82978

Conflict of Interest: The authors declare that the research was conducted in the absence of any commercial or financial relationships that could be construed as a potential conflict of interest.

frontiers in Physiology

ORIGINAL RESEARCH
published: 19 June 2020
doi: 10.3389/fphys.2020.00690

Mitochondrial Dysfunction Is an Early Consequence of Partial or Complete Dystrophin Loss in *mdx* Mice

*Timothy M. Moore[1,2], Amanda J. Lin[2], Alexander R. Strumwasser[2], Kevin Cory[2], Kate Whitney[2], Theodore Ho[2], Timothy Ho[2], Joseph L. Lee[2], Daniel H. Rucker[2], Christina Q. Nguyen[2], Aidan Yackly[2], Sushil K. Mahata[3,4], Jonathan Wanagat[5], Linsey Stiles[2], Lorraine P. Turcotte[1], Rachelle H. Crosbie[6,7,8] and Zhenqi Zhou[2]**

[1] Department of Biological Sciences, Dana & David Dornsife College of Letters, Arts, and Sciences, University of Southern California, Los Angeles, CA, United States, [2] Division of Endocrinology, Diabetes, and Hypertension, David Geffen School of Medicine, University of California, Los Angeles, Los Angeles, CA, United States, [3] VA San Diego Healthcare System, San Diego, CA, United States, [4] Department of Medicine, University of California, San Diego, La Jolla, CA, United States, [5] Division of Geriatrics, Department of Medicine, University of California, Los Angeles, Los Angeles, CA, United States, [6] Department of Integrative Biology and Physiology, University of California, Los Angeles, Los Angeles, CA, United States, [7] Department of Neurology, David Geffen School of Medicine, University of California, Los Angeles, Los Angeles, CA, United States, [8] Molecular Biology Institute, University of California, Los Angeles, Los Angeles, CA, United States

OPEN ACCESS

Edited by:
Libero Vitiello,
University of Padova, Italy

Reviewed by:
Eric Hoffman,
Binghamton University, United States
Peter P. Nghiem,
Texas A&M University, United States

***Correspondence:**
Zhenqi Zhou
zhenqizhou@mednet.ucla.edu

Specialty section:
This article was submitted to Striated Muscle Physiology, a section of the journal Frontiers in Physiology

Received: *01 April 2020*
Accepted: *27 May 2020*
Published: *19 June 2020*

Citation:
Moore TM, Lin AJ, Strumwasser AR, Cory K, Whitney K, Ho T, Ho T, Lee JL, Rucker DH, Nguyen CQ, Yackly A, Mahata SK, Wanagat J, Stiles L, Turcotte LP, Crosbie RH and Zhou Z (2020) Mitochondrial Dysfunction Is an Early Consequence of Partial or Complete Dystrophin Loss in mdx Mice. Front. Physiol. 11:690. doi: 10.3389/fphys.2020.00690

Duchenne muscular dystrophy (DMD) is characterized by rapid wasting of skeletal muscle. Mitochondrial dysfunction is a well-known pathological feature of DMD. However, whether mitochondrial dysfunction occurs before muscle fiber damage in DMD pathology is not well known. Furthermore, the impact upon heterozygous female *mdx* carriers (*mdx*/+), who display dystrophin mosaicism, has received little attention. We hypothesized that dystrophin deletion leads to mitochondrial dysfunction, and that this may occur before myofiber necrosis. As a secondary complication to mitochondrial dysfunction, we also hypothesized metabolic abnormalities prior to the onset of muscle damage. In this study, we detected aberrant mitochondrial morphology, reduced cristae number, and large mitochondrial vacuoles from both male and female *mdx* mice prior to the onset of muscle damage. Furthermore, we systematically characterized mitochondria during disease progression starting before the onset of muscle damage, noting additional changes in mitochondrial DNA copy number and regulators of mitochondrial size. We further detected mild metabolic and mitochondrial impairments in female *mdx* carrier mice that were exacerbated with high-fat diet feeding. Lastly, inhibition of the strong autophagic program observed in adolescent *mdx* male mice via administration of the autophagy inhibitor leupeptin did not improve skeletal muscle pathology. These results are in line with previous data and suggest that before the onset of myofiber necrosis, mitochondrial and metabolic abnormalities are present within the *mdx* mouse.

Keywords: muscular dystrophy, Duchenne muscular dystrophy, skeletal muscle, dystrophin, metabolism, mitochondria, autophagy

INTRODUCTION

Muscular dystrophies are a family of genetic disorders manifesting primarily by the progressive wasting of skeletal muscle. Duchenne muscular dystrophy (DMD) is the most severe and frequent muscular dystrophy with most patients having little, if any, detectable dystrophin within muscle (Monaco et al., 1988; Emery, 1989; Govoni et al., 2013; De Palma et al., 2014). DMD patients present with clinical manifestations early in life and experience progressively deteriorating muscles until eventual passing before age 30 (Davies et al., 1988; Pichavant et al., 2011). Currently, DMD treatments delay disease progression or mitigate its symptoms, but frequently produce adverse side effects (Muntoni et al., 2002; Dubowitz, 2005; Bushby et al., 2010a,b). Additional developing therapies hold promise, yet many challenges lay ahead with such treatments likely several years from the accepted standard of care and FDA approval (Marshall and Crosbie-Watson, 2013; Young et al., 2016; Jones, 2019). Therefore, there is a need for alternative strategies, including combination-based therapies, to be developed from a more complete understanding of the cellular and physiological impact of dystrophin loss upon the myofiber. The most commonly used mouse model to study DMD is the *mdx* mouse (Bulfield et al., 1984). Although *mdx* muscles share some histological features with DMD, the phenotype is less severe, particularly concerning the associated cardiomyopathy and respiratory dysfunction that is life-threatening in DMD (McIntosh et al., 1998a,b).

Recent studies indicate mitochondria can adapt in size and morphology to changes in the cellular environment in virtually all cell types assessed (Liesa et al., 2009; Twig and Shirihai, 2011; Lackner, 2014). Dysfunction of this adaptive response can lead to dysmorphology, impaired oxidative phosphorylation, metabolic dysfunction, and an inability to adapt to stressors (Taanman, 1999; Bach et al., 2003; Miller et al., 2003; Twig et al., 2008; Nochez et al., 2009; Chen et al., 2010; Jornayvaz and Shulman, 2010; Pejznochova et al., 2010; Seo et al., 2010; Westermann, 2010; Scarpulla, 2011; Chan, 2012; Dickinson et al., 2013; Shen et al., 2014; Montgomery and Turner, 2015). Evidence links muscular dystrophies with mitochondrial and metabolic dysfunction (Lucas-Héron et al., 1990; Kemp et al., 1993; Even et al., 1994; Mokhtarian et al., 1996; Sperl et al., 1997; Kuznetsov et al., 1998; McIntosh et al., 1998a; Cole et al., 2002; Angelin et al., 2007; Khairallah et al., 2007; Gulston et al., 2008; De Palma et al., 2012; Pauly et al., 2012). However, the timing of these defects with respect to DMD and *mdx* pathology is unknown. We sought to determine the impact of the loss of dystrophin on mitochondrial and metabolic dysfunction in both male and female *mdx* mice. We hypothesized that, due to the highly structured intracellular environment of muscle, lacking a structural protein (dystrophin) would lead to an aberrant mitochondrial and metabolic phenotype prior to myofiber necrosis. Our results indicate a mitochondrial and metabolic phenotype in both male and female *mdx* mice prior to the onset of muscle fiber abnormalities, potentially suggesting an early mitochondrial role in the etiology of this disease.

Abbreviations: 18S, 18S ribosomal RNA; AMPKa, protein kinase AMPK-activated catalytic subunit alpha 1; AUC, area under the curve; CI, mitochondrial complex 1 NADH:ubiquinone oxidoreductase subunit B8; CII or II-30, mitochondrial complex 2 succinate dehydrogenase complex iron sulfur subunit B; CIII, mitochondrial complex 3 ubiquinol-cytochrome C reductase core protein II; CIV, mitochondrial encoded cytochrome C oxidase I; CV or V-a, mitochondrial complex 5 ATP synthase alpha; COX, cytochrome C oxidase; DJ1, Parkinson disease 7; DNM1L, see Drp1; Drp1, dynamin related protein 1; Esr1, estrogen receptor 1; Fis1, fission, mitochondrial 1; GAPDH, glyceraldehyde-3-phosphate dehydrogenase; Gastroc, gastrocnemius; Gfm2, G elongation factor mitochondrial 2; gWAT, gonadal white adipose tissue; HE, hematoxylin and eosin; HSPA1A, heat shock protein family A member 1A; HSPA1B, heat shock protein family A member 1B; IFNy, interferon gamma; IL10, interleukin 10; IL6, interleukin 6; JNK1, mitogen-activated protein kinase 8; LC3B, see MAPLC3B; LPT, leupeptin; MAPK1, mitogen-activated protein kinase 1; MAPLC3B, microtubule associated protein 1 light chain 3 beta; *mdx*, Duchenne muscular dystrophy mouse model; MFF, mitochondrial fission factor; MFN1, mitofusin 1; MFN2, mitofusin 2; Mgme1, mitochondrial genome maintenance exonuclease 1; mtCO3, cytochrome C oxidase subunit III; mtDNA, mitochondrial DNA; Oma1, overlapping with the M-AAA protease 1; Opa1, optic atrophy protein 1; Parl, presenilin associated rhomboid like; Park2, Parkin RBR E3 ubiquitin protein ligase; Peo1, twinkle mtDNA helicase; PGC1a, PPARG coactivator 1 alpha; Pink1, PTEN induced putative kinase 1; PolGII, DNA polymerase gamma 2, accessory subunit; Polrmt, RNA polymerase mitochondrial; Quad, quadriceps; Ser, serine; SDH, succinate dehydrogenase; SQSTM1, sequestosome 1; TFAM, transcription factor A, mitochondrial; Thr, threonine; Tom20, translocase of outer mitochondrial member; TNFa, tumor necrosis factor alpha; wks, weeks.

MATERIALS AND METHODS

Ethical Approval

The University of California, Los Angeles Institutional Animal Care and Use Committee approved this study. All animal care, maintenance, surgeries, and euthanasia were conducted in accordance with this Institutional Animal Care and Use Committee and the National Institutes of Health.

Animals

Jackson Laboratories (Bar Harbor, ME, United States) 001801 (genotype: C57BL/10ScSn-*Dmd*^{mdx}/*J*) homozygous female laboratory mice were purchased and crossed with the recommended Jackson 000476 (genotype: C57BL/10ScSnJ) mice (Control) to generate hemizygous male (*mdx*) and female (*mdx* carrier) mice used for all studies. Mice were group-housed two to four per cage, fed chow diet *ad libitum* (8604, Teklad, calories: 25% protein, 14% fat, 54% carbohydrate) or high-fat diet (D12451, Research Diets, Inc., calories: 45% fat, 20% protein, 35% carbohydrates) *ad libitum* for 8 weeks where indicated, and on a 12-h light/dark cycle. Mice were fasted for 6 h prior to euthanasia. LPT (leupeptin) injections were given at 12 mg/kg every other day for 5 weeks, where indicated in 9-week-old mice.

Glucose and Insulin Tolerance Tests

Glucose and insulin tolerance tests (GTT or ITT) were performed following a 6 h fast as previously described (Ribas et al., 2016). Briefly, the GTT consisted of an intraperitoneal dextrose (1 g/kg) injection and glucose was assessed at 15-min intervals over the 120-min testing period. The ITT consisted of an intraperitoneal insulin injection (0.7 U/kg). Blood samples were drawn, and glucose was measured at 0, 15, 30, 45, 60, 90, and 120 min post-injection.

Plasma Analysis

Immediately following euthanasia, whole blood was removed via 27-gauge needle from the abdominal aorta and centrifuged at 2,000 × *g* for 2 min in EDTA-coated tubes. Plasma was analyzed for insulin and leptin using the Meso Scale Discovery (Rockville, MD, United States) platform following the manufacturer's recommended protocol. Assessment of plasma triglyceride was determined using the L-Type TG M Assay and Cholesterol E (Wako Diagnostics, Mountain View, CA, United States). Assessment of plasma glucose was determined using HemoCue Glucose 201 Systems glucometer. Assessment of plasma creatine kinase-MB (CKMB) was determined using mouse CKMB ELISA kit (LS-F5745-1, LSBio, WA, United States).

Ex vivo Skeletal Muscle Glucose Uptake

Whole-muscle *ex vivo* glucose uptake was assessed using 2-deoxyglucose uptake assay (Ribas et al., 2016). Briefly, soleus muscles were carefully excised from anesthetized animals and immediately incubated for 30 min in complete Krebs-Henseleit buffer with or without insulin (60 μU/ml) at 35°C. Muscles were then transferred to the same buffer containing [^{3}H] 2-deoxyglucose (3 μCi/ml) and [^{14}C] mannitol (0.053 μCi/ml), and incubated for 20 min before being blotted of excess liquid and frozen in liquid nitrogen. Muscles were homogenized in lysis buffer and counted for radioactivity. Glucose uptake was standardized to the non-specific uptake of mannitol and estimated as micromole of glucose uptake per gram of tissue.

Grip Strength, Maximal Running Speed, and Dynamic Hanging

The following experiments were performed as previously described without variation (Moore et al., 2019). Mouse genotypes were blinded to the experimenter for all tests. Grip strength was assessed using the GT3 Grip Strength Meter (BIOSEB, Pinellas Park, FL, United States). Each mouse performed five trials and the highest three trials were averaged. Maximal running speed was assessed as described previously (Lerman et al., 2002). Mice were acclimated to the running treadmill on two separate occasions prior to the maximal running speed test. On testing day, mice performed a 5-min warm-up at 5–10 m/min. Treadmill speed was increased by 3 m/min until mice were unable to maintain the speed for 10 consecutive seconds with gentle encouragement. Mice were given three attempts at each speed and approximately 60 s of rest after each increase in treadmill speed. Dynamic hanging as assessed by latency to fall test, an index of grip strength and muscle endurance, was performed as previously described (Mandillo et al., 2014). Mice were acclimated to the wire grid on two separate occasions prior to testing. Mice performed three trials and the data were averaged and reported as a Mean ± SEM. Mice were given 5 min of rest between each trial.

Nucleic Acid Extraction, cDNA Synthesis, and Quantitative RT-PCR

DNA and RNA were extracted from a portion of pulverized frozen muscle using DNeasy/RNeasy Isolation kits (Qiagen, Germantown, MD, United States) as described by the manufacturer. Isolated DNA and RNA were tested for concentration and purity using a NanoDrop Spectrophotometer (Thermo Scientific, Waltham, MA, United States). Isolated RNA was converted into cDNA, assessed for purity, and qPCR of the resulting cDNA levels was performed as previously described (Drew et al., 2014). All genes were normalized to the housekeeping genes Ppia or 18S. Mitochondrial DNA content was assessed as a ratio of mitochondrial DNA (mtCO2) to nuclear DNA (18S). Primers used for qPCR can be found in **Supplementary Table S1**.

Immunoblot Analyses

Pulverized frozen muscle was used for immunoblotting. Proteins from each individual whole cell homogenate were normalized (expressed relative to the pixel densitometry) to glyceraldehyde 3-phosphate dehydrogenase (GAPDH, AM4300, Ambion, Foster City, CA, United States). Phosphorylation-specific proteins were normalized (expressed relative to pixel densitometry) to the same unphosphorylated protein (i.e., phosphorylated Drp1 at Ser 616 was expressed relative to the pixel densitometry of Drp1 for each individual sample). See **Supplementary Table S2** for a list of the primary antibodies used.

Mitochondrial Isolation

Mitochondria were isolated from fresh gastrocnemius muscles using Mitochondria Isolation Kit (Thermo Scientific, Waltham, MA, United States) via Dounce homogenization for Hard Tissue protocol (Zhang et al., 2010; Benador et al., 2018). Briefly, 70 mg of fresh gastrocnemius muscles were rinsed by cold PBS twice. Then muscles were quickly minced, dounced, and centrifuged at 700 × *g* for 10 min at 4°C to discard tissue debris and nucleus. The supernatant was further centrifuged at 12,000 × *g* for 15 min at 4°C to acquire mitochondrial pellets. Subsequent immunoblotting underwent the same procedure described in the "Immunoblot Analyses" section.

Tissue Histology

Tibialis anterior or gastrocnemius muscles were sectioned and stained for HE, SDH, and COX as previously described (Wanagat et al., 2001). Semi-quantitative analyses were performed on a blind basis using a scale (high, medium, and low density of staining) for each slide by three individuals.

Transmission Electron Microscopy (TEM)

Soleus muscle was quickly and carefully excised from the lower hindlimb. Specifically, a small incision was made perpendicular to the distal end of the Achilles tendon. While cautiously preserving the underlying tissue, the skin was cut to expose the lower hindlimb muscle. The Achilles tendon was then cut and the entire muscle group consisting of the gastrocnemius, plantaris, and soleus was meticulously rotated uncovering the soleus muscle underneath. Great care was taken to ensure the muscle was not stretched or distorted. Using a surgical scalpel, small cuts were made around the visible soleus muscle removing it from the surrounding tissue. The soleus was examined for any remaining

tissue which was removed if present and then immersed in freshly prepared fixative containing 2.5% glutaraldehyde and 2% paraformaldehyde in 0.15 M cacodylate buffer and stored at 4°C until use as described previously (Doughty et al., 1995; Park et al., 2016). This fixative has been shown to preserve muscle architecture. After fixation, muscles were processed for TEM analysis as described previously (Zhou et al., 2018). Ultrathin (∼60 nm) sections were viewed using a JEOL 1200EX II (JEOL, Peabody, MA, United States) electron microscope and photographed using a Gatan digital camera (Gatan, Pleasanton, CA, United States) as previously described. Mitochondrial area, perimeter, Feret's diameter, and cristae numbers were analyzed and quantified in all images by three separate and blinded individuals using ImageJ (NIH).

Complex IV Enzyme Activity Assay

Mitochondrial complex IV enzymatic activity was measured as instructed (Complex IV Rodent Enzyme Activity Microplate Assay Kit, Abcam, ab109911). Briefly, same amounts of homogenized muscle sample were loaded on the plate and incubated at room temperature for 3 h. After rinsing wells twice with solution 1, the plate was read at OD550 with assay solution. Complex IV activity was determined by calculating the slope between two points within the linear region.

Mitochondrial Respirometry

Frozen skeletal muscle tissues were thawed on ice and homogenized in MAS (70 mM sucrose, 220 mM mannitol, 5 mM KH2PO4, 5 mM MgCl2, 1 mM EGTA, 2 mM HEPES, pH 7.4). The samples were mechanically homogenized with 60 strokes in a teflon-glass dounce homogenizer. All homogenates were centrifuged at 1000 × *g* for 10 min at 4°C then the supernatant was collected. Protein concentration was determined by BCA (Thermo Scientific, Waltham, MA, United States). Homogenates were loaded into Seahorse XF96 microplate in 20 μL of MAS at 6 μg/well. The loaded plate was centrifuged at 2,400 × *g* for 10 min at 4°C (no brake) and an additional 130 μL of MAS supplemented with 100 μg/mL cytochrome c was added to each well. Substrate injection were as follows: Port A: NADH (1 mM) or succinate + rotenone (5 mM + 2 μM); Port B: rotenone + antimycin A (2 μM + 2 μM); Port C: *N*,*N*,*N*′,*N*′-tetramethyl-p-phenylenediamine (TMPD) + ascorbic acid (0.5 mM + 1 mM); and Port D: azide (50 mM). These conditions allow for the determination of the maximal respiratory capacity of mitochondria through Complex I, Complex II, and Complex IV.

Statistical Analysis

Values are presented as mean ± SEM and expressed relative to the average value obtained for each experimental control group unless otherwise stated. Statistical analyses were performed using Student's *t*-test when comparing two groups of samples or one-way analysis of variance (ANOVA) with Tukey's *post hoc* comparison for identification of significance within and between groups using GraphPad Prism 5 (GraphPad Software, San Diego, CA, United States). Significance was set *a priori* at $P < 0.05$.

RESULTS

Regulators of the Mitochondrial Life Cycle Are Altered in Skeletal Muscle From 40-Week-Old, Male *mdx* Mice

To ascertain the impact of lacking dystrophin upon mitochondria, we quantified protein and RNA expression for several regulators of the mitochondrial network in gastrocnemius muscles from 40-week-old male mice (*mdx*-40wks), which represents the late, hypertrophic stage of disease. Gene expression for the inflammatory cytokines IFNγ, IL10, IL6, and TNFα were elevated by approximately 4.5 to 7.5-fold in *mdx* males compared with age-matched controls (**Figure 1A**). We also observed substantial reductions of genes related to mitochondrial fission (*Dnm1l*, *Mff*, and *Fis1*) and mitophagy (*Maplc3b* and *Pink1*) in *mdx* mice vs. age-matched controls (**Figure 1A**). Reduced phosphorylation of Drp1 at Serine 616, a pro mitochondrial fission signal, and elevated protein levels of mitochondrial fusion regulators (Mfn1 and Mfn2; **Figure 1B** and **Supplementary Figure S1**) were evident. Moreover, the protein levels of mitophagy related factors (Parkin and Lc3bI) were also elevated in *mdx* males compared with age-matched controls (**Figure 1B** and **Supplementary Figure S1**). In general, we found regulators of mitochondrial life cycle are altered in the skeletal muscle from 40-week-old, male *mdx* mice.

Dysfunction of Mitochondrial Enzymatic Activity and Morphology Are Evident at Early Stages of Dystrophin-Deficient Disease

Because of the large changes in the expression of regulators of the mitochondrial network observed in late stage of disease (*mdx*-40wks), we hypothesized that these responses resulted from widespread muscle damage and chronic inflammation that eventually causes muscle fiber apoptosis and necrosis. To test this hypothesis, we investigated 11-week-old, *mdx* male mice (*mdx*-11wks), which represents the active regeneration phase of the disease (prior to the onset of severe muscle damage, apoptosis, and necrosis) to determine if mitochondrial network alterations occur because of or as a precursor to severe muscle damage as observed previously (Ieronimakis et al., 2016). We found that quadriceps muscle from *mdx*-11wks male mice display reduced mitochondrial DNA copy number as well as reduced mitochondrial DNA derived transcript (mtCO3) relative to age-matched controls (**Figures 2A,B**). We observed no changes in the gene expression of regulators of mitochondrial DNA replication (*PolGII*, *Peo1*, and *Mgme1*), mitochondrial RNA polymerase (*Polrmt*), and protein translation (*Gfm2*; **Figure 2B**). At the protein level, several regulators of the mitochondrial network were altered including Lc3bI, Parkin, Pink1, Parl, Mfn2, mature and active Oma1, Fis1, Pgc1α, and Ampkα compared with age-matched controls (**Figure 2C** and **Supplementary Figure S2**). Active form of Ampkα (Phosphorylated threonine (Thr) 172) and Drp1 [serine (Ser) 616] were also significantly altered (**Figure 2C** and **Supplementary Figure S2**). Since changes in protein levels

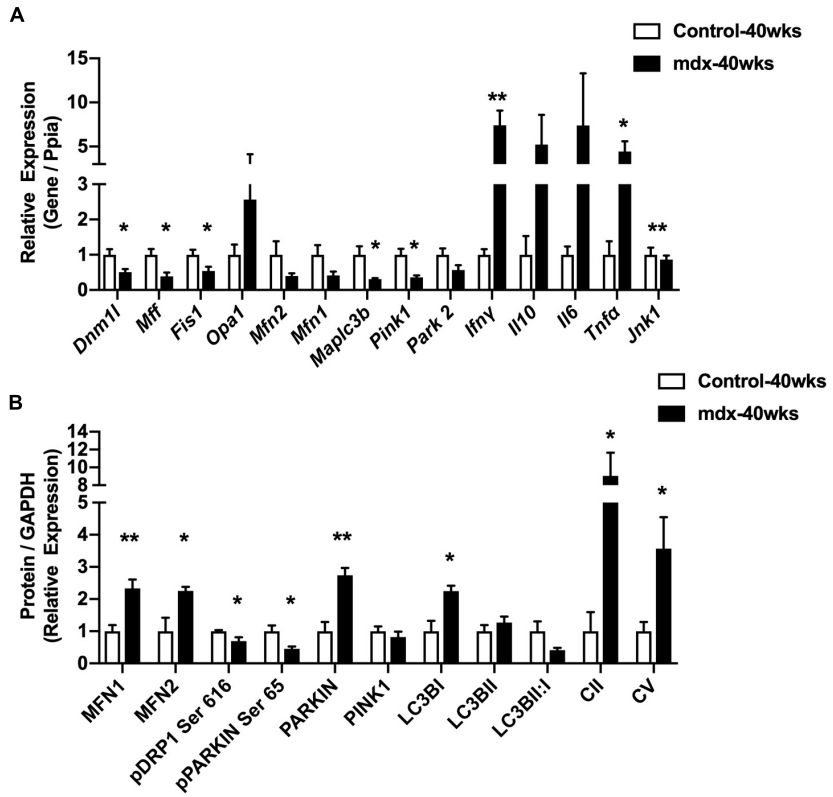

FIGURE 1 | 40-week-old *mdx* male muscles display altered regulators of the mitochondrial life cycle. **(A)** Gene expression from gastrocnemius muscle (N = 4–5). **(B)** Protein expression from gastrocnemius muscle (N = 4–5). Data presented as Mean ± SEM. *, **$P < 0.05$, 0.01, respectively.

observed in whole-cell lysates might not reflect proteins present within or on mitochondria, we immunoblotted for a select number of proteins in isolated mitochondria from the quadriceps muscle. Both Parkin and Drp1 were significantly increased, but no change of Mfn2 in the mitochondrial fraction from *mdx*-11wks vs. age-matched controls (**Figure 2D** and **Supplementary Figure S2**) was observed. Electron micrograph images from the soleus muscle depicted a highly altered mitochondria network that included aberrant structure and cristae numbers per area of mitochondria (**Figure 2E**). Muscle damage was also overtly visible via altered fiber and z-line orientation. As expected, centralized nuclei were abundant in myofibers from mdx samples, which is consistent with ongoing muscle degeneration and regeneration, a hallmark of DMD (**Figure 2F**). Such changes occur concomitantly with reduced percentage of muscle fibers with high density of SDH and COX staining indicative of reduced mitochondrial function (**Figure 2F**).

Mitochondria DNA Copy Number Is Reduced at the Onset of Tissue Abnormalities in 4-Week-Old, *mdx* Male Muscles

Having observed aberrant mitochondria in *mdx* muscle as early as 11 weeks of age, we extended our investigation to 4-week-old, *mdx* male mice (*mdx*-4wks), which represents the early state of the disease, just as the first signs of muscle regeneration are evident. Similar to our previous results, we observed a reduction in mitochondrial DNA copy number in quadriceps muscles of *mdx*-4wks vs. age-matched control mice (**Supplementary Figure S3A**). Histological staining of gastrocnemius muscle from these same animals revealed muscle fibers with centralized nuclei, localized reductions in fiber cross-sectional area, and regions of nuclei accumulation potentially indicative of inflammatory cell infiltration (**Supplementary Figure S3B**). Therefore, even at 4 weeks of age, *mdx* muscle exhibits reduced mitochondrial DNA copy number simultaneously with the onset of muscle fiber damage.

Mitochondria From Pre-necrotic 2-Week-Old, *mdx* Male Muscle Displays Altered Cristae Structure

To further test our hypothesis regarding the connection between mitochondria and muscle damage, we generated 2-week-old, *mdx* male mice (*mdx*-2wks), which represent the pre-necrotic stage of disease and is before the onset of overt muscle pathology. We measured mitochondrial DNA copy number in quadriceps muscles and found no difference between *mdx*-2wks and age-matched controls (**Figure 3A**). Quadriceps muscles were immunoblotted for several proteins related to mitochondria, mitophagy, fission, fusion, and biogenesis which showed no

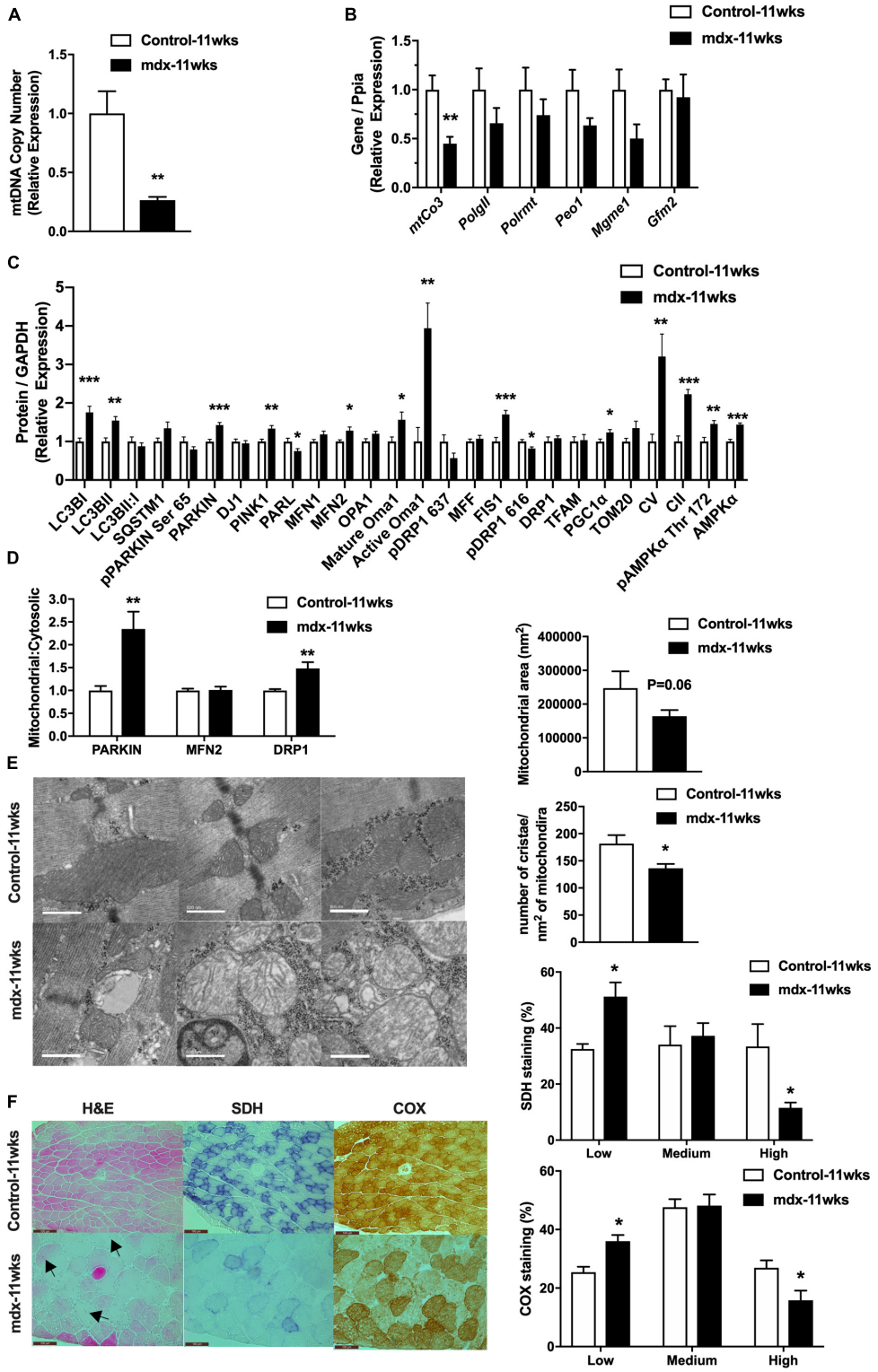

FIGURE 2 | 11-week-old, *mdx* male muscles display altered regulators of the mitochondrial life cycle, enzymatic activity, and mitochondrial shape. **(A)** Mitochondrial DNA copy number in quadriceps muscle (N = 6–8). **(B)** mRNA expression in quadriceps muscle (N = 5–8). **(C)** Protein expression in quadriceps muscle (N = 6–8). **(D)** Protein expression in mitochondria isolated from quadriceps muscle (N = 6–8). **(E)** Electron micrograph images of the soleus muscle with quantified mitochondrial area and cristae numbers per area of mitochondria shown right. **(F)** HE, SDH, and COX staining in tibialis anterior muscle with the percentage of muscle fiber density shown right (N = 13). Black arrow indicates fibers with centralized nuclei. Only some fibers are indicated. Scale bar = 0.1 mm. Data presented as Mean ± SEM. *, **, ***P < 0.05, 0.01, 0.001, respectively.

differences in levels of these marker proteins between the two groups (**Figure 3B**). Muscle fiber morphology was examined by histological staining of the gastrocnemius muscle, revealing no signs of muscle damage (**Figure 3C**). Despite observing no differences in mitochondrial DNA copy number, protein levels, and muscle fiber morphology, we found reduced cristae numbers per area of mitochondria and the presence of mitochondrial vacuoles in muscle from 2-week-old, *mdx* male mice in electron micrographs (**Figure 3D** and **Supplementary Figure S4**). Additionally, although mitochondrial oxygen consumption rate of complex I/II/IV were not altered, mitochondrial complex IV enzymatic activity was significantly decreased (**Figures 3E,F**). These results suggest the alteration of mitochondrial architecture and enzyme activity before the onset of muscle damage.

Autophagy Inhibition Did Not Improve Muscle or Mitochondrial Phenotype in *mdx* Male Mice

Our previous results in *mdx* mice at 40 and 11 weeks of age revealed elevated levels of genes and proteins related to mitophagy and autophagy. Furthermore, electron micrograph images of *mdx*-2wks displayed mitochondrial vacuoles. These observations and other results from the research community have supported the concept of autophagy inhibition as a potential therapy for muscle wasting conditions (Selsby et al., 2010; Childers et al., 2011; De Palma et al., 2012). Therefore, we treated *mdx* male mice via intraperitoneal injections of saline (*mdx* + saline) or the autophagy inhibitor, leupeptin (*mdx* + LPT) for 5 weeks, as described previously (Salminen, 1984; Haspel et al., 2011; Esteban-Martínez and Boya, 2015), starting at 9 weeks of age in an attempt to preserve mitochondrial degradation. Within quadriceps muscles, mitochondrial DNA copy number was not changed in *mdx* + LPT vs. saline-treated *mdx* mice (**Figure 4A**). Without changing gene expression, LPT treatment elevated the protein level of mitochondrial proteins (Drp1, Vdac1, Opa1, and Complex IV) and mitophagy related factors (Lc3bII/I, p62, and Pink1), validating robust autophagy inhibition by LPT (**Figure 4B** and **Supplementary Figures S5A,B**). However, mitochondrial enzymatic histochemical and activity analyses of the tibialis anterior muscle showed no differences in LPT treated animals suggesting LPT treatment did not ameliorate mitochondrial dysfunction in *mdx* mice (**Figures 4C,D**).

Female Asymptomatic *mdx* Carriers Present With Diet-Induced Obesity and Insulin Resistance

Women who are carriers of the DMD gene are largely asymptomatic with regard to skeletal muscle symptoms, but are susceptible to cardiomyopathy (Childers and Klaiman, 2017; Viggiano et al., 2017; Florian et al., 2018; Ishizaki et al., 2018; Zhong et al., 2019). Given our observation of mitochondrial defects in presymptomatic *mdx* male muscle, we sought to query the impact upon mitochondria, muscle, and metabolism in adult 24-week-old, female *mdx* carrier (*mdx* carriers) mice. Adult female *mdx* carriers were chosen because human female *mdx* carriers typically display symptoms during adult hood and because maximal muscle growth has nearly been achieved according to Jackson laboratory growth curves. We found that female *mdx* carriers displayed similar body weight to age-matched controls (**Figure 5A**). These mice showed a lower gonadal white adipose tissue mass (gWAT) although no differences in the weights of other metabolic organs (**Figure 5B**) were observed. Because of the role of muscle in glucose homeostasis, we performed glucose and insulin tolerance tests (GTT and ITT, respectively). Female *mdx* carrier mice showed slight impairments in glucose and insulin sensitivity although plasma insulin, leptin, and triglyceride values were not different compared to age-matched controls (**Figures 5C,D** and **Supplementary Figures S6A–C**). *Ex vivo* glucose uptake into excised soleus muscles revealed a similar modest reduction in insulin-stimulated glucose uptake in female *mdx* carriers, although this did not reach statistical significance (**Figure 5E**). We then performed functional muscle strength and endurance testing and found no differences between the two groups in these parameters (**Supplementary Figures S6D–F**). Our previous results indicated that a loss of dystrophin had an impact upon the expression of regulators of the mitochondria life cycle within skeletal muscle from male mice. However, female *mdx* carriers showed no differences in proteins related to mitophagy, autophagy, mitochondrial biogenesis, fission, or fusion (**Figure 5F**). Nevertheless, electron micrograph images from female *mdx* carriers consistently displayed mitochondrial vacuoles, similar to what was observed in presymptomatic 2-week-old, *mdx* male mice, despite no overt changes to the muscle fiber or z-line orientation (**Figure 5G**). Moreover, we performed both enzymatic and respirometry assays and observed a significant reduction of mitochondrial complex IV activity in female *mdx* carriers, suggesting a defect in mitochondrial function (**Figures 5H,I**). Interestingly, we found that high-fat diet (HFD) administration significantly reduced quadriceps and gastrocnemius muscle weights, dramatically elevated body weight, gWAT weight, impaired GTT, and elevated fat mass ratio without changing plasma triglyceride and lactate levels in female *mdx* carriers (**Figures 5J–L** and **Supplementary Figures S6G–I**). These results suggest female *mdx* carriers present with mild metabolic impairment that is exacerbated with HFD administration.

DISCUSSION

A greater understanding of the many consequences of loss of dystrophin are needed in order to inform the design of new therapies. Because of this, we sought to understand the biological impact of lacking functional dystrophin protein upon mitochondria and metabolism within male and female mice. Utilizing the *mdx* mouse, where males have little dystrophin expression and female carriers display dystrophin somatic mosaicism, we detected via electron microscopy, aberrant mitochondrial morphology, reduced cristae numbers, and large empty spaces within mitochondria in both male and female *mdx* mice prior to the onset of muscle fiber damage. To

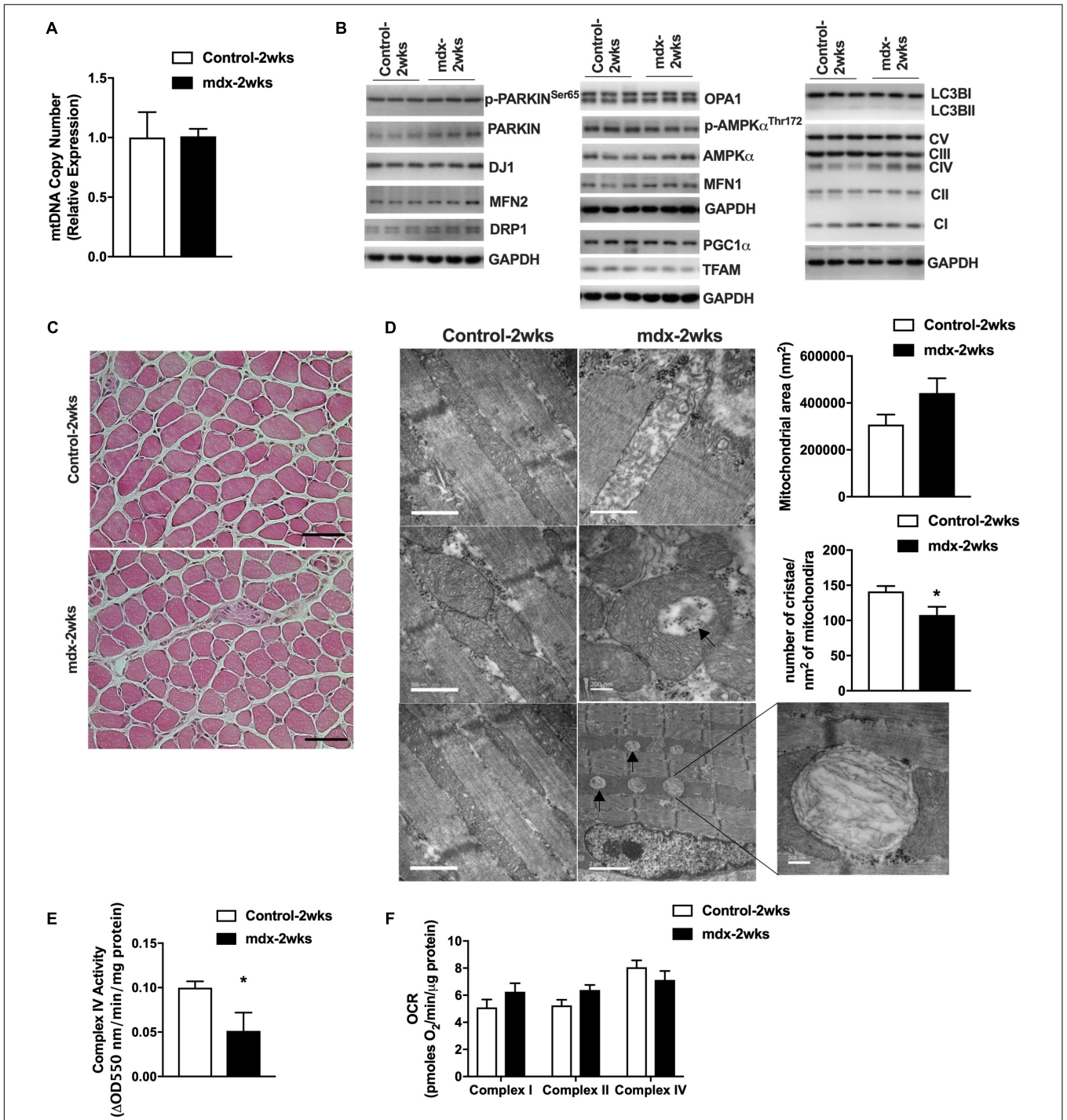

FIGURE 3 | Mitochondria from 2-week-old, *mdx* male muscles display altered size, cristae numbers per area of mitochondria, and enzymatic activity. **(A)** Mitochondrial DNA copy number in quadriceps muscle ($N = 5$). **(B)** Immunoblot images from quadriceps muscle ($N = 6$–8, showing $N = 3$). **(C)** HE stain of gastrocnemius muscle. Scale bar = 0.1 mm. **(D)** Electron micrograph images of the soleus muscle with quantified mitochondrial area and cristae numbers per area of mitochondria shown right. Black arrows indicate aberrant mitochondria. **(E)** Complex IV activity in quadriceps muscle ($N = 5$). Data presented as Mean ± SEM. **(F)** Mitochondrial respirometry analysis in frozen quadriceps muscle ($N = 6$–8). *$P < 0.05$.

our knowledge, this work represents the first to suggest that mitochondrial ultrastructure is impacted prior to muscle fiber damage. We further observed impaired complex IV enzymatic activity as previously described (Gaglianone et al., 2019). While not extensively tested, published research does suggest a mitochondrial phenotype occurring early in muscular dystrophy

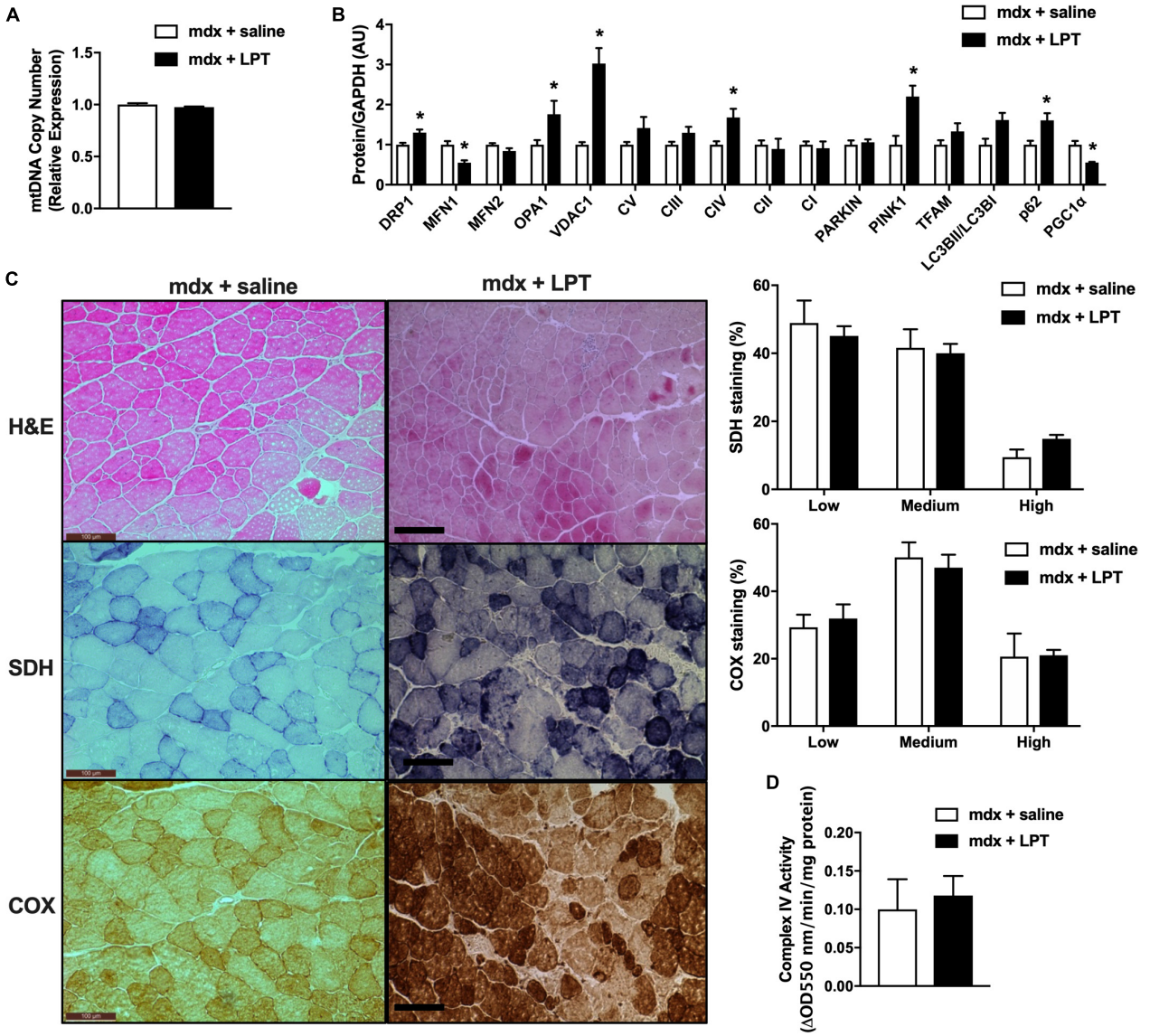

FIGURE 4 | Autophagy inhibition did not improve mitochondrial phenotype in 14-week-old *mdx* male mice. **(A)** Mitochondrial DNA copy number in quadriceps muscle ($N = 5$). **(B)** Protein expression in quadriceps muscle ($N = 5$). **(C)** HE, COX, and SDH staining in tibialis anterior muscle with the percentage of muscle fiber density shown right ($N = 12$). Scale bar = 0.1 mm. **(D)** Complex IV activity in quadriceps muscle ($N = 5$). Data presented as Mean ± SEM. *$P < 0.05$.

disease progression (Nghiem et al., 2017; Vila et al., 2017; Barker et al., 2018). These data suggest that a connection may exist between mitochondria, dystrophin, and muscle fiber damage, at least in a mouse model of muscular dystrophy. Our results are also in agreement with data showing genetic or pharmacological increases in PGC1α, a known master regulator of mitochondria, improving recovery from injury in *mdx* mice (Jahnke et al., 2012; Selsby et al., 2012; Chan et al., 2014).

Male *mdx* mice have already been shown to possess metabolic abnormalities after disease onset and during progression (Blanchet et al., 2012; Strakova et al., 2018). In alignment with these results, we additionally observed mitochondrial dysfunction and metabolic disorder in female *mdx* carrier mice that was exacerbated with high-fat diet feeding. These findings indicate mitochondrial and metabolic dysfunction in female *mdx* carriers with increased susceptibility to diet-induced obesity and insulin resistance despite possessing one functional copy of the dystrophin allele. To our knowledge, this is the first characterization of metabolism and mitochondria within female *mdx* carrier mice. Phenotypic abnormalities, particularly related to mild muscle weakness and cramping, have been noted in a small subset of human female dystrophin mutation carriers (Hoffman et al., 1992; Ceulemans et al., 2008; Ameen and Robson, 2010; Walcher et al., 2010; Yoon et al., 2011; Brioschi et al., 2012; van Putten et al., 2012). Nevertheless, epidemiological evidence linking female dystrophin mutation

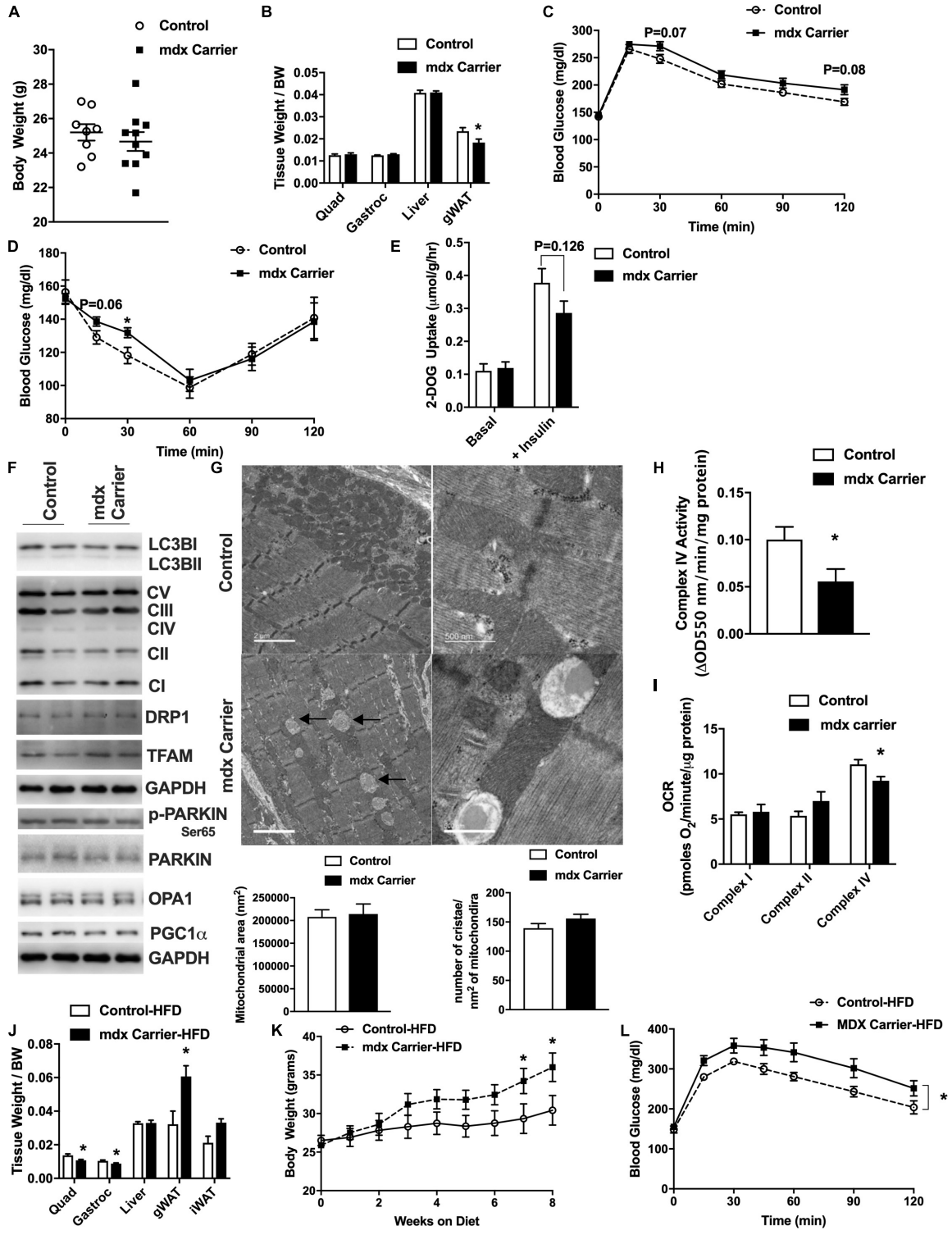

FIGURE 5 | Female *mdx* carriers present mild metabolic impairments that are exacerbated with high-fat diet feeding. Female *mdx* carriers fed with normal chow **(A–I)** (*N* = 6–10): **(A)** Tissue weight relative to body weight. **(B)** Body weight (grams). **(C,D)** Glucose and insulin tolerance tests with area under the curve (AUC) insert. **(E)** 2-Deoxyglucose uptake with or without insulin in excised soleus muscle. **(F)** Immunoblot images for respective proteins. **(G)** Electron micrograph images of the soleus muscle with quantified mitochondrial area and cristae numbers per area of mitochondria shown bottom. Black arrow indicates mitochondrial vacuoles. **(H)** Complex IV activity in quadriceps muscle. **(I)** Mitochondrial respirometry analysis in quadriceps muscle. Female *mdx* carriers fed with high-fat diet **(J–L)** (*N* = 6–7): **(J)** Tissue weight relative to body weight. **(K)** Body weight during high-fat diet feeding. **(L)** Glucose tolerance tests with area under the curve (AUC) insert. Data presented as Mean ± SEM. $^*P < 0.05$.

carriers with increased prevalence of obesity, type 2 diabetes, or metabolic dysfunction is lacking. Furthermore, while such metabolic changes are minor in female *mdx* carrier mice, they do suggest that female humans harboring dystrophin mutations could be susceptible to metabolic dysfunction particularly in the context of diet-induced obesity or aging. This is also supported by altered glucose handling and metabolism in a mixed sex canine model of muscular dystrophy (Schneider et al., 2018). Female carriers of DMD may present with associated cardiomyopathy, which has led to more widespread cardiac monitoring of women with DMD offspring (Florian et al., 2016). Interestingly, mitophagy has been implicated in DMD cardiac disease (Kyrychenko et al., 2015; Kang et al., 2018), further supporting that mitochondria dysfunction is a common feature of DMD.

Despite the novelty of our findings, there are several limitations. Our main finding of mitochondrial vacuoles within and adjacent to mitochondria is inconclusive. These structures could represent swollen mitochondria due to calcium influx, enlarged lipid droplets, or autophagic vesicles. In addition, it has been postulated that due to the reduced structural integrity of skeletal muscle cells in the *mdx* mouse, artifacts may occur more easily during assays (Bereiter-Hahn and Vöth, 1979). Thus, they could simply represent actual empty spaces as a result of tissue handling. Therefore, further work is needed to verify the identity of these structures. In addition, despite the connection between autophagy, mitochondria, and muscular dystrophy (De Palma et al., 2012, 2014; Whitehead, 2016; Piras and Boido, 2018), autophagy inhibition did not improve disease pathology in *mdx* male mice, similar to previous results (Selsby et al., 2010; Childers et al., 2011; De Palma et al., 2012; Sandri et al., 2013). The severity of the disease at this age could preclude the ability of autophagy inhibition to reverse symptoms. Moreover, the failure of autophagy inhibition to improve mitochondrial or muscle fiber damage could be related to the relatively low dose administered (12 mg/kg), the method of administration which did not specifically target skeletal muscle (intraperitoneal injection), the infrequent dosing scheme employed (Q.O.D, every other day), or the short duration of administration (5 weeks). Finally, while we observed reductions in mtDNA, previous results indicate *mdx* muscle having reduced numbers of nuclei per muscle fiber, smaller muscle fibers, and an increase in non-muscle cells potentially biasing our results and causing incorrect conclusions to be made (Duddy et al., 2015). Despite observing no difference in nuclear DNA number between groups in all experiments, more robust methods are needed to verify the legitimacy of these data.

Collectively, our results substantiate previous findings and further expound upon mitochondrial and metabolic abnormalities prior to the onset of muscle damage in both male and female *mdx* mice. While the precise connection between dystrophin and mitochondria is still unknown, lacking functional dystrophin is believed to increase the permeability of the cell to Ca^{2+}, promoting mitochondrial Ca^{2+} overload. Calcium overload leads to mitochondrial swelling, increased mitochondrial reactive oxygen species production, and mitochondrial permeability transition pore opening ultimately resulting in mitochondrial dysfunction (Millay et al., 2008; Perumal et al., 2015; Vila et al., 2017). In addition, because the sarcoendoplasmic reticulum (SR) physically interconnects with mitochondria within the muscle fiber and functions to store Ca^{2+}, Ca^{2+} overload can also result in SR stress further contributing to mitochondrial dysfunction in *mdx* mice (Pauly et al., 2017). In conclusion, the research presented here, as well as from other groups, supports future endeavors to improve mitochondrial function as a component of combination-based therapies to combat muscular dystrophy.

CONCLUSION

In line with previous data, prior to onset of muscle fiber damage, skeletal muscle from male *mdx* and female *mdx* carrier mice presented with aberrant mitochondrial structure, reduced cristae number, and large empty spaces within mitochondria in addition to reduced mitochondrial function. Moreover, female *mdx* carriers presented mild metabolic impairments that were exacerbated with high-fat diet feeding. These phenotypes prior to muscle damage suggest a mitochondrial component to the muscular dystrophy family of diseases. This insight can help shape future therapeutics to improve mitochondrial function and help mitigate the impact of this devastating group of diseases.

DATA AVAILABILITY STATEMENT

All datasets presented in this study are included in the article/**Supplementary Material**.

ETHICS STATEMENT

The animal study was reviewed and approved by The University of California, Los Angeles Institutional Animal Care and Use Committee.

AUTHOR CONTRIBUTIONS

TM and ZZ performed the conception and design. TM, AL, AS, KC, KW, ThH, TiH, JL, DR, CN, AY, JW, SM, LT, LS, RC, and ZZ conducted the animal experiments, sample collection, and subsequent experimental analysis. TM and ZZ drafted the original manuscript. All authors contributed to the final drafting of the manuscript.

FUNDING

This research was supported in part by the UCLA Claude Pepper Older Americans Independence Center funded by the National Institute of Aging (5P30AG028748), NIH/NCATS UCLA CTSI

Grant (UL1TR000124), and Wellstone NIH NIAMS Center of Excellence Grant (U54 AR052646) to ZZ. TM was supported by a Kirschstein-NRSA predoctoral fellowship (F31DK108657), a Carl V. Gisolfi Memorial Research grant from the American College of Sports Medicine, a predoctoral graduate student award from the Dornsife College at the University of Southern California, and a post-doctoral fellowship from the UCLA Intercampus Medical Genetics Training Program (T32GM008243). JW was supported by the American Federation for Aging Research, the Glenn Foundation for Medical Research, the UCLA Hartford Center of Excellence, National Institute on Aging Grants AG059847 and AG055518, UCLA Older Americans Independence Center P30 AG028748, UCSD/UCLA Diabetes Research Center Pilot and Feasibility Grant DK063491. LT was supported by a Gabilan Distinguished Fellowship from the Women in Science and Engineering program at USC. SM was supported by a grant from the Department of Veterans Affairs (I01BX000323). RC was supported by NIH R01AR048179 and R01HL126204.

ACKNOWLEDGMENTS

We would like to thank the UCLA Division of Laboratory Animal Medicine and Katie Moore for assisting us in animal welfare and data collection, respectively. This manuscript has been released as a pre-print at https://www.researchsquare.com/article/rs-14522/v1 (Moore et al., 2020).

SUPPLEMENTARY MATERIAL

The Supplementary Material for this article can be found online at: https://www.frontiersin.org/articles/10.3389/fphys.2020.00690/full#supplementary-material

FIGURE S1 | Immunoblot images from 40-week-old gastrocnemius muscle.

FIGURE S2 | Immunoblot images from 11-week-old quadriceps muscle.

FIGURE S3 | Mitochondria DNA copy number is reduced at the onset of tissue abnormalities in 4-week-old *mdx* male muscles. **(A)** Mitochondrial DNA copy number in quadriceps muscle (N = 8–10). **(B)** HE stain of gastrocnemius muscle. Black arrows indicate fibers with centralized nuclei. Only some fibers are indicated. Scale bar = 0.1 mm. Data presented as Mean ± SEM. $^{*}P < 0.05$.

FIGURE S4 | Electron micrograph images of the soleus muscle from 2-week-old control and *mdx* male mice.

FIGURE S5 | Immunoblot images and gene expression results from LPT treated quadriceps muscle. **(A)** Immunoblots of mitochondrial fission, fusion, mitophagy, and autophagy proteins in quadriceps muscle of *mdx* + saline and *mdx* + LPT (N = 5–6). **(B)** Gene expression of elevated protein targets in quadriceps muscle of *mdx* + saline and *mdx* + LPT (N = 5–6).

FIGURE S6 | Plasma metabolites and muscle strength and endurance measurements. Plasma **(A)** insulin, **(B)** leptin, **(C)** triglyceride of Control and *mdx* carrier fed with normal chow (N = 5–10). **(D)** Maximum running speed, **(E)** latency to fall, **(F)** fore + hindlimb grip strength of control and *mdx* carrier fed with normal chow (N = 8–10). Plasma **(G)** triglyceride, **(H)** lactate, and **(I)** fat mass/body weight ratio of control and *mdx* carrier fed with HFD (N = 6–7). $^{***}P < 0.001$.

TABLE S1 | Primers used for qPCR.

TABLE S2 | Antibodies used for immunoblotting.

REFERENCES

Ameen, V., and Robson, L. G. (2010). Experimental models of duchenne muscular dystrophy: relationship with cardiovascular disease. *Open Cardiovasc. Med. J.* 4, 265–277. doi: 10.2174/18741924010040 10265

Angelin, A., Tiepolo, T., Sabatelli, P., Grumati, P., Bergamin, N., Golfieri, C., et al. (2007). Mitochondrial dysfunction in the pathogenesis of Ullrich congenital muscular dystrophy and prospective therapy with cyclosporins. *Proc. Natl. Acad. Sci. U.S.A.* 104, 991–996. doi: 10.1073/pnas.0610 270104

Bach, D., Pich, S., Soriano, F. X., Vega, N., Baumgartner, B., Oriola, J., et al. (2003). Mitofusin-2 determines mitochondrial network architecture and mitochondrial metabolism. a novel regulatory mechanism altered in obesity. *J. Biol. Chem.* 278, 17190–17197. doi: 10.1074/jbc.m212754200

Barker, R. G., Wyckelsma, V. L., Xu, H., and Murphy, R. M. (2018). Mitochondrial content is preserved throughout disease progression in the mdx mouse model of Duchenne muscular dystrophy, regardless of taurine supplementation. *Am. J. Physiol. Cell Physiol.* 314, C483–C491.

Benador, I. Y., Veliova, M., Mahdaviani, K., Petcherski, A., Wikstrom, J. D., Assali, E. A., et al. (2018). Mitochondria bound to lipid droplets have unique bioenergetics, composition, and dynamics that support lipid droplet expansion. *Cell Metab* 27, 869–885e6.

Bereiter-Hahn, J., and Vöth, M. (1979). Metabolic state dependent preservation of cells by fixatives for electron microscopy. *Microsc. Acta* 82, 239–250.

Blanchet, E., Annicotte, J. S., Pradelli, L. A., Hugon, G., Matecki, S., Mornet, D., et al. (2012). E2F transcription factor-1 deficiency reduces pathophysiology in the mouse model of Duchenne muscular dystrophy through increased muscle oxidative metabolism. *Hum. Mol. Genet.* 21, 3910–3917. doi: 10.1093/hmg/dds219

Brioschi, S., Gualandi, F., Scotton, C., Armaroli, A., Bovolenta, M., Falzarano, M. S., et al. (2012). Genetic characterization in symptomatic female DMD carriers: lack of relationship between X-inactivation, transcriptional DMD allele balancing and phenotype. *BMC Med. Genet.* 13:73. doi: 10.1186/1471-2350-13-73

Bulfield, G., Siller, W. G., Wight, P. A., and Moore, K. J. (1984). X chromosome-linked muscular dystrophy (mdx) in the mouse. *Proc. Natl. Acad. Sci. U.S.A.* 81, 1189–1192.

Bushby, K., Finkel, R., Birnkrant, D. J., Case, L. E., Clemens, P. R., Cripe, L., et al. (2010a). Diagnosis and management of Duchenne muscular dystrophy, part 1: diagnosis, and pharmacological and psychosocial management. *Lancet Neurol.* 9, 77–93. doi: 10.1016/s1474-4422(09)70271-6

Bushby, K., Finkel, R., Birnkrant, D. J., Case, L. E., Clemens, P. R., Cripe, L., et al. (2010b). Diagnosis and management of Duchenne muscular dystrophy, part 2: implementation of multidisciplinary care. *Lancet Neurol.* 9, 177–189. doi: 10.1016/s1474-4422(09)70272-8

Ceulemans, B. P., Storm, K., Reyniers, E., Callewaert, L., and Martin, J. J. (2008). Muscle pain as the only presenting symptom in a girl with dystrophinopathy. *Pediatr. Neurol.* 38, 64–66. doi: 10.1016/j.pediatrneurol.2007.09.006

Chan, D. C. (2012). Fusion and fission: interlinked processes critical for mitochondrial health. *Annu. Rev. Genet.* 46, 265–287. doi: 10.1146/annurev-genet-110410-132529

Chan, M. C., Rowe, G. C., Raghuram, S., Patten, I. S., Farrell, C., and Arany, Z. (2014). Post-natal induction of PGC-1α protects against severe muscle dystrophy independently of utrophin. *Skelet. Muscle* 4:2. doi: 10.1186/2044-5040-4-2

Chen, H., Vermulst, M., Wang, Y. E., Chomyn, A., Prolla, T. A., McCaffery, J. M., et al. (2010). Mitochondrial fusion is required for mtDNA stability in skeletal muscle and tolerance of mtDNA mutations. *Cell* 141, 280–289. doi: 10.1016/j.cell.2010.02.026

Childers, M. K., Bogan, J. R., Bogan, D. J., Greiner, H., Holder, M., Grange, R. W., et al. (2011). Chronic administration of a leupeptin-derived calpain inhibitor fails to ameliorate severe muscle pathology in a canine model of

duchenne muscular dystrophy. *Front. Pharmacol.* 2:89. doi: 10.3389/fphar.2011.00089

Childers, M. K., and Klaiman, J. M. (2017). Cardiac involvement in female carriers of Duchenne or Becker muscular dystrophy. *Muscle Nerve* 55, 777–779. doi: 10.1002/mus.25661

Cole, M. A., Rafael, J. A., Taylor, D. J., Lodi, R., Davies, K. E., and Styles, P. (2002). A quantitative study of bioenergetics in skeletal muscle lacking utrophin and dystrophin. *Neuromuscul. Disord.* 12, 247–257. doi: 10.1016/s0960-8966(01)00278-4

Davies, K. E., Kenwrick, S. J., Patterson, M. N., Smith, T. J., Forrest, S. M., Dorkins, H. R., et al. (1988). Molecular analysis of muscular dystrophy. *J. Muscle Res. Cell Motil.* 9, 1–8.

De Palma, C., Morisi, F., Cheli, S., Pambianco, S., Cappello, V., Vezzoli, M., et al. (2012). Autophagy as a new therapeutic target in Duchenne muscular dystrophy. *Cell Death Dis.* 3:e418.

De Palma, C., Perrotta, C., Pellegrino, P., Clementi, E., and Cervia, D. (2014). Skeletal muscle homeostasis in duchenne muscular dystrophy: modulating autophagy as a promising therapeutic strategy. *Front. Aging Neurosci.* 6:188. doi: 10.3389/fnagi.2014.00188

Dickinson, A., Yeung, K. Y., Donoghue, J., Baker, M. J., Kelly, R. D., McKenzie, M., et al. (2013). The regulation of mitochondrial DNA copy number in glioblastoma cells. *Cell Death Differ.* 20, 1644–1653.

Doughty, M. J., Bergmanson, J. P., and Blocker, Y. (1995). Impact of glutaraldehyde versus glutaraldehyde-formaldehyde fixative on cell organization in fish corneal epithelium. *Tissue Cell* 27, 701–712. doi: 10.1016/s0040-8166(05)80025-4

Drew, B. G., Ribas, V., Le, J. A., Henstridge, D. C., Phun, J., Zhou, Z., et al. (2014). HSP72 is a mitochondrial stress sensor critical for Parkin action, oxidative metabolism, and insulin sensitivity in skeletal muscle. *Diabetes Metab Res. Rev.* 63, 1488–1505. doi: 10.2337/db13-0665

Dubowitz, V. (2005). Prednisone for Duchenne muscular dystrophy. *Lancet Neurol.* 4:264. doi: 10.1016/s1474-4422(05)70050-8

Duddy, W., Duguez, S., Johnston, H., Cohen, T. V., Phadke, A., Gordish-Dressman, H., et al. (2015). Muscular dystrophy in the mdx mouse is a severe myopathy compounded by hypotrophy, hypertrophy and hyperplasia. *Skelet. Muscle* 5:16.

Emery, A. E. (1989). Clinical and molecular studies in Duchenne muscular dystrophy. *Prog. Clin. Biol. Res.* 306, 15–28.

Esteban-Martínez, L., and Boya, P. (2015). Autophagic flux determination in vivo and ex vivo. *Methods* 75, 79–86. doi: 10.1016/j.ymeth.2015.01.008

Even, P. C., Decrouy, A., and Chinet, A. (1994). Defective regulation of energy metabolism in mdx-mouse skeletal muscles. *Biochem. J.* 304(Pt 2), 649–654. doi: 10.1042/bj3040649

Florian, A., Patrascu, A., Tremmel, R., Rösch, S., Sechtem, U., Schwab, M., et al. (2018). Identification of Cardiomyopathy-Associated Circulating miRNA Biomarkers in Muscular Dystrophy Female Carriers Using a Complementary Cardiac Imaging and Plasma Profiling Approach. *Front. Physiol.* 9:1770. doi: 10.3389/fphys.2018.01770

Florian, A., Rösch, S., Bietenbeck, M., Engelen, M., Stypmann, J., Waltenberger, J., et al. (2016). Cardiac involvement in female Duchenne and Becker muscular dystrophy carriers in comparison to their first-degree male relatives: a comparative cardiovascular magnetic resonance study. *Eur. Heart J. Cardiovasc. Imag.* 17, 326–333. doi: 10.1093/ehjci/jev161

Gaglianone, R. B., Santos, A. T., Bloise, F. F., Ortiga-Carvalho, T. M., Costa, M. L., et al. (2019). Reduced mitochondrial respiration and increased calcium deposits in the EDL muscle, but not in soleus, from 12-week-old dystrophic mdx mice. *Sci. Rep.* 9:1986.

Govoni, A., Magri, F., Brajkovic, S., Zanetta, C., Faravelli, I., Corti, S., et al. (2013). Ongoing therapeutic trials and outcome measures for Duchenne muscular dystrophy. *Cell Mol. Life. Sci.* 70, 4585–4602. doi: 10.1007/s00018-013-1396-z

Gulston, M. K., Rubtsov, D. V., Atherton, H. J., Clarke, K., Davies, K. E., Lilley, K. S., et al. (2008). A combined metabolomic and proteomic investigation of the effects of a failure to express dystrophin in the mouse heart. *J. Proteome Res.* 7, 2069–2077. doi: 10.1021/pr800070p

Haspel, J., Shaik, R. S., Ifedigbo, E., Nakahira, K., Dolinay, T., Englert, J. A., et al. (2011). Characterization of macroautophagic flux in vivo using a leupeptin-based assay. *Autophagy* 7, 629–642. doi: 10.4161/auto.7.6.15100

Hoffman, E. P., Arahata, K., Minetti, C., Bonilla, E., and Rowland, L. P. (1992). Dystrophinopathy in isolated cases of myopathy in females. *Neurology* 42, 967–975.

Ieronimakis, N., Hays, A., Prasad, A., Janebodin, K., Duffield, J. S., and Reyes, M. (2016). PDGFRα signalling promotes fibrogenic responses in collagen-producing cells in Duchenne muscular dystrophy. *J. Pathol.* 240, 410–424. doi: 10.1002/path.4801

Ishizaki, M., Kobayashi, M., Adachi, K., Matsumura, T., and Kimura, E. (2018). Female dystrophinopathy: review of current literature. *Neuromuscul. Disord.* 28, 572–581. doi: 10.1016/j.nmd.2018.04.005

Jahnke, V. E., Van Der Meulen, J. H., Johnston, H. K., Ghimbovschi, S., Partridge, T., Hoffman, E. P., et al. (2012). Metabolic remodeling agents show beneficial effects in the dystrophin-deficient mdx mouse model. *Skelet. Muscle* 2:16. doi: 10.1186/2044-5040-2-16

Jones, D. (2019). Duchenne muscular dystrophy awaits gene therapy. *Nat. Biotechnol.* 37, 335–337. doi: 10.1038/s41587-019-0103-5

Jornayvaz, F. R., and Shulman, G. I. (2010). Regulation of mitochondrial biogenesis. *Essays Biochem.* 47, 69–84.

Kang, C., Badr, M. A., Kyrychenko, V., Eskelinen, E. L., and Shirokova, N. (2018). Deficit in PINK1/PARKIN-mediated mitochondrial autophagy at late stages of dystrophic cardiomyopathy. *Cardiovasc. Res.* 114, 90–102. doi: 10.1093/cvr/cvx201

Kemp, G. J., Taylor, D. J., Dunn, J. F., Frostick, S. P., and Radda, G. K. (1993). Cellular energetics of dystrophic muscle. *J. Neurol. Sci.* 116, 201–206. doi: 10.1016/0022-510x(93)90326-t

Khairallah, M., Khairallah, R., Young, M. E., Dyck, J. R., Petrof, B. J., and Des Rosiers, C. (2007). Metabolic and signaling alterations in dystrophin-deficient hearts precede overt cardiomyopathy. *J. Mol. Cell Cardiol.* 43, 119–129. doi: 10.1016/j.yjmcc.2007.05.015

Kuznetsov, A. V., Winkler, K., Wiedemann, F. R., von Bossanyi, P., Dietzmann, K., and Kunz, W. S. (1998). Impaired mitochondrial oxidative phosphorylation in skeletal muscle of the dystrophin-deficient mdx mouse. *Mol. Cell. Biochem.* 183, 87–96.

Kyrychenko, V., Poláková, E., Janíèek, R., and Shirokova, N. (2015). Mitochondrial dysfunctions during progression of dystrophic cardiomyopathy. *Cell Calcium* 58, 186–195. doi: 10.1016/j.ceca.2015.04.006

Lackner, L. L. (2014). Shaping the dynamic mitochondrial network. *BMC Biol.* 12:35. doi: 10.1186/1741-7007-12-35

Lerman, I., Harrison, B. C., Freeman, K., Hewett, T. E., Allen, D. L., Robbins, J., et al. (2002). Genetic variability in forced and voluntary endurance exercise performance in seven inbred mouse strains. *J. Appl. Physiol. (1985)* 92, 2245–2255. doi: 10.1152/japplphysiol.01045.2001

Liesa, M., Palacín, M., and Zorzano, A. (2009). Mitochondrial dynamics in mammalian health and disease. *Physiol. Rev.* 89, 799–845. doi: 10.1152/physrev.00030.2008

Lucas-Héron, B., Schmitt, N., and Ollivier, B. (1990). Age-related calmitine distribution in mitochondria of normal and mdx mouse skeletal muscle. *J. Neurol. Sci.* 99, 349–353. doi: 10.1016/0022-510x(90)90169-n

Mandillo, S., Heise, I., Garbugino, L., Tocchini-Valentini, G. P., Giuliani, A., Wells, S., et al. (2014). Early motor deficits in mouse disease models are reliably uncovered using an automated home-cage wheel-running system: a cross-laboratory validation. *Dis Model Mech.* 7, 397–407. doi: 10.1242/dmm.013946

Marshall, J. L., and Crosbie-Watson, R. H. (2013). Sarcospan: a small protein with large potential for Duchenne muscular dystrophy. *Skelet. Muscle* 3:1. doi: 10.1186/2044-5040-3-1

McIntosh, L. M., Baker, R. E., and Anderson, J. E. (1998a). Magnetic resonance imaging of regenerating and dystrophic mouse muscle. *Biochem. Cell Biol.* 76, 532–541. doi: 10.1139/o98-033

McIntosh, L. M., Garrett, K. L., Megeney, L., Rudnicki, M. A., and Anderson, J. E. (1998b). Regeneration and myogenic cell proliferation correlate with taurine levels in dystrophin- and MyoD-deficient muscles. *Anat. Rec.* 252, 311–324. doi: 10.1002/(sici)1097-0185(199810)252:2<311::aid-ar17>3.0.co;2-q

Millay, D. P., Sargent, M. A., Osinska, H., Baines, C. P., Barton, E. R., Vuagniaux, G., et al. (2008). Genetic and pharmacologic inhibition of mitochondrial-dependent necrosis attenuates muscular dystrophy. *Nat. Med.* 14, 442–447. doi: 10.1038/nm1736

Miller, F. J., Rosenfeldt, F. L., Zhang, C., Linnane, A. W., and Nagley, P. (2003). Precise determination of mitochondrial DNA copy number in human skeletal and cardiac muscle by a PCR-based assay: lack of change of copy number with age. *Nucleic Acids Res.* 31:e61.

Mokhtarian, A., Decrouy, A., Chinet, A., and Even, P. C. (1996). Components of energy expenditure in the mdx mouse model of Duchenne muscular dystrophy. *Pflugers. Arch.* 431, 527–532. doi: 10.1007/bf02191899

Monaco, A. P., Bertelson, C. J., Liechti-Gallati, S., Moser, H., and Kunkel, L. M. (1988). An explanation for the phenotypic differences between patients bearing partial deletions of the DMD locus. *Genomics* 2, 90–95. doi: 10.1016/0888-7543(88)90113-9

Montgomery, M. K., and Turner, N. (2015). Mitochondrial dysfunction and insulin resistance: an update. *Endocr. Connect.* 4, R1–R15.

Moore, T. M., Lin, A., Strumwasser, A. R., Cory, K., Whitney, K., Ho, T., et al. (2020). Mitochondrial dysfunction is an early consequence of partial or complete dystrophin loss in *mdx* mice. doi: 10.21203/rs.2.23961/v1

Moore, T. M., Zhou, Z., Cohn, W., Norheim, F., Lin, A. J., Kalajian, N., et al. (2019). The impact of exercise on mitochondrial dynamics and the role of Drp1 in exercise performance and training adaptations in skeletal muscle. *Mol. Metab* 21, 51–67.

Muntoni, F., Fisher, I., Morgan, J. E., and Abraham, D. (2002). Steroids in Duchenne muscular dystrophy: from clinical trials to genomic research. *Neuromuscul. Disord.* 12(Suppl. 1), S162–S165.

Nghiem, P. P., Bello, L., Stoughton, W. B., López, S. M., Vidal, A. H., Hernandez, B. V., et al. (2017). Changes in muscle metabolism are associated with phenotypic variability in golden retriever muscular dystrophy. *Yale J. Biol. Med.* 90, 351–360.

Nochez, Y., Arsene, S., Gueguen, N., Chevrollier, A., Ferré, M., Guillet, V., et al. (2009). Acute and late-onset optic atrophy due to a novel OPA1 mutation leading to a mitochondrial coupling defect. *Mol. Vis.* 15, 598–608.

Park, C.-H., Kim, H.-W., Rhyu, I. J., and Uhm, C.-S. (2016). How to get well-preserved samples for transmission electron microscopy. *Appl. Microsc.* 46, 188–192. doi: 10.9729/am.2016.46.4.188

Pauly, M., Angebault-Prouteau, C., Dridi, H., Notarnicola, C., Scheuermann, V., Lacampagne, A., et al. (2017). ER stress disturbs SR/ER-mitochondria Ca. *Biochim. Biophys. Acta Mol. Basis Dis.* 1863, 2229–2239. doi: 10.1016/j.bbadis.2017.06.009

Pauly, M., Daussin, F., Burelle, Y., Li, T., Godin, R., Fauconnier, J., et al. (2012). AMPK activation stimulates autophagy and ameliorates muscular dystrophy in the mdx mouse diaphragm. *Am. J. Pathol.* 181, 583–592. doi: 10.1016/j.ajpath.2012.04.004

Pejznochova, M., Tesarova, M., Hansikova, H., Magner, M., Honzik, T., Vinsova, K., et al. (2010). Mitochondrial DNA content and expression of genes involved in mtDNA transcription, regulation and maintenance during human fetal development. *Mitochondrion* 10, 321–329. doi: 10.1016/j.mito.2010.01.006

Perumal, A. R., Rajeswaran, J., and Nalini, A. (2015). Neuropsychological profile of duchenne muscular dystrophy. *Appl. Neuropsychol. Child* 4, 49–57.

Pichavant, C., Aartsma-Rus, A., Clemens, P. R., Davies, K. E., Dickson, G., Takeda, S., et al. (2011). Current status of pharmaceutical and genetic therapeutic approaches to treat DMD. *Mol. Ther.* 19, 830–840. doi: 10.1038/mt.2011.59

Piras, A., and Boido, M. (2018). Autophagy inhibition: a new therapeutic target in spinal muscular atrophy. *Neural Regen. Res.* 13, 813–814.

Ribas, V., Drew, B. G., Zhou, Z., Phun, J., Kalajian, N. Y., Soleymani, T., et al. (2016). Skeletal muscle action of estrogen receptor alpha is critical for the maintenance of mitochondrial function and metabolic homeostasis in females. *Sci. Transl. Med.* 8:334ra354.

Salminen, A. (1984). Effects of the protease inhibitor leupeptin on proteolytic activities and regeneration of mouse skeletal muscles after exercise injuries. *Am. J. Pathol.* 117, 64–70.

Sandri, M., Coletto, L., Grumati, P., and Bonaldo, P. (2013). Misregulation of autophagy and protein degradation systems in myopathies and muscular dystrophies. *J. Cell Sci.* 126(Pt 23), 5325–5333. doi: 10.1242/jcs.114041

Scarpulla, R. C. (2011). Metabolic control of mitochondrial biogenesis through the PGC-1 family regulatory network. *Biochim. Biophys. Acta* 1813, 1269–1278. doi: 10.1016/j.bbamcr.2010.09.019

Schneider, S. M., Sridhar, V., Bettis, A. K., Heath-Barnett, H., Balog-Alvarez, C. J., Guo, L. J., et al. (2018). Glucose metabolism as a pre-clinical biomarker for the golden retriever model of duchenne muscular dystrophy. *Mol. Imaging Biol.* 20, 780–788. doi: 10.1007/s11307-018-1174-2

Selsby, J., Pendrak, K., Zadel, M., Tian, Z., Pham, J., Carver, T., et al. (2010). Leupeptin-based inhibitors do not improve the mdx phenotype. *Am. J. Physiol. Regul. Integr. Comp. Physiol.* 299, R1192–R1201.

Selsby, J. T., Morine, K. J., Pendrak, K., Barton, E. R., and Sweeney, H. L. (2012). Rescue of dystrophic skeletal muscle by PGC-1α involves a fast to slow fiber type shift in the mdx mouse. *PLoS One* 7:e30063. doi: 10.1371/journal.pone.0030063

Seo, A. Y., Joseph, A. M., Dutta, D., Hwang, J. C., Aris, J. P., and Leeuwenburgh, C. (2010). New insights into the role of mitochondria in aging: mitochondrial dynamics and more. *J. Cell Sci.* 123(Pt 15), 2533–2542. doi: 10.1242/jcs.070490

Shen, Q., Yamano, K., Head, B. P., Kawajiri, S., Cheung, J. T., Wang, C., et al. (2014). Mutations in Fis1 disrupt orderly disposal of defective mitochondria. *Mol. Biol. Cell* 25, 145–159. doi: 10.1091/mbc.e13-09-0525

Sperl, W., Skladal, D., Gnaiger, E., Wyss, M., Mayr, U., Hager, J., et al. (1997). High resolution respirometry of permeabilized skeletal muscle fibers in the diagnosis of neuromuscular disorders. *Mol. Cell. Biochem.* 174, 71–78. doi: 10.1007/978-1-4615-6111-8_11

Strakova, J., Kamdar, F., Kulhanek, D., Razzoli, M., Garry, D. J., Ervasti, J. M., et al. (2018). Integrative effects of dystrophin loss on metabolic function of the mdx mouse. *Sci. Rep.* 8:13624.

Taanman, J. W. (1999). The mitochondrial genome: structure, transcription, translation and replication. *Biochim. Biophys. Acta* 1410, 103–123. doi: 10.1016/s0005-2728(98)00161-3

Twig, G., Hyde, B., and Shirihai, O. S. (2008). Mitochondrial fusion, fission and autophagy as a quality control axis: the bioenergetic view. *Biochim. Biophys. Acta* 1777, 1092–1097. doi: 10.1016/j.bbabio.2008.05.001

Twig, G., and Shirihai, O. S. (2011). The interplay between mitochondrial dynamics and mitophagy. *Antioxid. Redox. Signal.* 14, 1939–1951. doi: 10.1089/ars.2010.3779

van Putten, M., Hulsker, M., Nadarajah, V. D., van Heiningen, S. H., van Huizen, E., van Iterson, M., et al. (2012). The effects of low levels of dystrophin on mouse muscle function and pathology. *PLoS One* 7:e31937. doi: 10.1371/journal.pone.0031937

Viggiano, E., Picillo, E., Ergoli, M., Cirillo, A., Del Gaudio, S., and Politano, L. (2017). Skewed X-chromosome inactivation plays a crucial role in the onset of symptoms in carriers of Becker muscular dystrophy. *J. Gene Med.* 19:e2952. doi: 10.1002/jgm.2952

Vila, M. C., Rayavarapu, S., Hogarth, M. W., Van der Meulen, J. H., Horn, A., Defour, A., et al. (2017). Mitochondria mediate cell membrane repair and contribute to Duchenne muscular dystrophy. *Cell Death. Differ.* 24, 330–342. doi: 10.1038/cdd.2016.127

Walcher, T., Kunze, M., Steinbach, P., Sperfeld, A. D., Burgstahler, C., Hombach, V., et al. (2010). Cardiac involvement in a female carrier of Duchenne muscular dystrophy. *Int. J. Cardiol.* 138, 302–305.

Wanagat, J., Cao, Z., Pathare, P., and Aiken, J. M. (2001). Mitochondrial DNA deletion mutations colocalize with segmental electron transport system abnormalities, muscle fiber atrophy, fiber splitting, and oxidative damage in sarcopenia. *FASEB J.* 15, 322–332. doi: 10.1096/fj.00-0320com

Westermann, B. (2010). Mitochondrial fusion and fission in cell life and death. *Nat. Rev. Mol. Cell Biol.* 11, 872–884. doi: 10.1038/nrm3013

Whitehead, N. P. (2016). Enhanced autophagy as a potential mechanism for the improved physiological function by simvastatin in muscular dystrophy. *Autophagy* 12, 705–706. doi: 10.1080/15548627.2016.1144005

Yoon, J., Kim, S. H., Ki, C. S., Kwon, M. J., Lim, M. J., Kwon, S. R., et al. (2011). Carrier woman of Duchenne muscular dystrophy mimicking inflammatory myositis. *J. Korean Med. Sci.* 26, 587–591.

Young, C. S., Hicks, M. R., Ermolova, N. V., Nakano, H., Jan, M., Younesi, S., et al. (2016). A Single CRISPR-Cas9 Deletion Strategy that Targets the Majority of DMD Patients Restores Dystrophin Function in hiPSC-Derived Muscle Cells. *Cell Stem Cell* 18, 533–540. doi: 10.1016/j.stem.2016.01.021

Zhang, Q., Raoof, M., Chen, Y., Sumi, Y., Sursal, T., Junger, W., et al. (2010). Circulating mitochondrial DAMPs cause inflammatory responses to injury. *Nature* 464, 104–107.

Zhong, J., Xie, Y., Bhandari, V., Chen, G., Dang, Y., Liao, H., et al. (2019). Clinical and genetic characteristics of female dystrophinopathy carriers. *Mol. Med. Rep.* 19, 3035–3044.

Zhou, Z., Ribas, V., Rajbhandari, P., Drew, B. G., Moore, T. M., Fluitt, A. H., et al. (2018). Estrogen receptor α protects pancreatic β-cells from apoptosis by preserving mitochondrial function and suppressing endoplasmic reticulum stress. *J. Biol. Chem.* 293, 4735–4751. doi: 10.1074/jbc.m117.805069

[†]We appreciate the contribution of all previous studies. Due to huge numbers of related references, we apologize that we did not cite those papers.

Conflict of Interest: The authors declare that the research was conducted in the absence of any commercial or financial relationships that could be construed as a potential conflict of interest.

frontiers in Physiology

MINI REVIEW
published: 23 June 2020
doi: 10.3389/fphys.2020.00662

Regulatory Role of the Transcription Factor Twist1 in Cancer-Associated Muscle Cachexia

Mohammed S. Razzaque[1] and Azeddine Atfi[2]*

[1] Department of Pathology, Lake Erie College of Osteopathic Medicine, Erie, PA, United States, [2] Department of Pathology, Virginia Commonwealth University, Richmond, VA, United States

Muscle cachexia is a catabolic response, usually takes place in various fatal diseases, such as sepsis, burn injury, and chronic kidney disease. Muscle cachexia is also a common co-morbidity seen in the vast majority of advanced cancer patients, often associated with low quality of life and death due to general organ dysfunction. The triggering events and underlying molecular mechanisms of muscle wasting are not yet clearly defined. Our recent study has shown that the ectopic expression of Twist1 in muscle progenitor cells is sufficient to drive muscle structural protein breakdown and attendant muscle atrophy, reminiscent of muscle cachexia. Intriguingly, muscle Twist1 expression is highly induced in cachectic muscles from several mouse models of pancreatic ductal adenocarcinoma (PDAC), raising the interesting possibility that Twist1 may mediate PDAC-driven muscle cachexia. Along these lines, both genetic and pharmacological inactivation of Twist1 function was highly significant at protecting against cancer cachexia, which translated into a significant survival benefit in the experimental PDAC animals. From a translational perspective, elevated expression of Twist1 is also detected in cancer patients with severe muscle wasting, implicating a role of Twist1 in cancer cachexia, and further providing a possible target for therapeutic attenuation of cachexia to improve cancer patient survival. In this article, we will briefly summarize how Twist1 acts as a master regulator of tumor-induced cachexia, and discuss the relevance of our findings to muscle wasting diseases in general. The mechanism of decreased muscle mass in various catabolic conditions is thought to rely on similar pathways, and, therefore, Twist1-induced cancer cachexia may benefit diverse groups of patients with clinical complications associated with loss of muscle mass and functions, beyond the expected benefits for cancer patients.

Keywords: activin A, twist1, MuRF1, atrogin1, muscle atrophy

OPEN ACCESS

Edited by:
Marcella Canton,
University of Padova, Italy

Reviewed by:
Xu Yan,
Victoria University, Australia
Yu-Chiang Lai,
University of Birmingham, United Kingdom

****Correspondence:***
Mohammed S. Razzaque
mrazzaque@lecom.edu;
mohammed.razzaque@umb.edu

Specialty section:
This article was submitted to Clinical and Translational Physiology, a section of the journal Frontiers in Physiology

Received: *14 February 2020*
Accepted: *25 May 2020*
Published: *23 June 2020*

Citation:
Razzaque MS and Atfi A (2020) Regulatory Role of the Transcription Factor Twist1 in Cancer-Associated Muscle Cachexia. Front. Physiol. 11:662. doi: 10.3389/fphys.2020.00662

Abbreviations: Atrogin1/MAFbx, atrogin1/muscle atrophy F-box; bHLH, basic helix-loop-helix Runx2; Elf-3f, eukaryotic initiation factor 3f FOXO1; HIV, human immunodeficiency viruses; IL-1, interleukin 1; IL-6, interleukin 6; INF-γ, interferon-gamma; MHC, myosin heavy chain; miR-206, microRNA-206; MuRF1, muscle RING finger 1; PDAC, pancreatic ductal adenocarcinoma; TGF-β, transforming growth factor-β; TNF-α, tumor necrosis factor-alpha; Twist1, twist family bHLH transcription factor 1.

INTRODUCTION

Cachexia, a hypercatabolic state, is a commonly encountered adverse effect of cancer, and markedly impairs the quality of life by harmfully impacting both the physical and psychosocial behaviors. An international consensus reached in 2011 explained cancer cachexia as a multifactorial condition with continuing skeletal muscle loss that is not reversible by standard nutritional support, ultimately leading to functional impairment (Fearon et al., 2011). A skeletal muscle index <7.26 kg/m^2 in males and <5.45 kg/m^2 in females is considered as cachexia. Of relevance, the majority of patients with pancreatic tumors display signs of cachexia at the time of diagnosis (Fearon et al., 2006). Even the overweight pancreatic cancer patients develop cachexia (sarcopenic obesity), and cachexia hidden in obesity causes extensive muscle loss, with the pathological accumulation of adipose tissue that influences the overall survival of the patients (Tan et al., 2009). In cancer patients, cachexia is a progressive process that evolves through various stages – from pre-cachexia to cachexia to refractory cachexia (irreversible stage). It is important to find measures to reverse from cachexia into pre-cachectic stages to provide relief to the affected patients. Besides cancer, cachexia can also occur in a wide range of disorders, ranging from infections to chronic kidney diseases to cerebrovascular diseases, including stroke and chronic obstructive pulmonary diseases (Reid et al., 2013; Scherbakov et al., 2013; Morley, 2014). Severe muscle wasting or cachexia is noted in up to 75% of chronic kidney disease patients undergoing hemodialysis treatment (Mak et al., 2011).

The underlying mechanism of cachexia, in tumor and other catabolic disorders, are not yet clearly understood. Various catabolic conditions are associated with altered expression and regulations of transcription factors and nuclear cofactors that induce a specific group of genes, which are believed to execute the final steps of muscle atrophy. Two muscle-specific ubiquitin ligases, MuRF1 and Atrogin1/MAFbx, are essential for the degradation of muscle proteins, including myosin heavy chain (MHC) and eukaryotic initiation factor 3f (Elf-3f) (Clarke et al., 2007; Lagirand-Cantaloube et al., 2008). Transcription factors, FOXO1 is an important regulator of muscle atrophy, and is shown to be affected by sepsis and elevated levels of glucocorticoids (Stitt et al., 2004; Crossland et al., 2008; Waddell et al., 2008; Reed et al., 2012; Xu et al., 2012; Huynh et al., 2013). It is a key regulator of genes involved in muscle wasting, including Atrogin-1 and MuRF1 (Li et al., 2007; Leger et al., 2009; Pomies et al., 2016). FOXO1 also regulates genes involved in the autophagy-lysosomal proteolytic pathway (Sengupta et al., 2009; Milan et al., 2015). MyoD is a muscle-specific transcription factor that regulates muscle cell differentiation (Davis et al., 1987). Recently, MyoD-induced muscle cell differentiation is shown to be mediated by Twist1 through miR-206 (Koutalianos et al., 2015). Our recent studies suggest that the transcription factor Twist1 is also actively involved in the regulation of cancer-induced muscle wasting presumably owing to its ability to induce the expression of MuRF1 and Atrogin1, thereby causing muscle protein degradation and attendant muscle cachexia (Parajuli et al., 2018).

Of particular clinical importance, developing effective treatments to curb cachexia and muscle wasting disorders are essential for improving the quality of health and survival of the cancer patients and beyond. Tumor necrosis factor-alpha (TNF-α), interleukin 1 (IL-1), interleukin 6 (IL-6) and interferon-gamma (IFN-γ) are the main cytokines that are thought to be involved in the evolvement of cachexia, in general (Fong et al., 1989; Strassmann et al., 1993; Kayacan et al., 2006; White, 2017). However, clinically targeting these cytokines showed mixed results. For instance, in a clinical trial, infliximab (anti-TNF-α monoclonal antibody) showed no improvement of cachexia in cancer patients (Jatoi et al., 2010). In contrast, treating tumor patients with a humanized monoclonal anti-IL-6 antibody increased hemoglobin levels and reduced muscle wasting (Rigas et al., 2010).

TWIST1

Twist was initially identified in Drosophila (Thisse et al., 1987). Later, Twist isoforms have been identified in humans and mice (Wolf et al., 1991; Wang et al., 1997). Twist1 is a member of the basic helix-loop-helix (bHLH) transcription factor family that controls the activity of genes essential for embryogenesis and organogenesis (el Ghouzzi et al., 1997; Wang et al., 1997; Pan et al., 2009). Human and mouse Twist1 proteins share a very high amino acid sequence identity (96%). The Twist1 protein is involved in the generation and maturation of cells that eventually form the musculoskeletal system. Notably, during development, Twist proteins transiently inhibit Runx2 function, causing osteoblast-specific gene expression that leads to osteoblast differentiation (Bialek et al., 2004). Of relevance, human Twist1 is highly expressed in fetal myoblasts, and its level diminishes in the later stages of development (Koutsoulidou et al., 2011). Mutations in the *TWIST1* gene in human is associated with craniosynostosis (premature closure of the sutures between the bones of the skull), as noted in the Saethre-Chotzen syndrome-affected individuals (Howard et al., 1997). Heterozygous *Twist1* knockout mice showed craniofacial and limb abnormalities, mimicking clinical features of Saethre-Chotzen syndrome patients. Of note, homozygous Twist1 knockout mice were embryonically lethal, suggesting a crucial role of this gene in embryonic survival and development (Chen and Behringer, 1995). In adult mice, Twist1 is expressed in a limited number of tissues, including fibroblasts of the mammary glands and dermal papilla cells of the hair follicles (Xu et al., 2013). Consequently, inducible knockout of *Twist1* in adult mice did not affect their overall health and viability, implicating a more important role of Twist1 during early development than in adult life (Xu et al., 2013).

Studies using breast cancer cell lines have shown an important role of Twist1 in epithelial-to-mesenchymal transformation, intravasation and metastasis (Xu et al., 2017); more importantly, genetically ablating the Twist1 function effectively inhibited

breast tumor cell intravasation and lung metastasis (Xu et al., 2017). In a similar line of study, Twist1 overexpression has shown to be associated with the progression of several human malignant tumors, including pancreatic ductal adenocarcinoma (PDAC) (Lee and Bar-Sagi, 2010; Qin et al., 2012).

The role of Twist1 in myogenesis is not clear. In Drosophila, Twist has been shown to enhance myogenesis, while in mouse myoblasts (C2C12) and human embryonic stem cells (embryoid bodies), Twist1 has shown to inhibit muscle cell differentiation (Hebrok et al., 1994; Rohwedel et al., 1995; Cao et al., 2008; Koutsoulidou et al., 2011). Moreover, overexpression of Twist1 reverses the process of muscle cell differentiation (Hjiantoniou et al., 2008; Mastroyiannopoulos et al., 2013). Recently, we have shown that induction of Twist1 is also related to muscle cachexia during the progression of cancer (Parajuli et al., 2018).

TWIST1 ACTIVATION AND CANCER-INDUCED CACHEXIA

Studies have shown that numerous hormones, cytokines, and tumor-derived factors play key roles in the initiation and propagation of cancer cachexia by involving several major intracellular signaling systems (Benny Klimek et al., 2010). ActRIIB is a high-affinity activin type two receptor that facilitates the signaling of various factors, including myostatin, and activin (Lee and McPherron, 2001; Souza et al., 2008). Induced expression of activin could cause cachexia in tumor-free mice (Chen et al., 2014). Myostatin is a secreted protein of the TGF-β family, which is mostly expressed in skeletal muscle, including muscle progenitor satellite cells. In a mouse model of pancreatic cancer-induced cachexia, therapeutic reduction of TGF-β resulted in reduced cachexia and increased survival (Greco et al., 2015). Furthermore, increased signaling activity through ActRIIB pathway has shown to be involved in both tumorigenesis and cancer-induced cachexia (Wildi et al., 2001; Costelli et al., 2008; Zhou et al., 2010). Intriguingly, blocking the bioactivities of ActRIIB has been shown to reverse cancer-induced cachexia and cardiac atrophy, and this response resulted in the extended lifespan of the experimental animals even without reducing the tumor growth (Zhou et al., 2010).

As mentioned, two muscle-specific ubiquitin ligases, MuRF1, and Atrogin1/MAFbx are essential to muscle protein degradation, including MHC and Elf-3f (Clarke et al., 2007; Lagirand-Cantaloube et al., 2008). Myostatin can induce the expression of MuRF1 and Atrogin1/MAFbx as well as Twist1 (Parajuli et al., 2018), and genetic inactivation of myostatin has shown to protect against cancer-induced cachexia (Gallot et al., 2014). Selectively inducing Twis1 in mesenchymal stem cells using mouse genetics tools caused severe hypotrophy of the skeletal muscle (Parajuli et al., 2018). Interestingly, when similar *in vivo* studies were conducted on muscle progenitor cells (satellite cells), overexpression of Twist1 resulted in the loss of muscle mass in adult mice. Morphological analysis of the Twist1 overexpressing atrophic muscle showed markedly reduced myofiber diameters, as compared to the control animals, clearly demonstrating the *in vivo* role of Twist1 hyperactivity in muscle atrophy (Parajuli et al., 2018).

THERAPEUTIC POTENTIAL OF TWIST1 IN CANCER

In a healthy-weight individual, skeletal muscle comprises almost 40% of total human body mass (Rolfe and Brown, 1997). Studies have shown that patients with pancreatic cancer have often developed severe cachexia, which is associated with substantial weight loss and skeletal muscle atrophy. Noteworthy, conventional nutritional support cannot fully reverse the loss of muscle function in these patients. Almost one-third of cachectic patients develop severe respiratory muscle dysfunction, causing death due to cardiopulmonary failure in pancreatic cancer patients (Bachmann et al., 2008). In experimental models of pancreatic cancer, reducing cachexia can improve overall survival, despite persistent tumor growth, suggesting that cachexia is an important determinant of survival in tumor patients (Tisdale, 2010).

Our studies have shown that tumor-derived Activin A acts on the muscle to upregulate the expression of Twist1, which in turn induces the synthesis of the muscle-specific ubiquitin ligases, MuRF1 and Atrogin1, thereby causing muscle cachexia by facilitating muscle protein degradation (**Figure 1**; Parajuli et al., 2018). In experimental studies, serum activin levels correlated with PDAC-induced cachexia and eventual mortality (Zhong et al., 2019). In the murine model of PDAC-induced cachexia, activins (activin-βA, or Inhba) are expressed, both in tumor cells and tumor stromal cells. Treatment with an activin inhibitor in a murine model of PDAC-induced cachexia reduced weight loss

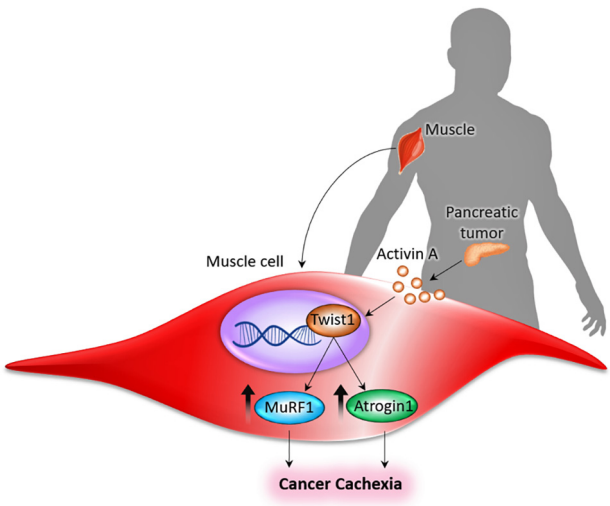

FIGURE 1 | Pancreas-muscle axis. Tumor-derived Activin A acts on the muscle to upregulate the expression of Twist1, which in turn induces the synthesis of the muscle-specific ubiquitin ligases (MuRF1 and Atrogin1), thereby causing cancer cachexia by facilitating muscle protein degradation (Parajuli et al., 2018).

and cachexia with the resultant effect being prolonged survival (Zhong et al., 2019). Moreover, using the pharmacological drug JQ1, a small molecule that suppresses Twist1 activity by blunting its binding to MuRF1 and Atrogin1 promoters, muscle cachexia could be reversed in PDAC mice deleted of Twist1, indicating that inhibition of Twist1 activity in muscle in indispensable for preventing muscle cachexia. Treatment with JQ1 prevented weight loss, which was associated with increased muscle mass and myofiber size, in turn resulting in improved muscle function and better survival of the PDAC-induced cachectic mice (Parajuli et al., 2018). It is important to emphasize that the apparent survival benefit of these experimentally induced tumor models (due to suppression of Twist1 activity) was mostly related to the reversal of muscle cachexia, and not due to shrinkage of tumor (Parajuli et al., 2018). These *in vivo* observations suggest that Twist1 could be a therapeutic target to reduce muscle mass loss in tumor and other chronic debilitating diseases, not only to improve quality of life, but also to increase disease-free survival.

In mice with chronic kidney disease, a two- to three-fold increase in myostatin expression was detected in muscle (Zhang et al., 2011); after 7 days of treatment with the anti-myostatin peptibody, muscle weights in mice with chronic kidney disease was significantly greater than those in vehicle-treated chronic kidney disease mice. Such gain of muscle mass was also reflected in the body weight gain of mice with chronic kidney disease that were treated with the anti-myostatin peptibody (Zhang et al., 2011). Furthermore, the elevated level of activin A was detected in various tissues in mice with chronic kidney disease (Williams et al., 2018). Interestingly, experimentally induced chronic kidney disease animals also showed higher expression of Atrogin-1 and MuRF-1 (Avin et al., 2016). Whether such an increase in the expression of activin A in chronic kidney disease leads to the activation of Twist1 to induce the expression of Atrogin-1 and MuRF-1 needs further studies.

Given the similarities in the general mechanisms governing muscle cachexia, one would surmise that the development of a therapeutic strategy to reduce the disease burden associated with reduced muscle function and cachexia would also benefit patients beyond tumor (**Table 1**). For instance, in chronic kidney disease patients undergoing hemodialysis treatment, the stable weight patients have better survival than those with weight loss (Villain et al., 2015). Of clinical importance, muscle wasting or cachexia occurs in up to 75% of chronic kidney disease patients on hemodialysis (Mak et al., 2011). Despite such widespread occurring of muscle wasting and its adverse impact on the survival of chronic kidney disease patients, there is no selective and effective clinical treatment of cachexia in patients with chronic kidney disease. Reducing the abundance of MuRF1 and atrogin-1 in skeletal muscles of the tumor and chronic diseases through targeting upstream regulators would likely to attenuate muscle cachexia (Zhang et al., 2018).

TABLE 1 | A partial list of the disorders associated with muscle wasting.

- Aging
- Anorexia nervosa
- Burns
- Cancer
- Chronic kidney disease
- Chronic obstructive pulmonary disease
- Congestive heart failure
- Cystic fibrosis
- Dermatomyositis
- Guillain-Barre Syndrome
- Lack of physical activity
- Long-term corticosteroid therapy
- Malnutrition (Kwashiorkor)
- Multiple sclerosis
- Osteoarthritis
- Peripheral neuropathy
- Polio (viral disease)
- Poliomyelitis
- Rheumatoid arthritis
- Sepsis
- Spinal cord injury

CONCLUSION

Cachexia occurs in many end-stage illnesses, including cancers, chronic kidney diseases, chronic cardiac diseases, chronic obstructive pulmonary diseases, chronic liver diseases, severe burns, HIV infections, rheumatoid arthritis, and aging (Mattox, 2017; von Haehling et al., 2017; Baracos et al., 2018; Scicchitano et al., 2018; Thakur et al., 2018). Roughly, 30% of patients with chronic lung, liver, heart or kidney diseases develop cachexia, while around 50% of cancer patients develop that syndrome, either as a direct consequence of the disease itself or as a consequence of treatment. Since cachexia cannot always be reversed by nutritional supplements, its underlying mechanism is different than that of an eating disorder, such as anorexia. Moreover, cachexia usually affects the loss of the muscular component of the body, while starvation initially initiates the loss of fat mass (Morley et al., 2006). The overall devastating impact of cachexia on patients with chronic diseases can not only reduce physical activities and quality of life but more importantly, can shorten survival (Farkas et al., 2013). Hence, developing effective treatments to reduce the progression of cachexia and muscle wasting disorders are essential clinical need to reduce disease burden and improve the quality of life and survival of the cancer patients and beyond. Twist1 promotes epithelial-mesenchymal transition, invasion, metastasis, and chemotherapy resistance in cancer cells and thus is a potential target for cancer therapy (Kang and Massague, 2004; Vernon and LaBonne, 2004; Yang et al., 2004; Lee et al., 2006; Yuen et al., 2007). Our recent identification of Twist1 as a master regulator of tumor-induced cachexia provides a promising therapeutic target to attenuate cachexia to improve cancer patient survival. In fact, pharmacological inactivation of the Twist1 function showed promising effects of protecting

cancer-induced cachexia, with a significant survival benefit in the experimental model of pancreatic carcinoma (Parajuli et al., 2018). Based on the inducible Twist1 knockout mice studies, it appears that Twist1 has rather a non-essential role in adult animals (Xu et al., 2013), and therefore, targeting Twist1 to manipulate tumor-induced cachexia would be a suitable drug target that is likely to exert minimal advert effects in adult patients. Further studies are needed to determine the effects of suppressing Twist1 function in muscle wasting diseases, in general.

AUTHOR CONTRIBUTIONS

MR and AA outlined and drafted the manuscript. Both authors contributed to the article and approved the submitted version.

ACKNOWLEDGMENTS

Thanks to Dr. Nuraly Akimbekov of Al-Farabi Kazakh National University (Kazakhstan) for help in drawing the illustration.

REFERENCES

Avin, K. G., Chen, N. X., Organ, J. M., Zarse, C., O'neill, K., Conway, R. G., et al. (2016). Skeletal muscle regeneration and oxidative stress are altered in chronic kidney disease. *PLoS One* 11:e0159411. doi: 10.1371/journal.pone.0159411

Bachmann, J., Heiligensetzer, M., Krakowski-Roosen, H., Buchler, M. W., Friess, H., and Martignoni, M. E. (2008). Cachexia worsens prognosis in patients with resectable pancreatic cancer. *J. Gastrointest. Surg.* 12, 1193–1201. doi: 10.1007/s11605-008-0505-z

Baracos, V. E., Martin, L., Korc, M., Guttridge, D. C., and Fearon, K. C. H. (2018). Cancer-associated cachexia. *Nat. Rev. Dis. Primers* 4:17105.

Benny Klimek, M. E., Aydogdu, T., Link, M. J., Pons, M., Koniaris, L. G., and Zimmers, T. A. (2010). Acute inhibition of myostatin-family proteins preserves skeletal muscle in mouse models of cancer cachexia. *Biochem. Biophys. Res. Commun.* 391, 1548–1554. doi: 10.1016/j.bbrc.2009.12.123

Bialek, P., Kern, B., Yang, X., Schrock, M., Sosic, D., Hong, N., et al. (2004). A twist code determines the onset of osteoblast differentiation. *Dev. Cell* 6, 423–435. doi: 10.1016/s1534-5807(04)00058-9

Cao, F., Wagner, R. A., Wilson, K. D., Xie, X., Fu, J. D., Drukker, M., et al. (2008). Transcriptional and functional profiling of human embryonic stem cell-derived cardiomyocytes. *PLoS One* 3:e3474. doi: 10.1371/journal.pone.0003474

Chen, J. L., Walton, K. L., Winbanks, C. E., Murphy, K. T., Thomson, R. E., Makanji, Y., et al. (2014). Elevated expression of activins promotes muscle wasting and cachexia. *FASEB J.* 28, 1711–1723. doi: 10.1096/fj.13-245894

Chen, Z. F., and Behringer, R. R. (1995). twist is required in head mesenchyme for cranial neural tube morphogenesis. *Genes Dev.* 9, 686–699. doi: 10.1101/gad.9.6.686

Clarke, B. A., Drujan, D., Willis, M. S., Murphy, L. O., Corpina, R. A., Burova, E., et al. (2007). The E3 Ligase MuRF1 degrades myosin heavy chain protein in dexamethasone-treated skeletal muscle. *Cell Metab.* 6, 376–385. doi: 10.1016/j.cmet.2007.09.009

Costelli, P., Muscaritoli, M., Bonetto, A., Penna, F., Reffo, P., Bossola, M., et al. (2008). Muscle myostatin signalling is enhanced in experimental cancer cachexia. *Eur. J. Clin. Invest.* 38, 531–538. doi: 10.1111/j.1365-2362.2008.01970.x

Crossland, H., Constantin-Teodosiu, D., Gardiner, S. M., Constantin, D., and Greenhaff, P. L. (2008). A potential role for Akt/FOXO signalling in both protein loss and the impairment of muscle carbohydrate oxidation during sepsis in rodent skeletal muscle. *J. Physiol.* 586, 5589–5600. doi: 10.1113/jphysiol.2008.160150

Davis, R. L., Weintraub, H., and Lassar, A. B. (1987). Expression of a single transfected cDNA converts fibroblasts to myoblasts. *Cell* 51, 987–1000. doi: 10.1016/0092-8674(87)90585-x

el Ghouzzi, V., Le Merrer, M., Perrin-Schmitt, F., Lajeunie, E., Benit, P., Renier, D., et al. (1997). Mutations of the TWIST gene in the Saethre-Chotzen syndrome. *Nat. Genet.* 15, 42–46.

Farkas, J., Von Haehling, S., Kalantar-Zadeh, K., Morley, J. E., Anker, S. D., and Lainscak, M. (2013). Cachexia as a major public health problem: frequent, costly, and deadly. *J. Cachexia Sarcopenia Muscle* 4, 173–178. doi: 10.1007/s13539-013-0105-y

Fearon, K., Strasser, F., Anker, S. D., Bosaeus, I., Bruera, E., Fainsinger, R. L., et al. (2011). Definition and classification of cancer cachexia: an international consensus. *Lancet Oncol.* 12, 489–495. doi: 10.1016/s1470-2045(10)70218-7

Fearon, K. C., Voss, A. C., and Hustead, D. S. (2006). Definition of cancer cachexia: effect of weight loss, reduced food intake, and systemic inflammation on functional status and prognosis. *Am. J. Clin. Nutr.* 83, 1345–1350. doi: 10.1093/ajcn/83.6.1345

Fong, Y., Moldawer, L. L., Marano, M., Wei, H., Barber, A., Manogue, K., et al. (1989). Cachectin/TNF or IL-1 alpha induces cachexia with redistribution of body proteins. *Am. J. Physiol.* 256, R659–R665.

Gallot, Y. S., Durieux, A. C., Castells, J., Desgeorges, M. M., Vernus, B., Plantureux, L., et al. (2014). Myostatin gene inactivation prevents skeletal muscle wasting in cancer. *Cancer Res.* 74, 7344–7356. doi: 10.1158/0008-5472.can-14-0057

Greco, S. H., Tomkotter, L., Vahle, A. K., Rokosh, R., Avanzi, A., Mahmood, S. K., et al. (2015). TGF-beta blockade reduces mortality and metabolic changes in a validated murine model of pancreatic cancer cachexia. *PLoS One* 10:e0132786. doi: 10.1371/journal.pone.0132786

Hebrok, M., Wertz, K., and Fuchtbauer, E. M. (1994). M-twist is an inhibitor of muscle differentiation. *Dev. Biol.* 165, 537–544. doi: 10.1006/dbio.1994.1273

Hjiantoniou, E., Anayasa, M., Nicolaou, P., Bantounas, I., Saito, M., Iseki, S., et al. (2008). Twist induces reversal of myotube formation. *Differentiation* 76, 182–192. doi: 10.1111/j.1432-0436.2007.00195.x

Howard, T. D., Paznekas, W. A., Green, E. D., Chiang, L. C., Ma, N., Ortiz De Luna, R. I., et al. (1997). Mutations in TWIST, a basic helix-loop-helix transcription factor, in Saethre-Chotzen syndrome. *Nat. Genet.* 15, 36–41. doi: 10.1038/ng0197-36

Huynh, T., Uaesoontrachoon, K., Quinn, J. L., Tatem, K. S., Heier, C. R., Van Der Meulen, J. H., et al. (2013). Selective modulation through the glucocorticoid receptor ameliorates muscle pathology in mdx mice. *J. Pathol.* 231, 223–235. doi: 10.1002/path.4231

Jatoi, A., Ritter, H. L., Dueck, A., Nguyen, P. L., Nikcevich, D. A., Luyun, R. F., et al. (2010). A placebo-controlled, double-blind trial of infliximab for cancer-associated weight loss in elderly and/or poor performance non-small cell lung cancer patients (N01C9). *Lung Cancer* 68, 234–239. doi: 10.1016/j.lungcan.2009.06.020

Kang, Y., and Massague, J. (2004). Epithelial-mesenchymal transitions: twist in development and metastasis. *Cell* 118, 277–279.

Kayacan, O., Karnak, D., Beder, S., Gullu, E., Tutkak, H., Senler, F. C., et al. (2006). Impact of TNF-alpha and IL-6 levels on development of cachexia in newly diagnosed NSCLC patients. *Am. J. Clin. Oncol.* 29, 328–335. doi: 10.1097/01.coc.0000221300.72657.e0

Koutalianos, D., Koutsoulidou, A., Mastroyiannopoulos, N. P., Furling, D., and Phylactou, L. A. (2015). MyoD transcription factor induces myogenesis by inhibiting Twist-1 through miR-206. *J. Cell Sci.* 128, 3631–3645. doi: 10.1242/jcs.172288

Koutsoulidou, A., Mastroyiannopoulos, N. P., Furling, D., Uney, J. B., and Phylactou, L. A. (2011). Endogenous TWIST expression and differentiation are opposite during human muscle development. *Muscle Nerve* 44, 984–986. doi: 10.1002/mus.22241

Lagirand-Cantaloube, J., Offner, N., Csibi, A., Leibovitch, M. P., Batonnet-Pichon, S., Tintignac, L. A., et al. (2008). The initiation factor eIF3-f is a major target for atrogin1/MAFbx function in skeletal muscle atrophy. *EMBO J.* 27, 1266–1276. doi: 10.1038/emboj.2008.52

Lee, K. E., and Bar-Sagi, D. (2010). Oncogenic KRas suppresses inflammation-associated senescence of pancreatic ductal cells. *Cancer Cell* 18, 448–458. doi: 10.1016/j.ccr.2010.10.020

Lee, S. J., and McPherron, A. C. (2001). Regulation of myostatin activity and muscle growth. *Proc. Natl. Acad. Sci. U.S.A.* 98, 9306–9311. doi: 10.1073/pnas.151270098

Lee, T. K., Poon, R. T., Yuen, A. P., Ling, M. T., Kwok, W. K., Wang, X. H., et al. (2006). Twist overexpression correlates with hepatocellular carcinoma metastasis through induction of epithelial-mesenchymal transition. *Clin. Cancer Res.* 12, 5369–5376. doi: 10.1158/1078-0432.ccr-05-2722

Leger, B., Senese, R., Al-Khodairy, A. W., Deriaz, O., Gobelet, C., Giacobino, J. P., et al. (2009). Atrogin-1, MuRF1, and FoXO, as well as phosphorylated GSK-3beta and 4E-BP1 are reduced in skeletal muscle of chronic spinal cord-injured patients. *Muscle Nerve* 40, 69–78. doi: 10.1002/mus.21293

Li, H. H., Willis, M. S., Lockyer, P., Miller, N., Mcdonough, H., Glass, D. J., et al. (2007). Atrogin-1 inhibits Akt-dependent cardiac hypertrophy in mice via ubiquitin-dependent coactivation of Forkhead proteins. *J. Clin. Invest.* 117, 3211–3223. doi: 10.1172/jci31757

Mak, R. H., Ikizler, A. T., Kovesdy, C. P., Raj, D. S., Stenvinkel, P., and Kalantar-Zadeh, K. (2011). Wasting in chronic kidney disease. *J. Cachexia Sarcopenia Muscle* 2, 9–25.

Mastroyiannopoulos, N. P., Antoniou, A. A., Koutsoulidou, A., Uney, J. B., and Phylactou, L. A. (2013). Twist reverses muscle cell differentiation through transcriptional down-regulation of myogenin. *Biosci. Rep.* 33:e00083.

Mattox, T. W. (2017). Cancer cachexia: cause, diagnosis, and treatment. *Nutr. Clin. Pract.* 32, 599–606. doi: 10.1177/0884533617722986

Milan, G., Romanello, V., Pescatore, F., Armani, A., Paik, J. H., Frasson, L., et al. (2015). Regulation of autophagy and the ubiquitin-proteasome system by the FoxO transcriptional network during muscle atrophy. *Nat. Commun.* 6:6670.

Morley, J. E. (2014). Chronic obstructive pulmonary disease: a disease of older persons. *J. Am. Med. Dir. Assoc.* 15, 151–153.

Morley, J. E., Thomas, D. R., and Wilson, M. M. (2006). Cachexia: pathophysiology and clinical relevance. *Am. J. Clin. Nutr.* 83, 735–743. doi: 10.1093/ajcn/83.4.735

Pan, D., Fujimoto, M., Lopes, A., and Wang, Y. X. (2009). Twist-1 is a PPARdelta-inducible, negative-feedback regulator of PGC-1alpha in brown fat metabolism. *Cell* 137, 73–86. doi: 10.1016/j.cell.2009.01.051

Parajuli, P., Kumar, S., Loumaye, A., Singh, P., Eragamreddy, S., Nguyen, T. L., et al. (2018). Twist1 activation in muscle progenitor cells causes muscle loss akin to cancer cachexia. *Dev. Cell.* 45, 712.e6–725.e6.

Pomies, P., Blaquiere, M., Maury, J., Mercier, J., Gouzi, F., and Hayot, M. (2016). Involvement of the FoxO1/MuRF1/Atrogin-1 signaling pathway in the oxidative stress-induced atrophy of cultured chronic obstructive pulmonary disease myotubes. *PLoS One* 11:e0160092. doi: 10.1371/journal.pone.0160092

Qin, Q., Xu, Y., He, T., Qin, C., and Xu, J. (2012). Normal and disease-related biological functions of Twist1 and underlying molecular mechanisms. *Cell Res.* 22, 90–106. doi: 10.1038/cr.2011.144

Reed, S. A., Sandesara, P. B., Senf, S. M., and Judge, A. R. (2012). Inhibition of FoxO transcriptional activity prevents muscle fiber atrophy during cachexia and induces hypertrophy. *FASEB J.* 26, 987–1000. doi: 10.1096/fj.11-189977

Reid, J., Noble, H. R., Porter, S., Shields, J. S., and Maxwell, A. P. (2013). A literature review of end-stage renal disease and cachexia: understanding experience to inform evidence-based healthcare. *J. Ren. Care* 39, 47–51. doi: 10.1111/j.1755-6686.2013.00341.x

Rigas, J. R., Schuster, M., Orlov, S. V., Milovanovic, B., Prabhash, K., and Smith, J. T. (2010). Efect of ALD518, a humanized anti-IL-6 antibody, on lean body mass loss and symptoms in patients with advanced non-small cell lung cancer (NSCLC): results of a phase II randomized, double-blind safety and efficacy trial. *J. Clin. Oncol.* 28(15_Suppl.):7622. doi: 10.1200/jco.2010.28.15_suppl.7622

Rohwedel, J., Horak, V., Hebrok, M., Fuchtbauer, E. M., and Wobus, A. M. (1995). M-twist expression inhibits mouse embryonic stem cell-derived myogenic differentiation in vitro. *Exp. Cell Res.* 220, 92–100. doi: 10.1006/excr.1995.1295

Rolfe, D. F., and Brown, G. C. (1997). Cellular energy utilization and molecular origin of standard metabolic rate in mammals. *Physiol. Rev.* 77, 731–758. doi: 10.1152/physrev.1997.77.3.731

Scherbakov, N., Von Haehling, S., Anker, S. D., Dirnagl, U., and Doehner, W. (2013). Stroke induced Sarcopenia: muscle wasting and disability after stroke. *Int. J. Cardiol.* 170, 89–94. doi: 10.1016/j.ijcard.2013.10.031

Scicchitano, B. M., Dobrowolny, G., Sica, G., and Musaro, A. (2018). Molecular insights into muscle homeostasis, atrophy and wasting. *Curr. Genomics* 19, 356–369. doi: 10.2174/1389202919666180101153911

Sengupta, A., Molkentin, J. D., and Yutzey, K. E. (2009). FoxO transcription factors promote autophagy in cardiomyocytes. *J. Biol. Chem.* 284, 28319–28331. doi: 10.1074/jbc.m109.024406

Souza, T. A., Chen, X., Guo, Y., Sava, P., Zhang, J., Hill, J. J., et al. (2008). Proteomic identification and functional validation of activins and bone morphogenetic protein 11 as candidate novel muscle mass regulators. *Mol. Endocrinol.* 22, 2689–2702. doi: 10.1210/me.2008-0290

Stitt, T. N., Drujan, D., Clarke, B. A., Panaro, F., Timofeyva, Y., Kline, W. O., et al. (2004). The IGF-1/PI3K/Akt pathway prevents expression of muscle atrophy-induced ubiquitin ligases by inhibiting FOXO transcription factors. *Mol. Cell.* 14, 395–403. doi: 10.1016/s1097-2765(04)00211-4

Strassmann, G., Masui, Y., Chizzonite, R., and Fong, M. (1993). Mechanisms of experimental cancer cachexia. Local involvement of IL-1 in colon-26 tumor. *J. Immunol.* 150, 2341–2345.

Tan, B. H., Birdsell, L. A., Martin, L., Baracos, V. E., and Fearon, K. C. (2009). Sarcopenia in an overweight or obese patient is an adverse prognostic factor in pancreatic cancer. *Clin. Cancer Res.* 15, 6973–6979. doi: 10.1158/1078-0432.ccr-09-1525

Thakur, S. S., Swiderski, K., Ryall, J. G., and Lynch, G. S. (2018). Therapeutic potential of heat shock protein induction for muscular dystrophy and other muscle wasting conditions. *Philos. Trans. R. Soc. Lond. B Biol. Sci.* 373:20160528. doi: 10.1098/rstb.2016.0528

Thisse, B., El Messal, M., and Perrin-Schmitt, F. (1987). The twist gene: isolation of a *Drosophila* zygotic gene necessary for the establishment of dorsoventral pattern. *Nucleic Acids Res.* 15, 3439–3453. doi: 10.1093/nar/15.8.3439

Tisdale, M. J. (2010). Reversing cachexia. *Cell* 142, 511–512. doi: 10.1016/j.cell.2010.08.004

Vernon, A. E., and LaBonne, C. (2004). Tumor metastasis: a new twist on epithelial-mesenchymal transitions. *Curr. Biol.* 14, R719–R721.

Villain, C., Ecochard, R., Genet, L., Jean, G., Kuentz, F., Lataillade, D., et al. (2015). Impact of BMI variations on survival in elderly hemodialysis patients. *J. Ren. Nutr.* 25, 488–493. doi: 10.1053/j.jrn.2015.05.004

von Haehling, S., Ebner, N., Dos Santos, M. R., Springer, J., and Anker, S. D. (2017). Muscle wasting and cachexia in heart failure: mechanisms and therapies. *Nat. Rev. Cardiol.* 14, 323–341. doi: 10.1038/nrcardio.2017.51

Waddell, D. S., Baehr, L. M., Van Den Brandt, J., Johnsen, S. A., Reichardt, H. M., Furlow, J. D., et al. (2008). The glucocorticoid receptor and FOXO1 synergistically activate the skeletal muscle atrophy-associated MuRF1 gene. *Am. J. Physiol. Endocrinol. Metab.* 295, E785–E797.

Wang, S. M., Coljee, V. W., Pignolo, R. J., Rotenberg, M. O., Cristofalo, V. J., and Sierra, F. (1997). Cloning of the human twist gene: its expression is retained in adult mesodermally-derived tissues. *Gene* 187, 83–92. doi: 10.1016/s0378-1119(96)00727-5

White, J. P. (2017). IL-6, cancer and cachexia: metabolic dysfunction creates the perfect storm. *Transl. Cancer Res.* 6, S280–S285.

Wildi, S., Kleeff, J., Maruyama, H., Maurer, C. A., Buchler, M. W., and Korc, M. (2001). Overexpression of activin A in stage IV colorectal cancer. *Gut* 49, 409–417. doi: 10.1136/gut.49.3.409

Williams, M. J., Sugatani, T., Agapova, O. A., Fang, Y., Gaut, J. P., Faugere, M. C., et al. (2018). The activin receptor is stimulated in the skeleton, vasculature, heart, and kidney during chronic kidney disease. *Kidney Int.* 93, 147–158. doi: 10.1016/j.kint.2017.06.016

Wolf, C., Thisse, C., Stoetzel, C., Thisse, B., Gerlinger, P., and Perrin-Schmitt, F. (1991). The M-twist gene of Mus is expressed in subsets of mesodermal cells and is closely related to the *Xenopus* X-twi and the *Drosophila* twist genes. *Dev. Biol.* 143, 363–373. doi: 10.1016/0012-1606(91)90086-i

Xu, J., Li, R., Workeneh, B., Dong, Y., Wang, X., and Hu, Z. (2012). Transcription factor FoxO1, the dominant mediator of muscle wasting in chronic kidney disease, is inhibited by microRNA-486. *Kidney Int.* 82, 401–411. doi: 10.1038/ki.2012.84

Xu, Y., Lee, D. K., Feng, Z., Bu, W., Li, Y., Liao, L., et al. (2017). Breast tumor cell-specific knockout of Twist1 inhibits cancer cell plasticity, dissemination, and lung metastasis in mice. *Proc. Natl. Acad. Sci. U.S.A.* 114, 11494–11499. doi: 10.1073/pnas.1618091114

Xu, Y., Liao, L., Zhou, N., Theissen, S. M., Liao, X. H., Nguyen, H., et al. (2013). Inducible knockout of Twist1 in young and adult mice prolongs hair growth cycle and has mild effects on general health, supporting Twist1 as a preferential

cancer target. *Am. J. Pathol.* 183, 1281–1292. doi: 10.1016/j.ajpath.2013.06.021

Yang, J., Mani, S. A., Donaher, J. L., Ramaswamy, S., Itzykson, R. A., Come, C., et al. (2004). Twist, a master regulator of morphogenesis, plays an essential role in tumor metastasis. *Cell* 117, 927–939. doi: 10.1016/j.cell.2004.06.006

Yuen, H. F., Chan, Y. P., Wong, M. L., Kwok, W. K., Chan, K. K., Lee, P. Y., et al. (2007). Upregulation of Twist in oesophageal squamous cell carcinoma is associated with neoplastic transformation and distant metastasis. *J. Clin. Pathol.* 60, 510–514. doi: 10.1136/jcp.2006.039099

Zhang, A., Li, M., Wang, B., Klein, J. D., Price, S. R., and Wang, X. H. (2018). miRNA-23a/27a attenuates muscle atrophy and renal fibrosis through muscle-kidney crosstalk. *J. Cachexia Sarcopenia Muscle* 9, 755–770. doi: 10.1002/jcsm.12296

Zhang, L., Rajan, V., Lin, E., Hu, Z., Han, H. Q., Zhou, X., et al. (2011). Pharmacological inhibition of myostatin suppresses systemic inflammation and muscle atrophy in mice with chronic kidney disease. *FASEB J.* 25, 1653–1663. doi: 10.1096/fj.10-176917

Zhong, X., Pons, M., Poirier, C., Jiang, Y., Liu, J., Sandusky, G. E., et al. (2019). The systemic activin response to pancreatic cancer: implications for effective cancer cachexia therapy. *J. Cachexia Sarcopenia Muscle* 10, 1083–1101. doi: 10.1002/jcsm.12461

Zhou, X., Wang, J. L., Lu, J., Song, Y., Kwak, K. S., Jiao, Q., et al. (2010). Reversal of cancer cachexia and muscle wasting by ActRIIB antagonism leads to prolonged survival. *Cell* 142, 531–543. doi: 10.1016/j.cell.2010.07.011

Conflict of Interest: The authors declare that the research was conducted in the absence of any commercial or financial relationships that could be construed as a potential conflict of interest.

frontiers in Physiology

REVIEW
published: 24 June 2020
doi: 10.3389/fphys.2020.00624

Genetic Animal Models for Arrhythmogenic Cardiomyopathy

Brenda Gerull[1,2*†] *and Andreas Brodehl*[3†]

[1] Comprehensive Heart Failure Center Wuerzburg, Department of Internal Medicine I, University Hospital Würzburg, Würzburg, Germany, [2] Department of Cardiac Sciences, Libin Cardiovascular Institute of Alberta, University of Calgary, Calgary, AB, Canada, [3] Erich and Hanna Klessmann Institute for Cardiovascular Research and Development, Heart and Diabetes Center NRW, University Hospitals of the Ruhr-University of Bochum, Bad Oeynhausen, Germany

Arrhythmogenic cardiomyopathy has been clinically defined since the 1980s and causes right or biventricular cardiomyopathy associated with ventricular arrhythmia. Although it is a rare cardiac disease, it is responsible for a significant proportion of sudden cardiac deaths, especially in athletes. The majority of patients with arrhythmogenic cardiomyopathy carry one or more genetic variants in desmosomal genes. In the 1990s, several knockout mouse models of genes encoding for desmosomal proteins involved in cell–cell adhesion revealed for the first time embryonic lethality due to cardiac defects. Influenced by these initial discoveries in mice, arrhythmogenic cardiomyopathy received an increasing interest in human cardiovascular genetics, leading to the discovery of mutations initially in desmosomal genes and later on in more than 25 different genes. Of note, even in the clinic, routine genetic diagnostics are important for risk prediction of patients and their relatives with arrhythmogenic cardiomyopathy. Based on improvements in genetic animal engineering, different transgenic, knock-in, or cardiac-specific knockout animal models for desmosomal and nondesmosomal proteins have been generated, leading to important discoveries in this field. Here, we present an overview about the existing animal models of arrhythmogenic cardiomyopathy with a focus on the underlying pathomechanism and its importance for understanding of this disease. Prospectively, novel mechanistic insights gained from the whole animal, organ, tissue, cellular, and molecular levels will lead to the development of efficient personalized therapies for treatment of arrhythmogenic cardiomyopathy.

Keywords: arrhythmogenic cardiomyopathy, desmosomes, animal models of human disease, sudden death, genetics, mouse, zebrafish

OPEN ACCESS

Edited by:
Martina Calore,
Maastricht University, Netherlands

Reviewed by:
Beata M. Wolska,
University of Illinois at Chicago, United States
Michelle S. Parvatiyar,
Florida State University, United States
Marina Cerrone,
New York University School of Medicine, United States

****Correspondence:***
Brenda Gerull
gerull_b@ukw.de

†ORCID:
Brenda Gerull
orcid.org/0000-0002-1363-8826
Andreas Brodehl
orcid.org/0000-0001-9202-2343

Specialty section:
This article was submitted to Striated Muscle Physiology, a section of the journal Frontiers in Physiology

Received: *18 March 2020*
Accepted: *18 May 2020*
Published: *24 June 2020*

Citation:
Gerull B and Brodehl A (2020) Genetic Animal Models for Arrhythmogenic Cardiomyopathy. Front. Physiol. 11:624. doi: 10.3389/fphys.2020.00624

INTRODUCTION

Arrhythmogenic cardiomyopathy (ACM) is a genetic cardiomyopathy characterized by ventricular arrhythmia often leading to sudden cardiac death in young people. Ventricular dysfunction often develops with progression of the disease leading to heart failure in some cases (Sen-Chowdhry and McKenna, 2010). ACM is frequently associated with fibro-fatty replacement of the myocardium (Slesnick et al., 2019). For a long time, the disease was referred to as arrhythmogenic right ventricular cardiomyopathy (ARVC) because the phenotype description was more focused on features of the right ventricle; however, increasing awareness of left ventricular and biventricular involvement led to the term "ACM" (Sen-Chowdhry et al., 2010). Because of the broad spectrum

of ACM-related phenotypes sometimes overlapping with other cardiomyopathies, we follow in this review the recommendations of the Heart Rhythm Society (HRS) and focus on the genetic etiology of this disease (Protonotarios and Elliott, 2019; Towbin et al., 2019). The estimated prevalence of ACM is 1 in between 1000 and 5000 (Basso et al., 2009).

Discovery of genetic causes of ACM started with two recessive cardio-cutaneous syndromes named Naxos disease and Carvajal syndrome (McKoy et al., 2000; Norgett et al., 2000), which guided the discovery of autosomal dominant inherited nonsyndromic cardiomyopathy in the direction of disturbed cell–cell adhesion, in particular desmosomes (**Figure 1**). Pathogenic mutations in genes encoding desmosomal proteins account for about 50% of the genetic etiology (Klauke et al., 2010; Gandjbakhch et al., 2013). However, genetic mutations in additional genes expressed in different subcellular systems have been discovered by various genetic approaches, indicating extensive genetic heterogeneity (**Figure 1**).

Moreover, genetic findings brought up that the same gene, and sometimes even the same genetic variant, can be causative for a wide range of clinical features, indicating that disease entities are indistinct or clinically overlapping. For ACM, the clinical overlap occurs in particular with dilated cardiomyopathy (DCM) with which, sometimes, ventricular arrhythmia are the predominant phenotype and also with primary arrhythmia syndromes such as Brugada syndrome, in which a potential structural phenotype may not be overt at the time of presentation (Cerrone et al., 2014; Zegkos et al., 2020). In addition, it became more and more evident that not only the primary genetic cause, but also many other factors, such as environment, comorbidities, age, genetic background, and epigenetic factors, are contributing to disease onset, progression, and prognosis in patients with ACM (Bondue et al., 2018). Therefore, animal models provide a defined genetic background and are suitable to study the cause of disease as well as confounding variables under controlled and standardized conditions.

On the other hand, animal models also have several limitations when applied to mimic human cardiac disease, in particular the commonly used mouse and zebrafish models. For example, neither mice nor zebrafish develop cardiac fatty tissue, which is a hallmark for human ACM. Mice seem to be less prone to genetic defects affecting the heart, which often requires homozygous (recessive) models for mutations appearing heterozygous (dominant) in humans. Even more limited is the two-chamber heart of the zebrafish, which regenerates and may not be an ideal system to mimic specific aspects (e.g., right ventricular involvement) of ACM but has some advantages to study electrophysiology (Vornanen and Hassinen, 2016). Despite those limitations, animal models have contributed to a better understanding of the pathophysiology and molecular pathways leading to cardiomyopathy and the susceptibility to arrhythmia. Initially, often the animal model was used to analyze the pathological effect of a gene with consequences for the whole organism, the organ, and at the cellular and molecular levels. The discovery of cardiac phenotypes in animal models followed by a forward genetic approach led to identification of the genetic defect in the underlying human disease (Gerull et al., 2004; Grossmann et al., 2004). With the advances in genetic technology, often the disease gene in humans was first identified and subsequently modeled according to the mutation and proposed genetic mechanism (Heuser et al., 2006; Brodehl et al., 2019d). In this review, we evaluate the current state of animal models for ACM according to the proposed human disease–associated genes (**Figure 1**) and briefly discuss relevant mechanistic insights and limitations obtained from these studies. Some genes are more established than others or display a broad spectrum of phenotypes as part of an overlap syndrome. In particular, in the latter, we focus on models of mutations that have been associated with the ACM phenotype or representing a general mechanistic concept.

ANIMAL MODELS FOR ACM ASSOCIATED WITH MUTATIONS IN DESMOSOMAL GENES

Desmosomes are multiple protein complexes mediating cell–cell adhesion (Patel and Green, 2014). Especially in tissue exposed to mechanical forces, such as the skin and the heart during contraction, they have an important function for structural integrity. In addition, desmosomes are indirectly involved in the electrochemical coupling of cardiomyocytes (Cerrone and Delmar, 2014) and in signal transduction (Zhao et al., 2019). The molecular composition between cardiac and dermal desmosomes differs significantly (Goossens et al., 2007). For example, in the skin, all three plakophilins 1–3 are expressed, whereas cardiomyocytes express exclusively plakophilin-2[1]. Proteins from three different families build the desmosomes. In myocardial tissue, two desmosomal cadherins, desmocollin-2 and desmoglein-2 (encoded by *DSC2* and *DSG2*), mediate the intercellular, Ca^{2+}-dependent adhesion (Harrison et al., 2016; **Figure 2**). The Ca^{2+} ion binding sites are localized in linker regions between the extracellular cadherin domains and are formed by aspartate and glutamate residues (Harrison et al., 2016). Both cadherins are type-I transmembrane proteins and carry several N-glycosylations and O-mannosylations in their extracellular domains (Harrison et al., 2016; Brodehl et al., 2019e; Debus et al., 2019). Their extracellular parts consist of five extracellular cadherin domains (ECD), mainly formed by β-sheets. Their first ECDs mediate this protein–protein interaction in *trans* position. Homophilic interactions between the desmosomal cadherins have relative high dissociation constants ($K_D > 400\ \mu M$), whereas heterophilic interactions have higher affinities ($K_D < 40\ \mu M$) (Harrison et al., 2016; Dieding et al., 2017). The intracellular domains of the desmosomal cadherins are bound in the heart by two proteins from the Armadillo family, which are called plakoglobin and plakophilin-2 (encoded by *JUP* and *PKP2*) (Chen et al., 2002; **Figure 2**). Central Armadillo domains consisting of several Armadillo repeats formed by a hairpin of two α-helices are the typical structural feature of these proteins (Choi et al., 2009; Kirchner et al., 2012). Plakoglobin and plakophilin-2 mediate the molecular

[1]https://www.proteinatlas.org/

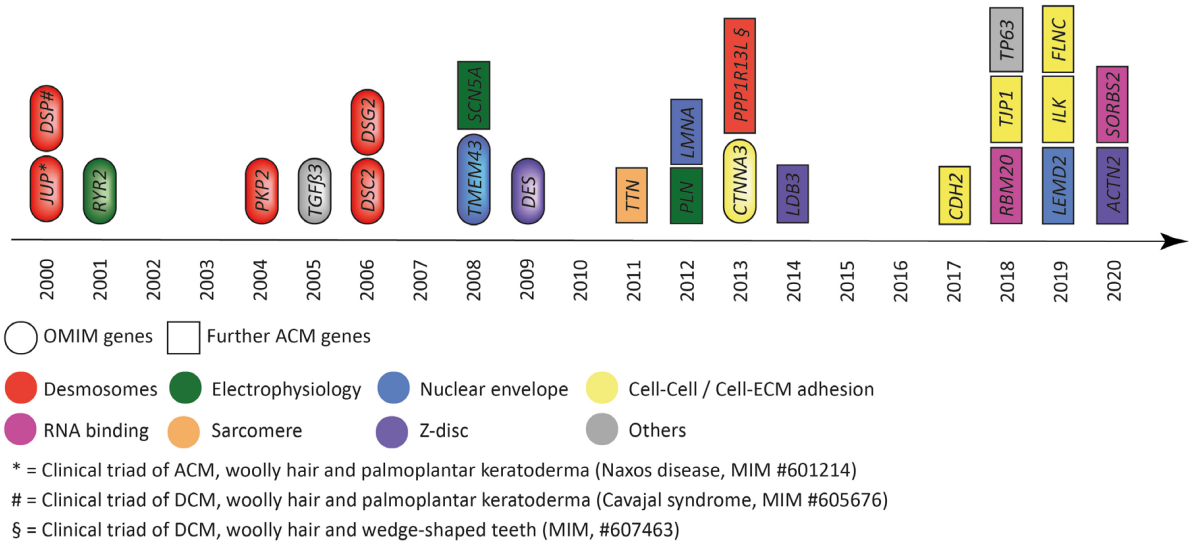

FIGURE 1 | Genes associated with arrhythmogenic cardiomyopathy according to the year of discovery. Colors indicate the subcellular location and/or functional association. Eclipses indicate genes listed by the Online Mendelian Inheritance in the Man (OMIM) database. Squares indicate further genes associated with arrhythmogenic cardiomyopathy. *JUP* = plakoglobin, *DSP* = desmoplakin, *RYR2* = ryanodine receptor-2, *PKP2* = plakophilin-2, *TGFβ3* = transforming growth factor β3, *DSC2* = desmocollin-2, *DSG2* = desmoglein-2, *TMEM43* = transmembrane protein member-43, *SCN5A* = sodium voltage-gated channel subunit 5α, *DES* = desmin, *TTN* = titin, *PLN* = phospholamban, *LMNA* = lamin A/C, *CTNNA3* = αT-catenin, *PPP1R13L* = protein phosphatase 1 regulatory subunit 13 like, *LDB3* = LIM domain binding 3, *CDH2* = N-cadherin, *RBM20* = RNA binding motif protein 20, *TJP1* = tight junction protein-1, *TP63* = tumor protein-63, *LEMD2* = LEM-domain containing protein-2, *SORBS2* = sorbin and SH3 domain containing protein-2, *ILK* = integrin linked kinase, *FLNC* = filamin-C, *ACTN2* = actinin α2, *SORBS2* = sorbin, and SH3 = domain containing protein-2.

interactions with the cytolinker protein desmoplakin (encoded by *DSP*) (Hofmann et al., 2000). Desmoplakin forms dimers and links the desmosomes to the intermediate filaments (IF), which consist in the heart mainly of the muscle-specific IF-protein desmin (encoded by *DES*) (Lapouge et al., 2006; Hatzfeld et al., 2017; **Figure 2**).

In the 1990s, the relevance of desmosomal genes for ACM was recognized by the attempt to generate global knockout mice. Independently, the groups of Kemler and Birchmeier demonstrated that global *Jup* deficiency causes embryonic lethality in mice due to severe cardiac defects (Bierkamp et al., 1996; Ruiz et al., 1996; **Figure 3** and **Supplementary Tables 1**, **2**). The number of cardiac desmosomes was significantly reduced in the *Jup*-deficient embryos. Correspondingly, it was also shown that the global knockout of *Dsp*, *Dsg2*, and *Pkp2* causes embryonic lethality in mice due to severe heart defects (Gallicano et al., 1998; Eshkind et al., 2002; Grossmann et al., 2004). Of note, these initial findings stimulated the human cardiovascular genetic field significantly. In consequence, genetic analyses of human-related ACM patients revealed pathogenic mutations in the desmosomal genes *JUP* (McKoy et al., 2000), *DSP* (Norgett et al., 2000), *PKP2* (Gerull et al., 2004), *DSG2* (Awad et al., 2006; Pilichou et al., 2006), and *DSC2* (Heuser et al., 2006; Syrris et al., 2006; **Figure 1**). Patients carrying a homozygous 2-bp *JUP* deletion presented, in addition to ACM, also wooly hair and palmoplantar keratoderma. Because these patients were from the Greek island Naxos, this clinical triad is also known as Naxos disease (MIM, #601214) (Protonotarios and Tsatsopoulou, 2006). Patients with pathogenic mutations in the *DSP* gene frequently presented with a comparable triad of clinical features consisting of DCM, wooly hair, and palmoplantar keratoderma, which is known as Carvajal syndrome (MIM, #605676) (Protonotarios and Tsatsopoulou, 2004). An additional skeletal muscle myopathy can contribute to the phenotype of patients with mutations in *DES* or *FLNC* (Klauke et al., 2010; Verdonschot et al., 2020).

In conclusion, initial findings in mice and humans led to the hypothesis that ACM is mainly a disease of cardiac desmosomes supported by the fact that about 50% of ACM patients carry one or multiple mutations in desmosomal genes (Xu et al., 2010). Despite the stimulating effects for human cardiovascular genetics, embryonic lethality associated with global desmosomal gene deficiency limited the molecular analyses of the underlying pathomechanisms involved in ACM. Cellular models, including cardiomyocytes derived from human-induced pluripotent stem cells (hiPSC), might be an alternative approach for *in vitro* analyses (for a review about hiPSC ACM models, see Brodehl et al. (2019a). In addition, different transgenic, knock-in (KI), and conditional cardiac-specific mouse models for the desmosomal genes have been developed to overcome embryonic lethality (**Figure 3** and **Supplementary Tables 1**, **2**). Different animal studies revealed that the number of cardiac desmosomes is decreased. In addition, the ultrastructure of the cardiac desmosomes is also significantly changed (Heuser et al., 2006). Both effects might contribute to a widening of the intercalated disc. In consequence, the electrical coupling of adhesive cardiomyocytes through gap junctions might be indirectly affected, which can explain an increased risk for ventricular arrhythmia in ACM patients. This hypothesis is

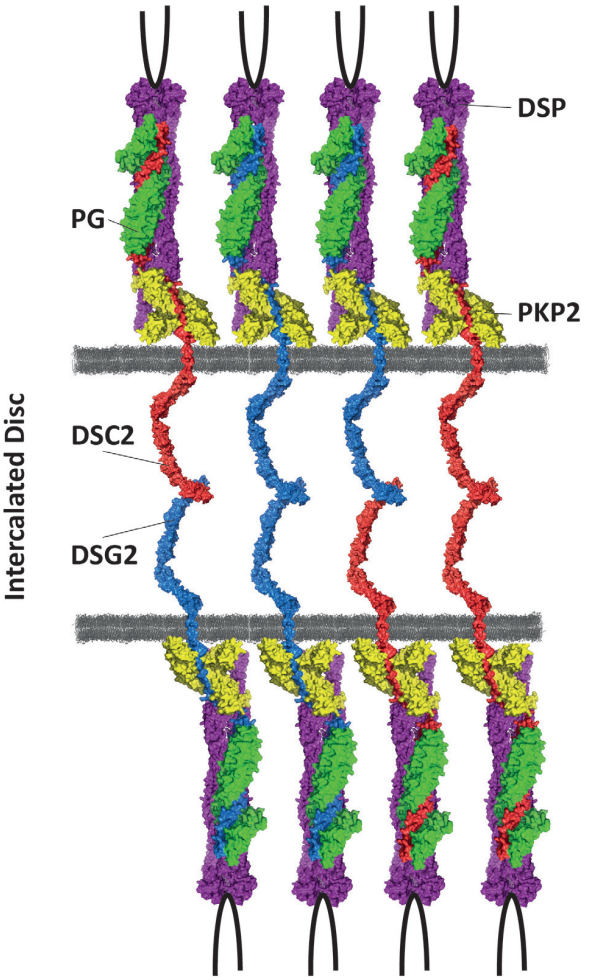

FIGURE 2 | Schematic overview of cardiac desmosomes. DSC2 = desmocollin-2, DSG2 = desmoglein-2, PKP2 = plakophilin-2, PG = plakoglobin, DSP = desmoplakin.

in good agreement with studies demonstrating a remarkable mislocalization of connexin-43 at the intercalated disc, which is the main cardiac gap junction protein (Gomes et al., 2012). More recently, molecular and functional crosstalk between plakophilin-2 and the voltage-gated sodium channel complex was discovered, indicating that the sodium channel current is decreased (Agullo-Pascual et al., 2013, 2014; Cerrone and Delmar, 2014).

In summary, the electrophysiological pathomechanisms caused by defects in desmosomal proteins are complex and still a matter of debate. Presumably, genetic, biochemical and electrophysiological changes contribute in combination to the complex disease phenotype of ACM.

Plakoglobin

In general, there is still an ongoing debate about if a loss-of-function (LOF) pathomechanism or a toxic effect of mutant plakoglobin is involved in ACM. More than 50 different rare human *JUP* variants are currently listed in the Human Gene Mutation Database (HGMD[2]) (Krawczak et al., 2000). For several of the known *JUP* missense variants, the significance is unknown, or they are even classified as (likely) benign. However, homozygous truncating mutations in *JUP* are almost certainly pathogenic (McKoy et al., 2000). To overcome the embryonic lethality of global *Jup* deficiency in mice, additional mice and zebrafish models have been generated (**Figure 3** and **Supplementary Tables 1**, **2**). Kirchhof and colleagues demonstrated that even heterozygous global *Jup* knockout mice developed right ventricular dilation, ventricular arrhythmia, and decreased right ventricular function without developing structural defects (Kirchhof et al., 2006; Fabritz et al., 2011). Interestingly, exercise strengthened and accelerated cardiac disease manifestation. For endurance training, the authors used a swimming approach over 8 weeks with an increasing time period (5–90 min) and observed an increased right ventricular dilation and dysfunction after 6 months (Kirchhof et al., 2006). In good agreement, knockdown via injection of morpholino oligonucleotides induced a cardiac phenotype consisting of cardiac edema, decreased heart size, and blood reflux between the two cardiac chambers in zebrafish (*Danio rerio*) (Martin et al., 2009). In addition, cardiac-specific or inducible cardiac-specific plakoglobin-deficient mice developed severe cardiac fibrosis in combination with cardiac dysfunction, ventricular arrhythmia, and dilation (Li et al., 2011; Li et al., 2011). These findings support an LOF pathomechanism for *JUP* mutations involved in ACM. In contrast, transgenic mice with a cardiac-specific overexpression of mutant or even wild-type plakoglobin under the control of the cardiac-specific *Myh6* promotor caused an increased mortality in mice (Lombardi et al., 2011). Likewise, transgenic zebrafish with an overexpression of mutant plakoglobin developed a comparable phenotype (Asimaki et al., 2014). In 2015, the Chen's group generated two remarkably different KI *Jup* mice, carrying a 2-bp deletion in exon 11 leading to a frame shift (*Jup*-c.2037-2038del) (Zhang et al., 2015). Regular knock-in mice died shortly after birth and showed decreased myocardial expression of mutant plakoglobin in comparison to the wild-type control mice, indicating that nonsense-mediated mRNA-decay (NMD) might be involved. Exon–exon junction complexes are involved in NMD (Dyle et al., 2020). In the second KI mice, carrying exactly the same 2-bp deletion in *Jup,* the introns 10–14 were deleted to block genetically NMD. Of note, this procedure rescued the expression of mutant and truncated plakoglobin and prevented the development of an ACM phenotype in these mice, supporting a clear LOF pathomechanism (Zhang et al., 2015). In conclusion, different animal models demonstrate that a balanced homeostasis of plakoglobin is necessary for normal cardiac function. There are several arguments that properties of pathogenic mutations in *JUP* might be caused by LOF. However, it cannot be completely excluded that *JUP* mutations have, in addition, toxic effects.

Desmoplakin

According to the HGMD, currently, nearly 200 different human cardiomyopathy-causing *DSP* mutations are known. In 5%–10% of all ACM patients, a pathogenic *DSP* mutation can be identified

[2]https://portal.biobase-international.com/hgmd/

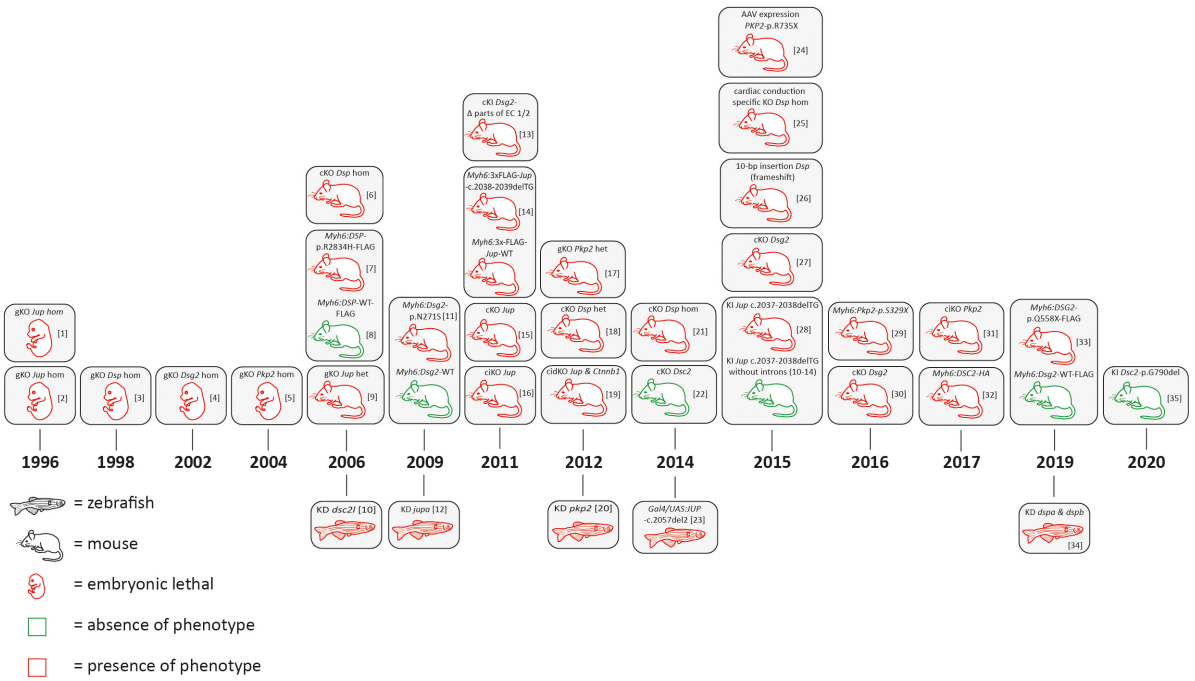

FIGURE 3 | Schematic overview of animal models for desmosomal genes according to the year of publication. AAV = adeno associated virus; bp = base pair, cKO = cardiac specific knockout; ciKO = cardiac specific, inducible knockout; cidKO = cardiac specific, inducible double knockout; gKO = global knockout; het = heterozygous; hom = homozygous; KD = knockdown; KI = knock-in. [1] (Ruiz et al., 1996); [2] (Bierkamp et al., 1996); [3] (Gallicano et al., 1998); [4] (Eshkind et al., 2002); [5] (Grossmann et al., 2004); [6] (Garcia-Gras et al., 2006; Cheedipudi et al., 2019); [7] (Yang et al., 2006); [8] (Kirchhof et al., 2006; Fabritz et al., 2011); [9] (Heuser et al., 2006); [10] (Pilichou et al., 2009; Rizzo et al., 2012); [11] (Martin et al., 2009); [12] (Krusche et al., 2011; Kant et al., 2012; Buck et al., 2018); [13] (Lombardi et al., 2011); [14] (Li et al., 2011); [15] (Li et al., 2011); [16] (Cerrone et al., 2012; Leo-Macias et al., 2015); [17] (Gomes et al., 2012); [18] (Swope et al., 2012); [19] (Moriarty et al., 2012); [20] (Lyon et al., 2014); [21] (Rimpler, 2014); [22] (Asimaki et al., 2014); [23] (Cruz et al., 2015); [24] (Mezzano et al., 2016); [25] (Herbert Pratt et al., 2015); [26] (Kant et al., 2015); [27] (Zhang et al., 2015); [28] (Moncayo-Arlandi et al., 2016); [29] (Chelko et al., 2016); [30] (Cerrone et al., 2017); [31] (Brodehl et al., 2017); [32] (Calore et al., 2019); [33] (Giuliodori et al., 2018); [34] (Hamada et al., 2020).

(Gerull et al., 2019). Homozygous and heterozygous truncating mutations spread over the total *DSP* length are common. In contrast to plakoglobin, the cardiac-specific overexpression of the wild-type desmoplakin is not toxic (Yang et al., 2006; **Figure 3**). However, transgenic mice with cardiac-specific overexpression of mutant desmoplakin (*Myh6:DSP*-p.R2834H-FLAG) developed cardiac fibrosis and apoptosis, leading to ventricular dilation in combination with cardiac dysfunction and ultrastructural changes of the intercalated disc (Yang et al., 2006). On the other hand, an LOF pathomechanism for *DSP* mutations is supported by generation and characterization of cardiac-specific *Dsp* deficient mice, which causes the homozygous status embryonic lethality (Garcia-Gras et al., 2006). Heterozygous, cardiac-specific *Dsp* knockout mice developed fibro-fatty replacement of the myocardium and increased cardiomyocyte death, leading to cardiac dysfunction and ventricular arrhythmia supporting haploinsufficiency as the underlying pathomechanism (Garcia-Gras et al., 2006). Interestingly, genes encoding inhibitors of the WNT pathway and inflammatory proteins were differently expressed in these mice (Cheedipudi et al., 2019). Knockdown of *dspa* and *dspb* in zebrafish using morpholino injections showed, in good agreement, altered WNT, TGFβ, and Hippo/YAP-TAZ signaling (Giuliodori et al., 2018). Downregulation of connexins, which are the protein building blocks of the gap junctions, was described in heterozygous and homozygous cardiac specific *Dsp*-deficient mice (Gomes et al., 2012; Lyon et al., 2014). In 2015, Mezzano et al. generated a mouse model with a cardiac conduction system–specific *Dsp* ablation, revealing the impact of desmoplakin for the cardiac pacemaker function (Mezzano et al., 2016). As human *DSP* mutations also cause Carvajal syndrome in addition to isolated ACM, a spontaneous homozygous Dsp^{rul} mouse model deserves attention. Dsp^{rul} mice carry a spontaneous 10-bp insertion, leading to a frame shift and, consequently, to a premature termination codon in the C-terminal part of desmoplakin. These mice developed abnormal coat and epidermal blistering and presented, in addition, electrophysiological alterations and cardiac fibrosis (Herbert Pratt et al., 2015). In summary, the majority of animal models demonstrate an LOF mechanism for *DSP*, which is, moreover, supported in humans by the relatively high amount (5%–10%) of pathogenic truncating *DSP* mutations associated with an ACM phenotype.

Plakophilin-2

Mutations in *PKP2* are common in ACM, and more than 250 different pathogenic mutations spread over the whole sequence are listed currently in the HGMD. The majority of *PKP2* mutations are truncating mutations although also

pathogenic missense mutations are known (Kirchner et al., 2012). Presumably, haploinsufficiency is the major pathomechanism caused by *PKP2* mutations (Kirchner et al., 2012; Rasmussen et al., 2014). However, even a homozygous deletion of *PKP2* was described in two siblings of a consanguineous family. Both siblings presented severe left-ventricular noncompaction cardiomyopathy (LVNC) instead of ACM (Ramond et al., 2017). Several different animal models support the concept of *PKP2* haploinsufficiency (**Figure 3**). Knockdown of *pkp2* in zebrafish caused cardiac edema, incomplete heart looping, and a decreased heart rate. The structure of the cardiac desmosomes was, moreover, altered in these zebrafish (Moriarty et al., 2012). Because homozygous global *Pkp2* deficiency is embryonically lethal in mice (Grossmann et al., 2004), heterozygous *Pkp2*-deficient mice were used for functional analyses (Cerrone et al., 2012; Leo-Macias et al., 2015). Although no histological phenotype was present in the heterozygous animals, they developed electrophysiological abnormalities and ultrastructural defects (Cerrone et al., 2012; Leo-Macias et al., 2015). However, two overexpression models of truncated plakophilin-2 might indicate a toxic effect in mice (Cruz et al., 2015; Moncayo-Arlandi et al., 2016). Cruz et al. used adeno-associated viruses (AAVs) to express mutant truncated plakophilin-2 (p.R375X). In combination with exercise, this overexpression led to right-ventricular dysfunction. Those findings are similar to a transgenic mouse model with a cardiac-specific overexpression of Pkp2-p.S329X. Although, no fibro-fatty replacement was present in these transgenic mice, electrophysiological abnormalities and ultrastructural defects were present. In addition, a decreased expression of the other desmosomal proteins and remodeling of connexin-43 was found (Moncayo-Arlandi et al., 2016). Recently, Cerrone et al. developed a cardiac-specific inducible *Pkp2* mice line presenting decreased ventricular function, severe cardiac fibrosis, and arrhythmia. Interestingly, remodeling of genes involved in Ca^{2+} handling was found using this mouse model (Cerrone et al., 2017). Overall, it may be summarized that there is high evidence that *Pkp2* haploinsufficiency is involved in the ACM-associated pathomechanism.

Desmoglein-2 and Desmocollin-2

Heterozygous and homozygous pathogenic mutations in *DSG2* and *DSC2*, encoding the two cardiac desmosomal cadherins, have been identified in human ACM patients responsible for about 5% of cases (Gerull et al., 2019; Brodehl et al., 2020). Using morpholino oligonucleotide injections, Heuser et al. knocked down *dsc2l* in zebrafish larvae causing cardiac edema, decreased fractional shortening, and altered desmosomal structure (Heuser et al., 2006). In contrast, homozygous conditional *Dsc2*-deficient mice were, under normal housing conditions, vital and did not develop cardiac dysfunction or show an increased mortality (Rimpler, 2014). Interestingly, homozygous knock-in mice carrying *Dsc2*-p.G790del did not develop a cardiac phenotype (Hamada et al., 2020). However, cardiac-specific overexpression of wild-type desmocollin-2 causes severe biventricular cardiomyopathy, including severe fibrotic scar formation, cardiac necrosis, calcification, and aseptic inflammation (Brodehl et al., 2017). Nevertheless, this mouse model cannot be directly transferred to the human condition of *DSC2* mutation carriers. Therefore, it is currently unknown if LOF or a pathogenic dosage effect of mutant desmocollin-2 contributes to ACM development.

The situation for desmoglein-2 is even more complex. Two transgenic mouse models with a cardiac-specific overexpression of Dsg2-p.N271S and DSG2-p.Q554X have been generated. The control mice with a cardiac-specific overexpression of the wild-type *DSG2* did not show any structural or functional abnormalities (Pilichou et al., 2009; Calore et al., 2019). In contrast, transgenic *Myh6:Dsg2*-p.N271S mice developed arrhythmia and ultrastructural defects of the intercalated disc (Pilichou et al., 2006). Correspondingly, *Myh6:*DSG2-p.Q554X mice developed cardiac fibrosis and had a reduced number of cardiac desmosomes. Interestingly, these mice had an increased expression of miRNAs signatures, which might be involved in the pathogenesis (Calore et al., 2019). The group of Krusche and Leube developed a mutant *Dsg2* mouse line missing parts of the first extracellular domains 1–2, mediating the homophilic and heterophilic intercellular protein–protein interactions. These mice developed cardiac fibrosis, necrosis, and calcification and showed an increased expression of cardiac stress markers. Ventricular arrhythmia and ultrastructural defects of the cardiac desmosomes were present in these mice (Krusche et al., 2011; Kant et al., 2012; Buck et al., 2018). Cardiac-specific *Dsg2* knockout mice were independently developed by two groups (Kant et al., 2015; Chelko et al., 2016). These mice present typical ACM features, leading to decreased cardiac function and arrhythmia. Of note, Chelko et al. demonstrated using *Dsg2*-deficient mice for which pharmacological inhibition of glycogen synthase kinase 3β (GSK3β) is able to improve cardiac function, indicating a putative therapeutic strategy for ACM as previously found in a transgenic zebrafish model (Asimaki et al., 2014; Chelko et al., 2016). However, whether inhibition of GSK3β serves as a therapeutic strategy in humans needs to be tested in future clinical trials. In addition, the molecular mechanism of GSK3ß inhibition in the context of ACM is currently unknown.

iASPP

Recently, Notari et al. demonstrated that the inhibitor of apoptosis-stimulating protein of p53 (iASPP) is a cardiac desmosomal protein by binding to desmoplakin and desmin (Notari et al., 2015). However, iASPP is also known as NFκB-interacting protein-1 (NKIP1) and has a widespread expression in different organs and cell types[3]. Of note, a different group identified a homozygous nonsense mutation in *PPP1R13L*, which encodes iASPP, in a consanguineous family by whole exome sequencing. The infant patients showed severe DCM, cardiac fibro-fatty replacement, tachycardia, wooly hair, and wedge-shaped teeth but no palmoplantar keratoderma (Falik-Zaccai et al., 2017). A spontaneous deletion affecting a splice site in *Ppp1r13l* in a mouse model caused abnormal coat, growth retardation, increased prenatal mortality, and biventricular cardiomyopathy with massive cardiac fibrosis (Herron et al., 2005). More recently, an inducible *Ppp1r13l*

[3]https://www.proteinatlas.org/ENSG00000104881-PPP1R13L/tissue

knockout mouse model was generated, which presented an ACM phenotype consisting of right ventricular dilation, ventricular tachycardia, and ultrastructural changes of the cardiac desmosomes (Notari et al., 2015). In addition, a homozygous 7-bp duplication in *PPP1R13L* leading to a frame shift and a premature stop codon is responsible in Poll Hereford cattle for correspondent cardiac and coat abnormalities, leading to prenatal death (Simpson et al., 2009).

ANIMAL MODELS FOR ACM ASSOCIATED WITH MUTATIONS IN NONDESMOSOMAL GENES

In addition to mutations in desmosomal genes, several rare mutations in nondesmosomal genes have been identified in human ACM patients. Those ACM-associated genes encode proteins involved in cardiac electrophysiology (encoded by *RYR2*, *SCN5A*, *PLN*), Z-band proteins (encoded by *DES*, *LDB3*, *ACTN2*), nuclear envelope proteins (encoded by *TMEM43*, *LMNA*, *LEMD2*), or proteins involved in cell–cell or cell to extracellular matrix (ECM) adhesion (encoded by *CTNNA3*, *CDH2, TJP1*, *ILK*, *FLNC*) (**Figures 1**, **4** and **Supplementary Tables 1**, **2**).

Animal Models for ACM Genes Involved in Cardiac Electrophysiology

The human ACM phenotype is associated with severe ventricular arrhythmia, often leading to sudden cardiac death at first presentation. Therefore, mutations in proteins regulating ion channels and calcium signaling have been proposed as part of overlapping phenotypes of ACM with primary arrhythmia syndromes and DCM. The three main representative genes are *RYR2*, *SCN5A*, and *PLN*.

Ryanodine Receptor 2

The cardiac ryanodine receptor 2 gene (*RYR2*) has been proposed as the first nonsyndromic autosomal dominant inherited disease gene for ACM (MIM #600996; Tiso et al., 2001). Although the separate entity ACM has been subsequently questioned as mutations in *RYR2* typically lead to exercise or emotion-induced ventricular tachycardia without overt cardiomyopathy, referred to as catecholaminergic ventricular tachycardia (CPVT). Interestingly, three of the four originally described human mutations have been modeled in mice. The Ryr2-*p*.R176Q$^{+/-}$ knock-in mouse (Kannankeril et al., 2006) mimics the human p.R176Q mutation and shows decreased right ventricular end-diastolic volumes without histological changes and ventricular tachycardia after beta-adrenergic stimulation. Two other human mutations related to ACM have been analyzed in mice (Shan et al., 2012). However, both Ryr2-p.L433P$^{+/-}$ and Ryr2-p.N2386I$^{+/-}$ knock-in mice demonstrated induced atrial fibrillation and leaky calcium channels in the sarcoplasmic reticulum of atrial myocytes but no structural or functional changes of cardiomyopathy. In contrast to mouse models of *Ryr2* representing gain-of-function mutations, the LOF of *Ryr2* in the global knockout mouse appears to be embryonically lethal at E10 with developmental defects, such as abnormalities in the heart tube morphology, large vacuolate sarcoplasmic reticulum, and structurally abnormal mitochondria (Takeshima et al., 1998). Moreover, an induced acute loss of half of the Ryr2 protein in the adult mouse hearts (Bround et al., 2012) leads to severe cardiac dysfunction, decreased heart rate, and ventricular arrhythmia, indicating that LOF not only causes fatal arrhythmia, but also has a role in heart rate control and cardiac remodeling contributing to heart failure.

Sodium Voltage-Gated Channel α Subunit 5

Mutations in *SCN5A* encoding the voltage-gated sodium channel subunit alpha Nav1.5 can cause cardiomyopathies and channelopathies. Functionally, there is a link to the desmosome as loss of *PKP2* expression alters the amplitude and kinetics of the sodium current (Sato et al., 2011; Cerrone et al., 2012). The first description of an ACM-like phenotype with an *SCN5A* variant came from a clinical study in which a coved-type ST-segment was provoked in ACM patients by a sodium channel blocker (Peters, 2008). Subsequently, a larger study found in almost 2% of ACM patients rare *SCN5A* variants and could show for *SCN5A*-p.R1898H reduced peak sodium current and abundance of NaV1.5 in clusters at the intercalated disc (Te Riele et al., 2017). Classically, gain-of-function *SCN5A* mutations cause Long QT syndrome, whereas LOF mutations are responsible for Brugada syndrome. However, both types of mutations may cause structural changes, usually in the form of DCM (Wilde and Amin, 2018). So far, the question remains whether the cardiomyopathy is a direct consequence of the mutation because Nav1.5 interacts with the proteins of the cytoskeleton and intercalated discs or may be secondary due to conduction defects caused by LOF effects. For example, mice with reduced 90% *Scn5a* expression develop conduction defects and severe biventricular cardiomyopathy (Hesse et al., 2007), also seen in a mouse and zebrafish model mimicking the human p.D1275N mutation. Mice homozygous (DN/DN) for the humanized mutation show conduction slowing and progressive cardiac dysfunction but no fibrosis (Watanabe et al., 2011). The transgenic zebrafish expressing the same human p.D1275N mutation exhibit bradycardia, conduction-system abnormalities, and premature death but no impaired cardiac function (Huttner et al., 2013).

Reduced *Scn5a* of about 50% as seen in heterozygous knockout hearts showed also impaired atrioventricular conduction and delayed intraventricular conduction, increased ventricular refractoriness, and ventricular tachycardia with characteristics of reentrant excitation. Homozygous mice were embryonically lethal with severe defects in ventricular morphology (Papadatos et al., 2002). Likewise, knockdown of cardiac sodium channels in zebrafish compromised both early chamber formation and normal patterned growth of the ventricle, suggesting that cardiac sodium channels in zebrafish affect heart development via a nonelectrophysiological mechanism (Chopra et al., 2010).

Another mouse model that modeled the human p.F1759A mutation showed that incomplete NaV1.5 channel inactivation is able to drive structural alterations, including atrial and

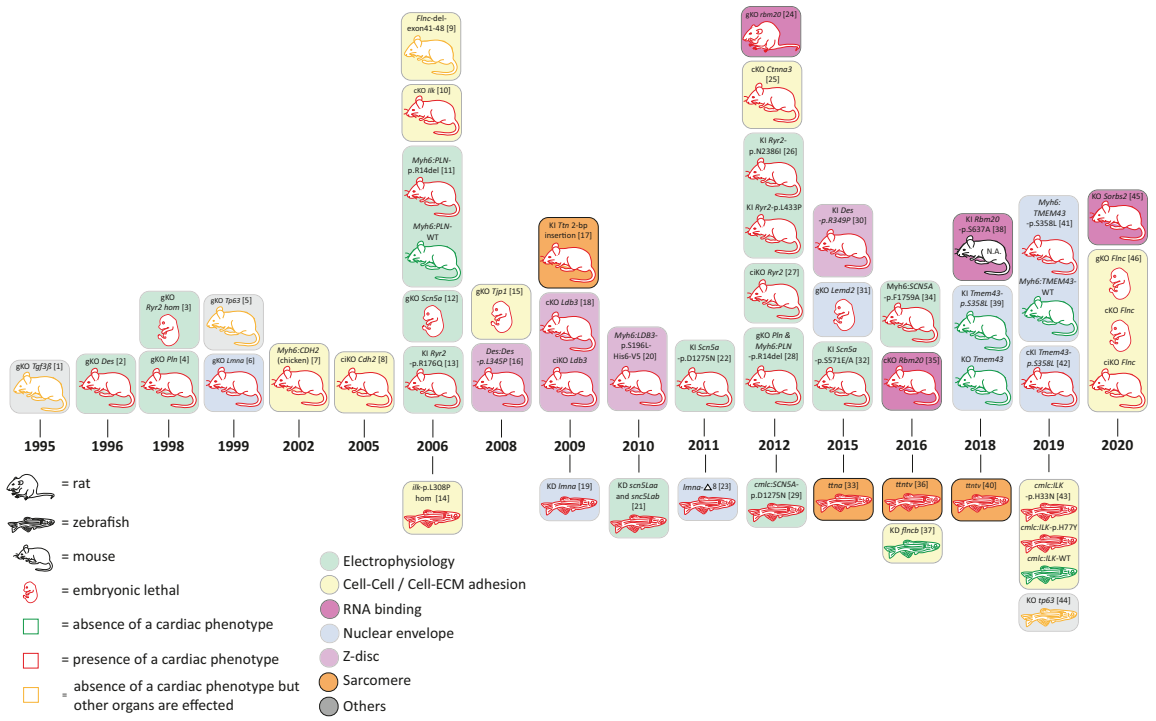

FIGURE 4 | Schematic overview of animal models for non-desmosomal genes according to the year of publication. bp = base pair, KD = knock-down; cKO = cardiac specific knock-out; ciKO = cardiac specific, inducible knock-out; gKO = global knock-out; hom = homozygous; KI = knock-in. N.A. = not assessed. [1] (Kaartinen et al., 1995); [2] (Li et al., 1996; Capetanaki et al., 1997); [3] (Takeshima et al., 1998); [4] (Chu et al., 1998); [5] (Mills et al., 1999); [6] (Sullivan et al., 1999; Nikolova et al., 2004); [7] (Ferreira-Cornwell et al., 2002); [8] (Kostetskii et al., 2005; Li et al., 2005); [9] (Dalkilic et al., 2006); [10] (White et al., 2006; Quang et al., 2015); [11] (Haghighi et al., 2006); [12] (Liu et al., 2006); [13] (Kannankeril et al., 2006); [14] (Bendig et al., 2006; Pott et al., 2018); [15] (Katsuno et al., 2008); [16] (Kostareva et al., 2008); [17] (Gramlich et al., 2009); [18] (Zheng et al., 2009); [19] (Vogel et al., 2009); [20] (Li et al., 2010); [21] (Chopra et al., 2010); [22] (Watanabe et al., 2011); [23] (Koshimizu et al., 2011); [24] (Guo et al., 2012); [25] (Li et al., 2012); [26] (Shan et al., 2012); [27] (Bround et al., 2012); [28] (Haghighi et al., 2012) [29] (Huttner et al., 2013); [30] (Clemen et al., 2015; Stockigt et al., 2020); [31] (Tapia et al., 2015); [32] (Glynn et al., 2015); [33] (Zou et al., 2015); [34] (Wan et al., 2016); [35] (Khan et al., 2016; van den Hoogenhof et al., 2018); [36] (Shih et al., 2016); [37] (Begay et al., 2018); [38] (Murayama et al., 2018); [39] (Stroud et al., 2018); [40] (Huttner et al., 2018); [41] (Padron-Barthe et al., 2019); [42] (Zheng et al., 2019); [43] (Brodehl et al., 2019d); [44] (Santos-Pereira et al., 2019); [45] (Ding et al., 2019); [46] (Zhou et al., 2020).

ventricular enlargement, myofibrillar disarray, fibrosis and mitochondrial injury, and electrophysiological dysfunctions (Wan et al., 2016). Moreover, a mouse model is focusing on the phosphorylation residue S571 in two *Scn5a* knock-in mouse models (p.S571E and p.S571A). Interestingly, the authors could demonstrate a binary molecular switch for CaMKII-dependent activation of $I_{Na,L}$ without affecting channel properties related to cardiac function (Glynn et al., 2015).

So far, none of the genetic variants found in typical ACM patients (Te Riele et al., 2017) have been analyzed in an animal model to specifically look at changes of the right ventricle; however, it is likely that LOF mutations are associated with cardiac dysfunction of the left or both ventricles even if whether a gain-of-function mechanism due to an interaction with desmosomal proteins exists remains unclear.

Phospholamban

Disturbed calcium homeostasis has been implicated as a mechanism for arrhythmogenesis as well as disturbed cardiac contractility. Phosholamban (encoded by *PLN*) regulates calcium handling by reversibly inhibiting the activity of the sarcoplasmic reticulum calcium ATPase 2 (SERCA2). This is based on the phosphorylation status through beta-adrenergic activation of protein kinase A (PKA). Although many human mutations have been described to cause DCM, an in-frame 3-bp deletion mutation leading to removal of R14 in phospholamban has been reported to cause both DCM and ACM, indicating the clinical overlap of both cardiomyopathies in particular for this mutation (van der Zwaag et al., 2012; Fish et al., 2016). *PLN*-p.R14del appears to be associated with high penetrance and severe disease. Two mouse models have been generated to mimic human disease. The transgenic mouse overexpressing the human PLN-p.R14del in the heart revealed ventricular dilation, myocyte disarray, and myocardial fibrosis. Mechanistically, it has been proposed that the dominant effect of the mutation leads to a nonreversible chronic suppression of SERCA activity based on its lack of PKA-mediated phosphorylation (Haghighi et al., 2006). Interestingly, when the wild-type phospholamban got removed by mating the transgenic mice with the *Pln* knockout mice, hearts are hypercontractile and show a progression to cardiac hypertrophy (Chu et al., 1998; Haghighi et al., 2012). More importantly, mutant phospholamban did not colocalize with SERCA2a and is

localized instead at the plasma membrane and alters function of the Na/K ATPase (NKA). Taken together, the p.R14del mutation has a complex effect on SR calcium homeostasis, impacting both PLN inhibition of SERCA and PKA-mediated phosphorylation of PLN via the beta-adrenergic pathway. In addition, a link between *PLN* mutations, disturbed calcium handling, and the intercalated discs has been postulated. The *PLN*-p.R14del mutation results in an accumulation of diastolic calcium, which, in turn, would be able directly or via an activation of Ca^{2+} sensitive proteins, such as calmodulin-dependent kinase II (CaMKII) and calcineurin (CnA), to affect the maladaptive remodeling of the macromolecular protein complex that forms the intercalated disc (van Opbergen et al., 2017). *PLN*-p.R14del may be a good example for a phenotype of arrhythmogenic dilated cardiomyopathy covering both entities of DCM and ACM.

Animal Models for ACM Genes Encoding Proteins of the Nuclear Envelope

Proteins of the nuclear envelope, which surround the nucleus and are continuous with the sarcoplasmic reticulum in the cell, are usually highly conserved and ubiquitously expressed. They have many distinct functions and are involved in the pathology of the heart and other organs. They contribute to the assembly of orderly structures and stability and strength of cells and participate in the regulation of DNA replication and transcription through chromatin structures (Stroud, 2018). Human mutations in *TMEM43*, *LMNA*, and *LEMD2* have been associated with often highly penetrant, aggressive disease with respect to ventricular arrhythmia and sudden cardiac death. In addition, the human phenotype mainly affects the left or both ventricles, whereas a predominant right ventricular involvement appears unusual.

Transmembrane Protein-43

The transmembrane protein-43 (TMEM43) localizes in the inner nuclear membrane, where it interacts with lamin and other proteins of the linker of nucleoskeleton and cytoskeleton (LINC) complex (Bengtsson and Otto, 2008). The best characterized human *TMEM43* missense mutation causing autosomal-dominant inherited ACM (#MIM 604400) is p.S358L. *TMEM43*-p.S358L generates a severe sex-influenced lethal ACM with left ventricular dilation, fibro-fatty replacement of cardiomyocytes, heart failure, and early death, especially in male patients (Merner et al., 2008; Hodgkinson et al., 2013; Milting et al., 2015). Currently, the exact molecular mechanism for earlier presentation and decreased life expectancy in males is unknown because *TMEM43* is not localized on a gonosome. Information about the role of TMEM43 in health and disease *in vivo* have been assessed just very recently in different mouse models. The first two mouse models have globally knocked out murine *Tmem43* as well as introduced the corresponding human mutation p.S358L via CRISPR/Cas9 knock-in into *Tmem43* (Stroud et al., 2018). Surprisingly, both mouse models did not show a cardiac phenotype at baseline and after pressure overload. In contrast, a very similar *Tmem43* knock-in mouse model carrying the p.S358L mutation, generated by traditional homologous recombination-mediated genomic targeting, shows features of cardiomyopathy with fibro-fatty infiltration but preserved cardiac function. The authors show activation of NFκB/TGFβ signaling, which may cause the fibrotic changes (Zheng et al., 2019). More importantly, cardiac-specific overexpression of human *TMEM43*-p.S358L in a transgenic model recapitulates the severe human phenotype. Transgenic hearts show severe biventricular cardiac dysfunction, fibro-fatty replacement of the myocardium, and decreased survival. Conduction defects precede the structural abnormalities. TMEM43-p.S358L showed partial delocalization to the cytoplasm and reduced interaction with emerin and β-actin, suggesting that a reduced interaction between the nucleus and the cytoskeleton contributes to cardiomyocyte death under biomechanical stress. Inhibition of the GSK3β pathway improved cardiac function (Padron-Barthe et al., 2019). However, a lot of questions still remain open, for example, with regards to the sex-specific effect and the mechanism of arrhythmia preceding the structural changes.

Lamin A/C

LMNA encodes nuclear proteins lamin A and C, which are widely expressed IF proteins within the inner nuclear membrane and a relatively common cause of familial DCM (Stroud, 2018). Cardiac manifestations are also part of isolated cardiomyopathy or associated with other syndromic features, ranging from skeletal myopathies, lipodystrophy, and neuropathy to premature aging. Patients with *LMNA* mutations affecting the heart present with conduction disease and ventricular arrhythmia, often preceding left and sometimes biventricular dysfunction. However, screening of typical ACM patients identified *LMNA* mutation carriers with severe right ventricular involvement, sudden cardiac death, and conduction abnormalities, suggesting a genetic overlap of DCM and ACM (Quarta et al., 2012; Valtuille et al., 2013). Mouse models carrying several missense mutations have been generated (Chen et al., 2019); however, a particular mutation with an overlapping phenotype to ACM has not been reported. More generally, homozygous *Lmna* knockout mice showed severely retarded postnatal growth with the appearance of muscular dystrophy and DCM and died by about 8 weeks of age mimicking a phenotype of Emery–Dreifuss muscular dystrophy, DCM, and progeria (Sullivan et al., 1999; Nikolova et al., 2004). However, human DCM is an autosomal-dominant disease and, therefore, heterozygous mice for *Lmna*+/- have been further evaluated and which demonstrate atrioventricular (AV) conduction defects, atrial and ventricular arrhythmia, and at an advanced age also impaired cardiac contractility, which mimics haploinsufficiency of human disease (Wolf et al., 2008). Knockdown of lamin during zebrafish development shows also a cardiomyopathic phenotype with significant bradycardia (Vogel et al., 2009), whereas another zebrafish model in which cryptic splicing of *lmna* generated a deletion of eight amino acids revealed embryonic senescence and S-phase accumulation/arrest as well as abnormal muscle and lipodystrophic phenotypes (Koshimizu et al., 2011). Finally, the underlying pathogenesis for *LMNA* mutations causing cardiac features is complex and part of a multisystem disease pathology. The type of *LMNA* mutation may modify the risk of disease progression and arrhythmia; however, many human missense mutations appear to be extensively heterogeneous, but in particular, truncating

mutations seem to have a higher risk for arrhythmia and sudden cardiac death (van Rijsingen et al., 2012).

LEM-Domain Containing Protein-2

More recently a human homozygous missense mutation (p.L13R) in another inner nuclear membrane protein, encoding the LEM-domain containing protein-2 (LEMD2), has been found to cause an ACM with juvenile cataract in the Hutterite population. The cardiac phenotype is characterized by ventricular arrhythmia and sudden cardiac death, which often precedes dilation and left-ventricular dysfunction (Abdelfatah et al., 2019). Interestingly, mutations in the same gene but a different domain cause a progeria-like phenotype (Marbach et al., 2019). So far, there is no mouse model simulating this specific mutation, but the global knockout of *Lemd2* in mice is embryonically lethal at E11.5 and shows reduced size of most tissues with thin myocardium and underdeveloped trabeculae, suggesting an importance of *Lemd2* during mouse development (Tapia et al., 2015). More specific data about the role of LEMD2 in the development of cardiomyopathy are required to explain the clinical phenotype and its pathology, which appears not to be neither classical for DCM nor ACM and may present an overlap of both forms.

Animal Models for ACM Genes Encoding Z-Band Proteins

Z-bands are multiple-protein structures responsible for anchoring thin sarcomeric filaments as well as the giant sarcomere protein titin (Luther, 2009) and impact the structural integrity of the sarcomeres. Mutations in several genes involved in Z-band formation are involved in genetic cardiomyopathies, including ACM (Gerull et al., 2019).

Desmin

Although desmin is not directly a Z-band protein, it forms cytoplasmic IF and is involved in connection of the Z-bands (Hijikata et al., 1999), desmosomes (Choi et al., 2002), mitochondria (Capetanaki, 2002), and also the nuclei (Heffler et al., 2020) in cardiomyocytes. Mutations in *DES* cause different skeletal and cardiac myopathies, including DCM (Li et al., 1999; Brodehl et al., 2016a), HCM (Harada et al., 2018), RCM (Brodehl et al., 2019c), LVNC (Marakhonov et al., 2019; Kubanek et al., 2020), and also ACM (Klauke et al., 2010; Bermudez-Jimenez et al., 2018). Desmin consists of a central α-helical rod domain flanked by nonhelical head and tail domains. The majority of pathogenic *DES* mutations are heterozygous missense or small in-frame deletion mutations spread over the whole rod domain (Brodehl et al., 2018). Many *DES* mutations disturb dominantly the filament assembly and cause an abnormal cytoplasmic desmin aggregation (Brodehl et al., 2012). In the 1990s, two groups independently generated *Des*-deficient mice models (Li et al., 1996; Capetanaki et al., 1997). *Des*-deficient mice develop severe fibrosis, cardiac calcification, and biventricular cardiomyopathy (Psarras et al., 2012). Correspondingly, knockdown of *desma* and *desmb* causes cardiac edema and structural disorganized muscles in zebrafish (Li et al., 2013). However, the major pathomechanism consisting of abnormal desmin aggregation is not modeled by this LOF animal model. In contrast, the Des-p.R349P knock-in mice developed toxic desmin aggregates and presented mitochondrial defects (Clemen et al., 2015; Winter et al., 2016; Stockigt et al., 2020). These mice developed skeletal myopathy in combination with DCM, including cardiac arrhythmia and conduction defects. In 2015, Ramspacher et al. inserted fluorescence proteins at position 460 in *desma* of the zebrafish (Ramspacher et al., 2015). These zebrafish developed cardiac arrhythmia and cardiac dysfunction, leading to decreased viability. In conclusion, desmin animal models suited for modeling of LOF and toxic dominant desmin accumulation are available and partially mimic human ACM.

LIM Domain Binding Protein-3

Mutations in *LDB3*, encoding LIM domain binding protein-3, which is also known as cipher or ZASP, cause myofibrillar myopathy and different cardiomyopathies in humans (Vatta et al., 2003; Selcen and Engel, 2005). ZASP binds to α-actinin-2 and is important for the structural integrity of the Z-bands (Lin et al., 2014). In 2015, Lopez-Ayala and coworkers identified the novel heterozygous missense mutation *LDB3*-c.1051A > G in the genome of an ACM index patient using a next-generation sequencing (NGS) gene panel. Cascade genetic screening revealed cosegregation of this mutation within the family supporting its pathogenicity (Lopez-Ayala et al., 2015). In 2009, Zheng et al. developed conditional cardiac-specific and inducible cardiac-specific *Ldb3* deficient mouse models (Zheng et al., 2009). Both mouse models presented severe biventricular dilation and cardiac dysfunction, leading to increased mortality. Of note, the Z-bands were highly disorganized in cardiomyocytes from *Ldb3*-deficient mice, and the ERK/Stat3 signaling was altered (Zheng et al., 2009). In addition, a transgenic mouse model with cardiac-specific overexpression of mutant LDB3-p.S196L was generated (Li et al., 2010). These mice developed DCM in combination with cardiac conduction defects and ventricular arrhythmia associated with ultrastructural defects of the sarcomeres.

α-Actinin-2

Recently, a novel missense mutation p.Y473C was identified in *ACTN2*, encoding α-actinin-2, in a family with left-dominant ACM (Good et al., 2020). Pathogenic mutations in *ACTN2* have been also identified in patients with HCM, DCM, and LVNC, indicating a genetic overlap of associated phenotypes (Mohapatra et al., 2003; Bagnall et al., 2014; Girolami et al., 2014). α-Actinin-2 anchors actin filaments and titin to the Z-bands. Gupta et al. knocked down *actn2* in zebrafish using morpholino oligonucleotide injections, revealing skeletal and cardiac muscle defects (Gupta et al., 2012). However, there is currently no specific mouse or zebrafish model available for ACM-associated human *ACTN2* mutations.

Animal Models for ACM Genes Encoding Proteins Involved in Cell–Cell and Cell-ECM Adhesion

Mutations in five genes (*CTNNA3*, *CDH2*, *TJP1*, *ILK*, *FLNC*) encoding proteins involved in cell–cell or ECM interaction are associated with human ACM (**Figure 1**). However, because these

mutations have been discovered recently, the amount and impact for ACM is currently inexplicit. Nevertheless, for some of them, specific animal models provide additional evidence for their pathogenicity (**Figure 4**).

αT-Catenin

Rampazzo's group identified a *CTNNA3* missense and a small in-frame 3-bp deletion in two ACM families (van Hengel et al., 2013). However, it seems that *CTNNA3* mutations are rare (Christensen et al., 2011; Gandjbakhch et al., 2013). *CTNNA3* encodes αT-Catenin, which is a structural protein involved in the area composita. Of note, conditional *Cttna3* knockout mice were viable and fertile but developed progressive cardiomyopathy, including left-ventricular dilation and decreased ejection fraction (Li et al., 2012). Despite that, the relevance of *CTNNA3* for ACM or other cardiomyopathies has to be investigated in more detail.

N-Cadherin

Recently, two independent groups identified *CDH2* missense variants (p.D407N and p.Q229P) in the genome of ACM patients (Mayosi et al., 2017; Turkowski et al., 2017; **Figure 1**). Cosegregation analyses within the families and absence in population databases might indicate pathogenicity of these *CDH2* mutations. Similar to the desmosomal cadherins, N-cadherin is localized in multiple-protein complexes in the intercalated disc, which are called adherens junctions or area composita (Franke et al., 2006; Zhao et al., 2019). The relevance of N-cadherin for ACM is additionally supported by two different mouse models (**Figure 4**). Cardiac-specific overexpression of chicken *CDH2* caused biventricular cardiomyopathy in combination with increased expression of stress markers and a decreased connexin-43 expression (Ferreira-Cornwell et al., 2002). Similarly, cardiac-specific inducible *Cdh2* knockout mice developed DCM in combination with ventricular arrhythmia and conduction abnormalities, leading to premature death after 2 months (Kostetskii et al., 2005; Li et al., 2005). Although no functional data about human *CDH2* mutations were currently available, both mouse models underline the impact of N-cadherin for normal heart function *in vivo*. However, future studies are needed to determine the pathomechanism of *CDH2* mutations at the molecular level.

Tight Junction Protein-1

Currently, there is one single report describing four different *TJP1* missense mutations in ACM patients (De Bortoli et al., 2018). *TJP1* encodes tight junction protein-1 localized at the intercalated disc, which is also known as zonula occludens-1 (ZO1). Global knockout of *TJP1* caused embryonic lethality in mice, limiting functional analyses (Katsuno et al., 2008). Because of the limited knowledge about the relevance of tight junction protein-1 in ACM, cardiac-specific conditional knockout or knock-in animal models might contribute to clinical interpretation of *TJP1* mutations in future.

Integrin-Linked Kinase

Recently, we identified two different missense mutations in *ILK* in the genome of ACM patients by NGS. One of these mutations occurred *de novo* (Brodehl et al., 2019d). Before, *ILK* mutations have been described for DCM patients (Knoll et al., 2007). *ILK* encodes integrin-linked kinase. There is still an ongoing debate about whether ILK is a real or pseudo kinase involved in linkage to the integrin system (Hannigan et al., 2011; Ghatak et al., 2013; Vaynberg et al., 2018). Transgenic zebrafish with a cardiac-specific overexpression of mutant ILK presented a decreased fractional shorting and showed premature death (Brodehl et al., 2019d). Correspondingly, a spontaneous homozygous *ilk* mutation (p.L308P) caused cardiac edema, decreased cardiac function, and premature death in the zebrafish (Bendig et al., 2006; Pott et al., 2018). Muscle-specific *Ilk* knockout mice showed an increased mortality, ventricular dilation, arrhythmia, and cardiac fibrosis (White et al., 2006; Quang et al., 2015). In addition, Akt phosphorylation was reduced, and connexin-43 was downregulated in these mice.

Filamin-C

Mutations in *FLNC* were initially identified in patients with myofibrillar myopathy (MFM) (Vorgerd et al., 2005; Shatunov et al., 2009). *FLNC* encodes filamin-c, which is a huge cytolinker protein involved in linkage of the area composita, costameres, and actin filaments. The relevance of *FLNC* mutations for development of different cardiomyopathies, such as HCM (Valdes-Mas et al., 2014), RCM (Brodehl et al., 2016b), and DCM (Begay et al., 2016; Nozari et al., 2018) has been more recently recognized. In addition, mutations in *FLNC* cause ACM (Begay et al., 2018; Hall et al., 2019, 2020; Augusto et al., 2020; Brun et al., 2020). Global or cardiac-specific *Flnc* deficiency was embryonically lethal in mice, limiting the functional analyses (Zhou et al., 2020). Mice expressing a mutant C-terminal truncated form of filamin-C died perinatal by respiratory failure, but no detailed cardiac analyses have been performed (Dalkilic et al., 2006). Therefore, Chen's group developed inducible cardiac-specific *Flnc*-deficient mice. These mice showed premature death, increased cardiac stress marker expression, cardiac fibrosis, and cardiac dysfunction. Interestingly, several proteins of the costameres, the intercalated discs, or the IFs were highly increased (Zhou et al., 2020). In summary, there is evidence from human and animal data that demonstrate the impact of filamin-C for heart function. However, the specific impact of *FLNC* mutations for ACM needs further investigation in the future.

Animal Models for ACM Genes Involved RNA Binding and Processing

Mutations in *RBM20*, encoding the RNA-binding motif protein 20 (RBM20), have been recently identified in patients with ACM (van den Hoogenhof et al., 2018; Parikh et al., 2019). Initially, pathogenic missense mutations in *RBM20* were described in DCM (Brauch et al., 2009) and LVNC patients (Sedaghat-Hamedani et al., 2017). RBM20 is a splicing factor and consists of one N-terminal leucine-rich domain, two zinc finger domains, a RNA recognition motif, an arginine- and serine-rich (RS) domain and a glutamate-rich region (Watanabe et al., 2018). The majority of pathogenic *RBM20* mutations is localized in the RS domain although also mutations in the glutamate-rich

region have been described (Beqqali et al., 2016). Using a spontaneous rat model carrying a homozygous large deletion affecting *rbm20*, Guo *et al. re*vealed that Rbm20 is involved in cardiac splicing of several genes, including *ttn* (titin) and *ldb3*. Of note, several of the known targets of Rbm20, such as *RYR2*, are ACM-associated genes. Maatz et al. determined further RBM20 target genes, such as *Myh7*, *Nexn*, *Tnnt2*, and *Ryr2* (Maatz et al., 2014). The *Rbm20*-deficient mice presented cardiomyopathy in combination with arrhythmia, leading to increased mortality. This phenotype in rats is in good agreement with the phenotype of cardiac-specific *Rbm20*-deficient mice, which developed arrhythmogenic DCM (Khan et al., 2016; van den Hoogenhof et al., 2018). Interestingly, adenovirus-mediated Rbm20 overexpression rescued the *ttn* splicing defect in *rbm20*-deficient cardiomyocytes, underlining a putative therapeutic strategy (Guo et al., 2012). Murayama and colleagues generated a knock-in mouse model carrying Rbm20-p.S647A in the RS domain. Although the detailed phenotype of these mice has yet not been described in detail, the authors demonstrated defects in splicing of titin in the murine heart (Murayama et al., 2018). Interestingly, mutations in the RS domain prevent nuclear transport of RBM20 (Murayama et al., 2018; Brodehl et al., 2019b). Another ACM-associated gene encoding a putative RNA-binding protein (Han et al., 2019) might be *SORBS2*, encoding sorbin and SH3 domain-containing protein-2 (Ding et al., 2019). The exact molecular function of *SORBS2* is currently unknown. However, in a preprinted manuscript, Ding et al. described several novel human *SORBS2* variants in ACM patients and generated cardiac-specific *Sorbs2*-deficient mice. These mice develop biventricular cardiomyopathy, leading to an increased mortality (Ding et al., 2019). However, it is currently unclear if SORBS2 is a RNA-binding protein or a desmosomal protein. Currently, it is difficult to predict the relevance of *SORBS2* in ACM.

Further Animal Models for Human ACM-Associated Genes

Few additional genes have been reported in association with ACM either as part of an overlap phenotype with other cardiomyopathies (*TTN*) or where the genes have been suggested as a candidate gene for ACM (*TGFβ3*) or as part of a complex syndrome (*TP63*). Their overall importance for the disease remains elusive.

Titin

Truncating mutations (TTNtv) in the sarcomeric gene *TTN* have been reported with a frequency of approximately 25% as the most common cause of DCM (Herman et al., 2012; Roberts et al., 2015). However, their role for other cardiomyopathies remains elusive (Gerull, 2015). Moreover, missense variants, which are predicted to be deleterious, are found in about 7% of DCM patients, which was comparable with the frequency in the reference population, suggesting that their causative relevance for DCM is not established (Akinrinade et al., 2019). For ACM, two studies have been published in which exclusively *TTN* missense variants have been suggested as a cause of ACM (Taylor et al., 2011; Brun et al., 2014), which might be, under current view, questionable although a modifying effect cannot be excluded.

Interestingly, in particular, the zebrafish has been used to mimic different TTNtv, but also a mouse model has been developed, which corresponds to a human A-band truncation mutation (Gerull et al., 2002). Mice homozygous for the truncation are embryonically lethal at E9.5 due to defects in the sarcomere formation, whereas heterozygous animals have no cardiac abnormalities at baseline but develop fibrotic remodeling under hemodynamic stress (Gramlich et al., 2009). Using different genome-editing approaches, truncation mutations have been introduced and analyzed at different locations of the zebrafish *ttn* gene (Zou et al., 2015; Shih et al., 2016; Huttner et al., 2018). Homozygous truncations at the N-terminal and C-terminal molecule caused severe defects in cardiac contractility, and the zebrafish died within 2 weeks. Interestingly, C-terminal truncations led to severe skeletal muscle myopathies but not N-terminal. A newly discovered internal promotor produces the so-called C-terminal titin isoform "Cronos," which is translated into a protein and explains the differences between the phenotypes, depending on the location of the truncation with or without a subsequent disruption of the "Cronos" isoform (Zou et al., 2015). Others also modeled truncation mutations in zebrafish and supported the exon usage hypothesis (Shih et al., 2016), which was previously suggested based on human studies (Roberts et al., 2015). The impact of heterozygous *ttn* truncations at an adult age was further investigated. Like in humans, heterozygous truncations led to spontaneous DCM with reduced baseline ventricular systolic function and failed to mount a hypercontractile response when challenged by hemodynamic stress (Huttner et al., 2018).

Transforming Growth Factor-ß3

The first genomic locus for ACM at 14q23-q24 (ARVD1; #MIM 107970) was discovered by linkage analysis in Italian families, but a pathogenic mutation in exonic sequences of several candidate genes was not detected (Rampazzo et al., 2003). Later on, two genetic variants in the untranslated regions of the transforming growth factor-β3 (TGFβ3) were identified; however, the role of *TGFβ3* as a causative gene for ACM (Beffagna et al., 2005) remains still open. Moreover, *Tgfβ3* knockout mice showed no specific cardiac phenotype but suffer from abnormal lung development and cleft palate at birth (Kaartinen et al., 1995; Proetzel et al., 1995). On the other hand, TGFβ signaling has been suggested to play a role in the disease process of ACM and has been shown to be activated in the pathogenesis of *TMEM43*-related disease as well as for mutant desmosomal proteins, such as plakoglobin and desmoplakin (Li et al., 2011; Giuliodori et al., 2018; Zheng et al., 2019).

Tumor Protein-63

Another interesting protein is the tumor protein p63 (*TP63*). Mutations in *TP63* can cause a range of overlapping syndromic ectodermal dysplasias (EDs). In some cases of EDs, a congenital heart defect was found; however, a case report described a missense mutation in *TP63* in a patient with ED and typical cardiac findings of ACM (Valenzise et al., 2008).

More recently, a novel heterozygous nonsense variant was reported in a typical nonsyndromic ACM case, suggesting that haploinsufficiency may play a role in the disease process (Poloni et al., 2019). Knockout of *Tp63* in mice and zebrafish are viable and indicate its role in development and ectodermal differentiation, but no obvious cardiac abnormalities have been detected in either homozygous or heterozygous animals (Mills et al., 1999; Santos-Pereira et al., 2019). A potential role for *TP63* as an ACM associated gene needs to be further defined.

ACM ANIMAL MODELS WITHOUT HUMAN GENETIC CORRELATION

Several animal models have been described for which the responsible gene is still unknown or no human genetic mutations have been associated with ACM. Asano et al. generated a spontaneous mouse model with massive right-ventricular fibrosis, calcification, and prolonged QRS duration with recessive inheritance. Linkage analyses revealed a 1031-bp retroposon in the *Rpsa* gene. *Rpsa* or *Lamr1* encodes the laminin receptor-1, which is also called ribosomal protein SA. Transgenic mice with cardiac-specific or systemic overexpression of this mutant form of the laminin receptor 1 caused ACM, supporting the pathogenicity of this mutant gene (Asano et al., 2004). In humans, heterozygous mutations in *RPSA* cause isolated congenital asplenia by haploinsufficiency (MIM, #271400) (Bolze et al., 2013).

Since the 1980s, it has been recognized that ACM occurred in Boxer dogs with similar clinical signs to humans, including ventricular arrhythmia, ventricular dilation, and fibro-fatty replacement of the myocardium (Miller et al., 1985; Harpster, 1991; Basso et al., 2004). Nearly all mouse and zebrafish models are unable to display fibro-fatty replacement of myocardial tissue, which is a typical hallmark of human ACM. In contrast, the Boxer ACM model is also able to mimic those pathological findings. In addition, inflammatory cell infiltration and apoptosis were present in this large-animal model (Basso et al., 2004). Meurs et al. analyzed pedigrees of Boxer dogs and suggested an autosomal dominant inheritance (Meurs et al., 1999). Based on a genome-wide association study, a deletion in the untranslated region of *STRN*, encoding striatin, was suggested as the pathogenic mutation causing Boxer ACM (Meurs et al., 2010). However, Cattanach et al. demonstrated that this *STRN* mutation is not causative for Boxer ACM, but might be genetically linked to the responsible gene on chromosome 17 (Cattanach et al., 2015). Currently, no *STRN* mutation for human ACM patients is listed in the HGMD or the ARVD/C Genetic Database[4]. In addition, ACM was described for English Bulldogs and Weimaraners (Eason et al., 2015; Cunningham et al., 2018). Corresponding to Boxer ACM, it was shown that ACM presented with right-ventricular dilation, thin right-ventricular wall diameter, ventricular tachycardia, and severe fibro-fatty replacement of the myocardium, which occurred spontaneously in domestic cats (Fox et al., 2000; Harvey et al., 2005; Ciaramella et al., 2009). However, the genetic mutations responsible for ACM in cats is currently unknown.

[4]https://molgenis136.gcc.rug.nl

SUMMARY AND OUTLOOK

Because the first disease genes of ACM were discovered more than 20 years ago, a substantial number of *in vivo* models have been generated and characterized to fill the important gap between the underlying genetic defect and the observed clinical phenotype. Those models often recapitulate at least partially pathological features of ACM and gain mechanistic insights into the disease pathogenesis with the opportunity to develop targeted therapies in the future. However, a past *in vivo* model strategy mimics LOF much better due to targeted knockouts of affected proteins, but it is limited in modeling missense mutations, often leading to a gain-of-function or toxic effect. Transgenic models used for missense mutations still mainly overexpress the human mutant proteins, which often have different effects in mice compared to the human phenotype. Knock-in animal models represent a much better system for studying human missense mutations as the mutation is inserted into the endogenous gene and works under the control of its own promotor. Nevertheless, even if the human disease mutation is conserved, it is still kept in mind that substantial differences exist between the human heart and mice or fish hearts. In particular in ACM, the hallmark of fatty tissue in the human right ventricle is almost never seen in the corresponding model system. From recent advances in genetic technology emerged the CRISPR/Cas9 genome-editing approach, which has simplified the generation of knockout and knock-in models and will become the technology of choice for studying human gene mutations in the future.

AUTHOR CONTRIBUTIONS

BG and AB contributed to the writing and visualization. Both authors agreed to be accountable for the content of this work.

FUNDING

Support was provided by the German Ministry of Education and Research (BMBF), Berlin, Germany, grant # 01EO1504.

ACKNOWLEDGMENTS

We thank Greta Pohl (Heart and Diabetes Center NRW) for reading and correcting the manuscript.

SUPPLEMENTARY MATERIAL

The Supplementary Material for this article can be found online at: https://www.frontiersin.org/articles/10.3389/fphys.2020.00624/full#supplementary-material

REFERENCES

Abdelfatah, N., Chen, R., Duff, H. J., Seifer, C. M., Buffo, I., Huculak, C., et al. (2019). Characterization of a unique form of arrhythmic cardiomyopathy caused by recessive mutation in LEMD2. *JACC Basic Transl. Sci.* 4, 204–221. doi: 10.1016/j.jacbts.2018.12.001

Agullo-Pascual, E., Lin, X., Leo-Macias, A., Zhang, M., Liang, F. X., Li, Z., et al. (2014). Super-resolution imaging reveals that loss of the C-terminus of connexin43 limits microtubule plus-end capture and NaV1.5 localization at the intercalated disc. *Cardiovasc. Res.* 104, 371–381. doi: 10.1093/cvr/cvu195

Agullo-Pascual, E., Reid, D. A., Keegan, S., Sidhu, M., Fenyo, D., Rothenberg, E., et al. (2013). Super-resolution fluorescence microscopy of the cardiac connexome reveals plakophilin-2 inside the connexin43 plaque. *Cardiovasc. Res.* 100, 231–240. doi: 10.1093/cvr/cvt191

Akinrinade, O., Helio, T., Lekanne Deprez, R. H., Jongbloed, J. D. H., Boven, L. G., Van Den Berg, M. P., et al. (2019). Relevance of titin missense and non-frameshifting insertions/deletions variants in dilated cardiomyopathy. *Sci. Rep.* 9:4093.

Asano, Y., Takashima, S., Asakura, M., Shintani, Y., Liao, Y., Minamino, T., et al. (2004). Lamr1 functional retroposon causes right ventricular dysplasia in mice. *Nat. Genet.* 36, 123–130. doi: 10.1038/ng1294

Asimaki, A., Kapoor, S., Plovie, E., Karin Arndt, A., Adams, E., Liu, Z., et al. (2014). Identification of a new modulator of the intercalated disc in a zebrafish model of arrhythmogenic cardiomyopathy. *Sci. Transl. Med.* 6:240ra274.

Augusto, J. B., Eiros, R., Nakou, E., Moura-Ferreira, S., Treibel, T. A., Captur, G., et al. (2020). Dilated cardiomyopathy and arrhythmogenic left ventricular cardiomyopathy: a comprehensive genotype-imaging phenotype study. *Eur. Heart J. Cardiovasc. Imaging* 21, 326–336.

Awad, M. M., Dalal, D., Cho, E., Amat-Alarcon, N., James, C., Tichnell, C., et al. (2006). DSG2 mutations contribute to arrhythmogenic right ventricular dysplasia/cardiomyopathy. *Am. J. Hum. Genet.* 79, 136–142. doi: 10.1086/504393

Bagnall, R. D., Molloy, L. K., Kalman, J. M., and Semsarian, C. (2014). Exome sequencing identifies a mutation in the ACTN2 gene in a family with idiopathic ventricular fibrillation, left ventricular noncompaction, and sudden death. *BMC Med. Genet.* 15:99. doi: 10.1186/s12881-014-0099-0

Basso, C., Corrado, D., Marcus, F. I., Nava, A., and Thiene, G. (2009). Arrhythmogenic right ventricular cardiomyopathy. *Lancet* 373, 1289–1300.

Basso, C., Fox, P. R., Meurs, K. M., Towbin, J. A., Spier, A. W., Calabrese, F., et al. (2004). Arrhythmogenic right ventricular cardiomyopathy causing sudden cardiac death in boxer dogs: a new animal model of human disease. *Circulation* 109, 1180–1185. doi: 10.1161/01.cir.0000118494.07530.65

Beffagna, G., Occhi, G., Nava, A., Vitiello, L., Ditadi, A., Basso, C., et al. (2005). Regulatory mutations in transforming growth factor-beta3 gene cause arrhythmogenic right ventricular cardiomyopathy type 1. *Cardiovasc. Res.* 65, 366–373. doi: 10.1016/j.cardiores.2004.10.005

Begay, R. L., Graw, S. L., Sinagra, G., Asimaki, A., Rowland, T. J., Slavov, D. B., et al. (2018). Filamin C truncation mutations are associated with arrhythmogenic dilated cardiomyopathy and changes in the cell-cell adhesion structures. *JACC Clin. Electrophysiol.* 4, 504–514. doi: 10.1016/j.jacep.2017.12.003

Begay, R. L., Tharp, C. A., Martin, A., Graw, S. L., Sinagra, G., Miani, D., et al. (2016). FLNC gene splice mutations cause dilated cardiomyopathy. *JACC Basic Transl. Sci.* 1, 344–359. doi: 10.1016/j.jacbts.2016.05.004

Bendig, G., Grimmler, M., Huttner, I. G., Wessels, G., Dahme, T., Just, S., et al. (2006). Integrin-linked kinase, a novel component of the cardiac mechanical stretch sensor, controls contractility in the zebrafish heart. *Genes Dev.* 20, 2361–2372. doi: 10.1101/gad.1448306

Bengtsson, L., and Otto, H. (2008). LUMA interacts with emerin and influences its distribution at the inner nuclear membrane. *J. Cell Sci.* 121, 536–548. doi: 10.1242/jcs.019281

Beqqali, A., Bollen, I. A., Rasmussen, T. B., van den Hoogenhof, M. M., Van Deutekom, H. W., Schafer, S., et al. (2016). A mutation in the glutamate-rich region of RNA-binding motif protein 20 causes dilated cardiomyopathy through missplicing of titin and impaired Frank-Starling mechanism. *Cardiovasc. Res.* 112, 452–463. doi: 10.1093/cvr/cvw192

Bermudez-Jimenez, F. J., Carriel, V., Brodehl, A., Alaminos, M., Campos, A., Schirmer, I., et al. (2018). Novel desmin mutation p.*Glu*401Asp impairs filament formation, disrupts cell membrane integrity, and causes severe arrhythmogenic left ventricular cardiomyopathy/dysplasia. *Circulation* 137, 1595–1610. doi: 10.1161/circulationaha.117.028719

Bierkamp, C., Mclaughlin, K. J., Schwarz, H., Huber, O., and Kemler, R. (1996). Embryonic heart and skin defects in mice lacking plakoglobin. *Dev. Biol.* 180, 780–785. doi: 10.1006/dbio.1996.0346

Bolze, A., Mahlaoui, N., Byun, M., Turner, B., Trede, N., Ellis, S. R., et al. (2013). Ribosomal protein SA haploinsufficiency in humans with isolated congenital asplenia. *Science* 340, 976–978. doi: 10.1126/science.1234864

Bondue, A., Arbustini, E., Bianco, A., Ciccarelli, M., Dawson, D., De Rosa, M., et al. (2018). Complex roads from genotype to phenotype in dilated cardiomyopathy: scientific update from the Working Group of Myocardial Function of the European Society of Cardiology. *Cardiovasc. Res.* 114, 1287–1303. doi: 10.1093/cvr/cvy122

Brauch, K. M., Karst, M. L., Herron, K. J., De Andrade, M., Pellikka, P. A., Rodeheffer, R. J., et al. (2009). Mutations in ribonucleic acid binding protein gene cause familial dilated cardiomyopathy. *J. Am. Coll. Cardiol.* 54, 930–941. doi: 10.1016/j.jacc.2009.05.038

Brodehl, A., Belke, D. D., Garnett, L., Martens, K., Abdelfatah, N., Rodriguez, M., et al. (2017). Transgenic mice overexpressing desmocollin-2 (DSC2) develop cardiomyopathy associated with myocardial inflammation and fibrotic remodeling. *PLoS One* 12:e0174019. doi: 10.1371/journal.pone.0174019

Brodehl, A., Dieding, M., Biere, N., Unger, A., Klauke, B., Walhorn, V., et al. (2016a). Functional characterization of the novel DES mutation p.*L136P* associated with dilated cardiomyopathy reveals a dominant filament assembly defect. *J. Mol. Cell. Cardiol.* 91, 207–214. doi: 10.1016/j.yjmcc.2015.12.015

Brodehl, A., Ebbinghaus, H., Deutsch, M. A., Gummert, J., Gartner, A., Ratnavadivel, S., et al. (2019a). Human induced pluripotent stem-cell-derived cardiomyocytes as models for genetic cardiomyopathies. *Int. J. Mol. Sci.* 20:4381. doi: 10.3390/ijms20184381

Brodehl, A., Ebbinghaus, H., Gaertner-Rommel, A., Stanasiuk, C., Klauke, B., and Milting, H. (2019b). Functional analysis of DES-p.*L398P* and RBM20-p.R636C. *Genet. Med.* 21, 1246–1247. doi: 10.1038/s41436-018-0291-2

Brodehl, A., Ferrier, R. A., Hamilton, S. J., Greenway, S. C., Brundler, M. A., Yu, W., et al. (2016b). Mutations in FLNC are associated with familial restrictive cardiomyopathy. *Hum. Mutat.* 37, 269–279.

Brodehl, A., Gaertner-Rommel, A., and Milting, H. (2018). Molecular insights into cardiomyopathies associated with desmin (DES) mutations. *Biophys. Rev.* 10, 983–1006. doi: 10.1007/s12551-018-0429-0

Brodehl, A., Hedde, P. N., Dieding, M., Fatima, A., Walhorn, V., Gayda, S., et al. (2012). Dual color photoactivation localization microscopy of cardiomyopathy-associated desmin mutants. *J. Biol. Chem.* 287, 16047–16057. doi: 10.1074/jbc.m111.313841

Brodehl, A., Pour Hakimi, S. A., Stanasiuk, C., Ratnavadivel, S., Hendig, D., Gaertner, A., et al. (2019c). Restrictive cardiomyopathy is caused by a novel homozygous desmin (DES) mutation p.Y122H leading to a severe filament assembly defect. *Genes* 10:918. doi: 10.3390/genes10110918

Brodehl, A., Rezazadeh, S., Williams, T., Munsie, N. M., Liedtke, D., Oh, T., et al. (2019d). Mutations in ILK, encoding integrin-linked kinase, are associated with arrhythmogenic cardiomyopathy. *Transl. Res.* 208, 15–29. doi: 10.1016/j.trsl.2019.02.004

Brodehl, A., Stanasiuk, C., Anselmetti, D., Gummert, J., and Milting, H. (2019e). Incorporation of desmocollin-2 into the plasma membrane requires N-glycosylation at multiple sites. *FEBS Open Biol.* 9, 996–1007. doi: 10.1002/2211-5463.12631

Brodehl, A., Weiss, J., Debus, J. D., Stanasiuk, C., Klauke, B., Deutsch, M. A., et al. (2020). A homozygous DSC2 deletion associated with arrhythmogenic cardiomyopathy is caused by uniparental isodisomy. *J. Mol. Cell Cardiol.* 141, 17–29. doi: 10.1016/j.yjmcc.2020.03.006

Bround, M. J., Asghari, P., Wambolt, R. B., Bohunek, L., Smits, C., Philit, M., et al. (2012). Cardiac ryanodine receptors control heart rate and rhythmicity in adult mice. *Cardiovasc. Res.* 96, 372–380. doi: 10.1093/cvr/cvs260

Brun, F., Barnes, C. V., Sinagra, G., Slavov, D., Barbati, G., Zhu, X., et al. (2014). Titin and desmosomal genes in the natural history of arrhythmogenic right ventricular cardiomyopathy. *J. Med. Genet.* 51, 669–676. doi: 10.1136/jmedgenet-2014-102591

Brun, F., Gigli, M., Graw, S. L., Judge, D. P., Merlo, M., Murray, B., et al. (2020). FLNC truncations cause arrhythmogenic right ventricular cardiomyopathy. *J Med Genet.* 57, 254–257. doi: 10.1136/jmedgenet-2019-106394

Buck, V. U., Hodecker, M., Eisner, S., Leube, R. E., Krusche, C. A., and Classen-Linke, I. (2018). Ultrastructural changes in endometrial desmosomes of desmoglein 2 mutant mice. *Cell Tissue Res.* 374, 317–327. doi: 10.1007/s00441-018-2869-z

Calore, M., Lorenzon, A., Vitiello, L., Poloni, G., Khan, M. A. F., Beffagna, G., et al. (2019). A novel murine model for arrhythmogenic cardiomyopathy points to a pathogenic role of Wnt signalling and miRNA dysregulation. *Cardiovasc. Res.* 115, 739–751. doi: 10.1093/cvr/cvy253

Capetanaki, Y. (2002). Desmin cytoskeleton: a potential regulator of muscle mitochondrial behavior and function. *Trends Cardiovasc. Med.* 12, 339–348. doi: 10.1016/s1050-1738(02)00184-6

Capetanaki, Y., Milner, D. J., and Weitzer, G. (1997). Desmin in muscle formation and maintenance: knockouts and consequences. *Cell Struct. Funct.* 22, 103–116. doi: 10.1247/csf.22.103

Cattanach, B. M., Dukes-Mcewan, J., Wotton, P. R., Stephenson, H. M., and Hamilton, R. M. (2015). A pedigree-based genetic appraisal of Boxer ARVC and the role of the Striatin mutation. *Vet. Rec.* 176:492. doi: 10.1136/vr.102821

Cerrone, M., and Delmar, M. (2014). Desmosomes and the sodium channel complex: implications for arrhythmogenic cardiomyopathy and Brugada syndrome. *Trends Cardiovasc. Med.* 24, 184–190. doi: 10.1016/j.tcm.2014.02.001

Cerrone, M., Lin, X., Zhang, M., Agullo-Pascual, E., Pfenniger, A., Chkourko Gusky, H., et al. (2014). Missense mutations in plakophilin-2 cause sodium current deficit and associate with a Brugada syndrome phenotype. *Circulation* 129, 1092–1103. doi: 10.1161/circulationaha.113.003077

Cerrone, M., Montnach, J., Lin, X., Zhao, Y. T., Zhang, M., Agullo-Pascual, E., et al. (2017). Plakophilin-2 is required for transcription of genes that control calcium cycling and cardiac rhythm. *Nat. Commun.* 8:106.

Cerrone, M., Noorman, M., Lin, X., Chkourko, H., Liang, F. X., Van Der Nagel, R., et al. (2012). Sodium current deficit and arrhythmogenesis in a murine model of plakophilin-2 haploinsufficiency. *Cardiovasc. Res.* 95, 460–468. doi: 10.1093/cvr/cvs218

Cheedipudi, S. M., Hu, J., Fan, S., Yuan, P., Karmouch, J., Czernuszewicz, G., et al. (2019). Exercise restores dysregulated gene expression in a mouse model of arrhythmogenic cardiomyopathy. *Cardiovasc. Res.* 116, 1199–1213. doi: 10.1093/cvr/cvz199

Chelko, S. P., Asimaki, A., Andersen, P., Bedja, D., Amat-Alarcon, N., Demazumder, D., et al. (2016). Central role for GSK3beta in the pathogenesis of arrhythmogenic cardiomyopathy. *JCI Insight* 1:e85923.

Chen, S. N., Sbaizero, O., Taylor, M. R. G., and Mestroni, L. (2019). Lamin A/C cardiomyopathy: implications for treatment. *Curr. Cardiol. Rep.* 21:160.

Chen, X., Bonne, S., Hatzfeld, M., Van Roy, F., and Green, K. J. (2002). Protein binding and functional characterization of plakophilin 2. Evidence for its diverse roles in desmosomes and beta -catenin signaling. *J. Biol. Chem.* 277, 10512–10522. doi: 10.1074/jbc.m108765200

Choi, H. J., Gross, J. C., Pokutta, S., and Weis, W. I. (2009). Interactions of plakoglobin and beta-catenin with desmosomal cadherins: basis of selective exclusion of alpha- and beta-catenin from desmosomes. *J. Biol. Chem.* 284, 31776–31788. doi: 10.1074/jbc.m109.047928

Choi, H. J., Park-Snyder, S., Pascoe, L. T., Green, K. J., and Weis, W. I. (2002). Structures of two intermediate filament-binding fragments of desmoplakin reveal a unique repeat motif structure. *Nat. Struct. Biol.* 9, 612–620.

Chopra, S. S., Stroud, D. M., Watanabe, H., Bennett, J. S., Burns, C. G., Wells, K. S., et al. (2010). Voltage-gated sodium channels are required for heart development in zebrafish. *Circ. Res.* 106, 1342–1350. doi: 10.1161/circresaha.109.213132

Christensen, A. H., Benn, M., Tybjaerg-Hansen, A., Haunso, S., and Svendsen, J. H. (2011). Screening of three novel candidate genes in arrhythmogenic right ventricular cardiomyopathy. *Genet. Test. Mol. Biomarkers* 15, 267–271. doi: 10.1089/gtmb.2010.0151

Chu, G., Ferguson, D. G., Edes, I., Kiss, E., Sato, Y., and Kranias, E. G. (1998). Phospholamban ablation and compensatory responses in the mammalian heart. *Ann. N. Y. Acad. Sci.* 853, 49–62. doi: 10.1111/j.1749-6632.1998.tb08256.x

Ciaramella, P., Basso, C., Di Loria, A., and Piantedosi, D. (2009). Arrhythmogenic right ventricular cardiomyopathy associated with severe left ventricular involvement in a cat. *J. Vet. Cardiol.* 11, 41–45. doi: 10.1016/j.jvc.2009.02.007

Clemen, C. S., Stockigt, F., Strucksberg, K. H., Chevessier, F., Winter, L., Schutz, J., et al. (2015). The toxic effect of R350P mutant desmin in striated muscle of man and mouse. *Acta Neuropathol.* 129, 297–315. doi: 10.1007/s00401-014-1363-2

Cruz, F. M., Sanz-Rosa, D., Roche-Molina, M., Garcia-Prieto, J., Garcia-Ruiz, J. M., Pizarro, G., et al. (2015). Exercise triggers ARVC phenotype in mice expressing a disease-causing mutated version of human plakophilin-2. *J. Am. Coll. Cardiol.* 65, 1438–1450. doi: 10.1016/j.jacc.2015.01.045

Cunningham, S. M., Sweeney, J. T., Macgregor, J., Barton, B. A., and Rush, J. E. (2018). Clinical features of english bulldogs with presumed arrhythmogenic right ventricular cardiomyopathy: 31 cases (2001-2013). *J. Am. Anim. Hosp. Assoc.* 54, 95–102. doi: 10.5326/jaaha-ms-6550

Dalkilic, I., Schienda, J., Thompson, T. G., and Kunkel, L. M. (2006). Loss of FilaminC (FLNc) results in severe defects in myogenesis and myotube structure. *Mol. Cell. Biol.* 26, 6522–6534. doi: 10.1128/mcb.00243-06

De Bortoli, M., Postma, A. V., Poloni, G., Calore, M., Minervini, G., Mazzotti, E., et al. (2018). Whole-exome sequencing identifies pathogenic variants in TJP1 gene associated with arrhythmogenic cardiomyopathy. *Circ. Genom. Precis Med.* 11:e002123.

Debus, J. D., Milting, H., Brodehl, A., Kassner, A., Anselmetti, D., Gummert, J., et al. (2019). In vitro analysis of arrhythmogenic cardiomyopathy associated desmoglein-2 (DSG2) mutations reveals diverse glycosylation patterns. *J. Mol. Cell. Cardiol.* 129, 303–313. doi: 10.1016/j.yjmcc.2019.03.014

Dieding, M., Debus, J. D., Kerkhoff, R., Gaertner-Rommel, A., Walhorn, V., Milting, H., et al. (2017). Arrhythmogenic cardiomyopathy related DSG2 mutations affect desmosomal cadherin binding kinetics. *Sci. Rep.* 7:13791.

Ding, Y., Yang, J., Chen, P., Lu, T., Jiao, K., Tester, D., et al. (2019). SORBS2 is a susceptibility gene to arrhythmogenic right ventricular cardiomyopathy. *bioRxiv* [Preprint]. doi: 10.1101/725077

Dyle, M. C., Kolakada, D., Cortazar, M. A., and Jagannathan, S. (2020). How to get away with nonsense: mechanisms and consequences of escape from nonsense-mediated RNA decay. *Wiley Interdiscip. Rev. RNA* 11:e1560.

Eason, B. D., Leach, S. B., and Kuroki, K. (2015). Arrhythmogenic right ventricular cardiomyopathy in a weimaraner. *Can. Vet. J.* 56, 1035–1039.

Eshkind, L., Tian, Q., Schmidt, A., Franke, W. W., Windoffer, R., and Leube, R. E. (2002). Loss of desmoglein 2 suggests essential functions for early embryonic development and proliferation of embryonal stem cells. *Eur. J. Cell Biol.* 81, 592–598. doi: 10.1078/0171-9335-00278

Fabritz, L., Hoogendijk, M. G., Scicluna, B. P., Van Amersfoorth, S. C., Fortmueller, L., Wolf, S., et al. (2011). Load-reducing therapy prevents development of arrhythmogenic right ventricular cardiomyopathy in plakoglobin-deficient mice. *J. Am. Coll. Cardiol.* 57, 740–750.

Falik-Zaccai, T. C., Barsheshet, Y., Mandel, H., Segev, M., Lorber, A., Gelberg, S., et al. (2017). Sequence variation in PPP1R13L results in a novel form of cardio-cutaneous syndrome. *EMBO Mol. Med.* 9:1326. doi: 10.15252/emmm.201708209

Ferreira-Cornwell, M. C., Luo, Y., Narula, N., Lenox, J. M., Lieberman, M., and Radice, G. L. (2002). Remodeling the intercalated disc leads to cardiomyopathy in mice misexpressing cadherins in the heart. *J. Cell Sci.* 115, 1623–1634.

Fish, M., Shaboodien, G., Kraus, S., Sliwa, K., Seidman, C. E., Burke, M. A., et al. (2016). Mutation analysis of the phospholamban gene in 315 South Africans with dilated, hypertrophic, peripartum and arrhythmogenic right ventricular cardiomyopathies. *Sci. Rep.* 6:22235.

Fox, P. R., Maron, B. J., Basso, C., Liu, S. K., and Thiene, G. (2000). Spontaneously occurring arrhythmogenic right ventricular cardiomyopathy in the domestic cat: a new animal model similar to the human disease. *Circulation* 102, 1863–1870. doi: 10.1161/01.cir.102.15.1863

Franke, W. W., Borrmann, C. M., Grund, C., and Pieperhoff, S. (2006). The area composita of adhering junctions connecting heart muscle cells of vertebrates. I. Molecular definition in intercalated disks of cardiomyocytes by immunoelectron microscopy of desmosomal proteins. *Eur. J. Cell. Biol.* 85, 69–82. doi: 10.1016/j.ejcb.2005.11.003

Gallicano, G. I., Kouklis, P., Bauer, C., Yin, M., Vasioukhin, V., Degenstein, L., et al. (1998). Desmoplakin is required early in development for assembly of desmosomes and cytoskeletal linkage. *J. Cell Biol.* 143, 2009–2022. doi: 10.1083/jcb.143.7.2009

Gandjbakhch, E., Vite, A., Gary, F., Fressart, V., Donal, E., Simon, F., et al. (2013). Screening of genes encoding junctional candidates in arrhythmogenic right ventricular cardiomyopathy/dysplasia. *Europace* 15, 1522–1525. doi: 10.1093/europace/eut224

Garcia-Gras, E., Lombardi, R., Giocondo, M. J., Willerson, J. T., Schneider, M. D., Khoury, D. S., et al. (2006). Suppression of canonical Wnt/beta-catenin

signaling by nuclear plakoglobin recapitulates phenotype of arrhythmogenic right ventricular cardiomyopathy. *J. Clin. Invest.* 116, 2012–2021. doi: 10.1172/jci27751

Gerull, B. (2015). The rapidly evolving role of titin in cardiac physiology and cardiomyopathy. *Can. J. Cardiol.* 31, 1351–1359. doi: 10.1016/j.cjca.2015.08.016

Gerull, B., Gramlich, M., Atherton, J., Mcnabb, M., Trombitas, K., Sasse-Klaassen, S., et al. (2002). Mutations of TTN, encoding the giant muscle filament titin, cause familial dilated cardiomyopathy. *Nat. Genet.* 30, 201–204. doi: 10.1038/ng815

Gerull, B., Heuser, A., Wichter, T., Paul, M., Basson, C. T., Mcdermott, D. A., et al. (2004). Mutations in the desmosomal protein plakophilin-2 are common in arrhythmogenic right ventricular cardiomyopathy. *Nat. Genet.* 36, 1162–1164. doi: 10.1038/ng1461

Gerull, B., Klaassen, S., and Brodehl, A. (2019). "The genetic landscape of cardiomyopathies," in *Genetic Causes of Cardiac Disease*, eds J. Erdmann, and A. Moretti (Cham: Springer), 45–91. doi: 10.1007/978-3-030-27371-2_2

Ghatak, S., Morgner, J., and Wickstrom, S. A. (2013). ILK: a pseudokinase with a unique function in the integrin-actin linkage. *Biochem. Soc. Trans.* 41, 995–1001. doi: 10.1042/bst20130062

Girolami, F., Iascone, M., Tomberli, B., Bardi, S., Benelli, M., Marseglia, G., et al. (2014). Novel alpha-actinin 2 variant associated with familial hypertrophic cardiomyopathy and juvenile atrial arrhythmias: a massively parallel sequencing study. *Circ. Cardiovasc. Genet.* 7, 741–750. doi: 10.1161/circgenetics.113.000486

Giuliodori, A., Beffagna, G., Marchetto, G., Fornetto, C., Vanzi, F., Toppo, S., et al. (2018). Loss of cardiac Wnt/beta-catenin signalling in desmoplakin-deficient AC8 zebrafish models is rescuable by genetic and pharmacological intervention. *Cardiovasc. Res.* 114, 1082–1097. doi: 10.1093/cvr/cvy057

Glynn, P., Musa, H., Wu, X., Unudurthi, S. D., Little, S., Qian, L., et al. (2015). Voltage-gated sodium channel phosphorylation at Ser571 regulates late current, arrhythmia, and cardiac function *in vivo*. *Circulation* 132, 567–577. doi: 10.1161/circulationaha.114.015218

Gomes, J., Finlay, M., Ahmed, A. K., Ciaccio, E. J., Asimaki, A., Saffitz, J. E., et al. (2012). Electrophysiological abnormalities precede overt structural changes in arrhythmogenic right ventricular cardiomyopathy due to mutations in desmoplakin-A combined murine and human study. *Eur. Heart J.* 33, 1942–1953. doi: 10.1093/eurheartj/ehr472

Good, J. M., Fellmann, F., Bhuiyan, Z. A., Rotman, S., Pruvot, E., and Schlapfer, J. (2020). ACTN2 variant associated with a cardiac phenotype suggestive of left-dominant arrhythmogenic cardiomyopathy. *Heart Rhythm Case Rep.* 6, 15–19. doi: 10.1016/j.hrcr.2019.10.001

Goossens, S., Janssens, B., Bonne, S., De Rycke, R., Braet, F., van Hengel, J., et al. (2007). A unique and specific interaction between alphaT-catenin and plakophilin-2 in the area composita, the mixed-type junctional structure of cardiac intercalated discs. *J. Cell Sci.* 120, 2126–2136. doi: 10.1242/jcs.004713

Gramlich, M., Michely, B., Krohne, C., Heuser, A., Erdmann, B., Klaassen, S., et al. (2009). Stress-induced dilated cardiomyopathy in a knock-in mouse model mimicking human titin-based disease. *J. Mol. Cell Cardiol.* 47, 352–358. doi: 10.1016/j.yjmcc.2009.04.014

Grossmann, K. S., Grund, C., Huelsken, J., Behrend, M., Erdmann, B., Franke, W. W., et al. (2004). Requirement of plakophilin 2 for heart morphogenesis and cardiac junction formation. *J. Cell Biol.* 167, 149–160. doi: 10.1083/jcb.200402096

Guo, W., Schafer, S., Greaser, M. L., Radke, M. H., Liss, M., Govindarajan, T., et al. (2012). RBM20, a gene for hereditary cardiomyopathy, regulates titin splicing. *Nat. Med.* 18, 766–773. doi: 10.1038/nm.2693

Gupta, V., Discenza, M., Guyon, J. R., Kunkel, L. M., and Beggs, A. H. (2012). alpha-Actinin-2 deficiency results in sarcomeric defects in zebrafish that cannot be rescued by alpha-actinin-3 revealing functional differences between sarcomeric isoforms. *FASEB J.* 26, 1892–1908. doi: 10.1096/fj.11-194548

Haghighi, K., Kolokathis, F., Gramolini, A. O., Waggoner, J. R., Pater, L., Lynch, R. A., et al. (2006). A mutation in the human phospholamban gene, deleting arginine 14, results in lethal, hereditary cardiomyopathy. *Proc. Natl. Acad. Sci. U.S.A.* 103, 1388–1393. doi: 10.1073/pnas.0510519103

Haghighi, K., Pritchard, T., Bossuyt, J., Waggoner, J. R., Yuan, Q., Fan, G. C., et al. (2012). The human phospholamban Arg14-deletion mutant localizes to plasma membrane and interacts with the Na/K-ATPase. *J. Mol. Cell Cardiol.* 52, 773–782. doi: 10.1016/j.yjmcc.2011.11.012

Hall, C. L., Akhtar, M. M., Sabater-Molina, M., Futema, M., Asimaki, A., Protonotarios, A., et al. (2019). Filamin C variants are associated with a distinctive clinical and immunohistochemical arrhythmogenic cardiomyopathy phenotype. *Int J Cardiol.* 307, 101–108. doi: 10.1016/j.ijcard.2019.09.048

Hall, C. L., Gurha, P., Sabater-Molina, M., Asimaki, A., Futema, M., Lovering, R. C., et al. (2020). RNA sequencing-based transcriptome profiling of cardiac tissue implicates novel putative disease mechanisms in FLNC-associated arrhythmogenic cardiomyopathy. *Int. J. Cardiol.* 302, 124–130. doi: 10.1016/j.ijcard.2019.12.002

Hamada, Y., Yamamoto, T., Nakamura, Y., Sufu-Shimizu, Y., Nanno, T., Fukuda, M., et al. (2020). G790del mutation in DSC2 alone is insufficient to develop the pathogenesis of ARVC in a mouse model. *Biochem. Biophys. Rep.* 21:100711. doi: 10.1016/j.bbrep.2019.100711

Han, L., Huang, C., and Zhang, S. (2019). The RNA-binding protein SORBS2 suppresses hepatocellular carcinoma tumourigenesis and metastasis by stabilizing RORA mRNA. *Liver Int.* 39, 2190–2203. doi: 10.1111/liv.14202

Hannigan, G. E., Mcdonald, P. C., Walsh, M. P., and Dedhar, S. (2011). Integrin-linked kinase: not so 'pseudo' after all. *Oncogene* 30, 4375–4385. doi: 10.1038/onc.2011.177

Harada, H., Hayashi, T., Nishi, H., Kusaba, K., Koga, Y., Koga, Y., et al. (2018). Phenotypic expression of a novel desmin gene mutation: hypertrophic cardiomyopathy followed by systemic myopathy. *J. Hum. Genet.* 63, 249–254. doi: 10.1038/s10038-017-0383-x

Harpster, N. K. (1991). Boxer cardiomyopathy. A review of the long-term benefits of antiarrhythmic therapy. *Vet. Clin. North Am. Small Anim. Pract.* 21, 989–1004.

Harrison, O. J., Brasch, J., Lasso, G., Katsamba, P. S., Ahlsen, G., Honig, B., et al. (2016). Structural basis of adhesive binding by desmocollins and desmogleins. *Proc. Natl. Acad. Sci. U.S.A.* 113, 7160–7165. doi: 10.1073/pnas.1606272113

Harvey, A. M., Battersby, I. A., Faena, M., Fews, D., Darke, P. G., and Ferasin, L. (2005). Arrhythmogenic right ventricular cardiomyopathy in two cats. *J. Small Anim. Pract.* 46, 151–156.

Hatzfeld, M., Keil, R., and Magin, T. M. (2017). Desmosomes and intermediate filaments: their consequences for tissue mechanics. *Cold Spring Harb. Perspect. Biol.* 9:a029157. doi: 10.1101/cshperspect.a029157

Heffler, J., Shah, P. P., Robison, P., Phyo, S., Veliz, K., Uchida, K., et al. (2020). A balance between intermediate filaments and microtubules maintains nuclear architecture in the cardiomyocyte. *Circ. Res.* 126, e10–e26.

Herbert Pratt, C., Potter, C. S., Fairfield, H., Reinholdt, L. G., Bergstrom, D. E., Harris, B. S., et al. (2015). Dsp rul: a spontaneous mouse mutation in desmoplakin as a model of Carvajal-Huerta syndrome. *Exp. Mol. Pathol.* 98, 164–172. doi: 10.1016/j.yexmp.2015.01.015

Herman, D. S., Lam, L., Taylor, M. R., Wang, L., Teekakirikul, P., Christodoulou, D., et al. (2012). Truncations of titin causing dilated cardiomyopathy. *N. Engl. J. Med.* 366, 619–628.

Herron, B. J., Rao, C., Liu, S., Laprade, L., Richardson, J. A., Olivieri, E., et al. (2005). A mutation in NFkB interacting protein 1 results in cardiomyopathy and abnormal skin development in wa3 mice. *Hum. Mol. Genet.* 14, 667–677. doi: 10.1093/hmg/ddi063

Hesse, M., Kondo, C. S., Clark, R. B., Su, L., Allen, F. L., Geary-Joo, C. T., et al. (2007). Dilated cardiomyopathy is associated with reduced expression of the cardiac sodium channel Scn5a. *Cardiovasc. Res.* 75, 498–509. doi: 10.1016/j.cardiores.2007.04.009

Heuser, A., Plovie, E. R., Ellinor, P. T., Grossmann, K. S., Shin, J. T., Wichter, T., et al. (2006). Mutant desmocollin-2 causes arrhythmogenic right ventricular cardiomyopathy. *Am. J. Hum. Genet.* 79, 1081–1088.

Hijikata, T., Murakami, T., Imamura, M., Fujimaki, N., and Ishikawa, H. (1999). Plectin is a linker of intermediate filaments to Z-discs in skeletal muscle fibers. *J. Cell Sci.* 112(Pt 6), 867–876.

Hodgkinson, K. A., Connors, S. P., Merner, N., Haywood, A., Young, T. L., Mckenna, W. J., et al. (2013). The natural history of a genetic subtype of arrhythmogenic right ventricular cardiomyopathy caused by a p.*S358L* mutation in TMEM43. *Clin. Genet.* 83, 321–331. doi: 10.1111/j.1399-0004.2012.01919.x

Hofmann, I., Mertens, C., Brettel, M., Nimmrich, V., Schnolzer, M., and Herrmann, H. (2000). Interaction of plakophilins with desmoplakin and intermediate filament proteins: an in vitro analysis. *J. Cell Sci.* 113(Pt 13), 2471–2483.

Huttner, I. G., Trivedi, G., Jacoby, A., Mann, S. A., Vandenberg, J. I., and Fatkin, D. (2013). A transgenic zebrafish model of a human cardiac sodium channel mutation exhibits bradycardia, conduction-system abnormalities and early death. *J. Mol. Cell Cardiol.* 61, 123–132. doi: 10.1016/j.yjmcc.2013.06.005

Huttner, I. G., Wang, L. W., Santiago, C. F., Horvat, C., Johnson, R., Cheng, D., et al. (2018). A-band titin truncation in zebrafish causes dilated cardiomyopathy and hemodynamic stress intolerance. *Circ. Genom Precis. Med.* 11:e002135.

Kaartinen, V., Voncken, J. W., Shuler, C., Warburton, D., Bu, D., Heisterkamp, N., et al. (1995). Abnormal lung development and cleft palate in mice lacking TGF-beta 3 indicates defects of epithelial-mesenchymal interaction. *Nat. Genet.* 11, 415–421. doi: 10.1038/ng1295-415

Kannankeril, P. J., Mitchell, B. M., Goonasekera, S. A., Chelu, M. G., Zhang, W., Sood, S., et al. (2006). Mice with the R176Q cardiac ryanodine receptor mutation exhibit catecholamine-induced ventricular tachycardia and cardiomyopathy. *Proc. Natl. Acad. Sci. U.S.A.* 103, 12179–12184. doi: 10.1073/pnas.0600268103

Kant, S., Holthofer, B., Magin, T. M., Krusche, C. A., and Leube, R. E. (2015). Desmoglein 2-dependent arrhythmogenic cardiomyopathy is caused by a loss of adhesive function. *Circ. Cardiovasc. Genet.* 8, 553–563. doi: 10.1161/circgenetics.114.000974

Kant, S., Krull, P., Eisner, S., Leube, R. E., and Krusche, C. A. (2012). Histological and ultrastructural abnormalities in murine desmoglein 2-mutant hearts. *Cell Tissue Res.* 348, 249–259. doi: 10.1007/s00441-011-1322-3

Katsuno, T., Umeda, K., Matsui, T., Hata, M., Tamura, A., Itoh, M., et al. (2008). Deficiency of zonula occludens-1 causes embryonic lethal phenotype associated with defected yolk sac angiogenesis and apoptosis of embryonic cells. *Mol. Biol. Cell.* 19, 2465–2475. doi: 10.1091/mbc.e07-12-1215

Khan, M. A., Reckman, Y. J., Aufiero, S., van den Hoogenhof, M. M., Van Der Made, I., Beqqali, A., et al. (2016). RBM20 regulates circular RNA production from the titin gene. *Circ. Res.* 119, 996–1003. doi: 10.1161/circresaha.116.309568

Kirchhof, P., Fabritz, L., Zwiener, M., Witt, H., Schafers, M., Zellerhoff, S., et al. (2006). Age- and training-dependent development of arrhythmogenic right ventricular cardiomyopathy in heterozygous plakoglobin-deficient mice. *Circulation* 114, 1799–1806. doi: 10.1161/circulationaha.106.624502

Kirchner, F., Schuetz, A., Boldt, L. H., Martens, K., Dittmar, G., Haverkamp, W., et al. (2012). Molecular insights into arrhythmogenic right ventricular cardiomyopathy caused by plakophilin-2 missense mutations. *Circ. Cardiovasc. Genet.* 5, 400–411. doi: 10.1161/circgenetics.111.961854

Klauke, B., Kossmann, S., Gaertner, A., Brand, K., Stork, I., Brodehl, A., et al. (2010). De novo desmin-mutation N116S is associated with arrhythmogenic right ventricular cardiomyopathy. *Hum. Mol. Genet.* 19, 4595–4607. doi: 10.1093/hmg/ddq387

Knoll, R., Postel, R., Wang, J., Kratzner, R., Hennecke, G., Vacaru, A. M., et al. (2007). Laminin-alpha4 and integrin-linked kinase mutations cause human cardiomyopathy via simultaneous defects in cardiomyocytes and endothelial cells. *Circulation* 116, 515–525. doi: 10.1161/circulationaha.107.689984

Koshimizu, E., Imamura, S., Qi, J., Toure, J., Valdez, D. M. Jr., Carr, C. E., et al. (2011). Embryonic senescence and laminopathies in a progeroid zebrafish model. *PLoS One* 6:e17688. doi: 10.1371/journal.pone.0017688

Kostareva, A., Sjoberg, G., Bruton, J., Zhang, S. J., Balogh, J., Gudkova, A., et al. (2008). Mice expressing L345P mutant desmin exhibit morphological and functional changes of skeletal and cardiac mitochondria. *J. Muscle Res. Cell Motil.* 29, 25–36. doi: 10.1007/s10974-008-9139-8

Kostetskii, I., Li, J., Xiong, Y., Zhou, R., Ferrari, V. A., Patel, V. V., et al. (2005). Induced deletion of the N-cadherin gene in the heart leads to dissolution of the intercalated disc structure. *Circ. Res.* 96, 346–354. doi: 10.1161/01.res.0000156274.72390.2c

Krawczak, M., Ball, E. V., Fenton, I., Stenson, P. D., Abeysinghe, S., Thomas, N., et al. (2000). Human gene mutation database-a biomedical information and research resource. *Hum. Mutat.* 15, 45–51. doi: 10.1002/(sici)1098-1004(200001)15:1<45::aid-humu10>3.0.co;2-t

Krusche, C. A., Holthofer, B., Hofe, V., Van De Sandt, A. M., Eshkind, L., Bockamp, E., et al. (2011). Desmoglein 2 mutant mice develop cardiac fibrosis and dilation. *Basic Res. Cardiol.* 106, 617–633. doi: 10.1007/s00395-011-0175-y

Kubanek, M., Schimerova, T., Piherova, L., Brodehl, A., Krebsova, A., Ratnavadivel, S., et al. (2020). Desminopathy: novel desmin variants, a new cardiac phenotype, and further evidence for secondary mitochondrial dysfunction. *J. Clin. Med.* 9:937. doi: 10.3390/jcm9040937

Lapouge, K., Fontao, L., Champliaud, M. F., Jaunin, F., Frias, M. A., Favre, B., et al. (2006). New insights into the molecular basis of desmoplakin- and desmin-related cardiomyopathies. *J. Cell Sci.* 119, 4974–4985. doi: 10.1242/jcs.03255

Leo-Macias, A., Liang, F. X., and Delmar, M. (2015). Ultrastructure of the intercellular space in adult murine ventricle revealed by quantitative tomographic electron microscopy. *Cardiovasc. Res.* 107, 442–452. doi: 10.1093/cvr/cvv182

Li, D., Liu, Y., Maruyama, M., Zhu, W., Chen, H., Zhang, W., et al. (2011). Restrictive loss of plakoglobin in cardiomyocytes leads to arrhythmogenic cardiomyopathy. *Hum. Mol. Genet.* 20, 4582–4596. doi: 10.1093/hmg/ddr392

Li, D., Tapscoft, T., Gonzalez, O., Burch, P. E., Quinones, M. A., Zoghbi, W. A., et al. (1999). Desmin mutation responsible for idiopathic dilated cardiomyopathy. *Circulation* 100, 461–464. doi: 10.1161/01.cir.100.5.461

Li, J., Goossens, S., van Hengel, J., Gao, E., Cheng, L., Tyberghein, K., et al. (2012). Loss of alphaT-catenin alters the hybrid adhering junctions in the heart and leads to dilated cardiomyopathy and ventricular arrhythmia following acute ischemia. *J. Cell Sci.* 125, 1058–1067. doi: 10.1242/jcs.098640

Li, J., Patel, V. V., Kostetskii, I., Xiong, Y., Chu, A. F., Jacobson, J. T., et al. (2005). Cardiac-specific loss of N-cadherin leads to alteration in connexins with conduction slowing and arrhythmogenesis. *Circ. Res.* 97, 474–481. doi: 10.1161/01.res.0000181132.11393.18

Li, J., Swope, D., Raess, N., Cheng, L., Muller, E. J., and Radice, G. L. (2011). Cardiac tissue-restricted deletion of plakoglobin results in progressive cardiomyopathy and activation of {beta}-catenin signaling. *Mol. Cell. Biol.* 31, 1134–1144. doi: 10.1128/mcb.01025-10

Li, M., Andersson-Lendahl, M., Sejersen, T., and Arner, A. (2013). Knockdown of desmin in zebrafish larvae affects interfilament spacing and mechanical properties of skeletal muscle. *J. Gen. Physiol.* 141, 335–345. doi: 10.1085/jgp.201210915

Li, Z., Ai, T., Samani, K., Xi, Y., Tzeng, H. P., Xie, M., et al. (2010). A ZASP missense mutation, S196L, leads to cytoskeletal and electrical abnormalities in a mouse model of cardiomyopathy. *Circ. Arrhythm Electrophysiol.* 3, 646–656. doi: 10.1161/circep.109.929240

Li, Z., Colucci-Guyon, E., Pincon-Raymond, M., Mericskay, M., Pournin, S., Paulin, D., et al. (1996). Cardiovascular lesions and skeletal myopathy in mice lacking desmin. *Dev. Biol.* 175, 362–366. doi: 10.1006/dbio.1996.0122

Lin, X., Ruiz, J., Bajraktari, I., Ohman, R., Banerjee, S., Gribble, K., et al. (2014). Z-disc-associated, alternatively spliced, PDZ motif-containing protein (ZASP) mutations in the actin-binding domain cause disruption of skeletal muscle actin filaments in myofibrillar myopathy. *J. Biol. Chem.* 289, 13615–13626. doi: 10.1074/jbc.m114.550418

Liu, K., Hipkens, S., Yang, T., Abraham, R., Zhang, W., Chopra, N., et al. (2006). Recombinase-mediated cassette exchange to rapidly and efficiently generate mice with human cardiac sodium channels. *Genesis* 44, 556–564. doi: 10.1002/dvg.20247

Lombardi, R., Da Graca Cabreira-Hansen, M., Bell, A., Fromm, R. R., Willerson, J. T., and Marian, A. J. (2011). Nuclear plakoglobin is essential for differentiation of cardiac progenitor cells to adipocytes in arrhythmogenic right ventricular cardiomyopathy. *Circ. Res.* 109, 1342–1353. doi: 10.1161/circresaha.111.255075

Lopez-Ayala, J. M., Ortiz-Genga, M., Gomez-Milanes, I., Lopez-Cuenca, D., Ruiz-Espejo, F., Sanchez-Munoz, J. J., et al. (2015). A mutation in the Z-line Cypher/ZASP protein is associated with arrhythmogenic right ventricular cardiomyopathy. *Clin. Genet.* 88, 172–176. doi: 10.1111/cge.12458

Luther, P. K. (2009). The vertebrate muscle Z-disc: sarcomere anchor for structure and signalling. *J. Muscle Res. Cell Motil.* 30, 171–185. doi: 10.1007/s10974-009-9189-6

Lyon, R. C., Mezzano, V., Wright, A. T., Pfeiffer, E., Chuang, J., Banares, K., et al. (2014). Connexin defects underlie arrhythmogenic right ventricular cardiomyopathy in a novel mouse model. *Hum. Mol. Genet.* 23, 1134–1150. doi: 10.1093/hmg/ddt508

Maatz, H., Jens, M., Liss, M., Schafer, S., Heinig, M., Kirchner, M., et al. (2014). RNA-binding protein RBM20 represses splicing to orchestrate cardiac pre-mRNA processing. *J. Clin. Invest.* 124, 3419–3430. doi: 10.1172/jci74523

Marakhonov, A. V., Brodehl, A., Myasnikov, R. P., Sparber, P. A., Kiseleva, A. V., Kulikova, O. V., et al. (2019). Noncompaction cardiomyopathy is caused by a novel in-frame desmin (DES) deletion mutation within the 1A coiled-coil rod segment leading to a severe filament assembly defect. *Hum. Mutat.* 40, 734–741. doi: 10.1002/humu.23747

Marbach, F., Rustad, C. F., Riess, A., Dukic, D., Hsieh, T. C., Jobani, I., et al. (2019). The discovery of a LEMD2-associated nuclear envelopathy with early progeroid appearance suggests advanced applications for ai-driven facial phenotyping. *Am. J. Hum. Genet.* 104, 749–757. doi: 10.1016/j.ajhg.2019.02.021

Martin, E. D., Moriarty, M. A., Byrnes, L., and Grealy, M. (2009). Plakoglobin has both structural and signalling roles in zebrafish development. *Dev. Biol.* 327, 83–96. doi: 10.1016/j.ydbio.2008.11.036

Mayosi, B. M., Fish, M., Shaboodien, G., Mastantuono, E., Kraus, S., Wieland, T., et al. (2017). Identification of Cadherin 2 (CDH2) mutations in arrhythmogenic right ventricular cardiomyopathy. *Circ. Cardiovasc. Genet.* 10:e001605.

McKoy, G., Protonotarios, N., Crosby, A., Tsatsopoulou, A., Anastasakis, A., Coonar, A., et al. (2000). Identification of a deletion in plakoglobin in arrhythmogenic right ventricular cardiomyopathy with palmoplantar keratoderma and woolly hair (Naxos disease). *Lancet* 355, 2119–2124. doi: 10.1016/s0140-6736(00)02379-5

Merner, N. D., Hodgkinson, K. A., Haywood, A. F., Connors, S., French, V. M., Drenckhahn, J. D., et al. (2008). Arrhythmogenic right ventricular cardiomyopathy type 5 is a fully penetrant, lethal arrhythmic disorder caused by a missense mutation in the TMEM43 gene. *Am. J. Hum. Genet.* 82, 809–821. doi: 10.1016/j.ajhg.2008.01.010

Meurs, K. M., Mauceli, E., Lahmers, S., Acland, G. M., White, S. N., and Lindblad-Toh, K. (2010). Genome-wide association identifies a deletion in the 3' untranslated region of striatin in a canine model of arrhythmogenic right ventricular cardiomyopathy. *Hum. Genet.* 128, 315–324. doi: 10.1007/s00439-010-0855-y

Meurs, K. M., Spier, A. W., Miller, M. W., Lehmkuhl, L., and Towbin, J. A. (1999). Familial ventricular arrhythmias in boxers. *J. Vet. Intern. Med.* 13, 437–439. doi: 10.1111/j.1939-1676.1999.tb01460.x

Mezzano, V., Liang, Y., Wright, A. T., Lyon, R. C., Pfeiffer, E., Song, M. Y., et al. (2016). Desmosomal junctions are necessary for adult sinus node function. *Cardiovasc. Res.* 111, 274–286. doi: 10.1093/cvr/cvw083

Miller, M. S., Saslow, N. J., and Tilley, L. P. (1985). ECG of the month. Boxer cardiomyopathy. *J. Am. Vet. Med. Assoc.* 187, 1002–1004.

Mills, A. A., Zheng, B., Wang, X. J., Vogel, H., Roop, D. R., and Bradley, A. (1999). p63 is a p53 homologue required for limb and epidermal morphogenesis. *Nature* 398, 708–713. doi: 10.1038/19531

Milting, H., Klauke, B., Christensen, A. H., Musebeck, J., Walhorn, V., Grannemann, S., et al. (2015). The TMEM43 Newfoundland mutation p.*S358L* causing ARVC-5 was imported from Europe and increases the stiffness of the cell nucleus. *Eur. Heart J.* 36, 872–881. doi: 10.1093/eurheartj/ehu077

Mohapatra, B., Jimenez, S., Lin, J. H., Bowles, K. R., Coveler, K. J., Marx, J. G., et al. (2003). Mutations in the muscle LIM protein and alpha-actinin-2 genes in dilated cardiomyopathy and endocardial fibroelastosis. *Mol. Genet. Metab.* 80, 207–215. doi: 10.1016/s1096-7192(03)00142-2

Moncayo-Arlandi, J., Guasch, E., Sanz-De La Garza, M., Casado, M., Garcia, N. A., Mont, L., et al. (2016). Molecular disturbance underlies to arrhythmogenic cardiomyopathy induced by transgene content, age and exercise in a truncated PKP2 mouse model. *Hum. Mol. Genet.* 25, 3676–3688. doi: 10.1093/hmg/ddw213

Moriarty, M. A., Ryan, R., Lalor, P., Dockery, P., Byrnes, L., and Grealy, M. (2012). Loss of plakophilin 2 disrupts heart development in zebrafish. *Int. J. Dev. Biol.* 56, 711–718. doi: 10.1387/ijdb.113390mm

Murayama, R., Kimura-Asami, M., Togo-Ohno, M., Yamasaki-Kato, Y., Naruse, T. K., Yamamoto, T., et al. (2018). Phosphorylation of the RSRSP stretch is critical for splicing regulation by RNA-Binding Motif Protein 20 (RBM20) through nuclear localization. *Sci. Rep.* 8:8970.

Nikolova, V., Leimena, C., Mcmahon, A. C., Tan, J. C., Chandar, S., Jogia, D., et al. (2004). Defects in nuclear structure and function promote dilated cardiomyopathy in lamin A/C-deficient mice. *J. Clin. Invest.* 113, 357–369. doi: 10.1172/jci200419448

Nikolova, V., Leimena, C., Mcmahon, A. C., Tan, J. C., Chandar, S., Jogia, D., et al. (2004). Defects in nuclear structure and function promote dilated cardiomyopathy in lamin A/C-deficient mice. *J. Clin. Invest.* 113, 357–369.

Norgett, E. E., Hatsell, S. J., Carvajal-Huerta, L., Cabezas, J. C., Common, J., Purkis, P. E., et al. (2000). Recessive mutation in desmoplakin disrupts desmoplakin-intermediate filament interactions and causes dilated cardiomyopathy, woolly hair and keratoderma. *Hum. Mol. Genet.* 9, 2761–2766.

Notari, M., Hu, Y., Sutendra, G., Dedeic, Z., Lu, M., Dupays, L., et al. (2015). iASPP, a previously unidentified regulator of desmosomes, prevents arrhythmogenic right ventricular cardiomyopathy (ARVC)-induced sudden death. *Proc. Natl. Acad. Sci. U.S.A.* 112, E973–E981.

Nozari, A., Aghaei-Moghadam, E., Zeinaloo, A., Mollazadeh, R., Majnoon, M. T., Alavi, A., et al. (2018). A novel splicing variant in FLNC gene responsible for a highly penetrant familial dilated cardiomyopathy in an extended Iranian family. *Gene* 659, 160–167.

Padron-Barthe, L., Villalba-Orero, M., Gomez-Salinero, J. M., Dominguez, F., Roman, M., Larrasa-Alonso, J., et al. (2019). Severe cardiac dysfunction and death caused by arrhythmogenic right ventricular cardiomyopathy type 5 are improved by inhibition of glycogen synthase kinase-3beta. *Circulation* 140, 1188–1204.

Papadatos, G. A., Wallerstein, P. M., Head, C. E., Ratcliff, R., Brady, P. A., Benndorf, K., et al. (2002). Slowed conduction and ventricular tachycardia after targeted disruption of the cardiac sodium channel gene Scn5a. *Proc. Natl. Acad. Sci. U.S.A.* 99, 6210–6215.

Parikh, V. N., Caleshu, C., Reuter, C., Lazzeroni, L. C., Ingles, J., Garcia, J., et al. (2019). Regional variation in RBM20 causes a highly penetrant arrhythmogenic cardiomyopathy. *Circ. Heart Fail.* 12:e005371.

Patel, D. M., and Green, K. J. (2014). Desmosomes in the heart: a review of clinical and mechanistic analyses. *Cell Commun. Adhes.* 21, 109–128.

Peters, S. (2008). Arrhythmogenic right ventricular dysplasia-cardiomyopathy and provocable coved-type ST-segment elevation in right precordial leads: clues from long-term follow-up. *Europace* 10, 816–820.

Pilichou, K., Nava, A., Basso, C., Beffagna, G., Bauce, B., Lorenzon, A., et al. (2006). Mutations in desmoglein-2 gene are associated with arrhythmogenic right ventricular cardiomyopathy. *Circulation* 113, 1171–1179.

Pilichou, K., Remme, C. A., Basso, C., Campian, M. E., Rizzo, S., Barnett, P., et al. (2009). Myocyte necrosis underlies progressive myocardial dystrophy in mouse dsg2-related arrhythmogenic right ventricular cardiomyopathy. *J. Exp. Med.* 206, 1787–1802.

Poloni, G., Calore, M., Rigato, I., Marras, E., Minervini, G., Mazzotti, E., et al. (2019). A targeted next-generation gene panel reveals a novel heterozygous nonsense variant in the TP63 gene in patients with arrhythmogenic cardiomyopathy. *Heart Rhythm* 16, 773–780.

Pott, A., Shahid, M., Kohler, D., Pylatiuk, C., Weinmann, K., Just, S., et al. (2018). Therapeutic chemical screen identifies phosphatase inhibitors to reconstitute PKB phosphorylation and cardiac contractility in ILK-deficient zebrafish. *Biomolecules* 8:153.

Proetzel, G., Pawlowski, S. A., Wiles, M. V., Yin, M., Boivin, G. P., Howles, P. N., et al. (1995). Transforming growth factor-beta 3 is required for secondary palate fusion. *Nat. Genet.* 11, 409–414.

Protonotarios, A., and Elliott, P. M. (2019). Arrhythmogenic cardiomyopathies (ACs): diagnosis, risk stratification and management. *Heart* 105, 1117–1128.

Protonotarios, N., and Tsatsopoulou, A. (2004). Naxos disease and Carvajal syndrome: cardiocutaneous disorders that highlight the pathogenesis and broaden the spectrum of arrhythmogenic right ventricular cardiomyopathy. *Cardiovasc. Pathol.* 13, 185–194.

Protonotarios, N., and Tsatsopoulou, A. (2006). Naxos disease: cardiocutaneous syndrome due to cell adhesion defect. *Orphanet J. Rare Dis.* 1:4.

Psarras, S., Mavroidis, M., Sanoudou, D., Davos, C. H., Xanthou, G., Varela, A. E., et al. (2012). Regulation of adverse remodelling by osteopontin in a genetic heart failure model. *Eur. Heart J.* 33, 1954–1963.

Quang, K. L., Maguy, A., Qi, X. Y., Naud, P., Xiong, F., Tadevosyan, A., et al. (2015). Loss of cardiomyocyte integrin-linked kinase produces an arrhythmogenic cardiomyopathy in mice. *Circ. Arrhythm Electrophysiol.* 8, 921–932.

Quarta, G., Syrris, P., Ashworth, M., Jenkins, S., Zuborne Alapi, K., Morgan, J., et al. (2012). Mutations in the Lamin A/C gene mimic arrhythmogenic right ventricular cardiomyopathy. *Eur. Heart J.* 33, 1128–1136.

Ramond, F., Janin, A., Di Filippo, S., Chanavat, V., Chalabreysse, L., Roux-Buisson, N., et al. (2017). Homozygous PKP2 deletion associated with neonatal left ventricle noncompaction. *Clin. Genet.* 91, 126–130.

Rampazzo, A., Beffagna, G., Nava, A., Occhi, G., Bauce, B., Noiato, M., et al. (2003). Arrhythmogenic right ventricular cardiomyopathy type 1 (ARVD1): confirmation of locus assignment and mutation screening of four candidate genes. *Eur. J. Hum. Genet.* 11, 69–76.

Ramspacher, C., Steed, E., Boselli, F., Ferreira, R., Faggianelli, N., Roth, S., et al. (2015). Developmental alterations in heart biomechanics and skeletal muscle function in desmin mutants suggest an early pathological root for desminopathies. *Cell. Rep.* 11, 1564–1576.

Rasmussen, T. B., Nissen, P. H., Palmfeldt, J., Gehmlich, K., Dalager, S., Jensen, U. B., et al. (2014). Truncating plakophilin-2 mutations in arrhythmogenic cardiomyopathy are associated with protein haploinsufficiency in both myocardium and epidermis. *Circ. Cardiovasc. Genet.* 7, 230–240.

Rimpler, U. (2014). *Funktionelle Charakterisierung von Desmocollin 2 während der Embryonalentwicklung und im adulten Herzen in der Maus*. Berlin: Humbold Universität zu Berlin.

Rizzo, S., Lodder, E. M., Verkerk, A. O., Wolswinkel, R., Beekman, L., Pilichou, K., et al. (2012). Intercalated disc abnormalities, reduced Na(+) current density, and conduction slowing in desmoglein-2 mutant mice prior to cardiomyopathic changes. *Cardiovasc. Res.* 95, 409–418.

Roberts, A. M., Ware, J. S., Herman, D. S., Schafer, S., Baksi, J., Bick, A. G., et al. (2015). Integrated allelic, transcriptional, and phenomic dissection of the cardiac effects of titin truncations in health and disease. *Sci. Transl. Med.* 7:270ra276.

Ruiz, P., Brinkmann, V., Ledermann, B., Behrend, M., Grund, C., Thalhammer, C., et al. (1996). Targeted mutation of plakoglobin in mice reveals essential functions of desmosomes in the embryonic heart. *J. Cell Biol.* 135, 215–225.

Santos-Pereira, J. M., Gallardo-Fuentes, L., Neto, A., Acemel, R. D., and Tena, J. J. (2019). Pioneer and repressive functions of p63 during zebrafish embryonic ectoderm specification. *Nat. Commun.* 10:3049.

Sato, P. Y., Coombs, W., Lin, X., Nekrasova, O., Green, K. J., Isom, L. L., et al. (2011). Interactions between ankyrin-G, Plakophilin-2, and Connexin43 at the cardiac intercalated disc. *Circ. Res.* 109, 193–201.

Sedaghat-Hamedani, F., Haas, J., Zhu, F., Geier, C., Kayvanpour, E., Liss, M., et al. (2017). Clinical genetics and outcome of left ventricular non-compaction cardiomyopathy. *Eur. Heart J.* 38, 3449–3460.

Selcen, D., and Engel, A. G. (2005). Mutations in ZASP define a novel form of muscular dystrophy in humans. *Ann. Neurol.* 57, 269–276.

Sen-Chowdhry, S., and McKenna, W. J. (2010). Reconciling the protean manifestations of arrhythmogenic cardiomyopathy. *Circ. Arrhythm Electrophysiol.* 3, 566–570.

Sen-Chowdhry, S., Morgan, R. D., Chambers, J. C., and Mckenna, W. J. (2010). Arrhythmogenic cardiomyopathy: etiology, diagnosis, and treatment. *Annu. Rev. Med.* 61, 233–253.

Shan, J., Xie, W., Betzenhauser, M., Reiken, S., Chen, B. X., Wronska, A., et al. (2012). Calcium leak through ryanodine receptors leads to atrial fibrillation in 3 mouse models of catecholaminergic polymorphic ventricular tachycardia. *Circ. Res.* 111, 708–717.

Shatunov, A., Olive, M., Odgerel, Z., Stadelmann-Nessler, C., Irlbacher, K., Van Landeghem, F., et al. (2009). In-frame deletion in the seventh immunoglobulin-like repeat of filamin C in a family with myofibrillar myopathy. *Eur. J. Hum. Genet.* 17, 656–663.

Shih, Y. H., Dvornikov, A. V., Zhu, P., Ma, X., Kim, M., Ding, Y., et al. (2016). Exon- and contraction-dependent functions of titin in sarcomere assembly. *Development* 143, 4713–4722.

Simpson, M. A., Cook, R. W., Solanki, P., Patton, M. A., Dennis, J. A., and Crosby, A. H. (2009). A mutation in NFkappaB interacting protein 1 causes cardiomyopathy and woolly haircoat syndrome of Poll Hereford cattle. *Anim. Genet.* 40, 42–46.

Slesnick, T., Parks, W. J., Poulik, J., Al-Haddad, E., Vickery, J., Eskarous, H., et al. (2019). Cardiac magnetic resonance imaging macroscopic fibro-fatty infiltration of the myocardium in pediatric patients with arrhythmogenic right ventricular cardiomyopathy/dysplasia. *Fetal Pediatr. Pathol.* doi: 10.1080/15513815.2019.1675108 [Epub ahead of print].

Stockigt, F., Eichhorn, L., Beiert, T., Knappe, V., Radecke, T., Steinmetz, M., et al. (2020). Heart failure after pressure overload in autosomal-dominant desminopathies: lessons from heterozygous DES-p.*R349P* knock-in mice. *PLoS One* 15:e0228913. doi: 10.1371/journal.pone.0228913

Stroud, M. J. (2018). Linker of nucleoskeleton and cytoskeleton complex proteins in cardiomyopathy. *Biophys. Rev.* 10, 1033–1051.

Stroud, M. J., Fang, X., Zhang, J., Guimaraes-Camboa, N., Veevers, J., Dalton, N. D., et al. (2018). Luma is not essential for murine cardiac development and function. *Cardiovasc. Res.* 114, 378–388.

Sullivan, T., Escalante-Alcalde, D., Bhatt, H., Anver, M., Bhat, N., Nagashima, K., et al. (1999). Loss of A-type lamin expression compromises nuclear envelope integrity leading to muscular dystrophy. *J. Cell Biol.* 147, 913–920.

Swope, D., Cheng, L., Gao, E., Li, J., and Radice, G. L. (2012). Loss of cadherin-binding proteins beta-catenin and plakoglobin in the heart leads to gap junction remodeling and arrhythmogenesis. *Mol. Cell. Biol.* 32, 1056–1067.

Syrris, P., Ward, D., Evans, A., Asimaki, A., Gandjbakhch, E., Sen-Chowdhry, S., et al. (2006). Arrhythmogenic right ventricular dysplasia/cardiomyopathy associated with mutations in the desmosomal gene desmocollin-2. *Am. J. Hum. Genet.* 79, 978–984.

Takeshima, H., Komazaki, S., Hirose, K., Nishi, M., Noda, T., and Iino, M. (1998). Embryonic lethality and abnormal cardiac myocytes in mice lacking ryanodine receptor type 2. *EMBO J.* 17, 3309–3316.

Tapia, O., Fong, L. G., Huber, M. D., Young, S. G., and Gerace, L. (2015). Nuclear envelope protein Lem2 is required for mouse development and regulates MAP and AKT kinases. *PLoS One* 10:e0116196. doi: 10.1371/journal.pone.0116196

Taylor, M., Graw, S., Sinagra, G., Barnes, C., Slavov, D., Brun, F., et al. (2011). Genetic variation in titin in arrhythmogenic right ventricular cardiomyopathy-overlap syndromes. *Circulation* 124, 876–885.

Te Riele, A. S., Agullo-Pascual, E., James, C. A., Leo-Macias, A., Cerrone, M., Zhang, M., et al. (2017). Multilevel analyses of SCN5A mutations in arrhythmogenic right ventricular dysplasia/cardiomyopathy suggest non-canonical mechanisms for disease pathogenesis. *Cardiovasc. Res.* 113, 102–111.

Tiso, N., Stephan, D. A., Nava, A., Bagattin, A., Devaney, J. M., Stanchi, F., et al. (2001). Identification of mutations in the cardiac ryanodine receptor gene in families affected with arrhythmogenic right ventricular cardiomyopathy type 2 (ARVD2). *Hum. Mol. Genet.* 10, 189–194.

Towbin, J. A., Mckenna, W. J., Abrams, D. J., Ackerman, M. J., Calkins, H., Darrieux, F. C. C., et al. (2019). 2019 HRS expert consensus statement on evaluation, risk stratification, and management of arrhythmogenic cardiomyopathy. *Heart Rhythm* 16, e301–e372.

Turkowski, K. L., Tester, D. J., Bos, J. M., Haugaa, K. H., and Ackerman, M. J. (2017). Whole exome sequencing with genomic triangulation implicates CDH2-encoded N-cadherin as a novel pathogenic substrate for arrhythmogenic cardiomyopathy. *Congenit Heart Dis.* 12, 226–235.

Valdes-Mas, R., Gutierrez-Fernandez, A., Gomez, J., Coto, E., Astudillo, A., Puente, D. A., et al. (2014). Mutations in filamin C cause a new form of familial hypertrophic cardiomyopathy. *Nat. Commun.* 5:5326.

Valenzise, M., Arrigo, T., De Luca, F., Privitera, A., Frigiola, A., Carando, A., et al. (2008). R298Q mutation of p63 gene in autosomal dominant ectodermal dysplasia associated with arrhythmogenic right ventricular cardiomyopathy. *Eur. J. Med. Genet.* 51, 497–500.

Valtuille, L., Paterson, I., Kim, D. H., Mullen, J., Sergi, C., and Oudit, G. Y. (2013). A case of lamin A/C mutation cardiomyopathy with overlap features of ARVC: a critical role of genetic testing. *Int. J. Cardiol.* 168, 4325–4327.

van den Hoogenhof, M. M. G., Beqqali, A., Amin, A. S., Van Der Made, I., Aufiero, S., Khan, M. A. F., et al. (2018). RBM20 mutations induce an arrhythmogenic dilated cardiomyopathy related to disturbed calcium handling. *Circulation* 138, 1330–1342.

van der Zwaag, P. A., van Rijsingen, I. A., Asimaki, A., Jongbloed, J. D., Van Veldhuisen, D. J., Wiesfeld, A. C., et al. (2012). Phospholamban R14del mutation in patients diagnosed with dilated cardiomyopathy or arrhythmogenic right ventricular cardiomyopathy: evidence supporting the concept of arrhythmogenic cardiomyopathy. *Eur. J. Heart Fail.* 14, 1199–1207.

van Hengel, J., Calore, M., Bauce, B., Dazzo, E., Mazzotti, E., De Bortoli, M., et al. (2013). Mutations in the area composita protein alphaT-catenin are associated with arrhythmogenic right ventricular cardiomyopathy. *Eur. Heart J.* 34, 201–210.

van Opbergen, C. J., Delmar, M., and Van Veen, T. A. (2017). Potential new mechanisms of pro-arrhythmia in arrhythmogenic cardiomyopathy: focus on calcium sensitive pathways. *Neth Heart J.* 25, 157–169.

van Rijsingen, I. A., Arbustini, E., Elliott, P. M., Mogensen, J., Hermans-Van Ast, J. F., Van Der Kooi, A. J., et al. (2012). Risk factors for malignant ventricular arrhythmias in lamin a/c mutation carriers a European cohort study. *J. Am. Coll. Cardiol.* 59, 493–500.

Vatta, M., Mohapatra, B., Jimenez, S., Sanchez, X., Faulkner, G., Perles, Z., et al. (2003). Mutations in Cypher/ZASP in patients with dilated cardiomyopathy and left ventricular non-compaction. *J. Am. Coll. Cardiol.* 42, 2014–2027.

Vaynberg, J., Fukuda, K., Lu, F., Bialkowska, K., Chen, Y., Plow, E. F., et al. (2018). Non-catalytic signaling by pseudokinase ILK for regulating cell adhesion. *Nat. Commun.* 9:4465.

Verdonschot, J. A. J., Vanhoutte, E. K., Claes, G. R. F., Helderman-Van Den Enden, A., Hoeijmakers, J. G. J., Hellebrekers, D., et al. (2020). A mutation update for the FLNC gene in myopathies and cardiomyopathies. *Hum. Mutat.* 41, 1091–1111.

Vogel, B., Meder, B., Just, S., Laufer, C., Berger, I., Weber, S., et al. (2009). In-vivo characterization of human dilated cardiomyopathy genes in zebrafish. *Biochem. Biophys. Res. Commun.* 390, 516–522.

Vorgerd, M., Van Der Ven, P. F., Bruchertseifer, V., Lowe, T., Kley, R. A., Schroder, R., et al. (2005). A mutation in the dimerization domain of filamin c causes a novel type of autosomal dominant myofibrillar myopathy. *Am. J. Hum. Genet.* 77, 297–304.

Vornanen, M., and Hassinen, M. (2016). Zebrafish heart as a model for human cardiac electrophysiology. *Channels* 10, 101–110.

Wan, E., Abrams, J., Weinberg, R. L., Katchman, A. N., Bayne, J., Zakharov, S. I., et al. (2016). Aberrant sodium influx causes cardiomyopathy and atrial fibrillation in mice. *J. Clin. Invest.* 126, 112–122.

Watanabe, H., Yang, T., Stroud, D. M., Lowe, J. S., Harris, L., Atack, T. C., et al. (2011). Striking In vivo phenotype of a disease-associated human SCN5A mutation producing minimal changes *in vitro*. *Circulation* 124, 1001–1011.

Watanabe, T., Kimura, A., and Kuroyanagi, H. (2018). Alternative splicing regulator RBM20 and cardiomyopathy. *Front. Mol. Biosci.* 5:105. doi: 10.3389/fmolb.2018.00105

White, D. E., Coutu, P., Shi, Y. F., Tardif, J. C., Nattel, S., St Arnaud, R., et al. (2006). Targeted ablation of ILK from the murine heart results in dilated cardiomyopathy and spontaneous heart failure. *Genes Dev.* 20, 2355–2360.

Wilde, A. A. M., and Amin, A. S. (2018). Clinical spectrum of SCN5A mutations: long QT syndrome, brugada syndrome, and cardiomyopathy. *JACC Clin. Electrophysiol.* 4, 569–579.

Winter, L., Wittig, I., Peeva, V., Eggers, B., Heidler, J., Chevessier, F., et al. (2016). Mutant desmin substantially perturbs mitochondrial morphology, function and maintenance in skeletal muscle tissue. *Acta Neuropathol.* 132, 453–473.

Wolf, C. M., Wang, L., Alcalai, R., Pizard, A., Burgon, P. G., Ahmad, F., et al. (2008). Lamin A/C haploinsufficiency causes dilated cardiomyopathy and apoptosis-triggered cardiac conduction system disease. *J. Mol. Cell Cardiol.* 44, 293–303.

Xu, T., Yang, Z., Vatta, M., Rampazzo, A., Beffagna, G., Pilichou, K., et al. (2010). Compound and digenic heterozygosity contributes to arrhythmogenic right ventricular cardiomyopathy. *J. Am. Coll. Cardiol.* 55, 587–597.

Yang, Z., Bowles, N. E., Scherer, S. E., Taylor, M. D., Kearney, D. L., Ge, S., et al. (2006). Desmosomal dysfunction due to mutations in desmoplakin causes arrhythmogenic right ventricular dysplasia/cardiomyopathy. *Circ. Res.* 99, 646–655.

Zegkos, T., Panagiotidis, T., Parcharidou, D., and Efthimiadis, G. (2020). Emerging concepts in arrhythmogenic dilated cardiomyopathy. *Heart Fail Rev.* doi: 10.1007/s10741-020-09933-z [Epub ahead of print].

Zhang, Z., Stroud, M. J., Zhang, J., Fang, X., Ouyang, K., Kimura, K., et al. (2015). Normalization of Naxos plakoglobin levels restores cardiac function in mice. *J. Clin. Invest.* 125, 1708–1712.

Zhao, G., Qiu, Y., Zhang, H. M., and Yang, D. (2019). Intercalated discs: cellular adhesion and signaling in heart health and diseases. *Heart Fail. Rev.* 24, 115–132.

Zheng, G., Jiang, C., Li, Y., Yang, D., Ma, Y., Zhang, B., et al. (2019). TMEM43-S358L mutation enhances NF-kappaB-TGFbeta signal cascade in arrhythmogenic right ventricular dysplasia/cardiomyopathy. *Protein Cell* 10, 104–119.

Zheng, M., Cheng, H., Li, X., Zhang, J., Cui, L., Ouyang, K., et al. (2009). Cardiac-specific ablation of Cypher leads to a severe form of dilated cardiomyopathy with premature death. *Hum. Mol. Genet.* 18, 701–713.

Zhou, Y., Chen, Z., Zhang, L., Zhu, M., Tan, C., Zhou, X., et al. (2020). Loss of filamin C is catastrophic for heart function. *Circulation* 141, 869–871.

Zou, J., Tran, D., Baalbaki, M., Tang, L. F., Poon, A., Pelonero, A., et al. (2015). An internal promoter underlies the difference in disease severity between N- and C-terminal truncation mutations of Titin in zebrafish. *eLife* 4:e09406.

Conflict of Interest: The authors declare that the research was conducted in the absence of any commercial or financial relationships that could be construed as a potential conflict of interest.

frontiers in Physiology

ORIGINAL RESEARCH
published: 24 June 2020
doi: 10.3389/fphys.2020.00604

Human Cardiac Mesenchymal Stromal Cells From Right and Left Ventricles Display Differences in Number, Function, and Transcriptomic Profile

*Ilaria Stadiotti[1], Luca Piacentini[2], Chiara Vavassori[2,3], Mattia Chiesa[2], Alessandro Scopece[1], Anna Guarino[4], Barbara Micheli[4], Gianluca Polvani[4], Gualtiero Ivanoe Colombo[2], Giulio Pompilio[1,3] and Elena Sommariva[1]**

[1] Unit of Vascular Biology and Regenerative Medicine, Centro Cardiologico Monzino IRCCS, Milan, Italy, [2] Unit of Immunology and Functional Genomics, Centro Cardiologico Monzino IRCCS, Milan, Italy, [3] Department of Clinical Sciences and Community Health, University of Milan, Milan, Italy, [4] Cardiovascular Tissue Bank, Centro Cardiologico Monzino IRCCS, Milan, Italy

OPEN ACCESS

Edited by:
Marcella Canton,
University of Padova, Italy

Reviewed by:
Morayma Reyes,
Montefiore Medical Center,
United States
Sabine J. van Dijk,
University of California, Davis,
United States

***Correspondence:**
Elena Sommariva
esommariva@ccfm.it

Specialty section:
This article was submitted to Striated Muscle Physiology, a section of the journal Frontiers in Physiology

Received: 23 December 2019
Accepted: 14 May 2020
Published: 24 June 2020

Citation:
Stadiotti I, Piacentini L, Vavassori C, Chiesa M, Scopece A, Guarino A, Micheli B, Polvani G, Colombo GI, Pompilio G and Sommariva E (2020) Human Cardiac Mesenchymal Stromal Cells From Right and Left Ventricles Display Differences in Number, Function, and Transcriptomic Profile. Front. Physiol. 11:604. doi: 10.3389/fphys.2020.00604

Background: Left ventricle (LV) and right ventricle (RV) are characterized by well-known physiological differences, mainly related to their different embryological origin, hemodynamic environment, function, structure, and cellular composition. Nevertheless, scarce information is available about cellular peculiarities between left and right ventricular chambers in physiological and pathological contexts. Cardiac mesenchymal stromal cells (C-MSC) are key cells affecting many functions of the heart. Differential features that distinguish LV from RV C-MSC are still underappreciated.

Aim: To analyze the physiological differential amount, function, and transcriptome of human C-MSC in LV versus (vs.) RV.

Methods: Human cardiac specimens of LV and RV from healthy donors were used for tissue analysis of C-MSC number, and for C-MSC isolation. Paired LV and RV C-MSC were compared as for surface marker expression, cell proliferation/death ratio, migration, differentiation capabilities, and transcriptome profile.

Results: Histological analysis showed a greater percentage of C-MSC in RV vs. LV tissue. Moreover, a higher C-MSC amount was obtained from RV than from LV after isolation procedures. LV and RV C-MSC are characterized by a similar proportion of surface markers. Functional studies revealed comparable cell growth curves in cells from both ventricles. Conversely, LV C-MSC displayed a higher apoptosis rate and RV C-MSC were characterized by a higher migration speed and collagen deposition. Consistently, transcriptome analysis showed that genes related to apoptosis regulation or extracellular matrix organization and integrins were over-expressed in LV and RV, respectively. Besides, we revealed additional pathways specifically associated with LV or RV C-MSC, including energy metabolism, inflammatory response, cardiac conduction, and pluripotency.

Conclusion: Taken together, these results contribute to the functional characterization of RV and LV C-MSC in physiological conditions. This information suggests a possible differential role of the stromal compartment in chamber-specific pathologic scenarios.

Keywords: cardiac mesenchymal stromal cells, cardiac ventricles, functional studies, transcriptome, left ventricle, right ventricle

INTRODUCTION

Left and right cardiac chambers retain well-known physiological differences, linked to their diverse embryological origin, hemodynamic environment, function, structure, and cellular composition (Friedberg and Redington, 2014; Penny and Redington, 2016).

Although cardiomyocytes occupy 75% of adult normal myocardial tissue volume, they represent 30–40% of cardiac cells only. The remaining cells are non-myocytes, including smooth muscle cells, endothelial cells, fibroblasts, and mesenchymal stromal cells (Camelliti et al., 2005; Gray et al., 2018; Perbellini et al., 2018). The distribution of these cell populations in the heart is not homogeneous: the myocardium exhibits distinct regional differences that influence heart physiology and disease development (Souders et al., 2009; Pinto et al., 2016). The different embryonic derivation of the cardiac chambers is the main responsible for this heterogeneity (Moorman et al., 2003). Indeed, the LV originates from the first heart field, while the RV, the intraventricular septum, and the outflow tract derive from the second heart field (Black, 2007; Kelly et al., 2014).

No univocal results have been reported about the cellular composition of the adult cardiac chambers (Zhou and Pu, 2016). The main limitations of the previous studies are the challenges in identifying cell type-specific markers and the different quantification techniques. The majority of the existing studies do not consider the LV and RV as separate entities (Banerjee et al., 2007; Pinto et al., 2016; Zhou and Pu, 2016). In addition, due to the difficulties of access to human tissues, several studies were carried out with murine samples (Banerjee et al., 2007; Pinto et al., 2016).

To the best of our knowledge, no studies so far have characterized the quantity and quality of C-MSC in LV and RV separately. C-MSC are a fibroblastoid cell blend, including fibroblasts, progenitor cells, pericytes, and fibrocytes (Souders et al., 2009), characterized by residual multipotency toward mesenchymal lineages (Pittenger et al., 1999). As stated by the International Society for Cellular Therapy (Dominici et al., 2006), C-MSC are defined by the positive expression of CD44, CD105, and CD29 surface antigens, whereas CD14, CD45, CD34, and CD31 hematopoietic and endothelial markers, and HLA-DR, involved in graft-vs.-host disease, are not expressed (Pilato et al., 2018). CD90 is a fibroblast surface marker (Hudon-David et al., 2007) whose expression in C-MSC is variable, due to the heterogeneity in the cell population, only partially represented by fibroblasts. C-MSC can differentiate into several cell types like adipocytes, chondrocytes, and osteoblasts, under standard differentiating conditions *in vitro* (Dominici et al., 2006).

C-MSC exert important functions in the heart in both physiological and pathologic conditions (Brown et al., 2005). They are essential to maintaining myocardial structure integrity and cardiac function, contributing to biochemical, mechanical, and electrical physiology in healthy hearts (Camelliti et al., 2005). The role of C-MSC in many cardiac diseases is increasingly recognized. In injury conditions, they can participate to wound healing and fibrotic remodeling (Long and Brown, 2002; Jugdutt, 2003). In addition, they can undergo adipogenic differentiation in the heart in particular diseases (Abel et al., 2008; Sommariva et al., 2016). Aside from a direct role, C-MSC influence cardiomyocyte function in pathological states (Takeda and Manabe, 2011). Interestingly, an immunomodulatory role of C-MSC has been described (Prockop and Oh, 2012; Czapla et al., 2016; Diedrichs et al., 2019). Moreover, high expectations are raised in the use of C-MSC in regenerative medicine scenarios (Pittenger and Martin, 2004; Bagno et al., 2018; Braunwald, 2018). For these reasons, a better characterization of C-MSC functions and properties may be clinically relevant, both as a target and as a tool for new therapies (Frangogiannis, 2017).

In this work, we describe, for the first time, differences in quantity, distinctive characteristics, functional properties, and resting transcriptome profile of C-MSC obtained from human RV and LV.

MATERIALS AND METHODS

Anonymized data and materials have been made publicly available at the NCBI's GEO repository and can be accessed at https://www.ncbi.nlm.nih.gov/geo/query/acc.cgi?acc=GSE142205.

Study Patients' Population

Human hearts are collected during multi-organ explants from heart-beating donors. Those excluded from organ transplantation for technical reasons (microbiological, serological reasons despite normal echocardiographic parameters) are sent to the "Cardiovascular Tissue Bank" of Centro Cardiologico Monzino IRCCS for aortic and pulmonary valve banking. Among the tissues discarded during

Abbreviations: C-MSC, cardiac mesenchymal stromal cells; DE, differentially expressed; FABP4, fatty acid-binding protein 4; FBS, fetal bovine serum; FDR, false discovery rate; GAPDH, glyceraldehyde 3-phosphate dehydrogenase; GLM, generalized linear model; GSEA, Gene Set Enrichment Analysis; IMDM, Iscove's Modified Dulbecco's Medium; LV, left ventricle; ORO, Oil Red O; PBS, phosphate-buffered saline; PCA, principal component analysis; PLIN1, perilipin-1; PPARγ, peroxisome proliferator-activated receptor gamma; qRT-PCR, quantitative reverse transcription polymerase chain reaction; RT, room temperature; RV, right ventricle; vs., versus.

valve preparation, transmural mid-chamber free wall samples from LV at the anterolateral mid-papillary level and RV at the anterior papillary muscle level, above moderator band insertion, were collected and processed for tissue sections. From six of the enrolled subjects, endocardial–myocardial ventricular tissue from the same origin was collected to isolate C-MSC (Pilato et al., 2018). See **Supplementary Figure S1**.

Supplementary Table S1 summarizes the clinical features of 13 healthy donors, dead due to accident, enrolled in this study. LV and RV autopsy samples, processed as described above, were obtained from all the enrolled individuals.

Heart Tissue Section Preparation and Immunofluorescence Analysis

Human ventricular samples were fixed in 4% paraformaldehyde (Santa Cruz) in PBS (Lonza) and processed for paraffin embedding. Paraffin-embedded sections (6 μm thick) were de-waxed in xylene and rehydrated in ascending alcohols. The immunofluorescence analysis was performed following antigen retrieval with incubation with target retrieval solution citrate pH 6/microwave (Dako). Sections were incubated at 4°C overnight with primary antibodies for the detection of mesenchymal surface markers (see **Supplementary Table S2**), namely, anti-CD29 (1:40; Leica), anti-CD44 (1:200; Abcam), and anti-CD105 (1:100; Abcam) diluted in 2% goat serum (Sigma–Aldrich). After washing with PBS, sections were incubated for 1 h at RT in the dark with proper secondary antibodies (see **Supplementary Table S3**). Nuclear staining was performed by incubating sections with Hoechst 33342 (1:1000; Life Technologies). Sections were observed by Zeiss Axio Observer.Z1, with Apotome technology, and images acquired with the software AxioVision Rel. 4.8. For each explanted heart patient, five slices and at least 10 fields for each slice were examined.

C-MSC Isolation and Culture

LV and RV C-MSC were isolated and cultured as previously reported (Sommariva et al., 2016; Pilato et al., 2018). Briefly, LV and RV samples were digested with 3 mg/ml collagenase NB4 (Serva) for 1.5 h under continuous agitation. Each LV and RV tissue sample used for C-MSC obtainment was weighted before the digestion process.

The digested tissue and cells were seeded onto uncoated Petri dishes (Corning) in a growth medium [IMDM supplemented with 20% FBS Hyclone (Euroclone), 10 ng/ml basic fibroblast growth factor (R&D Systems), 10,000 U/ml penicillin (Invitrogen), 10,000 μg/ml streptomycin (Invitrogen), and 20 mmol/l L-glutamine (Sigma–Aldrich)].

After 10 days, isolated C-MSC were detached and counted to determine the number of cells obtained from each sample. The counted number was normalized on the grams of digested tissue.

The medium used to prompt the adipogenic differentiation of C-MSC consists of IMDM supplemented with 10% FBS (Sigma–Aldrich), 0.5 mmol/l 3-isobutyl-1-methylxanthine (Sigma–Aldrich), 1 μmol/l hydrocortisone (Sigma–Aldrich), 0.1 mmol/l indomethacin (Sigma–Aldrich), 10,000 U/ml penicillin (Invitrogen), 10,000 μg/ml streptomycin (Invitrogen), and 20 mmol/L L-glutamine (Sigma–Aldrich).

The medium for the evaluation of collagen production and deposition consists of IMDM supplemented with 2% FBS (Sigma–Aldrich), 10 ng/ml basic fibroblast growth factor (R&D Systems), 10,000 U/ml penicillin (Invitrogen), 10,000 μg/ml streptomycin (Invitrogen), and 20 mmol/l L-glutamine (Sigma–Aldrich).

Flow Cytometry Analysis

To confirm the mesenchymal lineage of RV and LV C-MSC, cells cultured in the basal medium were detached with TrypLE™ Select Enzyme (Thermo Fisher Scientific), incubated with FITC/APC/PE-conjugated antibodies (see **Supplementary Table S2**) in 100 μl PBS, and analyzed by flow cytometry (Gallios, Beckman Coulter). The antibodies used are the following: CD29, CD44, CD105, CD90, (mesenchymal markers), CD14, CD31, CD34, CD45 (endothelial and hematopoietic markers), and HLA-DR (immunogenicity marker).

Cell Growth Analysis

LV and RV C-MSC were plated at a concentration of 10,000 cells/cm^2 in the growth medium (see section "C-MSC isolation and culture") in four replicates. After 24, 48, 72, and 96 h, cells were detached and counted to analyze their growth rate.

Apoptosis and Necrosis Assay

To evaluate apoptosis and necrosis rate in LV and RV C-MSC, Single-Channel Dead Cell Apoptosis Kit with Annexin V Alexa Fluor™ 488 and SYTOX™ Green Dyes (Thermo Fisher Scientific) has been used, according to the manufacturer's instructions. Briefly, cells were plated at a concentration of 20,000 cells/cm^2 in the growth medium for 24 h. Then, they were detached using TrypLE™ Select Enzyme (Thermo Fisher Scientific) and incubated with Annexin V Alexa Fluor® 488 and SYTOX® Green for 15 min at RT. The fluorescence emission at 530 nm corresponding to apoptotic and necrotic cells has been measured using flow cytometry. The population was separated into three groups: live cells with a low level of fluorescence, apoptotic cells with moderate fluorescence, and dead cells with high intensity of fluorescence.

To assess the apoptotic rate of LV and RV C-MSC during 5 days of culture, we used the IncuCyte live-cell analysis system (Essen BioScience). Briefly, 10,000 cells/cm^2 were plated in the growth medium in two replicates. After cell attachment, IncuCyte® Annexin V Green Reagent (Essen BioScience) for apoptosis detection was added to the plates. The IncuCyte analysis system scanned the plates every 2 h for 5 days. The Annexin V count normalized on the percentage of confluence was used to analyze the obtained results.

Motility Analysis

LV and RV C-MSC motility was assessed by scratch wound assay; 40,000 cells/cm^2 were plated in the growth medium in three replicates. After cell attachment, wounds were created simultaneously in all wells, using IncuCyte WoundMaker (Essen BioScience). The IncuCyte live-cell analysis system (Essen BioScience) scanned the plate every 2 h for 60 h, and the percentage of the dish area occupied by cells was quantified.

Adipogenic Differentiation and Oil-Red O Staining

LV and RV C-MSC were plated at a concentration of 20,000 cells/cm^2 in an adipogenic induction medium for 72 h or for 1 week. Lipid accumulation was tested by ORO staining (Fulka). qRT-PCR and Western blot for PPARγ, FABP4, and PLIN1 (for antibodies, see **Supplementary Tables S2, S3**—for primers, see **Supplementary Table S4**) were used to check adipogenic mediator expression. As control, ORO staining was performed also on LV and RV C-MSC plated at a density of 20,000 cells/cm^2 and cultured in the growth medium.

Cardiac mesenchymal stromal cells were fixed with 4% paraformaldehyde (Santa-Cruz) in PBS and then stained with 1% ORO solution (Fulka) in 60% isopropanol (Sigma–Aldrich) for 1 h. After PBS washes to remove the unbound dye, the images were acquired by Axiovert 200M supplied with Axiocam 503 (Zeiss) in black and white, using phase H, to highlight black lipid depots. The quantification was performed with the software AxioVision Rel. 4.8, evaluating at least 10 fields per sample.

Quantitative Reverse Transcriptase-Polymerase Chain Reaction (qRT-PCR)

LV and RV C-MSC total RNA extracted using TRIzol Reagent (Thermo Fisher Scientific) was reversely transcribed using SuperScript III Reverse Transcriptase (Invitrogen). Each sample was analyzed in duplicates with each primer pair, using 10 ng of cDNA, with CFX96 Touch Real-Time PCR Detection System (Bio-Rad) using iQ SYBR Green Supermix (Bio-Rad). Threshold cycles were normalized against the expression of the housekeeping gene *GAPDH* (ΔCt). Primer sequences are reported in **Supplementary Table S4**.

Western Blot

Total proteins from LV and RV C-MSC were obtained by Cell Lysis Buffer (Cell Signaling). After quantification with DC protein assay (Bio-Rad), proteins were run on SDS-PAGE gel (NuPAGE precast 4–12%, Invitrogen) and transferred to the Trans-Blot® Turbo™ nitrocellulose membrane (Bio-Rad) with the Trans-Blot® Turbo™ transfer system. The membrane was blocked in PBS containing 0.05% Tween® 20 (Sigma–Aldrich) and 5% skimmed milk (ChemCruz) for 1 h at RT and incubated overnight at 4°C with the primary antibodies against GAPDH and the main adipogenic proteins PPARγ, PLIN1, and FABP4 (see **Supplementary Table S2**). After washes in PBS containing 0.05% Tween® 20 (Sigma–Aldrich), the membranes were incubated 1 h at RT with the appropriate HRP-conjugated secondary antibody (see **Supplementary Table S3**). Blots were washed and developed with the ECL system (Amersham) and images acquired and quantified with the UVItec Cambridge system. The normalization was performed on the housekeeping protein GAPDH.

Collagen Production

LV and RV C-MSC were plated at a concentration of 30,000 cells/cm^2 in the growth medium with a reduced amount of FBS (2%; see section "C-MSC Isolation and Culture") for 5 days, without medium change. The collagen production and myofibroblast differentiation were assessed through Sircol collagen analysis (Biocolor Life Science Assays), Western Blot, and qRT-PCR. Sircol Collagen Assay was performed on LV and RV C-MSC lysates and supernatants, after their collection in low-protein-binding tubes. The cellular lysates underwent collagen isolation and concentration step overnight. Both C-MSC lysates and supernatants were then mixed with 1 ml of Sircol Dye Reagent at RT for 30 min to ensure the precipitation of collagen. The obtained pellet was dissolved in Alkali Reagent, and the amount of collagen was determined at 540 nm using a microplate reader (Mithras LB 940; Berthold Technologies) and calculated based on a standard curve of soluble collagen.

RNA-Seq Analysis and Data Processing

Total RNA of 300,000 cultured, amplified C-MSC from LV (n = 6) and RV (n = 6) was isolated using TRIzol™ Reagent (Thermo Fisher Scientific), precipitated through the ammonium acetate/ethanol method and, then, treated with DNAse (TURBO DNAse; Thermo Fisher Scientific) to remove genomic DNA contamination. The total RNA concentration and quality were assessed, respectively, by micro-volume spectrophotometry on an Infinite M200 PRO Multimode microplate reader (Tecan, Mannedorf, Switzerland) and by microfluidics electrophoresis using the RNA 6000 Nano Assay Kit on the 2100 Bioanalyzer system (Agilent Technologies, Santa Clara, CA, United States). Poly(A)$^+$ RNA enrichment was performed using Dynabeads mRNA DIRECT Micro Kit (Thermo Fisher Scientific) starting from 6 μg of total RNA. Barcoded libraries were constructed using Ion Total RNA-Seq Kit v2.0 and Ion Express RNA-Seq Barcode kit (Thermo Fisher Scientific) following the manufacturer's instructions. Briefly, after poly(A)$^+$ RNA fragmentation using RNAse III, hybridization and ligation of barcoded adapters for stranded RNA sequencing were performed, followed by reverse transcription. cDNA fragments of 200 bp of each sample were amplified by 16 cycles of PCR using the specific "Barcode BC primers" for library demultiplexing and quantified on the 2100 Bioanalyzer system (Agilent Technologies, Santa Clara, CA, United States). One hundred pM diluted libraries were randomly pooled (six samples per pool). Templated Ion sphere particles preparation and chip loading were, then, performed by the automated Ion Chef System and Ion 550 Kit-Chef reagents and disposables. Loaded Ion 550 Chips were run on Ion GeneStudio S5 Prime System (all kits and instruments for sequencing were provided by Thermo Fisher Scientific).

Sequential aligning of raw reads was performed against the GRCh38 Human Genome reference (last release) with the most updated version of the "Spliced Transcripts Alignment to a Reference (STAR)" software (Dobin et al., 2013) and with "Bowtie2" (Langmead and Salzberg, 2012) to align locally any reads not mapped by STAR. Gene expression quantification and annotation were computed by "featureCounts" (Liao et al., 2014).

Raw count data were imported into the R software v3.5.0. and filtered to retain genes with a minimum of 10 counts in at least 50% of the samples. Differential expression analysis was performed by a negative binomial GLM approach (using

the edgeR/Bioconductor package) (Robinson and Oshlack, 2010; McCarthy et al., 2012) along with the estimation of latent variables, technical batch effects, or biological confounding variables, for adjusting the statistical model (using the RUVSeq R/Bioconductor package) (Risso et al., 2014). The number of K factors was chosen by comparing unadjusted vs. adjusted expression data by the use of diagnostic plots, i.e., relative log expression (RLE) plot, scatter plot of the first two principal components derived from PCA performed on total data, and histogram of the *P*-value distribution for testing the differential expression between LV vs. RV. A $K = 3$ factor of "unwanted variation" showed the best trade-off between data adjustment and the risk of data overcorrection and was, thus, used as covariates for model adjustment in a paired-sample data analysis. Genes were deemed as significantly different for FDR-adjusted P-value < 0.05. The reliability of the differential expression analysis results was further assessed by exploring the histograms of the *P*-value distribution, which showed a uniformly flat distribution across the unit interval (null *P*-values) with a peak near zero (*P*-values for alternative hypotheses) (Leek and Storey, 2008).

Functional inference analysis took advantage of prior biological knowledge of genes grouped by pathways and used for GSEA (software v4.0) (Subramanian et al., 2005). Gene sets of various pathway repositories were retrieved as a unique, merged Gene Matrix Transposed file format (*.gmt) from the Bader Lab gene-set collections[1] to perform a single GSEA run. A combined gene rank score (cs) was applied to weigh the relevance of the genes by taking into consideration both the magnitude [i.e., log2 fold change (FC)] and the statistical score of the gene expression differences [likelihood ratio (LR)] and was used as the gene-ranking metric for the GSEA pre-ranked tool option. Other GSEA parameters included 10,000 permutations and gene-set size limit ranging from 10 to 250 genes. To reduce redundancy and highlight grouping of functionally related gene sets, GSEA results were visualized through an enrichment network of the most significant pathways (FDR q-value < 0.05) with the Enrichment Map Software v.3.2.1 (Merico et al., 2010), implemented as a plug-in in the Cytoscape v.3.7.1 platform (Shannon et al., 2003).

Statistical Analysis

Continuous variables are reported as mean ± standard error. Comparisons between groups were performed using two-tailed paired Student's *t*-test. Dissimilarities in the growth rate between LV and RV C-MSC were evaluated by testing the difference between the two linear regression slopes with the following method: $t = (b1\text{-}b2)/sb1,b2$ where b1 and b2 are the two slope coefficients and sb1,b2 the pooled standard error of the slope. To test if the distribution of the migration curves of LV and RV cells was diverse, we performed a Kolmogorov–Smirvov test, followed by fitting analyses with linear and quadratic regression models. Statistics were performed using GraphPad Prism 5 software. Results were considered statistically significant for *P*-values < 0.05.

[1]http://download.baderlab.org/EM_Genesets/

RESULTS

Quantitative Analysis of C-MSC in LV and RV Tissues

To characterize the amount of C-MSC in the two cardiac ventricles, we analyzed LV and RV serial slices from 13 healthy donors (see **Supplementary Table S1** for donor characteristics) for CD44, CD29, and CD105 mesenchymal marker expression. RV presented a higher percentage of positive cells compared with LV ($n = 13$; % LV $CD44^+$ cells 11.05 ± 1.450 vs. % RV $CD44^+$ cells 19.75 ± 2.210, $P = 0.001$; % LV $CD29^+$ cells 6.764 ± 1.285 vs. % RV $CD29^+$ cells 11.31 ± 2.178, $P = 0.020$; % LV $CD105^+$ cells 2.638 ± 0.7078 vs. % RV $CD105^+$ cells 6.269 ± 1.627, $P = 0.011$; **Figure 1A**).

We then proceeded with a quantitative evaluation of C-MSC isolated from LV and RV tissues through the digestion procedure, already described in Pilato et al. (2018). A significantly greater amount of RV C-MSC has been obtained from the same quantity of source tissue ($n = 6$; LV C-MSC 396,047 ± 165,909 vs. RV C-MSC 1564,440 ± 366,220; $P = 0.040$; **Figure 1B**), in line with the physiological higher number of C-MSC in the RV (**Figure 1A**).

Immuno-Phenotyping of Isolated LV and RV C-MSC

We characterized the obtained cells for surface marker expression (**Figure 2**; please see **Supplementary Table S2** for the list of used antibodies). Both LV and RV C-MSC were near 100% positive for the mesenchymal markers CD44, CD29, and CD105, whereas they displayed negligible values for CD14, CD45, CD34, and CD31 markers, which were assessed to exclude hematopoietic and endothelial cell contamination. Moreover, HLA-DR, a marker of alloreactivity, was not detected in either LV or RV cells. The percentage of $CD90^+$ cells was measured to define the number of fibroblasts in the heterogeneous population of C-MSC (Hudon-David et al., 2007). As shown in **Figure 2**, the percentage of $CD90^+$ cells was comparable in the two populations. In conclusion, for all the surface markers screened, we found a similar pattern of expression in LV and RV C-MSC, indicating no differences in the mesenchymal identity of the two populations (see **Supplementary Table S5**).

Functional Analysis on LV and RV C-MSC

Growth Rate of LV and RV C-MSC

We performed growth curves of LV and RV C-MSC in culture medium for 4 days, up to growth plateau achievement. As shown in **Figure 3A**, the comparison between the growth curve slopes revealed that both LV and RV C-MSC have a similar growth trend ($n = 6$; $P = 0.67$).

Cell Death of LV and RV C-MSC

We evaluated the number of apoptotic and necrotic cultured LV and RV C-MSC. **Figure 3B** shows that LV cells presented a higher percentage of apoptotic cells if compared with RV C-MSC ($n = 6$; LV C-MSC 15.66 ± 1.62 vs. RV C-MSC 10.91 ± 1.035%; $P = 0.049$), while no differences in marker of necrosis were found

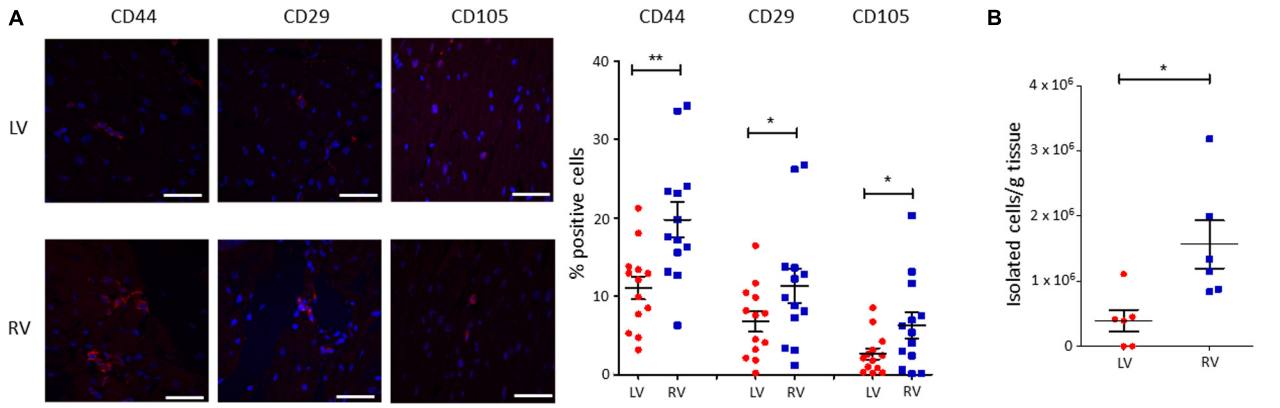

FIGURE 1 | A higher amount of cardiac mesenchymal stromal cells (C-MSC) is present in the RV when compared to the left one. **(A)** Immunofluorescence staining on human left ventricular (LV) and right ventricular (RV) total tissue for the mesenchymal markers CD29, CD44, and CD105. On the left, representative images are shown. The red staining is relative to the mesenchymal markers, the blue signal marks the nuclei (Hoechst 33342). On the right, the quantification of the percentage of positive cells is reported. The scale bar indicates 50 μm. $n = 13$ each; $^{*}p < 0.05$ (paired t-test). **(B)** C-MSC were isolated from either LV or RV human samples. A higher amount of C-MSC was obtained from RV samples. $n = 6$ each; $^{*}p < 0.05$, $^{**}p < 0.01$ (paired t-test).

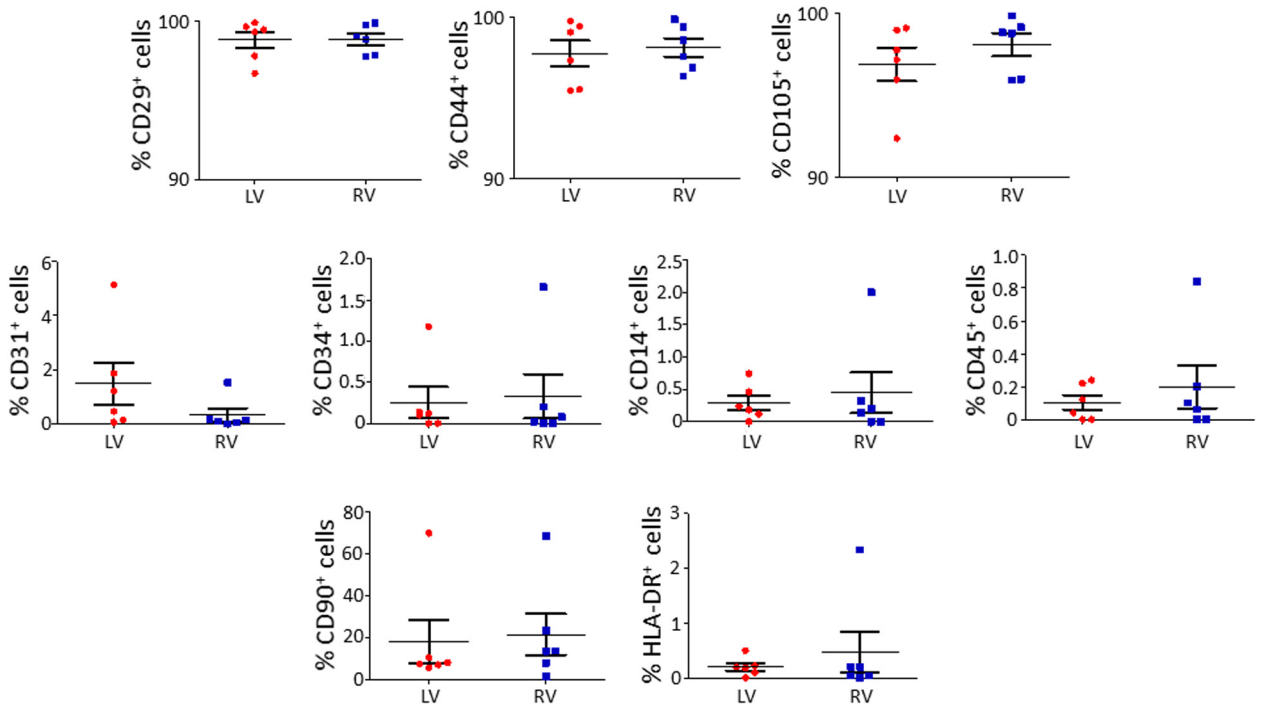

FIGURE 2 | The isolated left ventricle (LV) and right ventricle (RV) cardiac mesenchymal stromal cells (C-MSC) are not different for surface marker expression. LV and RV C-MSC were characterized for surface marker expression, showing no differences. Mesenchymal markers CD29, CD44, and CD105, endothelial markers CD31 and CD34, hematopoietic markers CD14 and CD45, the fibroblast marker CD90, and the alloreactivity marker HLA-DR have been used. $n = 6$ each (paired t-test).

between the two cell populations ($n = 6$; LV C-MSC 10.56 ± 2.37 vs. RV C-MSC 9.43 ± 1.98%; $P = 0.711$).

Basing on this result, we followed LV and RV C-MSC with a live-imaging technique for 5 days in culture conditions and we assessed their apoptotic rate. **Figure 3C** shows that LV C-MSC presented a higher apoptosis rate if compared with RV cells at all time-points, confirming **Figure 3B** results.

LV and RV C-MSC Motility

By performing the scratch wound assay, we assessed the migration capability of LV and RV C-MSC. As reported in **Figure 3D**, the percentage of confluence detected in the two cell populations during the 60 h of measurements revealed a different migration rate in LV and RV cells, with a significant discrepancy in the distributions ($P < 0.001$). In particular, for

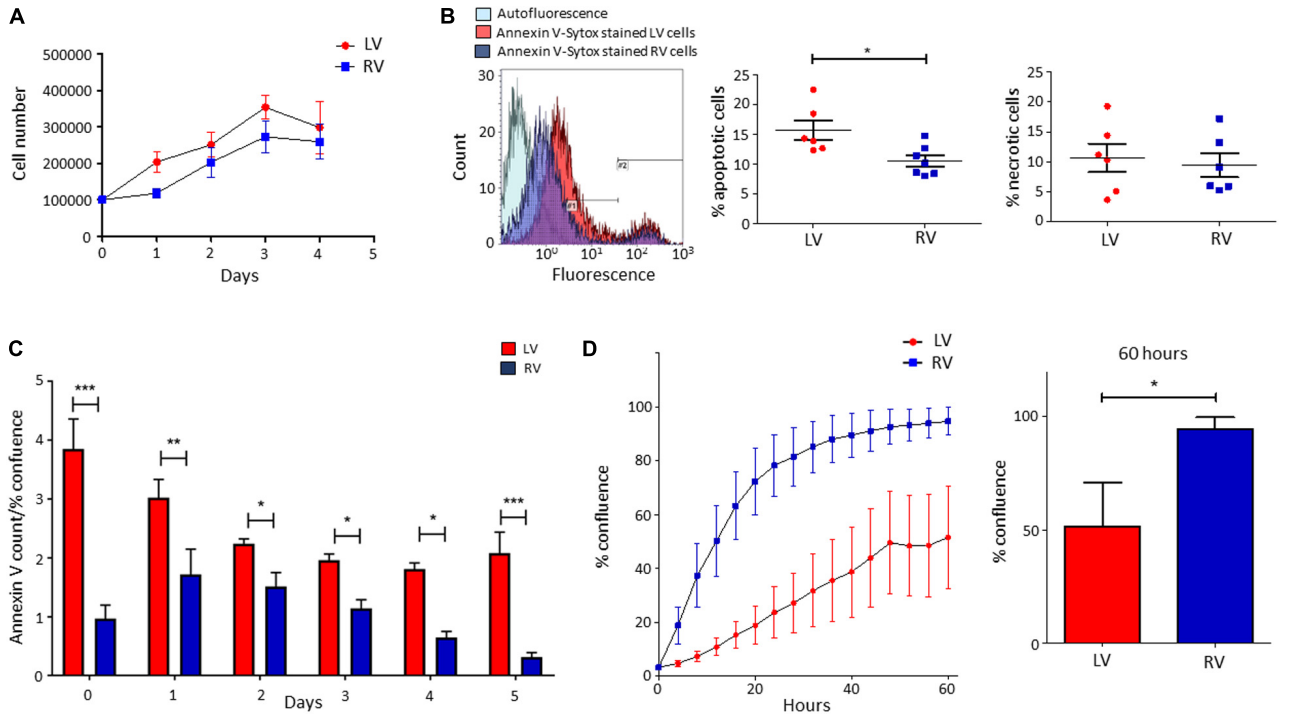

FIGURE 3 | Higher apoptosis in growth conditions characterizes left ventricle (LV) cardiac mesenchymal stromal cells (C-MSC) with respect to right ventricle (RV) cells. RV C-MSC show greater motility when compared to LV cells. **(A)** The growth curves of LV and RV C-MSC in the culture medium are reported. Cells were cultured for 4 days, and the number of cells was counted every 24 h. No differences in growth curve slopes have been obtained. $n = 6$ each (linear regression slope comparison). **(B)** The percentage of apoptotic and necrotic cells was evaluated in the culture medium. In the left panel, representative flow cytometry histograms comparing LV and RV C-MSC patterns are shown. As shown in the right graphs, a higher percentage of apoptotic (measured in #1 interval) LV C-MSC than RV cells has been found. No differences between the necrotic (measured in #2 interval) cell amount were recorded. $n = 6$ each; $^{*}p < 0.05$ (paired t-test). **(C)** The apoptosis rate of LV and RV C-MSC for different time-points is reported. Cells were cultured for 5 days in growth medium. The Annexin V count normalized on the percentage of confluence is shown. For all the time-points, a trend of higher apoptosis was measured in LV cells, significantly different from RV C-MSC apoptotic rate at days 0, 1, 2, 3, 4, and 5. $n = 6$ each; $^{*}p < 0.05$, $^{**}p < 0.01$, $^{***}p < 0.001$ (two-way ANOVA). **(D)** The mean values of confluence percentage of LV and RV cells during scratch wound assay are reported (left panel). Higher motility of RV C-MSC, if compared to LV cells, has been found. Cell confluence was recorded for 60 h. The right graph depicts the difference in confluence percentage at 60 h. $n = 6$ each; $^{*}p < 0.05$ (paired t-test).

LV cells, the distribution was linear ($R^2 = 0.98$), whereas, for RV cells, the distribution was not linear ($R^2 = 0.79$) but fitted a quadratic curve ($R^2 = 0.98$). In addition, RV C-MSC reached a significantly higher percentage of confluence if compared with LV cells at 60 h ($n = 6$; LV C-MSC 51.56 ± 19.15 vs. RV C-MSC 94.64 ± 5.17%; $P = 0.046$).

LV and RV C-MSC Adipogenic Differentiation

LV and RV C-MSC were cultured in adipogenic conditions for 72 h or 1 week, to understand their capability to accumulate lipids and differentiate in adipocytes. The ORO staining, which quantifies the intracellular neutral lipid accumulation, revealed similar lipid accumulation between LV and RV C-MSC, both after 72 h ($n = 6$; relative lipid accumulation LV C-MSC 1.00 ± 0.21 vs. RV C-MSC 1.24 ± 0.33; $P = 0.754$; **Figure 4A**) and 1 week ($n = 6$; relative lipid accumulation LV C-MSC 1.66 ± 0.12 vs. 1.70 ± 0.28; $P = 0.99$; **Figure 4A**). In agreement with the comparable levels of lipid accumulation between LV and RV cells, also the expression of the adipogenic genes *PPARγ*, *FABP4*, and *PLIN1* were similar in the two cell populations at the considered time-points (**Figure 4B** and **Supplementary Table S6**). Moreover, the correspondent adipogenic proteins showed analogous levels (**Figure 4C** and **Supplementary Table S6**). As control, we performed the ORO staining also in LV and RV C-MSC cultured in the growth medium, obtaining a very small amount of lipid accumulation and no differences in the two cell populations (**Supplementary Figure S2**).

LV and RV C-MSC Collagen Production and Deposition

C-MSC are known to produce collagen. Comparing LV and RV cells, we found a higher collagen production in RV cells after 5 days of culture, both evaluating total collagen quantity in supernatants (left panel LV C-MSC 0.64 ± 0.22 μg collagen/cell number*100,000 vs. RV C-MSC 1.24 ± 0.41 μg collagen/cell number*100,000; $P = 0.04$; **Figure 5A**) and in the deposited extracellular matrix (right panel LV C-MSC 4.41 ± 1.21 vs. RV C-MSC 7.65 ± 1.54 μg collagen/cell number*100,000; $P = 0.05$; **Figure 5A**). On protein lysates, we evaluated the levels of the more expressed collagen type, COL1A1, normalized on the housekeeping protein GAPDH, finding a trend of increased expression in RV cells, according with the analysis of total

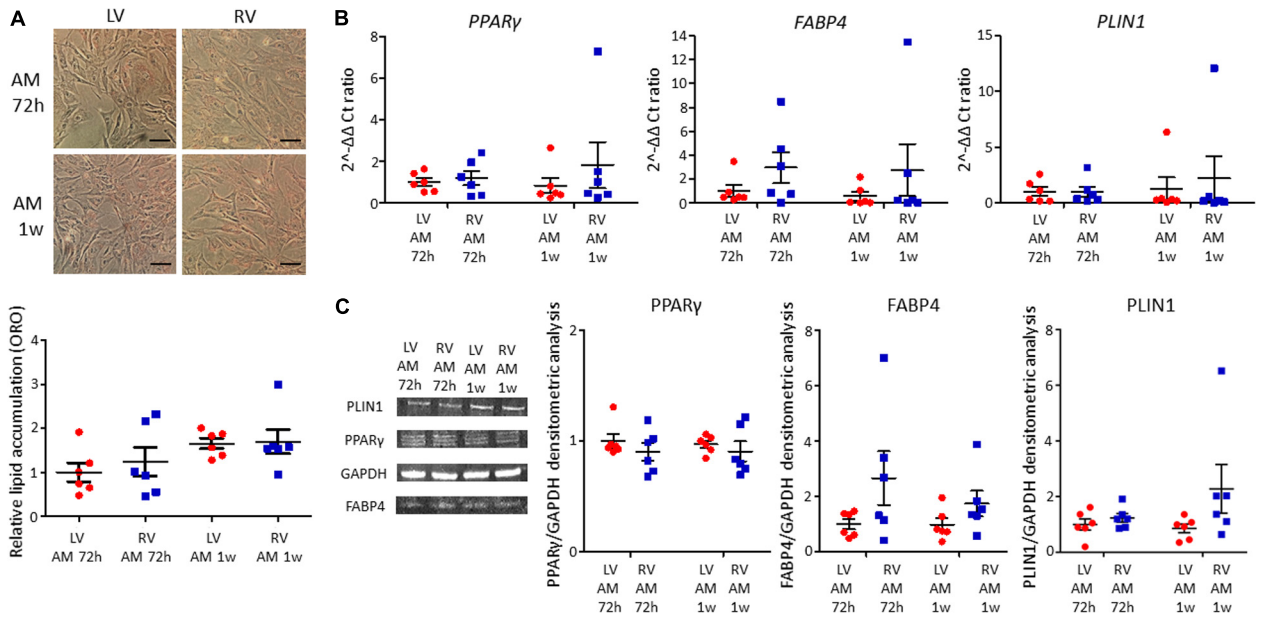

FIGURE 4 | No differences in adipogenic differentiation between left ventricle (LV) and right ventricle (RV) cardiac mesenchymal stromal cells (C-MSC) have been observed. **(A)** The upper panels show Oil Red O staining representative images of LV and RV C-MSC cultured for 72 h and 1 week in the adipogenic medium (AM). The scale bar indicates 50 μm. The quantification of cell lipid accumulation is provided in the bottom panel. $n = 6$ each (paired t-test). **(B)** qRT-PCR analysis of *PPARγ*, *FABP4*, and *PLIN1* expression in LV and RV C-MSC cultured for 72 h and 1 week in AM, normalized on the housekeeping gene *GAPDH*. $2^{-\Delta\Delta}$ Ct ratio is shown: $2^{-\Delta\Delta}$ Cts of each group are normalized on $2^{-\Delta\Delta}$ Ct values of LV C-MSC cultured in AM for 72 h. $n = 6$ each (paired t-test). **(C)** The protein extracts of LV and RV C-MSC cultured for 72 h and 1 week have been analyzed by Western blot. The densitometric analysis of PPARγ, FABP4, and PLIN1 normalized on the housekeeping protein GAPDH is shown. $n = 6$ each (paired t-test).

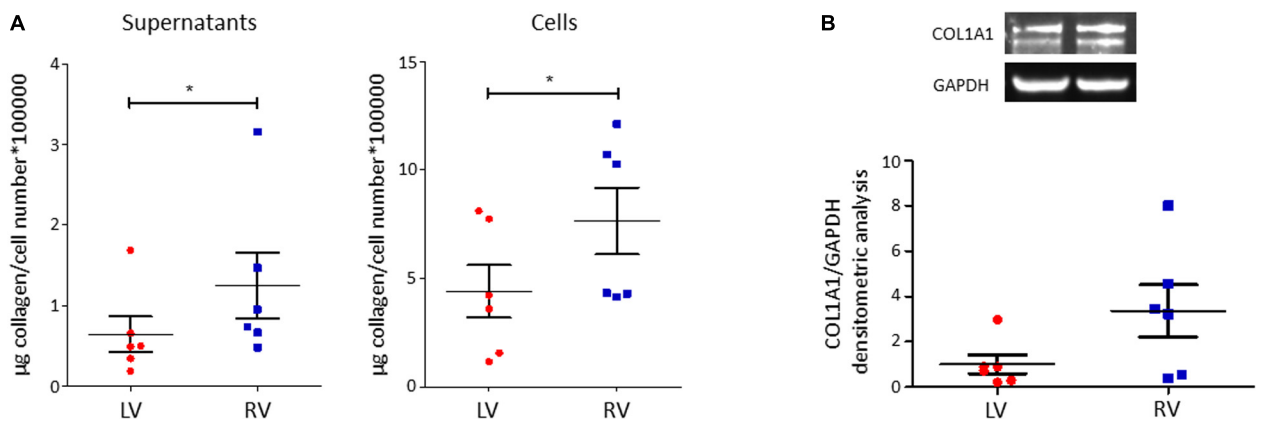

FIGURE 5 | Right ventricle (RV) cardiac mesenchymal stromal cells (C-MSC) produce more collagen than left ventricle (LV) cells. **(A)** Collagen production quantification with Sircol assay in supernatants (left graph) and cells (right graph) of LV and RV C-MSC cultured for 5 days in the basal medium with 2% serum. As shown in the graphs, RV cells produce more collagen than LV cells. *$p < 0.05$; $n = 6$ each (paired t-test). **(B)** Western blot analysis of COL1A1, the more expressed collagen type, confirmed Sircol result. A trend of higher expression of COL1A1 was evaluated in RV C-MSC. $n = 6$ each (paired t-test).

collagens (LV C-MSC 1.00 ± 0.41 vs. RV C-MSC 3.36 ± 1.15; $P = 0.11$; **Figure 5B**).

Transcriptomic Analysis of LV and RV C-MSC

To extend the characterization of LV and RV C-MSC, we performed transcriptomic profiling in resting conditions.

Following data processing and raw count filtering, we identified 14,486 expressed genes, which include 11,942 protein-coding genes, 1754 pseudogenes, 768 long non-coding genes, and 22 short non-coding genes (**Supplementary Figure S3**; see annotation in **Supplementary File S1** for details).

Paired-sample analysis and adjustment for confounding "latent" variables allowed reducing the effects of heterogeneity among subjects, thus unveiling specific changes between LV vs.

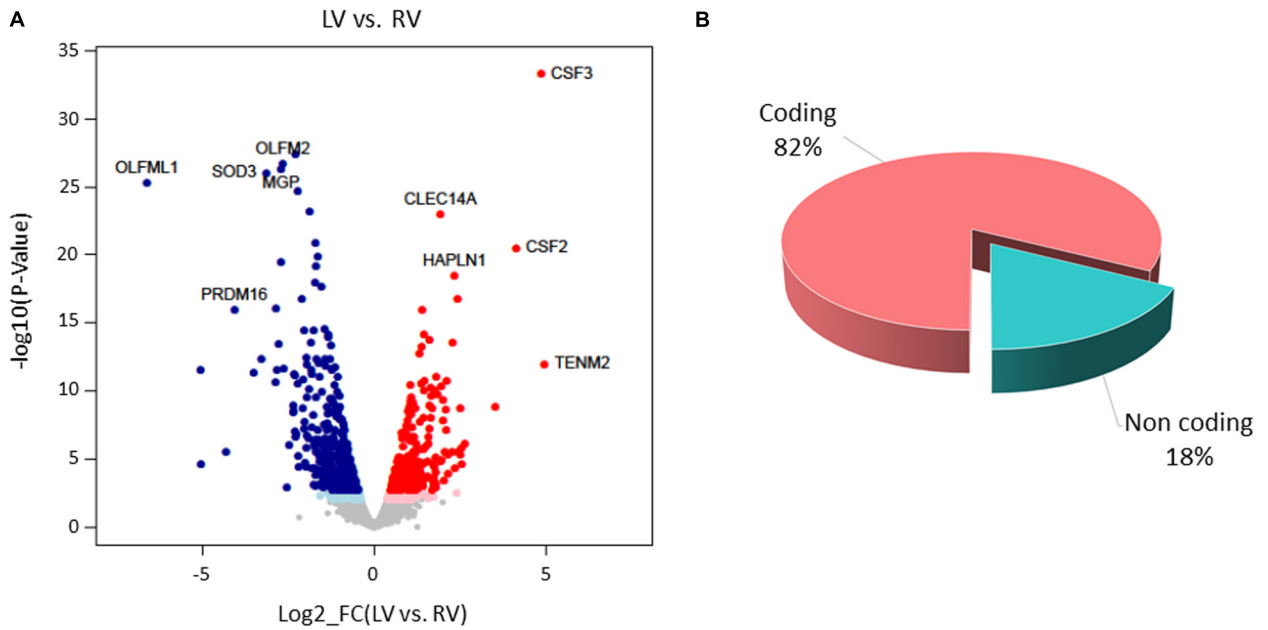

FIGURE 6 | Differential gene expression between left ventricle (LV) and right ventricle (RV) cardiac mesenchymal stromal cells (C-MSC). **(A)** Scatterplot of the log2 fold change (FC) vs. the significance (*x*- and *y*-axes, respectively) for the paired comparison of LV vs. RV C-MSC. Red and blue dots represent genes overexpressed in LV and RV C-MSC, respectively. Light red and light blue dots are genes significant at the nominal *P*-value < 0.01, whereas red and blue dots represent significant differentially expressed (DE) genes that withstood adjustment for multiple testing (adjusted *P*-value < 0.05). Ten of the top DE genes with the highest combined rank score (the product of the log2 FC $\times$ likelihood ratio) are shown. **(B)** Pie chart of the percentage of coding (pink) and non-coding (light blue) differentially expressed genes; more than 80% of DE genes are protein coding.

RV. We detected 652 DE genes with log2 FCs ranging from −6.6 to 4.9 at FDR < 0.05. Among them, 271 genes presented higher expression levels in LV and 381 in RV samples (**Figure 6** and **Supplementary File S1**). The histogram of *P*-value distribution confirmed the reliability of differential expression (DE) analysis (**Supplementary Figure S4**).

By GSEA, we identified a considerable number of significant pathways that characterize LV or RV C-MSC. To facilitate result interpretation and visualize the relationships among the most significant gene sets, we drew an enrichment network of GSEA results for the paired comparison between LV vs. RV (**Figure 7**). The most representative pathways associated with LV are suggestive for mRNA and rRNA processing, signaling by ROBO receptors, regulation of apoptosis, glucose metabolism, mitochondrial translation, and cytokine and inflammatory response. Conversely, the most representative pathways associated with RV (and negatively associated with LV) were related to extracellular matrix organization; collagen biosynthesis; integrin cell surface interactions; cardiac conduction; regulation of cholesterol biosynthesis by SREBP (SREBF); binding and uptake of ligands by scavenger receptors; arrhythmogenic right ventricular cardiomyopathy; GPCR Class A 1 rhodopsin-like receptor, neurotransmitter receptor and postsynaptic signal transmission; and interferon-alpha and beta signaling. Overall, these findings suggest profound differences in the transcriptional programs involved in remodeling, energy metabolism, responses to cytokines or inflammatory stimuli, electrical conduction, pluripotency, repair, and regeneration between LV and RV C-MSC.

DISCUSSION

To date, the literature on human cardiac cell composition provides few and conflicting data (Zhou and Pu, 2016). Despite the increasingly recognized importance of the non-myocyte compartment (Tian and Morrisey, 2012), the C-MSC population has not been previously in-depth investigated in this regard. In addition, C-MSC differential role within the cardiac chambers, with particular regard to the left and right human ventricles, is underinvestigated. A more robust definition is required to distinguish subsets of stromal cells with specialized functions in diverse tissues. In fact, due to morphology, immunophenotype, and differentiation potential similarity, the nomenclature of MSC and fibroblasts is often used indistinctively (Hematti, 2012) to name the same cell type isolated with the same method (Rockel et al., 2019).

In this study, by using samples obtained from cadaveric donors, we performed a better characterization of human C-MSC quantity, distinctive transcriptional configuration, and functional properties, focusing on differences related to the two cardiac ventricular chambers.

Although all of the cardiac samples used for this study were obtained following a reproducible procedure, using proper

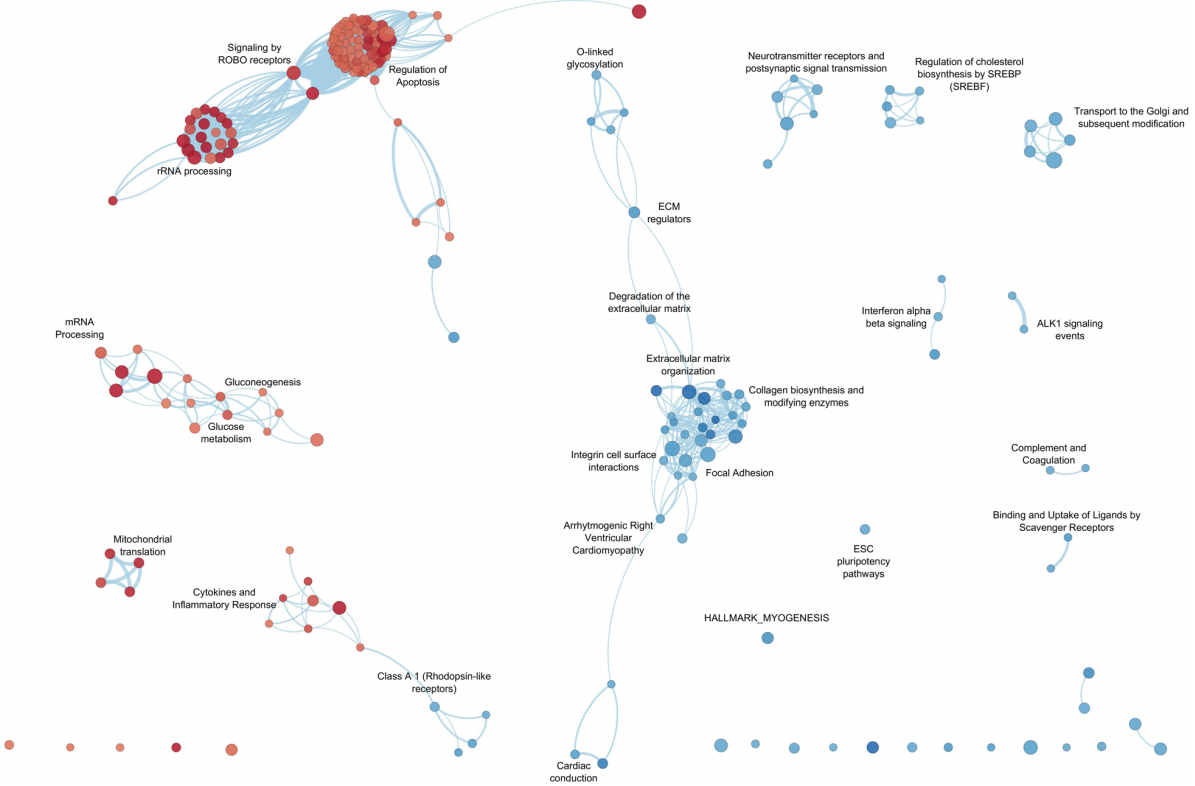

FIGURE 7 | Enrichment map for left ventricle (LV) and right ventricle (RV) cardiac mesenchymal stromal cells (C-MSC). The enrichment network shows the pathway gene sets (nodes) that are significantly associated either with LV or RV ventricles (false discovery rate < 0.05). Node color refers to the association with the phenotype (LV = red, RV = blue); node gradient color is proportional to the gene-set normalized enrichment score (NES), from lower (light) to higher (dark); node size is proportional to the gene-set size. Edges connect related pathways. Edge thickness is proportional to the similarity between two pathways, for a cutoff = 0.25 of the combined Jaccard plus overlap coefficient.

references to ensure the collection of comparable samples, a residual heterogeneity between samples cannot be excluded, comprising imbalanced representation of gender.

The immunofluorescence analysis of human cardiac left and right ventricular tissues showed a higher percentage of cells positive for the mesenchymal markers CD29, CD44, and CD105 in the RV. In general, the total number of C-MSC resulted proportionally low in both ventricles. The majority of non-myocytes was previously thought to be fibroblasts (Camelliti et al., 2005). However, this information has been recently questioned by Pinto et al. (2016). Indeed, the authors demonstrate that endothelial cells outnumber the other non-myocyte cardiac cell types in the adult ventricles, representing >60% of cells. Specifically, fibroblasts accounted for less than 20% of the non-myocytes. Overall, our results concur with this evidence and add a clear definition of the differential C-MSC abundance in the two ventricular chambers.

In accordance with tissue analysis, a higher amount of C-MSC can be isolated from the human RV than from the left one. Although RV or LV C-MSC have been used and characterized alternatively (Chong et al., 2013; Czapla et al., 2016; Sommariva et al., 2016; Le et al., 2018, 2019), no previous study performed a direct comparison of cells obtained from the two ventricles of the same individual. This novel approach is useful for a better C-MSC characterization in the human heart. Although the sample size used for *in vitro* experiments is relatively low, it is sufficient to ensure a good statistical power of the analyses, as in a paired-sample design the effects of heterogeneity among subjects are reduced.

Noteworthily, isolated LV and RV C-MSC showed comparable expression of surface markers, despite important differences unveiled with other assays. This indicates, as previously observed (Lv et al., 2014), that surface markers are not sufficient to determine the functional property potential and transcriptomic configuration of C-MSC.

Remarkable concordance was found between functional assays and transcriptome results. No significant difference was detected in C-MSC growth rate. Indeed, no pathway associated with cell growth or proliferation was specifically enriched in LV or RV C-MSC. Instead, a higher apoptosis rate was found in LV C-MSC, in accordance with the fact that LV C-MSC transcripts resulted to be enriched in genes associated with pathways of apoptosis regulation. Moreover, RV cells showed higher motility by scratch wound assay. This is in line with RV C-MSC enrichment of pathways related to integrins, which allow adhesion to promote cell traction (Huttenlocher and Horwitz, 2011). No differences were found between LV and RV C-MSC upon stimulation for adipogenic differentiation, while fibrosis and collagen production

were higher in RV C-MSC compared to LV cells. Both results are in line with the transcriptome analysis, in which extracellular matrix organization and collagen production genes were found significantly upregulated in the RV. Interestingly, in healthy hearts, exercise triggers RV profibrotic remodeling (La Gerche et al., 2012).

Furthermore, LV C-MSC transcriptome revealed enrichment in genes associated with cytokines and inflammatory response pathways. C-MSC from the RV are instead enriched in nodes linked to innate immunity mechanisms, such as complement and interferon type 1 signaling pathways. In fact, C-MSC can both amplify inflammatory stimuli and act as anti-inflammatory mediators (Smith et al., 1997; McGettrick et al., 2012; Coulson-Thomas et al., 2016). In this regard, the differential potential of C-MSC from the two chambers in eliciting either innate or cytokine-mediated inflammatory response has never been described and could be of importance for the substrate response to regenerative therapy (Vagnozzi et al., 2019).

A distinctive feature of the LV is the high workload environment. It should not, therefore, be surprising to observe an LV-specific enrichment for pathways linked to energy production and use, such as those related to mitochondria and glucose metabolism (Stanley et al., 2005; Pham et al., 2019).

As expected, given the embryologic origin and the developmental program of the RV (Clapham et al., 2019), we found in RV C-MSC a significant upregulation of the transcription factor *MEF2C*. Moreover, the antisense long-non-coding HAND2-AS1 is specifically more expressed in the LV, pointing to an RV-associated gene downregulation in LV determination (Tsuchihashi et al., 2011).

Taken together, these results highlight relevant physiological differences between LV and RV C-MSC.

In light of this information, the design of new targeted therapeutic strategies to promote heart repair and regeneration could be reconsidered (Pinto et al., 2016). MSC represent a promising tool in the field of regenerative medicine for their therapeutic potential (Pittenger and Martin, 2004; Karantalis and Hare, 2015; Bagno et al., 2018; Braunwald, 2018). Their beneficial properties have been attributed to their capability to migrate to injured areas eliciting immunomodulatory function, to their multipotency, and to their secretion of bioactive compounds (e.g., cytokines, chemokines, growth factors) inducing repair of damaged tissues (Pittenger and Martin, 2004; Caplan and Dennis, 2006; Karantalis and Hare, 2015; Czapla et al., 2016; Bagno et al., 2018). Only few clinical studies, to date, have focused on cardiac-derived MSC, due to the critical access to human cardiac specimens (Miteva et al., 2011; Chugh et al., 2012; Malliaras et al., 2014; Czapla et al., 2016; Detert et al., 2017; Sanz-Ruiz et al., 2017). However, the beneficial effects of cells obtained from the heart are deemed stronger than those obtained using mesenchymal cells from other sources (Rossini et al., 2010; Czapla et al., 2016). Our data on RV enrichment in genes associated with pluripotency allow us to speculate about a greater potential of RV C-MSC in cardiac regeneration.

Moreover, C-MSC are involved in several cardiac conditions. Understanding the healthy state of the human heart, with particular regard to the dissection of cell component properties, may offer a new perspective to heart diseases, which remain the leading cause of death worldwide (Doll et al., 2017). Several diseases differentially affect the two heart chambers. Since determinants of the preferential involvement of LV vs. RV are still unknown, this work may add clues to understand the relative contribution of the stromal compartment.

In particular, our results are of interest for arrhythmogenic cardiomyopathy (ACM), where the role of C-MSC in disease pathogenesis has been increasingly recognized by our group and others (Lombardi et al., 2016; Sommariva et al., 2016). Indeed, the transcriptome analysis showed in RV C-MSC an association with the ACM pathway. For ACM vs. control C-MSC differential transcriptomics, see Rainer et al. (2018).

Pulmonary hypertension is another example of a disease with fibrotic drift mostly affecting the RV (Egemnazarov et al., 2018; Andersen et al., 2019). On top of the anatomical proximity of the trigger, leading to RV pressure overload, the RV maladaptive fibrotic remodeling may partly depend on C-MSC number and specific characteristics. In addition, various arrhythmic diseases, such as Brugada syndrome, ACM, right ventricular outflow tract tachycardia, and Uhl's anomaly are hallmarked by arrhythmias originating preferentially from the RV (Hoch and Rosenfeld, 1992). Accordingly, we found that RV C-MSC associate with "cardiac conduction" pathways, which include many ion channel genes (Di Resta and Becchetti, 2010). We speculate about the potential involvement of C-MSC in contributing to the altered RV electrical environment. Indeed, a regional difference (RV vs. LV) in current handling is known for cardiomyocytes (Kondo et al., 2006). Given cardiomyocyte–stromal cell coupling (Nattel, 2018), a contribution of stromal cells in RV arrhythmia predisposition cannot be excluded.

Similarly, a contribution of C-MSC characteristics cannot be excluded in disease with preferential LV involvement. An example is constituted by cardiomyopathies of genetic origin, which develop mainly in the LV, while RV dysfunction is an expression of advanced disease progression (Merlo et al., 2016). These inherited cardiomyopathies also involve metabolic and mitochondrial abnormalities (Sacchetto et al., 2019), in agreement with our data showing LV C-MSC enrichment in mitochondrial-associated pathways. Accordingly, multi-organ diseases caused by mitochondrial mutations prevalently cause LV non-compaction cardiomyopathy or LV dilated cardiomyopathy (Towbin and Jefferies, 2017).

CONCLUSION

We found that RV and LV differ for quantity and quality of C-MSC. We speculate that these findings may have pathophysiological implications in different areas. Appropriate LV vs. RV C-MSC can be used in disease modeling. Similarly, tissue engineering could benefit from the origin-correspondent C-MSC and gain from our description of cell composition percentage. Regenerative medicine and pharmacological screening, using C-MSC, may take advantage of a responsible choice of the appropriate cell product or derivative, either from the LV or the RV, depending on the application. Moreover, the awareness of the baseline LV or RV C-MSC differences can contribute to a proper understanding of

chamber-specific diseases, where C-MSC possibly contribute to regional phenotypic disease expression.

DATA AVAILABILITY STATEMENT

The dataset has been deposited to the GEO-GSE142205.

ETHICS STATEMENT

This study was approved and reviewed by the Ethics Committee of the IRCCS Istituto Europeo di Oncologia e Centro Cardiologico Monzino (R1020/19-CCM1072). Autoptic donor cardiac samples were obtained from the "Cardiovascular Tissue Bank" of Centro Cardiologico Monzino IRCCS (MTA signed 5/11/2019). Donor heart tissue was collected only after signature of informed consent by relatives, authorizing transplantation and research on the remaining tissue, not suitable for human clinical use.

AUTHOR CONTRIBUTIONS

IS, ES, and GiuP conceived the study. IS isolated the cells and performed the experiments to characterize differential C-MSC functions. AS performed immunofluorescence on tissue samples. CV, LP, MC, and GC performed and supervised sequencing and transcriptome analysis. BM, AG, and GiaP provided samples from cadaveric donors and collected clinical data. All authors critically reviewed the manuscript.

FUNDING

The project was funded by Italian Ministry of Health (RC2019 EF5C ID: 2754330).

ACKNOWLEDGMENTS

We are deeply grateful to heart donors' families, who consented the donation for both transplantation and research use. We also acknowledge the fundamental help of Dr. Paolo Poggio, Dr. Gianluca Perrucci, and Dr. Rosaria Santoro for data acquisition and analysis.

SUPPLEMENTARY MATERIAL

The Supplementary Material for this article can be found online at: https://www.frontiersin.org/articles/10.3389/fphys.2020.00604/full#supplementary-material

FIGURE S1 | Methodological approach. Transmural samples of left (LV) and right (RV) ventricles have been obtained from mid-chamber free walls of LV at the anterolateral mid-papillary level and of RV at the anterior papillary muscle level, above moderator band insertion. From these samples, total tissue was embedded for immunofluorescence analysis and endocardial–myocardial tissue from the same origin was collected to obtain C-MSC.

FIGURE S2 | Lipid accumulation in growth conditions. The left panels show Oil Red O staining representative images of left (LV) and right (RV) cardiac mesenchymal stromal cells (C-MSC) cultured in growth medium (GM). The scale bar indicates 50 μm. The quantification of cell lipid accumulation in comparison to the results obtained in adipogenic medium is provided in the right panel. $n = 6$ each (paired *t*-test).

FIGURE S3 | Distribution of gene expression. **(A)** Density distribution of the gene expression levels, grouped by coding (pink) and non-coding (light blue) expressed genes. The protein-coding genes show a higher average expression value than non-coding genes. **(B)** Pie chart of the percentage of coding (pink) and non-coding (light blue) expressed genes; more than 80% of expressed genes are protein-coding.

FIGURE S4 | Histogram *P*-value. The histogram of *P*-values distribution for non-DE genes is ideally uniformly distributed across the unit interval, whereas the *P*-values for DE genes present a spike near zero.

TABLE S1 | Summary of the clinical features of the healthy controls from which LV and RV samples were obtained.

TABLE S2 | Primary antibodies.

TABLE S3 | Secondary antibodies.

TABLE S4 | Primers.

TABLE S5 | Detailed FACS analysis of LV and RV C-MSC.

TABLE S6 | Summary of gene and protein expression during LV and RV C-MSC adipogenic differentiation for 72 h and 1 week. $2^{-\Delta\Delta}$Ct ratio is reported for qRT-PCR analysis. The densitometric analysis for each protein normalized on GAPDH expression is shown for WB data.

FILE S1 | (a) Differential gene expression analysis in pair-wise left vs. right ventricle samples. The list shows annotations and statistics for all the genes detected by transcriptome RNA-Sequencing (IonS5, Thermo Fisher Scientific). Significant comparisons for an adjusted *P*-value < 0.05 are highlighted in green. Combined rank-score is calculated as the log2 fold-change (logFC) × LR. **(b)** Gene-set enrichment analysis (GSEA) using AllPathways on combined rank score of pair-wise differential expression analysis. The table lists AllPathways Gene Set Name, Database ID terms, and GSEA statistics for LEFT vs. RIGHT ventricles. Significant tests for a false discovery rate (FDR) < 0.05 are highlighted in green. **(c)** Legend_DE_analysis and Legend_GSEA.

REFERENCES

Abel, E. D., Litwin, S. E., and Sweeney, G. (2008). Cardiac remodeling in obesity. *Physiol. Rev.* 88, 389–419. doi: 10.1152/physrev.00017.2007

Andersen, S., Nielsen-Kudsk, J. E., Vonk Noordegraaf, A., and de Man, F. S. (2019). Right ventricular fibrosis. *Circulation* 139, 269–285.

Bagno, L., Hatzistergos, K. E., Balkan, W., and Hare, J. M. (2018). Mesenchymal stem cell-based therapy for cardiovascular disease: progress and challenges. *Mol. Ther.* 26, 1610–1623. doi: 10.1016/j.ymthe.2018.05.009

Banerjee, I., Fuseler, J. W., Price, R. L., Borg, T. K., and Baudino, T. A. (2007). Determination of cell types and numbers during cardiac development in the neonatal and adult rat and mouse. *Am. J. Physiol. Heart Circ. Physiol.* 293, H1883–H1891.

Black, B. L. (2007). Transcriptional pathways in second heart field development. *Semin. Cell Dev. Biol.* 18, 67–76. doi: 10.1016/j.semcdb.2007.01.001

Braunwald, E. (2018). Cell-based therapy in cardiac regeneration: an overview. *Circ. Res.* 123, 132–137. doi: 10.1161/circresaha.118.313484

Brown, R. D., Ambler, S. K., Mitchell, M. D., and Long, C. S. (2005). The cardiac fibroblast: therapeutic target in myocardial remodeling and failure. *Annu. Rev. Pharmacol. Toxicol.* 45, 657–687. doi: 10.1146/annurev.pharmtox.45.120403.095802

Camelliti, P., Borg, T. K., and Kohl, P. (2005). Structural and functional characterisation of cardiac fibroblasts. *Cardiovasc. Res.* 65, 40–51. doi: 10.1016/j.cardiores.2004.08.020

Caplan, A. I., and Dennis, J. E. (2006). Mesenchymal stem cells as trophic mediators. *J. Cell Biochem.* 98, 1076–1084. doi: 10.1002/jcb.20886

Chong, J. J., Reinecke, H., Iwata, M., Torok-Storb, B., Stempien-Otero, A., and Murry, C. E. (2013). Progenitor cells identified by PDGFR-alpha expression in the developing and diseased human heart. *Stem. Cells Dev.* 22, 1932–1943. doi: 10.1089/scd.2012.0542

Chugh, A. R., Beache, G. M., Loughran, J. H., Mewton, N., Elmore, J. B., Kajstura, J., et al. (2012). Administration of cardiac stem cells in patients with ischemic cardiomyopathy: the SCIPIO trial: surgical aspects and interim analysis of myocardial function and viability by magnetic resonance. *Circulation* 126(11 Suppl. 1), S54–S64.

Clapham, K. R., Singh, I., Capuano, I. S., Rajagopal, S., and Chun, H. J. (2019). MEF2 and the right ventricle: from development to disease. *Front. Cardiovasc. Med.* 6:29. doi: 10.3389/fcvm.2019.00029

Coulson-Thomas, V. J., Coulson-Thomas, Y. M., Gesteira, T. F., and Kao, W. W. (2016). Extrinsic and intrinsic mechanisms by which mesenchymal stem cells suppress the immune system. *Ocul. Surf.* 14, 121–134. doi: 10.1016/j.jtos.2015.11.004

Czapla, J., Matuszczak, S., Wisniewska, E., Jarosz-Biej, M., Smolarczyk, R., Cichoń, T., et al. (2016). Human cardiac mesenchymal stromal cells with CD105+CD34-phenotype enhance the function of post-infarction heart in mice. *PLoS One* 11:e0158745. doi: 10.1371/journal.pone.0158745

Detert, S., Stamm, C., Beez, C., Diedrichs, F., Ringe, J., Van Linthout, S., et al. (2017). The atrial appendage as a suitable source to generate cardiac-derived adherent proliferating cells for regenerative cell-based therapies. *J. Tissue Eng. Regen. Med.* 2, e1404–e1417.

Di Resta, C., and Becchetti, A. (2010). Introduction to ion channels. *Adv. Exp. Med. Biol.* 674, 9–21. doi: 10.1007/978-1-4419-6066-5_2

Diedrichs, F., Stolk, M., Jurchott, K., Haag, M., Sittinger, M., and Seifert, M. (2019). Enhanced immunomodulation in inflammatory environments favors human cardiac mesenchymal stromal-like cells for allogeneic cell therapies. *Front. Immunol.* 10:1716. doi: 10.3389/fimmu.2019.01716

Dobin, A., Davis, C. A., Schlesinger, F., Drenkow, J., Zaleski, C., Jha, S., et al. (2013). STAR. *Bioinformatics* 29, 15–21.

Doll, S., Dressen, M., Geyer, P. E., Itzhak, D. N., Braun, C., Doppler, S. A., et al. (2017). Region and cell-type resolved quantitative proteomic map of the human heart. *Nat. Commun.* 8:1469.

Dominici, M., Le Blanc, K., Mueller, I., Slaper-Cortenbach, I., Marini, F., Krause, D., et al. (2006). Minimal criteria for defining multipotent mesenchymal stromal cells. the international society for cellular therapy position statement. *Cytotherapy* 8, 315–317. doi: 10.1080/14653240600855905

Egemnazarov, B., Crnkovic, S., Nagy, B. M., Olschewski, H., and Kwapiszewska, G. (2018). Right ventricular fibrosis and dysfunction: actual concepts and common misconceptions. *Matrix Biol.* 6, 507–521. doi: 10.1016/j.matbio.2018.01.010

Frangogiannis, N. G. (2017). Fibroblasts and the extracellular matrix in right ventricular disease. *Cardiovasc. Res.* 113, 1453–1464. doi: 10.1093/cvr/cvx146

Friedberg, M. K., and Redington, A. N. (2014). Right versus left ventricular failure: differences, similarities, and interactions. *Circulation* 129, 1033–1044. doi: 10.1161/circulationaha.113.001375

Gray, G. A., Toor, I. S., Castellan, R., Crisan, M., and Meloni, M. (2018). Resident cells of the myocardium: more than spectators in cardiac injury, repair and regeneration. *Curr. Opin. Physiol.* 1, 46–51. doi: 10.1016/j.cophys.2017.08.001

Hematti, P. (2012). Mesenchymal stromal cells and fibroblasts: a case of mistaken identity? *Cytotherapy* 14, 516–521. doi: 10.3109/14653249.2012.677822

Hoch, D. H., and Rosenfeld, L. E. (1992). Tachycardias of right ventricular origin. *Cardiol. Clin.* 10, 151–164. doi: 10.1016/s0733-8651(18)30260-1

Hudon-David, F., Bouzeghrane, F., Couture, P., and Thibault, G. (2007). Thy-1 expression by cardiac fibroblasts: lack of association with myofibroblast contractile markers. *J. Mol. Cell Cardiol.* 42, 991–1000. doi: 10.1016/j.yjmcc.2007.02.009

Huttenlocher, A., and Horwitz, A. R. (2011). Integrins in cell migration. *Cold Spring Harb. Perspect. Biol.* 3, a005074.

Jugdutt, B. I. (2003). Ventricular remodeling after infarction and the extracellular collagen matrix: when is enough enough? *Circulation* 108, 1395–1403. doi: 10.1161/01.cir.0000085658.98621.49

Karantalis, V., and Hare, J. M. (2015). Use of mesenchymal stem cells for therapy of cardiac disease. *Circ. Res.* 116, 1413–1430. doi: 10.1161/circresaha.116.303614

Kelly, R. G., Buckingham, M. E., and Moorman, A. F. (2014). Heart fields and cardiac morphogenesis. *Cold Spring Harb. Perspect. Med.* 4:a015750. doi: 10.1101/cshperspect.a015750

Kondo, R. P., Dederko, D. A., Teutsch, C., Chrast, J., Catalucci, D., Chien, K. R., et al. (2006). Comparison of contraction and calcium handling between right and left ventricular myocytes from adult mouse heart: a role for repolarization waveform. *J. Physiol.* 571(Pt 1), 131–146. doi: 10.1113/jphysiol.2005.101428

La Gerche, A., Burns, A. T., Mooney, D. J., Inder, W. J., Taylor, A. J., Bogaert, J., et al. (2012). Exercise-induced right ventricular dysfunction and structural remodelling in endurance athletes. *Eur. Heart J.* 33, 998–1006. doi: 10.1093/eurheartj/ehr397

Langmead, B., and Salzberg, S. L. (2012). Fast gapped-read alignment with Bowtie 2. *Nat. Methods* 9, 357–359. doi: 10.1038/nmeth.1923

Le, T. Y. L., Pickett, H. A., Dos Remedios, C. G., Barbaro, P. M., Kizana, E., and Chong, J. J. H. (2018). Platelet-derived growth factor receptor-alpha expressing cardiac progenitor cells can be derived from previously cryopreserved human heart samples. *Stem. Cells Dev.* 27, 184–198. doi: 10.1089/scd.2017.0082

Le, T. Y. L., Pickett, H. A., Yang, A., Ho, J. W. K., Thavapalachandran, S., Igoor, S., et al. (2019). Enhanced cardiac repair by telomerase reverse transcriptase over-expression in human cardiac mesenchymal stromal cells. *Sci. Rep.* 9:10579.

Leek, J. T., and Storey, J. D. (2008). A general framework for multiple testing dependence. *Proc. Natl. Acad. Sci. U.S.A.* 105, 18718–18723. doi: 10.1073/pnas.0808709105

Liao, Y., Smyth, G. K., and Shi, W. (2014). featureCounts: an efficient general purpose program for assigning sequence reads to genomic features. *Bioinformatics* 30, 923–930. doi: 10.1093/bioinformatics/btt656

Lombardi, R., Chen, S. N., Ruggiero, A., Gurha, P., Czernuszewicz, G. Z., Willerson, J. T., et al. (2016). Cardiac fibro-adipocyte progenitors express desmosome proteins and preferentially differentiate to adipocytes upon deletion of the desmoplakin gene. *Circ. Res.* 119, 41–54. doi: 10.1161/circresaha.115.308136

Long, C. S., and Brown, R. D. (2002). The cardiac fibroblast, another therapeutic target for mending the broken heart? *J. Mol. Cell Cardiol.* 34, 1273–1278. doi: 10.1006/jmcc.2002.2090

Lv, F. J., Tuan, R. S., Cheung, K. M., and Leung, V. Y. (2014). Concise review: the surface markers and identity of human mesenchymal stem cells. *Stem. Cells* 32, 1408–1419. doi: 10.1002/stem.1681

Malliaras, K., Makkar, R. R., Smith, R. R., et al. (2014). Intracoronary cardiosphere-derived cells after myocardial infarction: evidence of therapeutic regeneration in the final 1-year results of the CADUCEUS trial (CArdiosphere-Derived aUtologous stem CElls to reverse ventricUlar dySfunction). *J. Am. Coll. Cardiol.* 63, 110–122.

McCarthy, D. J., Chen, Y., and Smyth, G. K. (2012). Differential expression analysis of multifactor RNA-Seq experiments with respect to biological variation. *Nucleic Acids Res.* 40, 4288–4297. doi: 10.1093/nar/gks042

McGettrick, H. M., Butler, L. M., Buckley, C. D., Rainger, G. E., and Nash, G. B. (2012). Tissue stroma as a regulator of leukocyte recruitment in inflammation. *J. leukoc.Biol.* 91, 385–400. doi: 10.1189/jlb.0911458

Merico, D., Isserlin, R., Stueker, O., Emili, A., and Bader, G. D. (2010). Enrichment map: a network-based method for gene-set enrichment visualization and interpretation. *PLoS One* 5:e13984. doi: 10.1371/journal.pone.0013984

Merlo, M., Gobbo, M., Stolfo, D., Losurdo, P., Ramani, F., Barbati, G., et al. (2016). The Prognostic Impact of the Evolution of RV Function in Idiopathic DCM. *JACC Cardiovasc. Imaging* 9, 1034–1042. doi: 10.1016/j.jcmg.2016.01.027

Miteva, K., Haag, M., Peng, J., Savvatis, K., Becher, P. M., Seifert, M., et al. (2011). Human cardiac-derived adherent proliferating cells reduce murine acute Coxsackievirus B3-induced myocarditis. *PLoS One* 6:e28513. doi: 10.1371/journal.pone.0028513

Moorman, A., Webb, S., Brown, N. A., Lamers, W., and Anderson, R. H. (2003). Development of the heart: (1) formation of the cardiac chambers and arterial trunks. *Heart* 89, 806–814. doi: 10.1136/heart.89.7.806

Nattel, S. (2018). Electrical coupling between cardiomyocytes and fibroblasts: experimental testing of a challenging and important concept. *Cardiovasc Res.* 114, 349–352. doi: 10.1093/cvr/cvy003

Penny, D. J., and Redington, A. N. (2016). Function of the left and right ventricles and the interactions between them. *Pediatr. Crit. Care Med.* 17(8 Suppl. 1), S112–S118.

Perbellini, F., Watson, S. A., Bardi, I., and Terracciano, C. M. (2018). Heterocellularity and cellular cross-talk in the cardiovascular system. *Front. Cardiovasc. Med.* 5:143. doi: 10.3389/fcvm.2018.00143

Pham, T., Zgierski-Johnston, C. M., Tran, K., Taberner, A. J., Loiselle, D. S., and Han, J. C. (2019). Energy expenditure for isometric contractions of right and left ventricular trabeculae over a wide range of frequencies at body temperature. *Sci. Rep.* 9:8841.

Pilato, C. A., Stadiotti, I., Maione, A. S., Saverio, V., Catto, V., Tundo, F., et al. (2018). Isolation and characterization of cardiac mesenchymal stromal cells from endomyocardial bioptic samples of arrhythmogenic cardiomyopathy patients. *J. Vis. Exp.* 132:57263.

Pinto, A. R., Ilinykh, A., Ivey, M. J., Kuwabara, J. T., D'Antoni, M. L., Debuque, R., et al. (2016). Revisiting cardiac cellular composition. *Circ. Res.* 118, 400–409. doi: 10.1161/circresaha.115.307778

Pittenger, M. F., Mackay, A. M., Beck, S. C., Jaiswal, R. K., Douglas, R., Mosca, J. D., et al. (1999). Multilineage potential of adult human mesenchymal stem cells. *Science* 284, 143–147. doi: 10.1126/science.284.5411.143

Pittenger, M. F., and Martin, B. J. (2004). Mesenchymal stem cells and their potential as cardiac therapeutics. *Circ. Res.* 95, 9–20. doi: 10.1161/01.res.0000135902.99383.6f

Prockop, D. J., and Oh, J. Y. (2012). Mesenchymal stem/stromal cells (MSCs): role as guardians of inflammation. *Mol. Ther.* 20, 14–20. doi: 10.1038/mt.2011.211

Rainer, J., Meraviglia, V., Blankenburg, H., Piubelli, C., Pramstaller, P. P., Paolin, A., et al. (2018). The arrhythmogenic cardiomyopathy-specific coding and non-coding transcriptome in human cardiac stromal cells. *BMC Genom.* 19:491. doi: 10.1186/s12864-018-4876-6

Risso, D., Ngai, J., Speed, T. P., and Dudoit, S. (2014). Normalization of RNA-seq data using factor analysis of control genes or samples. *Nat. Biotechnol.* 32, 896–902. doi: 10.1038/nbt.2931

Robinson, M. D., and Oshlack, A. (2010). A scaling normalization method for differential expression analysis of RNA-seq data. *Genome Biol.* 11, R25.

Rockel, J. S., Rabani, R., and Viswanathan, S. (2019). Anti-fibrotic mechanisms of exogenously-expanded mesenchymal stromal cells for fibrotic diseases. *Semin. Cell Dev. Biol.* 101, 87–103. doi: 10.1016/j.semcdb.2019.10.014

Rossini, A., Frati, C., Lagrasta, C., Graiani, G., Scopece, A., Cavalli, S., et al. (2010). Human cardiac and bone marrow stromal cells exhibit distinctive properties related to their origin. *Cardiovasc. Res.* 89, 650–660. doi: 10.1093/cvr/cvq290

Sacchetto, C., Sequeira, V., Bertero, E., Dudek, J., Maack, C., and Calore, M. (2019). Metabolic Alterations in Inherited Cardiomyopathies. Journal of clinical medicine. *J. Clin. Med.* 8:2195. doi: 10.3390/jcm8122195

Sanz-Ruiz, R., Casado Plasencia, A., Borlado, L. R., Fernández-Santos, M. E., Al-Daccak, R., Claus, P., et al. (2017). Rationale and design of a clinical trial to evaluate the safety and efficacy of intracoronary infusion of allogeneic human cardiac stem cells in patients with acute myocardial infarction and left ventricular dysfunction: the randomized multicenter double-blind controlled CAREMI trial (Cardiac stem cells in patients with acute myocardial infarction). *Circ. Res.* 121, 71–80. doi: 10.1161/circresaha.117.310651

Shannon, P., Markiel, A., Ozier, O., Baliga, N. S., Wang, J. T., Ramage, D., et al. (2003). Cytoscape: a software environment for integrated models of biomolecular interaction networks. *Genome Res.* 13, 2498–2504. doi: 10.1101/gr.1239303

Smith, R. S., Smith, T. J., Blieden, T. M., and Phipps, R. P. (1997). Fibroblasts as sentinel cells. synthesis of chemokines and regulation of inflammation. *Am. J. Pathol.* 151, 317–322.

Sommariva, E., Brambilla, S., Carbucicchio, C., Gambini, E., Meraviglia, V., Dello Russo, A., et al. (2016). Cardiac mesenchymal stromal cells are a source of adipocytes in arrhythmogenic cardiomyopathy. *Eur. Heart J.* 37, 1835–1846. doi: 10.1093/eurheartj/ehv579

Souders, C. A., Bowers, S. L., and Baudino, T. A. (2009). Cardiac fibroblast: the renaissance cell. *Circ. Res.* 105, 1164–1176. doi: 10.1161/circresaha.109.209809

Stanley, W. C., Recchia, F. A., and Lopaschuk, G. D. (2005). Myocardial substrate metabolism in the normal and failing heart. *Physiol. Rev.* 85, 1093–1129. doi: 10.1152/physrev.00006.2004

Subramanian, A., Tamayo, P., Mootha, V. K., Mukherjee, S., Ebert, B. L., Gillette, M. A., et al. (2005). Gene set enrichment analysis: a knowledge-based approach for interpreting genome-wide expression profiles. *Proc. Natl. Acad. Sci. U.S.A.* 102, 15545–15550. doi: 10.1073/pnas.0506580102

Takeda, N., and Manabe, I. (2011). Cellular interplay between cardiomyocytes and nonmyocytes in cardiac remodeling. *Int. J. Inflamm.* 2011:535241. doi: 10.4061/2011/535241

Tian, Y., and Morrisey, E. E. (2012). Importance of myocyte-nonmyocyte interactions in cardiac development and disease. *Circ. Res.* 110, 1023–1034. doi: 10.1161/circresaha.111.243899

Towbin, J. A., and Jefferies, J. L. (2017). cardiomyopathies due to left ventricular noncompaction, mitochondrial and storage diseases, and inborn errors of metabolism. *Circ. Res.* 121, 838–854. doi: 10.1161/circresaha.117.310987

Tsuchihashi, T., Maeda, J., Shin, C. H., Ivey, K. N., Black, B. L., Olson, E. N., et al. (2011). Hand2 function in second heart field progenitors is essential for cardiogenesis. *Dev. Biol.* 351, 62–69. doi: 10.1016/j.ydbio.2010.12.023

Vagnozzi, R. J., Maillet, M., Sargent, M. A., Khalil, H., Johansen, A. K., Schwanekamp, J. A., et al. (2019). An acute immune response underlies the benefit of cardiac stem-cell therapy. *Nature* 577, 405–409. doi: 10.1038/s41586-019-1802-2

Zhou, P., and Pu, W. T. (2016). Recounting cardiac cellular composition. *Circ. Res.* 118, 368–370. doi: 10.1161/circresaha.116.308139

Conflict of Interest: The authors declare that the research was conducted in the absence of any commercial or financial relationships that could be construed as a potential conflict of interest.

frontiers in Physiology

MINI REVIEW
published: 03 July 2020
doi: 10.3389/fphys.2020.00761

The Broad Spectrum of *LMNA* Cardiac Diseases: From Molecular Mechanisms to Clinical Phenotype

Silvia Crasto[1,2†], *Ilaria My*[1†] *and Elisa Di Pasquale*[1,2*]

[1] Humanitas Clinical and Research Center – IRCCS, Rozzano, Italy, [2] Institute of Genetic and Biomedical Research (IRGB) – UOS of Milan, National Research Council (CNR), Milan, Italy

Mutations of Lamin A/C gene (*LMNA*) cause laminopathies, a group of disorders associated with a wide spectrum of clinically distinct phenotypes, affecting different tissues and organs. Heart involvement is frequent and leads to cardiolaminopathy LMNA-dependent cardiomyopathy (LMNA-CMP), a form of dilated cardiomyopathy (DCM) typically associated with conduction disorders and arrhythmias, that can manifest either as an isolated event or as part of a multisystem phenotype. Despite the recent clinical and molecular developments in the field, there is still lack of knowledge linking specific *LMNA* gene mutations to the distinct clinical manifestations. Indeed, the severity and progression of the disease have marked interindividual variability, even amongst members of the same family. Studies conducted so far have described Lamin A/C proteins involved in diverse biological processes, that span from a structural role in the nucleus to the regulation of response to mechanical stress and gene expression, proposing various mechanistic hypotheses. However, none of those is *per se* able to fully justify functional and clinical phenotypes of LMNA-CMP; therefore, the role of Lamin A/C in cardiac pathophysiology still represents an open question. In this review we provide an update on the state-of-the-art studies on cardiolaminopathy, in the attempt to draw a line connecting molecular mechanisms to clinical manifestations. While investigators in this field still wonder about a clear genotype/phenotype correlation in LMNA-CMP, our intent here is to recapitulate common mechanistic hypotheses that link different mutations to similar clinical presentations.

Keywords: *LMNA* gene, cardiolaminopathy, Lamin A/C, clinical phenotype, molecular mechanisms

OPEN ACCESS

Edited by:
Martina Calore,
Maastricht University, Netherlands

Reviewed by:
J. Carter Ralphe,
University of Wisconsin-Madison, United States
Michelle S. Parvatiyar,
Florida State University, United States

***Correspondence:**
Elisa Di Pasquale
elisa.dipasquale@humanitasresearch.it;
elisadipa@gmail.com

[†] These authors have contributed equally to this work

Specialty section:
This article was submitted to Striated Muscle Physiology, a section of the journal Frontiers in Physiology

Received: *26 February 2020*
Accepted: *11 June 2020*
Published: *03 July 2020*

Citation:
Crasto S, My I and Di Pasquale E (2020) The Broad Spectrum of LMNA Cardiac Diseases: From Molecular Mechanisms to Clinical Phenotype. Front. Physiol. 11:761. doi: 10.3389/fphys.2020.00761

INTRODUCTION

LMNA Gene and Its Products

LMNA gene maps to chromosome 1q21.1-21.2 and is composed of 12 exons spanning around 25 kb. It encodes A-type nuclear lamins via alternative splicing (Lin and Worman, 1993; Wydner et al., 1996): Lamin A and C (Lamin A/C) represents the two main isoforms, while Lamin C2 and AD10 are described in germ cells and cancer cells, respectively (Machiels et al., 1996; Alsheimer et al., 2000). A-type lamin proteins have a tripartite domain organization with a central rod domain, a short N-terminal head domain and a tail C-terminal domain. Unlike Lamin C, Lamin A is translated as Prelamin A, containing a carboxyl-terminal CaaX motif, which is then modified by carboxymethylation and farnesylation and undergoes sequential post-translational modifications to form mature Lamin A (Herrmann and Aebi, 2004; Young et al., 2005). Nuclear lamins are classified

as type V intermediate filament (IF) proteins and represent the major elements that constitute the nuclear lamina (NL). In addition to their well-known structural role in the nucleus, Lamin A/C are increasingly considered as key players in regulating gene transcription through both direct and indirect modulation of chromatin organization, DNA replication and signal transduction pathways (Gruenbaum et al., 2005; Dechat et al., 2008; Dittmer and Misteli, 2011).

Unlike B-type lamins, the expression of A-type lamins is developmentally regulated and mostly occurs in differentiated cells (Worman and Bonne, 2007). During mouse embryogenesis, Lamin A/C start to be expressed around day 8–9 in extra-embryonic tissues and few days later (day 10–12) in the embryo (Dittmer and Misteli, 2011). The cell-specific and temporally regulated expression of these proteins supports a fundamental role of Lamin A/C in cell differentiation, lineage specification and tissue development (Worman and Bonne, 2007; Butin-Israeli et al., 2012).

Laminopathies

Mutations in the *LMNA* gene cause laminopathies, a group of disorders characterized by phenotypically heterogeneous manifestations. Up to now a total of 498 *LMNA* mutations have been described[1] associated to more than 15 different phenotypes. Indeed, laminopathies can either specifically affect distinct tissues, including striated muscles, the peripheral nerves, or the adipose tissue, or present as a systemic disease affecting concomitantly several organs similar to premature aging syndromes. However, there is growing evidence of overlapping phenotypes, suggesting the presence of a real continuum within the disease.

Among the different phenotypes, cardiac involvement is one of the most prevalent and severe manifestations, being a hallmark of several laminopathies, such as Emery-Dreifuss muscular dystrophy, Limb-girdle muscular dystrophy 1B and Hutchinson-Gilford Progeria Syndrome (HGPS) (Fatkin et al., 1999; Arbustini et al., 2002; van Tintelen et al., 2007a). Despite the recent developments in the field, the understanding of the pathogenetic role of Lamin A/C in cardiac disease is still incomplete.

In this review we aim to provide an update on the state-of-the-art investigations in this area of research, drawing a definite line from the molecular mechanisms toward the clinical manifestations. Although investigators are still working on defining genotype/phenotype correlations, our goal is to highlight common molecular features that could link different *LMNA* variants to a similar clinical presentation.

FROM *LMNA* VARIANTS TO CARDIAC PHENOTYPES

LMNA Variants

The first reports that associate *LMNA* mutations to cardiac diseases date back to 1999 (Bonne et al., 1999; Fatkin et al., 1999): these reports represented a revolution in the field, identifying for the first time *LMNA* mutations as responsible for dilated cardiomyopathy (DCM) associated with conduction system disease. Jakobs et al. (2001) described several novel *LMNA* mutations, one missense (p.E203K, nucleotide c.G607A) in 14 individuals and one nonsense (p.R225X, nucleotide c.C673T) in 10 subjects: these patients were diagnosed with DCM and variable conduction system disease, and were free from any skeletal muscle phenotype. Few years later, other mutations in *LMNA* gene were described (van Tintelen et al., 2007a,van Tintelen et al., 2007b; Saga et al., 2009): one nonsense mutation (815_818delinsCCAGAC) and some missense variants (p.N195K; p.Y259H; p.R166P). Overtime, *LMNA* gene emerged as the second most commonly mutated gene associated to familial cardiomyopathy (CMP), accounting for ∼6–8% of the cases (Hershberger and Siegfried, 2011) of idiopathic DCM, with this number raising up to 33% for cases presenting with both DCM and conduction defects (McNally and Mestroni, 2017).

Cardiolaminopathy

Cardiomyopathy caused by mutations in *LMNA* gene is referred to as cardiolaminopathy (LMNA-CMP). The disease is generally characterized by variable extent of ventricular dilation (Bonne et al., 1999; Fatkin et al., 1999) or, less frequently, by left ventricular (LV) non-compaction (Sedaghat-Hamedani et al., 2017).

LMNA-CMP has been linked to 165 unique mutations, distributed along the entire gene (Tesson et al., 2014). However, the majority of the mutations occur in the head and in the rod domains and rarely in the tail domain (Fatkin et al., 1999; Jakobs et al., 2001). Pathogenic variants are mainly missense and nonsense mutations, while fewer small deletions/insertions have been identified (Dittmer et al., 2014; Zahr and Jaalouk, 2018). Haploinsufficiency has been suggested as mechanism of disease in patients carrying truncating variants, while missense mutations have been proposed to act mainly through a dominant negative pathway. Subjects with truncating mutations have been associated to an earlier onset of cardiac conduction defects and atrial arrhythmias and a lower LV ejection fraction (EF), than those with missense mutations (Nishiuchi et al., 2017). However, so far there is still lack of knowledge explaining the link between specific *LMNA* mutations and a defined phenotype, and the severity and the progression of the disease have marked interindividual variability, not only among unrelated probands, but also within members of the same family. This supports the concept that the final phenotype results not only from the single *LMNA* mutation, but is also influenced by modifying genes or environmental cues, similarly to what has been reported in some families with titin and desmin mutations (Muntoni et al., 2008; Granger et al., 2011; Roncarati et al., 2013). Whole-exome and whole-genome sequencing studies will unequivocally facilitate the investigation of the genetics behind the disease and allow a comprehensive understanding of the mechanisms underlying the final clinical presentation.

[1] http://www.umd.be/LMNA/

Cardiac Conduction System Disease and Arrhythmias

The clinical course of LMNA-CMP is characterized by a high rate of major cardiac events such as sudden cardiac death (SCD), malignant ventricular tachycardia (VT), extreme bradycardia due to a high degree of atrioventricular block (AVB) and end-stage heart failure. What is intriguing is the common finding that laminopathies often manifest as primary arrhythmia. Bradyarrhythmias and supraventricular tachyarrhythmias as atrial fibrillation and flutter often anticipate by decades the development of DCM. For this reason, genetic screening should be considered in young patients presenting with new AVB or atypical atrial arrhythmias, even in the absence of LV dysfunction. In the study by Kumar et al. (2016), only one-half of patients have an LVEF < 50% at the initial medical consultation.

The pathophysiological mechanisms underlying the arrhythmic phenotype are still not well elucidated. Systolic dysfunction, male sex, non-missense mutations and non-sustained VT are considered predictors of malignant ventricular arrhythmias in LMNA-CMP (Van Rijsingen et al., 2012; Hasselberg et al., 2014; Kumar et al., 2016; Nishiuchi et al., 2017). However, such risk factors are debated in some studies (Nishiuchi et al., 2017; Peretto et al., 2019) and it was recently shown in a large cohort of DCM patients, that carriers of *LMNA* variants experience the highest rates of SCD/VT/ventricular fibrillation (VF), which was independent of the LV EF (Gigli et al., 2019). Further studies need to be conducted in order to clarify to which extent phenotypic differences among the different cohorts of patients are dependent on genetic background rather than on specific *LMNA* variants.

Clinical Presentation

The presentation of DCM does not show specific characteristics and the expression of the DCM pattern was found to be age-dependent, with development of the phenotype between 20 and 39 years of age in two thirds of the cases and complete penetrance by 60 years (Arbustini et al., 2002). The "red flags" predicting higher chance of *LMNA* mutations are the concomitant presence of conduction defects and skeletal muscle involvement, even if creatine phosphokinase (CPK – serum marker of muscular damage) is elevated only in one third of the cases (Fatkin et al., 1999; Rapezzi et al., 2013). Arbustini et al. (2002) showed that approximately 33% of patients with AVB and cardiomyopathy carries a *LMNA* mutation. For this reason, screening for *LMNA* mutations in young patients with idiopathic DCM, especially when it is associated with atrial arrhythmias and/or AVB, is important for prognosis and genetic counseling.

Patients who have both cardiac and neuromuscular manifestations more commonly experience bradyarrhythmias and atrial fibrillation compared to patients with solely cardiac phenotypes, despite having no differences in structural heart disease. In this group of patients cardiac abnormalities do not strictly correlate with the severity of the neuromuscular involvement, which may suggest distinct pathogenetic mechanisms (Benedetti et al., 2007; Hasselberg et al., 2018; Peretto et al., 2019). However, a recent study on a small cohort of patients showed that the neuromuscular presentation was associated with earlier cardiac involvement, characterized by a linear and progressive evolution from rhythm disorders to cardiomyopathy (Ditaranto et al., 2019).

Prognosis and Risk Stratification

Cardiolaminopathy often presents an aggressive and rapid evolution, with a worse natural history compared to other forms of non-ischemic dilated cardiomyopathies and have higher prevalence of malignant arrhythmias and cardiac transplantation (Pasotti et al., 2008; Kayvanpour et al., 2017).

Positive genetic testing for *LMNA* mutations has crucial clinical and prognostic implications. Mortality in patients with LMNA-CMP is estimated to be 40% at 5 years (Pasotti et al., 2008), whereas 45% suffered SCD or aborted SCD. Currently, *LMNA* mutations represent the only genetic background in DCM that influences international guidelines-based timing of ICD therapy in primary prevention, regardless of LV EF values (Priori et al., 2013; Priori and Blomström-Lundqvist, 2015).

Recently, a new 5-year prediction model for life threatening ventricular tachyarrhythmia (LTVTA) has been proposed (Wahbi et al., 2019) to assist us in deciding whether or not a candidate is eligible for the placement of an ICD implantation (online calculator available at http://lmna-risk-vta.fr/). Predictors of LTVTA in the analyzed sample were male sex, non-missense *LMNA* mutation, 1st degree and higher AV block, non-sustained VT and LV EF. The risk threshold used enabled reclassification of 28.8% of patients compared with the guidelines-based approach.

New Molecular Targets Under Clinical Investigation

Currently, three new molecular targets, emerged from biochemical studies, are under investigation as possible pharmacological strategies to treat LMNA-CMP. The first approach involves a selective oral inhibitor of the p38 MAPK pathway is currently under a phase III clinical trial[2]. The second approach regards the application of mTOR pathway inhibitors that have shown promising improvements in terms of LV size and function in animal models (Choi et al., 2012), and the third approach focuses on PDGFR blockers and their ability to ameliorate the arrhythmic phenotype in *in vitro* models (Lee et al., 2019).

MOLECULAR HYPOTHESES BEHIND THE "CLINICAL SCENARIO"

As mentioned above, 498 different mutations in *LMNA* gene have been reported, of which 165 associated with LMNA-CMP. Since the discovery of the *LMNA* gene as causative of laminopathies, more than 1000 research and clinical studies have been published, aiming to establish a causal correlation between morphological and functional defects of laminopathic cells and the heterogeneous clinical phenotypes of this group of disorders. Although several hypotheses on the potential mechanisms have

[2]www.clinicalTrials.gov identifier NCT03439514

emerged from these studies, a unique view on the role of Lamin A/C defects in laminopathies is still missing. The same scenario also applies to CMPs due to *LMNA* mutations and the functional role of A-type lamins in the mammalian heart. Studies on animal models either lacking *Lmna* gene or transgenic for specific human *LMNA* variants, together with evidence from human cardiac models generated through iPSC (induced Pluripotent Stem Cell) technology have significantly contributed to increase our knowledge in the field of cardiolaminopathy. Independent investigations have proposed several hypotheses to explain molecular mechanisms underlying Lamin A/C action in the heart and their link to disease traits.

Nikolova et al. (2004) proposed that the softer nuclei's structure associated to *LMNA* mutations and the resulting morphological abnormalities may be the molecular events at the basis of the Lamin-related cardiac phenotypes. This has been specifically referred to as the "structural hypothesis," attributing the lamin-associated phenotypes to structural defects. Furthermore, being an integral part of the LINC complex (Linker of Nucleoskeleton and Cytoskeleton), A-type lamins may also contribute in regulating the structural architecture of the contractile tissue, conferring resistance and protection against any mechanical stress (Swift et al., 2013); this view was later referred to as the "mechano-transduction hypothesis."

Alongside these "structural hypotheses," a "gene transcription hypothesis" also emerged, starting from previous evidence suggesting a role of the inner nuclear membrane in regulating chromatin organization (and gene expression). A study from Ye and Worman (1996) provided the first piece of evidence of a link between NL and chromatin regulation: the authors finely demonstrated a specific binding between the human chromodomain proteins HP1 and the integral protein of the inner nuclear membrane LBR (Lamin B Receptor) in *Drosophila*, portraying for the first time, the association between heterochromatin and the inner nuclear membrane in eukaryotic cells. These findings added a new function to Lamin A/C proteins, demonstrating that their biological role is not just restricted to the control of nuclear shape and mechano-transduction, but extends to the active regulation of gene transcription. Following this trail, many other studies subsequently showed that several binding factors are able to simultaneously interact with the chromatin and the NL (Cohen et al., 2001; Wilson et al., 2001; Wilson and Foisner, 2010; Cesarini et al., 2015). This gene transcription hypothesis relies on a two-step model, in which the NL regulates transcription factors, either by sequestering them to the nuclear periphery – usually transcriptionally inactive – or by a mechanism that involves activation of specific signaling pathways, such as ERK1/2 (Arimura et al., 2005; Muchir et al., 2007; Chatzifrangkeskou et al., 2018). In addition to this, Lamin A/C is also able to directly bind chromatin, modulating its spatial organization. The interaction between chromatin and A-type lamins occurs at definite genomic regions, defined as lamin-associated domains (LADs) (Pickersgill et al., 2006). Interestingly, there is evidence showing a remodeling of LADs, in particular those tissue-specific (facultative LADs), in presence of Lamin A/C mutations. These rearrangements do not exclusively occur at the nuclear periphery, but also affect expression of genes located at the nuclear interior (Briand and Collas, 2018). For example, repositioning of *T/BRACHYURY* gene from the nuclear periphery toward the nuclear interior has been reported in fibroblasts of patients affected by familial partial lipodystrophy of Dunnigan type 2 (FPLD2) (Briand et al., 2018). Muck et al. (2012) also showed that knockdown of Lamin A/C in human HeLa cells, cause relocation of *CFTR* gene in the nuclear interior, without affecting the position of the neighboring *GASZ* and *CORTBP2* genes. On the contrary, we recently demonstrated a preferential localization of *SCN5A* gene by the nuclear periphery in human iPSC-CMs carrying the p.K219T *LMNA* mutation, resulting in the inhibition of the expression of the gene and thus leading to reduction of sodium currents and impaired cell excitability (Salvarani et al., 2019).

In addition to this, lamin-chromatin interactions may also occur through several binding factors, identified as interacting-mediators between Lamin A/C and chromatin compartments (Kubben et al., 2010); interestingly some of these have been described as essential elements to regulate transcription of key tissue-specific genes, also in the heart (Briand et al., 2018; Salvarani et al., 2019). From this perspective, this mechanistic model of Lamin A/C action can be more accurately defined as "chromatin hypothesis"; importantly, Lamin A/C-driven chromatin regulation has been recently started to be addressed also in the field of cardiolaminopathy by studies from different research groups including ours (Bertero et al., 2019; Mozzetta and Tedesco, 2019; Salvarani et al., 2019). The general view emerging from chromosome conformation capture studies (HiC), a method to study three-dimensional architecture of genomes enabling to distinguish between transcriptionally active (A) and inactive (B) compartments, is that Lamin A/C haploinsufficiency is associated to an increase of intra-chromosomal interactions (meaning interactions between two active compartments – A-A), without interfering with inter-chromosome interactions (with different transcriptional status – A-B) or inducing massive changes in gene transcription (Bertero et al., 2019). According to that, four dimensional genome conformation (referred as spatial assemblies of heterochromatic topological associated domains – TADs, or "TAD cliques") showed silencing of developmental genes in human adipose-derived stromal cells (ASCs), without reporting any A to B switch (Paulsen et al., 2019). On the other hand, the study from Lee et al. (2019) associated Lamin A/C haploinsufficiency, caused by a different frameshift *LMNA* mutation, with relevant LAD alterations, that are responsible for substantial changes in gene expression profile leading to altered activation of PDGF pathway. Although the "chromatin hypothesis" has been associated so far to few specific variants, it is likely that similar regulatory mechanisms are driven also by other Lamin A/C mutations, reinforcing the link between changes in transcriptional regulation and chromatin organization occurring in Lamin A/C mutant cells and the respective clinical phenotype.

Consistently, chromatin remodeling and the associated transcriptional changes of disease-relevant genes, is also the prevalent model proposed for the HGPS, the most severe *LMNA*-dependent disease (Goldman et al., 2004; Gordon et al., 2014; Aguado et al., 2019). Interestingly, a very recent study by Ikegami et al. (2020) further contributed to the field describing

a new regulatory mechanism by Lamin A/C. Specifically, the authors describe a new regulatory function of the nucleoplasmic Ser22-phosphorylated (pS22) Lamin A/C, that they found specifically bound to a subset of active enhancers, and show the acquisition of new pS22-Lamin A/C binding site in HGPS cells, leading to upregulation of clinically relevant genes and potentially underlying the mechanism behind the disease phenotype.

Overall, data obtained so far from different studies in the field support a model by which all the proposed hypotheses can be causally connected, rather than mutually exclusive. As suggested by Osmanagic-Myers and Foisner (2019) in their Perspective, it is likely that a robust link between the structural abnormalities of laminopathic nuclei (Nikolova et al., 2004; Galiová et al., 2008) and either chromatin modifications or reorganization exists, thus contributing to a multifaceted mechanistic model underlying the pathogenesis of the disease.

MOUSE MODELS

In the past two decades, several mouse models have been generated, either reproducing patients' mutations (*LMNA* transgenic mice) or studying the consequences of *Lmna* deficiency (*Lmna* knockout mice). $Lmna^{-/-}$ mouse developed muscular dystrophy, DCM, neuropathy and displayed retarded growth rate, reduced stores of white fat and cardiac arrhythmia (Sullivan et al., 1999). These mice generally die by 8 weeks of age.

The heterozygous ($Lmna^{\pm}$), with 50% of Lamin A/C expression, manifest conduction system diseases, ventricular dilatation later in adult life and generally die by 8 months of age (Chandar et al., 2010). At the molecular level, both the *Lmna* null and the *Lmna* haploinsufficiency mice showed altered desmin pathway and defective force transmission, leaning toward the mechano-transduction hypothesis. Furthermore, those models also showed an increase of pro-adipogenic factors (PPAPγ and CEBP/α), whereas Wnt-10/β-catenin levels were decreased (Tong et al., 2011). Another two *Lmna* knock-out models, $Lmna^{GT-/-}$ and $Lmna^{delK32/delK32}$, have also contributed significantly to establish the role of Lamin A/C in postnatal maturation, showing developmental impairment and growth retardation, that mostly affect the adipose tissue, the skeletal muscle and the heart (Kubben et al., 2011; Bertrand et al., 2012).

Recently, the generation of $Lmna^{H222P}$ and $Lmna^{N195K}$ transgenic mice (Arimura et al., 2005; Mounkes et al., 2005) successfully recapitulated a faithful model of skeletal muscle and DCM, with no phenotype at neonatal stage and displaying disease traits similar to patients. The pathogenesis of $Lmna^{H222P}$ mice was linked to elevated MAP kinase 1/2 (ERK1/2) and AKT/mTor signaling pathways (Muchir et al., 2007; Chatzifrangkeskou et al., 2016). Antoku et al. (2019) recently further characterized this model, describing a novel relationship between the elevated levels of ERK1/2 and nuclear positioning in cardiomyocytes (CMs) isolated from $Lmna^{H222P/H222P}$. The authors showed that a single phosphorylation site in the formin homology domain-containing proteins (FHOD) can be targeted by ERK1/2, changing cell polarity and negatively regulating cell migration. Nuclear positioning is strictly linked to the formation of the sarcomeres during skeletal muscle maturation (Sewry et al., 2001). Consistently, the authors showed that H222P mutation in the *LMNA* gene is associated to altered nuclear positioning and formation and function of sarcomeres, contributing to the pathogenesis of cardiomyopathy. On the other hand, $Lmna^{N195K}$ mice displayed an abnormal expression and/or localization of connexin 40 and connexin 43 and sarcomeres disorganization associated to the main DCM phenotype and conduction system defects (Mounkes et al., 2005). A complete list of the described mouse models and their relevant cardiac phenotypes and molecular characteristics are provided in the **Table 1**.

To conclude, despite likely species-specific limitations, studies conducted so far using mouse models have been fundamental to identify signaling pathways relevant to development of new therapeutics, such as the previously mentioned p38 inhibitor ARRY-371797 – already in Phase III clinical trial (NCT02057341) – and the N-acetyltransferare 10 (NAT10) inhibitor, Remodelin (Balmus et al., 2018). However, although these are important achievements, there is still an important lack of knowledge on the pathogenetic mechanisms underlying this complex disease and therefore further research in the field is mandatory to comprehensively tackle its molecular basis and develop more specific and effective therapies (Stewart et al., 2007; Zhang et al., 2013).

CARDIOMYOCYTES FROM iPSCs: A POWERFUL PLATFORM TO MODEL HUMAN CARDIOLAMINOPATHY

The development of iPSC technology has been a groundbreaking revolution in all areas of research, allowing us to generate *in vitro* any cell type of interest, including human CMs, in which pathogenic mechanisms of diseases may be fully investigated (Xu et al., 2002; Moretti et al., 2010; Lodola et al., 2016; Lee J.H. et al., 2017). Research in the cardiolaminopathy field has also benefit of this technology, since use of iPSC-based models allowed us to overcome the major limitations linked to investigation on animal models and non-cardiac primary cells. Indeed, recreating human phenotypes in mice may not be feasible, due to species-specific differences between mice and humans, especially in relation to the cardiovascular system (i.e., electrophysiological properties of cardiac cells) (Davis et al., 2011). On the other hand, obtaining cells from the human heart may be difficult, due to the limited access the organ and the poor survival of the heart cells grown *ex vivo*. For these reasons studies on cardiolaminopathies so far have been mainly conducted on other somatic cell types, such as fibroblasts, skeletal muscle cells and adipocytes, which are easy to access and to maintain *in vitro* (Ho et al., 2011).

Thus far seven independent studies have investigated human LMNA-CMP using iPSCs either derived from patients carrying different *LMNA* mutations or generated through genome editing (**Supplementary Table S1**). The first set of studies – those published from 2011 to late 2018 – were mainly descriptive, reporting morphological and functional characteristics of cardio-laminopathic cells: these studies thus

TABLE 1 | Mouse models of cardiolaminopathy.

Mouse model	Phenotype	Molecular mechanism	References
Lmna$^{-/-}$	Muscular dystrophy; DCM; signs of axonal neuropathy; reduction of adipose tissue; death by 8 weeks of age	Structural and Mechano-transduction hypotheses based on abnormal desmin network and defective force transmission	Sullivan et al., 1999; De Sandre-Giovannoli et al., 2002; Nikolova et al., 2004
Lmna$^{+/-}$ (Haploinsufficiency)	Phenotypes are less severe than in *Lmna*$^{-/-}$Conduction system defects; DCM; apoptosis of the conduction tissue; death by 8 months of age	Structural and Mechano-transduction hypotheses: – Abnormal desmin network and defective force transmission; – Mechanical-stress induced apoptosis	Wolf et al., 2008; Chandar et al., 2010; Cupesi et al., 2010
		Gene transcription hypothesis: – Reduced expression of *Egr-1* gene due to a direct interaction between Lamin A/C and c-Fos in response to pressure overload	Cupesi et al., 2010
Lmna^{N195K} knock-in	DCM-CD	Structural and Signaling hypotheses: – Misexpression/mislocalization of Cx40 and Cx43 – Abnormal desmin organization	Mounkes et al., 2005
Lmna^{H222P}	Muscular dystrophy and DCM-CD	Structural and signaling hypotheses: – Alteration of ERK/MAPK pathway	Arimura et al., 2005; Muchir et al., 2007; Choi et al., 2012; Muchir et al., 2012; Chatzifrangkeskou et al., 2016; Chatzifrangkeskou et al., 2018; Antoku et al., 2019
		– Link between ERK1/2 and repositioning of cell nuclei	Antoku et al., 2019
Lmna$^{GT-/-}$ (*Lmna* null mouse to study cardiac development)	Growth retardation; defects in heart development; decreased amount of subcutaneous fat; death by 2–3 weeks of age	Alteration in gene transcription profile: delayed muscle and cardiac differentiation/maturation.	Kubben et al., 2011
Lmna$^{delK32/delK32}$ (*Lmna* null mouse to study cardiac development)	Growth retardation; defects in heart development; decreased amount of subcutaneous fat; death by 2–3 weeks of age	Gene transcription profile defects: deregulation of genes involved in cell metabolism and adipogenesis.	Bertrand et al., 2012

DCM, dilated cardiomyopathy; DCM-CD, dilated cardiomyopathy-conduction defect; Cx40, Connexin 40; Cx43, Connexin 43.

confirmed the abnormal morphology of cell nuclei and investigated the susceptibility to electrical and mechanical stresses and the alteration of excitation-contraction coupling in contractile cardiac cells (Ho et al., 2011; Siu et al., 2012; Lee Y.K. et al., 2017). The reported phenotypes were generally ascribed to a structural and/or mechano-transduction hypotheses, in which a generated physical force is responsible for the sarcomeres' disorganization and contribute to alter the NL structure. In a few studies, defects due to *LMNA* mutations were associated to alteration of ERK1/2 signaling pathway, that itself influences the correct assembly of the sarcomeres (Siu et al., 2012; Chatzifrangkeskou et al., 2018).

More recently, similarly to what reported in other cellular models of laminopathy, the pathogenesis of the LMNA-CMP has been linked to the "gene expression/chromatin organization hypothesis," showing a causal association between *LMNA* mutations, transcription and specific cell phenotypes (Bertero et al., 2019; Lee et al., 2019; Salvarani et al., 2019). More specifically, these studies utilized models of cardiolaminopathy carrying different mutations (i.e., K219T, R225X, and R190W) and found an altered expression of genes of key pathways for CMs functionality. Whether these effects on gene expression are preferentially mediated by remodeling of LADs or the results of a rearrangement at a different level of chromatin organization/regulation (i.e., TADs; change of affinity of mutant Lamin A/C for chromatin binding proteins) still need to be clearly determined.

What is important to highlight, from the functional point of view, is that the robust association between the disease phenotypes and *LMNA* defects was supported by the experiments conducted in isogenic iPSC paired lines, in which the *LMNA* mutations were corrected or inserted through CRISPR/Cas9-based (Bertero et al., 2019; Salvarani et al., 2019) or TALEN (Lee et al., 2019) technologies. Also, these studies provided the identification of new potential therapeutic targets (*SCN5A* gene and PDGF pathway) to treat cardiolaminopathy.

These are important achievements in the field but, with the constant amelioration of the protocols for CM differentiation, we expect to improve even further and to gain more insights into the pathogenetic mechanisms of the disease. Indeed, data available so far come from studies on human CMs obtained from iPSCs mostly through 2D-based differentiation protocols, known to generate CMs with an immature fetal-like phenotype, meaning that they lack some of the structural (i.e., T-tubules, sarcomeric

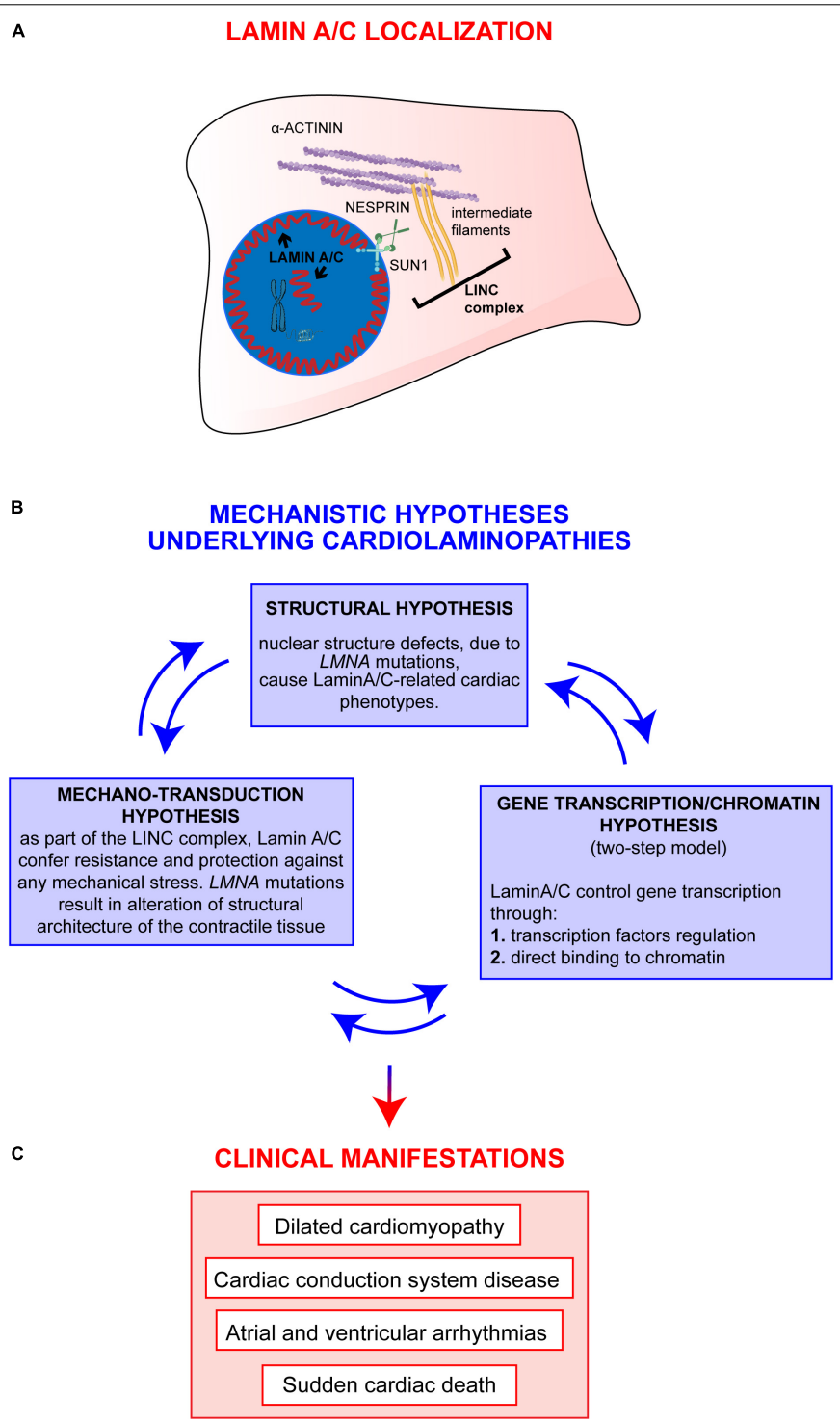

FIGURE 1 | Overview on Lamin A/C proteins localization and on major mechanistic hypotheses underlying cardiac phenotypes. **(A)** Graphic representation of Lamin A/C proteins localization within the cell: Lamin A/C can be found both, at the periphery and in the nuclear interior. In the nucleus, Lamin A/C have a key structural function and are also involved in chromatin organization and regulation of genes transcription. This latter function can be mediated by both peripheral and nucleoplasmic Lamin A/C forms. Besides their role inside the nucleus, Lamin A/C also impact on cellular processes taking place at the outer part of the nuclear envelope: Lamin A/C indeed interact with the nucleo-cytoskeletal proteins, here indicated as LINC complex (i.e., SUN1, NESPRIN, intermediate filaments). The LINC proteins, in turn, interact with other cytoskeletal proteins (i.e., alpha-actinin), contributing to the maintenance of nuclear and cytoskeletal structure and effectors of specific signaling pathways. **(B)** The diagram shows the main mechanistic hypotheses underlying clinical manifestations of cardiolaminopathies. The arrows connecting the blue boxes indicate that these hypotheses are not mutually exclusive, but, instead, are potentially interconnected and all contribute to the final phenotype. **(C)** Clinical manifestations typically associated to LMNA-CMP.

alignment), functional (i.e., calcium handling and contractile properties differences) and metabolic (i.e., glycolysis vs. fatty acid oxidation) properties typical of an adult CM. These properties are highly desirable for drug screening and for modeling specific, adult-onset traits of disease (Karbassi et al., 2020; Mazzola and Di Pasquale, 2020). Given the developmentally regulated expression of Lamin A/C and the complexity of disease phenotype, cell immaturity is likely to impact also on LMNA-CMP modeling, and some important traits of the disease may have been missed so far. The iPSC field is now moving toward the application of 3D-based differentiation protocols, shown to improve maturation of the differentiated CMs, enhancing the potential of iPSC-based cardiac platforms for both disease modeling and drug screening purposes, and from which the cardiolaminopathy field will also benefit in the near future.

CONCLUSION

Consensus has yet to be reached on the pathogenetic mechanism of cardiolaminopathy and researchers in the field are still trying to finely dissect the molecular role of A-type lamins in the heart and to establish clear genotype/phenotype correlations. Indeed, cardiolaminopathy is a quite complex diseases, with patients exhibiting extremely variable phenotypes, as regards of either specific clinical manifestations or the severity and progression of the disease.

Decades of studies in the field clearly sustain a view in which epigenetic regulations and environmental stimuli are likely to act alongside a single *LMNA* mutation in determining the final cardiolaminopathy phenotype. More recent studies have started to unravel those mechanisms showing (a) the involvement of other "actors" cooperating with a defective Lamin A/C (Salvarani et al., 2019) and (b) the dual impairment of mechano-signaling and gene expression in laminopathies (Osmanagic-Myers and Foisner, 2019), supporting a holistic model in which the different mechanistic hypotheses cooperate with different extents to the final clinical phenotypes observed in patients (**Figure 1**).

We strongly believe that future studies will further support this global model, unveiling novel disease-relevant pathways and specific targets to treat LMNA-CMP.

AUTHOR CONTRIBUTIONS

SC and IM performed the bibliographic search and wrote the manuscript. ED wrote and revised the manuscript, provided funding. All authors contributed to the article and approved the submitted version.

FUNDING

SC was supported by the Italian Ministry of Education, University and Research (2015583WMX), and European Union (ERC-CoG-2017 under the grant agreement no. 772168).

ACKNOWLEDGMENTS

We thank Dr. Andrew Kadies for language editing and proofreading.

SUPPLEMENTARY MATERIAL

The Supplementary Material for this article can be found online at: https://www.frontiersin.org/articles/10.3389/fphys.2020.00761/full#supplementary-material

REFERENCES

Aguado, J., Sola-Carvajal, A., Cancila, V., Revˆechon, G., Ong, P. F., Jones-Weinert, C. W., et al. (2019). Inhibition of DNA damage response at telomeres improves the detrimental phenotypes of Hutchinson–Gilford Progeria Syndrome. *Nat. Commun.* 10, 1–11.

Alsheimer, M., von Glasenapp, E., Schnölzer, M., Heid, H., and Benavente, R. (2000). Meiotic lamin C2: the unique amino-terminal hexapeptide GNAEGR is essential for nuclear envelope association. *Proc. Natl. Acad. Sci. U.S.A.* 97, 13120–13125. doi: 10.1073/pnas.240466597

Antoku, S., Wu, W., Joseph, L. C., Morrow, J. P., Worman, H. J., and Gundersen, G. G. (2019). ERK1/2 phosphorylation of FHOD connects signaling and nuclear positioning alternations in cardiac laminopathy. *Dev. Cell.* 51, 602.e12–616.e12.

Arbustini, E., Pilotto, A., Repetto, A., Grasso, M., Negri, A., Diegoli, M., et al. (2002). Autosomal dominant dilated cardiomyopathy with atrioventricular block: a lamin A/C defect-related disease. *J. Am. Coll. Cardiol.* 39, 981–990. doi: 10.1016/s0735-1097(02)01724-2

Arimura, T., Helbling-Leclerc, A., Massart, C., Varnous, S., Niel, F., Lacène, E., et al. (2005). Mouse model carrying H222P-Lmna mutation develops muscular dystrophy and dilated cardiomyopathy similar to human striated muscle laminopathies. *Hum. Mol. Genet.* 14, 155–169. doi: 10.1093/hmg/ddi017

Balmus, G., Larrieu, D., Barros, A. C., Collins, C., Abrudan, M., Demir, M., et al. (2018). Targeting of NAT10 enhances healthspan in a mouse model of human accelerated aging syndrome. *Nat. Commun.* 9:1700.

Benedetti, S., Menditto, I., Degano, M., Rodolico, C., Merlini, L., D'Amico, A., et al. (2007). Phenotypic clustering of lamin A/C mutations in neuromuscular patients. *Neurology* 69, 1285–1292. doi: 10.1212/01.wnl.0000261254.87181.80

Bertero, A., Fields, P. A., Smith, A. S., Leonard, A., Beussman, K., Sniadecki, N. J., et al. (2019). Chromatin compartment dynamics in a haploinsufficient model of cardiac laminopathy. *J. Cell Biol.* 218, 2919–2944. doi: 10.1083/jcb.201902117

Bertrand, A. T., Renou, L., Papadopoulos, A., Beuvin, M., Lacène, E., Massart, C., et al. (2012). DelK32-lamin A/C has abnormal location and induces incomplete tissue maturation and severe metabolic defects leading to premature death. *Hum. Mol. Genet.* 21, 1037–1048. doi: 10.1093/hmg/ddr534

Bonne, G., Di Barletta, M. R., Varnous, S., Bécane, H.-M., Hammouda, E.-H., Merlini, L., et al. (1999). Mutations in the gene encoding lamin A/C cause autosomal dominant Emery-Dreifuss muscular dystrophy. *Nat. Genet.* 21, 285–288. doi: 10.1038/6799

Briand, N., and Collas, P. (2018). Laminopathy-causing lamin A mutations reconfigure lamina-associated domains and local spatial chromatin conformation. *Nucleus* 9, 216–226. doi: 10.1080/19491034.2018.1449498

Briand, N., Guénantin, A.-C., Jeziorowska, D., Shah, A., Mantecon, M., Capel, E., et al. (2018). The lipodystrophic hotspot lamin A p. R482W mutation deregulates the mesodermal inducer T/Brachyury and early vascular differentiation gene networks. *Hum. Mol. Genet.* 27, 1447–1459. doi: 10.1093/hmg/ddy055

Butin-Israeli, V., Adam, S. A., Goldman, A. E., and Goldman, R. D. (2012). Nuclear lamin functions and disease. *Trends Genet.* 28, 464–471. doi: 10.1016/j.tig.2012.06.001

Cesarini, E., Mozzetta, C., Marullo, F., Gregoretti, F., Gargiulo, A., Columbaro, M., et al. (2015). Lamin A/C sustains PcG protein architecture, maintaining transcriptional repression at target genes. *J. Cell Biol.* 211, 533–551. doi: 10.1083/jcb.201504035

Chandar, S., Yeo, L. S., Leimena, C., Tan, J.-C., Xiao, X.-H., Nikolova-Krstevski, V., et al. (2010). Effects of mechanical stress and carvedilol in lamin A/C-deficient dilated cardiomyopathy. *Circ. Res.* 106:573. doi: 10.1161/circresaha.109.204388

Chatzifrangkeskou, M., Le Dour, C., Wu, W., Morrow, J. P., Joseph, L. C., Beuvin, M., et al. (2016). ERK1/2 directly acts on CTGF/CCN2 expression to mediate myocardial fibrosis in cardiomyopathy caused by mutations in the lamin A/C gene. *Hum. Mol. Genet.* 25, 2220–2233. doi: 10.1093/hmg/ddw090

Chatzifrangkeskou, M., Yadin, D., Marais, T., Chardonnet, S., Cohen-Tannoudji, M., Mougenot, N., et al. (2018). Cofilin-1 phosphorylation catalyzed by ERK1/2 alters cardiac actin dynamics in dilated cardiomyopathy caused by lamin A/C gene mutation. *Hum. Mol. Genet.* 27, 3060–3078. doi: 10.1093/hmg/ddy215

Choi, J. C., Muchir, A., Wu, W., Iwata, S., Homma, S., Morrow, J. P., et al. (2012). Temsirolimus activates autophagy and ameliorates cardiomyopathy caused by lamin A/C gene mutation. *Sci. Transl. Med.* 4:144ra102. doi: 10.1126/scitranslmed.3003875

Cohen, M., Gruenbaum, Y., Lee, K. K., and Wilson, K. L. (2001). Transcriptional repression, apoptosis, human disease and the functional evolution of the nuclear lamina. *Trends Biochem. Sci.* 26, 41–47. doi: 10.1016/s0968-0004(00)01727-8

Cupesi, M., Yoshioka, J., Gannon, J., Kudinova, A., Stewart, C. L., and Lammerding, J. (2010). Attenuated hypertrophic response to pressure overload in a lamin A/C haploinsufficiency mouse. *J. Mol. Cell Cardiol.* 48, 1290–1297. doi: 10.1016/j.yjmcc.2009.10.024

Davis, R. P., van den Berg, C. W., Casini, S., Braam, S. R., and Mummery, C. L. (2011). Pluripotent stem cell models of cardiac disease and their implication for drug discovery and development. *Trends Mol. Med.* 17, 475–484. doi: 10.1016/j.molmed.2011.05.001

De Sandre-Giovannoli, A., Chaouch, M., Kozlov, S., Vallat, J.-M., Tazir, M., Kassouri, N., et al. (2002). Homozygous defects in LMNA, encoding lamin A/C nuclear-envelope proteins, cause autosomal recessive axonal neuropathy in human (Charcot-Marie-Tooth disorder type 2) and mouse. *J. Peripher. Nerv. Syst.* 7, 205–205. doi: 10.1046/j.1529-8027.2002.02026_2.x

Dechat, T., Pfleghaar, K., Sengupta, K., Shimi, T., Shumaker, D. K., Solimando, L., et al. (2008). Nuclear lamins: major factors in the structural organization and function of the nucleus and chromatin. *Genes Dev.* 22, 832–853. doi: 10.1101/gad.1652708

Ditaranto, R., Boriani, G., Biffi, M., Lorenzini, M., Graziosi, M., Ziacchi, M., et al. (2019). Differences in cardiac phenotype and natural history of laminopathies with and without neuromuscular onset. *Orphanet J. Rare Dis.* 14:263.

Dittmer, T. A., and Misteli, T. (2011). The lamin protein family. *Genome Biol.* 12:222. doi: 10.1186/gb-2011-12-5-222

Dittmer, T. A., Sahni, N., Kubben, N., Hill, D. E., Vidal, M., Burgess, R. C., et al. (2014). Systematic identification of pathological lamin A interactors. *Mol. Biol. Cell* 25, 1493–1510. doi: 10.1091/mbc.e14-02-0733

Fatkin, D., MacRae, C., Sasaki, T., Wolff, M. R., Porcu, M., Frenneaux, M., et al. (1999). Missense mutations in the rod domain of the lamin A/C gene as causes of dilated cardiomyopathy and conduction-system disease. *New Engl. J. Med.* 341, 1715–1724. doi: 10.1056/nejm199912023412302

Galiová, G., Bártová, E., Raška, I., Krejèí, J., and Kozubek, S. (2008). Chromatin changes induced by lamin A/C deficiency and the histone deacetylase inhibitor trichostatin A. *Eur. J. Cell Biol.* 87, 291–303. doi: 10.1016/j.ejcb.2008.01.013

Gigli, M., Merlo, M., Graw, S. L., Barbati, G., Rowland, T. J., Slavov, D. B., et al. (2019). Genetic risk of arrhythmic phenotypes in patients with dilated cardiomyopathy. *J. Am. Coll. Cardiol.* 74, 1480–1490. doi: 10.1016/j.jacc.2019.06.072

Goldman, R. D., Shumaker, D. K., Erdos, M. R., Eriksson, M., Goldman, A. E., Gordon, L. B., et al. (2004). Accumulation of mutant lamin A causes progressive changes in nuclear architecture in Hutchinson–Gilford progeria syndrome. *Proc. Natl. Acad. Sci. U.S.A.* 101, 8963–8968. doi: 10.1073/pnas.0402943101

Gordon, L. B., Rothman, F. G., López-Otín, C., and Misteli, T. (2014). Progeria: a paradigm for translational medicine. *Cell* 156, 400–407. doi: 10.1016/j.cell.2013.12.028

Granger, B., Gueneau, L., Drouin-Garraud, V., Pedergnana, V., Gagnon, F., Yaou, R. B., et al. (2011). Modifier locus of the skeletal muscle involvement in Emery–Dreifuss muscular dystrophy. *Hum. Genet.* 129, 149–159. doi: 10.1007/s00439-010-0909-1

Gruenbaum, Y., Margalit, A., Goldman, R. D., Shumaker, D. K., and Wilson, K. L. (2005). The nuclear lamina comes of age. *Nat. Rev. Mol. Cell Biol.* 6, 21–31. doi: 10.1038/nrm1550

Hasselberg, N. E., Edvardsen, T., Petri, H., Berge, K. E., Leren, T. P., Bundgaard, H., et al. (2014). Risk prediction of ventricular arrhythmias and myocardial function in Lamin A/C mutation positive subjects. *Europace* 16, 563–571. doi: 10.1093/europace/eut291

Hasselberg, N. E., Haland, T. F., Saberniak, J., Brekke, P. H., Berge, K. E., Leren, T. P., et al. (2018). Lamin A/C cardiomyopathy: young onset, high penetrance, and frequent need for heart transplantation. *Eur. Heart J.* 39, 853–860. doi: 10.1093/eurheartj/ehx596

Herrmann, H., and Aebi, U. (2004). Intermediate filaments: molecular structure, assembly mechanism, and integration into functionally distinct intracellular scaffolds. *Annu. Rev. Biochem.* 73, 749–789. doi: 10.1146/annurev.biochem.73.011303.073823

Hershberger, R. E., and Siegfried, J. D. (2011). Update 2011: clinical and genetic issues in familial dilated cardiomyopathy. *J. Am. Coll. Cardiol.* 57, 1641–1649. doi: 10.1016/j.jacc.2011.01.015

Ho, J. C., Zhou, T., Lai, W.-H., Huang, Y., Chan, Y.-C., Li, X., et al. (2011). Generation of induced pluripotent stem cell lines from 3 distinct laminopathies bearing heterogeneous mutations in lamin A/C. *Aging* 3:380. doi: 10.18632/aging.100277

Ikegami, K., Secchia, S., Almakki, O., Lieb, J. D., and Moskowitz, I. P. (2020). Phosphorylated Lamin A/C in the nuclear interior binds active enhancers associated with abnormal transcription in progeria. *Dev. Cell* 52, 699.e11–713.e11.

Jakobs, P. M., Hanson, E. L., Crispell, K. A., Toy, W., Keegan, H., Schilling, K., et al. (2001). Novel lamin A/C mutations in two families with dilated cardiomyopathy and conduction system disease. *J. Card. Fail.* 7, 249–256. doi: 10.1054/jcaf.2001.26339

Karbassi, E., Fenix, A., Marchiano, S., Muraoka, N., Nakamura, K., Yang, X., et al. (2020). Cardiomyocyte maturation: advances in knowledge and implications for regenerative medicine. *Nat. Rev. Cardiol.* 17, 341–359. doi: 10.1038/s41569-019-0331-x

Kayvanpour, E., Sedaghat-Hamedani, F., Amr, A., Lai, A., Haas, J., Holzer, D. B., et al. (2017). Genotype-phenotype associations in dilated cardiomyopathy: meta-analysis on more than 8000 individuals. *Clin. Res. Cardiol.* 106, 127–139. doi: 10.1007/s00392-016-1033-6

Kubben, N., Voncken, J. W., Konings, G., van Weeghel, M., van den Hoogenhof, M. M., Gijbels, M., et al. (2011). Post-natal myogenic and adipogenic developmental: defects and metabolic impairment upon loss of A-type lamins. *Nucleus* 2, 195–207. doi: 10.4161/nucl.2.3.15731

Kubben, N., Voncken, J. W., and Misteli, T. (2010). Mapping of protein-and chromatin-interactions at the nuclear lamina. *Nucleus* 1, 460–471. doi: 10.4161/nucl.1.6.13513

Kumar, S., Baldinger, S. H., Gandjbakhch, E., Maury, P., Sellal, J.-M., Androulakis, A. F., et al. (2016). Long-term arrhythmic and nonarrhythmic outcomes of lamin A/C mutation carriers. *J. Am. Coll. Cardiol.* 68, 2299–2307. doi: 10.1016/j.jacc.2016.08.058

Lee, J., Termglinchan, V., Diecke, S., Itzhaki, I., Lam, C. K., Garg, P., et al. (2019). Activation of PDGF pathway links LMNA mutation to dilated cardiomyopathy. *Nature* 572, 335–340. doi: 10.1038/s41586-019-1406-x

Lee, J. H., Protze, S. I., Laksman, Z., Backx, P. H., and Keller, G. M. (2017). Human pluripotent stem cell-derived atrial and ventricular cardiomyocytes develop from distinct mesoderm populations. *Cell Stem Cell* 21, 179.e4–194.e4.

Lee, Y. K., Lau, Y. M., Cai, Z. J., Lai, W. H., Wong, L. Y., Tse, H. F., et al. (2017). Modeling treatment response for lamin A/C related dilated cardiomyopathy in human induced pluripotent stem cells. *J. Am. Heart Assoc.* 6:e005677.

Lin, F., and Worman, H. J. (1993). Structural organization of the human gene encoding nuclear lamin A and nuclear lamin C. *J. Biol. Chem.* 268, 16321–16326.

Lodola, F., Morone, D., Denegri, M., Bongianino, R., Nakahama, H., Rutigliano, L., et al. (2016). Adeno-associated virus-mediated CASQ2 delivery rescues phenotypic alterations in a patient-specific model of recessive catecholaminergic polymorphic ventricular tachycardia. *Cell Death Dis.* 7:e2393. doi: 10.1038/cddis.2016.304

Machiels, B. M., Zorenc, A. H., Endert, J. M., Kuijpers, H. J., van Eys, G. J., Ramaekers, F. C., et al. (1996). An alternative splicing product of the lamin A/C gene lacks exon 10. *J. Biol. Chem.* 271, 9249–9253. doi: 10.1074/jbc.271.16.9249

Mazzola, M., and Di Pasquale, E. (2020). Toward cardiac regeneration: combination of pluripotent stem cell-based therapies and bioengineering strategies. *Front. Bioeng. Biotechnol.* 8:455. doi: 10.3389/fbioe.2020.00455

McNally, E. M., and Mestroni, L. (2017). Dilated cardiomyopathy: genetic determinants and mechanisms. *Circ. Res.* 121, 731–748. doi: 10.1161/circresaha.116.309396

Moretti, A., Bellin, M., Welling, A., Jung, C. B., Lam, J. T., Bott-Flügel, L., et al. (2010). Patient-specific induced pluripotent stem-cell models for long-QT syndrome. *New Engl. J. Med.* 363, 1397–1409.

Mounkes, L. C., Kozlov, S. V., Rottman, J. N., and Stewart, C. L. (2005). Expression of an LMNA-N195K variant of A-type lamins results in cardiac conduction defects and death in mice. *Hum. Mol. Genet.* 14, 2167–2180. doi: 10.1093/hmg/ddi221

Mozzetta, C., and Tedesco, F. S. (2019). Challenging the "chromatin hypothesis" of cardiac laminopathies with LMNA mutant iPS cells. *J. Cell Biol.* 218, 2826–2828. doi: 10.1083/jcb.201907166

Muchir, A., Pavlidis, P., Bonne, G., Hayashi, Y. K., and Worman, H. J. (2007). Activation of MAPK in hearts of EMD null mice: similarities between mouse models of X-linked and autosomal dominant Emery–Dreifuss muscular dystrophy. *Hum. Mol. Genet.* 16, 1884–1895. doi: 10.1093/hmg/ddm137

Muchir, A., Wu, W., Choi, J. C., Iwata, S., Morrow, J., Homma, S., et al. (2012). Abnormal p38α mitogen-activated protein kinase signaling in dilated cardiomyopathy caused by lamin A/C gene mutation. *Hum. Mol. Genet.* 21, 4325–4333. doi: 10.1093/hmg/dds265

Muck, J. S., Kandasamy, K., Englmann, A., Günther, M., and Zink, D. (2012). Perinuclear positioning of the inactive human cystic fibrosis gene depends on CTCF, A-type lamins and an active histone deacetylase. *J. Cell. Biochem.* 113, 2607–2621. doi: 10.1002/jcb.24136

Muntoni, F., Torelli, S., and Brockington, M. (2008). Muscular dystrophies due to glycosylation defects. *Neurotherapeutics* 5, 627–632. doi: 10.1016/j.nurt.2008.08.005

Nikolova, V., Leimena, C., McMahon, A. C., Tan, J. C., Chandar, S., Jogia, D., et al. (2004). Defects in nuclear structure and function promote dilated cardiomyopathy in lamin A/C–deficient mice. *J. Clin. Invest.* 113, 357–369. doi: 10.1172/jci200419448

Nishiuchi, S., Makiyama, T., Aiba, T., Nakajima, K., Hirose, S., Kohjitani, H., et al. (2017). Gene-based risk stratification for cardiac disorders in LMNA mutation carriers. *Circ. Cardiovasc. Genet.* 10:e001603.

Osmanagic-Myers, S., and Foisner, R. (2019). The structural and gene expression hypotheses in laminopathic diseases—not so different after all. *Mol. Biol. Cell* 30, 1786–1790. doi: 10.1091/mbc.e18-10-0672

Pasotti, M., Klersy, C., Pilotto, A., Marziliano, N., Rapezzi, C., Serio, A., et al. (2008). Long-term outcome and risk stratification in dilated cardiolaminopathies. *J. Am. Coll. Cardiol.* 52, 1250–1260. doi: 10.1016/j.jacc.2008.06.044

Paulsen, J., Ali, T. M. L., Nekrasov, M., Delbarre, E., Baudement, M.-O., Kurscheid, S., et al. (2019). Long-range interactions between topologically associating domains shape the four-dimensional genome during differentiation. *Nat. Genet.* 51, 835–843. doi: 10.1038/s41588-019-0392-0

Peretto, G., Di Resta, C., Perversi, J., Forleo, C., Maggi, L., Politano, L., et al. (2019). Cardiac and neuromuscular features of patients with LMNA-related cardiomyopathy. *Ann. Intern. Med.* 171, 458–463.

Pickersgill, H., Kalverda, B., De Wit, E., Talhout, W., Fornerod, M., and van Steensel, B. (2006). Characterization of the *Drosophila melanogaster* genome at the nuclear lamina. *Nat. Genet.* 38, 1005–1014. doi: 10.1038/ng1852

Priori, S. G., and Blomström-Lundqvist, C. (2015). 2015 European Society of Cardiology Guidelines for the management of patients with ventricular arrhythmias and the prevention of sudden cardiac death summarized by co-chairs. *Eur. Heart J.* 36, 2757–2759.

Priori, S. G., Wilde, A. A., Horie, M., Cho, Y., Behr, E. R., Berul, C., et al. (2013). HRS/EHRA/APHRS expert consensus statement on the diagnosis and management of patients with inherited primary arrhythmia syndromes: document endorsed by HRS, EHRA, and APHRS in May 2013 and by ACCF, AHA, PACES, and AEPC in June 2013. *Heart Rhythm* 10, 1932–1963. doi: 10.1016/j.hrthm.2013.05.014

Rapezzi, C., Arbustini, E., Caforio, A. L., Charron, P., Gimeno-Blanes, J., Heliö, T., et al. (2013). Diagnostic work-up in cardiomyopathies: bridging the gap between clinical phenotypes and final diagnosis. A position statement from the ESC Working Group on Myocardial and Pericardial Diseases. *Eur. Heart J.* 34, 1448–1458. doi: 10.1093/eurheartj/ehs397

Roncarati, R., Anselmi, C. V., Krawitz, P., Lattanzi, G., Von Kodolitsch, Y., Perrot, A., et al. (2013). Doubly heterozygous LMNA and TTN mutations revealed by exome sequencing in a severe form of dilated cardiomyopathy. *Eur. J. Hum. Genet.* 21, 1105–1111. doi: 10.1038/ejhg.2013.16

Saga, A., Karibe, A., Otomo, J., Iwabuchi, K., Takahashi, T., Kanno, H., et al. (2009). Lamin A/C gene mutations in familial cardiomyopathy with advanced atrioventricular block and arrhythmia. *Tohoku J. Exp. Med.* 218, 309–316. doi: 10.1620/tjem.218.309

Salvarani, N., Crasto, S., Miragoli, M., Bertero, A., Paulis, M., Kunderfranco, P., et al. (2019). The K219T-Lamin mutation induces conduction defects through epigenetic inhibition of SCN5A in human cardiac laminopathy. *Nat. Commun.* 10, 1–16.

Sedaghat-Hamedani, F., Haas, J., Zhu, F., Geier, C., Kayvanpour, E., Liss, M., et al. (2017). Clinical genetics and outcome of left ventricular non-compaction cardiomyopathy. *Eur. Heart J.* 38, 3449–3460.

Sewry, C., Brown, S., Mercuri, E., Bonne, G., Feng, L., Camici, G., et al. (2001). Skeletal muscle pathology in autosomal dominant Emery-Dreifuss muscular dystrophy with lamin A/C mutations. *Neuropathol. Appl. Neurobiol.* 27, 281–290. doi: 10.1046/j.0305-1846.2001.00323.x

Siu, C.-W., Lee, Y.-K., Ho, J. C.-Y., Lai, W.-H., Chan, Y.-C., Ng, K.-M., et al. (2012). Modeling of lamin A/C mutation premature cardiac aging using patient-specific induced pluripotent stem cells. *Aging* 4:803. doi: 10.18632/aging.100503

Stewart, C. L., Kozlov, S., Fong, L. G., and Young, S. G. (2007). Mouse models of the laminopathies. *Exp. Cell Res.* 313, 2144–2156. doi: 10.1016/j.yexcr.2007.03.026

Sullivan, T., Escalante-Alcalde, D., Bhatt, H., Anver, M., Bhat, N., Nagashima, K., et al. (1999). Loss of A-type lamin expression compromises nuclear envelope integrity leading to muscular dystrophy. *J. Cell Biol.* 147, 913–920. doi: 10.1083/jcb.147.5.913

Swift, J., Ivanovska, I. L., Buxboim, A., Harada, T., Dingal, P. D. P., Pinter, J., et al. (2013). Nuclear lamin-A scales with tissue stiffness and enhances matrix-directed differentiation. *Science* 341:1240104. doi: 10.1126/science.1240104

Tesson, F., Saj, M., Uvaize, M. M., Nicolas, H., Płoski, R., and Biliñska, Z. (2014). Lamin A/C mutations in dilated cardiomyopathy. *Cardiol. J.* 21, 331–342. doi: 10.5603/cj.a2014.0037

Tong, J., Li, W., Vidal, C., Yeo, L. S., Fatkin, D., and Duque, G. (2011). Lamin A/C deficiency is associated with fat infiltration of muscle and bone. *Mech. Ageing Dev.* 132, 552–559. doi: 10.1016/j.mad.2011.09.004

Van Rijsingen, I. A., Arbustini, E., Elliott, P. M., Mogensen, J., Hermans-van Ast, J. F., Van Der Kooi, A. J., et al. (2012). Risk factors for malignant ventricular arrhythmias in lamin A/C mutation carriers: a European cohort study. *J. Am. Coll. Cardiol.* 59, 493–500.

van Tintelen, J. P., Hofstra, R. M., Katerberg, H., Rossenbacker, T., Wiesfeld, A. C., du Marchie, et al. (2007a). High yield of LMNA mutations in patients with dilated cardiomyopathy and/or conduction disease referred to cardiogenetics outpatient clinics. *Am. Heart. J.* 154, 1130–1139. doi: 10.1016/j.ahj.2007.07.038

van Tintelen, J. P., Tio, R. A., Kerstjens-Frederikse, W. S., van Berlo, J. H., Boven, L. G., Suurmeijer, A. J., et al. (2007b). Severe myocardial fibrosis caused by a deletion of the 5'end of the lamin A/C gene. *J. Am. Coll. Cardiol.* 49, 2430–2439. doi: 10.1016/j.jacc.2007.02.063

Wahbi, K., Ben Yaou, R., Gandjbakhch, E., Anselme, F., Gossios, T., Lakdawala, N. K., et al. (2019). Development and validation of a new risk prediction score for life-threatening ventricular tachyarrhythmias in laminopathies. *Circulation* 140, 293–302.

Wilson, K. L., and Foisner, R. (2010). Lamin-binding proteins. *Cold Spring Harb. Perspect. Biol.* 2:a000554. doi: 10.1101/cshperspect.a000554

Wilson, K. L., Zastrow, M. S., and Lee, K. K. (2001). Lamins and disease: insights into nuclear infrastructure. *Cell* 104, 647–650. doi: 10.1016/s0092-8674(02)01452-6

Wolf, C. M., Wang, L., Alcalai, R., Pizard, A., Burgon, P. G., Ahmad, F., et al. (2008). Lamin A/C haploinsufficiency causes dilated cardiomyopathy and apoptosis-triggered cardiac conduction system disease. *J. Mol. Cell Cardiol.* 44, 293–303. doi: 10.1016/j.yjmcc.2007.11.008

Worman, H. J., and Bonne, G. (2007). "Laminopathies": a wide spectrum of human diseases. *Exp. Cell Res.* 313, 2121–2133. doi: 10.1016/j.yexcr.2007.03.028

Wydner, K. L., McNeil, J. A., Lin, F., Worman, H. J., and Lawrence, J. B. (1996). Chromosomal assignment of human nuclear envelope protein genes LMNA, LMNB1, and LBR by fluorescencein situhybridization. *Genomics* 32, 474–478. doi: 10.1006/geno.1996.0146

Xu, C., Police, S., Rao, N., and Carpenter, M. K. (2002). Characterization and enrichment of cardiomyocytes derived from human embryonic stem cells. *Circ. Res.* 91, 501–508. doi: 10.1161/01.res.0000035254.80718.91

Ye, Q., and Worman, H. J. (1996). Interaction between an integral protein of the nuclear envelope inner membrane and human chromodomain proteins homologous to *Drosophila* HP1. *J. Biol. Chem.* 271, 14653–14656. doi: 10.1074/jbc.271.25.14653

Young, S. G., Fong, L. G., and Michaelis, S. (2005). Prelamin A, Zmpste24, misshapen cell nuclei, and progeria—new evidence suggesting that protein farnesylation could be important for disease pathogenesis. *J. Lipid Res.* 46, 2531–2558. doi: 10.1194/jlr.r500011-jlr200

Zahr, H. C., and Jaalouk, D. E. (2018). Exploring the crosstalk between LMNA and splicing machinery gene mutations in dilated cardiomyopathy. *Front. Genet.* 9:231. doi: 10.3389/fgene.2018.00231

Zhang, H., Kieckhaefer, J. E., and Cao, K. (2013). Mouse models of laminopathies. *Aging Cell* 12, 2–10. doi: 10.1111/acel.12021

Conflict of Interest: The authors declare that the research was conducted in the absence of any commercial or financial relationships that could be construed as a potential conflict of interest.

frontiers in Physiology

REVIEW
published: 30 July 2020
doi: 10.3389/fphys.2020.00834

Arrhythmogenic Cardiomyopathy and Skeletal Muscle Dystrophies: Shared Histopathological Features and Pathogenic Mechanisms

Shanshan Gao[1†], Suet Nee Chen[1†], Carlo Di Nardo[2] and Raffaella Lombardi[1,2]*

[1] Division of Cardiology, Department of Medicine, University of Colorado, Aurora, CO, United States, [2] Division of Cardiology, Department of Advanced Biomedical Sciences, Federico II University of Naples, Naples, Italy

Arrhythmogenic cardiomyopathy (ACM) is a heritable cardiac disease characterized by fibrotic or fibrofatty myocardial replacement, associated with an increased risk of ventricular arrhythmias and sudden cardiac death. Originally described as a disease of the right ventricle, ACM is currently recognized as a biventricular entity, due to the increasing numbers of reports of predominant left ventricular or biventricular involvement. Research over the last 20 years has significantly advanced our knowledge of the etiology and pathogenesis of ACM. Several etiopathogenetic theories have been proposed; among them, the most attractive one is the dystrophic theory, based on the observation of similar histopathological features between ACM and skeletal muscle dystrophies (SMDs), such as progressive muscular degeneration, inflammation, and tissue replacement by fatty and fibrous tissue. This review will describe the pathophysiological and molecular similarities shared by ACM with SMDs.

Keywords: arrhythmogenic cardiomyopathy, skeletal muscle dystrophies, fibroadiposis, inflammation, molecular pathogenesis

OPEN ACCESS

Edited by:
Marcella Canton, University of Padua, Italy

Reviewed by:
Marina Bouche, Sapienza University of Rome, Italy
Farah Sheikh, University of California, San Diego, United States

****Correspondence:***
Raffaella Lombardi
raffaella.lombardi@unina.it

† These authors have contributed equally to this work

Specialty section:
This article was submitted to Striated Muscle Physiology, a section of the journal Frontiers in Physiology

Received: *11 March 2020*
Accepted: *22 June 2020*
Published: *30 July 2020*

Citation:
Gao S, Chen SN, Di Nardo C and Lombardi R (2020) Arrhythmogenic Cardiomyopathy and Skeletal Muscle Dystrophies: Shared Histopathological Features and Pathogenic Mechanisms. Front. Physiol. 11:834. doi: 10.3389/fphys.2020.00834

INTRODUCTION

Arrhythmogenic cardiomyopathy (ACM) is a primary heritable disease of the myocardium, clinically characterized by increased risk of ventricular arrhythmias and sudden cardiac death (SCD) (Towbin et al., 2019).

ACM includes arrhythmogenic right ventricular cardiomyopathy (ARVC), which affects the right ventricle (RV); left dominant arrhythmogenic cardiomyopathy (LD-ACM), in which the left ventricle is the first chamber to be affected; and biventricular ACM (Sen-Chowdhry et al., 2008; Miles et al., 2019).

The histological feature of ACM is the progressive replacement of the myocardium with fibrotic or fibrofatty tissue, typically starting from the epicardium (Lombardi and Marian, 2010; Basso et al., 2011).

Three main etiopathogenetic theories have been proposed to explain the origin and development of the ACM phenotype: (Basso et al., 1996; Towbin et al., 2019) the dysontogenetic (dysplasia) theory considers ACM as a developmental disorder of the RV (Marcus et al., 1982; Sen-Chowdhry et al., 2008), the myocarditis theory based on the evidence of inflammation in ACM hearts (Basso et al., 1996; Campian et al., 2010; Miles et al., 2019; Protonotarios et al., 2019) and the dystrophic theory, based on the histopathological similarities between ACM and skeletal muscle dystrophies (SMDs)

(Pearce et al., 1981; Hadar et al., 1983; Lombardi and Marian, 2010; Basso et al., 2011). According to the dysontogenetic theory, the disease was interpreted as a congenital defect of the development of the right ventricular myocardium and hence called "right ventricular dysplasia" (Marcus et al., 1982). Later on, evidence from genetic, morphological, and clinical studies showed that ACM was not a structural defect present at birth but a genetic progressive disease of the myocardium, associated with a high risk of life-threatening arrhythmias (Basso et al., 1996, 2010, 2011). For this reason, the term dysplasia was replaced, and the condition became known as "arrhythmogenic RV cardiomyopathy," and the disease was listed, together with hypertrophic, restrictive, and dilated variants, in the WHO classification of cardiomyopathies in 1995 (Richardson et al., 1996).

Although ACM is a cardiac pathology while SMD affects mainly the skeletal muscle, the two diseases share histological features as well as molecular and cellular pathogenic mechanisms.

ACM and SMD are both genetically transmitted and show similar histopathological hallmarks, namely muscle degeneration, inflammation, and tissue replacement by fibrosis and fat.

Myocardium loss in ACM is the consequence of myocyte death by apoptosis and/or necrosis, which is accompanied by inflammation followed by abnormal fibrofatty repair (Basso et al., 1996, 2011; Pilichou et al., 2009). Similarly, muscle degeneration, inflammation, fat infiltration, and fibrosis have been detected in the muscles of patients and mouse models of SMD, mainly in Duchenne muscle dystrophy (DMD) (Pearce et al., 1981; Hadar et al., 1983; Nowak and Davies, 2004; Consalvi et al., 2013).

Inflammation is a key feature of both diseases and precedes the fibrofatty infiltration (Basso et al., 1996; Lombardi and Marian, 2010). Nevertheless, whether inflammation plays a primary role or is a secondary response to cell death remains elusive.

Although the primary presenting symptom in SMDs is skeletal muscle weakness, cardiac muscle may also be similarly affected. Indeed, cardiomyopathies are an increasingly recognized manifestation of SMDs and contribute significantly to the morbidity and mortality (Kamdar and Garry, 2016).

DMD is the most common form of SMD. DMD is inherited in a X-linked recessive manner and is caused by out-of-frame mutations, which result in the absence of functional dystrophin protein. Becker muscular dystrophy (BMD) is another X-linked muscular dystrophy showing a milder clinical course than DMD. BMD is also caused by mutations in the *DMD* gene, but mutations in BMD tend to be in-frame and result in abnormal and less functional dystrophin instead than in the complete absence of the protein (Monaco et al., 1988; Kamdar and Garry, 2016). Research over the last 20 years has significantly advanced our knowledge of the etiology and pathogenesis of both ACM and SMD. Two main pathways, the Wnt signaling and the Hippo pathway, are affected in both diseases (Garcia-Gras et al., 2006; Lombardi et al., 2011; Chen et al., 2014). Furthermore, the heart and skeletal muscle contain a subset of analogous resident mesenchymal progenitor cells, identified by the surface marker platelet-derived growth factor receptor alpha (PDGFRA) and called fibroadipocyte progenitors, which, in the presence of chronic myocyte injury induced by the causal mutation, differentiate to adipocytes and fibroblasts (Uezumi et al., 2010, 2011; Gurha et al., 2016; Lombardi et al., 2016; Malecova et al., 2018).

This review describes similarities in genetics, histology/imaging features, and pathogenic mechanisms between ACM and SMD.

Genetics

Despite that the familial background of ACM was known from late 1980s (Nava et al., 1988, 2000), the first causal mutation was identified 20 years later in a rare recessive syndrome known as Naxos disease, characterized by typical ARVC associated with wooly hair and palmoplantar keratoderma (McKoy et al., 2000). The mutation was a 2 bp deletion in the gene encoding for plakoglobin (*JUP*) (McKoy et al., 2000), a protein of the desmosomes and adherens junctions, which are part of a more complex functional unit, responsible for structural integrity and synchronized contraction of the cardiac tissue, named intercalated disk (ID). IDs include, in addition to desmosomes, several other specialized structures, mainly fascia adherens and gap junctions (Sheikh et al., 2009; Swope et al., 2013). Desmosomes are complex structures not only responsible for cell-cell attachment but also regulators of signaling pathways (Swope et al., 2013).

After the discovery of *JUP* gene, additional causal autosomal dominant mutations were identified in desmosome genes, such as plakophilin-2 (*PKP2*) (Gerull et al., 2004; den Haan et al., 2009), desmoplakin (*DSP*) (Rampazzo et al., 2002), desmoglein-2 (*DSG2*) (Pilichou et al., 2006; Gehmlich et al., 2010), and desmocollin-2 (*DSC2*) (Syrris et al., 2006); in addition, ACM autosomal dominant forms due to *JUP* (De Deyne et al., 2006) and recessive forms due to *DSP* (Norgett et al., 2000) and *DSC2* (Al-Sabeq et al., 2014) mutations have been identified, usually in the context of cardiocutaneous syndromes. Mutations in desmosomal genes are identified in approximately two-thirds of the affected probands; hence ACM is commonly considered a disease of the desmosomes.

ACM mutations have also been identified in non-desmosomal genes encoding for adherens junction components such as catenin-α3 and cadherin 2 (van Hengel et al., 2013; Mayosi et al., 2017; Turkowski et al., 2017); nuclear lamina proteins lamin A/C (*LMNA*) (Quarta et al., 2012) and transmembrane protein 43 (*TMEM43*) (Merner et al., 2008); cytoskeletal proteins desmin (*DES*) (van Tintelen et al., 2009; Klauke et al., 2010; Bermudez-Jimenez et al., 2018) and filamin C (*FLNC*) (Ortiz-Genga et al., 2016; Hall et al., 2019; Brun et al., 2020); the sarcomere protein titin (*TTN*) (Taylor et al., 2011); ion channels such as phospholamban (*PLN*) (van der Zwaag et al., 2012, 2013; van der Heijden and Hassink, 2013), ryanodine receptor 2 (*RYR2*) (Tiso et al., 2001), and sodium voltage-gated channel alpha subunit 5 (SCN5A) (Te Riele et al., 2017); and transforming growth factor β3 (*TGFB3*) (Beffagna et al., 2005; **Table 1**).

Interestingly, *DES* (Melberg et al., 1999; van Spaendonck-Zwarts et al., 2011; Hedberg et al., 2012), *LMNA* (Capell and Collins, 2006; Quarta et al., 2012), *TMEM43* (Merner et al., 2008; Liang et al.,; 2011 Mukai et al., 2019), and *TTN*

TABLE 1 | List of causal genes for ACM.

Gene	Encoded protein	Estimated frequency (%)	Features	Mode of inheritance	References
			Desmosome		
PKP2	Plakophilin 2	∼40	Haploinsufficiency; ACM	AD, AR	Nava et al., 1988, 2000
DSP	Desmoplakin	∼16	Associated with LV-dominant disease; Carvajal syndrome	AD, AR	McKoy et al., 2000; Rampazzo et al., 2002
DSG2	Desmoglein 2	∼10	Overlap with DCM	AD	Sheikh et al., 2009; Swope et al., 2013
DSC2	Desmocollin 2	∼8	ACM	AD, AR	Gerull et al., 2004; Pilichou et al., 2006
JUP	Junction plakoglobin	Rare	Naxos disease; autosomal dominant ACM	AD, AR	den Haan et al., 2009; Joe et al., 2010
			Adherens junction		
CTNNA3	Catenin-α3	Rare	Incomplete penetrance; normal plakoglobin localization	AD	Gehmlich et al., 2010
CDH2	Cadherin 2	Rare	No specific genotype–phenotype relationship identified	AD	De Deyne et al., 2006; Syrris et al., 2006
			Nucleus/ Cytoskeleton		
LMNA	Lamin A/C	Rare	DCM phenotype, conduction defects, arrhythmias and high risk of sudden cardiac death; muscle dystrophies; lipodystrophies; progeria	–	Norgett et al., 2000; Te Riele et al., 2017
TMEM43	Transmembrane protein 43	Rare	Fully penetrant; affected men more severely than women; LV involvement; muscle dystrophy	AD	Al-Sabeq et al., 2014
DES	Desmin	Rare	Fully penetrant; associated with LV and RV-dominant ACM, DCM and skeletal myopathies	AD	Tiso et al., 2001; van Hengel et al., 2013; van der Zwaag et al., 2013; van der Heijden and Hassink, 2013; Mayosi et al., 2017; Turkowski et al., 2017
FLNC	Filamin C	Rare	Associated with Left-dominant ACM, high risk of arrhythmias and sudden death	–	Merner et al., 2008; Klauke et al., 2010; Quarta et al., 2012
			Sarcomere		
TTN	Titin	Rare	Higher risk of supraventricular tachycardia and progression to heart failure; tibial muscular dystrophy	–	van Tintelen et al., 2009
			Ion transport		
PLN	Phospholamban	Rare	Low prevalent and cause DCM and ACM	–	Ortiz-Genga et al., 2016; Bermudez-Jimenez et al., 2018; Hall et al., 2019
RYR2	Ryanodine receptor 2	Rare	Overlap with DCM	AD	Brun et al., 2020
SCN5A	Nav1.5	Rare	Prolonged QRS interval	–	Taylor et al., 2011
			Cytokines		
TGFB3	Transforming growth factor-β3	Rare	No specific genotype–phenotype relationship identified	–	van der Zwaag et al., 2012

AD, autosomal dominant; AR, autosomal recessive; ACM, Arrhythmogenic cardiomyopathy; DCM, Dilatative Cardiomyopathy; LV, left ventricle; RV, right ventricle; SCN5A, Sodium Voltage-Gated Channel Alpha Subunit 5; Nav1.5, α-subunit of the cardiac sodium channel complex.

(Hackman et al., 2002, 2008; Pollazzon et al., 2010; Taylor et al., 2011; Misaka et al., 2019) have been associated with either cardiomyopathies or SMD. Hence, patients with primary myopathy due to a mutation in one of these genes should be screened for cardiac involvement.

Desmin is the main intermediate filament and is highly expressed in both skeletal and cardiac muscle cells; therefore, *DES* mutations frequently cause concomitant skeletal-muscle and cardiac phenotype (van Spaendonck-Zwarts et al., 2011).

Mutations in the *LMNA* gene, encoding lamin A and lamin C, cause a wide range of diseases: Emery-Dreifuss muscular dystrophy (EDMD) types 2 and 3, limb girdle muscular dystrophy (LGMD) type 1B, cardiomyopathy, lipodystrophies, peripheral neuropathies, and progeria syndromes. These diseases are

collectively known as laminopathies (Capell and Collins, 2006). Conduction disorders, atrial fibrillation, ventricular tachycardia, and increased risk of sudden cardiac death are typical features of LMNA-associated cardiomyopathies. Mutations in *TMEM43* may cause ACM and EDMD (Merner et al., 2008; Liang et al., 2011; Mukai et al., 2019). It is not clear how defects in these nuclear membrane proteins result in the phenotype development; possibly, the mutant proteins may increase mechanical stress to the nucleus or alter gene expression through interaction with the chromatin (Chen et al., 2019; Cheedipudi et al., 2019).

TTN mutations cause different skeletal phenotypes (such as tibial muscular dystrophy, LGMD type 2J, EDMD, hereditary myopathy with early respiratory failure, central core myopathy, centronuclear myopathy), collectively known as titinopathies. The severity of the myopathy and the cardiac involvement in titinopathies are determined by the position and type of *TTN* mutation (Hackman et al., 2008; Misaka et al., 2019). Moreover, some *TTN* mutations cause isolated cardiomyopathy, mainly DCM but also HCM or ACM, without skeletal muscle involvement (Taylor et al., 2011; Misaka et al., 2019).

DMD and BMD are caused by mutations in the gene encoding dystrophin, a rod-shaped cytoplasmic protein, which is part of the dystroglycan complex (DGC), the multimeric complex that forms a structural link between the filamentous (F)-actin cytoskeleton and the extracellular matrix (ECM) in both cardiac and skeletal muscle and provides mechanical support to the skeletal or cardiac plasma membrane during contraction (Ervasti and Campbell, 1993; Rybakova et al., 2000). It has been shown that the specific dystrophin mutations affect the incidence and severity of cardiomyopathy and response to treatment (Jefferies et al., 2005).

Histological Features and Inflammation

ACM and SMD share similar histopathological features consisting of progressive muscular degeneration due to apoptosis or necrosis, inflammatory infiltrates, and fibrofatty tissue replacement (Pearce et al., 1981; Hadar et al., 1983; Basso et al., 1996, 2011; Mallat et al., 1996; Corrado et al., 1997; Nowak and Davies, 2004; Pilichou et al., 2009; Consalvi et al., 2013; **Figure 1**). Interestingly, fibrosis in ACM is present not only in the form of fibrofatty infiltration but also as interstitial fibrosis, with or without adiposis (Basso et al., 2008; Marcus et al., 2010).

Inflammation is a key feature of both ACM and SMD and is usually detected at the early stages of the disease before the development of fibroadiposis.

Infiltration of inflammatory cells in the heart has been found in over 70% of ARVC patients and in ACM mouse models (Thiene et al., 1991; Basso et al., 1996, 2011; Corrado et al., 1997; Pilichou et al., 2009; Li et al., 2011; Elliott et al., 2019): patchy mononuclear inflammatory infiltrates of CD3 + T lymphocytes (Elliott et al., 2019) and CD45 +; CD68 + (Basso et al., 1996; Elliott et al., 2019) macrophages are observed in association with dying myocytes, suggesting that the pathological process may be immunologically mediated (Thiene et al., 1991; Basso et al., 1996; Corrado et al., 1997; Elliott et al., 2019).

Similarly, the presence of macrophages, CD4 + and CD8 + T cells, natural killer T cells, neutrophils, and eosinophils has been described in the skeletal muscle of patients with DMD and of mdx mice, a widely used animal model of DMD (Arahata and Engel, 1984; Spencer and Tidball, 2001; Spencer et al., 2001; Vetrone et al., 2009; Lozanoska-Ochser et al., 2018). A recent study has shown that T lymphocytes infiltrate mdx mouse dystrophic muscles prior to the occurrence of necrosis, suggesting a primary role of this cell type in the onset of the disease. Furthermore, the same study demonstrated that inhibition of the protein kinase C θ, a key regulator of T-cell activation, markedly diminishes the size of the inflammatory cell infiltrates and reduces muscle damage (Lozanoska-Ochser et al., 2018).

Inflammation in ARVC patients has also been confirmed by detection of increased plasma levels of interleukin (IL)-1β, IL-6, and tumor necrosis factor alpha (TNF-α) (Campian et al., 2010). Similarly, DMD patients and mdx mice present with higher serum levels of inflammatory cytokines as compared with healthy subjects (Barros Maranhao et al., 2015; Cruz-Guzman Odel et al., 2015; Pelosi et al., 2015).

The empirical observation that immunosuppressive drugs, such as glucocorticoids, can improve muscle strength in patients and in animal models of DMD furthers supports a role for the immune system in the pathogenesis of the disease (Wehling-Henricks et al., 2004; Hussein et al., 2006).

Although the presence of inflammation is widely recognized in both ACM and SMD, its origin and role as a primary event or secondary response to myocyte damage is unknown.

The role of autoimmunity as a trigger for inflammation is a new research field in both ACM and SMD. However, so far, the evidence supporting the involvement of autoimmune response in the pathogenesis of these diseases is still limited, and further studies are needed for the identification of specific molecular and cellular players.

Although the infiltration of immune cells in dystrophic muscle is viewed as a generalized inflammatory response (Arahata and Engel, 1984; Spencer and Tidball, 2001; Spencer et al., 2001; Vetrone et al., 2009), several studies suggest that an autoimmune T-cell-mediated response to specific ill-muscle antigens may also be involved in the pathogenesis of SMDs (Gussoni et al., 1994; Vetrone et al., 2009; Burzyn et al., 2013; Villalta et al., 2015).

Recent deep-sequencing studies examining the T-cell receptor (TCR) repertoire of regulatory T cells (Tregs) in mdx muscle revealed an enrichment of several TCR rearrangements (Burzyn et al., 2013), suggesting that Tregs react to multiple self-antigens in dystrophic muscle. Thus, patients may retain a pool of dystrophin-reactive T cells, which may be further activated by expression of mutant dystrophin or dystrophin introduced exogenously by gene therapy. Indeed, the presence of an autoimmune response in muscle dystrophies was described in a clinical gene therapy trial in 2010 in which circulating antidystrophin T cells were unexpectedly detected in DMD patients before transgene delivery (Mendell et al., 2010). The autoimmune response was induced by epitopes contained in the truncated dystrophin encoded by the endogenous gene after spontaneous in-frame splicing (Mendell et al., 2010).

Another recent study has confirmed that a substantial number of DMD patients present with a pre-existing pool of circulating dystrophin-reactive T cells (Flanigan et al., 2013).

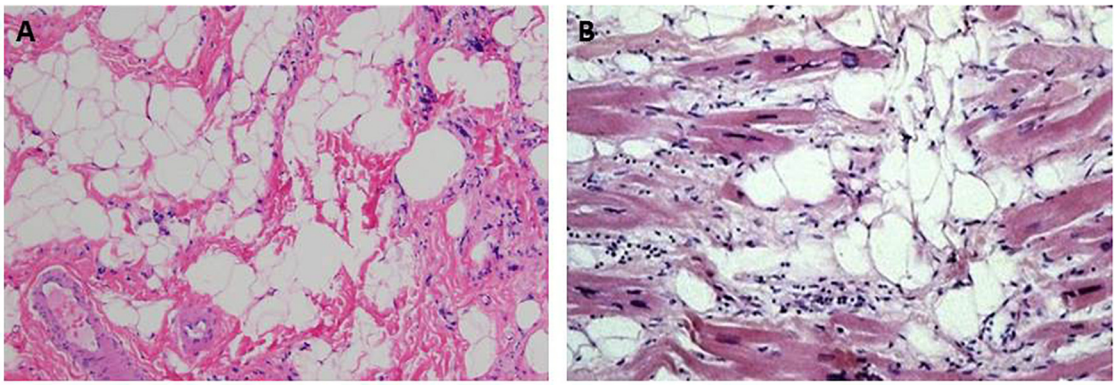

FIGURE 1 | Hematoxylin & eosin images showing fibroadiposis in human skeletal muscle dystrophies (SMD) and in arrhythmogenic cardiomyopathy (ACM). **(A)** The pathological aspect of the skeletal muscle observed in Duchenne muscle dystrophy. **(B)** shows the typical histological aspect of the heart tissue in ACM. Panel (A) from Hiser (2020). Panel (B) from Thiene et al. (2007).

Likewise, the cause of the non-infectious myocarditis in ACM could plausibly be due to autoimmunity. Specific serum antidesmoglein-2 autoantibodies have been detected in ARVC patients regardless of the underlying mutation as compared with normal subjects and non-ARVC cardiomyopathies (Chatterjee et al., 2018). A recent study has shown the presence of serum antiheart autoantibodies (AHAs) and anti-intercalated disk autoantibodies (AIDAs) in the majority of familial and in almost half of sporadic ARVC cases, including some healthy relatives (Caforio et al., 2020). Furthermore, the serum levels of these autoantibodies in affected individuals were associated with disease severity (Caforio et al., 2020). The findings suggest a primary role of autoimmunity in the pathogenesis of ACM, as observed previously in primary dilated cardiomyopathy (Caforio et al., 1994), and open the stage to the potential therapeutic use of immunosuppression in biopsy-proven virus-negative autoantibody-positive inflammatory ACM.

The pathobiology responsible for an autoimmune response in ACM patients is still unknown; likewise, further studies are necessary to establish to what degree autoimmunity participates in the pathophysiology of the disease. One hypothesis is that the ACM causal mutation may induce the expression of a protein with unmasked "cryptic" epitopes; alternatively, myocyte damage may lead to the release of autoantigens that stimulate the immune system to generate autoantibodies.

Longitudinal studies will eventually clarify whether AHA and AIDA may be used as biomarkers to predict the development of the disease in healthy relatives.

Non-invasive Tissue Characterization

Currently, the preferred imaging technique in both ACM and SMD is magnetic resonance imaging (MRI), which combines structural and functional evaluation with non-invasive tissue characterization (Parsai et al., 2012).

Tissue characterization by MRI is mainly based on the detection of changes in proton relaxation times T1 (also known as longitudinal relaxation) and T2 (also known as transverse relaxation). T1-weighted sequences are used to identify fat infiltration and diffuse fibrosis, while T2-weighted imaging is mainly used to detect the presence of edema. Moreover, T1-weighted imaging after infusion of gadolinium, also known as late gadolinium enhancement (LGE), is used to detect focal fibrosis. In cardiology, this technique is essential in the differential diagnosis of ischemic cardiomyopathy, in which LGE is localized in an area of coronary artery distribution and always involves the subendocardial region, versus non-ischemic cardiomyopathy, in which LGE does not occur in a specific coronary artery territory and is often midwall or epicardial rather than subendocardial or transmural (Parsai et al., 2012). Moreover, from the LGE distribution patterns, it is possible to make an etiological diagnosis (Kramer, 2015; Patel and Kramer, 2017).

Cardiac MRI has an important role in the clinical management of ACM because it allows the identification of minor tissue abnormalities, before the onset of morphofunctional abnormalities observed by echocardiography (Sen-Chowdhry et al., 2007, 2008; Sen-Chowdhry and McKenna, 2008). Furthermore, it has been shown that LGE distribution pattern differs among ACM subtypes and between carriers of desmosomal versus non-desmosomal pathogenic variants (Sen-Chowdhry et al., 2007; Sen-Chowdhry and McKenna, 2008; Segura-Rodriguez et al., 2019). Septal LGE is present in > 50% of cases of LD-ACM, unlike ARVC in which septal involvement is rare (Sen-Chowdhry et al., 2008). Furthermore, ACM patients with non-desmosomal variants usually show a circumferential subepicardial LV-LGE pattern, while those with desmosomal variants are more likely to have RV-LGE (Segura-Rodriguez et al., 2019).

Tissue characterization of skeletal muscle by MRI has an important role in disease staging and evaluation of therapeutic response for a number of neuromuscular diseases, including DMD (Finanger et al., 2012). T1-weighted imaging in the skeletal muscle of DMD patients shows higher T1 values at the early stages of the disease, which go down with increasing fatty replacement and clinical deterioration (Matsumura et al., 1988; Finanger et al., 2012). Moreover, it has been shown that the mean T2 relaxation time of thigh muscles in DMD correlates

significantly with the mean fat fraction (Yin et al., 2019) and the severity of muscle weakness (Kim H.K. et al., 2013).

Gadolinium, which in normal muscle remains extracellular, is taken up into the muscle fibers with damaged membranes (Thibaud et al., 2007). Hence, because dystrophin deficiency renders muscle fibers susceptible to contraction-induced injury, a higher amount of gadolinium uptake has been found in the muscles of DMD patients after stepping exercise as compared with controls (Garrood et al., 2009).

It is known that patients with dystrophinopathies may develop dilated cardiomyopathy. Cardiac MRI provides accurate assessments of left ventricular size and function in patients with DMD and BMD (Hagenbuch et al., 2010). Cardiac MRI, with the use of strain technique, allows to identify cardiac involvement in the early stages, before the evidence of functional impairment at the echocardiography. The presence of LGE in the dystrophic heart is a sensitive early detection tool, as it usually precedes LV systolic dysfunction; moreover, the extent of fibrosis has been associated with an increased risk of progression toward ventricular dysfunction and increased mortality (Silva et al., 2007; Patel and Kramer, 2017). DMD and BMD patients with associated cardiomyopathy present a characteristic non-ischemic LGE pattern localized in the posterobasal region of the left ventricle, which starts from the subepicardium. Over the years, with the deterioration of the cardiac dysfunction, the LGE extends toward transmurality and to other myocardial segments (i.e., septum) (Puchalski et al., 2009); the late involvement of the septum differentiate the DMD cardiomyopathy from left-sided ACM, in which the septum is already affected in the early stages of the disease.

Pathogenic Molecular Pathways

Mutations in desmosomal genes account for about two-thirds of ACM cases (Lombardi and Marian, 2010; Basso et al., 2011). Thus, ACM is considered a disease of desmosomes, structures responsible not only for myocytes-myocyte attachment but also hubs of molecular pathways regulated at the cell junctions. Indeed, it has been shown that desmosomal proteins are not only structural proteins but have also signaling functions as they regulate cellular proliferation, differentiation, apoptosis, and gene expression (Garcia-Gras et al., 2006; Bass-Zubek et al., 2009; Lombardi and Marian, 2010; Delmar and McKenna, 2010; Lombardi et al., 2011; Chen et al., 2014; Gurha et al., 2016; van Opbergen et al., 2019).

Animal and cellular models indicate abnormal biomechanical properties, and crosstalks from the desmosome to the cytoskeleton, nucleus, gap junctions, and ion channels are implicated in the pathobiology of ACM (Garcia-Gras et al., 2006; Bass-Zubek et al., 2009; Lombardi and Marian, 2010; Delmar and McKenna, 2010; Lombardi et al., 2011; Chen et al., 2014; Gurha et al., 2016; van Opbergen et al., 2019; Puzzi et al., 2019).

Fibrofatty infiltration is a common feature of SMD and ACM (Pearce et al., 1981; Hadar et al., 1983; Lombardi and Marian, 2010; Basso et al., 2011) and may be considered an anomaly of cell differentiation. This observation has prompted researchers to investigate the role of the canonical Wnt signaling and the Hippo pathway, two molecular pathways known to regulate embryonic development and adult tissue homeostasis, on the development of fibroadiposis in both conditions.

Wnt Signaling in ACM and SMD

The Wnt signaling network controls embryonic development and adult tissue homeostasis, through the regulation of proliferation, cell polarity and migration, and cell fate specification (Komiya and Habas, 2008). It includes three highly conserved signaling pathways: the canonical β-catenin-dependent Wnt pathway and the two non-canonical β-catenin independent pathways (the non-canonical Wnt planar cell polarity and the non-canonical Wnt/calcium pathways) (Komiya and Habas, 2008). Wnt ligands are a family of secreted glycoproteins with autocrine and paracrine functions (Komiya and Habas, 2008).

Canonical and non-canonical Wnt pathways are known to compete between each other; the predominance of a pathway over the other depends on the expression of specific Wnt ligands and cell-surface receptors [Frizzled receptors (Fzd)] and coreceptors in a given cell or tissue, at a given time point (Grumolato et al., 2010; MacDonald and He, 2012).

β-Catenin is the main effector of the canonical Wnt signaling (Grumolato et al., 2010). In the absence of Wnt signals, β-catenin is incorporated in the so-called destruction complex where β-catenin is phosphorylated by the glycogen synthase kinase 3-beta (GSK3β) and degraded (Grumolato et al., 2010). Upon Wnt binding to Fzd receptors and the coreceptor Lrp5/6, the components of the destruction complex are recruited to the plasma membrane preventing the degradation of β-catenin that translocates to the nucleus and binds the TCF/LEF transcription factor (MacDonald et al., 2009; MacDonald and He, 2012).

Suppression of the canonical Wnt/β-catenin signaling is known to provoke adipogenesis, fibrogenesis, and apoptosis (Ross et al., 2000; Chen et al., 2001; Longo et al., 2002).

We have identified suppression of the canonical Wnt signaling as an important mechanism for the enhanced adipogenesis in desmosomal ACM (Garcia-Gras et al., 2006; Lombardi and Marian, 2010; Lombardi et al., 2011; Chen et al., 2014). We showed that mutations in desmosome genes alter assembly of the desmosomes and cause partial relocalization of JUP to the nucleus where it competes with β-catenin for binding to the transcription factor TCF/LEF, resulting in suppression of the canonical Wnt signaling (Garcia-Gras et al., 2006; Lombardi et al., 2011), which in turn determines a switch from myogenesis to adipogenesis in cardiac progenitors (Lombardi et al., 2009, 2011).

Inhibition of canonical Wnt signaling because of the activation of GSK3β and increased degradation of β-catenin has been also shown in a non-desmosomal form of ACM caused by a *TMEM43* mutation (Padron-Barthe et al., 2019). Another study in an ACM transgenic mouse model with cardiomyocyte-specific overexpression of a FLAG-tagged human desmoglein-2 harboring the Q558* nonsense mutation has confirmed inhibition of Wnt signaling in the pathogenesis of the disease (Calore et al., 2019). Moreover, a zebrafish model of DSP deficiency has been recently generated for *in vivo* cell signaling screen, using pathway-specific reporter transgenes. Out of nine considered, three pathways (Wnt/β-catenin, TGFβ/Smad3, and

Hippo/YAP-TAZ) were significantly altered, with Wnt as the most dramatically affected (Giuliodori et al., 2018). The findings of all these papers point to Wnt/β-catenin as the final common pathway underlying the ACM pathogenesis, independently from the causal gene. The role of the nuclear translocation of plakoglobin as the main mechanism for the inhibition of Wnt signaling in ACM is still uncertain. A paper on a mouse model with cardiac-specific deletion of JUP showed that despite the model largely recapitulated the phenotype of human ACM, the Wnt/β-catenin-mediated signaling was not altered, while transforming growth factor-beta-mediated signaling was found significantly elevated (Li et al., 2011). Furthermore, a 2009 paper reported that endomyocardial biopsies from patients with ACM, but not controls, present with a marked reduction in immune-reactive signal levels for plakoglobin, suggesting that routine immunohistochemical analysis for plakoglobin expression of conventional endomyocardial biopsy samples could be a highly sensitive and specific diagnostic test for ACM (Asimaki et al., 2009). However, later on, subsequent studies revealed that plakoglobin-signal reduction was not a sensitive (Ermakov et al., 2014) nor a specific diagnostic marker for ACM, as it could also be demonstrated in other cardiac diseases, such as in sarcoidosis and giant-cell myocarditis (Asimaki et al., 2011).

Published data on the impact of Wnt signaling in the pathogenesis of muscular dystrophies have been conflicting. Increased β-catenin/Tcf transcriptional activity has been detected in the circulation, along with increased protein levels of β-catenin and enhanced DNA-binding activity of β-catenin/TCF in the skeletal muscle of DMD patients, suggestive of negative effects of activation of the canonical Wnt signaling pathway in DMD (Liu et al., 2016). On the contrary, activation of the canonical Wnt signaling pathway by intramuscular injection of Wnt3a in mdx mice has been proven to be beneficial as it attenuated the dystrophic phenotype (Shang et al., 2016). The inconsistence of these reports is most likely due to differences in the timing in which the Wnt signaling was assessed with regard to the state of cellular differentiation or to the interaction with other signaling pathways.

Hippo Signaling in ACM and SMD

The Hippo signaling is an evolutionally conserved pathway consisting of a cascade of serine/threonine kinases: the tumor suppressor Hippo (MST1/2), large tumor suppressor kinases 1/2 (LATS1/2), and Yes-associated protein (YAP) (Pan, 2010; Halder and Johnson, 2011). YAP, the effector of Hippo pathway, is negatively regulated by phosphorylation by its upstream kinases. Non-phosphorylated/active YAP migrates to the nucleus, where it interacts with TEA domain family member (TEAD) transcription factor and regulates cell fate, muscle growth, regeneration, and wasting (Pan, 2010; Halder and Johnson, 2011; Zhou et al., 2015). So far, only limited studies have explored the relationship between the Hippo pathway and the pathogenesis of ACM or muscular dystrophies.

A study from our group in human hearts with ACM and two independent mouse and cell culture ACM models identified activation of the Hippo pathway as a major mechanism in the pathogenesis of ACM (Chen et al., 2014). We showed that, in ACM, mutations in genes encoding desmosome proteins, by impairing cell–cell attachment, activate neurofibromin 2 (NF2), the upstream molecule of the Hippo pathway. Active NF2 initiates the cascade of the Hippo kinases downstream to NF2, which culminates in YAP phosphorylation/inactivation. As a result, gene expression through TEAD is suppressed (Chen et al., 2014). In addition, we showed that activation of the Hippo pathway contributes to suppress the canonical Wnt signaling as phosphorylated YAP sequestrates β-catenin in the cytosol, preventing its translocation into the nucleus (Chen et al., 2014). Collectively, these findings provide a mechanistic link between the mutant desmosome protein and enhanced adipogenesis through the Hippo and the canonical Wnt signaling pathways in ACM. Activation of Hippo/YAP-TAZ in the pathogenesis of ACM has also been confirmed by a recent study on a novel zebrafish model of DSP deficiency (Giuliodori et al., 2018).

In the skeletal muscle, YAP has a major role in myoblast proliferation, atrophy/hypertrophy, and mechanotransduction (Judson et al., 2012; Wei et al., 2013; Fischer et al., 2016).

A reduction in active YAP protein expression and increased LATS1/2 kinase activity has been found in skeletal muscle specimens from DMD patients but not in muscles from patients with other types of muscular dystrophy (Vita et al., 2018). However, these results from DMD patients have not been completely reproduced in mdx mice in which, although the increase in LATS1/2 activity was confirmed, the levels of total YAP and phosphorylated YAP were found to be elevated or not changed (Vita et al., 2018). The findings suggest that activation of Hippo is implicated in the pathogenesis of DMD, but the specific functions of key molecular regulators remain largely unknown.

A recent paper has shown that, in cardiac myocytes, dystroglycan 1 (DAG1), a component of the DGC, directly binds to YAP and inhibits cardiomyocyte proliferation; moreover, Hippo-induced YAP phosphorylation promotes YAP–DAG1 interaction, suggesting cooperation between Hippo pathway and DGC in preventing the nuclear localization of YAP (Morikawa et al., 2017). In the same paper, the authors show that, in the absence of dystrophin (like in DMD), the interaction of YAP with DGC is disrupted (Morikawa et al., 2017); however, the mechanism through which phosphorylated YAP is sequestered to the cell membrane in the absence of dystrophin and sarcoglycan-δ is not identified.

Membrane Channels and Calcium Signaling in ACM and SMD

Several studies suggest dysregulation of ion channels and of the Ca^{2+} signaling machinery in ACM, not only as direct effect of causal mutations located in genes encoding components of the Ca^{2+} cycling machinery (such as PLN) but also as a consequence of mutations in desmosomal genes (Noorman et al., 2013).

In vitro and *in vivo* studies have shown that decreased expression of PKP2 and DSP in cardiomyocytes affects expression levels, phosphorylation, and function of connexin 40 and connexin 43 independently of the cell–cell detachment and prior to the fibrofatty infiltration of the myocardium

(Oxford et al., 2007; Noorman et al., 2013; Lyon et al., 2014). Additionally, mutations in desmosomal proteins have been shown to affect the sodium channel function prior to cardiomyopathic changes (Sato et al., 2009; Rizzo et al., 2012; Cerrone et al., 2014). These data suggest a role for desmosomal proteins as stabilizers of the gap junction integrity and highlight the molecular mechanisms of early electrical defects found in ACM patients.

ACM causal mutations in the non-desmosomal gene encoding PLN directly impair the calcium handling machinery (van der Zwaag et al., 2012; van der Zwaag et al., 2013). On the other hand, recent studies in induced pluripotent stem cell-derived cardiomyocytes (hIPSC-CMs) and mouse models have shown that cardiomyocyte PKP2 deficiency causes calcium handling dysregulation by affecting the transcription of genes and the function of components of intracellular calcium cycling machinery (Kim C. et al., 2013; Cerrone et al., 2017; Kim et al., 2019).

Abnormal calcium homeostasis has also been described in the pathogenesis of cardiac disease in the course of dystrophinopathies (Whitehead et al., 2006; Williams and Allen, 2007; Fanchaouy et al., 2009). The absence of dystrophin in the heart renders cardiomyocytes more sensitive to stretch-induced damage leading to loss of plasma membrane integrity, which results in an increased calcium influx into the cell (Yasuda et al., 2005; Yeung et al., 2005; Whitehead et al., 2006; Williams and Allen, 2007; Fanchaouy et al., 2009). Elevation in intracellular Ca^{2+} has several negative effects: mitochondrial deregulation, induction of protease calpain-mediated necrosis, activation of Ca^{2+}/calmodulin (CaM) and CaM kinase II (CaMKII) and protein kinase A (PKA), and activation of nuclear factor kappa B (NF-κB) and of neuronal nitric oxide synthase (nNOS) (Yeung et al., 2005; Whitehead et al., 2006; Williams and Allen, 2007; Fanchaouy et al., 2009). The resulting cell damage causes degeneration of the cardiomyocytes and fibrosis, which are responsible of development of dilated cardiomyopathy.

Cell Origin of Fibroadiposis in ACM and SMD

Skeletal muscle consists of fascicles of elongated multinucleate cells, called myofibers, while the myocardium is composed of single binucleate cardiomyocytes connected through the intercalated disks, unique structures that enable them to work as a single functional syncytium. Both adult skeletal and cardiac muscle cells do not divide; however, while skeletal muscle is able to have a considerable amount of regeneration, cardiac myocytes have a limited regeneration capacity after injury.

Upon skeletal muscle injury, satellite cells (SCs) promptly re-enter the cell-cycle, proliferate and differentiate in order to repair the damaged myofibers, and, at the same time, repopulate the SC reserve pool by self-renewing (Feige et al., 2018). On the other hand, myocyte death due to chronic cardiac injury is not followed by replacement with new cardiomyocytes but results in activation of the extracellular matrix and consequent fibrosis.

Genetic mutations in ACM and in SMD cause persistent muscle damage; the resulting progressive-chronic injury induces abnormal tissue repair ending in fibroadiposis.

In the skeletal muscle, effective repair requires functional crosstalk of SCs with other resident cell types including motor neurons, endothelial cells, immune cells, fibrogenic cells, and adipogenic precursors (Tatsumi et al., 2009; Uezumi et al., 2010, 2011; Heredia et al., 2013; Verma et al., 2018). Among them, mesenchymal progenitors identified by the surface marker PDGFRA have recently emerged as important players in skeletal muscle regeneration, but they have also been identified as the main source of intramuscular fibro/adipogenesis in pathological conditions (Joe et al., 2010; Uezumi et al., 2010, 2011). PDGFRα + cells are also known as fibroadipocyte progenitors (FAPs) because of their fibrogenic and adipogenic potential (Uezumi et al., 2010, 2011). Upon acute muscle injury, FAPs are activated and, in normal conditions, act in synergy with SCs to promote efficient muscle regeneration (Joe et al., 2010; Uezumi et al., 2010, 2011; Heredia et al., 2013). In contrast, when the muscle injury is persistent, like in muscular dystrophies, activated FAPs differentiate to fibroblasts and adipocytes (Joe et al., 2010; Uezumi et al., 2010, 2011; Heredia et al., 2013).

In ACM, the cell source of adipocytes has been an enigma for many years. Recently, our group has shown that cardiac progenitor cells (CPCs) from the second heart field are a source of adipocytes in ACM (Lombardi et al., 2009, 2011; Lombardi and Marian, 2010, 2011); however, these cells are rare in the heart and account for only a small fraction of the adipocytes. Thus, cardiac cells other than CPCs might contribute to fibroadiposis in ACM.

Since ACM and SMD show similar fibroadipocytic replacement of muscle, we surmised that the heart, like skeletal muscle, might contain resident FAPs, which could differentiate to adipocytes in the presence of chronic injury due to the presence of mutant desmosomal proteins. Therefore, we isolated from human and mouse heart a population of progenitor cells, positive for PDGFRA and negative for other lineage and fibroblast markers, which we named cardiac FAPs (Lombardi et al., 2016). Cardiac FAPs express desmosomal proteins (which are encoded by most of ACM causal genes) and are bipotential as the majority express the fibroblast marker collagen 1 α-1, while a small subset expresses the adipogenic marker CCAAT/enhancer-binding protein α (Lombardi et al., 2016). *In vivo* genetic fate-mapping experiments demonstrated ∼40% of adipocytes in the heart of a mouse model of ACM originates from FAPs, through a Wnt-dependent mechanism (Lombardi et al., 2016). The findings expand the cellular spectrum of ACM, commonly recognized as a disease of cardiomyocytes, to include non-myocyte cells in the heart.

CONCLUSION

Arrhythmogenic cardiomyopathy and SMDs share many histological and molecular/cellular pathogenic mechanisms; for this reason, research findings from either pathology are expected

to have significant reciprocal impact. Muscle degeneration, inflammation, and fibroadipocytic replacement have been described, and common molecular pathways (such as Wnt and Hippo signaling) and cell types have been shown to play a pathogenic role in both diseases. Moreover autoimmunity is an emerging research area with important translational promises for the clinical management and treatment of affected individual in both conditions.

In this review, we summarize for the first time the analogies between studies on skeletal muscle dystrophies and arrhythmogenic cardiomyopathy, with a particular focus on the findings with the highest potential for knowledge exchange between the two research fields.

AUTHOR CONTRIBUTIONS

SG, SC, and RL contributed to the preparation of the whole manuscript. CD wrote the MRI paragraph. All authors contributed to the article and approved the submitted version.

FUNDING

This work was supported by the Research Projects of National Interest (PRIN) grant from the Italian Ministry of University and Research (20173ZWACS) to RL and by the Career Development Award from American Heart Association (19CDA34660035) to SC.

REFERENCES

Al-Sabeq, B., Krahn, A. D., Conacher, S., Klein, G. J., and Laksman, Z. (2014). Arrhythmogenic right ventricular cardiomyopathy with recessive inheritance related to a new homozygous desmocollin-2 mutation. *Can. J. Cardiol.* 30, e1–e3.

Arahata, K., and Engel, A. G. (1984). Monoclonal antibody analysis of mononuclear cells in myopathies. I: quantitation of subsets according to diagnosis and sites of accumulation and demonstration and counts of muscle fibers invaded by T cells. *Ann. Neurol.* 16, 193–208. doi: 10.1002/ana.410160206

Asimaki, A., Tandri, H., Duffy, E. R., Winterfield, J. R., Mackey-Bojack, S., Picken, M. M., et al. (2011). Altered desmosomal proteins in granulomatous myocarditis and potential pathogenic links to arrhythmogenic right ventricular cardiomyopathy. *Circ. Arrhythm. Electrophysiol.* 4, 743–752. doi: 10.1161/circep.111.964890

Asimaki, A., Tandri, H., Huang, H., Halushka, M. K., Gautam, S., Basso, C., et al. (2009). A new diagnostic test for arrhythmogenic right ventricular cardiomyopathy. *N Engl. J. Med.* 360, 1075–1084.

Barros Maranhao, J., de Oliveira Moreira, D., Mauricio, A. F., de Carvalho, S. C., Ferretti, R., Pereira, J. A., et al. (2015). Changes in calsequestrin, TNF-alpha, TGF-beta and MyoD levels during the progression of skeletal muscle dystrophy in mdx mice: a comparative analysis of the quadriceps, diaphragm and intrinsic laryngeal muscles. *Int. J. Exp. Pathol.* 96, 285–293. doi: 10.1111/iep.12142

Basso, C., Bauce, B., Corrado, D., and Thiene, G. (2011). Pathophysiology of arrhythmogenic cardiomyopathy. *Nat. Rev. Cardiol.* 9, 223–233. doi: 10.1038/nrcardio.2011.173

Basso, C., Corrado, D., and Thiene, G. (2010). Arrhythmogenic right ventricular cardiomyopathy: what's in a name? From a congenital defect (dysplasia) to a genetically determined cardiomyopathy (dystrophy). *Am. J. Cardiol.* 106, 275–277. doi: 10.1016/j.amjcard.2010.03.055

Basso, C., Ronco, F., Marcus, F., Abudureheman, A., Rizzo, S., Frigo, A. C., et al. (2008). Quantitative assessment of endomyocardial biopsy in arrhythmogenic right ventricular cardiomyopathy/dysplasia: an in vitro validation of diagnostic criteria. *Eur. Heart J.* 29, 2760–2771. doi: 10.1093/eurheartj/ehn415

Basso, C., Thiene, G., Corrado, D., Angelini, A., Nava, A., and Valente, M. (1996). Arrhythmogenic right ventricular cardiomyopathy. Dysplasia, dystrophy, or myocarditis? *Circulation* 94, 983–991. doi: 10.1161/01.cir.94.5.983

Bass-Zubek, A. E., Godsel, L. M., Delmar, M., and Green, K. J. (2009). Plakophilins: multifunctional scaffolds for adhesion and signaling. *Curr. Opin. Cell. Biol.* 21, 708–716. doi: 10.1016/j.ceb.2009.07.002

Beffagna, G., Occhi, G., Nava, A., Vitiello, L., Ditadi, A., Basso, C., et al. (2005). Regulatory mutations in transforming growth factor-beta3 gene cause arrhythmogenic right ventricular cardiomyopathy type 1. *Cardiovasc. Res.* 65, 366–373. doi: 10.1016/j.cardiores.2004.10.005

Bermudez-Jimenez, F. J., Carriel, V., Brodehl, A., Alaminos, M., Campos, A., Schirmer, I., et al. (2018). novel desmin mutation p.Glu401Asp impairs filament formation, disrupts cell membrane integrity, and causes severe arrhythmogenic left ventricular cardiomyopathy/dysplasia. *Circulation* 137, 1595–1610. doi: 10.1161/circulationaha.117.028719

Brun, F., Gigli, M., Graw, S. L., Judge, D. P., Merlo, M., Murray, B., et al. (2020). FLNC truncations cause arrhythmogenic right ventricular cardiomyopathy. *J. Med. Genet.* 57, 254–257. doi: 10.1136/jmedgenet-2019-106394

Burzyn, D., Kuswanto, W., Kolodin, D., Shadrach, J. L., Cerletti, M., Jang, Y., et al. (2013). A special population of regulatory T cells potentiates muscle repair. *Cell* 155, 1282–1295. doi: 10.1016/j.cell.2013.10.054

Caforio, A. L., Keeling, P. J., Zachara, E., Mestroni, L., Camerini, F., Mann, J. M., et al. (1994). Evidence from family studies for autoimmunity in dilated cardiomyopathy. *Lancet* 344, 773–777. doi: 10.1016/s0140-6736(94)92339-6

Caforio, A. L. P., Re, F., Avella, A., Marcolongo, R., Baratta, P., Seguso, M., et al. (2020). Evidence from family studies for autoimmunity in arrhythmogenic right ventricular cardiomyopathy: associations of circulating anti-heart and anti-intercalated disk autoantibodies with disease severity and family history. *Circulation* 141, 1238–1248. doi: 10.1161/circulationaha.119.043931

Calore, M., Lorenzon, A., Vitiello, L., Poloni, G., Khan, M. A. F., Beffagna, G., et al. (2019). A novel murine model for arrhythmogenic cardiomyopathy points to a pathogenic role of Wnt signalling and miRNA dysregulation. *Cardiovasc. Res.* 115, 739–751. doi: 10.1093/cvr/cvy253

Campian, M. E., Verberne, H. J., Hardziyenka, M., de Groot, E. A., van Moerkerken, A. F., van Eck-Smit, B. L., et al. (2010). Assessment of inflammation in patients with arrhythmogenic right ventricular cardiomyopathy/dysplasia. *Eur. J. Nucl. Med. Mol. Imaging.* 37, 2079–2085.

Capell, B. C., and Collins, F. S. (2006). Human laminopathies: nuclei gone genetically awry. *Nat. Rev. Genet.* 7, 940–952. doi: 10.1038/nrg1906

Cerrone, M., Lin, X., Zhang, M., Agullo-Pascual, E., Pfenniger, A., Chkourko Gusky, H., et al. (2014). Missense mutations in plakophilin-2 cause sodium current deficit and associate with a Brugada syndrome phenotype. *Circulation* 129, 1092–1103. doi: 10.1161/circulationaha.113.003077

Cerrone, M., Montnach, J., Lin, X., Zhao, Y. T., Zhang, M., Agullo-Pascual, E., et al. (2017). Plakophilin-2 is required for transcription of genes that control calcium cycling and cardiac rhythm. *Nat. Commun.* 8:106.

Chatterjee, D., Fatah, M., Akdis, D., Spears, D. A., Koopmann, T. T., Mittal, K., et al. (2018). An autoantibody identifies arrhythmogenic right ventricular cardiomyopathy and participates in its pathogenesis. *Eur. Heart J.* 39, 3932–3944. doi: 10.1093/eurheartj/ehy567

Cheedipudi, S. M., Matkovich, S. J., Coarfa, C., Hu, X., Robertson, M. J., Sweet, M., et al. (2019). Genomic reorganization of lamin-associated domains in cardiac myocytes is associated with differential gene expression and DNA methylation in human dilated cardiomyopathy. *Circ. Res.* 124, 1198–1213. doi: 10.1161/circresaha.118.314177

Chen, S., Guttridge, D. C., You, Z., Zhang, Z., Fribley, A., Mayo, M. W., et al. (2001). Wnt-1 signaling inhibits apoptosis by activating beta-catenin/T cell factor-mediated transcription. *J. Cell Biol.* 152, 87–96. doi: 10.1083/jcb.152.1.87

Chen, S. N., Gurha, P., Lombardi, R., Ruggiero, A., Willerson, J. T., and Marian, A. J. (2014). The hippo pathway is activated and is a causal mechanism for adipogenesis in arrhythmogenic cardiomyopathy. *Circ. Res.* 114, 454–468. doi: 10.1161/circresaha.114.302810

Chen, S. N., Lombardi, R., Karmouch, J., Tsai, J. Y., Czernuszewicz, G., Taylor, M. R. G., et al. (2019). DNA damage response/TP53 pathway is activated

and contributes to the pathogenesis of dilated cardiomyopathy associated with LMNA (Lamin A/C) mutations. *Circ. Res.* 124, 856–873. doi: 10.1161/circresaha.118.314238

Consalvi, S., Mozzetta, C., Bettica, P., Germani, M., Fiorentini, F., Del Bene, F., et al. (2013). Preclinical studies in the mdx mouse model of duchenne muscular dystrophy with the histone deacetylase inhibitor givinostat. *Mol. Med.* 19, 79–87. doi: 10.2119/molmed.2013.00011

Corrado, D., Basso, C., Thiene, G., McKenna, W. J., Davies, M. J., Fontaliran, F., et al. (1997). Spectrum of clinicopathologic manifestations of arrhythmogenic right ventricular cardiomyopathy/dysplasia: a multicenter study. *J. Am. Coll. Cardiol.* 30, 1512–1520. doi: 10.1016/s0735-1097(97)00332-x

Cruz-Guzman Odel, R., Rodriguez-Cruz, M., and Escobar Cedillo, R. E. (2015). Systemic inflammation in duchenne muscular dystrophy: association with muscle function and nutritional status. *Biomed Res Int.* 2015:891972.

De Deyne, S., De la Gastine, B., Gras, G., Dargere, S., Verdon, R., and Coquerel, A. (2006). Acute renal failure with acyclovir in a 42-year-old patient without previous renal dysfunction. *Rev. Med. Interne* 27, 892–894.

Delmar, M., and McKenna, W. J. (2010). The cardiac desmosome and arrhythmogenic cardiomyopathies: from gene to disease. *Circ. Res.* 107, 700–714. doi: 10.1161/circresaha.110.223412

den Haan, A. D., Tan, B. Y., Zikusoka, M. N., Llado, L. I., Jain, R., Daly, A., et al. (2009). Comprehensive desmosome mutation analysis in north americans with arrhythmogenic right ventricular dysplasia/cardiomyopathy. *Circ. Cardiovasc. Genet.* 2, 428–435. doi: 10.1161/circgenetics.109.858217

Elliott, P. M., Anastasakis, A., Asimaki, A., Basso, C., Bauce, B., Brooke, M. A., et al. (2019). Definition and treatment of arrhythmogenic cardiomyopathy: an updated expert panel report. *Eur. J. Heart Fail.* 21, 955–964. doi: 10.1002/ejhf.1534

Ermakov, S., Ursell, P. C., Johnson, C. J., Meadows, A., Zhao, S., Marcus, G. M., et al. (2014). Plakoglobin immunolocalization as a diagnostic test for arrhythmogenic right ventricular cardiomyopathy. *PACE* 37, 1708–1716. doi: 10.1111/pace.12492

Ervasti, J. M., and Campbell, K. P. (1993). A role for the dystrophin-glycoprotein complex as a transmembrane linker between laminin and actin. *J. Cell Biol.* 122, 809–823.

Fanchaouy, M., Polakova, E., Jung, C., Ogrodnik, J., Shirokova, N., and Niggli, E. (2009). Pathways of abnormal stress-induced Ca2+ influx into dystrophic mdx cardiomyocytes. *Cell Calcium.* 46, 114–121.

Feige, P., Brun, C. E., Ritso, M., and Rudnicki, M. A. (2018). Orienting muscle stem cells for regeneration in homeostasis. aging, and disease. *Cell Stem. Cell.* 23, 653–664.

Finanger, E. L., Russman, B., Forbes, S. C., Rooney, W. D., Walter, G. A., and Vandenborne, K. (2012). Use of skeletal muscle MRI in diagnosis and monitoring disease progression in Duchenne muscular dystrophy. *Phys. Med. Rehabil. Clin. N. Am.* 23, 1–10.

Fischer, M., Rikeit, P., Knaus, P., and Coirault, C. Y. A. P. - (2016). Mediated mechanotransduction in skeletal muscle. *Front. Physiol.* 7:41. doi: 10.3389/fphys.2016.00041

Flanigan, K. M., Campbell, K., Viollet, L., Wang, W., Gomez, A. M., Walker, C. M., et al. (2013). Anti-dystrophin T cell responses in Duchenne muscular dystrophy: prevalence and a glucocorticoid treatment effect. *Hum. Gene Ther.* 24, 797–806.

Garcia-Gras, E., Lombardi, R., Giocondo, M. J., Willerson, J. T., Schneider, M. D., Khoury, D. S., et al. (2006). Suppression of canonical Wnt/beta-catenin signaling by nuclear plakoglobin recapitulates phenotype of arrhythmogenic right ventricular cardiomyopathy. *J. Clin. Invest.* 116, 2012–2021.

Garrood, P., Hollingsworth, K. G., Eagle, M., Aribisala, B. S., Birchall, D., Bushby, K., et al. (2009). MR imaging in Duchenne muscular dystrophy: quantification of T1-weighted signal, contrast uptake, and the effects of exercise. *J. Magn. Reson. Imaging.* 30, 1130–1138.

Gehmlich, K., Asimaki, A., Cahill, T. J., Ehler, E., Syrris, P., Zachara, E., et al. (2010). Novel missense mutations in exon 15 of desmoglein-2: role of the intracellular cadherin segment in arrhythmogenic right ventricular cardiomyopathy? *Heart Rhythm.* 7, 1446–1453.

Gerull, B., Heuser, A., Wichter, T., Paul, M., Basson, C. T., McDermott, D. A., et al. (2004). Mutations in the desmosomal protein plakophilin-2 are common in arrhythmogenic right ventricular cardiomyopathy. *Nat Genet.* 36, 1162–1164.

Giuliodori, A., Beffagna, G., Marchetto, G., Fornetto, C., Vanzi, F., Toppo, S., et al. (2018). Loss of cardiac Wnt/beta-catenin signalling in desmoplakin-deficient AC8 zebrafish models is rescuable by genetic and pharmacological intervention. *Cardiovasc. Res.* 114, 1082–1097.

Grumolato, L., Liu, G., Mong, P., Mudbhary, R., Biswas, R., Arroyave, R., et al. (2010). Canonical and noncanonical Wnts use a common mechanism to activate completely unrelated coreceptors. *Genes Dev.* 24, 2517–2530.

Gurha, P., Chen, X., Lombardi, R., Willerson, J. T., and Marian, A. J. (2016). Knockdown of plakophilin 2 downregulates miR-184 through CpG hypermethylation and suppression of the E2F1 pathway and leads to enhanced adipogenesis in vitro. *Circ. Res.* 119, 731–750.

Gussoni, E., Pavlath, G. K., Miller, R. G., Panzara, M. A., Powell, M., Blau, H. M., et al. (1994). Specific T cell receptor gene rearrangements at the site of muscle degeneration in Duchenne muscular dystrophy. *J. Immunol.* 153, 4798–4805.

Hackman, P., Marchand, S., Sarparanta, J., Vihola, A., Penisson-Besnier, I., Eymard, B., et al. (2008). Truncating mutations in C-terminal titin may cause more severe tibial muscular dystrophy (TMD). *Neuromuscul. Disord.* 18, 922–928.

Hackman, P., Vihola, A., Haravuori, H., Marchand, S., Sarparanta, J., De Seze, J., et al. (2002). Tibial muscular dystrophy is a titinopathy caused by mutations in TTN, the gene encoding the giant skeletal-muscle protein titin. *Am. J. Hum. Genet.* 71, 492–500.

Hadar, H., Gadoth, N., and Heifetz, M. (1983). Fatty replacement of lower paraspinal muscles: normal and neuromuscular disorders. *AJR Am. J. Roentgenol.* 141, 895–898.

Hagenbuch, S. C., Gottliebson, W. M., Wansapura, J., Mazur, W., Fleck, R., Benson, D. W., et al. (2010). Detection of progressive cardiac dysfunction by serial evaluation of circumferential strain in patients with Duchenne muscular dystrophy. *Am. J. Cardiol.* 105, 1451–1455.

Halder, G., and Johnson, R. L. (2011). Hippo signaling: growth control and beyond. *Development* 138, 9–22.

Hall, C. L., Akhtar, M. M., Sabater-Molina, M., Futema, M., Asimaki, A., Protonotarios, A., et al. (2019). Filamin C variants are associated with a distinctive clinical and immunohistochemical arrhythmogenic cardiomyopathy phenotype. *Int. J. Cardiol.* 307, 101–108.

Hedberg, C., Melberg, A., Kuhl, A., Jenne, D., and Oldfors, A. (2012). Autosomal dominant myofibrillar myopathy with arrhythmogenic right ventricular cardiomyopathy 7 is caused by a DES mutation. *Eur. J. Hum. Genet.* 20, 984–985.

Heredia, J. E., Mukundan, L., Chen, F. M., Mueller, A. A., Deo, R. C., Locksley, R. M., et al. (2013). Type 2 innate signals stimulate fibro/adipogenic progenitors to facilitate muscle regeneration. *Cell* 153, 376–388.

Hiser, W. (2020). *Duchenne Muscular Dystrophy*. Available online at: http://www.pathologyoutlines.com/topic/muscleduchennemusculardystrophy.html

Hussein, M. R., Hamed, S. A., Mostafa, M. G., Abu-Dief, E. E., Kamel, N. F., and Kandil, M. R. (2006). The effects of glucocorticoid therapy on the inflammatory and dendritic cells in muscular dystrophies. *Int. J. Exp. Pathol.* 87, 451–461.

Jefferies, J. L., Eidem, B. W., Belmont, J. W., Craigen, W. J., Ware, S. M., Fernbach, S. D., et al. (2005). Genetic predictors and remodeling of dilated cardiomyopathy in muscular dystrophy. *Circulation* 112, 2799–2804.

Joe, A. W., Yi, L., Natarajan, A., Le Grand, F., So, L., Wang, J., et al. (2010). Muscle injury activates resident fibro/adipogenic progenitors that facilitate myogenesis. *Nat. Cell. Biol.* 12, 153–163.

Judson, R. N., Tremblay, A. M., Knopp, P., White, R. B., Urcia, R., De Bari, C., et al. (2012). The Hippo pathway member Yap plays a key role in influencing fate decisions in muscle satellite cells. *J. Cell Sci.* 125(Pt 24), 6009–6019.

Kamdar, F., and Garry, D. J. (2016). Dystrophin-deficient cardiomyopathy. *J. Am. Coll. Cardiol.* 67, 2533–2546.

Kim, C., Wong, J., Wen, J., Wang, S., Wang, C., Spiering, S., et al. (2013). Studying arrhythmogenic right ventricular dysplasia with patient-specific iPSCs. *Nature* 494, 105–110.

Kim, H. K., Merrow, A. C., Shiraj, S., Wong, B. L., Horn, P. S., and Laor, T. (2013). Analysis of fatty infiltration and inflammation of the pelvic and thigh muscles in boys with Duchenne muscular dystrophy (DMD): grading of disease involvement on MR imaging and correlation with clinical assessments. *Pediatr. Radiol.* 43, 1327–1335.

Kim, J. C., Perez-Hernandez, M., Alvarado, F. J., Maurya, S. R., Montnach, J., Yin, Y., et al. (2019). Disruption of Ca(2+)i homeostasis and connexin 43

hemichannel function in the right ventricle precedes overt arrhythmogenic cardiomyopathy in plakophilin-2-deficient mice. *Circulation* 140, 1015–1030.

Klauke, B., Kossmann, S., Gaertner, A., Brand, K., Stork, I., Brodehl, A., et al. (2010). De novo desmin-mutation N116S is associated with arrhythmogenic right ventricular cardiomyopathy. *Hum. Mol. Genet.* 19, 4595–4607.

Komiya, Y., and Habas, R. (2008). Wnt signal transduction pathways. *Organogenesis* 4, 68–75.

Kramer, C. M. (2015). Role of Cardiac MR Imaging in cardiomyopathies. journal of nuclear medicine : official publication. *Soc. Nuclear Med.* 56(Suppl. 4), 39S–45S.

Li, J., Swope, D., Raess, N., Cheng, L., Muller, E. J., and Radice, G. L. (2011). Cardiac tissue-restricted deletion of plakoglobin results in progressive cardiomyopathy and activation of {beta}-catenin signaling. *Mol. Cell Biol.* 31, 1134–1144.

Liang, W. C., Mitsuhashi, H., Keduka, E., Nonaka, I., Noguchi, S., Nishino, I., et al. (2011). TMEM43 mutations in Emery-Dreifuss muscular dystrophy-related myopathy. *Ann. Neurol.* 69, 1005–1013.

Liu, F., Liang, Z., Xu, J., Li, W., Zhao, D., Zhao, Y., et al. (2016). Activation of the wnt/beta-catenin signaling pathway in polymyositis, dermatomyositis and Duchenne muscular dystrophy. *J. Clin. Neurol.* 12, 351–360.

Lombardi, R., Chen, S. N., Ruggiero, A., Gurha, P., Czernuszewicz, G. Z., Willerson, J. T., et al. (2016). Cardiac fibro-adipocyte progenitors express desmosome proteins and preferentially differentiate to adipocytes upon deletion of the desmoplakin gene. *Circ. Res.* 119, 41–54.

Lombardi, R., da Graca Cabreira-Hansen, M., Bell, A., Fromm, R. R., Willerson, J. T., and Marian, A. J. (2011). Nuclear plakoglobin is essential for differentiation of cardiac progenitor cells to adipocytes in arrhythmogenic right ventricular cardiomyopathy. *Circ. Res.* 109, 1342–1353.

Lombardi, R., Dong, J., Rodriguez, G., Bell, A., Leung, T. K., Schwartz, R. J., et al. (2009). Genetic fate mapping identifies second heart field progenitor cells as a source of adipocytes in arrhythmogenic right ventricular cardiomyopathy. *Circ. Res.* 104, 1076–1084.

Lombardi, R., and Marian, A. J. (2010). Arrhythmogenic right ventricular cardiomyopathy is a disease of cardiac stem cells. *Curr. Opin. Cardiol.* 25, 222–228.

Lombardi, R., and Marian, A. J. (2011). Molecular genetics and pathogenesis of arrhythmogenic right ventricular cardiomyopathy: a disease of cardiac stem cells. *Pediatr. Cardiol.* 32, 360–365.

Longo, K. A., Kennell, J. A., Ochocinska, M. J., Ross, S. E., Wright, W. S., and MacDougald, O. A. (2002). Wnt signaling protects 3T3-L1 preadipocytes from apoptosis through induction of insulin-like growth factors. *J. Biol. Chem.* 277, 38239–38244.

Lozanoska-Ochser, B., Benedetti, A., Rizzo, G., Marrocco, V., Di Maggio, R., Fiore, P., et al. (2018). Targeting early PKCtheta-dependent T-cell infiltration of dystrophic muscle reduces disease severity in a mouse model of muscular dystrophy. *J. Pathol.* 244, 323–333.

Lyon, R. C., Mezzano, V., Wright, A. T., Pfeiffer, E., Chuang, J., Banares, K., et al. (2014). Connexin defects underlie arrhythmogenic right ventricular cardiomyopathy in a novel mouse model. *Hum. Mol. Genet.* 23, 1134–1150.

MacDonald, B. T., and He, X. (2012). Frizzled and LRP5/6 receptors for Wnt/beta-catenin signaling. *Cold Spring Harb. Perspect.Biol.* 4:a007880.

MacDonald, B. T., Tamai, K., and He, X. (2009). Wnt/beta-catenin signaling: components, mechanisms, and diseases. *Dev. Cell* 17, 9–26.

Malecova, B., Gatto, S., Etxaniz, U., Passafaro, M., Cortez, A., Nicoletti, C., et al. (2018). Dynamics of cellular states of fibro-adipogenic progenitors during myogenesis and muscular dystrophy. *Nat. Commun.* 9, 3670.

Mallat, Z., Tedgui, A., Fontaliran, F., Frank, R., Durigon, M., and Fontaine, G. (1996). Evidence of apoptosis in arrhythmogenic right ventricular dysplasia. *N. Engl. J. Med.* 335, 1190–1196.

Marcus, F. I., Fontaine, G. H., Guiraudon, G., Frank, R., Laurenceau, J. L., Malergue, C., et al. (1982). Right ventricular dysplasia: a report of 24 adult cases. *Circulation* 65, 384–398.

Marcus, F. I., McKenna, W. J., Sherrill, D., Basso, C., Bauce, B., Bluemke, D. A., et al. (2010). Diagnosis of arrhythmogenic right ventricular cardiomyopathy/dysplasia: proposed modification of the task force criteria. *Eur. Heart J.* 31, 806–814.

Matsumura, K., Nakano, I., Fukuda, N., Ikehira, H., Tateno, Y., and Aoki, Y. (1988). Proton spin-lattice relaxation time of Duchenne dystrophy skeletal muscle by magnetic resonance imaging. *Muscle Nerve* 11, 97–102.

Mayosi, B. M., Fish, M., Shaboodien, G., Mastantuono, E., Kraus, S., Wieland, T., et al. (2017). Identification of cadherin 2 (CDH2) mutations in arrhythmogenic right ventricular cardiomyopathy. *Circ. Cardiovasc. Genet.* 10:e001605.

McKoy, G., Protonotarios, N., Crosby, A., Tsatsopoulou, A., Anastasakis, A., Coonar, A., et al. (2000). Identification of a deletion in plakoglobin in arrhythmogenic right ventricular cardiomyopathy with palmoplantar keratoderma and woolly hair (Naxos disease). *Lancet.* 355, 2119–2124.

Melberg, A., Oldfors, A., Blomstrom-Lundqvist, C., Stalberg, E., Carlsson, B., Larrson, E., et al. (1999). Autosomal dominant myofibrillar myopathy with arrhythmogenic right ventricular cardiomyopathy linked to chromosome 10q. *Ann. Neurol.* 46, 684–692.

Mendell, J. R., Campbell, K., Rodino-Klapac, L., Sahenk, Z., Shilling, C., Lewis, S., et al. (2010). Dystrophin immunity in Duchenne's muscular dystrophy. *N. Engl. J. Med.* 363, 1429–1437.

Merner, N. D., Hodgkinson, K. A., Haywood, A. F., Connors, S., French, V. M., Drenckhahn, J. D., et al. (2008). Arrhythmogenic right ventricular cardiomyopathy type 5 is a fully penetrant, lethal arrhythmic disorder caused by a missense mutation in the TMEM43 gene. *Am. J. Hum. Genet.* 82, 809–821.

Miles, C., Finocchiaro, G., Papadakis, M., Gray, B., Westaby, J., Ensam, B., et al. (2019). Sudden death and left ventricular involvement in arrhythmogenic cardiomyopathy. *Circulation* 139, 1786–1797.

Misaka, T., Yoshihisa, A., and Takeishi, Y. (2019). Titin in muscular dystrophy and cardiomyopathy: urinary titin as a novel marker. *Clin. Chim. Acta* 495, 123–128.

Monaco, A. P., Bertelson, C. J., Liechti-Gallati, S., Moser, H., and Kunkel, L. M. (1988). An explanation for the phenotypic differences between patients bearing partial deletions of the DMD locus. *Genomics* 2, 90–95.

Morikawa, Y., Heallen, T., Leach, J., Xiao, Y., and Martin, J. F. (2017). Dystrophin-glycoprotein complex sequesters Yap to inhibit cardiomyocyte proliferation. *Nature* 547, 227–231.

Mukai, T., Mori-Yoshimura, M., Nishikawa, A., Hokkoku, K., Sonoo, M., Nishino, I., et al. (2019). Emery-Dreifuss muscular dystrophy-related myopathy with TMEM43 mutations. *Muscle Nerve* 59, E5–E7.

Nava, A., Bauce, B., Basso, C., Muriago, M., Rampazzo, A., Villanova, C., et al. (2000). Clinical profile and long-term follow-up of 37 families with arrhythmogenic right ventricular cardiomyopathy. *J. Am. Coll. Cardiol.* 36, 2226–2233.

Nava, A., Thiene, G., Canciani, B., Scognamiglio, R., Daliento, L., Buja, G., et al. (1988). Familial occurrence of right ventricular dysplasia: a study involving nine families. *J. Am. Coll. Cardiol.* 12, 1222–1228.

Noorman, M., Hakim, S., Kessler, E., Groeneweg, J. A., Cox, M. G., Asimaki, A., et al. (2013). Remodeling of the cardiac sodium channel, connexin43, and plakoglobin at the intercalated disk in patients with arrhythmogenic cardiomyopathy. *Heart Rhythm* 10, 412–419.

Norgett, E. E., Hatsell, S. J., Carvajal-Huerta, L., Cabezas, J. C., Common, J., Purkis, P. E., et al. (2000). Recessive mutation in desmoplakin disrupts desmoplakin-intermediate filament interactions and causes dilated cardiomyopathy, woolly hair and keratoderma. *Hum. Mol. Genet.* 9, 2761–2766.

Nowak, K. J., and Davies, K. E. (2004). Duchenne muscular dystrophy and dystrophin: pathogenesis and opportunities for treatment. *EMBO Rep.* 5, 872–876.

Ortiz-Genga, M. F., Cuenca, S., Dal Ferro, M., Zorio, E., Salgado-Aranda, R., Climent, V., et al. (2016). Truncating FLNC mutations are associated with high-risk dilated and arrhythmogenic cardiomyopathies. *J. Am. Coll. Cardiol.* 68, 2440–2451.

Oxford, E. M., Musa, H., Maass, K., Coombs, W., Taffet, S. M., and Delmar, M. (2007). Connexin43 remodeling caused by inhibition of plakophilin-2 expression in cardiac cells. *Circ. Res.* 101, 703–711.

Padron-Barthe, L., Villalba-Orero, M., Gomez-Salinero, J. M., Dominguez, F., Roman, M., Larrasa-Alonso, J., et al. (2019). Severe cardiac dysfunction and death caused by arrhythmogenic right ventricular cardiomyopathy type 5 are improved by inhibition of glycogen synthase kinase-3beta. *Circulation* 140, 1188–1204.

Pan, D. (2010). The hippo signaling pathway in development and cancer. *Dev. Cell.* 19, 491–505.

Parsai, C., O'Hanlon, R., Prasad, S. K., and Mohiaddin, R. H. (2012). Diagnostic and prognostic value of cardiovascular magnetic resonance in non-ischaemic cardiomyopathies. *J. Cardiovasc. Magn. Reson.* 14:54.

Patel, A. R., and Kramer, C. M. (2017). Role of cardiac magnetic resonance in the diagnosis and prognosis of nonischemic cardiomyopathy. *JACC Cardiovasc. Imaging* 10(10 Pt A), 1180–1193.

Pearce, P. H., Johnsen, R. D., Wysocki, S. J., and Kakulas, B. A. (1981). Muscle lipids in Duchenne muscular dystrophy. *Aust. J. Exp. Biol. Med. Sci.* 59, 77–90.

Pelosi, L., Berardinelli, M. G., Forcina, L., Spelta, E., Rizzuto, E., Nicoletti, C., et al. (2015). Increased levels of interleukin-6 exacerbate the dystrophic phenotype in mdx mice. *Hum. Mol. Genet.* 24, 6041–6053.

Pilichou, K., Nava, A., Basso, C., Beffagna, G., Bauce, B., Lorenzon, A., et al. (2006). Mutations in desmoglein-2 gene are associated with arrhythmogenic right ventricular cardiomyopathy. *Circulation* 113, 1171–1179.

Pilichou, K., Remme, C. A., Basso, C., Campian, M. E., Rizzo, S., Barnett, P., et al. (2009). Myocyte necrosis underlies progressive myocardial dystrophy in mouse dsg2-related arrhythmogenic right ventricular cardiomyopathy. *J. Exp. Med.* 206, 1787–1802.

Pollazzon, M., Suominen, T., Penttila, S., Malandrini, A., Carluccio, M. A., Mondelli, M., et al. (2010). The first Italian family with tibial muscular dystrophy caused by a novel titin mutation. *J. Neurol.* 257, 575–579.

Protonotarios, A., Wicks, E., Ashworth, M., Stephenson, E., Guttmann, O., Savvatis, K., et al. (2019). Prevalence of (18)F-fluorodeoxyglucose positron emission tomography abnormalities in patients with arrhythmogenic right ventricular cardiomyopathy. *Int. J. Cardiol.* 284, 99–104.

Puchalski, M. D., Williams, R. V., Askovich, B., Sower, C. T., Hor, K. H., Su, J. T., et al. (2009). Late gadolinium enhancement: precursor to cardiomyopathy in Duchenne muscular dystrophy? *Int. J. Cardiovasc. Imaging* 25, 57–63.

Puzzi, L., Borin, D., Gurha, P., Lombardi, R., Martinelli, V., Weiss, M., et al. (2019). Knock down of plakophillin 2 dysregulates adhesion pathway through upregulation of miR200b and alters the mechanical properties in cardiac cells. *Cells* 8:1639.

Quarta, G., Syrris, P., Ashworth, M., Jenkins, S., Zuborne Alapi, K., Morgan, J., et al. (2012). Mutations in the Lamin A/C gene mimic arrhythmogenic right ventricular cardiomyopathy. *Eur. Heart J.* 33, 1128–1136.

Rampazzo, A., Nava, A., Malacrida, S., Beffagna, G., Bauce, B., Rossi, V., et al. (2002). Mutation in human desmoplakin domain binding to plakoglobin causes a dominant form of arrhythmogenic right ventricular cardiomyopathy. *Am. J. Hum. Genet.* 71, 1200–1206.

Richardson, P., McKenna, W., Bristow, M., Maisch, B., Mautner, B., O'Connell, J., et al. (1996). Report of the 1995 world health organization/international society and federation of cardiology task force on the definition and classification of cardiomyopathies. *Circulation* 93, 841–842.

Rizzo, S., Lodder, E. M., Verkerk, A. O., Wolswinkel, R., Beekman, L., Pilichou, K., et al. (2012). Intercalated disc abnormalities, reduced Na(+) current density, and conduction slowing in desmoglein-2 mutant mice prior to cardiomyopathic changes. *Cardiovasc. Res.* 95, 409–418.

Ross, S. E., Hemati, N., Longo, K. A., Bennett, C. N., Lucas, P. C., Erickson, R. L., et al. (2000). Inhibition of adipogenesis by Wnt signaling. *Science* 289, 950–953.

Rybakova, I. N., Patel, J. R., and Ervasti, J. M. (2000). The dystrophin complex forms a mechanically strong link between the sarcolemma and costameric actin. *J. Cell Biol.* 150, 1209–1214.

Sato, P. Y., Musa, H., Coombs, W., Guerrero-Serna, G., Patino, G. A., Taffet, S. M., et al. (2009). Loss of plakophilin-2 expression leads to decreased sodium current and slower conduction velocity in cultured cardiac myocytes. *Circ. Res.* 105, 523–526.

Segura-Rodriguez, D., Bermudez-Jimenez, F. J., Carriel, V., Lopez-Fernandez, S., Gonzalez-Molina, M., Oyonarte Ramirez, J. M., et al. (2019). Myocardial fibrosis in arrhythmogenic cardiomyopathy: a genotype-phenotype correlation study. *Eur. Heart J. Cardiovasc. Imaging* 21, 378–386.

Sen-Chowdhry, S., and McKenna, W. J. (2008). The utility of magnetic resonance imaging in the evaluation of arrhythmogenic right ventricular cardiomyopathy. *Curr. Opin. Cardiol.* 23, 38–45.

Sen-Chowdhry, S., Syrris, P., Prasad, S. K., Hughes, S. E., Merrifield, R., Ward, D., et al. (2008). Left-dominant arrhythmogenic cardiomyopathy: an under-recognized clinical entity. *J. Am. Coll. Cardiol.* 52, 2175–2187.

Sen-Chowdhry, S., Syrris, P., Ward, D., Asimaki, A., Sevdalis, E., and McKenna, W. J. (2007). Clinical and genetic characterization of families with arrhythmogenic right ventricular dysplasia/cardiomyopathy provides novel insights into patterns of disease expression. *Circulation* 115, 1710–1720.

Shang, Y. C., Wang, S. H., Xiong, F., Peng, F. N., Liu, Z. S., Geng, J., et al. (2016). Activation of Wnt3a signaling promotes myogenic differentiation of mesenchymal stem cells in mdx mice. *Acta Pharmacol. Sin.* 37, 873–881.

Sheikh, F., Ross, R. S., and Chen, J. (2009). Cell-cell connection to cardiac disease. *Trends Cardiovasc. Med.* 19, 182–190.

Silva, M. C., Meira, Z. M., Gurgel Giannetti, J., da Silva, M. M., Campos, A. F., Barbosa Mde, M., et al. (2007). Myocardial delayed enhancement by magnetic resonance imaging in patients with muscular dystrophy. *J. Am. Coll. Cardiol.* 49, 1874–1879.

Spencer, M. J., Montecino-Rodriguez, E., Dorshkind, K., and Tidball, J. G. (2001). Helper (CD4(+)) and cytotoxic (CD8(+)) T cells promote the pathology of dystrophin-deficient muscle. *Clin. Immunol.* 98, 235–243.

Spencer, M. J., and Tidball, J. G. (2001). Do immune cells promote the pathology of dystrophin-deficient myopathies? *Neuromuscul. Disord.* 11, 556–564.

Swope, D., Li, J., and Radice, G. L. (2013). Beyond cell adhesion: the role of armadillo proteins in the heart. *Cell Signal.* 25, 93–100.

Syrris, P., Ward, D., Evans, A., Asimaki, A., Gandjbakhch, E., Sen-Chowdhry, S., et al. (2006). Arrhythmogenic right ventricular dysplasia/cardiomyopathy associated with mutations in the desmosomal gene desmocollin-2. *Am. J. Hum. Genet.* 79, 978–984.

Tatsumi, R., Sankoda, Y., Anderson, J. E., Sato, Y., Mizunoya, W., Shimizu, N., et al. (2009). Possible implication of satellite cells in regenerative motoneuritogenesis: HGF upregulates neural chemorepellent Sema3A during myogenic differentiation. *Am. J. Physiol. Cell Physiol.* 297, C238–C252.

Taylor, M., Graw, S., Sinagra, G., Barnes, C., Slavov, D., Brun, F., et al. (2011). Genetic variation in titin in arrhythmogenic right ventricular cardiomyopathy-overlap syndromes. *Circulation* 124, 876–885.

Te Riele, A. S., Agullo-Pascual, E., James, C. A., Leo-Macias, A., Cerrone, M., Zhang, M., et al. (2017). Multilevel analyses of SCN5A mutations in arrhythmogenic right ventricular dysplasia/cardiomyopathy suggest non-canonical mechanisms for disease pathogenesis. *Cardiovasc. Res.* 113, 102–111.

Thibaud, J. L., Monnet, A., Bertoldi, D., Barthelemy, I., Blot, S., and Carlier, P. G. (2007). Characterization of dystrophic muscle in golden retriever muscular dystrophy dogs by nuclear magnetic resonance imaging. *Neuromuscul. Disord.* 17, 575–584.

Thiene, G., Corrado, D., and Basso, C. (2007). Arrhythmogenic right ventricular cardiomyopathy/dysplasia. *Orphanet. J. Rare Dis.* 2:45. doi: 10.1186/1750-1172-2-45

Thiene, G., Corrado, D., Nava, A., Rossi, L., Poletti, A., Boffa, G. M., et al. (1991). Right ventricular cardiomyopathy: is there evidence of an inflammatory aetiology?. *Eur. Heart J.* 12(Suppl. D), 22–25.

Tiso, N., Stephan, D. A., Nava, A., Bagattin, A., Devaney, J. M., Stanchi, F., et al. (2001). Identification of mutations in the cardiac ryanodine receptor gene in families affected with arrhythmogenic right ventricular cardiomyopathy type 2 (ARVD2). *Hum. Mol. Genet.* 10, 189–194.

Towbin, J. A., McKenna, W. J., Abrams, D. J., Ackerman, M. J., Calkins, H., Darrieux, F. C. C., et al. (2019). 2019 HRS expert consensus statement on evaluation, risk stratification, and management of arrhythmogenic cardiomyopathy: Executive summary. *Heart Rhythm* 16, e373–e407.

Turkowski, K. L., Tester, D. J., Bos, J. M., Haugaa, K. H., and Ackerman, M. J. (2017). Whole exome sequencing with genomic triangulation implicates CDH2-encoded N-cadherin as a novel pathogenic substrate for arrhythmogenic cardiomyopathy. *Congenit. Heart Dis.* 12, 226–235.

Uezumi, A., Fukada, S., Yamamoto, N., Takeda, S., and Tsuchida, K. (2010). Mesenchymal progenitors distinct from satellite cells contribute to ectopic fat cell formation in skeletal muscle. *Nat. Cell Biol.* 12, 143–152.

Uezumi, A., Ito, T., Morikawa, D., Shimizu, N., Yoneda, T., Segawa, M., et al. (2011). Fibrosis and adipogenesis originate from a common mesenchymal progenitor in skeletal muscle. *J. Cell Sci.* 124(Pt 21), 3654–3664.

van der Heijden, J. F., and Hassink, R. J. (2013). The phospholamban p.Arg14del founder mutation in Dutch patients with arrhythmogenic cardiomyopathy. *Neth Heart J.* 21, 284–285.

van der Zwaag, P. A., van Rijsingen, I. A., Asimaki, A., Jongbloed, J. D., van Veldhuisen, D. J., Wiesfeld, A. C., et al. (2012). Phospholamban R14del mutation in patients diagnosed with dilated cardiomyopathy or arrhythmogenic right ventricular cardiomyopathy: evidence supporting

the concept of arrhythmogenic cardiomyopathy. *Eur. J. Heart Fail.* 14, 1199–1207.

van der Zwaag, P. A., van Rijsingen, I. A., de Ruiter, R., Nannenberg, E. A., Groeneweg, J. A., Post, J. G., et al. (2013). Recurrent and founder mutations in the Netherlands-phospholamban p.Arg14del mutation causes arrhythmogenic cardiomyopathy. *Neth. Heart J.* 21, 286–293.

van Hengel, J., Calore, M., Bauce, B., Dazzo, E., Mazzotti, E., De Bortoli, M., et al. (2013). Mutations in the area composita protein alphaT-catenin are associated with arrhythmogenic right ventricular cardiomyopathy. *Eur. Heart J.* 34, 201–210.

van Opbergen, C. J. M., Noorman, M., Pfenniger, A., Copier, J. S., Vermij, S. H., Li, Z., et al. (2019). Plakophilin-2 haploinsufficiency causes calcium handling deficits and modulates the cardiac response towards stress. *Int. J. Mol. Sci.* 20:4076.

van Spaendonck-Zwarts, K. Y., van Hessem, L., Jongbloed, J. D., de Walle, H. E., Capetanaki, Y., van der Kooi, A. J., et al. (2011). Desmin-related myopathy. *Clin. Genet.* 80, 354–366.

van Tintelen, J. P., Van Gelder, I. C., Asimaki, A., Suurmeijer, A. J., Wiesfeld, A. C., Jongbloed, J. D., et al. (2009). Severe cardiac phenotype with right ventricular predominance in a large cohort of patients with a single missense mutation in the DES gene. *Heart Rhythm* 6, 1574–1583.

Verma, M., Asakura, Y., Murakonda, B. S. R., Pengo, T., Latroche, C., Chazaud, B., et al. (2018). Muscle satellite cell cross-talk with a vascular niche maintains quiescence via VEGF and notch signaling. *Cell Stem Cell.* 23, 530–43e9.

Vetrone, S. A., Montecino-Rodriguez, E., Kudryashova, E., Kramerova, I., Hoffman, E. P., Liu, S. D., et al. (2009). Osteopontin promotes fibrosis in dystrophic mouse muscle by modulating immune cell subsets and intramuscular TGF-beta. *J. Clin. Invest.* 119, 1583–1594.

Villalta, S. A., Rosenberg, A. S., and Bluestone, J. A. (2015). The immune system in Duchenne muscular dystrophy: Friend or foe. *Rare Dis.* 3:e1010966.

Vita, G. L., Polito, F., Oteri, R., Arrigo, R., Ciranni, A. M., Musumeci, O., et al. (2018). Hippo signaling pathway is altered in Duchenne muscular dystrophy. *PLoS One* 13:e0205514. doi: 10.1371/journal.pone.0205514

Wehling-Henricks, M., Lee, J. J., and Tidball, J. G. (2004). Prednisolone decreases cellular adhesion molecules required for inflammatory cell infiltration in dystrophin-deficient skeletal muscle. *Neuromuscul. Disord.* 14, 483–490.

Wei, B., Dui, W., Liu, D., Xing, Y., Yuan, Z., and Ji, G. (2013). MST1, a key player, in enhancing fast skeletal muscle atrophy. *BMC Biol.* 11:12. doi: 10.1186/1741-7007-11-12

Whitehead, N. P., Yeung, E. W., and Allen, D. G. (2006). Muscle damage in mdx (dystrophic) mice: role of calcium and reactive oxygen species. *Clin. Exp. Pharmacol. Physiol.* 33, 657–662.

Williams, I. A., and Allen, D. G. (2007). Intracellular calcium handling in ventricular myocytes from mdx mice. *Am. J. Phys. Heart Circ. Physiol.* 292, H846–H855.

Yasuda, S., Townsend, D., Michele, D. E., Favre, E. G., Day, S. M., and Metzger, J. M. (2005). Dystrophic heart failure blocked by membrane sealant poloxamer. *Nature* 436, 1025–1029.

Yeung, E. W., Whitehead, N. P., Suchyna, T. M., Gottlieb, P. A., Sachs, F., and Allen, D. G. (2005). Effects of stretch-activated channel blockers on [Ca2+]i and muscle damage in the mdx mouse. *J. Physiol.* 562(Pt 2), 367–380.

Yin, L., Xie, Z. Y., Xu, H. Y., Zheng, S. S., Wang, Z. X., Xiao, J. X., et al. (2019). T2 mapping and fat quantification of thigh muscles in children with duchenne muscular dystrophy. *Curr. Med. Sci.* 39, 138–145.

Zhou, Q., Li, L., Zhao, B., and Guan, K. L. (2015). The hippo pathway in heart development, regeneration, and diseases. *Circ. Res.* 116, 1431–1447.

Conflict of Interest: The authors declare that the research was conducted in the absence of any commercial or financial relationships that could be construed as a potential conflict of interest.

frontiers in Physiology

REVIEW
published: 09 September 2020
doi: 10.3389/fphys.2020.00738

Non-coding RNAs in Cardiac Intercellular Communication

Raquel Figuinha Videira[1,2,3] *and Paula A. da Costa Martins*[1,2,4]*

[1] CARIM School for Cardiovascular Diseases, Faculty of Health, Medicine and Life Sciences, Maastricht University, Maastricht, Netherlands, [2] Department of Molecular Genetics, Faculty of Science and Engineering, Maastricht University, Maastricht, Netherlands, [3] Cardiovascular Research and Development Center, Faculty of Medicine, University of Porto, Porto, Portugal, [4] Department of Physiology and Cardiothoracic Surgery, Faculty of Medicine, University of Porto, Porto, Portugal

Intercellular communication allows for molecular information to be transferred from cell to cell, in order to maintain tissue or organ homeostasis. Alteration in the process due to changes, either on the vehicle or the cargo information, may contribute to pathological events, such as cardiac pathological remodeling. Extracellular vesicles (EVs), namely exosomes, are double-layer vesicles secreted by cells to mediate intercellular communication, both locally and systemically. EVs can carry different types of cargo, including non-coding RNAs (ncRNAs), which, are major regulators of physiological and pathological processes. ncRNAs transported in EVs are functionally active and trigger a cascade of processes in the recipient cells. Upon cardiac injury, exosomal ncRNAs can derive from and target different cardiac cell types to initiate cellular and molecular remodeling events such as hypertrophic growth, cardiac fibrosis, endothelial dysfunction, and inflammation, all contributing to cardiac dysfunction and, eventually, heart failure. Exosomal ncRNAs are currently accepted as crucial players in the process of cardiac pathological remodeling and alterations in their presence profile in EVs may attenuate cardiac dysfunction, suggesting that exosomal ncRNAs are potential new therapeutic targets. Here, we review the current research on the role of ncRNAs in intercellular communication, in the context of cardiac pathological remodeling.

Keywords: non-coding RNAs, extracellular vesicles, cardiac intercellular communication, cardiac pathological remodeling, heart failure

OPEN ACCESS

Edited by:
Marcella Canton,
University of Padua, Italy

Reviewed by:
Jop Van Berlo,
University of Minnesota Twin Cities, United States
Nazareno Paolocci,
Johns Hopkins University, United States

***Correspondence:**
Paula A. da Costa Martins
p.dacostamartins@maastrichtuniversity.nl

Specialty section:
This article was submitted to Striated Muscle Physiology, a section of the journal Frontiers in Physiology

Received: *26 February 2020*
Accepted: *08 June 2020*
Published: *09 September 2020*

Citation:
Videira RF and da Costa Martins PA (2020) Non-coding RNAs in Cardiac Intercellular Communication. Front. Physiol. 11:738. doi: 10.3389/fphys.2020.00738

INTRODUCTION

Cardiac homeostasis is achieved through a complex network of interactions between the different cells of the myocardium, including cardiomyocytes, cardiac fibroblasts, neurons, cardiac endothelial, and immune cells. Upon injury, this homeostatic state is damaged and intercellular communications are rearranged toward cardiac maladaptive remodeling (Xin et al., 2013), normally characterized by cardiac hypertrophic growth, capillary rarefaction, and scar-induced events such as exacerbated inflammation, interstitial fibrosis, and ventricular dilation (Xin et al., 2013).

Cardiac communication between different types of cells can occur *via* (i) cell–matrix interactions, where cells respond to mechanical and extracellular matrix (ECM) stress; (ii) synaptic signaling, usually associated with electric and chemical neuronal signals released at the synapse site; (iii) endocrine signaling, a long distance communication where signaling factors are released into the blood stream (Kamo et al., 2015); but mostly (iv) *via* paracrine signaling, a short-range crosstalk mechanism where signals are diffused through the extracellular space before being incorporated in

recipient cells and instigating a response (Bang et al., 2015). While paracrine factors have been confined for a long-time to soluble factors released from the cells, such as cytokines, in the past few years, growing evidence suggests more controlled and protected signaling mechanisms mediated by extracellular vesicles (EVs) (Hervera et al., 2019).

The classic concept of EVs containing cell debris or being markers of cell death was recently revolutionized when healthy cells were also shown to be capable of releasing these vesicles and, today, they are considered crucial mediators of both physiological and pathological cellular and molecular events. While EV is a generic term to describe a double-layer vesicle endogenously secreted by cells, their different origin, size and surface markers allow us to categorize them into three main groups: microvesicles, exosomes, and apoptotic bodies (Raposo and Stoorvogel, 2013). In contrast to microvesicles (100–1000 nm in diameter, MVs), which are formed by direct budding of the plasma membrane and, therefore, express selectins, integrins, and CD40l; exosomes (40–120 nm in diameter) originate through the cellular endocytic pathway and express markers such as CD81, CD63, CD9 (tetraspanins), flotillin, and Alix (Raposo and Stoorvogel, 2013). To date, only MVs and exosomes have been associated with intercellular communication.

Recently, a new class of EVs named exomeres has been characterized as non-encapsulated nanoparticles due to the absence of an external membrane structure, a low lipidic composition and a smaller size (up to 50 nm in diameter) (Zhang et al., 2018). The same study also distinguished two subtypes of exosomes: small exosomes (exo-S) and large exosomes (exo-L), primarily according to their size which varies from 60 to 80 nm and 90 to 120 nm, respectively. Although exo-S and exo-L present the typical exosome marker proteins Alix and Tsg101, exo-S preferentially express tetraspanins and their cargo is mainly composed of proteins associated with endosomes, multivesicular bodies, vacuoles, and phagocytic vesicles whereas Exo-L are enriched in proteins that make up the plasma membrane, cell junctions, late-endosome, and *trans*-Golgi network (Zhang et al., 2018). Given that a distinct set of proteins is found among the different exosomes, it is not surprising that they also show different degrees of stiffness and charge (Zhang et al., 2018). Due to their novelty, differences among exosomes subtypes were not taking into consideration on the studies reported in this review and, therefore, discrimination between exo-S and exo-L was not included in their reported analysis. Indeed, exosomes are generalized and referred to as a major class, without differentiation according to their subtypes, throughout this review.

Notably, exosomes can transport both proteomic and genetic cargo that are functionally active once within the recipient cell (Raposo and Stoorvogel, 2013). A great component of exosomal cargo is made up of non-coding RNAs (ncRNAs), which are major regulators of cell homeostasis and are the main players in a variety of diseases, namely cardiovascular diseases and heart failure (Dhanoa et al., 2018). ncRNAs are a heterogenous class of RNAs, classified mostly according to their size: small (miRNAs) or long (lncRNAs); shape: linear or circular (circRNAs), and cell position: nucleolar (snoRNAs) or cytoplasmic (Santosh et al., 2015; **Figure 1**). From bacteria to humans, ncRNAs are present in a wide range of organisms, in fact, the "baby boom" of ncRNAs occurred after the first report on the *lin-4* gene in *Caenorhabditis elegans* (Lee et al., 1993). Since then, multiple reports have implicated miRNAs in the negative regulation of gene expression at a post-transcriptional level, in biological processes ranging from cellular proliferation, migration, and apoptosis and thus, also in pathological processes such as maladaptive cardiac remodeling leading to heart failure (Liao et al., 2018; Huang S. et al., 2019; Yang et al., 2019). Typically, a miRNA selectively binds to the 3′UTR of mRNA targets and either induces their degradation or prevents them from being translated into protein, in a process that is dependent on the complementarity between the miRNA and the respective mRNA target (Li and Rana, 2014). In turn, miRNAs can be regulated by linear lncRNAs that present multiple miRNA-binding sites and which, by allowing the recruitment of several molecules at once, generate a sponge-like effect (Greene et al., 2017; Zhou and Yu, 2017). lncRNAs can also structurally facilitate mRNA decay, mRNA splicing, and translation by functioning as a dock for the "mRNA-lncRNA-Staufen-1," a complex responsible for mRNA degradation and accumulation/assembly of specific factors of the splicing machinery by promoting the association of the mRNA 5′UTR with the polysome (Gong and Maquat, 2011; Uchida and Dimmeler, 2015). At the DNA level, lncRNAs can contribute to epigenetic modifications, namely histone and DNA methylation, by recruiting chromatin remodeling complexes such as the polycomb repressive complex 2 (PRC2) or H3K27me3 and lead to transcriptional repression (Gupta et al., 2010). In contrast to miRNAs, with their exclusive non-coding function, recent reports described a potential dual role for lncRNA as both non-coding and protein coding genes (Matsumoto et al., 2017). Recently, several lncRNAs were found to be enriched in EVs secreted by colorectal cancer cells and were shown to control gene expression patterns in the recipient cells (Hinger et al., 2018). The export of RNAs through exosomes seems to be a controlled rather than a passive or random mechanism. Despite miRNAs and lncRNAs being both incorporated in EVs, miRNAs are exported in greater quantities, and often intact, suggesting a more regulated control of exosomal miRNA content (Hinger et al., 2018).

Exosome-mediated shuttling of ncRNAs between cells is not the only mechanism of ncRNAs transference, as shown for miRNAs which can also leave the cell bound to either lipid particles such as cholesterol (Tabet et al., 2014), ribonucleic complex (Arroyo et al., 2011), and other vesicles (Chen et al., 2019). Being incorporated into vesicles grants higher miRNA longevity by conferring protection from degradation by nucleases (Arroyo et al., 2011). However, the relative abundance of cardiac secreted miRNAs within exosomes and/or other vesicles remains debatable. While Chen et al. (2020) described higher plasma levels of miR-126 in the exosomal fraction compared to the non-exosomal fraction, another study suggests that plasmatic exosomal miRNAs are only a minority, with 90% of the plasmatic miRNAs being present in a non-membrane-bound form, possibly bound to a ribonucleoprotein complex (Arroyo et al., 2011).

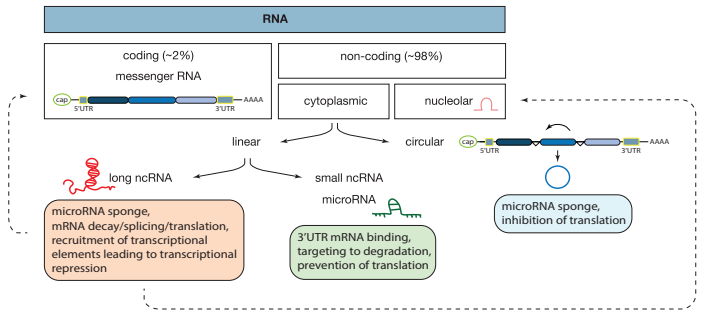

FIGURE 1 | Classes of RNAs and their mechanisms of action. In our genome, approximately 98% of the transcribed RNA is ncRNA, a diverse class of RNAs that does not encode for a protein. ncRNAs are divided according to their localization: nucleus or cytoplasm; shape: circular or linear and size: small or long. Each ncRNA is a unique form and mechanism of action, as described inside of each box. In this review we focused on microRNAs, long non-coding, and circular RNAs. Dashed lines represent findings that need further validation.

Similar to lncRNAs, circular RNAs (circRNAs) can also inhibit miRNAs using the "sponge" effect strategy. circRNAs are ncRNAs (exon- or intron-derived) where the 3′ and 5′ ends, usually free in a linear RNA, are linked together forming a continuous loop (Greene et al., 2017). Recently, these structurally different RNAs were associated with cardiovascular diseases and were shown to also serve as EV cargo (Zhou and Yu, 2017; Huang S. et al., 2019). In fact, an altered circRNA pattern was found in EVs derived from ischemic heart tissue when compared to EVs derived from healthy myocardium (Ge et al., 2019). The enriched circRNAs in ischemic heart tissue were associated with the metabolic process of vesicle generation while the depleted circRNAs were involved in transforming growth factor beta (TGF-β) signaling, commonly, associated with cardiac fibrosis and inflammation (Ge et al., 2019).

Here, we review the current research on the role of ncRNAs in intercellular communication, in the context of cardiac pathological remodeling.

CROSS TALK OF ncRNAs IN CARDIAC HYPERTROPHY

Cardiomyocytes, the most prominent cell type of the myocardium (Zhou and Pu, 2016) can grow either *via* hyperplasia, which results in increased number of cells, or *via* hypertrophy where cell size increases while the cell number remains the same. In mammalians, adult cardiac growth occurs mainly through cardiomyocyte hypertrophy as cardiomyocytes exit the cell cycle, shortly after birth, hampering them to proliferate as an adult (Xin et al., 2013). Although physiological hypertrophic growth may be necessary to prevent cardiac atrophy during pregnancy or intense exercise, (Pu et al., 2003) hypertrophic growth is normally a maladaptive remodeling process that eventually progresses toward heart failure, depending on the nature, length, and intensity of the initial cardiac stress (Samak et al., 2016).

Intense exercise and pregnancy often result in cardiac hypertrophic growth through a process regulated by the phosphoinositide 3-kinase/protein kinase B (PI3K/AKT) signaling pathway and insulin growth factor (IGF) (Frey and Olson, 2003). As cardiac morphology and contractile function are both preserved, this is considered to be an adaptive or physiological process (Frey and Olson, 2003). In pathologic hypertrophy, where contractile function is compromised, activation of G-protein coupled receptors (GPCRs), mitogen-activated protein kinase (MAPK), and the calcineurin/nuclear factor activated cells (Cn/NFAT) pathway leads to suppression of fatty acid oxidation, increased cell growth, fibrosis, and inflammation toward heart failure (Frey and Olson, 2003). Pathological hypertrophy often develops as a consequence of chronic hypertension, valvular disease, or cardiomyopathies. Briefly, the ventricular wall is exposed to elevated mechanical stress which is perceived by the sarcomeric Z-disks in the cardiac muscle cells to trigger the activation of signaling pathways including the Cn/NFAT pathway, inducing, in turn, cardiomyocytes to become hypertrophic and ventricle walls to reach excessive dimensions (Lyon et al., 2015). Initially, an increase in size is matched with a higher heart rate as the heart tries to maintain its normal cardiac output. However, if the pathologic stimuli remains, the heart can no longer cope with the stress, and without enough oxygen due to insufficient coronary perfusion, hypertrophy becomes a maladaptive, rather than an adaptive process (Frey and Olson, 2003). In fact, the Heart Outcomes Prevention Evaluation (*HOPE*) trial, a study assessing the efficiency of ramipril, an angiotensin-converting enzyme (ACE) inhibitor, in preventing future cardiovascular events in high-risk patients, showed that inhibition or regression of cardiac hypertrophy is able to decrease heart failure and stroke events as well as increase survival rate, thus questioning whether hypertrophy is ever an adaptive process at all (Mathew et al., 2001).

Not only cardiomyocytes but also cardiac fibroblasts and endothelial cells are affected by hypertrophic stimuli, and their orchestrated response can promote cardiomyocyte growth mostly by the release of a variety of pro-hypertrophic paracrine factors. In line with this, lower levels of such factors will hamper cell growth. Inhibition of nitric oxide (NO) synthesis by endothelial cells is followed by a reduction in cardiomyocyte size (Jaba et al., 2013). Another well-described paracrine factor is TGF-β, secreted

by cardiac fibroblasts. Conditioned medium of cardiac pressure overload-derived fibroblasts was shown to be sufficient to induce hypertrophic growth of cardiomyocytes in culture – an effect that could be abrogated by blockade of TGF- β receptors (Cartledge et al., 2015). These findings highlight the role of intercellular communication in the heart and its importance in the cardiac response to stress.

Hypertrophic signaling is also influenced by the transfer of ncRNAs through crosstalk between cardiomyocytes and non-cardiomyocytes (**Figure 2**). Fibroblast-derived exosomes were shown to be enriched in miR-21* which can be taken up by cardiomyocytes and can induce their hypertrophic growth by targeting cytoskeletal proteins, namely sorbin and SH3 domain-containing protein 2 (SORBS2) and PDZ and LIM domain 5 (PDLIM5) (Tian et al., 2018). In line with this, blocking of miR-21* in mice subjected to chronic administration of angiotensin II (AngII) reduced cardiomyocyte growth, underlining fibroblast-derived miR-21* as a key player toward a pathologic cardiac response to chronic stress (Tian et al., 2018). More recently, miR-34a, along with miR-27a and miR-28a were reported to be preferentially incorporated into exosomes secreted by cardiac fibroblasts after tumor necrosis factor alpha (TNF-α) treatment (Tian et al., 2018). These miRNAs are secreted from cardiac fibroblasts and transferred to cardiomyocytes where they not only induce expression of hypertrophic genes but also have as a common target an antioxidant enzyme, Kelch-like ECH-associated protein 1-nuclear factor erythroid 2-related factor 2 (Nrf2), previously shown to be downregulated in chronic heart failure (Tian et al., 2018). By being upregulated in chronic heart failure, miR-27a, miR-28a, and miR-34a may contribute to the development of the disease through the inhibition of Nrf2 (Tian et al., 2018).

Similarly, macrophages are also able to influence the cardiomyocyte response to stress by transferring macrophage-derived miR-155 (Halkein et al., 2013). *In vitro*, the hypertrophic phenotype of cardiomyocytes treated with the pro-hypertrophic factor endothelin 1 (ET1) was attenuated by exposing the cells to conditioned media derived from miR-155-deficient macrophages (Wang C. et al., 2017). *In vivo*, specific genetic ablation of miR-155 on macrophages hampered cardiac hypertrophy and inflammation in a mouse model of hypertrophy (Wang C. et al., 2017). Regarding endothelial cells, it was shown that in peripartum cardiomyopathy, a cardiac disease initiated by a cleaved prolactin fragment (16-kDa N-terminal prolactin fragment, 16K PRL), increased expression of miR-146 hampering angiogenesis (Halkein et al., 2013). However, miR-146 was also found in endothelial cell-derived exosomes and was shown to be transferred to cardiomyocytes where it negatively regulates Erb-B2 Receptor Tyrosine Kinase 4 (*Erbb4*), known to be involved in cardiac hypertrophy and metabolism. Chemical inhibition of miR-146 in a mouse model of peripartum cardiomyopathy attenuated cardiac dysfunction (Halkein et al., 2013).

Cardiac hypertrophy, a fundamental risk factor for heart failure, develops as an orchestrated response of several types of cells where ncRNAs act as paracrine factors manipulating the behavior of both donor and recipient cells (**Figure 2**).

CROSS TALK OF ncRNAs IN CARDIAC CAPILLARY RAREFACTION

As shown for several vascular diseases such as atherosclerosis, vessel restenosis, and primary hypertension, the vasculature is mostly capable of adapting itself in response to different stimuli to maintain vascular function and structure after injury (Su et al., 2017). However, pathologic stimulation of the cardiac vessels results in increased rigidity and a decline of vessel compliance as maladaptive vascular remodeling that will ultimately further contribute to cardiomyocyte hypertrophy and fibrosis (Su et al., 2017). Larger cardiomyocytes require more oxygen and nutrients and to cope with this increased demand, the cardiac vasculature must expand accordingly. In an initial phase, proangiogenic signals are released from damaged cardiomyocytes and capillaries are able to adapt to the increased demand, however, if the stress persists leading to exaggerated hypertrophy, these mechanisms fail to further stimulate vascular growth (Gogiraju et al., 2019). In pressure overload-induced hypertrophy, an increase in p53 expression leads to apoptosis of endothelial cells, deficient vasculature, and diminished capillary density – all contributing to tissue hypoxia and subsequent scar formation (Gogiraju et al., 2019).

One of the mainstays of cardiac vascularization and function is the vascular endothelial growth factor (VEGF) signaling pathway. Constitutive expression of VEGF-A in mice is able to enhance cardiac angiogenesis and improve basal cardiac function and *vice versa*, while its depletion results in defective vascularization, thinner cardiac walls, and contractile dysfunction (Lee et al., 2017). The VEGF signaling is also under the control of miRNAs including miR-374, shown to target VEGF receptor 1 (VEGFR1) and its downstream factor protein kinase G1 (PKG1), a regulator of calcium release from endoplasmatic reticulum that, indirectly, promotes hypertrophy (Lee et al., 2017). Depletion of miR-126, another miRNA regulating angiogenesis, in endothelial cells leads to partial embryonic lethality (40%) due to vascular defects (Wang et al., 2008). Similarly, in mice subjected to myocardial infarction (MI), miR-126 deletion contributed to a decrease in the VEGF signaling pathway (Yang et al., 2017). Following MI, the ischemic myocardium responds by increasing VEGF and fibroblast growth factor (FGF) expression, two potent angiogenic factors that are crucial for the development of collateral vessels and contribute to the reperfusion of the damaged myocardium (Cochain et al., 2013). MiR-126 silencing promotes the expression of its target Sprouty Related EVH1 Domain Containing 1 (SPRED1), an inhibitor of the RAF proto-oncogene serine/threonine-protein kinase (RAF1) and VEGF/ERK angiogenic pathway (Fish et al., 2008). Interestingly, miR-126 was reported to be depleted in exosomes derived from type 2 diabetic rat cardiomyocytes, while miR-320 was found to be highly enriched (Wang et al., 2014). Uptake of these miR-320-enriched exosomes by cardiac endothelial cells compromised their proliferative, migratory, and tube formation capacity (Wang et al., 2014). In contrast, inhibition of miR-320 or pharmacological inhibition of exosome formation were sufficient to abrogate the deleterious effects of miR-320 expression on

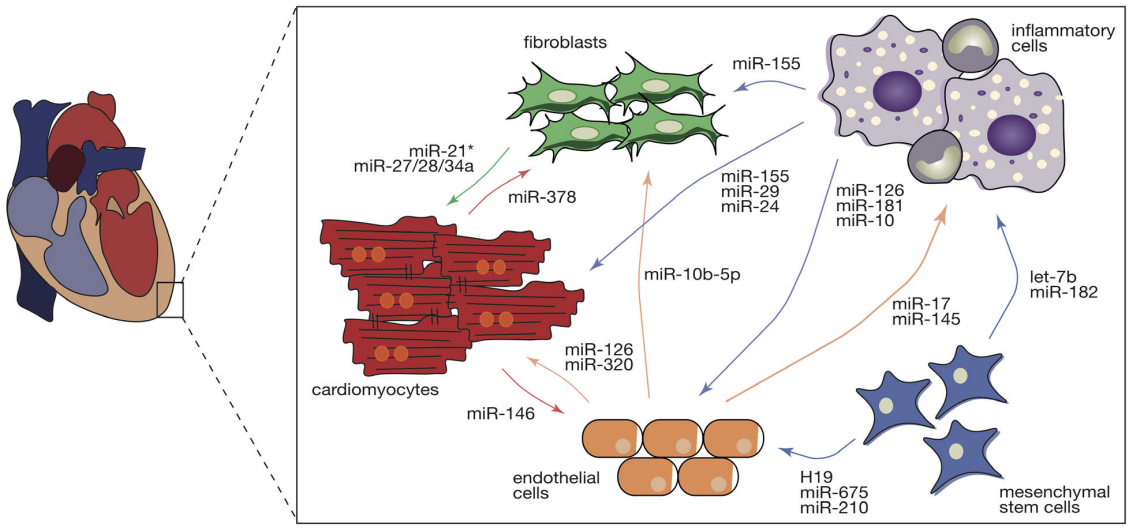

FIGURE 2 | Intercellular transfer of ncRNAs during cardiac pathological remodeling. Cardiac pathological stimuli promote the various cardiac cell types to release exosomes that are enriched in several ncRNA species including miRs, circRNAs, and lncRNAs. Intercellular transfer of ncRNAs in the heart regulates diverse types of remodeling cellular and molecular processes in the recipient cells (cardiomyocytes, endothelial cells, cardiac fibroblasts, inflammatory, and mesenchymal stem cells), contributing to cardiac hypertrophy, microvascular dysfunction, capillary rarefaction, fibrosis, and inflammation. Intercellular communication is a bidirectional complex and the direction of the arrows represents the direction of the transference. Colors of the arrows symbolize the donor cell: red- cardiomyocytes, green- cardiac fibroblasts, light brown – endothelial cells, purple – inflammatory cells, and blue – mesenchymal stem cells.

angiogenesis – indicative of an anti-angiogenic and exosome-dependent role for this miRNA (Wang et al., 2014).

Moreover, depletion of miR-17 and miR-145 from exosomes derived from macrophages that were exposed to AngII, interferes with the capacity of cells to incorporate those exosomes (Leisegang et al., 2017). In endothelial cells, exosomal depletion of miR-17 and miR-145 increased the expression of two previously described targets known to be involved in inflammation, intercellular adhesion molecule 1 (ICAM-1), and plasminogen activator inhibitor 1 (PAI-1) (Osada-Oka et al., 2017). These results underline miRNAs as pathological cargo of exosomes, emphasizing their role in promoting pro-inflammatory signaling pathways in endothelial cells.

Similar to miRNAs, lncRNAs can also act as regulators of angiogenesis. CRISPR/Cas9-mediated genetic deletion of a lncRNA that is normally found upregulated in vascular pathologies (Leisegang et al., 2017), *MANTIS*, in human umbilical vein endothelial cells (HUVECs), compromised their tube formation and sprouting capacity through the downregulation of several angiogenic-related genes (Leisegang et al., 2017).

Interestingly, exposing neonatal rat cardiomyocytes to hypoxic conditions induced the release of exosomes that are enriched in circRNAs, namely, circHIPK3 (Wang et al., 2019b). Conditioned media derived from hypoxic cardiomyocytes led to upregulation of this circRNA in cardiac microvascular endothelial cells (CMVECs). In contrast, circHIPK3 is downregulated when CMVECs are exposed to H_2O_2. In these cells, circHIPK3 acts as a sponge for miR-29, that in turn, targets the insulin-like growth factor 1 (IGF-1) pathway, involved in reactive oxygen species (ROS) production and apoptosis (Yanagisawa-Miwa et al., 1992). In fact, re-expression of IGF-1, due to enrichment of circHIPK3, promoted survival of CMVECs exposed to H_2O_2 and decreased ROS production, suggesting that cardiomyocyte exosome-derived circHIPK3 is a regulator of endothelial function and capillary rarefaction during hypoxic conditions (Wang et al., 2019b).

A defective vasculature is typical of the maladaptive cardiac remodeling process observed in different pathologies, including MI, hypertension, or cardiomyopathy (Cochain et al., 2013). Increased capillary density after cardiac injury has been shown to prevent cardiac remodeling and improve cardiac function, establishing angiogenesis as an appealing therapeutic target (Yanagisawa-Miwa et al., 1992). Besides being effective regulators of angiogenesis, incorporation of ncRNAs into exosomes protects them and facilitates their intercellular transfer, making them attractive tools for angiogenic therapy (Huang P. et al., 2019).

CROSSTALK OF ncRNAs IN CARDIAC FIBROSIS

The very limited regenerative capacity of the mammalian adult heart due to low proliferative capacity and defective angiogenesis leads to the formation of a permanent scar after ischemic injury (Xin et al., 2013). Cardiac fibrosis is the main cellular event leading to scar formation and is characterized by an accumulation of ECM in the myocardium (Beltrami et al., 2003). In healthy conditions, ECM is responsible for transmission of the contractile force and serves as scaffolding for cardiac cells conferring mechanical support to the heart, and as such, cardiac contraction and relaxation firmly depends

on ECM (Michel, 2003; Bildyug, 2019). Cardiac ECM is predominantly composed of collagens I and III (ColI and ColIII), glycosaminoglycans, glycoproteins, latent growth factors, and proteases (Kong et al., 2014), and is under constant turnover of sustained degradation and synthesis processes (Lajiness and Conway, 2014). Dysregulation of this tightly controlled process may impair both systolic and diastolic function as result of uncoordinated cardiomyocyte contraction, and/or cardiomyocyte displacement associated with ventricular dilation, and, ultimately cause ventricular stiffness and arrhythmias. The hallmarks of the cardiac fibrotic response include activation of fibrillary collagen and myofibroblast differentiation from either fibroblasts, hematopoietic, or endothelial cells (Davis and Molkentin, 2014). Myofibroblasts display contractile stress fibers and a large endoplasmic reticulum – associated with secretion of large amounts of ECM proteins – and are very sensitive to growth factors and pro-inflammatory molecules (Davis and Molkentin, 2014). Despite being essential for myocardium repair, continuous presence of myofibroblasts in response to persistent inflammatory signals may result in excessive scarring and impairment of both systolic and diastolic function (Davis and Molkentin, 2014).

The molecular mechanisms underlying cardiac fibrosis are very dependent on the type of primary myocardial injury; however, there are fibrogenic signals consistently activated during fibrosis such as increased levels of TGF-β and AngII, among several others (Kong et al., 2014). TGF-β is a cytokine present as three different isoforms (TGF-β1, 2, and 3) and, while in the heart TGF-β1 is mainly present as a latent complex, once it is activated upon injury through the matrix metalloproteases 9 and 2 (MMP-9, MMP-2), it will cause alterations in the ECM composition (Ignotz and Massague, 1986). While overexpression of TGF-β1 promotes collagen deposition and ventricular fibrosis, its loss of function attenuates myocardial fibrosis in a rat model of pressure-overload (Koitabashi et al., 2011).

Several studies have indicated cardiac fibrosis to be under control of ncRNAs. In fact, TGF-β1 activity is regulated by miR-21, which by targeting Jagged1, a ligand for Notch receptor 1, affects *trans*-differentiation of cardiac fibroblasts into myofibroblasts and subsequently, myocardial fibrosis (Zhou et al., 2018).

Global lncRNA expression profiling in cardiac fibroblasts revealed lncRNA *Meg3* to be specifically enriched in cardiac fibroblasts (Piccoli et al., 2017). Upon pressure overload, *Meg3* regulates MMP-2 expression by stabilizing p53 at its binding site on the MMP-2 promoter, resulting in cardiac fibrosis and diastolic dysfunction (Piccoli et al., 2017). Silencing of lncRNA *Meg3* with gapmers, prevented MMP2 activation and had a protective effect in pressure-overloaded hearts, partially due to attenuation of fibrosis (Piccoli et al., 2017). Given the emerging importance of circRNAs in myocardial function, Zhou and Yu (2017) analyzed the circRNA expression pattern in myocardial tissue of diabetic mice. A circRNA microarray screening identified circRNA_010567 as one of the top upregulated circRNAs in cardiac fibroblasts and its inhibition in cardiac fibroblasts exposed to AngII suppressed fibrosis-associated genes such as *Col I, Col III, and* alpha smooth muscle actin (α-*SMA)* (Zhou and Yu, 2017). circRNA_010567 was shown to have multiple binding sites for miR-141, that in turn targets TGF-β1. In fact, silencing of circRNA_010567, increased miR-141 expression, decreased TGF-β1 expression and its downstream targets, attenuating myocardial fibrosis (Zhou and Yu, 2017).

Apart from fibroblast-derived ncRNAs, there are other ncRNAs that originate from different cell types and are implicated in cardiac fibrosis through paracrine signaling. A recent study demonstrated that mechanical stress due to pressure-overload promotes transfer of cardiomyocyte-derived miR-378 to cardiac fibroblasts in an EV-dependent manner (Yuan et al., 2018). Loss- and gain-of function of miR-378 in cardiomyocytes, *via* targeting of the TGF-β1 pathway, accentuated collagen deposition but inhibited cardiac fibroblast proliferation. Similar effects were observed when EV secretion was impaired by administration of a sphingomyelin phosphodiesterase inhibitor, GW4869 (Yuan et al., 2018), suggesting that the mechanism used by cardiomyocytes to release miR-378 and to exert its function in cardiac fibroblasts, is dependent on intercellular communication *via* exosomes.

As mentioned, myofibroblast activation is a key contributor to cardiac fibrosis and cardiac pathological remodeling, and the transition between fibroblasts and myofibroblast can be regulated by exosomal miRNAs, namely, cardiomyocyte-derived miR-195 (Morelli et al., 2019). Upon cardiac ischemic injury, cardiomyocytes release exosomes that are enriched in miR-195. *In vitro* exposure of cardiac fibroblasts to conditioned medium derived from myocardial infarction (MI)-hypoxic cardiomyocytes, led to an increase in the levels of miR-195, as well as in myofibroblast and fibrotic markers such as periostatin, alpha smooth muscle actin (α-SMA), and ColI and III on cardiac fibroblasts. Mechanistically, miR-195 targets the α-SMA inhibitor mothers against decapentaplegic homolog 7 (SMAD7), promoting the transcription of α-SMA and other myofibroblast associated genes (Morelli et al., 2019). Inhibition of EV release or inhibition of miR-195, *via* administration of the GW4869 or miR-195 inhibitor, respectively, abrogated myofibroblast activation. These observations established miR-195 as an important player during MI-induced pathological remodeling through myocyte-fibroblast communication (Morelli et al., 2019).

Macrophages, in turn, are able to affect cardiac fibrosis by transferring miR-155 into cardiac fibroblasts (Wang C. et al., 2017). An increment in exosome secretion by macrophages is accompanied by an increase in miR-155 expression in cardiac fibroblasts while deletion of miR-155 on macrophages leads to a reduction of miR-155 levels in cardiac fibroblasts. However, abrogation of miR-155 expression in cardiac fibroblasts did not interfere with their endogenous levels of miR-155, suggesting that the origin of miR-155 in cardiac fibroblasts derives from an external source, namely, macrophages. In cardiac fibroblasts, increased miR-155 expression prevents cell proliferation and increases inflammation by targeting fibrotic and inflammatory genes, simultaneously. Genetic deletion of miR-155 *in vivo* attenuated inflammation but accelerated cardiac fibroblast proliferation after MI, inhibiting myocardial rupture and improving cardiac function (Wang C. et al., 2017).

While the concept of exosomal miRNAs in myocardial fibrosis is well established, implication of exosomal lncRNAs and/or exosomal circRNAs transfer during cardiac fibrosis were still not reported, highlighting the need for better understanding of the molecular mechanisms driving cardiac fibrosis as a dichotomous event, in order to pursue more efficient therapeutic targets.

CROSSTALK OF ncRNAs IN CARDIAC INFLAMMATION

Inflammation is a common ground for maladaptive cardiac remodeling, independent of the disease etiology. Inflammation occurs in all stages of tissue repair including initiation, maintenance, resolution, and clearing out the damaged tissue. A vast variety of cells, including monocytes, macrophages, dendritic cells, T-cells, B-cells, NK cells, and others, compose the immune system and regulate the inflammatory response. Both MI and hypertension activate an inflammatory cardiac response; however, the mechanisms induced by these two types of injury are very distinct.

In MI, inflammation is initiated following the typical hallmarks of ischemic injury, cardiomyocyte death, and interstitial fibrosis, both involved in the generation of reactive oxidative species and activation of the complement pathway (Prabhu and Frangogiannis, 2016). Subsequently, endothelial dysfunction leads to increased vessel permeability followed by leukocyte infiltration. Finally, remodeling of the ECM, along with damaged cardiac cells' release of interleukins (IL) like IL one alpha (IL-1α) and heat shock proteins (HSP) that act as damage-associated molecular patterns (DAMPs), takes place (Prabhu and Frangogiannis, 2016). When secreted to the extracellular environment these danger signals bind to pattern recognition receptors activating leukocytes (Prabhu and Frangogiannis, 2016). Hearts subjected to pressure overload either by hypertension or aortic stenosis, show a profound vascular remodeling accompanied by perivascular fibrosis and inflammation but no significant cardiomyocyte loss (Xia et al., 2009). Cardiac hypertrophy is followed by transient activation of the inflammatory response, starting with the release of pro-inflammatory cytokines such as IL-1β, IL-6, and TNF-α and rapidly progressing to macrophage infiltration and upregulation of TGF-β. Long term inflammation is replaced by fibrosis and the initial cardiac response develops into both diastolic and systolic dysfunction (Xia et al., 2009).

Macrophages display different inflammatory states. Usually, M1 macrophages are associated with a pro-inflammatory phenotype by releasing IL-1β, IL-6, and TNF-α, while M2 phenotype transition is linked to immunomodulation and secretion of anti-inflammatory cytokines such as IL-10. Notably, M1 to M2 macrophage transition might be influenced by bone marrow-derived mesenchymal stem cells (BMSCs)-derived exosomes (Xu et al., 2019) as myocardial injection of such exosomes in the border zone of ischemic hearts, significantly decreased M1/M2 ratio and attenuated cardiac inflammation. These protective effects were enhanced by exosomes derived from BMSCs after preconditioning with lipopolysaccharide (LPS) stimulation (Xu et al., 2019). Similar to BMSCs, LPS preconditioning of mesenchymal stromal cells can also guide M1 to M2 macrophage activation along with the upregulation of anti-inflammatory cytokines through exosomal release (Ti et al., 2015). Interestingly, exosomes derived from LPS-activated MSCs are enriched with let-7b which regulates macrophage plasticity *via* toll-like receptor 4 (TLR4), and *in vivo,* increases diabetic cutaneous wound healing and attenuates inflammation (Ti et al., 2015). Another report on mesenchymal stromal cells-derived exosomes highlighted the cardioprotective and immunomodulatory effect of exosomal miRNAs on M1/M2 macrophage shuttle (Zhao et al., 2019). Under inflammatory conditions, such as myocardial ischemia/reperfusion, miR-182 is loaded in MSCs-derived exosomes and further incorporated into macrophages (Zhao et al., 2019). Similar to let-7b, miR-182 also targets the TLR4 pathway and activates the PI3K/AKT signaling pathway, an important step in the conversion of M1 into anti-inflammatory M2 phenotype (Zhao et al., 2019).

Reduction of the inflammatory process and improved immunomodulatory response were shown upon addition of endothelial cell-derived EV to monocytes (Njock et al., 2015). Endothelial cells exert their anti-inflammatory effect by secreting EVs loaded with miR-126, miR-181b, and miR-10. Once taken up by monocytes, miR-10 induced the strongest anti-inflammatory effect by repressing the nuclear factor κB (NF-κB) pathway and increasing the levels of immunomodulatory genes (Njock et al., 2015). This supports an essential role of the crosstalk between different cell types such as endothelial cells and monocytes, during cardiac inflammation cardiac, mediated by miRNAs enclosed in secreted EVs.

INTER-ORGAN CROSSTALK

The primary function of the heart is to pump blood to the rest of the body, yet, recent studies demonstrate that the heart could have other functions and acts as an endocrine organ (de Bold et al., 1981; Nakamura et al., 1991). Through endocrine signaling, the heart is able to maintain whole body homeostasis and, in this way, peripheral organs are able to respond to stress stimuli that originate in the heart (**Figure 3**).

Most likely, the best described cardiac endocrine factor is the atrial natriuretic peptide (ANP), the expression of which is increased after myocardial stretching (Hardy-Rando and Fernandez-Patron, 2019). A previous study reported that upon corticosterone stimulation, astrocytes release "ANPergic vesicles" (vesicles enriched in ANP) (Chatterjee and Sikdar, 2013). In the brain, ANP acts as an inhibitory signal that regulates astrocyte mobility, neuron signaling and blood flow to the brain due to its vasoregulatory action (Chatterjee and Sikdar, 2013). Although no evidence of ANP vesicles has been reported in the heart, it is possible that ANP-containing vesicles constitutes a mechanism of ANP transport and action within the cardiovascular system, as well as modulators of heart-kidney communication and particularly, blood pressure-control.

Atrial natriuretic peptide can influence and suppress the sympathetic activity in the heart through a decrease in the activity

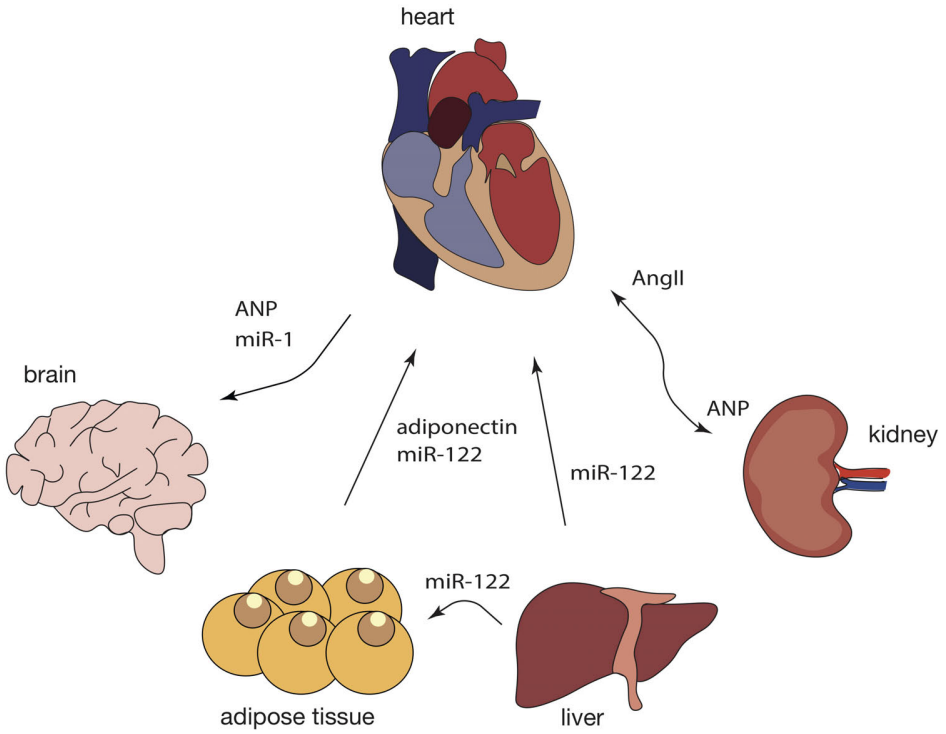

FIGURE 3 | Crosstalk between the heart and peripheral organs during cardiac pathological remodeling. Response to cardiac injury is a multi-organ process as it affects not only the heart but also the brain, kidneys, adipose tissue, and the liver, among others. In turn, a variety of other tissues can contribute to cardiac pathological remodeling, not only by secreting specific chemokines but also by releasing exosomal ncRNAs into the blood stream and further affecting cardiac function through intricate signaling networks. Dashed lines represent findings that need further validation.

of chemo and baroreceptors, which leads to lower heart rate and cardiac output (McGrath et al., 2005). Since adipose tissue presents ANP receptors, the release of ANP by the heart, can trigger lipolysis, energy expenditure and shifting of adipokine production and release (Gruden et al., 2014). In mice subjected to MI, miR-214, typically enriched in adipose-derived regenerative cells (ADRCs), is transferred into cardiomyocytes, where it suppresses apoptotic gene expression such as Bcl-2-like protein 11 (*Bcl2l11*) and solute carrier family 8 member A1 (*Slc8a1*), preventing cardiac rupture (Eguchi et al., 2019). Cardiomyocytes can also uptake miR-214 derived from ADRCs, suggesting that EVs containing miR-214 are endocytosed through a clathrin-mediated endocytosis process triggered by MI-induced hypoxia (Eguchi et al., 2019).

However, the opposite can also occur. For example, in obesity, metabolic stress induces changes in adipose tissue, and increased secretion of adipokines is perceived by the heart and impacts on its function. One of these adipokines, adiponectin, is decrease in several cardiovascular diseases, including MI (Shojaie et al., 2009), and hypertension (Wang et al., 2012; Brambilla et al., 2013). In cardiomyocytes, adiponectin is able to activate the adenosine monophosphate-activated protein kinase signaling pathway inhibiting pressure-overload induced hypertrophy (Turdi et al., 2011).

An increase in heart rate and contractility is regulated by the sympathetic system, namely, postganglionic efferent neurons that communicate with cardiomyocytes by releasing noradrenaline and cause the activation of β-adrenergic receptors (Bang et al., 2015). In contrast, heart rate decrease is under the control of the parasympathetic system *via* acetylcholine, which binds to muscarinic receptors, and dysregulation of these hormones could lead to arrhythmias (Bang et al., 2015).

Besides the adipose tissue and the brain, the heart also communicates with the kidneys through the renin-angiotensin system (RAS), mainly associated with regulation of blood pressure (Jahng et al., 2016). In a healthy heart, low blood pressure stimulates the kidneys to produce renin, which, in turn, leads to increased AngII, followed by sodium and water retention. Finally, an increase in blood volume and increased pressure stimulate cardiomyocytes to release ANP into the circulation, through which it will reach the kidneys (Song et al., 2015). Here, ANP activates excretion of salts and water reducing both blood volume and pressure. In hypertension, this system is overly activated and the heart is not able to decrease the blood pressure, causing continuous secretion of ANP and subsequently maladaptive cardiac remodeling (Orsborne et al., 2017).

Interestingly, not only proteins participate in cardiac inter-organ communication. In obese mice, cardiac injury can be induced by liver-derived exosomal miR-122 (Wang et al., 2019a). MiR-122 is liver-specific and, upon accumulation of visceral fat, miR-122 is released in liver-derived exosomes and transported to the heart, where it interferes with mitochondrial adenosine

triphosphate (ATP) production, and eventually, left ventricle (LV) function (Wang et al., 2019a). Deletion of hepatic miR-122 significantly improved LV function parameters in obese mice (Wang et al., 2019a). This miRNA, by also being enriched in plasmatic exosomes from obese humans, is a promising target against obese-induced cardiac injury.

As discussed before, the heart can also send signals to other organs, including the brain. Upon MI, cardiomyocytes increase the release of exosomes enriched in miR-1 (Sun et al., 2018). These exosomes are carried through the blood flow and incorporated by the hippocampus to induce neuronal microtubule damage (Sun et al., 2018). Genetic ablation of cardiomyocyte-derived miR-1 significantly attenuated neuronal damage in mice subjected to MI, suggesting that miR-1 acts as an endocrine factor (Sun et al., 2018).

To date no other classes of ncRNAs have been reported to have an endocrine effect to or from the heart.

THERAPEUTIC POTENTIAL OF CARDIAC EXOSOMAL ncRNAs

Exosomal ncRNAs constitute a new form of paracrine signaling that seems to be more protected, directed, and therefore, most likely also more efficient. Naturally, exosomes are endogenously produced by cells, but systemic isolation of exosomes that are secreted by one specific cell type is still difficult. Therefore, all the studies reported in this review are based on exosomes that were produced *in vitro* and then administrated *in vivo*. Consequently, these cell culture-derived exosomes are of exogenous origin, relative to the recipient mouse, which, in turn are also able to naturally produce endogenous exosomes. These exogenous exosomes may have an enormous therapeutic potential. In fact, exosomes revolutionized the delivery strategies of therapeutics as the use of these vectors in cell-free medicine will, most likely, overcome the barriers associated with cell transplantation such as contamination and cell death (Toma et al., 2002) and decrease the risk of tumorigenicity and immune rejection (Chen Y. et al., 2017). The smaller size of exosomes allows immediate and easy circulation through capillaries, opposed to what was observed for cell-based therapies such as mesenchymal stem cell (MSC) transplantation, where many cells do not manage to pass the first capillary bed (Phinney and Pittenger, 2017). Exosomes can potentially carry the same miRNA profile of the donor cell, which may potentiate the beneficial effects observed in traditional cell transplantation (Shao et al., 2017). Likewise, in a mouse model of MI it was shown that the protective effect of MSC transplantation was promoted by exosomal miR-125, which, by targeting p53 reduced the apoptotic flux and, consequently, cell death, while its deletion abrogated these effects (Xiao et al., 2018). Transplantation of MSC-derived exosomes alone, revealed to be sufficient to recapitulate MSC-associated beneficial effects. Furthermore, exosomal ncRNA content can be, partially, modulated by transfecting donor cells with a specific ncRNA mimic or inhibitor (Xiao et al., 2018) that will be, in turn, naturally released in exosomes, improving therapy efficacy, as demonstrated by Zhu et al. (2019). The presence of lncRNA *MALAT-1* in exosomes derived from umbilical cord MSCs is able to alter NF-κB signaling and exert cardioprotection in an *in vitro* model of aging (Zhu et al., 2019). The facility in obtaining MSCs, isolating their released exosomes and modeling their miRNA content, are particularly attractive features for their therapeutic use.

In fact, MSCs, have been extensively studied as therapeutic targets for MI, due to their reparative capacity (Przybyt and Harmsen, 2013; Chen L. et al., 2017; Luger et al., 2017). Since transplantation of MSCs has high risks, a therapy based on EVs could be advantageous. Analysis of the MSC-derived exosome contents revealed enrichment of miR-24 and miR-29 and depletion of miR-130, miR-378, and miR-34 (Shao et al., 2017). While the enriched miRNAs positively associate with the regulation of cardiac function, the depleted miRNAs were negative regulators. Interestingly, addition of MSCs-derived exosomes to cardiomyocyte cultures was sufficient to stimulate cardiomyocyte proliferation (Shao et al., 2017). Another study reported that hypoxic preconditioning enhances the protective effect of MSCs, manifested by decreased scar size and improved cardiac function after MI, through exosome-mediated signaling (Zhu et al., 2018). Exosomes secreted by MSCs can be incorporated into cardiac endothelial cells, increase their angiogenic capacity and, ultimately, improve cardiac function (Zhu et al., 2018). MSC-derived exosomes are also enriched in miR-210, known as the "master hypoxamir," (Chan et al., 2012) which overexpression promotes to tube formation but its depletion fails to promote angiogenesis on endothelial cells (Zhu et al., 2018). Furthermore, Wang K. et al. (2017) unraveled that the mechanism whereby endometrium-derived MSCs (EndMSC) can exert their cardiac protective effect is by exosomal release of miRNAs, namely, miR-21. EndMSC secrete miR-21 that is shuttled to both cardiomyocytes and endothelial cells, preventing apoptosis and promoting angiogenesis after MI, respectively (Wang K. et al., 2017).

In turn, lncRNA *H19* was shown to have a paracrine effect upon atorvastatin (AT)-conditioned (MSC) treatment, as AT treatment induced MSCs to produce exosomes that were enriched in lncRNA H19 and miR-675, that once internalized by endothelial cells enhanced their migratory, proliferative and sprouting capacity and therefore, angiogenesis (Huang P. et al., 2019). In fact, in a mouse model of MI, administration of H19-enriched, MSC-derived exosomes, significantly reduced infarct size and increased left ventricle ejection fraction (Huang P. et al., 2019).

Due to their high proliferative capacity, endothelial colony forming-cells (ECFCs), progenitor of endothelial cells, are able to reduce fibrosis after MI, making them an attractive target for cell-based therapies, even though their beneficial effect is hampered under hypoxic conditions (Liu et al., 2018). ECFCs have shown to enhance vascularization by stabilizing the perivascular area and secretion of angiogenic molecules (e.g., VEGF-A), to attenuate fibrosis, and to increase cardiomyocyte survival possibly due to increased expression of IGF-1, an anti-apoptotic factor (Liu et al., 2018). ECFC-derived exosomes are thought to be the mediators of the observed protective effects. Adding exosomes derived from ECFCs exposed to normoxia to cardiac fibroblast cultures, significantly reduced fibroblast activation, TGF-β stimulation, and the fibroblast expression levels of *Col-I*α and α-*SMA*

(Liu et al., 2018). Exposing cardiac fibroblasts to hypoxic ECFCs-derived exosomes increased fibrosis and showed a similar effect to treatment of TGF-β alone. miRNA content analysis revealed miR-10b-5p as the most enriched miRNA in normoxia ECFCs-derived exosomes when compared to hypoxia ECFCs-derived exosomes, which, curiously, targets the downstream factors of the TGF-β pathway, SMAD ubiquitylation regulatory factor 1 (SMURF1) and histone deacetylase 4 (HDAC4) (Liu et al., 2018).

A study reported that intravenously and intraperitoneal injections of exogenous exosomes does not induce toxicity (no body weight or behavioral changes) nor an alteration of hematological and biochemical parameters (Zhu et al., 2017). As EVs were only detectable at low levels in the spleen and not detectable at all in the liver or spleen, this indeed suggests that there is no toxicity or severe immune response (Zhu et al., 2017). Nevertheless, not only is more research needed to draw a conclusion on exosome cardiotoxicity, a better understanding of miRNA off-targets effects is also necessary before exomiRs reach clinical practice.

CONCLUSION

Intercellular communication in the heart contributes to both the maintenance of cardiac function and the development of cardiac pathologies, characterized by cardiac hypertrophy, fibrosis, inflammation, and deficient vasculature. Communication between cardiomyocytes, fibroblasts, inflammatory cells, and endothelial cells in the heart is not unidirectional but bi/multidirectional, as each cell type profoundly influences each other's behavior. Most of the mechanisms driving this cell-to-cell crosstalk are relatively unknown, thus, analyzing the changes in cell signaling upon a pathological stimulus may yield new information to prevent or reverse pathological remodeling. Although intercellular communication can occur in a variety of forms, here we focused on the paracrine signaling through EVs, namely, exosomes. Many reports have been focused on how the modulation of ncRNAs can successfully prevent and even reverse cardiac maladaptive remodeling. Despite the promising value of several miRNAs, lncRNAs, and circRNAs, as new therapeutic targets, to date, miR-122 is the only ncRNA that has reached a phase II clinical trial.

Interestingly, ncRNAs can be loaded into EVs and further incorporated into others cell types, where they are still capable of efficiently exert their action and consequently, trigger a response. However, since the majority of the current studies were based on the isolation of vesicles from cellular cultures, there is a considerable gap in the *in vivo* EV characterization, as well as in understanding their spatial and temporal secretion in the heart. Furthermore, exosomal ncRNAs have an unpredictable toxicity when administrated *in vivo* due to the short-observation span of the majority of the studies. Finally, we believe that understanding and mimicking the action of EVs, by modifying EV ncRNA content, will constitute a future therapeutic target.

AUTHOR CONTRIBUTIONS

RV and PC wrote the manuscript and designed the figures. PC revised the manuscript. Both authors contributed to the article and approved the submitted version.

FUNDING

RV was supported by the Foundation for Science and Technology of Portugal (FCT) grant (SFRH/BD/129507/2017). PC was supported by a Dutch Heart Foundation grant (NHS2015T066).

REFERENCES

Arroyo, J. D., Chevillet, J. R., Kroh, E. M., Ruf, I. K., Pritchard, C. C., Gibson, D. F., et al. (2011). Argonaute2 complexes carry a population of circulating microRNAs independent of vesicles in human plasma. *Proc. Natl. Acad. Sci. U.S.A.* 108, 5003–5008. doi: 10.1073/pnas.1019055108

Bang, C., Antoniades, C., Antonopoulos, A. S., Eriksson, U., Franssen, C., Hamdani, N., et al. (2015). Intercellular communication lessons in heart failure. *Eur. J. Heart Fail.* 17, 1091–1103. doi: 10.1002/ejhf.399

Beltrami, A. P., Barlucchi, L., Torella, D., Baker, M., Limana, F., Chimenti, S., et al. (2003). Adult cardiac stem cells are multipotent and support myocardial regeneration. *Cell* 114, 763–776. doi: 10.1016/s0092-8674(03)00687-1

Bildyug, N. (2019). Extracellular matrix in regulation of contractile system in cardiomyocytes. *Int. J. Mol. Sci.* 20:5054. doi: 10.3390/ijms20205054

Brambilla, P., Antolini, L., Street, M. E., Giussani, M., Galbiati, S., Valsecchi, M. G., et al. (2013). Adiponectin and hypertension in normal-weight and obese children. *Am. J. Hypertens* 26, 257–264. doi: 10.1093/ajh/hps033

Cartledge, J. E., Kane, C., Dias, P., Tesfom, M., Clarke, L., McKee, B., et al. (2015). Functional crosstalk between cardiac fibroblasts and adult cardiomyocytes by soluble mediators. *Cardiovasc. Res.* 105, 260–270. doi: 10.1093/cvr/cvu264

Chan, Y. C., Banerjee, J., Choi, S. Y., and Sen, C. K. (2012). miR-210: the master hypoxamir. *Microcirculation* 19, 215–223. doi: 10.1111/j.1549-8719.2011.00154.x

Chatterjee, S., and Sikdar, S. K. (2013). Corticosterone treatment results in enhanced release of peptidergic vesicles in astrocytes via cytoskeletal rearrangements. *Glia* 61, 2050–2062. doi: 10.1002/glia.22576

Chen, L., Zhang, Y., Tao, L., Yang, Z., and Wang, L. (2017). Mesenchymal stem cells with eNOS over-expression enhance cardiac repair in rats with myocardial infarction. *Cardiovasc. Drugs Ther.* 31, 9–18. doi: 10.1007/s10557-016-6704-z

Chen, M., Xu, R., Rai, A., Suwakulsiri, W., Izumikawa, K., Ishikawa, H., et al. (2019). Distinct shed microvesicle and exosome microRNA signatures reveal diagnostic markers for colorectal cancer. *PLoS One* 14:e0210003. doi: 10.1371/journal.pone.0210003

Chen, S., Shiesh, S. C., Lee, G. B., and Chen, C. (2020). Two-step magnetic bead-based (2MBB) techniques for immunocapture of extracellular vesicles and quantification of microRNAs for cardiovascular diseases: a pilot study. *PLoS One* 15:e0229610. doi: 10.1371/journal.pone.0229610

Chen, Y., Zhao, Y., Chen, W., Xie, L., Zhao, Z. A., Yang, J., et al. (2017). MicroRNA-133 overexpression promotes the therapeutic efficacy of mesenchymal stem cells on acute myocardial infarction. *Stem Cell Res. Ther.* 8:268.

Cochain, C., Channon, K. M., and Silvestre, J. S. (2013). Angiogenesis in the infarcted myocardium. *Antioxid Redox Signal.* 18, 1100–1113. doi: 10.1089/ars.2012.4849

Davis, J., and Molkentin, J. D. (2014). Myofibroblasts: trust your heart and let fate decide. *J. Mol. Cell Cardiol.* 70, 9–18. doi: 10.1016/j.yjmcc.2013.10.019

de Bold, A. J., Borenstein, H. B., Veress, A. T., and Sonnenberg, H. (1981). A rapid and potent natriuretic response to intravenous injection of atrial myocardial extract in rats. *Life Sci.* 28, 89–94. doi: 10.1016/0024-3205(81)90370-2

Dhanoa, J. K., Sethi, R. S., Verma, R., Arora, J. S., and Mukhopadhyay, C. S. (2018). Long non-coding RNA: its evolutionary relics and biological implications in mammals: a review. *J. Anim. Sci. Technol.* 60:25. doi: 10.1016/b978-1-78548-265-6.50002-2

Eguchi, S., Takefuji, M., Sakaguchi, T., Ishihama, S., Mori, Y., Tsuda, T., et al. (2019). Cardiomyocytes capture stem cell-derived, anti-apoptotic microRNA-214 via clathrin-mediated endocytosis in acute myocardial infarction. *J. Biol. Chem.* 294, 11665–11674. doi: 10.1074/jbc.ra119.007537

Fish, J. E., Santoro, M. M., Morton, S. U., Yu, S., Yeh, R. F., Wythe, J. D., et al. (2008). miR-126 regulates angiogenic signaling and vascular integrity. *Dev. Cell* 15, 272–284. doi: 10.1016/j.devcel.2008.07.008

Frey, N., and Olson, E. N. (2003). Cardiac hypertrophy: the good, the bad, and the ugly. *Annu. Rev. Physiol.* 65, 45–79. doi: 10.1146/annurev.physiol.65.092101.142243

Ge, X., Meng, Q., Zhuang, R., Yuan, D., Liu, J., Lin, F., et al. (2019). Circular RNA expression alterations in extracellular vesicles isolated from murine heart post ischemia/reperfusion injury. *Int. J. Cardiol.* 296, 136–140. doi: 10.1016/j.ijcard.2019.08.024

Gogiraju, R., Bochenek, M. L., and Schafer, K. (2019). Angiogenic endothelial cell signaling in cardiac hypertrophy and heart failure. *Front. Cardiovasc. Med.* 6:20. doi: 10.3389/fcvm.2019.00020

Gong, C., and Maquat, L. E. (2011). lncRNAs transactivate STAU1-mediated mRNA decay by duplexing with 3' UTRs via Alu elements. *Nature* 470, 284–288. doi: 10.1038/nature09701

Greene, J., Baird, A. M., Brady, L., Lim, M., Gray, S. G., McDermott, R., et al. (2017). Circular RNAs: biogenesis, function and role in human diseases. *Front. Mol. Biosci.* 4:38. doi: 10.3389/fmolb.2017.00038

Gruden, G., Landi, A., and Bruno, G. (2014). Natriuretic peptides, heart, and adipose tissue: new findings and future developments for diabetes research. *Diabetes Care* 37, 2899–2908. doi: 10.2337/dc14-0669

Gupta, R. A., Shah, N., Wang, K. C., Kim, J., Horlings, H. M., Wong, D. J., et al. (2010). Long non-coding RNA HOTAIR reprograms chromatin state to promote cancer metastasis. *Nature* 464, 1071–1076. doi: 10.1038/nature08975

Halkein, J., Tabruyn, S. P., Ricke-Hoch, M., Haghikia, A., Nguyen, N. Q., Scherr, M., et al. (2013). MicroRNA-146a is a therapeutic target and biomarker for peripartum cardiomyopathy. *J. Clin. Invest.* 123, 2143–2154. doi: 10.1172/jci64365

Hardy-Rando, E., and Fernandez-Patron, C. (2019). Emerging pathways of communication between the heart and non-cardiac organs. *J. Biomed. Res.* 33, 145–155.

Hervera, A., Santos, C. X., De Virgiliis, F., Shah, A. M., and Di Giovanni, S. (2019). Paracrine mechanisms of redox signalling for postmitotic cell and tissue regeneration. *Trends Cell Biol.* 29, 514–530. doi: 10.1016/j.tcb.2019.01.006

Hinger, S. A., Cha, D. J., Franklin, J. L., Higginbotham, J. N., Dou, Y., Ping, J., et al. (2018). Diverse long RNAs are differentially sorted into extracellular vesicles secreted by colorectal cancer Cells. *Cell Rep.* 25, 715.e4–725.e4.

Huang, P., Wang, L., Li, Q., Tian, X., Xu, J., Xu, J., et al. (2019). Atorvastatin enhances the therapeutic efficacy of mesenchymal stem cells derived exosomes in acute myocardial infarction via up-regulating long non-coding RNA H19. *Cardiovasc. Res.* 116, 353–367.

Huang, S., Li, X., Zheng, H., Si, X., Li, B., Wei, G., et al. (2019). Loss of super-enhancer-regulated circRNA Nfix induces cardiac regeneration after myocardial infarction in adult mice. *Circulation* 139, 2857–2876. doi: 10.1161/circulationaha.118.038361

Ignotz, R. A., and Massague, J. (1986). Transforming growth factor-beta stimulates the expression of fibronectin and collagen and their incorporation into the extracellular matrix. *J. Biol. Chem.* 261, 4337–4345.

Jaba, I. M., Zhuang, Z. W., Li, N., Jiang, Y., Martin, K. A., Sinusas, A. J., et al. (2013). NO triggers RGS4 degradation to coordinate angiogenesis and cardiomyocyte growth. *J. Clin. Invest.* 123, 1718–1731. doi: 10.1172/jci65112

Jahng, J. W., Song, E., and Sweeney, G. (2016). Crosstalk between the heart and peripheral organs in heart failure. *Exp. Mol. Med.* 48:e217. doi: 10.1038/emm.2016.20

Kamo, T., Akazawa, H., and Komuro, I. (2015). Cardiac nonmyocytes in the hub of cardiac hypertrophy. *Circ. Res.* 117, 89–98. doi: 10.1161/circresaha.117.305349

Koitabashi, N., Danner, T., Zaiman, A. L., Pinto, Y. M., Rowell, J., Mankowski, J., et al. (2011). Pivotal role of cardiomyocyte TGF-beta signaling in the murine pathological response to sustained pressure overload. *J. Clin. Invest.* 121, 2301–2312. doi: 10.1172/jci44824

Kong, P., Christia, P., and Frangogiannis, N. G. (2014). The pathogenesis of cardiac fibrosis. *Cell Mol. Life Sci.* 71, 549–574.

Lajiness, J. D., and Conway, S. J. (2014). Origin, development, and differentiation of cardiac fibroblasts. *J. Mol. Cell Cardiol.* 70, 2–8. doi: 10.1016/j.yjmcc.2013.11.003

Lee, J. S., Song, D. W., Park, J. H., Kim, J. O., Cho, C., and Kim, D. H. (2017). miR-374 promotes myocardial hypertrophy by negatively regulating vascular endothelial growth factor receptor-1 signaling. *BMB Rep.* 50, 208–213. doi: 10.5483/bmbrep.2017.50.4.165

Lee, R. C., Feinbaum, R. L., and Ambros, V. (1993). The *C. elegans* heterochronic gene lin-4 encodes small RNAs with antisense complementarity to lin-14. *Cell* 75, 843–854. doi: 10.1016/0092-8674(93)90529-y

Leisegang, M. S., Fork, C., Josipovic, I., Richter, F. M., Preussner, J., Hu, J., et al. (2017). Long noncoding RNA MANTIS facilitates endothelial angiogenic function. *Circulation* 136, 65–79. doi: 10.1161/circulationaha.116.026991

Li, Z., and Rana, T. M. (2014). Therapeutic targeting of microRNAs: current status and future challenges. *Nat. Rev. Drug Discov.* 13, 622–638. doi: 10.1038/nrd4359

Liao, B., Chen, R., Lin, F., Mai, A., Chen, J., Li, H., et al. (2018). Long noncoding RNA HOTTIP promotes endothelial cell proliferation and migration via activation of the Wnt/beta-catenin pathway. *J. Cell Biochem.* 119, 2797–2805. doi: 10.1002/jcb.26448

Liu, W., Zhang, H., Mai, J., Chen, Z., Huang, T., Wang, S., et al. (2018). Distinct anti-fibrotic effects of exosomes derived from endothelial colony-forming cells cultured under normoxia and hypoxia. *Med. Sci. Monit.* 24, 6187–6199. doi: 10.12659/msm.911306

Luger, D., Lipinski, M. J., Westman, P. C., Glover, D. K., Dimastromatteo, J., Frias, J. C., et al. (2017). Intravenously delivered mesenchymal stem cells: systemic anti-inflammatory effects improve left ventricular dysfunction in acute myocardial infarction and ischemic cardiomyopathy. *Circ. Res.* 120, 1598–1613. doi: 10.1161/circresaha.117.310599

Lyon, R. C., Zanella, F., Omens, J. H., and Sheikh, F. (2015). Mechanotransduction in cardiac hypertrophy and failure. *Circ. Res.* 116, 1462–1476. doi: 10.1161/circresaha.116.304937

Mathew, J., Sleight, P., Lonn, E., Johnstone, D., Pogue, J., Yi, Q., et al. (2001). Reduction of cardiovascular risk by regression of electrocardiographic markers of left ventricular hypertrophy by the angiotensin-converting enzyme inhibitor ramipril. *Circulation* 104, 1615–1621. doi: 10.1161/hc3901.096700

Matsumoto, A., Pasut, A., Matsumoto, M., Yamashita, R., Fung, J., Monteleone, E., et al. (2017). mTORC1 and muscle regeneration are regulated by the LINC00961-encoded SPAR polypeptide. *Nature* 541, 228–232. doi: 10.1038/nature21034

McGrath, M. F., de Bold, M. L., and de Bold, A. J. (2005). The endocrine function of the heart. *Trends Endocrinol. Metab.* 16, 469–477.

Michel, J. B. (2003). Anoikis in the cardiovascular system: known and unknown extracellular mediators. *Arterioscler Thromb. Vasc. Biol.* 23, 2146–2154. doi: 10.1161/01.atv.0000099882.52647.e4

Morelli, M. B., Shu, J., Sardu, C., Matarese, A., and Santulli, G. (2019). Cardiosomal microRNAs are essential in post-infarction myofibroblast phenoconversion. *Int. J. Mol. Sci.* 21:201. doi: 10.3390/ijms21010201

Nakamura, S., Naruse, M., Naruse, K., Kawana, M., Nishikawa, T., Hosoda, S., et al. (1991). Atrial natriuretic peptide and brain natriuretic peptide coexist in the secretory granules of human cardiac myocytes. *Am. J. Hypertens* 4, 909–912. doi: 10.1093/ajh/4.11.909

Njock, M. S., Cheng, H. S., Dang, L. T., Nazari-Jahantigh, M., Lau, A. C., Boudreau, E., et al. (2015). Endothelial cells suppress monocyte activation through secretion of extracellular vesicles containing antiinflammatory microRNAs. *Blood* 125, 3202–3212. doi: 10.1182/blood-2014-11-611046

Orsborne, C., Chaggar, P. S., Shaw, S. M., and Williams, S. G. (2017). The renin-angiotensin-aldosterone system in heart failure for the non-specialist: the past, the present and the future. *Postgrad. Med. J.* 93, 29–37. doi: 10.1136/postgradmedj-2016-134045

Osada-Oka, M., Shiota, M., Izumi, Y., Nishiyama, M., Tanaka, M., Yamaguchi, T., et al. (2017). Macrophage-derived exosomes induce inflammatory factors in endothelial cells under hypertensive conditions. *Hypertens Res.* 40, 353–360. doi: 10.1038/hr.2016.163

Phinney, D. G., and Pittenger, M. F. (2017). Concise review: MSC-Derived exosomes for cell-free therapy. *Stem Cells* 35, 851–858. doi: 10.1002/stem.2575

Piccoli, M. T., Gupta, S. K., Viereck, J., Foinquinos, A., Samolovac, S., Kramer, F. L., et al. (2017). Inhibition of the cardiac fibroblast-enriched lncRNA Meg3 prevents cardiac fibrosis and diastolic dysfunction. *Circ. Res.* 121, 575–583. doi: 10.1161/circresaha.117.310624

Prabhu, S. D., and Frangogiannis, N. G. (2016). The biological basis for cardiac repair after myocardial infarction: from inflammation to fibrosis. *Circ. Res.* 119, 91–112. doi: 10.1161/circresaha.116.303577

Przybyt, E., and Harmsen, M. C. (2013). Mesenchymal stem cells: promising for myocardial regeneration? *Curr. Stem Cell Res. Ther.* 8, 270–277. doi: 10.2174/1574888x11308040002

Pu, W. T., Ma, Q., and Izumo, S. (2003). NFAT transcription factors are critical survival factors that inhibit cardiomyocyte apoptosis during phenylephrine stimulation in vitro. *Circ. Res.* 92, 725–731. doi: 10.1161/01.res.0000069211.82346.46

Raposo, G., and Stoorvogel, W. (2013). Extracellular vesicles: exosomes, microvesicles, and friends. *J. Cell Biol.* 200, 373–383. doi: 10.1083/jcb.201211138

Samak, M., Fatullayev, J., Sabashnikov, A., Zeriouh, M., Schmack, B., Farag, M., et al. (2016). Cardiac hypertrophy: an introduction to molecular and cellular basis. *Med. Sci. Monit. Basic Res.* 22, 75–79.

Santosh, B., Varshney, A., and Yadava, P. K. (2015). Non-coding RNAs: biological functions and applications. *Cell Biochem. Funct.* 33, 14–22. doi: 10.1002/cbf.3079

Shao, L., Zhang, Y., Lan, B., Wang, J., Zhang, Z., Zhang, L., et al. (2017). MiRNA-sequence indicates that mesenchymal stem cells and exosomes have similar mechanism to enhance cardiac repair. *Biomed. Res. Int.* 2017:4150705.

Shojaie, M., Sotoodah, A., and Shafaie, G. (2009). Is adiponectin associated with acute myocardial infarction in Iranian non obese patients? *Lipids Health Dis.* 8:17. doi: 10.1186/1476-511x-8-17

Song, W., Wang, H., and Wu, Q. (2015). Atrial natriuretic peptide in cardiovascular biology and disease (NPPA). *Gene* 569, 1–6. doi: 10.1016/j.gene.2015.06.029

Su, S. A., Xie, Y., Fu, Z., Wang, Y., Wang, J. A., and Xiang, M. (2017). Emerging role of exosome-mediated intercellular communication in vascular remodeling. *Oncotarget* 8, 25700–25712. doi: 10.18632/oncotarget.14878

Sun, L. L., Duan, M. J., Ma, J. C., Xu, L., Mao, M., Biddyut, D., et al. (2018). Myocardial infarction-induced hippocampal microtubule damage by cardiac originating microRNA-1 in mice. *J. Mol. Cell Cardiol.* 120, 12–27. doi: 10.1016/j.yjmcc.2018.05.009

Tabet, F., Vickers, K. C., Cuesta Torres, L. F., Wiese, C. B., Shoucri, B. M., Lambert, G., et al. (2014). HDL-transferred microRNA-223 regulates ICAM-1 expression in endothelial cells. *Nat. Commun.* 5:3292.

Ti, D., Hao, H., Tong, C., Liu, J., Dong, L., Zheng, J., et al. (2015). LPS-preconditioned mesenchymal stromal cells modify macrophage polarization for resolution of chronic inflammation via exosome-shuttled let-7b. *J. Transl. Med.* 13:308.

Tian, C., Gao, L., Zimmerman, M. C., and Zucker, I. H. (2018). Myocardial infarction-induced microRNA-enriched exosomes contribute to cardiac Nrf2 dysregulation in chronic heart failure. *Am. J. Physiol. Heart Circ. Physiol.* 314, H928–H939.

Toma, C., Pittenger, M. F., Cahill, K. S., Byrne, B. J., and Kessler, P. D. (2002). Human mesenchymal stem cells differentiate to a cardiomyocyte phenotype in the adult murine heart. *Circulation* 105, 93–98. doi: 10.1161/hc0102.101442

Turdi, S., Kandadi, M. R., Zhao, J., Huff, A. F., Du, M., and Ren, J. (2011). Deficiency in AMP-activated protein kinase exaggerates high fat diet-induced cardiac hypertrophy and contractile dysfunction. *J. Mol. Cell Cardiol.* 50, 712–722. doi: 10.1016/j.yjmcc.2010.12.007

Uchida, S., and Dimmeler, S. (2015). Long noncoding RNAs in cardiovascular diseases. *Circ. Res.* 116, 737–750. doi: 10.1161/circresaha.116.302521

Wang, C., Zhang, C., Liu, L., Xi, A., Chen, B., Li, Y., et al. (2017). Macrophage-derived mir-155-containing exosomes suppress fibroblast proliferation and promote fibroblast inflammation during cardiac injury. *Mol. Ther.* 25, 192–204. doi: 10.1016/j.ymthe.2016.09.001

Wang, K., Jiang, Z., Webster, K. A., Chen, J., Hu, H., Zhou, Y., et al. (2017). Enhanced cardioprotection by human endometrium mesenchymal stem cells driven by exosomal MicroRNA-21. *Stem Cells Transl. Med.* 6, 209–222. doi: 10.5966/sctm.2015-0386

Wang, L., Manson, J. E., Gaziano, J. M., Liu, S., Cochrane, B., Cook, N. R., et al. (2012). Plasma adiponectin and the risk of hypertension in white and black postmenopausal women. *Clin. Chem.* 58, 1438–1445. doi: 10.1373/clinchem.2012.191080

Wang, S., Aurora, A. B., Johnson, B. A., Qi, X., McAnally, J., Hill, J. A., et al. (2008). The endothelial-specific microRNA miR-126 governs vascular integrity and angiogenesis. *Dev. Cell* 15, 261–271. doi: 10.1016/j.devcel.2008.07.002

Wang, X., Huang, W., Liu, G., Cai, W., Millard, R. W., Wang, Y., et al. (2014). Cardiomyocytes mediate anti-angiogenesis in type 2 diabetic rats through the exosomal transfer of miR-320 into endothelial cells. *J. Mol. Cell Cardiol.* 74, 139–150. doi: 10.1016/j.yjmcc.2014.05.001

Wang, Y., Jin, P., Liu, J., and Xie, X. (2019a). Exosomal microRNA-122 mediates obesity-related cardiomyopathy through suppressing mitochondrial ADP-ribosylation factor-like 2. *Clin. Sci.* 133, 1871–1881. doi: 10.1042/cs20190558

Wang, Y., Zhao, R., Liu, W., Wang, Z., Rong, J., Long, X., et al. (2019b). Exosomal circHIPK3 released from hypoxia-pretreated cardiomyocytes regulates oxidative damage in cardiac microvascular endothelial Cells via the miR-29a/IGF-1 pathway. *Oxid Med. Cell Longev.* 2019:7954657.

Xia, Y., Lee, K., Li, N., Corbett, D., Mendoza, L., and Frangogiannis, N. G. (2009). Characterization of the inflammatory and fibrotic response in a mouse model of cardiac pressure overload. *Histochem. Cell Biol.* 131, 471–481. doi: 10.1007/s00418-008-0541-5

Xiao, C., Wang, K., Xu, Y., Hu, H., Zhang, N., Wang, Y., et al. (2018). Transplanted mesenchymal stem cells reduce autophagic flux in infarcted hearts via the exosomal transfer of miR-125b. *Circ. Res.* 123, 564–578. doi: 10.1161/circresaha.118.312758

Xin, M., Olson, E. N., and Bassel-Duby, R. (2013). Mending broken hearts: cardiac development as a basis for adult heart regeneration and repair. *Nat. Rev. Mol. Cell Biol.* 14, 529–541. doi: 10.1038/nrm3619

Xu, R., Zhang, F., Chai, R., Zhou, W., Hu, M., Liu, B., et al. (2019). Exosomes derived from pro-inflammatory bone marrow-derived mesenchymal stem cells reduce inflammation and myocardial injury via mediating macrophage polarization. *J. Cell Mol. Med.* 23, 7617–7631. doi: 10.1111/jcmm.14635

Yanagisawa-Miwa, A., Uchida, Y., Nakamura, F., Tomaru, T., Kido, H., Kamijo, T., et al. (1992). Salvage of infarcted myocardium by angiogenic action of basic fibroblast growth factor. *Science* 257, 1401–1403. doi: 10.1126/science.1382313

Yang, H. H., Chen, Y., Gao, C. Y., Cui, Z. T., and Yao, J. M. (2017). Protective effects of MicroRNA-126 on human cardiac microvascular endothelial cells against Hypoxia/Reoxygenation-induced injury and inflammatory response by activating PI3K/Akt/eNOS signaling pathway. *Cell Physiol. Biochem.* 42, 506–518. doi: 10.1159/000477597

Yang, W., Han, Y., Yang, C., Chen, Y., Zhao, W., Su, X., et al. (2019). MicroRNA-19b-1 reverses ischaemia-induced heart failure by inhibiting cardiomyocyte apoptosis and targeting Bcl2 l11/BIM. *Heart Vessels* 34, 1221–1229. doi: 10.1007/s00380-018-01336-3

Yuan, J., Liu, H., Gao, W., Zhang, L., Ye, Y., Yuan, L., et al. (2018). MicroRNA-378 suppresses myocardial fibrosis through a paracrine mechanism at the early stage of cardiac hypertrophy following mechanical stress. *Theranostics* 8, 2565–2582. doi: 10.7150/thno.22878

Zhang, H., Freitas, D., Kim, H. S., Fabijanic, K., Li, Z., Chen, H., et al. (2018). Identification of distinct nanoparticles and subsets of extracellular vesicles by asymmetric flow field-flow fractionation. *Nat. Cell Biol.* 20, 332–343.

Zhao, J., Li, X., Hu, J., Chen, F., Qiao, S., Sun, X., et al. (2019). Mesenchymal stromal cell-derived exosomes attenuate myocardial ischaemia-reperfusion injury through miR-182-regulated macrophage polarization. *Cardiovasc. Res.* 115, 1205–1216. doi: 10.1093/cvr/cvz040

Zhou, B., and Yu, J. W. (2017). A novel identified circular RNA, circRNA_010567, promotes myocardial fibrosis via suppressing miR-141 by targeting TGF-beta1. *Biochem. Biophys. Res. Commun.* 487, 769–775. doi: 10.1016/j.bbrc.2017.04.044

Zhou, P., and Pu, W. T. (2016). Recounting cardiac cellular composition. *Circ. Res.* 118, 368–370. doi: 10.1161/circresaha.116.308139

Zhou, X. L., Xu, H., Liu, Z. B., Wu, Q. C., Zhu, R. R., and Liu, J. C. (2018). miR-21 promotes cardiac fibroblast-to-myofibroblast transformation and myocardial fibrosis by targeting Jagged1. *J. Cell Mol. Med.* 22, 3816–3824. doi: 10.1111/jcmm.13654

Zhu, B., Zhang, L., Liang, C., Liu, B., Pan, X., Wang, Y., et al. (2019). Stem cell-derived exosomes prevent aging-induced cardiac dysfunction through a novel exosome/lncRNA MALAT1/NF-kappaB/TNF-alpha signaling pathway. *Oxid. Med. Cell Longev.* 2019:9739258.

Zhu, J., Lu, K., Zhang, N., Zhao, Y., Ma, Q., Shen, J., et al. (2018). Myocardial reparative functions of exosomes from mesenchymal stem cells are enhanced by hypoxia treatment of the cells via transferring microRNA-210 in an nSMase2-dependent way. *Artif. Cells Nanomed. Biotechnol.* 46, 1659–1670.

Zhu, X., Badawi, M., Pomeroy, S., Sutaria, D. S., Xie, Z., Baek, A., et al. (2017). Comprehensive toxicity and immunogenicity studies reveal minimal effects in mice following sustained dosing of extracellular vesicles derived from HEK293T cells. *J. Extracell Vesicles.* 6:1324730. doi: 10.1080/20013078.2017.1324730

Conflict of Interest: PC is a cofounder of Mirabilis Therapeutics.

The remaining author declares that the research was conducted in the absence of any commercial or financial relationships that could be construed as a potential conflict of interest.

frontiers in Physiology

BRIEF RESEARCH REPORT
published: 16 September 2020
doi: 10.3389/fphys.2020.553198

Skeletal Muscle-Derived Human Mesenchymal Stem Cells: Influence of Different Culture Conditions on Proliferative and Myogenic Capabilities

Stefano Testa[1†], Carles Sánchez Riera[1†], Ersilia Fornetti[1], Federica Riccio[1], Claudia Fuoco[1], Sergio Bernardini[1], Jacopo Baldi[2], Marco Costantini[3], Maria Laura Foddai[2], Stefano Cannata[1]* and Cesare Gargioli[1]**

[1]Department of Biology, University of Rome Tor Vergata, Rome, Italy, [2]IRCCS Regina Elena National Cancer Institute, Rome, Italy, [3]Institute of Physical Chemistry, Polish Academy of Sciences, Warsaw, Poland

Skeletal muscle tissue is characterized by restrained self-regenerative capabilities, being ineffective in relation to trauma extension both in time span (e.g., chronic diseases) and in size (e.g., large trauma). For these reasons, tissue engineering and/or cellular therapies represent a valuable solution in the cases where the physiological healing process failed. Satellite cells, the putative skeletal muscle stem cells, have been the first solution explored to remedy the insufficient self-regeneration capacity. Nevertheless, some limitation related to donor age, muscle condition, expansion hitch, and myogenic potentiality maintenance have limited their use as therapeutic tool. To overcome this hindrance, different stem cells population with myogenic capabilities have been investigated to evaluate their real potentiality for therapeutic approaches, but, as of today, the perfect cell candidate has not been identified yet. In this work, we analyze the characteristics of skeletal muscle-derived human Mesenchymal Stem Cells (hMSCs), showing the maintenance/increment of myogenic activity upon differential culture conditions. In particular, we investigate the influence of a commercial enriched growth medium (Cyto-Grow), and of a medium enriched with either human-derived serum (H.S.) or human Platelet-rich Plasma (PrP), in order to set up a culture protocol useful for employing this cell population in clinical therapeutic strategies. The presented results reveal that both the enriched medium (Cyto-Grow) and the human-derived supplements (H.S. and PrP) have remarkable effects on hMSCs proliferation and myogenic differentiation compared to standard condition, uncovering the real possibility to exploit these human derivatives to ameliorate stem cells yield and efficacy.

Keywords: skeletal muscle, mesenchymal stem cells, myogenic differentiation, human serum, platelet-rich plasma

OPEN ACCESS

Edited by:
Martina Calore,
Maastricht University, Netherlands

Reviewed by:
Xu Yan,
Victoria University, Australia
Alberto Malerba,
Royal Holloway, University of London, United Kingdom

***Correspondence:**
Maria Laura Foddai
marialaura.foddai@ifo.gov.it;
marialaura.foddai@gmail.com
Stefano Cannata
cannata@uniroma2.it
Cesare Gargioli
cesare.gargioli@uniroma2.it

[†]These authors have contributed equally to this work

Specialty section:
This article was submitted to Clinical and Translational Physiology, a section of the journal Frontiers in Physiology

Received: *17 April 2020*
Accepted: *12 August 2020*
Published: *16 September 2020*

Citation:
Testa S, Riera CS, Fornetti E, Riccio F, Fuoco C, Bernardini S, Baldi J, Costantini M, Foddai ML, Cannata S and Gargioli C (2020) Skeletal Muscle-Derived Human Mesenchymal Stem Cells: Influence of Different Culture Conditions on Proliferative and Myogenic Capabilities. Front. Physiol. 11:553198. doi: 10.3389/fphys.2020.553198

INTRODUCTION

The self-regenerative process of skeletal muscle tissue is a complex phenomenon that engages several types of resident and circulating stem cells with different potentialities (Yin et al., 2013; Čamernik et al., 2018). Among all of these cell types, the most important involved in the repairing process are satellite (Mauro, 1961) and non-satellite cell populations (Crisan et al., 2008; Sacchetti et al., 2016). While the former has been well characterized in the last decades and their activation mechanism unraveled relying on satellite cell niche regulation by the complex interaction among Notch, Collagen V, and Calcitonin receptor (Baghdadi et al., 2018), the latter are gaining increasing interest in the research community thanks to readiness of isolation and expansion, and last but not least the better migratory capacity (Rando et al., 1995; Ferrari et al., 1998; Sacco et al., 2008).

Notably, mesenchymal stem cells (MSCs) are a heterogeneous population composed of satellite and non-satellite cells, the latter including interstitial cells called $PW1^+/Pax7^-$ interstitial cells (PICs; Mitchell et al., 2010), fibro-adipogenic progenitors (FAPs; Uezumi et al., 2010), muscle side population cells (SP), and muscle resident pericytes (Gussoni et al., 1999; Kumar et al., 2017).

MSCs were initially described in the bone marrow as bone marrow-derived mesenchymal stromal/stem cells (BM-MSCs) for their unique combination of features, which include fibroblast-like morphology, clonogenicity, multipotency, and *in vitro* adherence on plastic surface unlike the hematopoietic counterpart (Friedenstein et al., 1970; Pittenger et al., 1999). Cells with similar *in vitro* abilities have been isolated from numerous adult tissues and organs, including skeletal muscle, both from small mammals and human biopsies (Hass et al., 2011; Čamernik et al., 2018). So far, the most popular and studied tissue source employed for MSC isolation has been the bone marrow thanks to its availability and accessibility in the human body. Nevertheless, over the last decade other tissue sources have been explored such as fat tissue, umbilical cord, dental pulp, skin, placenta, and even brain (Yamada et al., 2010; Appaix, 2014; Orciani et al., 2014; Li et al., 2015; Bieback and Netsch, 2016; Pelekanos et al., 2016; Amati et al., 2017). Despite heterogeneity primarily due to different isolation tissue sources, MSCs maintain characteristic expression markers such as CD90, CD44, CD73, CD29, and CD105 while missing the hematopoietic ones such as CD34, CD45, and CD11 (Haynesworth et al., 1992; Lodie et al., 2002; Suva et al., 2004). Besides, they retain and share similar differentiation potential in mesoderm-lineage tissues including bone, fat, cartilage, and skeletal muscle (Okamoto et al., 2002; Sottile et al., 2002; Zhang et al., 2009; Almalki and Agrawal, 2016; Kozlowska et al., 2019).

As regards skeletal muscle tissue, BM-MSCs differentiate into myogenic lineage exclusively upon exposure to demethylating agent 5-azacytidine (Wakitani et al., 1995; Jackson et al., 2007) or in co-culture with myocytes (Lee et al., 2005). More recently, Sacchetti and collaborators have demonstrated that skeletal muscle-derived MSCs have, beyond an intrinsic heterogeneity, spontaneous and important myogenic capabilities *in vitro* and *in vivo*. Moreover, the authors have shown that the differentiation potentiality may vary radically according with the tissue origin and that MSCs immune-profile does not reflect identical cells and function (Sacchetti et al., 2016). Human MSCs (hMSCs), due to their multiple potentialities, could still represent a good candidate for cell therapy (De Bari et al., 2003; Oppermann et al., 2014; Klimczak et al., 2018; Pittenger et al., 2019). Hence, in order to translate MSCs into the actual clinical scenario, researchers still need to address a long-standing challenge: to produce *in vitro* a clinically relevant number of cells without affecting their differentiation capacity. Moreover, culture conditions should be standardized to fulfill good manufacturing practice (GMP) protocols and to avoid possible contamination or immunological reactions due to xenogeneic medium supplement, e.g., animal derived sera (Tonti and Mannello, 2008). In fact, as demonstrated in numerous studies, the expansion of hMSCs strongly depends on the culture conditions, being anchorage-dependent and requiring medium supplemented with 10–20% serum (De Bari et al., 2003; Meuleman et al., 2006; Čamernik et al., 2018; Musiał-Wysocka et al., 2019). Additionally, interactions among cells, growth surface, and surrounding medium influence many aspects of cell behavior, such as efficiency of isolation, proliferation rate, maintenance in culture, stemness, and differentiation potentiality (Kozlowska et al., 2019; Musiał-Wysocka et al., 2019).

Given all these key aspects, over the past years a growing interest has been focused on biologic agents such as platelet-rich plasma (PrP) to complement the cell culture medium and/or significantly ameliorate musculoskeletal tissue healing (Hamid et al., 2014; Kunze et al., 2019). However, their real beneficial effect is still questioned (Grassi et al., 2018).

In order to shed some light on the potentialities of skeletal muscle-derived hMSCs for skeletal muscle regeneration, here we compare different culture conditions evaluating immunophenotypical aspect, cell growth, and myogenic differentiation capability. The obtained results show the possibility to ameliorate hMSCs proliferation and differentiation capabilities adding human-derived supplements (H.S. and PrP) to basic medium or employing enriched growth medium (Cyto-Grow) for human stem cells culturing.

MATERIALS AND METHODS

Isolation of Mesenchymal Stem Cells From Muscle Biopsies and Cell Culture and Differentiation

hMSCs were isolated from skeletal muscle tissue using a protocol that includes mechanical mincing, enzymatic digestion with type II collagenase, filtration, and selection of the colonies on plastic surface at low confluence (Sacchetti et al., 2016; Vono et al., 2016). Briefly, human skeletal muscle biopsies were finely minced with a surgical knife and collected in a solution of collagenase type II (100 U/ml in PBS Ca^{2+}/Mg^{2+}), subsequently left to incubate in a thermal shaker for 45 min at 37°C. After digestion, the solution was centrifuged at 300 *g* for 10 min at room temperature (RT) and then aspirated without disturbing the pellet. The pellet was then resuspended in 15 ml of PBS and filtered through progressively finer cell strainers: 100, 70, and 40 μm. Cells were counted with a Burker

counting chamber and plated on conventional Petri dishes (BD Falcon) at low confluence (10^3 cells/cm^2) to promote the growth of cells that had clonogenicity and therefore stem potentiality. The freshly isolated MSCs were divided into two experimental groups respectively cultured in either α-MEM (Gibco) supplemented with 20% heat-inactivated fetal bovine serum (FBS, EuroClone), penicillin (100 IU/ml, Gibco) and streptomycin (100 mg/ml, Gibco), or Cyto-Grow medium (Resnova) supplemented with penicillin (100 IU/ml, Gibco) and streptomycin (100 mg/ml, Gibco). In both conditions, cells were cultured at 37°C and 5% CO_2 and left to incubate for 15 days, the time required for colonies formation. After colonies formation, cells were expanded for both flow cytometric and differentiation analysis. In particular, differentiation was achieved spontaneously once the culture reached a cell confluence of 80%, without needing differentiation medium or specific factors. Alternatively, freshly isolated cells and colonies were harvested and used for flow cytometry analysis.

Flow Cytometry Analysis

The 1×10^6 cells for each experimental condition were harvested with Lonza™ Trypsin-Versene™-Trypsin-EDTA (Fisher Scientific, #BE17-161E), resuspended and centrifuged at 300 *g* for 10 min at RT. Cells were washed twice with PBS supplemented with BSA 0.5% (Bovine Serum Albumin, AppliChem, #A1391) and EDTA 2 mM at 300 g for 10 min at 4°C. Samples were then resuspended in PBS and incubated with APC-A700 anti-human CD56 (N901, #B92446 Beckman Coulter), APC-A750 anti-human CD90 (Thy-1/310, #B36121 Beckman Coulter), and Vioblue anti-human CD45 antibodies (REA747, #5180719178 Miltenyi Biotec) for 30 min at 4°C. After incubation, cells were washed in PBS, centrifuged at 300 *g* for 10 min at 4°C, and resuspended in PBS. Samples were visualized on Cytoflex S, 3 lasers (488, 405, and 638 nm), and 13 detectors (Beckman Coulter). Live cells were gated based on side scatter and forward scatter. Data were analyzed by CytExpert software (Beckman Coulter).

Growth Curves

Growth curves were obtained using 48-well plates containing 2×10^4 cells/well. Three wells of the 48-well plates were prepared for every experimental point (2, 5, 7, and 9 days) and every experimental condition: (i) α-MEM supplemented with 20% FBS (control), (ii) 5% human serum (low-H.S.), (iii) 10% human serum (medium-H.S.), (iv) 20% human serum (high-H.S.), (v) 5×10^5 platelets/ml (low-PrP), (vi) 1×10^6 platelets/ml (medium-PrP) and 1.5×10^6 platelets/ml (high-PrP). Human serum (H.S.) and PrP were provided by Dr. Foddai. Serum was obtained from a sample of whole blood donor (ranging from 30 to 60 years old). Ten milliliter of venous blood is yielded without addition of anticoagulant, and each blood sample is prepared by centrifugation (5' at 3000 RPM and 15°C) to separate red blood cells from serum. The obtained serum was transferred to an empty sterile tube and criopreserved at −80°C.

The PrP was a cell concentrate of leucodepleted platelets suspended in plasma, obtained from single donor of blood subjected to a platelet apheresis procedure using a Fresenius Kabi Amicus cell separator. An aliquot of cell concentrate is transferred into a sterile falcon and brought to different concentration: 0.5×10^5/ml, 1.0×10^5/ml, and 1.5×10^5/ml. Cellular proliferation was evaluated by harvesting cells at each time point and scoring the media in a Burker counting chamber.

Immunofluorescence Analysis

Cells were fixed with 4% PFA in PBS for 10 min at 4°C and processed for immunofluorescence analysis as previously described (Testa et al., 2017). Briefly, cells were washed with PBS and blocked with 10% goat serum in PBS for 1 h at RT. Subsequently, cells were incubated with the primary antibody anti-myosin heavy chain (MF20, mouse monoclonal, DHSB, diluted 1:2) or anti-ki67 (rabbit polyclonal, Novus Biologicals #NB110-89717, diluted 1:200) for 1 h, followed by incubation with Alexa Fluor 555-conjugated goat anti-mouse IgG (H + L; Thermo Fisher Scientific #A21422, diluted 1:400) and 488-conjugated goat anti-rabbit IgG (H + L; Thermo Fisher Scientific #A11008, diluted 1:400) for 1 h. Finally, nuclei were stained with 300 nM DAPI (Thermo Fisher Scientific) for 10 min. Specimens were viewed using a Nikon TE 2000 epifluorescence microscope equipped with a Photometrics Cool SNAP MYO CCD camera.

Statistical Analysis

All experiments were performed in biological and technical triplicate ($n = 9$). Data were analyzed using GraphPad Prism 7, and values were expressed as means ± standard error (SEM). Statistical significance was tested using either ONE WAY ANOVA and Tukey's *post hoc* test or *t*-test when only two parameters were compared. A probability of less than 5% ($p < 0.05$) was considered to be statistically significant.

RESULTS

Influence of Different Culture Media on CD90 Expression, Proliferation, and Myogenic Capabilities of Skeletal Muscle-Derived hMSCs

Mononucleated cells from human derived skeletal muscle biopsies were examined at different time points by flow cytometry analysis in order to test whether different culture media would affect cell populations heterogeneity and behavior. In this regard, hMSCs were divided in two experimental groups according to the differential culture conditions: (i) α-MEM supplemented with 20% of FBS (standard medium) or (ii) Cyto-Grow (rich medium). The two experimental groups were analyzed at different time points (t0–t3) starting from isolation up to late doubling time, namely: total mononucleated cells soon after isolation from fresh muscle biopsy (t0), colonies formation stage according to MSCs conduct (after 15 days on standard plastic culture; Sacchetti et al., 2007, 2016; t1), expansion passage 3 (t2), and expansion passage 9 (t3; **Figure 1**). Cells were, accordingly, analyzed by flow cytometry analysis to evaluate the expression of hMSCs stemness marker CD90 as indicated by Kisselbach and colleagues (Kisselbach et al., 2009) and the human muscle

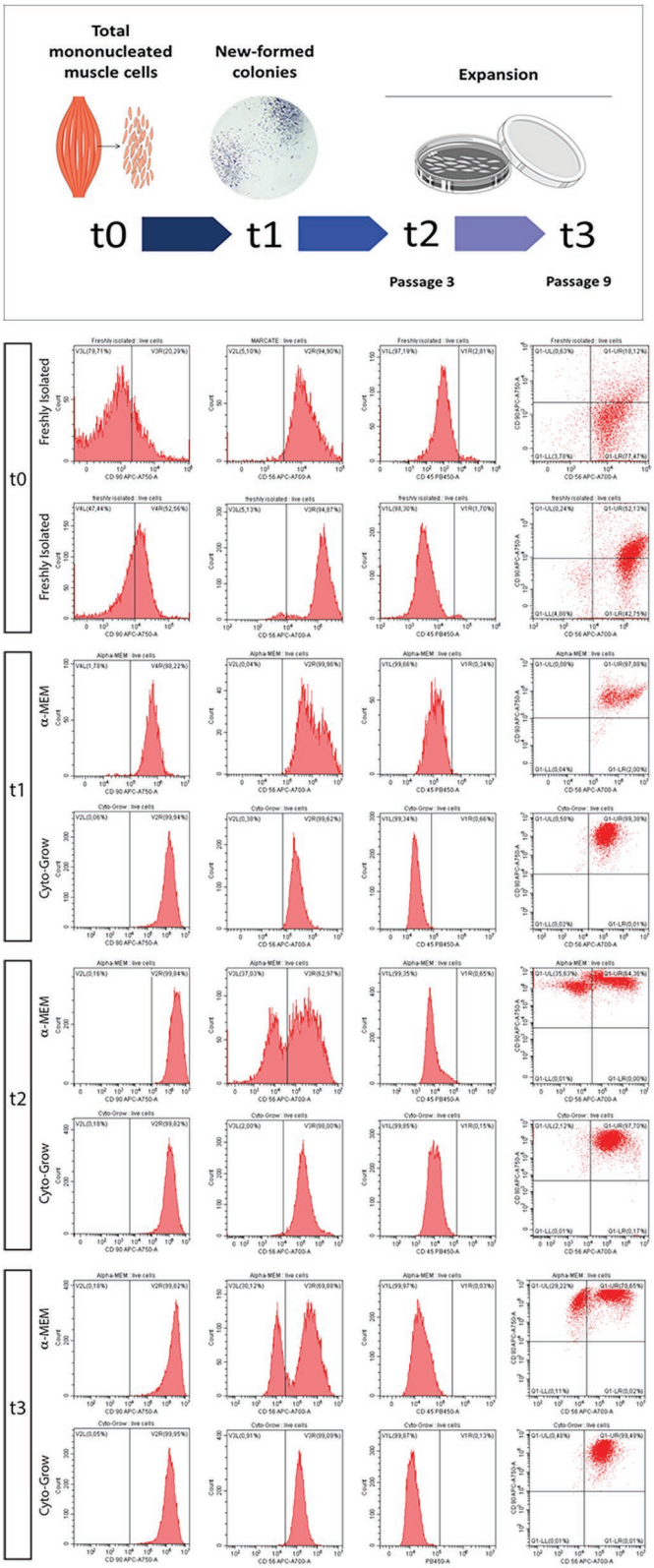

FIGURE 1 | Human MSC (hMSC) characterization by flow cytometric analysis. Scheme representing the time points analyzed in the flow cytometric analysis, from skeletal muscle-derived hMSCs isolation up to late doubling time: total mononucleated cells freshly isolated from the tissue (t0), new formed colonies after 15 days (t1), expansion passage 3 (t2), and expansion passage 9 (t3). Flow cytometry analysis for CD56, CD90, and CD45 in relation to different culture media: α-MEM and Cyto-Grow, showing the histograms of the signal for each antibody used and the dot plot displaying the double positivity for CD90 and CD56.

marker CD56 (labeling human myogenic cells), further using CD45 as a negative marker (hematopoietic compartment). Analysis at t0 revealed a heterogeneous population of mononucleated cells, presenting several stem cells CD90$^+$ (15.75%) together with abundant myogenic cells CD56$^+$ (76.65%) displayed in the dot-plot, besides hematopoietic stem cells positive for CD45 (11.45%; **Figure 1**, t0). Hence, t0 population has been split and cultured in two different media (α-MEM or Cyto-Grow, used in the following stages) revealing differences in terms of marker expression already at t1. Here, the colonies formed in standard medium presented the tendency to segregate in two subpopulations: one exclusively CD90$^+$ and the other one double positive CD56$^+$/CD90$^+$. Differently, cells cultured in rich medium formed a more homogeneous double positive population CD56$^+$/CD90$^+$ (**Figure 1**, t1). At t2, in standard medium, two well distinct cell subpopulations became more evident reaching at t3 29.22% of CD90$^+$ cells and 70.65% of double positive CD56$^+$/CD90$^+$ cells, while expansion in rich medium selected myogenic CD56$^+$ cell population at the expenses of CD90$^+$/CD56$^+$ double positive one (**Figure 1**, t2 and t3). The CD45$^+$ hematopoietic stem cells are lost on both groups already at t1 (**Figure 1**).

To evaluate the influence of the two different media on proliferation rate and myogenic differentiation, immunofluorescence analysis against the proliferation marker Ki67 and the muscle terminal differentiation marker myosin heavy chain (MyHC) has been performed on both experimental groups. Results show a significative increase of Ki67$^+$ nuclei in rich medium grown cells (**Figure 2**) implying a higher proliferation rate. Moreover, in both media a spontaneous myogenic capability was observed in skeletal muscle-derived hMSC culture with a higher efficiency in rich medium (**Figure 2**). This evidence was confirmed by fusion index analysis, a quantitative indicator of the cell differentiation level that is calculated by dividing the number of nuclei present in the myotubes (threshold: 3 nuclei per myotube) by the number of total nuclei (**Figure 2**).

Employment of Different Human Serum Concentration as Medium Supplement for hMSCs Culturing

In order to test whether human serum could be employed as medium supplement for hMSCs growth and thus satisfy the need of MSC culture standardization avoiding animal derivatives, different concentration of this compound has been used to investigate its efficacy. Therefore, hMSCs have been cultured in α-MEM supplemented with 20% FBS as standard (control) medium, or at increasing concentration of human serum: low (5%), medium (10%), and high (20%). At different time points (2, 5, 7, and 9 days of culture) the cells were harvested to score proliferation rate. hMSCs growth revealed a significant dependence on human serum concentration: in particular, low concentration (5%) of human serum was comparable to the control medium (20% FBS) growth rate, while already at medium concentration (10%) it was possible to observe a remarkable enhancement in the hMSCs proliferation, reaching a statistically significant increment at high concentration (20%) in every analyzed time point up to a more than 5-fold increase at day 9 (**Figure 3**).

Myogenic differentiation has been assessed by MyHC expression by means of immunofluorescence analysis at culturing

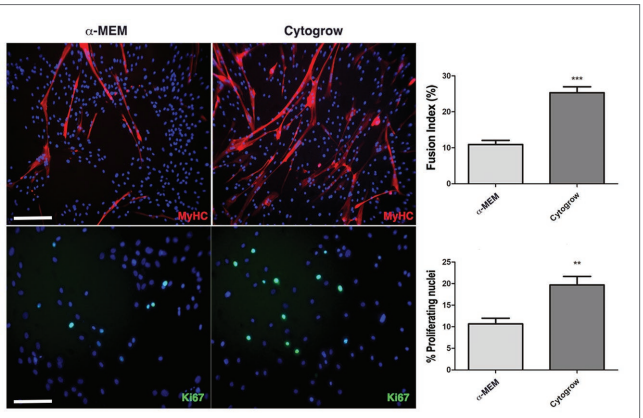

FIGURE 2 | Culture conditions influence cell behavior. Immunofluorescences against MyHC (red) and Ki67 (green) reveal the remarkable differences in terms of differentiation and proliferation employing Cyto-Grow commercial medium compared with α-MEM (nuclei labeled in blue by DAPI). The respective quantifications are reported as fusion index and rate of proliferating nuclei (Ki67 positive). Statistical analysis: one-way ANOVA and Tukey's test. $^{**}p < 0.01$, $^{***}p < 0.001$ ($n = 3$). Scale bars: MyHC = 200 μm; Ki67 = 100 μm.

day 9, a suitable time allowing cells to fuse and differentiate into myotubes. A clear trend was also observed for the number of formed myotubes, with the highest number of myotubes obtained with the highest human serum concentration (**Figure 3**). These observations have been further confirmed by the fusion index analysis showing the effect of human serum enhancing significatively myogenic differentiation, revealing the higher concentration being more efficient to the control (4-fold increase) and the other two concentrations (**Figure 3**).

The effect of human serum supplementation on hMSCs heterogeneity has also been evaluated. Flow cytometry assay was performed employing the higher H.S. concentration tested in the previous experiments, indicating the formation of a homogeneous myogenic population CD90$^+$/CD56$^+$ double positive (**Supplementary Figure 1**).

Influence of Different Platelet-Rich Plasma Concentrations on hMSCs Proliferation and Differentiation

In order to test PrP effect on cell division rate and myogenic differentiation, hMSCs have been cultured with low (5×10^5 platelets/ml), medium (1×10^6 platelets/ml), and high (1.5×10^6 platelets/ml) concentrations of PrP as medium supplement. To evaluate the proliferation under PrP influence, cells were harvested and counted at 2, 5, 7, and 9 days upon PrP exposure. The resulting growth curves revealed that medium supplementation with high concentration of PrP significantly increased cell division for 7 days, while a decrease was observed at day 9 (**Figure 4**). The other concentrations of PrP demonstrated a relative moderate and progressive increase up to day 7, reaching the plateau at day 9. The PrP effect on hMSCs proliferation has been further confirmed by immunofluorescence analysis for Ki67 at day 9 (**Figure 4**). The obtained results, plotted scoring Ki67$^+$ nuclei, were consistent with the cell growth curves

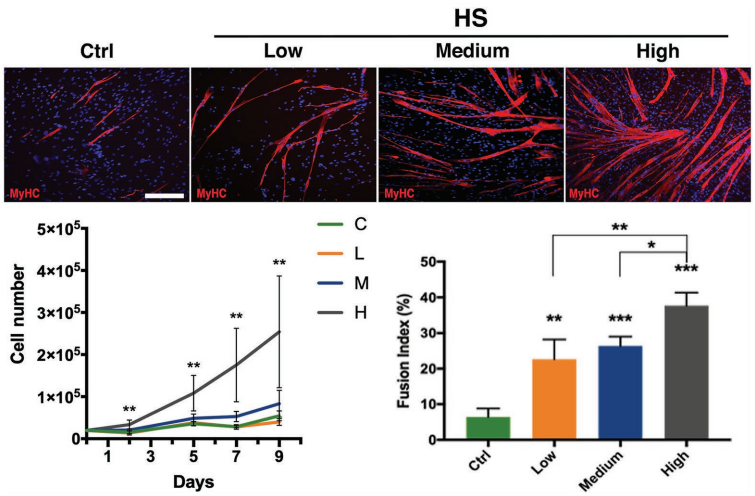

FIGURE 3 | Effect of human serum on hMSC proliferation and differentiation. hMSC proliferation and differentiation analyzed upon different medium supplementations exposure. α-MEM medium added with: Ctrl (20% FBS), Low (5% Human Serum), Medium (10% Human Serum), and High (20% Human Serum). Anti MyHC (red) immunolabeling on hMSCs cultured in different conditions as indicated; nuclei were marked with DAPI (blue). Cell growth is indicated as proliferation curve evaluated up to 9 days. Myogenic evaluation relative to MyHC signal is represented as fusion index at day 9 of culturing in the investigated conditions. Statistical analysis: one-way ANOVA and Tukey's test. $^{*}p < 0.05$, $^{**}p < 0.01$, $^{***}p < 0.001$ ($n = 3$). C–F: scale bar 250 μm.

showing a raise of proliferating nuclei at every PrP concentration compared to the control, being significant at low and medium concentrations (**Figure 4**). As regards the PrP effect on myogenic differentiation, fusion index assay was performed revealing a significative increment of myotube formation as a consequence of PrP addition, despite the fact that the effect is not concentration-dependent in a significative way (**Figure 4**). Moreover, the cell population heterogeneity exposed to the higher dose of PrP tested was assessed by flow cytometry assay, yielding a homogeneous and myogenic population $CD90^{+}/CD56^{+}$ double positive (**Supplementary Figure 1**).

DISCUSSION

Today, one of the most challenging tasks in skeletal muscle regenerative medicine is to find a suitable stem cells source for a large and easy cellular expansion, avoiding losing the myogenic potential (Errico et al., 2018). In fact, satellite cells, despite being the effective muscle stem cells, present a low isolation rate and can be kept in culture only for a few passages without losing myogenic potentiality. This has prompted researchers to investigate other stem cell populations (Fuoco et al., 2016a,b). However, despite the efforts of the last decades leading to the characterization of several stem cell populations with mesenchymal origin and promising myogenic potentiality, obtaining a large amount of human myogenic primary cells for tissue engineering or cell therapy approaches is still an unmet need (Torrente et al., 2007; Skuk et al., 2014; Sacchetti et al., 2016). For this reason, in this work we evaluated how culture conditions can modulate different basic features of skeletal muscle-derived hMSCs, such as proliferation rate, myogenic potential efficacy, and maintenance.

Here, we tested whether different growth media can directly influence hMSCs – freshly isolated from human skeletal muscle biopsies – heterogeneity, expansion potentiality, and differentiation capabilities. In particular, we employed different culture conditions comprising different media (α-MEM and Cyto-Grow) and different supplements (Human Serum and PrP). To monitor the effect of the two different media on hMSCs heterogeneity, we performed a time course analysis by cytofluorimetric assay, investigating CD90 positivity, a MSCs marker, and myogenic potential (CD56 positivity). The obtained results revealed that both media were able to maintain the positivity to the stem cell marker CD90 for many doubling times (up to passage 9). Interestingly, while in standard medium (α-MEM + 20% FBS) we observed the formation of two distinct subpopulations (single positive $CD90^{+}$ and double positive $CD90^{+}/CD56^{+}$), in the rich medium a more homogeneous population double positive was formed and maintained, showing to directly promote the maintenance of the myogenic properties right from the early stages. Thus, in order to obtain a large number of myogenic stem/progenitor cells, the use of a rich medium – such as Cyto-Grow – would ameliorate remarkably the isolation and expansion procedures. Moreover, Cyto-grow proved to be a better medium choice for promoting proliferation and a robust myotubes formation compared to standard medium, as confirmed by $Ki67^{+}$ nuclei scoring and fusion index assay.

In parallel, we investigated the possibility to employ human-derived medium supplements in order to avoid animal derivatives and then guaranteeing completely species-specific cell condition, the "humanizing supplement" (Roberts et al., 2012; Shanbhag et al., 2017). These supplements were employed to replace animal derived serum to the standard medium (α-MEM + 20% FBS) and then to identify the best in terms of CD90 expression maintenance *in vitro*, proliferation, and differentiation ability in relation to what is considered the standard condition in

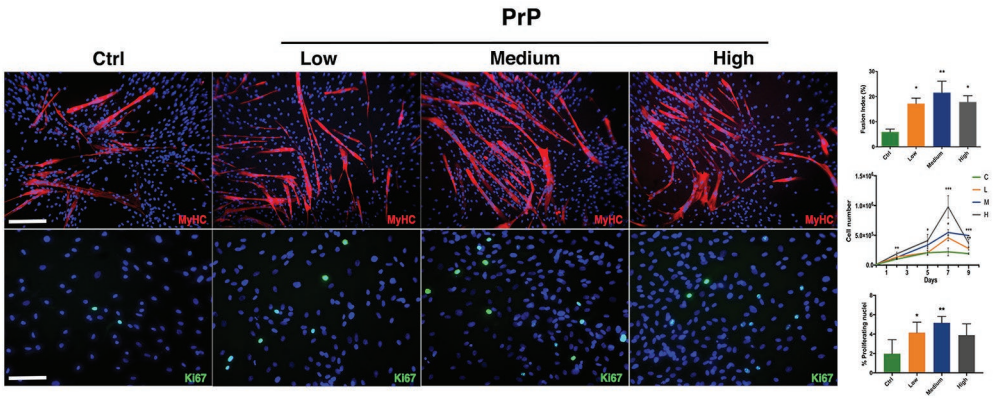

FIGURE 4 | platelet-rich plasma (PrP) affects hMSC proliferation and myogenesis. Immunofluorescences against MyHC (red) and Ki67 (green) revealing differences in proliferation and differentiation in relation to different PrP concentration. α-MEM supplemented with: Ctrl (20% FBS), Low (5×10^5 platelets/ml), Medium (1×10^6 platelets/ml), and High (1.5×10^6 platelets/ml); nuclei were counterstained in blue by DAPI. The relative quantification is reported as fusion index for muscle differentiation, proliferating curve, and rate of Ki67 positive nuclei for cell doubling. Statistical analysis: one-way ANOVA and Tukey's test. $^*p < 0.05$, $^{**}p < 0.01$, $^{***}p < 0.001$ ($n = 3$). Scale bars: MyHC = 200 μm; Ki67 = 100 μm.

literature (Shahdadfar et al., 2005). Hence, we tested different human serum concentration (ranging from 5 to 20%), observing that at higher concentration (20%) the hMSCs proliferation rate was about 5-fold greater than control (20% FBS). The medium dose (10%) had just a slight effect, while the lower concentration (5%) was comparable with the control in terms of proliferation rate. These results demonstrated the possibility to exploit human serum to ameliorate human cell proliferation rate and then to reduce the cellular expansion time. This strategy has a great clinical potential as it avoids the use of animal-derived supplements and, on the other hand, lays the basis for the development of a culturing protocol that fulfill GMP regulations essential for human cell clinical application. Additionally, we have also investigated the impact of the human serum on hMSCs myogenic capabilities, showing – upon 9 days of culture – a noteworthy enhancement of the differentiated myotubes in relation to the serum concentration, with a significant increment (up to 4-fold increase) of the fusion index at high concentration (20%).

Taken together these results suggest a strong direct correlation between human cell physiological processes, such as proliferation and differentiation, and medium supplementation with increasing doses of a pool of human sera. Interestingly, unlike what was reported by Shahdadfar et al. (2005), we observed that the beneficial effect of the human serum is independent from the autologous donor derivation. This divergence could rely on the different MSC isolation origin skeletal muscle versus bone marrow (Shahdadfar et al., 2005).

Furthermore, we tested PrP action on hMSCs to exploit another humanizing medium supplement largely used in clinical therapeutic approach for pathologies affecting the musculoskeletal system (Roberts et al., 2012; Shanbhag et al., 2017). In this case, we observed that cell proliferation rate increases with the increase of PrP concentration, reaching the maximum at day 7 for the highest PrP concentration (approx. 4-fold increase compared to the control), further confirmed by Ki67 expression quantification (**Figure 4**). Nevertheless, at day 9 we noticed a dramatic decrease in the proliferation rate, with a more pronounced effect for the highest dose of PrP, probably due to the excessive over-confluence compromising cell health. PrP addition also promoted increased myotubes formation, although dose-independent.

Finally, we have evaluated the effect of human-derivates addition on hMSCs heterogeneity, observing that this aspect is not affected. These results suggested that the medium used during isolation is more crucial than the subsequent addition of derivates in the determination of cellular population fate.

The presented results display a better effect of human serum on hMSCs myogenic differentiation compared to PrP. Also, the readiness of serum isolation and availability contrasting with the industrious PrP isolation and with the different formulations (Shanbhag et al., 2017) make it a preferable choice.

In this study, we demonstrated the possibility to directly influence skeletal muscle-derived hMSCs isolation and behavior improving cell proliferation rate and myogenic efficacy by formulating specific culture media. Moreover, we have shown that by exploiting human blood derivates such as serum or PrP, one can achieve efficient and robust culture protocols for hMSCs expansion and differentiation that do not require animal derived supplements and can be easily translated into the clinical scenarios fulfilling GMP requirement.

DATA AVAILABILITY STATEMENT

The raw data supporting the conclusions of this article will be made available by the authors, without undue reservation.

ETHICS STATEMENT

The studies involving human participants were reviewed and approved by IFO ethics committee. The patients/participants provided their written informed consent to participate in this study.

AUTHOR CONTRIBUTIONS

CG and MF conceived and designed the experiments. ST, CR, EF, SB, and CF carried out experiments. CG and SC supervised the project. ST and ER isolated and cultured human primary MSC besides critical reading. FR performed FACS analysis. JB provided muscle biopsies beside critical reading. MC, ST, EF, CR, and CG wrote the manuscript. All authors contributed to the article and approved the submitted version.

FUNDING

This study was supported by the National Science Centre – Poland (NCN) within the POLONEZ 3 fellowship number 2016/23/P/NZ1/03604 which has received funding from the European Union's Horizon 2020 research and innovation program under the Marie Skłodowska-Curie grant agreement No. 665778.

ACKNOWLEDGMENTS

We thank FUNDACION ONCE – fundation for the cooperation and inclusion of people with disabilities - to support Dr. Carles Sánchez Riera research with "Talent opportunity" scholarship.

SUPPLEMENTARY MATERIAL

The Supplementary Material for this article can be found online at: https://www.frontiersin.org/articles/10.3389/fphys.2020.553198/full#supplementary-material

REFERENCES

Almalki, S. G., and Agrawal, D. K. (2016). Key transcription factors in the differentiation of mesenchymal stem cells. *Differentiation* 92, 41–51. doi: 10.1016/j.diff.2016.02.005

Amati, E., Sella, S., Perbellini, O., Alghisi, A., Bernardi, M., Chieregato, K., et al. (2017). Generation of mesenchymal stromal cells from cord blood: evaluation of in vitro quality parameters prior to clinical use. *Stem Cell Res. Ther.* 8:14. doi: 10.1186/s13287-016-0465-2

Appaix, F. (2014). Brain mesenchymal stem cells: the other stem cells of the brain? *World J. Stem Cells* 6, 134–143. doi: 10.4252/wjsc.v6.i2.134

Baghdadi, M. B., Castel, D., Machado, L., Fukada, S. I., Birk, D. E., Relaix, F., et al. (2018). Reciprocal signalling by notch-collagen V-CALCR retains muscle stem cells in their niche. *Nature* 557, 714–718. doi: 10.1038/s41586-018-0144-9

Bieback, K., and Netsch, P. (2016). Isolation, culture, and characterization of human umbilical cord blood-derived mesenchymal stromal cells. *Methods Mol. Biol.* 1416, 245–258. doi: 10.1007/978-1-4939-3584-0_14

Čamernik, K., Barlič, A., Drobnič, M., Marc, J., Jeras, M., and Zupan, J. (2018). Mesenchymal stem cells in the musculoskeletal system: from animal models to human tissue regeneration? *Stem Cell Rev. Rep.* 14, 346–369. doi: 10.1007/s12015-018-9800-6

Crisan, M., Deasy, B., Gavina, M., Zheng, B., Huard, J., Lazzari, L., et al. (2008). Purification and long-term culture of multipotent progenitor cells affiliated with the walls of human blood vessels: myoendothelial cells and pericytes. *Methods Cell Biol.* 86, 295–309. doi: 10.1016/S0091-679X(08)00013-7

De Bari, C., Dell'Accio, F., Vandenabeele, F., Vermeesch, J. R., Raymackers, J. M., and Luyten, F. P. (2003). Skeletal muscle repair by adult human mesenchymal stem cells from synovial membrane. *J. Cell Biol.* 160, 909–918. doi: 10.1083/jcb.200212064

Errico, V., Arrabito, G., Fornetti, E., Fuoco, C., Testa, S., Saggio, G., et al. (2018). High-density ZnO nanowires as a reversible myogenic-differentiation switch. *ACS Appl. Mater. Interfaces* 10, 14097–14107. doi: 10.1021/acsami.7b19758

Ferrari, G., Cusella-De Angelis, G., Coletta, M., Paolucci, E., Stornaiuolo, A., Cossu, G., et al. (1998). Muscle regeneration by bone marrow-derived myogenic progenitors. *Science* 279, 1528–1530. doi: 10.1126/science.279.5356.1528

Friedenstein, A. J., Chailakhjan, R. K., and Lalykina, K. S. (1970). The development of fibroblast colonies in monolayer cultures of guinea-pig bone marrow and spleen cells. *Cell Tissue Kinet.* 3, 393–403. doi: 10.1111/j.1365-2184.1970.tb00347.x

Fuoco, C., Cannata, S., and Gargioli, C. (2016a). Could a functional artificial skeletal muscle be useful in muscle wasting? *Curr. Opin. Clin. Nutr. Metab. Care* 19, 182–187. doi: 10.1097/MCO.0000000000000271

Fuoco, C., Petrilli, L. L., Cannata, S., and Gargioli, C. (2016b). Matrix scaffolding for stem cell guidance toward skeletal muscle tissue engineering. *J. Orthop. Surg. Res.* 11:86. doi: 10.1186/s13018-016-0421-y

Grassi, A., Napoli, F., Romandini, I., Samuelsson, K., Zaffagnini, S., Candrian, C., et al. (2018). Is platelet-rich plasma (PRP) effective in the treatment of acute muscle injuries? A systematic review and meta-analysis. *Sports Med.* 48, 971–989. doi: 10.1007/s40279-018-0860-1

Gussoni, E., Soneoka, Y., Strickland, C. D., Buzney, E. A., Khan, M. K., Flint, A. F., et al. (1999). Dystrophin expression in the mdx mouse restored by stem cell transplantation. *Nature* 401, 390–394. doi: 10.1038/43919

Hamid, M. S. A., Yusof, A., and Mohamed Ali, M. R. (2014). Platelet-rich plasma (PRP) for acute muscle injury: a systematic review. *PLoS One* 9:e90538. doi: 10.1371/journal.pone.0090538

Hass, R., Kasper, C., Böhm, S., and Jacobs, R. (2011). Different populations and sources of human mesenchymal stem cells (MSC): a comparison of adult and neonatal tissue-derived MSC. *Cell Commun. Signal.* 9:12. doi: 10.1186/1478-811X-9-12

Haynesworth, S. E., Barer, M. A., and Caplan, A. I. (1992). Cell surface antigens on human marrow-derived mesenchymal cells are detected by monoclonal antibodies. *Bone* 13, 69–80. doi: 10.1016/8756-3282(92)90363-2

Jackson, L., Jones, D., Scotting, P., and Sottile, V. (2007). Adult mesenchymal stem cells: differentiation potential and therapeutic applications. *J. Postgrad. Med.* 53, 121–127. doi: 10.4103/0022-3859.32215

Kisselbach, L., Merges, M., Bossie, A., and Boyd, A. (2009). CD90 expression on human primary cells and elimination of contaminating fibroblasts from cell cultures. *Cytotechnology* 59, 31–44. doi: 10.1007/s10616-009-9190-3

Klimczak, A., Kozlowska, U., and Kurpisz, M. (2018). Muscle stem/progenitor cells and mesenchymal stem cells of bone marrow origin for skeletal muscle regeneration in muscular dystrophies. *Arch. Immunol. Ther. Exp.* 66, 341–354. doi: 10.1007/s00005-018-0509-7

Kozlowska, U., Krawczenko, A., Futoma, K., Jurek, T., Rorat, M., Patrzalek, D., et al. (2019). Similarities and differences between mesenchymal stem/progenitor cells derived from various human tissues. *World J. Stem Cells* 11, 347–374. doi: 10.4252/wjsc.v11.i6.347

Kumar, A., D'Souza, S. S., Moskvin, O. V., Toh, H., Wang, B., Zhang, J., et al. (2017). Specification and diversification of pericytes and smooth muscle cells from mesenchymoangioblasts. *Cell Rep.* 19, 1902–1916. doi: 10.1016/j.celrep.2017.05.019

Kunze, K. N., Hannon, C. P., Fialkoff, J. D., Frank, R. M., and Cole, B. J. (2019). Platelet-rich plasma for muscle injuries: a systematic review of the basic science literature. *World J. Orthop.* 10, 278–291. doi: 10.5312/wjo.v10.i7.278

Lee, J. H., Kosinski, P. A., and Kemp, D. M. (2005). Contribution of human bone marrow stem cells to individual skeletal myotubes followed by myogenic gene activation. *Exp. Cell Res.* 307, 174–182. doi: 10.1016/j.yexcr.2005.03.008

Li, C. Y., Wu, X. Y., Tong, J. B., Yang, X. X., Zhao, J. L., Zheng, Q. F., et al. (2015). Comparative analysis of human mesenchymal stem cells from bone marrow and adipose tissue under xeno-free conditions for cell therapy. *Stem Cell Res. Ther.* 6:55. doi: 10.1186/s13287-015-0066-5

Lodie, T. A., Blickarz, C. E., Devarakonda, T. J., Chufa, H. E., Dash, A. B., Clarke, J., et al. (2002). Systematic analysis of reportedly distinct populations of multipotent bone marrow-derived stem cells reveals a lack of distinction. *Tissue Eng.* 8, 739–751. doi: 10.1089/10763270260424105

Mauro, A. (1961). Satellite cell of skeletal muscle fibers. *J. Biophys. Biochem. Cytol.* 9, 493–495. doi: 10.1083/jcb.9.2.493

Meuleman, N., Tondreau, T., Delforge, A., Dejeneffe, M., Massy, M., Libertalis, M., et al. (2006). Human marrow mesenchymal stem cell culture: serum-free medium allows better expansion than classical α-MEM medium. *Eur. J. Haematol.* 76, 309–316. doi: 10.1111/j.1600-0609.2005.00611.x

Mitchell, K. J., Pannérec, A., Cadot, B., Parlakian, A., Besson, V., Gomes, E. R., et al. (2010). Identification and characterization of a non-satellite cell muscle resident progenitor during postnatal development. *Nat. Cell Biol.* 12, 257–266. doi: 10.1038/ncb2025

Musiał-Wysocka, A., Kot, M., and Majka, M. (2019). The pros and cons of mesenchymal stem cell-based therapies. *Cell Transplant.* 28, 801–812. doi: 10.1177/0963689719837897

Okamoto, R., Yajima, T., Yamazaki, M., Kanai, T., Mukai, M., Ikeda, Y., et al. (2002). Damaged epithelia regenerated by bone marrow-derived cells in the human gastrointestinal tract. *Nat. Med.* 8, 1011–1017. doi: 10.1038/nm755

Oppermann, T., Leber, J., Elseberg, C., Salzig, D., and Czermak, P. (2014). HMSC production in disposable bioreactors in compliance with cGMP guidelines and PAT. *Am. Pharm. Rev.* 17, 42–47.

Orciani, M., Bolletta, E., Campanati, A., Di Benedetto, G., and Di Primio, R. (2014). The response of breast cancer cells to mesenchymal stem cells: a possible role of inflammation by breast implants. *Plast. Reconstr. Surg.* 134, 994e–996e. doi: 10.1097/PRS.0000000000000665

Pelekanos, R. A., Sardesai, V. S., Futrega, K., Lott, W. B., Kuhn, M., and Doran, M. R. (2016). Isolation and expansion of mesenchymal stem/stromal cells derived from human placenta tissue. *J. Vis. Exp.* 6:54204. doi: 10.3791/54204

Pittenger, M. F., Discher, D. E., Péault, B. M., Phinney, D. G., Hare, J. M., and Caplan, A. I. (2019). Mesenchymal stem cell perspective: cell biology to clinical progress. *NPJ Regen. Med.* 4:22. doi: 10.1038/s41536-019-0083-6

Pittenger, M. F., Mackay, A. M., Beck, S. C., Jaiswal, R. K., Douglas, R., Mosca, J. D., et al. (1999). Multilineage potential of adult human mesenchymal stem cells. *Science* 284, 143–147. doi: 10.1126/science.284.5411.143

Rando, T. A., Pavlath, G. K., and Blau, H. M. (1995). The fate of myoblasts following transplantation into mature muscle. *Exp. Cell Res.* 220, 383–389. doi: 10.1006/excr.1995.1329

Roberts, I., Baila, S., Rice, R. B., Janssens, M. E., Nguyen, K., Moens, N., et al. (2012). Scale-up of human embryonic stem cell culture using a hollow fibre bioreactor. *Biotechnol. Lett.* 34, 2307–2315. doi: 10.1007/s10529-012-1033-1

Sacchetti, B., Funari, A., Michienzi, S., Di Cesare, S., Piersanti, S., Saggio, I., et al. (2007). Self-renewing osteoprogenitors in bone marrow sinusoids can organize a hematopoietic microenvironment. *Cell* 131, 324–336. doi: 10.1016/j.cell.2007.08.025

Sacchetti, B., Funari, A., Remoli, C., Giannicola, G., Kogler, G., Liedtke, S., et al. (2016). No identical "mesenchymal stem cells" at different times and sites: human committed progenitors of distinct origin and differentiation potential are incorporated as adventitial cells in microvessels. *Stem Cell Reports* 6, 897–913. doi: 10.1016/j.stemcr.2016.05.011

Sacco, A., Doyonnas, R., Kraft, P., Vitorovic, S., and Blau, H. M. (2008). Self-renewal and expansion of single transplanted muscle stem cells. *Nature* 456, 502–506. doi: 10.1038/nature07384

Shahdadfar, A., Frønsdal, K., Haug, T., Reinholt, F. P., and Brinchmann, J. E. (2005). In vitro expansion of human mesenchymal stem cells: choice of serum is a determinant of cell proliferation, differentiation, gene expression, and transcriptome stability. *Stem Cells* 23, 1357–1366. doi: 10.1634/stemcells.2005-0094

Shanbhag, S., Stavropoulos, A., Suliman, S., Hervig, T., and Mustafa, K. (2017). Efficacy of humanized mesenchymal stem cell cultures for bone tissue engineering: a systematic review with a focus on platelet derivatives. *Tissue Eng. Part B Rev.* 23, 552–569. doi: 10.1089/ten.teb.2017.0093

Skuk, D., Goulet, M., and Tremblay, J. P. (2014). Intramuscular transplantation of myogenic cells in primates: importance of needle size, cell number, and injection volume. *Cell Transplant.* 23, 13–25. doi: 10.3727/096368912X661337

Sottile, V., Halleux, C., Bassilana, F., Keller, H., and Seuwen, K. (2002). Stem cell characteristics of human trabecular bone-derived cells. *Bone* 30, 699–704. doi: 10.1016/S8756-3282(02)00674-9

Suva, D., Garavaglia, G., Menetrey, J., Chapuis, B., Hoffmeyer, P., Bernheim, L., et al. (2004). Non-hematopoietic human bone marrow contains long-lasting, pluripotential mesenchymal stem cells. *J. Cell. Physiol.* 198, 110–118. doi: 10.1002/jcp.10396

Testa, S., Costantini, M., Fornetti, E., Bernardini, S., Trombetta, M., Seliktar, D., et al. (2017). Combination of biochemical and mechanical cues for tendon tissue engineering. *J. Cell. Mol. Med.* 21, 2711–2719. doi: 10.1111/jcmm.13186

Tonti, G. A., and Mannello, F. (2008). From bone marrow to therapeutic applications: different behaviour and genetic/epigenetic stability during mesenchymal stem cell expansion in autologous and foetal bovine sera? *Int. J. Dev. Biol.* 52, 1023–1032. doi: 10.1387/ijdb.082725gt

Torrente, Y., Belicchi, M., Marchesi, C., D'Antona, G., Cogiamanian, F., Pisati, F., et al. (2007). Autologous transplantation of muscle-derived CD133+ stem cells in Duchenne muscle patients. *Cell Transplant.* 16, 563–577. doi: 10.3727/000000007783465064

Uezumi, A., Fukada, S. I., Yamamoto, N., Takeda, S., and Tsuchida, K. (2010). Mesenchymal progenitors distinct from satellite cells contribute to ectopic fat cell formation in skeletal muscle. *Nat. Cell Biol.* 12, 143–152. doi: 10.1038/ncb2014

Vono, R., Fuoco, C., Testa, S., Pirrò, S., Maselli, D., McCollough, D. F., et al. (2016). Activation of the pro-oxidant PKCβIIp66Shc signaling pathway contributes to pericyte dysfunction in skeletal muscles of patients with diabetes with critical limb ischemia. *Diabetes* 65, 3691–3704. doi: 10.2337/db16-0248

Wakitani, S., Saito, T., and Caplan, A. I. (1995). Myogenic cells derived from rat bone marrow mesenchymal stem cells exposed to 5-azacytidine. *Muscle Nerve* 18, 1417–1426. doi: 10.1002/mus.880181212

Yamada, Y., Nakamura, S., Ito, K., Sugito, T., Yoshimi, R., Nagasaka, T., et al. (2010). A feasibility of useful cell-based therapy by bone regeneration with deciduous tooth stem cells, dental pulp stem cells, or bone-marrow-derived mesenchymal stem cells for clinical study using tissue engineering technology. *Tissue Eng. Part A* 16, 1891–1900. doi: 10.1089/ten.tea.2009.0732

Yin, H., Price, F., and Rudnicki, M. A. (2013). Satellite cells and the muscle stem cell niche. *Physiol. Rev.* 93, 23–67. doi: 10.1152/physrev.00043.2011

Zhang, J., Wilson, G. F., Soerens, A. G., Koonce, C. H., Yu, J., Palecek, S. P., et al. (2009). Functional cardiomyocytes derived from human induced pluripotent stem cells. *Circ. Res.* 104, e30–e41. doi: 10.1161/CIRCRESAHA.108.192237

Conflict of Interest: The authors declare that the research was conducted in the absence of any commercial or financial relationships that could be construed as a potential conflict of interest.

frontiers in Physiology

REVIEW
published: 12 November 2020
doi: 10.3389/fphys.2020.568535

Mechanotransduction and Adrenergic Stimulation in Arrhythmogenic Cardiomyopathy: An Overview of *in vitro* and *in vivo* Models

*Giorgia Beffagna[1,2], Elena Sommariva[3] and Milena Bellin[2,4,5]**

[1] Department of Cardio-Thoraco-Vascular Sciences and Public Health, University of Padua, Padua, Italy, [2] Department of Biology, University of Padua, Padua, Italy, [3] Vascular Biology and Regenerative Medicine Unit, Centro Cardiologico Monzino IRCCS, Milan, Italy, [4] Veneto Institute of Molecular Medicine, Padua, Italy, [5] Department of Anatomy and Embryology, Leiden University Medical Center, Leiden, Netherlands

Arrhythmogenic Cardiomyopathy (AC) is a rare inherited heart disease, manifesting with progressive myocardium degeneration and dysfunction, and life-threatening arrhythmic events that lead to sudden cardiac death. Despite genetic determinants, most of AC patients admitted to hospital are athletes or very physically active people, implying the existence of other disease-causing factors. It is recognized that AC phenotypes are enhanced and triggered by strenuous physical activity, while excessive mechanical stretch and load, and repetitive adrenergic stimulation are mechanisms influencing disease penetrance. Different approaches have been undertaken to recapitulate and study both mechanotransduction and adrenergic signaling in AC, including the use of *in vitro* cellular and tissue models, and the development of *in vivo* models (particularly rodents but more recently also zebrafish). However, it remains challenging to reproduce mechanical load stimuli and physical activity in laboratory experimental settings. Thus, more work to drive the innovation of advanced AC models is needed to recapitulate these subtle physiological influences. Here, we review the state-of-the-art in this field both in clinical and laboratory-based modeling scenarios. Specific attention will be focused on highlighting gaps in the knowledge and how they may be resolved by utilizing novel research methodology.

Keywords: arrhythmogenic cardiomyopathy, mechanotransduction, adrenergic signaling, cell models of disease, animal models

OPEN ACCESS

Edited by:
Martina Calore,
Maastricht University, Netherlands

Reviewed by:
Michelle S. Parvatiyar,
Florida State University, United States
Xiongwen Chen,
Lewis Katz School of Medicine at Temple University, United States

***Correspondence:**
Milena Bellin
milena.bellin@unipd.it;
m.bellin@lumc.nl

Specialty section:
This article was submitted to Striated Muscle Physiology, a section of the journal Frontiers in Physiology

Received: *01 June 2020*
Accepted: *19 October 2020*
Published: *12 November 2020*

Citation:
Beffagna G, Sommariva E and Bellin M (2020) Mechanotransduction and Adrenergic Stimulation in Arrhythmogenic Cardiomyopathy: An Overview of in vitro and in vivo Models. Front. Physiol. 11:568535. doi: 10.3389/fphys.2020.568535

INTRODUCTION

Arrhythmogenic cardiomyopathy (AC) is a rare disease, which commonly manifests during late childhood or adolescence with malignant arrhythmias and causes sudden cardiac death (SCD) in otherwise healthy young individuals (Thiene et al., 1988; Thiene and Basso, 2001; Basso et al., 2009). Progressive fibro-fatty replacement of the myocardium is the histopathological hallmark of the disease, although in the early concealed stages, electrophysiological changes may precede structural changes (Basso et al., 1996; Kaplan et al., 2004b; Bauce et al., 2005; Gomes et al., 2012;

Rizzo et al., 2012). A major breakthrough in the understanding of AC came with the realization that this disease is associated with mutations in desmosomal proteins (Gerull et al., 2004; Yang et al., 2006), resulting in impaired mechanical properties of cardiac cells. This discovery fueled several studies aimed at uncovering the relationship between desmosome abnormalities and AC pathological and clinical findings (Thiene, 2015).

The heart is indeed constantly challenged by mechanical stress and both its function and mechanical integrity strictly depends on correct cell-cell and cell-extracellular matrix (ECM) connections. Desmosomes are junctional complexes that interconnect adjacent cells, and therefore are highly expressed in tissues subject to mechanical stretch and load, such as skin and heart. Together with integrins and cadherins, desmosomes are coupled to structural mechanoresponsive cytoskeletal elements, such as F-actin, microtubules, and intermediate filaments, which allow cardiomyocytes (CMs) to adapt to external and internal physical stimuli. These mechanoresponsive elements are necessary for correct dissipation of mechanical loads and for efficient mechanotransduction. Mechanotransduction is the mechanism by which force transmission between cells and between cell-ECM is translated into a series of dynamic intracellular signaling events (Hoffman et al., 2011). In addition, cell shape can influence cell lineage commitment through ROCK-mediated cytoskeletal tension (McBeath et al., 2004), since cell-cell and cell-ECM adhesions translate into soluble intracellular signals, influencing cell fate.

In AC, genetic defects in desmosomes and other mechanosensitive or mechanotransduction proteins lead to altered response to physiologic mechanical load and even more to exercise. In AC, mechanical load causes intracellular signaling changes (mainly in Wnt/βcatenin and Hippo pathways) driving alternative cell fate, such as fibrotic or adipogenic signaling.

In addition, competitive sports expose the heart to adrenergic stress, which may lead to electrical and functional destabilization. Indeed, exercise is one of the main triggers for life-threatening arrhythmias and SCD in several inherited heart conditions, including AC (Furlanello et al., 1998; Firoozi et al., 2002; Thiene et al., 2016; Corrado and Zorzi, 2018), as recently demonstrated by the tragic events of top-level athletes (Catto et al., 2019).

Once the genetic causes of AC were discovered, several *in vitro* and *in vivo* models were quickly established. Cell models include CMs, the primary cell type affected by AC-linked mutations, and non-CM cell types, and both human and non-human models. *In vivo* models mainly include transgenic mice and, to a lesser extent, zebrafish knock-down models and the spontaneous AC feline and canine models were studied. Both *in vitro* and *in vivo* models helped to reveal the major pathogenic mechanisms underlying AC. However, in AC, the genetic substrate is not sufficient for a comprehensive disease modeling. Therefore, different mechanical and adrenergic stimuli have been applied to cell and animal models to mimic the effect of exercise on AC pathogenesis and to understand their finer molecular determinants. This aspect is the main focus of this review.

Abbreviations: AA, Aortic Aneurism; AC, Arrhythmogenic Cardiomyopathy; ACC, American College of Cardiology; ACTN1, α-actinin-1; ACTN2, α-actinin-2; AFM, Atomic force microscopy; AHA, American Heart Association; AP, Action potential; BS, Brugada Syndrome; Ca^{2+}, Calcium; CaMKII, Calcium/calmodulin-dependent protein kinase II; cAMP, Cyclic AMP; CDH2, N-caderin (Cadherin-2); CM, Cardiomyocyte; CPVT, Catecholaminergic Ventricular Tachycardia; CRISPR/Cas9, Clustered Regularly Interspaced Short Palindromic Repeats/CRISPR associated protein 9; CTNNA3, αT-catenin; CX43, Connexin 43; DC, Dilated Cardiomyopathy; DES, Desmin; DSC, Desmocollin; DSG, Desmoglein; DSP, Desmoplakin; E, Embryonic day; ECM, Extracellular matrix; EDMD, Emery-Dreifuss muscular dystrophy; EMT, Epithelial-mesenchymal transition; FLNC, Filamin C; FOS, Fos proto-oncogene, AP-1 transcription factor subunit; GSK3b, Glycogen synthase kinase 3 beta; HC, Hypertrophic Cardiomyopathy; Hippo, Salvador-Warts-Hippo signaling pathway; hiPSC, Human induced pluripotent stem cells; HRS, heart rhythm society; I_{KATP}, K -selective, inward rectifier current; I_{Kr}, Rapidly Activating Delayed Rectifier Potassium current; I_{Na}, Voltage-gated sodium current; I_{NCX}, Sodium/Calcium exchanger current; I_{SK}, Small conductance Calcium-activated potassium current; I_{to}, Transient outward potassium current; JUN, Jun Proto-Oncogene, AP-1 Transcription Factor Subunit; JUP, Plakoglobin; LDB3, LIM Domain Binding 3 (ZASP); LDS, Loeys-Dietz syndrome; LMNA, Lamin A/C; LVNC, Left Ventricular non-compaction; miR, microRNA; MYH10, Myosin Heavy Chain 10; Nav1.5, Cardiac sodium channel; NMIIB, Non-muscle myosin IIB; NTg, Non-transgenic; PKA, Protein kinase A; PKP, Plakophilin; PLN, Phospholamban; PPAR, Peroxisome proliferator-activated receptor; RCM, Restrictive Cardiomyopathy; ROCK, Rho-associated protein kinase; RYR2, Ryanodine Receptor-2; SAP97, Synapse-associated protein 97; SCD, Sudden cardiac death; SCN5A, Sodium voltage-gated channel alpha subunit 5; SERCA, Sarco-Endoplasmic Reticulum Calcium ATPase; Smad, Small mother against decapentaplegic; STRN, Striatin; TAZ, Tafazzin; Tg, Transgenic; TGFβ3, Transforming growth factor β3; TJP1, Tight Junction Protein ZO-1; TMEM43, Transmembrane protein-43; TTN, Titin; Wnt, Wingless-type pathway; YAP, Yes-associated protein.

CLINICAL ASPECTS OF MECHANICAL LOAD AND ADRENERGIC STRESS IN AC PATIENTS

Most AC Causal Genes Have Mechanic and Adrenergic-Response Functions

Cardiac tissue is constantly exposed to different external forces such as mechanical load and stretch, in addition to intrinsic forces from the contraction machinery of single CMs. These extrinsic and intrinsic forces contribute to tissue morphogenesis, homeostasis, and regeneration and affect different aspects, such as cell size and shape, proliferation, differentiation, and migration (Evans et al., 2013).

Cardiac output and rhythm are tightly regulated by the autonomic nervous system (Silvani et al., 2016). Adrenergic nerves are in contact with cardiac cells (Kawashima, 2005) and signal transmission is based on neuro-cardiac synapses. The stimulation signals include the release of the adrenergic hormones catecholamines (noradrenaline and adrenaline), which in turn are sensed by cardiac cells through adrenoceptors, resulting in a positive inotropic response of the heart (Mary-Rabine et al., 1978; Hedberg et al., 1985; Chamberlain et al., 1999).

Arrhythmogenic cardiomyopathy is an inherited cardiomyopathy characterized by a high degree of genetic heterogeneity (Celeghin and Pilichou, 2019). To date, many genes have been associated with the disease, although some very rarely. **Tables 1**, **2** summarize the desmosomal and non-desmosomal genes, respectively, for which a causative role in AC has reached consensus and the corresponding proteins are graphically represented in **Figure 1**. However, additional genes

were associated to AC and are reviewed elsewhere (Towbin et al., 2019). Interestingly, some of these genes are associated to more than one channelopathy or cardiomyopathy (e.g., *LMNA*, *SCN5A*, and *TITIN*), and other genes (e.g., *RYR2*) display phenotypical overlap with other cardiac diseases which raises questions regarding their association to AC. The more likely scenario is that the concept of one gene-one disease paradigm does not hold (Cerrone et al., 2019). Importantly, although mutations in the *RYR2* gene were initially recognized in phenocopy AC (Tiso et al., 2001), they rather belong to the morbid entity clinically reported by Philippe Coumel in Paris, characterized by effort-induced polymorphic ventricular arrhythmias and SCD with a structurally normal heart, later named catecholaminergic polymorphic ventricular tachycardia (Prof. G. Thiene, personal communication). Nevertheless, the majority of genes involved in AC encode for proteins related to cardiac tissue extrinsic and/or intrinsic forces (**Tables 1**, **2**), making stretch and mechanosensing of fundamental importance for understanding the pathogenic mechanisms of AC (Padrón-Barthe et al., 2019). In addition, some AC-associated genes have adrenergic-dependent functions (**Tables 2**, making AC phenotypes vulnerable to autonomic signals (Shen and Zipes, 2014).

About 50% of AC probands are carriers of mutations in genes encoding desmosomes (Pilichou et al., 2016). Desmosomes are intercellular junctions composed of three protein families essential for mediating strong intercellular cohesion (Garrod, 2010; Green et al., 2010; Kowalczyk and Green, 2013). These three protein families are: (i) desmosomal cadherins (ii) armadillo proteins and (iii) plakins. The desmosomal cadherins, named desmogleins (DSGs) and desmocollins (DSCs), are transmembrane proteins whose extracellular domains form the adhesive interface of the desmosome, whereas their cytoplasmic tails anchor the armadillo proteins to the desmosomal plaque. The armadillo proteins, plakoglobin (JUP) and plakophilins 1–3 (PKP1-3) in turn, bind to desmoplakin (DSP), a member of the plakin family of cytoskeleton-associated proteins. DSP links the desmosome to the desmin filament network which is essential to provide tensile strength (Hatzfeld et al., 2017). All genes encoding desmosomal proteins are involved in the genetic determination of AC (Celeghin and Pilichou, 2019).

Autosomal dominant is the most common pattern of inheritance in AC but desmosomal recessive forms have also been reported to present a cardio-cutaneous phenotype, named Naxos disease (Kaplan et al., 2004b) when *JUP* carries a homozygous mutation (McKoy et al., 2000), and Carvajal syndrome when *DSP* carries a homozygous mutation (Carvajal-Huerta, 1998; Norgett et al., 2000). Further analysis of the structural and molecular pathology of the heart in Carvajal syndrome showed a distinct cardiomyopathy characterized by focal ventricular aneurysms and reduced expression of desmosomal proteins DSP and plakoglobin, and the gap junction protein connexin 43 (CX43) at intercalated disks. These abnormal protein–protein interactions cause both contractile and electrical dysfunction in Carvajal syndrome (Kaplan et al., 2004a).

Two adherens junction proteins, N-cadherin (CDH2; Mayosi et al., 2017) and αT-catenin (CTNNA3; van Hengel et al., 2013), have been associated with AC, that broadens cell-cell adhesion disease pathogenesis beyond the desmosomes. In the extracellular space, cadherins of adjacent cells bind together, while the cytoplasmic domains of cadherins are linked to the actin cytoskeleton through β-catenin, plakoglobin, and αT-catenin (Janssens et al., 2001; Kobielak and Fuchs, 2004). Since N-cadherin and αT-catenin co-localize with the area composita and not desmosomes, AC could also be considered as an "area composita disease" rather than a classical "desmosomal disease" (van Hengel et al., 2013). In addition, variants in the tight junction protein zonula occludens-1 (*TJP1*) gene have recently been described in AC cases (De Bortoli et al., 2018). The translation product of *TJP1*, ZO-1 is an adapter protein that interacts with gap junctions and area composita proteins and plays a crucial role in the cardiac functional syncytium (Zhang et al., 2020).

Junctional complexes mediate cell-cell adhesion tethering adjacent cells and anchoring them to the ECM (Gumbiner, 1996). Junctional proteins provide tensile strength and resilience to the tissue as well as mechanical, electrical, and chemical continuity between cells. This function is of particular importance for cardiac cells, allowing the mechanical work of individual myocytes to integrate into the pumping function of the heart, continuously subjected to contraction and relaxation cycles of different intensity (McCain et al., 2012). Moreover, desmosomes and adherens junctions constitute a mechanotransduction hub (Pannekoek et al., 2019). AC-causing mutations that modify junctions might thus alter cardiac cell tethering or signaling functions (Hariharan et al., 2014).

The cytoplasmic face of desmosomes and adherens junctions are connected to cytoskeleton proteins, e.g., actin. Mutations in some cytoskeleton-associated proteins (Titin or TTN, Filamin or FLNC, and Desmin or DES) were also found in some AC patients (Klauke et al., 2010; Taylor et al., 2011; Hall et al., 2020). Moreover, variants in two proteins of the sarcomere stabilizing the Z-line, namely α-actinin-1 (ACTN1; Good et al., 2020), which is a cytoskeleton protein binding actin filaments and stabilizing the contractile apparatus, and lim domain binding 3 (LDB3 or ZASP; Lopez-Ayala et al., 2015), which is an α-actinin interacting protein, have also been described in AC patients. Cytoskeleton proteins are in charge of structural preservation and mechanotransduction.

Similarly, transmembrane protein 43 (TMEM43) and Lamin A/C (LMNA), both involved in preserving the structural integrity continuum at the nuclear membrane level, are rarely mutated in AC (Merner et al., 2008; Quarta et al., 2012).

Calcium (Ca^{2+}) handling proteins, such as PLN and RYR2, regulating Ca^{2+} storage in the sarcoplasmic-endoplasmic reticulum of cardiac cells, have been implicated in AC pathogenesis (Tiso et al., 2001; van der Zwaag et al., 2012). They are involved in regulating excitation-contraction coupling and many Ca^{2+}-dependent functions. Ca^{2+} is the major second messenger mediating response to sympathetic stimuli through beta adrenergic receptor activation, cyclic AMP (cAMP) formation and Ca^{2+}-dependent kinases activation (de Lucia et al., 2018). Furthermore, through the action of stretch-activated

TABLE 1 | Desmosomal genes associated to AC.

Gene	Chromosomal location	Protein	Prevalence	Mainly associated to:	References
DSP	6p24	Desmoplakin	10–15%	AC	Rampazzo et al., 2002
PKP2	12p11	Plakophilin-2	10–45%	AC	Gerull et al., 2004
DSG2	18q12	Desmoglein-2	7–10%	AC	Pilichou et al., 2006
DSC2	18q12	Desmocollin-2	Rare	AC	Syrris et al., 2006; Beffagna et al., 2007
JUP	17q23	Plakoglobin	Rare	AC	McKoy et al., 2000

TABLE 2 | Non-desmosomal genes also associated with AC phenocopies.

Gene	Chromosomal location	Protein	Prevalence	Mainly associated to:	References
CTNNA3	10q21	α-T-Catenin	Rare	AC	van Hengel et al., 2013
CDH2	18q12	Cadherin-2	Rare	–	Turkowski et al., 2017
TJP1	15q13	Tight Junction Protein ZO-1	Rare	–	De Bortoli et al., 2018
DES	2q35	Desmin	Rare	DC	Klauke et al., 2010
TTN	2q31	Titin	Rare	DC	Taylor et al., 2011
FLNC	7q32.1	Filamin C	Rare	HC; RC	Hall et al., 2020
LMNA	1q21	Lamin A/C	Rare		Quarta et al., 2012
TMEM43	3p23	Transmembrane protein-43	Rare	AC; EDMD	Merner et al., 2008
ACTN2	1q43	α-actinin-2	Rare	DC; HC	Good et al., 2020
LDB3	10q23	Lim domain binding 3 or ZASP	Rare	DC; HC; LVNC	Lopez-Ayala et al., 2015
RYR2	1q43	Ryanodine Receptor-2	Rare	CPVT	Tiso et al., 2001
PLN	6p21	Phospholamban	Rare	DC; HC	van der Zwaag et al., 2012
TGFβ3	14q24	Transforming growth factor β3	Rare	LDS; AC	Beffagna et al., 2005
SCN5A	3p22	Sodium voltage-gated channel alpha subunit 5	Rare	BS	Yu et al., 2014

Green, genes with mechanical function; yellow, genes with a function in response to adrenergic stimuli. Association based on Online Mendelian Inheritance in Man catalog. AA, Aortic Aneurism; AC, Arrhythmogenic Cardiomyopathy; BS, Brugada Syndrome; CPVT, Catecholaminergic Polymorphic Ventricular Tachycardia; LDS, Loeys-Dietz Syndrome; DC, Dilated Cardiomyopathy; HC, Hypertrophic Cardiomyopathy; RC, Restrictive Cardiomyopathy; ED-MD, Emery-Dreifuss Muscular Dystrophy; and LVNC, Left Ventricular Non-Compaction.

channels, mechanical forces are transduced into ion fluxes including Ca^{2+} (Martinac, 2004).

Interestingly, positron emission tomography showed that the AC myocardium displayed reduced β-adrenergic receptor density, which was hypothesized to be the result of a secondary downregulation in response to either local increased firing rates or impaired presynaptic catecholamine reuptake in efferent sympathetic nerves (Wichter et al., 2000). These data suggest a link between sympathetic hyperactivity and life-threatening arrhythmias triggering in patients with AC.

Despite such deep understanding of AC-linked genetics, AC diagnosis is mainly based on clinical parameters and it remains challenging to be unambiguously identified due to non-specific clinical features and the variable clinical presentation of the disease. Diagnostic criteria were established by an international task force in 1994 and revised in 2010 due to the use of emerging diagnostic modalities and the discovery of genes involved in AC (McKenna et al., 1994; Marcus et al., 2010). Recently, the criteria have been better defined and widened to include left dominant AC and pediatric cases (Corrado et al., 2020). However, once a causative mutation is identified in a proband, predictive genetic testing is advisable for relatives, in order to adopt either clinical follow-up or preventive strategies, such as sport restriction and beta-blockers or ICD therapy in individuals at risk (Corrado et al., 2015; Stadiotti et al., 2019).

AC Penetrance Is Dependent on Physical Exercise

Exercise is associated with modulation of cardiac sympathetic activation. As a consequence, aerobic exercise promotes beneficial effects on the treatment of diseases such as arterial hypertension, atherosclerosis, venous insufficiency, and peripheral arterial disease (Leosco et al., 2013). However, a small but significant proportion of athletes die suddenly (Corrado and Zorzi, 2018), with exercise being particularly deleterious in AC. Despite its genetic determinants, AC penetrance is largely affected by high-intensity physical activity. While the most accepted view is that exercise enhances a genetic predisposition, others theorize that genetic and environmental stressors may combine to variable extent resulting in overt disease with inconsistent phenotype severity (Prior and La Gerche, 2020).

Undoubtedly, exercise is a strong predictor of life-threatening ventricular arrhythmias in AC (Lie et al., 2018b). Accordingly, the risk of SCD was increased five-fold in AC athletes (Corrado et al., 2003) and arrhythmic events often occurred during exercise (Thiene et al., 1988).

For this reason, some countries worldwide, supported by expert consensus of the major cardiology societies, have defined a pre-participation screening program for competitive athletes, in order to avoid the combination of intense exercise and the presence of underlying cardiomyopathy (among which AC;

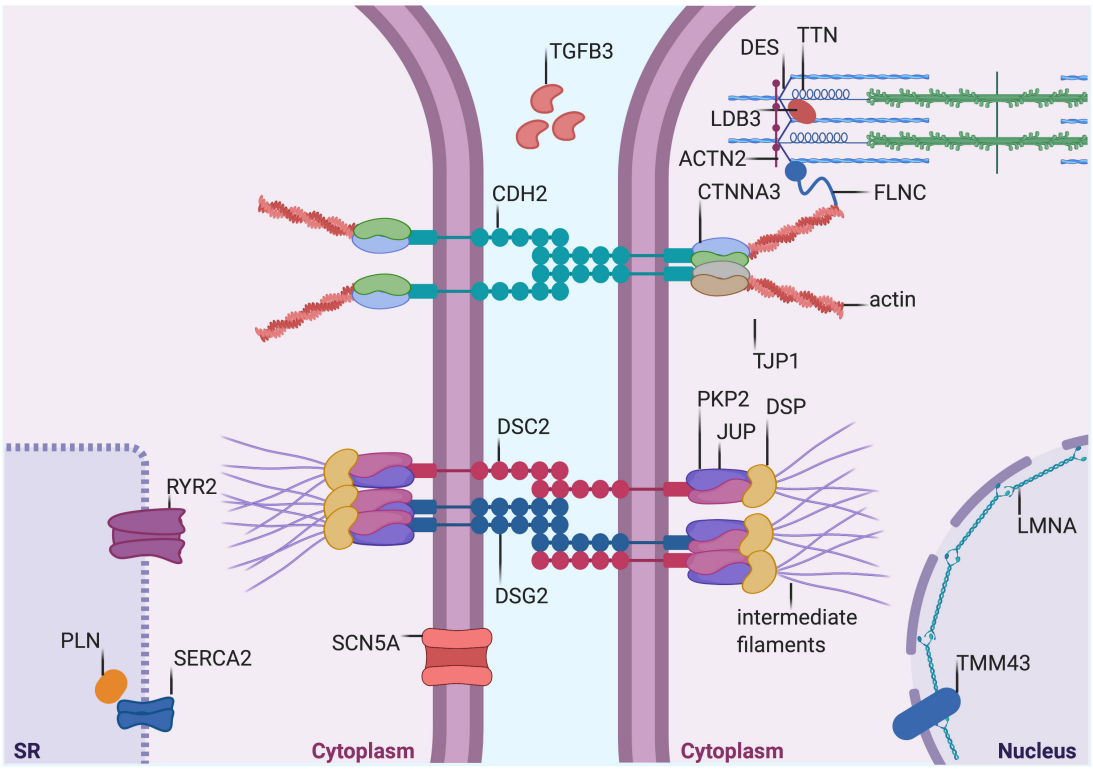

FIGURE 1 | Proteins mutated in AC. Graphical representation of proteins that are mutated in AC. Both proteins desmosomal (see **Table 1**) and non-desmosomal proteins (see **Table 2**) are depicted in this figure. DSP, desmoplakin; PKP2, plakophilin-2; DSG2, desmoglein-2; DSC2, desmocollin-2; JUP, plakoglobin; CTNNA3, α-T-Catenin; CDH2, cadherin-2; TJP1, tight Junction Protein ZO-1; DES, desmin; TTN, titin; FLMN, filamin C; LMNA, lamin A/C; TMEM43, transmembrane protein-43; ACTN2, α-actinin-2; LDB3, lim domain binding 3 or ZASP; RYR2, ryanodine Receptor-2; PLN, phospholamban; TGFβ3, transforming growth factor β3; and SCN5A, sodium voltage-gated channel alpha subunit 5. SERCA2, sarcoplasmic/endoplasmic reticulum calcium ATPase 2. The figure was redrawn from Austin et al., 2019.

Maron et al., 2015; Mont et al., 2017). This has drastically reduced the occurrence of SCD (Corrado et al., 2006), as ECG alone can effectively recognize most individuals requiring sport disqualification (Mont et al., 2017). However, management and costs of the screening do not allow a thorough analysis on such a large population and the transition to secondary tests, including genetics, does improve the recognition yield of individuals at risk (Limongelli et al., 2020).

In clinical settings, exercise testing can be used to mimic, under controlled circumstances, the effect of exercise. Such tests could reveal latent electrocardiogram abnormalities and electrical instability in a significant number of asymptomatic AC gene carriers (Perrin et al., 2013).

Strenuous exercise increases both mechanical load (stretch and volume) and adrenergic stress in humans, the two types of stimulation that AC patients are particularly vulnerable to (**Figure 2**).

The arrhythmogenic effect of exercise on AC hearts is likely due to sympathetic induction, which, *per se*, can affect electrophysiological mechanisms of arrhythmia initiation and/or maintenance (Johnson and Antoons, 2018). β-adrenergic receptor activation increases sarcoplasmic reticulum Ca^{2+} load, triggering pro-arrhythmogenic effects, and in the AC setting can exacerbate existing Ca^{2+} defects (Moccia et al., 2019). This is supported by the fact that isoproterenol testing can sensibly unveil arrhythmias in AC patients, particularly in the early concealed stages of the disease (Denis et al., 2014).

Additionally, different studies have associated intense endurance exercise with earlier onset and more severe expression of AC disease substrate phenotype (La Gerche, 2015), broadening the effect of sport beyond arrhythmic burden. In AC mutation carriers with a history of endurance exercise, symptoms occur at a younger age than in sedentary individuals, and athletes are more likely to develop heart failure and to meet Task Force criteria for AC (James et al., 2013). Moreover, imaging studies revealed that left and right ventricular function was reduced and right ventricle volume enlarged in athletes when compared to non-athletes (Sen-Chowdhry et al., 2007). Interestingly, an apparent direct dose-response relationship has been established between exercise intensity and severity of AC phenotypes in AC-mutation carriers, where exercise intensity is more damaging than exercise duration (Lie et al., 2018a).

Intense exercise increases ventricular wall stress and the forces to which desmosomes, adherens junctions and the whole cytoskeletal continuum are subjected. In the AC context, defects in these proteins provide susceptibility to mechanical

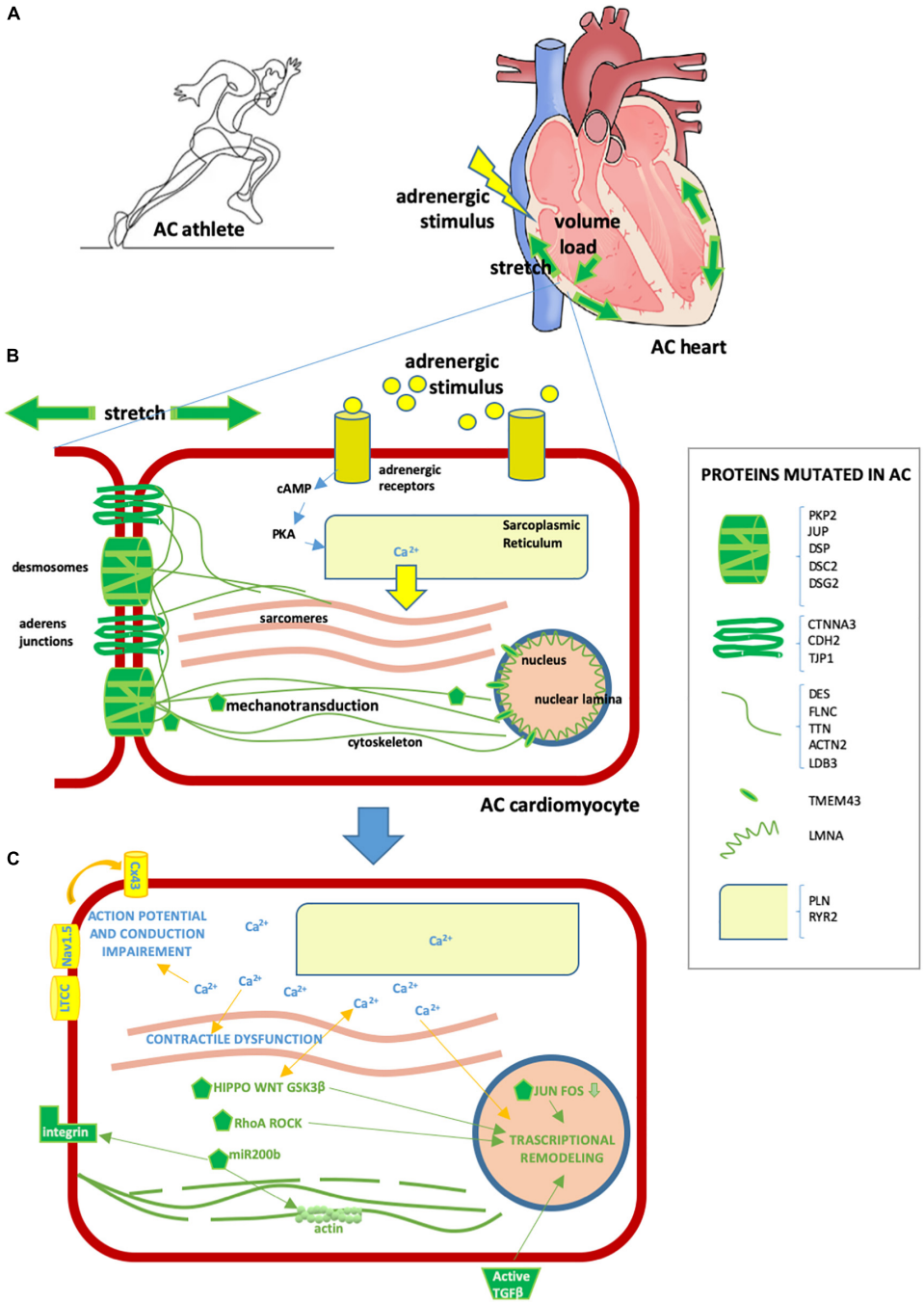

FIGURE 2 | Effect of exercise on the AC heart. **(A)** Exercise involves hyperactivation of adrenergic stimuli and augmented mechanical forces, including stretch and volume load. These physiological mechanisms can exacerbate AC heart remodeling and arrhythmia predisposition, already induced by AC mutations. **(B)** AC cardiomyocyte. In yellow/light blue, adrenergic stimuli or proteins implicated in adrenergic response [some proteins regulating calcium (Ca^{2+}) fluxes can be mutated in AC, as detailed in the box on the right]; in green, stretch or mechanical stretch responsive proteins (some proteins implicated in mechanical force management can be mutated in AC, as detailed in the box on the right). **(C)** Consequences of cytoplasmic Ca^{2+} excess and activation of mechanotransduction molecules in AC cardiomyocytes are as follows:
– contractile dysfunction due to excitation-contraction coupling defect;
– transcriptional remodeling including cell fate change, apoptosis, pro-inflammatory, pro-adipogenic and pro-fibrotic program activation;
– intercalated disk remodeling with abnormal activation of the NaV1.5 channel and other Ca^{2+}-dependent ion channels, leading to action potential shortening;
– lateralization of CX43 and altered permeability leading to conduction defects;
– cytoskeleton alteration/disruption, integrins and TGFβ activation.
Some of these consequences are mediated by several Ca^{2+}-sensitive or mechano-sensitive pathways (namely Hippo, WNT, GSK3β, RhoA ROCK, JUN-FOS, miR-200b, TGFβ, ion channels, and CX43 modulation) which combine with those already genetically active in AC, resulting in a strong additive effect.

damages and/or alter signal mechanotransduction. Interestingly, AC phenotype may involve both the right and left ventricles with variable expressivity, but the associated mechanisms that are still not well understood. Intriguingly, physiological difference between right and left ventricle thickness and wall tension might result in different mechanotransduction signaling (Mestroni and Sbaizero, 2018); being the right ventricle wall more volume-loaded (La Gerche et al., 2011), this provides an explanation for the predominant right ventricle involvement in both arrhythmias and fibro-fatty remodeling in AC (Thiene and Marcus, 2013). Indeed, the observation that the thin walled right ventricle and the thinnest segment of the left ventricle (posterior wall) are most often involved may reflect these areas being more vulnerable to physical stress or stretch, where, according to Laplace's law, wall tension is particularly high (Thiene and Marcus, 2013). Accordingly, right ventricular strain measured by echocardiography is associated with worst structural degeneration in AC patients (Malik et al., 2020).

AC Therapies Include Beta Blocker Administration and Exercise Limitation

Therapeutic options for AC are aimed both at prevention of SCD and at limiting heart failure and symptoms. They mainly consist on lifestyle changes, pharmacological treatment, catheter ablation, implantable cardioverter defibrillator graft, and, in the worst cases, heart transplantation.

Lifestyle changes consist of exercise restrictions, which effectively limited disease progression and reduced the likelihood of sustained ventricular arrhythmias (Calkins et al., 2017). The main pharmacological therapy used with AC patients is β-blocker administration. According to the 2017 AHA/ACC/HRS guidelines for the management of ventricular arrhythmias, a strong recommendation is made both for the use of β-blockers and for avoiding intense exercise (Al-Khatib et al., 2018). While these recommendations and approaches are based on several well-structured studies deemed effective in clinical practice, no systematic randomized studies are available to date.

β-blockers are competitive antagonists of endogenous catecholamines that block receptor sites on adrenergic beta receptors. By binding stress hormone receptors, they weaken the fight-or-flight reaction (Szentmiklosi et al., 2015). Bursts of adrenergic stimulation promote hyperphosphorylation of RYR2 in the myocardium, leading to excess Ca^{2+} influx into the cytoplasm which contributes to electrical instability, thus triggering arrhythmias (Landstrom et al., 2017). This mechanism is particularly relevant for catecholaminergic ventricular tachycardia (CPVT), where arrhythmia occurs in the context of a structurally-normal heart and only in response to adrenergic stress, thus supporting the essential role of β-blockade therapy in these patients. In addition, excessive catecholamine activity is responsible for a number of deleterious effects on the heart, including increased oxygen demand, propagation of inflammatory mediators, and abnormal cardiac tissue remodeling, all of which decrease the efficiency of cardiac contraction and contribute to heart failure progression (de Lucia et al., 2018). The antiarrhythmic of effects β-blockers are based on counteracting the effects of adrenergic stress by: (i) slowing down the heart rate, decreasing spontaneous depolarization of pacemaker cells of the sinus node; (ii) slowing atrio-ventricular conduction, which increases the refractory period of the atrio-ventricular node; (iii) reducing myocardial contractility, thus preventing action potential (AP) duration shortening of myocardial cells; (iv) suppressing catecholamine-induced hypokalemia (Gorre and Vandekerckhove, 2010). Importantly, ventricular structure and function can be modulated by β-blockade. Myocardial ischemia can be reduced though vasodilation, and heart failure can be reduced by modulating gene expression, ultimately inhibiting myocardial oxidative stress and apoptosis (López-Sendón et al., 2004).

Arrhythmogenic Cardiomyopathy guidelines and expert consensus documents generally advise β-blocker use for AC, without indication about β-receptor selectivity (Al-Khatib et al., 2018; Towbin et al., 2019). Indeed, no randomized studies have been performed on specific β-blockers in AC. Recent advances in the pharmacological selectivity of β-blockers has defined three generations: first-generation β-blockers, non-selective, blocking both β1 and β2 receptors, thus acting also in non-cardiac sites; second-generation β-blockers, more cardio-selective since they present higher affinity for β1-receptors; third-generation β-blockers with selectivity for β1 receptors and α1-adrenoreceptors while activating β3-adrenergic receptors. The latter group showed vasodilation, antioxidant, antihypertrophic, and antiapoptotic activities (do Vale et al., 2019). In principle, third-generation β-blockers may be more appropriate for AC by potentially targeting other AC dysfunctions. Accordingly, the MADIT-CRT trial showed that the third generation β-blocker carvedilol was the most effective agent that reduced the number of inappropriate ICD shocks for patients who received an ICD (Ruwald et al., 2013). Also, a case report suggests that carvedilol improved left ventricular function in an AC patient (Hiroi et al., 2004). Specific clinical studies in AC patients are needed to unveil the most effective class of β-blocker.

IN VITRO AC CELLULAR MODELS

Arrhythmogenic Cardiomyopathy cellular models represent extremely useful tools to recapitulate AC-specific traits *in vitro*, to investigate cellular and molecular mechanisms involved in disease onset and progression, and in testing potential treatments. In this section, we focus on the cellular models that supported the link between AC and either mechanical load or adrenergic signaling (**Table 3**). A complete overview of the cellular models used to study AC have been previously reviewed (Sommariva et al., 2017).

In vitro Models of Mechanical Load in AC

Here we provide an overview of how mechanical load was integrated in cellular models to support the concept that stretch may impair cell adhesion, intracellular signaling, and intercellular conduction of excitation in AC cells.

Non-Human Models

New insights into the molecular basis of altered mechanosensing in AC have come from biophysical measurements in heterologous

TABLE 3 | Animal and cellular AC models linking mechanical load/mechanotransduction and adrenergic stimulation with AC pathogenesis.

Model		Gene/Mutation	Phenotype	Type of stress	Conclusions	References
Animal models	Murine	*Dsp* / Cardiac-specific p.R2834H Dsp overexpression	Ventricular enlargement and biventricular cardiomyopathy at rest; right ventricle dilation and focal fat infiltration in response to exercise	Physical exercise (daily running regimen for 12 week)	DSP expression in cardiomyocytes contributes to maintaining cardiac tissue integrity; exercise accelerates cardiac remodeling	Yang et al., 2006; Martherus et al., 2016
		Dsp / cardiac-specific Dsp-KO	No phenotype within 2-months after birth. By 6 months of age, cardiac systolic dysfunction and mild myocardial fibrosis. By 1-month increased mortality, cardiac systolic dysfunction and exercise-inducible ventricular arrhythmias.	Early and long treadmill exercise	Treadmill exercise restored transcript levels of dysregulated genes in cardiomyocytes, reducedmyocardial apoptosis, and induced cardiac hypertrophy without affecting cardiac dysfunction	Garcia-Gras et al., 2006; Cheedipudi et al., 2020
		Dsp / Cardiomyocyte-specific Dsp-KO	Ultrastructural defects in desmosomal integrity and cardiomyopathy; cell death and fibro-fatty replacement; biventricular dysfunction, failure and death; arrhythmias	Physical exercise (horizontal treadmill at incrementally faster running speeds). Adrenergic stress (intraperitoneal injection of high or low dose epinephrine)	Exercise causes catecholamine-induced arrhythmias	Lyon et al., 2014
		Pkp2 deficiency	Flecainide and exercise-induced arrhythmia and cardiac remodeling	One-month voluntary running on a treadmill	Exercise-induced pro-arrhythmic behavior due to impaired Ca^{2+} cycling and electrical conduction	Grossmann et al., 2004; van Opbergen et al., 2019
		PKP2 / card-ac-specific p.R735* overexpression	No AC phenotype at rest; strenuous swimming induced right ventricular dysfunction	Endurance exercise training (10 months strenuous swimming protocol)	Endurance training triggers AC-like phenotype in mice	Cruz et al., 2015
		Dsg2 / exons 4 and 5 deletion	No phenotype at rest; myocyte injury and redistribution of intercalated disk proteins in response to exercise	Starting from 3 weeks of age, gradually incremented exercise training (swimming)	Exercise reduces survival of Dsg2 mutant mice	Chelko et al., 2016
		Dsc2 / Embryonic Dsc2-knock-down	Reduction in the desmosomal plaque area, loss of desmosome extracellular electron-dense midlines, and myocardial contractility defects	–	Dsc2 is necessary for normal myocardial structure and function	Heuser et al., 2006
		Jup / Jup-KO	Genetic background-dependent embryonic lethality (heart defects) or late-embryonic/perinatal lethality (cardiac dysfunction and severe skin phenotype); thin and detached epidermis; altered physical properties of the skin	Mechanical stress (skin rubbing and cutting)	Jup mutations are responsible of different skin physical properties and susceptibility to mechanical stress	Bierkamp et al., 1996; Bierkamp et al., 1999
		Jup / 2057del2 heterozygous mutation	No phenotype at rest; myocyte injury and redistribution of intercalated disk proteins in response to exercise	Starting from 3 weeks of age, gradually exercise training increment (swimming)	Exercise reduces survival of Jup mutant mice	Chelko et al., 2016
		PLN / Cardiac-specific heterozygous expression of PLN Arg14Del	By middle age, *het* individuals developed left ventricular dilation, contractile dysfunction, and episodic ventricular arrhythmias, with overt heart failure; cardiomyopathy and heart failure upon adrenergic stimulation	Adrenergic stimulation (chronic suppression of either basal SERCA2a activity or the stimulatory effect of the β-adrenergic signaling pathway)	Chronic suppression of SERCA2 may lead to premature death	Haghighi et al., 2006
	Zebrafish	*Dsp* / transient Dsp-knock-down	Mild developmental delay, signs of microcephaly, pericardial effusion, and decreased heart rate	–	Wnt/β-catenin and Hippo are the final common pathways underlying different desmosomal AC forms	Giuliodori et al., 2018
		Pkp2 / Pkp2-konck-down	Decreased heart rate, reduced number of intercalated disks, increased intracellular space	–	Pkp2 has structural and signaling roles in heart development	Moriarty et al., 2012

(Continued)

TABLE 3 | Continued

Model		Gene/Mutation	Phenotype	Type of stress	Conclusions	References
		Jup / Jup-knock-down	Reduced number of adhesion junction proteins	–	Loss of Jup leads to altered desmosome structure. Jup antagonizes β-catenin signaling in the heart	Martin et al., 2009
		JUP / cardiomyocyte-specific over-expression c.2057del2	Heart enlargement with marked thinning of atrial and ventricular walls, cachexia, and peripheral edema	–	Mortality, reduced I_{Na} current density. SB216763 rescued the AC phenotypes	Asimaki et al., 2014
		STRN / 8 bp deletion in the 3' UTR	Syncope or SCD or heart failure	Exposure to risk factors similar to those of humans may be one of the reasons for spontaneous AC occurrence	STRN co-localizes with desmosomal proteins and interferes with the Wnt pathway thus STRN is a potential contributor to mechanotransduction and downstream sympathetic signaling	Meurs et al., 2010; Oxford et al., 2014; Cattanach et al., 2015
	Canine	Spontaneous model, genetic alterations were unknown	Cardiomyopathy that closely mimics AC in humans	Exposure to risk factors similar to those of humans	Spontaneous canine model is s useful tool to study pathophysiological mechanisms in AC	Fox et al., 2000
	Feline	*PKP2* / c.2386T > C (p.C796R)	Unstable PKP2 proteins that fail to interact with DSP and undergo targeted degradation involving calpain and other proteases	–	PKP2 mutations induce loss of function effects by intrinsic instability and calpain protease- mediated degradation	Kirchner et al., 2012
Cellular models	HL-1	*Pkp2* knock-down	Changes in cytoskeleton organization including perturbation of the actin network and focal adhesions, decreased stiffness, reduced work of detachment	Mechanical load	Pkp2 mutation impact on cardiomyocyte-ECM interactions; miR200b is one of the mediators	Puzzi et al., 2019
		Pkp2 knock-down	Increased separation of microtubules from the cell extremities	–	Compromised adhesion networks and impaired mechanotransduction	Cerrone et al., 2014
		Dsg2 / p.D154E, p.D264E, p.N266S, p.D494N, p.A517V, p.G812S, p.G812C, p.C813R, and p.V920G	Reduced cell-cell cohesion	Force of detachment / shear stress	Desmoglein-2 interaction is crucial for cardiomyocyte cohesion	Schlipp et al., 2014
		LMNA / c.418_438dup (p. Leu140_Ala146dup)	Decreased mechanical resistance of the nuclear envelope	–	*LMNA* mutations cause decreased cardiomyocyte tolerance to mechanical stress	Forleo et al., 2015
	Murine ventricular myocytes	*Jup* 2057del2 over-expression	Increased apoptosis	Uniaxial cyclic stretch	Aberrant trafficking of intercalated disk proteins is a central mechanism in AC myocyte injury	Asimaki et al., 2014
	Neonatal rat ventricular myocytes	*DSP* / homozygous C-terminaltruncation	Altered morphology, elasticity, adhesion and viscoelastic properties	–	*DSP* mutations lead to cellular biomechanics impairment	Puzzi et al., 2018
	Human keratinocytes	*PKP2* / c.1760delT (p.V587Afs*655)	Accumulated lipid droplets, disarray of myofilaments	Physiological substrate stiffness and electrical stimulation	Cell-cell adhesion and mechanical sensing influences cell identity	Dorn et al., 2018
	hiPSC-CMs	*PKP2* / homozygous c.2484C > T	Lipid accumulation and apoptosis	Transplant into neonatal rat hearts	hiPSC maturation uncovers some of the AC phenotypes	Cho et al., 2017
		PKP2 / homozygous c.2484C > T	Reduced gene expression response to mechanical stress	Physical confinement and cyclic uniaxial elongation	Transcriptional response to mechanical load is impaired	Martewicz et al., 2019

(Continued)

TABLE 3 | Continued

Model	Gene/Mutation	Phenotype	Type of stress	Conclusions	References
	PKP2 / c.971_972InsT (p.A324fs335X/N)	Changes in gene expression, lipid accumulation, action potential shortening, re-entrant arrhythmia	Electrical stimulation	Syncytial constructs and matrix cues enable better modeling of heart tissue	Blazeski et al., 2019
	PKP2 / homozygous c.2484C > T	Increased apoptosis and lipid accumulation	Hormonal treatment (testosterone)	Sex hormones can influence disease pathology	Akdis et al., 2017
	DSG2 / p.G638R	Increased action potential shortening, arrhythmic events	Adrenergic stimulation	*DSG2* mutations influence cardiac ion currents and cause arrhythmia	El-Battrawy et al., 2018
	TMEM3 / p.S358L	Decrease in the rising and decay time of Ca^{2+} transients, changes in contraction properties	Adrenergic stimulation	Isoprenaline induced abnormal Ca^{2+} transients	Padrón-Barthe et al., 2019
hiPSC-cardiac microtissues	*PKP2* / c.2013delC (p.K672RfsX12)	Arrhythmias	Electrical stimulation	hiPSC-cardiac fibroblasts influence adjacent cardiomyocyte electrical behavior	Giacomelli et al., 2020

cell systems and murine cellular models. These systems proved useful in studying biomechanical properties of cells in the presence of altered or reduced desmosomal proteins.

The mouse atrial CM HL-1 cell-line has been widely used to study AC causing mutations. Overexpression of mutant PKP2 in HL-1 cells revealed that mutated PKP2 failed to interact with DSP (Kirchner et al., 2012), supporting the concept that mechanotransduction is impaired in AC (Mestroni and Sbaizero, 2018).

Atomic force microscopy (AFM) can be used to assess morphology and mechanical properties in single living cells, including cell-ECM interactions. Using a cantilever system, cell elasticity and viscoelasticity behavior toward externally applied forces can be measured, since alterations of cellular tension elements have an impact on cell stiffness. Pkp2 was knocked-down in these cells using short hairpin RNA (Puzzi et al., 2019) and single-cell force spectroscopy by AFM was used to determine cell-ECM interactions in Pkp2-deficient HL-1 cells. Specifically, Pkp2-knock-down was sufficient to induce changes in cytoskeleton organization with perturbation of the actin network and changes in focal adhesions. As a consequence, CM stiffness decreased, along with a reduction in work of detachment, suggesting an impact on CM-ECM interactions. Interestingly, the authors identified miR200b as one of the mediators of these effects, since miR200b predicted targets belong to the focal adhesion pathways. In line with this, downregulation of miR200b partially rescued the mechanical properties of Pkp2-deficient cells, with restoration of cellular stiffness but only partial actin network rescue, indicating that likely additional factors regulate the cytoskeleton organization.

HL-1 cells were also used to demonstrate that some Dsg2 mutations affect cell cohesion, which was measured using a liberase-based dissociation-assay. In addition, Dsc2 and N-cadherin interactions were measured using AFM and compared with cell-free single-molecule measurements (Schlipp et al., 2014).

Overexpression of mutated LMNA in HL-1 cells revealed decreased mechanical resistance of the nuclear envelope, again supporting the idea that one of the main pathological mechanisms in AC include decreased CM tolerance to mechanical stress (Forleo et al., 2015).

Among the murine cellular models, super-resolution fluorescence microscopy was used in single isolated mouse ventricular myocytes with *Pkp2*-heterozygous *null* genotype and identified increased separation between the microtubule plus end (marked by the protein EB-1) and N-cadherin. This supported the concept that defective desmosomal proteins interfere with adhesion networks resulting in impaired mechanotransduction properties of the cells (Cerrone et al., 2014).

Finally, a mutant *Jup* was overexpressed in neonatal rat ventricular myocytes that showed increased levels of apoptosis when subjected to brief intervals of uniaxial cyclical stretch for 4 h (Asimaki et al., 2014).

Human AC Cellular Models

Human tissue for studying AC is not easily obtained and it is limited to small biopsies, which are, however, mainly used

for diagnostic purposes, and rare explanted hearts. From small biopsies, it is possible to isolate cardiac stromal cells that can be used to assess contribution to adipocyte differentiation (Sommariva et al., 2016; Pilato et al., 2018), while CMs isolated from biopsies cannot be kept very long in culture without de-differentiation. However, epithelial cells also express junctional and desmosomal proteins, therefore keratinocytes or buccal mucosa epithelial cells from AC patients represent an alternative cell source to investigate especially the localization of mutated proteins.

Similarly to the heart, the skin is a tissue that experiences continuous mechanical stress. It is therefore not unexpected that mutations in DSP, which is an essential component of cell-cell junctions both in CMs and keratinocytes, cause cardio-cutaneous syndrome (Carvajal syndrome; Norgett et al., 2000). Single cell force spectroscopy based-AFM was applied to human keratinocytes carrying a homozygous DSP mutation, which displayed altered morphology, elasticity, adhesion capabilities and viscoelastic properties compared to wild type keratinocytes, highlighting the tight interconnection between adhesion proteins and the intermediate filament scaffold (Puzzi et al., 2018).

After their discovery, human induced pluripotent stem cells (hiPSC) were soon differentiated into CMs and used to model several inherited cardiac diseases (Bellin et al., 2012; Giacomelli et al., 2017), including AC (Caspi et al., 2013; Kim et al., 2013; Ma et al., 2013). The majority of these models used hiPSCs from patients carrying mutations in *PKP2*, the most commonly mutated gene in AC. The first studies used hiPSC-CMs differentiated in embryoid bodies or in two-dimensional monolayer cultures, and the main focus of the AC phenotype was apoptosis and lipid accumulation. Importantly, under basic culture conditions, only some typical signs of the disease were detectable *in vitro*, including identification of defects of hiPSC-CMs in establishing cell-cell junctions (such as enlarged desmosomes at electron microscopy analysis, reduced immune-signal for desmosomal proteins). To uncover the AC phenotypes of CM apoptosis and lipid accumulation *in vitro* using AC hiPSC-CMs, both induction of metabolic maturation from glycolytic to fatty acid oxidation energetics was necessary and further co-activation of normal PPAR-alpha and abnormal PPAR-gamma pathways (Kim et al., 2013; Wen et al., 2015).

In standard CM cultures *in vitro*, the physical cues of the human heart are not sufficiently reproduced, and the capability of modeling the dynamic and highly organized environment of such a complex organ is limited. A well-recognized limitation of hiPSC-CMs is indeed their fetal-like phenotype, with disorganized sarcomeres and lack of T-tubules (where connexosomes are located) to mention some junctional proteins that are most relevant for AC modeling. Therefore, later studies used different strategies to reproduce the biophysical and mechanical characteristics typical of the heart, including mechanical load and stretch, continuous electrical stimulation, and anisotropic tissue organization.

By culturing 3-month old hiPSC-CMs under conditions mimicking the mechanical load of the heart (50 kPa substrate stiffness and 1 Hz electrical pacing), together with maturation/adipogenic medium, PKP2 mutant hiPSC-CMs not only accumulated lipid droplets, but also displayed disarrayed myofilaments, with progressive acquisition of fat cell identity (Dorn et al., 2018). This work highlighted the role of cell-cell adhesion and mechanical sensing in determining (cardiac) cell identity. This work is an exemplar of how changes in cell-cell contacts may induce changes in transcriptional programs and, in this particular case, control myocyte/adipocyte identity. Interestingly, by exome sequencing, the authors identified a mutation in the *MYH10* gene in a patient diagnosed with AC but without mutations in classical AC-causing genes. *MYH10* encodes the non-muscle myosin IIB (NMIIB) of the actomyosin cytoskeleton, which regulates both actin dynamics and accumulation of active RhoA-GTP at adherens junctions, thereby supporting the role of the mechanosignaling cascade in the pathogenesis of AC. hiPSC-CMs were also generated from this patient and they recapitulated AC traits *in vitro*, including reduced levels of NMIIB protein at the cell membrane, accompanied by decreased membrane RhoA and compromised cell-cell junctions. Importantly, the link between RhoA regulation by PKP2 and impact on CX43 was previously demonstrated in AC patients' samples and HL-1 cells (Wang et al., 2015). However, a clear link between MYH10 and AC has not been firmly established yet. Notwithstanding, this work provided evidence that by using culture conditions more closely mimicking the mechanical strain of the heart, it was possible to reveal lineage conversion under pathological conditions and lipogenic stimuli.

Maturation to adult-like phenotype could be achieved by *in vivo* transplantation of *PKP2* mutated hiPSC-CMs into neonatal rat hearts, which allowed the recapitulation of lipid accumulation and apoptosis after 1 month (Cho et al., 2017). The elements that permitted maturation and development of AC pathological features in this experimental setting might be multifold and likely include microenvironment, cardiac-specific secreted factors, cardiac ECM, electrical pulses or even stiffness and mechanical load and stretch.

Cell-cell interactions play key roles in normal and pathological heart physiology and, electrophysiological and histopathological manifestations at tissue level may not be evident in single cells *in vitro*. To properly model these features *in vitro*, both precisely oriented syncytium-like structure and cyclic biomechanical stimuli must be accurately mimicked. Two multicellular syncytial models were used to study AC using hiPSC-CMs (Blazeski et al., 2019; Martewicz et al., 2019).

To specifically analyze how hiPSC-CMs reacted to mechanical load in the settings of AC, Martewicz et al. (2019) integrated both controlled substrate topology (50-μm wide linear confinement) and a stretching system to apply cyclic uniaxial elongation. Physical confinement resulted in a regular and organized sarcomeric structure, and in a more physiological distribution of desmosomal proteins, i.e., PKP2 was mainly localized at inter-cellular junctions. Without stretching system, the main difference in gene expression between AC and control hiPSC-CMs was found in ECM genes (including collagen and fibronectin encoding genes), cell-cell communication and cell adhesion. When 60 min cyclic anisotropic (parallel to the pattern) stretch was applied, the very early response of both control and AC

hiPSC-CMs to mechanical stress was identified. Importantly, control but not AC hiPSC-CMs upregulated genes belonging to the response to mechanical stimulus, such as Jun proto-oncogene, AP-1 transcription factor subunit (JUN) and FOS proto-oncogene, AP-1 transcription factor subunit (FOS). The design of this study allowed for the identification of early response genes, however, it would be informative to capture the adaptive changes by analyzing responses to different magnitudes and duration of stretch, and how biophysical parameters, such as cellular and tissue viscoelasticity properties impact cellular consequences of mechanical stimuli.

Engineered heart slices built by seeding AC hiPSC-CMs (carrying a *PKP2* mutation) in de-cellularized porcine myocardium sections (Blazeski et al., 2019) which within 2 weeks formed spontaneously beating multi-layered syncytia, with aligned and sometimes multinucleated CMs, organized sarcomeric structures and elongated nuclei. The engineered slices could be stimulated at different frequencies (namely from 0.5 to 2 Hz). In these settings several AC-related features were confirmed. In particular, anisotropic propagation of contraction allowed for the identification of re-entrant arrhythmias. This is a disease-relevant phenotype of important physiological significance that could not be recapitulated in other standard culture formats.

In vitro AC Models of Adrenergic Stress

Several *in vitro* cell models were used to address the electrical aspects of AC and some tried to recapitulate the effects of adrenergic stimulation.

Among these, *DSG2*-mutated hiPSCs-CMs were used to investigate the connection between desmosome mutations and arrhythmia (El-Battrawy et al., 2018). Electrophysiology was the main focus in this study and AC hiPSC-CMs displayed reduced I_{Na} impacting on a slower upstroke velocity of the AP. Furthermore, I_{Na}, I_{NCX}, I_{to}, I_{SK}, and I_{KATP} were decreased, while I_{Kr} was enhanced in AC hiPSC-CMs compared with control hiPSC-CMs. Interestingly, AC hiPSC-CMs were more sensitive to adrenergic stimulation by isoprenaline, which caused a more pronounced AP shortening but also a higher incidence of arrhythmic events (both early-after depolarization and delayed after depolarizations). These results support the hypothesis that enhanced AP shortening by adrenergic stimulation may increase arrhythmia susceptibility in this cell model, thus recapitulating what happens in AC patients under catecholamine stress, where enhanced AP shortening increases the propensity to arrhythmias.

Human induced pluripotent stem cells with mutated TMEM43 were generated by CRISPR/Cas9 (Padrón-Barthe et al., 2019). Although TMEM43 is not a protein of the desmosome but a transmembrane protein of the nuclear envelope, hiPSC-CM stimulation with isoprenaline caused a decrease in the rising and decay time of the Ca^{2+} transients. Interestingly, contraction properties of the mutated iPSC-CMs were changed under basal conditions. GSK3β inhibition using CHIR99021 partially rescued the contraction properties. It is interesting to note that GSK3β is both a crucial component of the Wnt/β-catenin pathway, which has been shown to play a crucial role in AC (Lorenzon et al., 2017), and a central regulator of the β-adrenergic response (Zhou et al., 2010). Interestingly, hiPSCs with truncation mutations in PKP2 showed reduced immunofluorescence signal for PKP2 itself, CX43, Nav1.5 channel, and SAP97 (Asimaki et al., 2014), features that were reverted by treatment with another GSK3β inhibitor (SB216763).

As discussed above, early AC hiPSC-CM studies used media compositions able to activate both PPAR-alpha and PPAR-gamma pathways (Caspi et al., 2013; Kim et al., 2013; Ma et al., 2013). Furthermore, despite adrenergic stimulation not being directly addressed in these studies, it is worthwhile noting that some compounds in the lipogenic media not only impact cell metabolism, but might also have modulated cAMP levels (dexamethasone, IBMX, which in turn is a second messenger belonging to the signaling cascade of adrenergic stimulation), and β-adrenergic receptors (insulin and rosiglitazone). This highlights a major limitation of studies in hiPSC-CMs using adipogenic induction protocols which are inherently artificial in composition and have different time-scales. Indeed, fibro-fatty substitution in the AC myocardium progresses over years to decades and is likely incrementally influenced by various prevailing endogenous and exogenous factors.

Arrhythmogenic Cardiomyopathy shows gender imbalance and it has already been shown for other cardiovascular diseases that there might be a direct role of sex hormones in influencing disease pathology and arrhythmogenesis. In line with this, AC hiPSCs generated by Kim and colleagues (carrying a *PKP2* homozygous mutations) were used to show that testosterone was increased while estradiol decreased apoptosis and lipid accumulation in AC hiPSC-CMs (Akdis et al., 2017). This is interesting as some studies suggested that testosterone has pro-arrhythmic effects by modulating cardiac contraction and Ca^{2+} homeostasis whereas estradiol has anti-arrhythmic effects. In addition, arrhythmias may occur due to adrenergic-induced apoptosis which would worsen AC pathophysiology (Veldhuis et al., 2009; Tsai et al., 2014).

There is a close functional association between NaV1.5 and mechanical junctional proteins, supported by NaV1.5 co-precipitation with PKP2 (Cerrone et al., 2012) and with N-cadherin (Sato et al., 2011). This supports the presence of an adhesion/excitability node in cardiac myocytes. hiPSC-CMs carrying the p.R1898H missense substitution variant showed reduced I_{Na} density compared with isogenic corrected controls and reduced density of NaV1.5 and N-cadherin clusters at the site of cell contact (Te Riele et al., 2017). NaV1.5 might then not only be a cardiac ion channel, but also a multifunctional protein in an active adhesion/excitability complex with mechanical junctions that orchestrates the interaction between mechanical and electrical junctions (Te Riele et al., 2017). Lastly, the link between mutated PKP2 and I_{Na} has also been shown (Cerrone et al., 2014).

We have recently described a novel cardiac microtissue model entirely derived from hiPSCs, where fixed ratios of hiPSC-CMs, -cardiac fibroblasts and -cardiac endothelial cells were combined in a 3D spheroid structure. To mimic the high frequency ranges that are reached following beta-adrenergic stimulation during physical exercise, these microtissues were paced at increasing beat frequencies. Interestingly, replacing wild-type

with PKP2-defective hiPSC-cardiac fibroblasts was sufficient to induce an arrhythmic phenotype in the cardiac microtissues, despite the CMs being healthy (Giacomelli et al., 2020). This illustrated the crucial role that cardiac fibroblasts, although non-excitable themselves, have in modulating active and passive electrical properties of adjacent CMs (Gaudesius et al., 2003; Miragoli et al., 2006; Ongstad and Kohl, 2016) and that PKP2-defective cardiac fibroblasts were integral contributors to the AC phenotype. The mechanism for the arrhythmic behavior could be related to the overall reduced CX43 expression and/or remodeling observed throughout cardiac microtissues containing AC hiPSC-cardiac fibroblasts, even though further studies are needed to clearly identify the histological and functional effects of these heterocellular interactions *in vitro*.

Limitations of AC *in vitro* Cellular Models and Possible Solutions

Although *in vitro* cellular models have contributed to our understanding of the pathogenic mechanisms underlying AC, including genetic factors, cellular contributions, signaling pathways, and molecular defects, they also bring some limitations that need attention.

First, isolated cells lack the physiological realism of *in vivo* tissues, where different cell types are organized in functional units and both homo- and hetero-cellular interactions contribute to tissue homeostasis, including biophysical, mechanical, and electrical properties. Importantly, cell-cell communication is essential for the proper propagation of electrical impulses and mechanical strains. Second, cell-ECM interactions are essential for maintaining tissue structure and dynamics, where the ECM contributes to heart stiffness, which includes viscosity and elasticity. Furthermore, ECM is a crucial organizer of the cellular microenvironment, where hormones, growth factors, and other molecules travel in the extracellular space (Valiente-Alandi et al., 2016). This brings us to the third limitation of *in vitro* cellular models, the lack of systemic regulatory stimuli such as cytokines, hormones, neuro-hormones, and microRNAs that can act in both autocrine and paracrine manners. Finally, some specific clinical features, like predisposition of the right or left ventricle as seen in certain AC patients and the appearance of re-entrant arrhythmia are difficult to model and recapitulate *in vitro*.

Multicellular interactions play key roles in heart physiology and pathophysiology, but *in vitro* models often include only one cell type. Some pathological signs might depend or develop only in the presence of cell-cell interactions, and their electrophysiological and histopathological manifestations at the tissue level may not be evident in single cells. It is then still difficult that all the aspects of the disease can be faithfully studied *in vitro* in one cell type in isolation, but solutions are starting to emerge.

A key step in the field is the development of micro-environments that more closely mimic the bio-physical properties of the native heart, by employing biomechanical devices able to integrate physical cues in biological models, providing tools to better understand *in vivo* environment.

Some limitations are restricted to hiPSC tools and are discussed here. In the majority of the studies, hiPSCs from unrelated healthy donors were used as controls, however, it is known that a high degree of variability is observed in iPSC-CMs from different hiPSC lines (Volpato and Webber, 2020), and even among wild-type control hiPSC-CMs, especially with regards to AP properties (Sala et al., 2017) but also cardiac ion currents (Hoekstra et al., 2012). The solution here is to use gene-corrected hiPSCs (Meraviglia et al., 2020) as a control or introduce the mutation of interest in a wild-type hiPSC line (Padrón-Barthe et al., 2019). Another limitation well-known to the hiPSC community is the immaturity of hiPSC-CMs. Ion channels are indeed not expressed at the same levels as adult cardiac myocytes, sarcomeres are disorganized, contraction force is small with non-physiological force-frequency relationship, mitochondria-to-cell volume is low, and energetics mainly rely on glycolysis versus beta-oxidation of fatty acids (Hoekstra et al., 2012; Veerman et al., 2015). Therefore hiPSC-CMs may not be completely representative of diseases (such as AC) with adolescence-adulthood onset. In this respect, methods to enhance structural, mechanical, electrical and metabolic maturation of hiPSC-CMs are all useful for obtaining meaningful insights.

Exercise-like conditions are difficult to reproduce comprehensively *in vitro*, but electrical stimulation, mechanical stretch, or substrate stiffness change and addition of pharmacological compounds can be used to investigate the effects of individual aspects of exercise physiology, such as cardiac muscle contraction or activation of exercise-responsive signaling pathways, similar to what is performed for skeletal muscle (Carter and Solomon, 2019). Whilst a few studies using AC hiPSC-CMs have used such an approach, to our knowledge other AC cellular systems have not been challenged in this way. In the future, it will be important to identify the exact metabolic, inflammatory, and signaling changes induced by exercise *in vivo*, to be able to mimic those *in vitro*. Indeed, "exercise-in-a-dish" approaches allow investigations into different aspects of exercise with a level of abstraction not possible *in vivo*, either directly upon a specific cell type, or as exercise-mediated cross-talk between different cell types.

Cardiac tissue engineering may provide a solution to the challenge of faithfully recapitulating *in vitro* factors that are recognized as playing a role in AC pathogenesis, as discussed above. Ideally, advanced systems will be needed, where distinct cardiac cell types are organized in multicellular three-dimensional syncytia, built using cardiac-specific ECM, and subjected to physiological mechanical load (cyclic stretch and contraction against resistance) and electrical stimulation. In this respect, recent advancements in hiPSC technology provide precious resources for investigating electromechanical training in AC such as: cardiac tissues that can be subjected to physical conditioning with increasing intensity over time (Ronaldson-Bouchard et al., 2018); tissue slices similar to those generated by Blazeski et al. (2019) but replacing porcine with human ECM and higher frequency stimulating to mimic strenuous exercise; engineered heart tissues of different formats which enhanced I_{Na} density (Lemoine et al., 2017; Tiburcy et al., 2017), *t*-tubule formation together physiological contractile force responses

(Mannhardt et al., 2016), and inotropic responses to β-adrenergic stimulation mediated via canonical β1- and β2-adrenoceptor signaling pathways (Tiburcy et al., 2017); thin cardiac muscle films (together with optogenetics and optical mapping) and high pacing rate and β-adrenergic stimulation to uncover re-entry arrhythmias as rotors in these tissues (Park et al., 2019).

AC ANIMAL MODELS

In cardiovascular research, *in vivo* models mainly include rodent models (Camacho et al., 2016) and the teleost zebrafish which have become increasingly important for studying developmental cardiovascular diseases (Beffagna, 2019).

The discovery of genes linked to AC and advances in genetic engineering made it possible to create transgenic, knock-in, and cardiac-specific knockout animal models for both desmosomal and non-desmosomal proteins (for a comprehensive overview, readers are referred to Gerull and Brodehl, 2020). These models contributed to confirm AC causative roles for many gene mutations and provided novel mechanistic insights into AC pathogenesis. The advantage of animal models is that they provide a defined genetic background which allows to clearly identify the cause of AC. However, some limitations apply to animal models, especially with regards to disease onset, progression, and prognosis that in patients are influenced by a variety of factors including environment, comorbidities, age, genetic background, and epigenetic factors, which are difficult to recapitulate in animals. As an example, mice and zebrafish do not show fatty substitution of the myocardium, one of the hallmarks linked to AC progression in humans.

Importantly, animal models represent a precious tool to help unravel the molecular mechanisms underlying AC in relation to mechanical load and adrenergic stimulation. Under physiological conditions, the heart is constantly challenged by cyclic mechanical stress. The study of many AC models at rest, i.e., without exercise simulation etc., suggested that AC phenotype, although genetically determined, develops postnatally and progresses with age, probably due to the temporal action of cardiac tissue extrinsic and/or intrinsic mechanical forces. While exercise training in these animals highlighted the role of physical stress in accelerating disease onset and precipitating arrhythmic events.

Here we focus on *in vivo* models that investigated the connection between AC and physical exercise, mechanical load and adrenergic stimulation (**Table 3**). More general overviews on all AC animal models can be found in (McCauley and Wehrens, 2009; Pilichou et al., 2011; Padrón-Barthe et al., 2017; Austin et al., 2019).

Physical Exercise and Mechanical Load in AC Animal Models

Research on the effects of exercise and adrenergic signaling as a trigger for AC pathological phenotype is limited by the experimental difficulties in implementing training protocols for animal models. Nevertheless a few studies successfully linked strenuous physical activity and accelerated phenotype progression in AC.

Homozygous mice with a germline Pkp2 deficiency showed severe heart defects during cardiac development due to reduced architectural stability of the intercalated disks (Grossmann et al., 2004). However, the heterozygous mouse was viable and three- or six-month-old Pkp2 heterozygous mice displayed no structural or electrical abnormalities but arrhythmic susceptibility to flecainide. In Pkp2 heterozygous mice, protein levels of Ca^{2+} handling proteins were reduced compared to wild-type siblings. However, when 12-week-old mice were subjected to 1-month voluntary running on a treadmill, their hearts showed lateralization of Cx43 in right ventricular myocytes, right ventricular conduction slowing, and a higher susceptibility toward arrhythmias (van Opbergen et al., 2019). This suggested a cross-talk between the desmosomal integrity and Nav1.5 complexes and a possible contribution of sodium current (I_{Na}) dysfunction to arrhythmias. Moreover, exercise induced a pro-arrhythmic cardiac remodeling based on impaired Ca^{2+} cycling and electrical conduction. As for structural remodeling, physical exercise exacerbated the fibrotic response.

A novel PKP2 R735X nonsense mutation dominant-negative mouse model was generated using adeno-associated virus gene delivery. Expression of the mutant protein was induced after a single AAV9-R735X intravenous injection and stable cardiac expression of mutant Pkp2 was achieved 4 weeks after. Endurance exercise training (swimming endurance training protocol) was started 2 weeks later. After 10 months of strenuous swimming, trained but not sedentary one-year-old mice developed RV regional and global dysfunction, as well as an altered localization and punctate distribution of Cx43 at intercalated disks (Cruz et al., 2015).

Different mouse models were generated to mimic Naxos disease, showing defects in embryonic skin architecture and extreme sensitivity to mechanical stress (Bierkamp et al., 1996, 1999; Zhang et al., 2015). Bierkamp and colleagues demonstrated that plakoglobin *null* mutant embryos with a 129/Sv genetic background, died due to severe heart defects, starting from embryonic day (E) 10.5. Histological sections of E10.5 and E12.5 embryos revealed that mutant hearts were structurally less well developed, with thin and weak walls. Coagulated blood was often found in atria, ventricles, and pericardium, suggesting cardiac dysfunction. In a different genetic background, such as C57BL/6, embryos developed and died around birth, due to cardiac dysfunction and to a severe skin phenotype. The superficial layer of the epidermis in different body districts was detached, leading to regions with a very thin epidermis. The skin showed altered physical properties; it dried more quickly and was extremely sensitive to mechanical stress such as rubbing and cutting (Bierkamp et al., 1996). Unfortunately, mutant mice die during late embryogenesis or soon after birth, indicating that there could be differences in the mutant *JUP* expression levels between human patients and mouse models. Interestingly, a stable zebrafish model of AC with CM-specific expression of the human *JUP* 2057del2 mutation responsible for Naxos disease was created in order to study the pathogenesis of the disease (Asimaki et al., 2014). By 4 to 6 weeks of age,

the mutant animals showed heart enlargement with marked thinning of atrial and ventricular walls, cachexia, peripheral edema, and high mortality. A reduction of the I_{Na} current density was also described. This stable AC zebrafish model was used in a chemical screen leading to the identification of a small molecule named SB216763 that was able to rescue AC phenotypes (Asimaki et al., 2014). SB216763 is described as an inhibitor of GSK3β, increasing canonical Wnt/β catenin signaling (Coghlan et al., 2000). Interestingly, SB216763 was subsequently used to prevent myocyte injury and cardiac dysfunction in two AC mouse models both at baseline and in response to physical exercise (Chelko et al., 2016). In this study the following mice were used: (i) a mouse model related to the zebrafish model described above with transgenic overexpression of mutant *Jup* 2057del2 mutation, encoding human Naxos JUP, named Jup2157del2 and (ii) another mouse model, named Dsg2 mut, the loss of exons 4 and 5 of murine *Dsg2*, causes a frameshift mutation and premature termination of translation. Mice began SB216763 treatment at 3 weeks of age, and a subset of these mice began a gradually incremented exercise training protocol (swimming) at 5 weeks of age. Heterozygous Dsg2mut/+ mice did not show an overt AC phenotype at rest but developed myocyte injury and redistribution of ID proteins in response to endurance exercise. Importantly, activation of a common disease pathway in Dsg2mut/+ animals subjected to swimming was blocked by SB216763. Treatment with SB216763 improved cardiac function, myocardial injury, and survival in exercised mice, implicating a central role for GSK3β signaling in the pathogenesis and progression of AC in response to exercise (Chelko et al., 2016).

While systemic *Dsp-null* mutations but also cardiac-specific overexpression of heterozygous V30M or Q90R mutant *Dsp* resulted in embryonic lethality (Gallicano et al., 1998; Yang et al., 2006), cardiac-specific overexpression of the C-terminal mutant R2834H *Dsp* resulted in viable mice that developed ventricular enlargement and biventricular cardiomyopathy. This last transgenic cardiac-specific model was used by Martherus and colleagues to investigate how chronic endurance exercise may lead to AC pathogenesis. Transgenic mice that overexpressed wild-type or R2834H mutant DSP (Tg-Dsp^{WT} or Tg-Dsp^{R2834H}) along with control non-transgenic (NTg) littermates were kept sedentary or exposed to a daily running regimen for 12 weeks. Accelerated cardiac remodeling was evident upon exercise in comparison with non-exercised mice and mutant animals showed RV dilation and focal fat infiltration whereas cardiac function was preserved in NTg and Tg-Dsp^{WT} littermates. Hearts obtained from trained Tg-Dsp^{R2834H} mice showed focal fat infiltrations in the right ventricle, cytoplasmic aggregations consisting of Dsp, Jup, and Cx43 and the disruption of the intercalated disks, intermediate filaments, and microtubules (Martherus et al., 2016). These results confirmed the role of physical training in precipitating cardiac remodeling and dysfunction in AC.

The AC mouse model carrying a cardiac-specific disrupted form of DSP did not show any discernible AC phenotype within the first couple of months after birth but exhibited cardiac systolic dysfunction and myocardial fibrosis starting from 6 months of age which correlated with plakoglobin delocalization to the nucleus where it is able to suppresses Wnt/β-catenin canonical signaling (Garcia-Gras et al., 2006). Intriguingly, treadmill exercise in these mice did not accelerate AC progression, rather it restored transcript levels of the majority of dysregulated genes in CMs (particularly those involved in inflammation, epithelial to mesenchymal transition (EMT), and oxidative phosphorylation), reduced apoptosis, and induced cardiac hypertrophy without affecting cardiac function (Cheedipudi et al., 2020). It is important to note that these findings should not be interpreted to encourage sport activity in AC patients, rather they raise the hypothesis that only strenuous exercise and not physical activity *per se* is detrimental in AC. Indeed, these *Dsp* mutant mice were exposed to 60-min regular treadmill run for 3 months. In the future it will be important to include short- and long-term treadmill exercise in AC models to discern between the molecular mechanisms involved in onset and acceleration of the disease phenotype from protective mechanisms linked to mechanical load.

Lyon and colleagues generated a CM-specific *Dsp*-knockout mouse model using a ventricular myosin light chain-2-Cre construct. Homozygous *Dsp*-knockout mice were viable but showed early ultrastructural defects in desmosomal integrity leading to a biventricular form of AC. The myocardium alterations included cell death and fibro-fatty replacement within the ventricle leading to biventricular dysfunction, heart failure and premature death. In these mice, to establish if in *Dsp*-cKO hearts the loss of Cx43 is a primary or secondary consequence of Dsp depletion, authors evaluated the dose-dependent effects of loss of DSP versus controls, analyzing Cx43, plakophilin-2 and N-cadherin in neonatal CM cultures generated from Dsp-floxed mice. They demonstrated that the level of Cx43: (i) follows the dose-dependent knock-down of DSP and (ii) is found independent from any molecular dissociation of the desmosomal and fascia adherens junction complex, as evidenced by the maintained levels of plakophilin-2 and N-cadherin in neonatal CMs following DSP knock-down (Lyon et al., 2014). The down regulation of Cx43 in this mouse model, results in conduction abnormalities prior to mechanical junction complex damage, and fibro-fatty replacement (Lyon et al., 2014). Interestingly, these mice exhibited ventricular arrhythmias that were exacerbated with exercise and catecholamine stimulation, supporting the idea that vulnerability to adrenergic stress can be captured with AC animal models.

In order to study AC, different zebrafish models have also been used (Heuser et al., 2006; Martin et al., 2009; Moriarty et al., 2012) without a specific training protocols. However, unlike mouse models, fish swim actively throughout their life even if they are not forced to swim-training. *Dsp*-knock-down zebrafish models were generated with antisense morpholino, confirming specific and disruptive effects on desmosomes, like those identified in AC patients (Giuliodori et al., 2018). Dsp-deficient zebrafish models were used for an *in vivo* cell-signaling screen, using pathway-specific reporter zebrafish lines. This work demonstrated that Wnt/β-catenin, TGFβ/Smad3, and Hippo/YAP-TAZ pathways were significantly altered in AC zebrafish models, with Wnt as the most dramatically

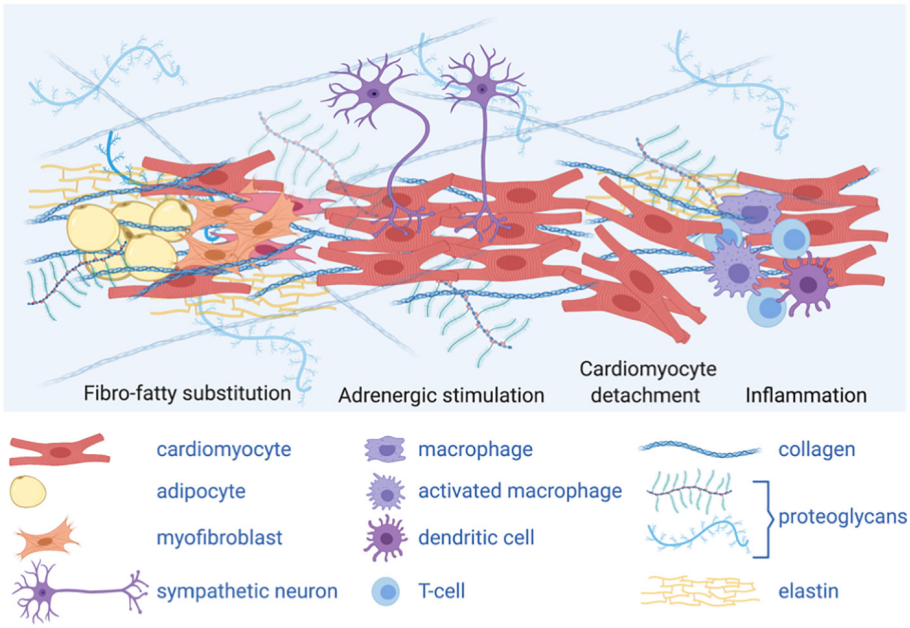

FIGURE 3 | A complex extracellular environment influences intracellular signaling in AC. Graphical representation of different cell types and extracellular matrix (ECM) composing AC heart micro-environment: adipocytes and ECM protein deposition, including collagen, secreted by activated fibroblasts (myofibroblasts) change the stiffness of the heart tissue, thus impacting mechanical stimuli; fibro-fatty substitution is likely secondary to cardiomyocyte damage and death; sympathetic neurons release catecholamines, acting as adrenergic stimuli; inflammatory cells are also present in the AC myocardium. The complex cardiac micro-environment is sensed by the cells and influences intracellular signaling and cell fate.

affected. Involvement of Wnt/β-catenin signaling in the pathogenesis of AC (Garcia-Gras et al., 2006) and the ability of mechanotransduction to activate canonical Wnt/β-catenin signaling (Warboys, 2018) was also confirmed in zebrafish. Furthermore, other authors demonstrated that YAP/TAZ play a central role in delivering information of mechanical environments surrounding cells to the nucleus transcriptional machinery suggesting a link between mechanotransduction and hippo pathway (Dobrokhotov et al., 2018). Interestingly, under persistent Dsp deficiency, Wnt signaling is rescuable both by genetic and pharmacological approaches, which may suggest new therapeutic scenarios (Giuliodori et al., 2018).

The study of AC molecular mechanisms has also made use of spontaneous animal disease models. AC is a spontaneous and manifest disease in the Boxer breed of dogs with striking histopathological, anatomical, genetic, and biomolecular similarities with AC in humans (Vischer et al., 2017).

Proprietary Boxer dogs are free to move and thus subjected to exercise-induced stimuli. Exposure to risk factors similar to those of humans may be one reason for spontaneous AC occurrence. The evidences for Striatin gene (*STRN*) as causative gene for AC canine disease is still under debate (Meurs et al., 2010; Cattanach et al., 2015). Intriguingly, STRN co-localizes with desmosomal proteins, interferes with the Wnt pathway and is involved in intracellular Ca^{2+} regulation (Oxford et al., 2014; Montnach et al., 2018), thus potentially contributing to mechanotransduction and downstream adrenergic signaling.

In 2000 a spontaneously occurring cardiac disease in domestic cats was reported, that shared remarkable similarities with human AC, both for clinical and pathological features (Fox et al., 2000). The histopathological analysis of the cats' hearts showed evidence of myocardial cell injury and cell-death as well as repair in the right ventricle, closely resembling AC patients. Subsequent reports described two AC cats with right predominant AC (Harvey et al., 2005), and an AC cat model with severe left ventricular involvement (Ciaramella et al., 2009). This feline model is considered a potentially important investigative tool that could enhance the understanding of the complex clinical and pathophysiological AC mechanisms, as well as the genetic factors and molecular mechanisms responsible for its genesis.

PLN is a crucial regulatory protein for Ca^{2+}-cycling and an important mediator of the adrenergic effects resulting in enhanced cardiac output. A mouse model with cardiac-specific expression of the heterozygous human PLN Arg14Del mutation recapitulated the human phenotype and suggested the inhibition of SERCA2a activity, likely mediated through a disturbance in the structure of PLN, as a mechanism of action (Haghighi et al., 2006). Interestingly, phospholamban content in murine was increased in denervated skeletal muscles (Komatsu et al., 2018). Cardiac sympathetic denervation represents a well-established intervention in patients with ventricular arrhythmias refractory to pharmacotherapy and ablation, especially long QT-syndrome, but its role in other cardiomyopathies including AC is less clear (Coleman et al., 2012; Schwartz, 2014). Nevertheless, when applied to mouse models, this technique could help understanding the role of innervation in the progression of AC. It is interesting to note that the interface between neuron and CMs, also called neuro-cardiac junction, could explain the heart ability

to function with precision, specificity and elevated temporal resolution to mechanical stretch and adrenergic stimulation in mouse models (Zaglia and Mongillo, 2017). Interestingly, *ex vivo* murine hearts were used to demonstrate the existence of a tight link between impaired desmosomal binding and a reduced response to adrenergic stimulation by isoprenaline, probably *via* disruption of β1-adrenergic receptor localization (Schlipp et al., 2014).

Altogether, these studies support the concept that in the presence of AC causing mutations, exercise is a trigger associated with aggravation of AC phenotype and a more rapid progression of the disease. However, it is worthwhile mentioning that, in line with some human studies, certain pre-clinical models also support the idea that extreme exercise may cause AC-like changes, even in the absence of a genetic predisposition. In male Wistar rats without known AC gene mutations, vigorous running exercise alone was able to induce fibrosis in the right ventricle and predispose to right ventricular arrhythmias with programmed electrical stimulation (Benito et al., 2011).

Finally, evidence that inflammatory mediators might play an important role in AC onset and progression are leading to exploring anti-inflammatory drug therapy as a potential effective strategy to reduce myocardial damage and risk of SCD. In Dsg2-mutant mice, anti-inflammatory treatment through inhibition of the NFκB signaling pathways was effective in reducing the structural and functional signs associated with AC disease progression (myocardial fibrosis, necrosis, inflammation, and arrhythmias; Chelko et al., 2019). Moreover, cytokines implicated in granulomatous inflammation led to intracellular translocation of junctional plakoglobin in cultured neonatal rat ventricular myocytes (Asimaki et al., 2011). Emerging evidence linking systemic inflammatory stress with perturbed desmosome function in both heart and skin (Paller et al., 2018) and the increasing understanding of the interplay between inflammation and physical exercise, might provide further insights into the mechanisms involved in AC disease progression due to exercise (Elliott et al., 2019).

CONCLUSION

Exercise is one of the main triggers for life-threatening arrhythmias and SCD in several conditions that are vulnerable to adrenergic stress, in particular inherited diseases syndromes including AC (Cerrone, 2018). In the setting of AC, this can be mechanistically linked to: (i) a direct mechanical stress in cells with weakened cell-cell junctions, (ii) adrenergic surge, and (iii) electrophysiological remodeling.

Importantly, a complex extracellular environment influences intracellular signaling in AC (**Figure 3**). Structural weakening of the desmosome is a hallmark of AC pathogenesis, which predisposes the right ventricle to fibrosis and dilation (Stokes, 2007). The underlying molecular mechanisms include impairment of the mechanical CM-CM and CM/non-CM junctions, released desmosomal transcription regulators and adipogenic differentiation of mesenchymal cells. Both inhibition of canonical Wnt/β-catenin and activation of the Hippo signaling pathways have emerged as active players in AC pathogenesis. Interestingly, the Hippo pathway, which responds to cell polarity and mechanotransduction, is able to regulate cell proliferation, apoptosis and cell fate.

Activation of the adrenergic signaling cascade is a precipitating event which is involved in different forms of heart failure, as β-receptor blockers are a favorable pharmacological treatment of heart failure (Waagstein, 1993; Port and Bristow, 2001; Ponikowski et al., 2016). Furthermore, adrenergic signaling is a worsening factor for primary arrhythmic syndromes, such as long-QT syndrome, where left cardiac sympathetic denervation represents a therapeutic option (Schwartz et al., 2004).

In the early concealed stages, electrical abnormalities can be observed in the absence of overt structural changes, such as fibro-fatty replacement of the myocardium (Kaplan et al., 2004b; Rizzo et al., 2012).

Importantly, the I_{Na} current depends on the expression and structural integrity of desmosomes. A clear link between proteins of the desmosome and electrical stability of CMs is evident by several evidence that show reduced I_{Na} in the presence of reduced or mutated PKP2 and DSP and explain how impaired mechanical coupling may affect electrical properties of CMs (Zhang et al., 2013). In this view, correction of the mechanical coupling or removing the external stressor of mechanical load could prevent electrical dysfunction.

Heart failure in general has been associated with both elevated sympathetic tone and mechanical load (Lohse et al., 2003). Both systems activate signaling transduction pathways that increase cardiac output, but adversely contribute to electrical stability, at least partially *via* modulation of Ca^{2+} handling. PKA and CaMKII are key to the regulation of L-type Ca^{2+} channels and RYR2 in the β-adrenergic and stretch response. PKA targets L-type Ca^{2+} and RYR2 *via* A-kinase anchoring proteins, and transmits signals from β-adrenergic receptors *via* cAMP (Catterall, 2015; Landstrom et al., 2017).

In the early concealed stages of the disease, AC patients can be asymptomatic even if they are at high risk for SCD. The study of such patients is hampered by the difficulty in obtaining cardiac samples at the early stages of AC disease. Both *in vitro* cellular and *in vivo* animal models represent precious tools for modeling also the early stages of the disease to identify the initial molecular events triggering disease manifestation and therefore identify novel potential targets for therapies. Indeed, while AC manifestation progresses over the years in patients, documented early changes in AC animal models include electrical remodeling and electrical instability, along with desmosome loosening. Advanced technology including sophisticated intravital imaging systems applied to animal models and tissue engineering to mimic the highly organized 3D multicellular structure of the heart have the potential to advance our knowledge of AC pathogenesis, including untangling the link between physical exercise/adrenergic stress and molecular/electrical changes. Although complementary studies in AC human patients will be required, the need for novel therapeutic options that can prevent disease manifestation remains an open challenge and is one of the most important tasks to address to improve patients' survival.

AUTHOR CONTRIBUTIONS

GB, ES, and MB conceptualization, writing original draft, and reviewing. All authors contributed to the article and approved the submitted version.

FUNDING

This work was supported by the following grants: Transnational Research Project on Cardiovascular Diseases (JTC2016_FP-40-021 ACM-HF); Italian Ministry of Health grant GR-2016-02362024; CARIPARO Foundation project SHoCD; and Italian Ministry of Education, University and Research PRIN 20173ZWACS.

ACKNOWLEDGMENTS

The authors are grateful to Prof. Gaetano Thiene and Prof. Cristina Basso (University of Padova) for critical comments on the manuscript and to Dr. Aoife Gowran (Centro Cardiologico Monzino) for proofreading. **Figures 1**, **3** were created with BioRender.com.

REFERENCES

Akdis, D., Saguner, A. M., Shah, K., Wei, C., Medeiros-Domingo, A., von Eckardstein, A., et al. (2017). Sex hormones affect outcome in arrhythmogenic right ventricular cardiomyopathy/dysplasia: from a stem cell derived cardiomyocyte-based model to clinical biomarkers of disease outcome. *Eur. Heart Journal* 38, 1498–1508. doi: 10.1093/eurheartj/ehx011

Al-Khatib, S. M., Stevenson, W. G., Ackerman, M. J., Bryant, W. J., Callans, D. J., Curtis, A. B., et al. (2018). 2017 AHA/ACC/HRS guideline for management of patients with ventricular arrhythmias and the prevention of sudden cardiac death: a report of the American College of Cardiology/American Heart Association task force on clinical practice guidelines and the heart rhythm society. *Circulation* 138, e272–e391. doi: 10.1161/CIR.0000000000000549

Asimaki, A., Kapoor, S., Plovie, E., Karin Arndt, A., Adams, E., Liu, Z., et al. (2014). Identification of a new modulator of the intercalated disc in a zebrafish model of arrhythmogenic cardiomyopathy. *Sci. Transl. Med.* 6:240ra74. doi: 10.1126/scitranslmed.3008008

Asimaki, A., Tandri, H., Duffy, E. R., Winterfield, J. R., Mackey-Bojack, S., Picken, M. M., et al. (2011). Altered desmosomal proteins in granulomatous myocarditis and potential pathogenic links to arrhythmogenic right ventricular cardiomyopathy. *Circ. Arrhythm Electrophysiol.* 4, 743–752. doi: 10.1161/CIRCEP.111.964890

Austin, K. M., Trembley, M. A., Chandler, S. F., Sanders, S. P., Saffitz, J. E., Abrams, D. J., et al. (2019). Molecular mechanisms of arrhythmogenic cardiomyopathy. *Nat. Rev. Cardiol.* 16, 519–537. doi: 10.1038/s41569-019-0200-7

Basso, C., Corrado, D., Marcus, F. I., Nava, A., and Thiene, G. (2009). Seminar Arrhythmogenic right ventricular cardiomyopathy. *Lancet* 373, 1289–1300. doi: 10.1016/S0140-6736(09)60256-7

Basso, C., Thiene, G., Corrado, D., Angelini, A., Nava, A., and Valente, M. (1996). Arrhythmogenic right ventricular cardiomyopathy. Dysplasia, dystrophy, or myocarditis? *Circulation* 94, 983—991. doi: 10.1161/01.cir.94.5.983

Bauce, B., Basso, C., Rampazzo, A., Beffagna, G., Daliento, L., Frigo, G., et al. (2005). Clinical profile of four families with arrhythmogenic right ventricular cardiomyopathy caused by dominant desmoplakin mutations. *Eur. Heart J.* 26, 1666–1675. doi: 10.1093/eurheartj/ehi341

Beffagna, G. (2019). Zebrafish as a smart model to understand regeneration after heart injury: how fish could help humans. *Front. Cardiovasc. Med.* 6:107. doi: 10.3389/fcvm.2019.00107

Beffagna, G., De Bortoli, M., Nava, A., Salamon, M., Lorenzon, A., Zaccolo, M., et al. (2007). Missense mutations in desmocollin-2 N-terminus, associated with arrhythmogenic right ventricular cardiomyopathy, affect intracellular localization of desmocollin-2 in vitro. *BMC Med. Genet.* 8:65. doi: 10.1186/1471-2350-8-65

Beffagna, G., Occhi, G., Nava, A., Vitiello, L., Ditadi, A., Basso, C., et al. (2005). Regulatory mutations in transforming growth factor-beta3 gene cause arrhythmogenic right ventricular cardiomyopathy type 1. *Cardiovasc. Res.* 65, 366—373. doi: 10.1016/j.cardiores.2004.10.005

Bellin, M., Marchetto, M. C., Gage, F. H., and Mummery, C. L. (2012). Induced pluripotent stem cells: the new patient? *Nat. Rev. Mol. Cell Biol.* 13, 713–726. doi: 10.1038/nrm3448

Benito, B., Gay-Jordi, G., Serrano-Mollar, A., Guasch, E., Shi, Y., Tardif, J.-C., et al. (2011). Cardiac arrhythmogenic remodeling in a rat model of long-term intensive exercise training. *Circulation* 123, 13–22. doi: 10.1161/CIRCULATIONAHA.110.938282

Bierkamp, C., Mclaughlin, K. J., Schwarz, H., Huber, O., and Kemler, R. (1996). Embryonic heart and skin defects in mice lacking plakoglobin. *Dev. Biol.* 180, 780–785. doi: 10.1006/dbio.1996.0346

Bierkamp, C., Schwarz, H., Huber, O., and Kemler, R. (1999). Desmosomal localization of beta-catenin in the skin of plakoglobin null-mutant mice. *Development* 126, 371–381.

Blazeski, A., Lowenthal, J., Wang, Y., Teuben, R., Zhu, R., Gerecht, S., et al. (2019). Engineered heart slice model of arrhythmogenic cardiomyopathy using plakophilin-2 mutant myocytes. *Tissue Eng. Part A* 25, 725–735. doi: 10.1089/ten.tea.2018.0272

Calkins, H., Corrado, D., and Marcus, F. (2017). Risk stratification in arrhythmogenic right ventricular cardiomyopathy. *Circulation* 136, 2068–2082. doi: 10.1161/CIRCULATIONAHA.117.030792

Camacho, P., Fan, H., Liu, Z., and He, J. Q. (2016). Small mammalian animal models of heart disease. *Am. J. Cardiovasc. Dis.* 6, 70—80.

Carter, S., and Solomon, T. P. J. (2019). In vitro experimental models for examining the skeletal muscle cell biology of exercise: the possibilities, challenges and future developments. *Pflugers Arch.* 471, 413–429. doi: 10.1007/s00424-018-2210-4

Carvajal-Huerta, L. (1998). Epidermolytic palmoplantar keratoderma with woolly hair and dilated cardiomyopathy. *J. Am. Acad. Dermatol.* 39, 418–421. doi: 10.1016/s0190-9622(98)70317-2

Caspi, O., Huber, I., Gepstein, A., Arbel, G., Maizels, L., Boulos, M., et al. (2013). Modeling of arrhythmogenic right ventricular cardiomyopathy with human induced pluripotent stem cells. *Circ. Cardiovasc. Genet.* 6, 557–568. doi: 10.1161/CIRCGENETICS.113.000188

Cattanach, B. M., Dukes-McEwan, J., Wotton, P. R., Stephenson, H. M., and Hamilton, R. M. (2015). A pedigree-based genetic appraisal of Boxer ARVC and the role of the Striatin mutation. *Vet. Rec.* 176, 492–492. doi: 10.1136/vr.102821

Catterall, W. A. (2015). Regulation of cardiac calcium channels in the fight-or-flight response. *Curr. Mol. Pharmacol.* 8, 12–21. doi: 10.2174/1874467208666150507103417

Catto, V., Dessanai, M. A., Sommariva, E., Tondo, C., and Dello Russo, A. (2019). S-ICD is effective in preventing sudden death in arrhythmogenic cardiomyopathy athletes during exercise. *Pacing Clin. Electrophysiol.* 42, 1269–1272. doi: 10.1111/pace.13702

Celeghin, R., and Pilichou, K. (2019). The complex molecular genetics of arrhythmogenic cardiomyopathy. *Int. J. Cardiol.* 284, 59–60. doi: 10.1016/j.ijcard.2018.11.004

Cerrone, M. (2018). Exercise: a risky subject in arrhythmogenic cardiomyopathy. *J. Am. Heart Assoc.* 7, 1–3. doi: 10.1161/JAHA.118.009611

Cerrone, M., Lin, X., Zhang, M., Agullo-Pascual, E., Pfenniger, A., Chkourko Gusky, H., et al. (2014). Missense mutations in plakophilin-2 cause sodium current deficit and associate with a Brugada syndrome phenotype. *Circulation* 129, 1092–1103. doi: 10.1161/CIRCULATIONAHA.113.003077

Cerrone, M., Noorman, M., Lin, X., Chkourko, H., Liang, F.-X., van der Nagel, R., et al. (2012). Sodium current deficit and arrhythmogenesis in a murine

model of plakophilin-2 haploinsufficiency. *Cardiovasc. Res.* 95, 460–468. doi: 10.1093/cvr/cvs218

Cerrone, M., Remme, C. A., Tadros, R., Bezzina, C. R., and Delmar, M. (2019). Beyond the one gene-one disease paradigm: complex genetics and pleiotropy in inheritable cardiac disorders. *Circulation* 140, 595–610. doi: 10.1161/CIRCULATIONAHA.118.035954

Chamberlain, P. D., Jennings, K. H., Paul, F., Cordell, J., Berry, A., Holmes, S. D., et al. (1999). The tissue distribution of the human beta3-adrenoceptor studied using a monoclonal antibody: direct evidence of the beta3-adrenoceptor in human adipose tissue, atrium and skeletal muscle. *Int. J. Obes. Relat. Metab. Disord.* 23, 1057–1065. doi: 10.1038/sj.ijo.0801039

Cheedipudi, S. M., Hu, J., Fan, S., Yuan, P., Karmouch, J., Czernuszewicz, G., et al. (2020). Exercise restores dysregulated gene expression in a mouse model of arrhythmogenic cardiomyopathy. *Cardiovasc. Res.* 116, 1199–1213. doi: 10.1093/cvr/cvz199

Chelko, S. P., Asimaki, A., Andersen, P., Bedja, D., Amat-Alarcon, N., DeMazumder, D., et al. (2016). Central role for GSK3β in the pathogenesis of arrhythmogenic cardiomyopathy. *JCI Insight* 1:e85923. doi: 10.1172/jci.insight.85923

Chelko, S. P., Asimaki, A., Lowenthal, J., Bueno-Beti, C., Bedja, D., Scalco, A., et al. (2019). Therapeutic modulation of the immune response in arrhythmogenic cardiomyopathy. *Circulation* 140, 1491–1505. doi: 10.1161/CIRCULATIONAHA.119.040676

Cho, G.-S., Lee, D. I., Tampakakis, E., Murphy, S., Andersen, P., Uosaki, H., et al. (2017). Neonatal transplantation confers maturation of PSC-derived cardiomyocytes conducive to modeling cardiomyopathy. *CellReports* 18, 571–582. doi: 10.1016/j.celrep.2016.12.040

Ciaramella, P., Basso, C., Di Loria, A., and Piantedosi, D. (2009). Arrhythmogenic right ventricular cardiomyopathy associated with severe left ventricular involvement in a cat. *J. Vet. Cardiol.* 11, 41–45. doi: 10.1016/j.jvc.2009.02.007

Coghlan, M. P., Culbert, A. A., Cross, D. A., Corcoran, S. L., Yates, J. W., Pearce, N. J., et al. (2000). Selective small molecule inhibitors of glycogen synthase kinase-3 modulate glycogen metabolism and gene transcription. *Chem. Biol.* 7, 793–803. doi: 10.1016/s1074-5521(00)00025-9

Coleman, M. A., Bos, J. M., Johnson, J. N., Owen, H. J., Deschamps, C., Moir, C., et al. (2012). Videoscopic left cardiac sympathetic denervation for patients with recurrent ventricular fibrillation/malignant ventricular arrhythmia syndromes besides congenital long-QT syndrome. *Circ. Arrhythm Electrophysiol.* 5, 782–788. doi: 10.1161/CIRCEP.112.971754

Corrado, D., Basso, C., Pavei, A., Michieli, P., Schiavon, M., and Thiene, G. (2006). Trends in sudden cardiovascular death in young competitive athletes after implementation of a preparticipation screening program. *JAMA* 296, 1593–1601. doi: 10.1001/jama.296.13.1593

Corrado, D., Basso, C., Rizzoli, G., Schiavon, M., and Thiene, G. (2003). Does sports activity enhance the risk of sudden death in adolescents and young adults? *J. Am. College Cardiol.* 42, 1959–1963. doi: 10.1016/j.jacc.2003.03.002

Corrado, D., van Tintelen, P. J., McKenna, W. J., Hauer, R. N. W., Anastastakis, A., Asimaki, A., et al. (2020). Arrhythmogenic right ventricular cardiomyopathy: evaluation of the current diagnostic criteria and differential diagnosis. *Eur. Heart J.* 41, 1414–1429. doi: 10.1093/eurheartj/ehz669

Corrado, D., Wichter, T., Link, M. S., Hauer, R. N., Marchlinski, F. E., Anastasakis, A., et al. (2015). Treatment of arrhythmogenic right ventricular cardiomyopathy/dysplasia: an international task force consensus statement. *Circulation*. 132, 441–453. doi: 10.1161/CIRCULATIONAHA.115.017944

Corrado, D., and Zorzi, A. (2018). Sudden cardiac death in young people and athletes. *Ital. J. Med.* 12, 74–87. doi: 10.4081/itjm.2018.1027

Cruz, F. M., Sanz-Rosa, D., Roche-Molina, M., García-Prieto, J., García-Ruiz, J. M., Pizarro, G., et al. (2015). Exercise triggers ARVC phenotype in mice expressing a disease-causing mutated version of human plakophilin-2. *J. Am. Coll. Cardiol.* 65, 1438–1450. doi: 10.1016/j.jacc.2015.01.045

De Bortoli, M., Postma, A. V., Poloni, G., Calore, M., Minervini, G., Mazzotti, E., et al. (2018). Whole-Exome sequencing identifies pathogenic variants in TJP1gene associated with arrhythmogenic cardiomyopathy. *Circ. Genom. Precis. Med.* 11, 1–10. doi: 10.1161/CIRCGEN.118.002123

de Lucia, C., Eguchi, A., and Koch, W. J. (2018). New insights in cardiac β-adrenergic signaling during heart failure and aging. *Front. Pharmacol.* 9:904. doi: 10.3389/fphar.2018.00904

Denis, A., Sacher, F., Derval, N., Lim, H. S., Cochet, H., Shah, A. J., et al. (2014). Diagnostic value of isoproterenol testing in arrhythmogenic right ventricular cardiomyopathy. *Circ. Arrhythm Electrophysiol.* 7, 590–597. doi: 10.1161/CIRCEP.113.001224

do Vale, G. T., Ceron, C. S., Gonzaga, N. A., Simplicio, J. A., and Padovan, J. C. (2019). Three Generations of β-blockers: history, class differences and clinical applicability. *Curr. Hypertens Rev.* 15, 22–31. doi: 10.2174/1573402114666180918102735

Dobrokhotov, O., Samsonov, M., Sokabe, M., and Hirata, H. (2018). Mechanoregulation and pathology of YAP/TAZ via Hippo and non-Hippo mechanisms. *Clin. Transl. Med.* 7:23. doi: 10.1186/s40169-018-0202-9

Dorn, T., Kornherr, J., Parrotta, E. I., Zawada, D., Ayetey, H., Santamaria, G., et al. (2018). Interplay of cell–cell contacts and RhoA/ MRTF-A signaling regulates cardiomyocyte identity. *EMBO J.* 37:e98133. doi: 10.15252/embj.201798133

El-Battrawy, I., Zhao, Z., Lan, H., Cyganek, L., Tombers, C., Li, X., et al. (2018). Electrical dysfunctions in human-induced pluripotent stem cell-derived cardiomyocytes from a patient with an arrhythmogenic right ventricular cardiomyopathy. *EP Europace* 20, f46–f56. doi: 10.1093/europace/euy042

Elliott, P. M., Anastasakis, A., Asimaki, A., Basso, C., Bauce, B., Brooke, M. A., et al. (2019). Definition and treatment of arrhythmogenic cardiomyopathy: an updated expert panel report. *Eur. J. Heart Fail.* 21, 955–964. doi: 10.1002/ejhf.1534

Evans, N. D., Oreffo, R. O. C., Healy, E., Thurner, P. J., and Man, Y. H. (2013). Epithelial mechanobiology, skin wound healing, and the stem cell niche. *J. Mech. Behav. Biomed. Mater.* 28, 397–409. doi: 10.1016/j.jmbbm.2013.04.023

Firoozi, S., Sharma, S., Hamid, M. S., and McKenna, W. J. (2002). Sudden death in young athletes: HCM or ARVC? *Cardiovasc. Drugs Ther.* 16, 11–17. doi: 10.1023/a:1015307229339

Forleo, C., Carmosino, M., Resta, N., Rampazzo, A., Valecce, R., Sorrentino, S., et al. (2015). Clinical and functional characterization of a novel mutation in lamin a/c gene in a multigenerational family with arrhythmogenic cardiac laminopathy. *PLoS One* 10:e0121723. doi: 10.1371/journal.pone.0121723

Fox, P. R., Maron, B. J., Basso, C., Liu, S. K., and Thiene, G. (2000). Spontaneously occurring arrhythmogenic right ventricular cardiomyopathy in the domestic cat: a new animal model similar to the human disease. *Circulation* 102, 1863−1870. doi: 10.1161/01.cir.102.15.1863

Furlanello, F., Bertoldi, A., Dallago, M., Furlanello, C., Fernando, F., Inama, G., et al. (1998). Cardiac arrest and sudden death in competitive athletes with arrhythmogenic right ventricular dysplasia. *Pacing Clin. Electrophysiol.* 21, 331–335. doi: 10.1111/j.1540-8159.1998.tb01116.x

Gallicano, G. I., Kouklis, P., Bauer, C., Yin, M., Vasioukhin, V., Degenstein, L., et al. (1998). Desmoplakin is required early in development for assembly of desmosomes and cytoskeletal linkage. *J. Cell Biol.* 143, 2009–2022. doi: 10.1083/jcb.143.7.2009

Garcia-Gras, E., Lombardi, R., Giocondo, M. J., Willerson, J. T., Schneider, M. D., Khoury, D. S., et al. (2006). Suppression of canonical Wnt/beta-catenin signaling by nuclear plakoglobin recapitulates phenotype of arrhythmogenic right ventricular cardiomyopathy. *J. Clin. Invest.* 116, 2012–2021. doi: 10.1172/JCI27751

Garrod, D. (2010). Desmosomes in vivo. *Dermatol. Res. Pract.* 2010:212439. doi: 10.1155/2010/212439

Gaudesius, G., Miragoli, M., Thomas, S. P., and Rohr, S. (2003). Coupling of cardiac electrical activity over extended distances by fibroblasts of cardiac origin. *Circ. Res.* 93, 421–428. doi: 10.1161/01.RES.0000089258.40661.0C

Gerull, B., and Brodehl, A. (2020). Genetic animal models for arrhythmogenic cardiomyopathy. *Front. Physiol.* 11:624. doi: 10.3389/fphys.2020.00624

Gerull, B., Heuser, A., Wichter, T., Paul, M., Basson, C. T., McDermott, D. A., et al. (2004). Mutations in the desmosomal protein plakophilin-2 are common in arrhythmogenic right ventricular cardiomyopathy. *Nat. Genet.* 36, 1162–1164. doi: 10.1038/ng1461

Giacomelli, E., Meraviglia, V., Campostrini, G., Cochrane, A., Cao, X., van Helden, R. W. J., et al. (2020). Human-iPSC-derived cardiac stromal cells enhance maturation in 3D cardiac microtissues and reveal non-cardiomyocyte contributions to heart disease. *Cell Stem Cell* 26, 862–879.e11. doi: 10.1016/j.stem.2020.05.004

Giacomelli, E., Mummery, C. L., and Bellin, M. (2017). Human heart disease: lessons from human pluripotent stem cell-derived cardiomyocytes. *Cell. Mol. Life Sci.* 74, 3711–3739. doi: 10.1007/s00018-017-2546-5

Giuliodori, A., Beffagna, G., Marchetto, G., Fornetto, C., Vanzi, F., Toppo, S., et al. (2018). Loss of cardiac Wnt/β-catenin signalling in desmoplakin-deficient AC8 zebrafish models is rescuable by genetic and pharmacological intervention. *Cardiovasc. Res.* 114, 1082–1097. doi: 10.1093/cvr/cvy057

Gomes, J., Finlay, M., Ahmed, A. K., Ciaccio, E. J., Asimaki, A., Saffitz, J. E., et al. (2012). Electrophysiological abnormalities precede overt structural changes in arrhythmogenic right ventricular cardiomyopathy due to mutations in desmoplakin-A combined murine and human study. *Eur. Heart J.* 33, 1942–1953. doi: 10.1093/eurheartj/ehr472

Good, J.-M., Fellmann, F., Bhuiyan, Z. A., Rotman, S., Pruvot, E., and Schläpfer, J. (2020). ACTN2 variant associated with a cardiac phenotype suggestive of left-dominant arrhythmogenic cardiomyopathy. *HeartRhythm Case Rep.* 6, 15–19. doi: 10.1016/j.hrcr.2019.10.001

Gorre, F., and Vandekerckhove, H. (2010). Beta-blockers: focus on mechanism of action. Which beta-blocker, when and why? *Acta Cardiol.* 65, 565–570. doi: 10.1080/ac.65.5.2056244

Green, K. J., Getsios, S., Troyanovsky, S., and Godsel, L. M. (2010). Intercellular junction assembly, dynamics, and homeostasis. *Cold Spring Harb. Perspect. Biol.* 2:a000125. doi: 10.1101/cshperspect.a000125

Grossmann, K. S., Grund, C., Huelsken, J., Behrend, M., Erdmann, B., Franke, W. W., et al. (2004). Requirement of plakophilin 2 for heart morphogenesis and cardiac junction formation. *J. Cell Biol.* 167, 149–160. doi: 10.1083/jcb.200402096

Gumbiner, B. M. (1996). Cell adhesion: the molecular basis of tissue architecture and morphogenesis. *Cell* 84, 345–357. doi: 10.1016/s0092-8674(00)81279-9

Haghighi, K., Kolokathis, F., Gramolini, A. O., Waggoner, J. R., Pater, L., Lynch, R. A., et al. (2006). A mutation in the human phospholamban gene, deleting arginine 14, results in lethal, hereditary cardiomyopathy. *Proc. Natl. Acad. Sci. U.S.A.* 103, 1388–1393. doi: 10.1073/pnas.0510519103

Hall, C. L., Akhtar, M. M., Sabater-Molina, M., Futema, M., Asimaki, A., Protonotarios, A., et al. (2020). Filamin C variants are associated with a distinctive clinical and immunohistochemical arrhythmogenic cardiomyopathy phenotype. *Int. J. Cardiol.* 307, 101–108. doi: 10.1016/j.ijcard.2019.09.048

Hariharan, V., Asimaki, A., Michaelson, J. E., Plovie, E., MacRae, C. A., Saffitz, J. E., et al. (2014). Arrhythmogenic right ventricular cardiomyopathy mutations alter shear response without changes in cell-cell adhesion. *Cardiovasc. Res.* 104, 280–289. doi: 10.1093/cvr/cvu212

Harvey, A. M., Battersby, I. A., Faena, M., Fews, D., Darke, P. G., and Ferasin, L. (2005). Arrhythmogenic right ventricular cardiomyopathy in two cats. *J. Small Anim. Pract.* 46, 151–156. doi: 10.1111/j.1748-5827.2005.tb00306.x

Hatzfeld, M., Keil, R., and Magin, T. M. (2017). Desmosomes and intermediate filaments: their consequences for tissue mechanics. *Cold Spring Harb. Perspect. Biol.* 9:a029157. doi: 10.1101/cshperspect.a029157

Hedberg, A., Kempf, F., Josephson, M. E., and Molinoff, P. B. (1985). Coexistence of beta-1 and beta-2 adrenergic receptors in the human heart: effects of treatment with receptor antagonists or calcium entry blockers. *J. Pharmacol. Exp. Ther.* 234, 561–568.

Heuser, A., Plovie, E. R., Ellinor, P. T., Grossmann, K. S., Shin, J. T., Wichter, T., et al. (2006). Mutant desmocollin-2 causes arrhythmogenic right ventricular cardiomyopathy. *Am. J. Hum. Genet.* 79, 1081–1088. doi: 10.1086/509044

Hiroi, Y., Fujiu, K., Komatsu, S., Sonoda, M., Sakomura, Y., Imai, Y., et al. (2004). Carvedilol therapy improved left ventricular function in a patient with arrhythmogenic right ventricular cardiomyopathy. *Jpn. Heart J.* 45, 169–177. doi: 10.1536/jhj.45.169

Hoekstra, M., Mummery, C. L., Wilde, A. A. M., Bezzina, C. R., and Verkerk, A. O. (2012). Induced pluripotent stem cell derived cardiomyocytes as models for cardiac arrhythmias. *Front. Physiol.* 3:346. doi: 10.3389/fphys.2012.00346

Hoffman, B. D., Grashoff, C., and Schwartz, M. A. (2011). Dynamic molecular processes mediate cellular mechanotransduction. *Nature* 475, 316–323. doi: 10.1038/nature10316

James, C. A., Bhonsale, A., Tichnell, C., Murray, B., Russell, S. D., Tandri, H., et al. (2013). Exercise increases age-related penetrance and arrhythmic risk in arrhythmogenic right ventricular dysplasia/cardiomyopathy-associated desmosomal mutation carriers. *J. Am. Coll. Cardiol.* 62, 1290–1297. doi: 10.1016/j.jacc.2013.06.033

Janssens, B., Goossens, S., Staes, K., Gilbert, B., van Hengel, J., Colpaert, C., et al. (2001). alphaT-catenin: a novel tissue-specific beta-catenin-binding protein mediating strong cell-cell adhesion. *J. Cell Sci.* 114, 3177–3188.

Johnson, D. M., and Antoons, G. (2018). Arrhythmogenic mechanisms in heart failure: linking β-adrenergic stimulation, stretch, and calcium. *Front. Physiol.* 9:1453. doi: 10.3389/fphys.2018.01453

Kaplan, S. R., Gard, J. J., Carvajal-Huerta, L., Ruiz-Cabezas, J. C., Thiene, G., Saffitz, J. E. (2004a). Structural and molecular pathology of the heart in carvajal syndrome. *Cardiovasc Pathol.* 13, 26–32. doi: 10.1016/S1054-8807(03)00107-8

Kaplan, S. R., Gard, J. J., Protonotarios, N., Tsatsopoulou, A., Spiliopoulou, C., Anastasakis, A., et al. (2004b). Remodeling of myocyte gap junctions in arrhythmogenic right ventricular cardiomyopathy due to a deletion in plakoglobin (Naxos disease). *Heart Rhythm* 1, 3–11. doi: 10.1016/j.hrthm.2004.01.001

Kawashima, T. (2005). The autonomic nervous system of the human heart with special reference to its origin, course, and peripheral distribution. *Anat. Embryol.* 209, 425–438. doi: 10.1007/s00429-005-0462-1

Kim, C., Wong, J., Wen, J., Wang, S., Wang, C., Spiering, S., et al. (2013). Studying arrhythmogenic right ventricular dysplasia with patient-specific iPSCs. *Nature* 494, 105–110. doi: 10.1038/nature11799

Kirchner, F., Schuetz, A., Boldt, L.-H., Martens, K., Dittmar, G., Haverkamp, W., et al. (2012). Molecular insights into arrhythmogenic right ventricular cardiomyopathy caused by plakophilin-2 missense mutations. *Circ. Cardiovasc. Genet.* 5, 400–411. doi: 10.1161/CIRCGENETICS.111.961854

Klauke, B., Kossmann, S., Gaertner, A., Brand, K., Stork, I., Brodehl, A., et al. (2010). De novo desmin-mutation N116S is associated with arrhythmogenic right ventricular cardiomyopathy. *Hum. Mol. Genet.* 19, 4595–4607. doi: 10.1093/hmg/ddq387

Kobielak, A., and Fuchs, E. (2004). Alpha-catenin: at the junction of intercellular adhesion and actin dynamics. *Nat. Rev. Mol. Cell Biol.* 5, 614–625. doi: 10.1038/nrm1433

Komatsu, M., Nakada, T., Kawagishi, H., Kato, H., and Yamada, M. (2018). Increase in phospholamban content in mouse skeletal muscle after denervation. *J. Muscle Res. Cell Motil.* 39, 163–173. doi: 10.1007/s10974-019-09504-2

Kowalczyk, A. P., and Green, K. J. (2013). Structure, function, and regulation of desmosomes. *Prog. Mol. Biol. Transl. Sci.* 116, 95–118. doi: 10.1016/B978-0-12-394311-8.00005-4

La Gerche, A. (2015). Defining the interaction between exercise and arrhythmogenic right ventricular cardiomyopathy. *Eur. J. Heart Fail.* 17, 128–131. doi: 10.1002/ejhf.224

La Gerche, A., Heidbüchel, H., Burns, A. T., Mooney, D. J., Taylor, A. J., Pfluger, H. B., et al. (2011). Disproportionate exercise load and remodeling of the athlete's right ventricle. *Med. Sci. Sports Exerc.* 43, 974–981. doi: 10.1249/MSS.0b013e31820607a3

Landstrom, A. P., Dobrev, D., and Wehrens, X. H. T. (2017). Calcium signaling and cardiac arrhythmias. *Circ. Res.* 120, 1969–1993. doi: 10.1161/CIRCRESAHA.117.310083

Lemoine, M. D., Mannhardt, I., Breckwoldt, K., Prondzynski, M., Flenner, F., Ulmer, B. X. R., et al. (2017). Human iPSC-derived cardiomyocytes cultured in 3D engineered heart tissue show physiological upstroke velocity and sodium current density. *Sci. Rep.* 7:5464. doi: 10.1038/s41598-017-05600-w

Leosco, D., Parisi, V., Femminella, G. D., Formisano, R., Petraglia, L., Allocca, E., et al. (2013). Effects of exercise training on cardiovascular adrenergic system. *Front. Physiol.* 4:348. doi: 10.3389/fphys.2013.00348

Lie, ØH., Dejgaard, L. A., Saberniak, J., Rootwelt, C., Stokke, M. K., Edvardsen, T., et al. (2018a). Harmful effects of exercise intensity and exercise duration in patients with arrhythmogenic cardiomyopathy. *JACC Clin. Electrophysiol.* 4, 744–753. doi: 10.1016/j.jacep.2018.01.010

Lie, ØH., Rootwelt-Norberg, C., Dejgaard, L. A., Leren, I. S., Stokke, M. K., Edvardsen, T., et al. (2018b). Prediction of life-threatening ventricular arrhythmia in patients with arrhythmogenic cardiomyopathy: a primary prevention cohort study. *JACC Cardiovasc. Imaging* 11, 1377–1386. doi: 10.1016/j.jcmg.2018.05.017

Limongelli, G., Nunziato, M., D'Argenio, V., Esposito, M. V., Monda, E., Mazzaccara, C., et al. (2020). Yield and clinical significance of genetic screening in elite and amateur athletes. *Eur. J. Prev. Cardiol.* doi: 10.1177/2047487320934265 [Epub ahead of print].

Lohse, M. J., Engelhardt, S., and Eschenhagen, T. (2003). What is the role of beta-adrenergic signaling in heart failure? *Circ. Res.* 93, 896–906. doi: 10.1161/01.RES.0000102042.83024.CA

Lopez-Ayala, J. M., Ortiz-Genga, M., Gomez-Milanes, I., Lopez-Cuenca, D., Ruiz-Espejo, F., Sanchez-Munoz, J. J., et al. (2015). A mutation in the Z-line Cypher/ZASP protein is associated with arrhythmogenic right ventricular cardiomyopathy. *Clin. Genet.* 88, 172–176. doi: 10.1111/cge.12458

López-Sendón, J., Swedberg, K., McMurray, J., Tamargo, J., Maggioni, A. P., Dargie, H., et al. (2004). Expert consensus document on angiotensin converting enzyme inhibitors in cardiovascular disease. The Task Force on ACE-inhibitors of the European Society of Cardiology. *Eur. Heart J.* 25, 1454–1470. doi: 10.1016/j.ehj.2004.06.003

Lorenzon, A., Calore, M., Poloni, G., de Windt, L. J., Braghetta, P., and Rampazzo, A. (2017). Wnt/β-catenin pathway in arrhythmogenic cardiomyopathy. *Oncotarget* 8, 60640–60655. doi: 10.18632/oncotarget.17457

Lyon, R. C., Mezzano, V., Wright, A. T., Pfeiffer, E., Chuang, J., Banares, K., et al. (2014). Connexin defects underlie arrhythmogenic right ventricular cardiomyopathy in a novel mouse model. *Hum. Mol. Genet.* 23, 1134–1150. doi: 10.1093/hmg/ddt508

Ma, D., Wei, H., Lu, J., Ho, S., Zhang, G., Sun, X., et al. (2013). Generation of patient-specific induced pluripotent stem cell-derived cardiomyocytes as a cellular model of arrhythmogenic right ventricular cardiomyopathy. *Eur. Heart J.* 34, 1122–1133. doi: 10.1093/eurheartj/ehs226

Malik, N., Win, S., James, C. A., Kutty, S., Mukherjee, M., Gilotra, N. A., et al. (2020). Right ventricular strain predicts structural disease progression in patients with arrhythmogenic right ventricular cardiomyopathy. *J. Am. Heart Assoc.* 9:e015016. doi: 10.1161/JAHA.119.015016

Mannhardt, I., Breckwoldt, K., Letuffe-Brenière, D., Schaaf, S., Schulz, H., Neuber, C., et al. (2016). Human engineered heart tissue: analysis of contractile force. *Stem Cell Rep.* 7, 29–42. doi: 10.1016/j.stemcr.2016.04.011

Marcus, F. I., McKenna, W. J., Sherrill, D., Basso, C., Bauce, B., Bluemke, D. A., et al. (2010). Diagnosis of arrhythmogenic right ventricular cardiomyopathy/dysplasia: proposed modification of the task force criteria. *Eur. Heart J.* 31, 806–814. doi: 10.1093/eurheartj/ehq025

Maron, B. J., Zipes, D. P., and Kovacs, R. J. (2015). Eligibility and disqualification recommendations for competitive athletes with cardiovascular abnormalities: preamble, principles, and general considerations: a scientific statement from the American Heart Association and American College of cardiology. *J. Am. Coll. Cardiol.* 66, 2343–2349. doi: 10.1016/j.jacc.2015.09.032

Martewicz, S., Luni, C., Serena, E., Pavan, P., Chen, H.-S. V., Rampazzo, A., et al. (2019). Transcriptomic characterization of a human in vitro model of arrhythmogenic cardiomyopathy under topological and mechanical stimuli. *Ann. Biomed. Eng.* 47, 852–865. doi: 10.1007/s10439-018-02134-8

Martherus, R., Jain, R., Takagi, K., Mendsaikhan, U., Turdi, S., Osinska, H., et al. (2016). Accelerated cardiac remodeling in desmoplakin transgenic mice in response to endurance exercise is associated with perturbed Wnt/β-catenin signaling. *Am. J. Physiol. Heart Circ. Physiol.* 310, H174–H187. doi: 10.1152/ajpheart.00295.2015

Martin, E. D., Moriarty, M. A., Byrnes, L., and Grealy, M. (2009). Plakoglobin has both structural and signalling roles in zebrafish development. *Dev. Biol.* 327, 83–96. doi: 10.1016/j.ydbio.2008.11.036

Martinac, B. (2004). Mechanosensitive ion channels: molecules of mechanotransduction. *J. Cell Sci.* 117, 2449–2460. doi: 10.1242/jcs.01232

McKenna, W. J., Thiene, G., Nava, A., Fontaliran, F., Blomstrom-Lundqvist, C., Fontaine, G., et al. (1994). Diagnosis of arrhythmogenic right ventricular dysplasia/cardiomyopathy. Task force of the working group myocardial and pericardial disease of the european society of cardiology and of the scientific council on cardiomyopathies of the international society and federation of cardiology. *Br. Heart J.* 71, 215–218. doi: 10.1136/hrt.71.3.215

Mary-Rabine, L., Hordof, A. J., Bowman, F. O., Malm, J. R., and Rosen, M. R. (1978). Alpha and beta adrenergic effects on human atrial specialized conducting fibers. *Circulation* 57, 84–90. doi: 10.1161/01.cir.57.1.84

Mayosi, B. M., Fish, M., Shaboodien, G., Mastantuono, E., Kraus, S., Wieland, T., et al. (2017). Identification of cadherin 2 (CDH2) mutations in arrhythmogenic right ventricular cardiomyopathy. *Circ. Cardiovasc. Genet.* 10:11. doi: 10.1161/CIRCGENETICS.116.001605

McBeath, R., Pirone, D. M., Nelson, C. M., Bhadriraju, K., and Chen, C. S. (2004). Cell shape, cytoskeletal tension, and RhoA regulate stem cell lineage commitment. *Dev. Cell* 6, 483–495. doi: 10.1016/s1534-5807(04)00075-9

McCain, M. L., Lee, H., Aratyn-Schaus, Y., Kleber, A. G., and Parker, K. K. (2012). Cooperative coupling of cell-matrix and cell-cell adhesions in cardiac muscle. *Proc. Natl. Acad. Sci. U.S.A.* 109, 9881–9886. doi: 10.1073/pnas.1203007109

McCauley, M. D., and Wehrens, X. H. T. (2009). Animal models of arrhythmogenic cardiomyopathy. *Dis. Model. Mech.* 2, 563–570. doi: 10.1242/dmm.002840

McKoy, G., Protonotarios, N., Crosby, A., Tsatsopoulou, A., Anastasakis, A., Coonar, A., et al. (2000). Identification of a deletion in plakoglobin in arrhythmogenic right ventricular cardiomyopathy with palmoplantar keratoderma and woolly hair (Naxos disease). *Lancet* 355, 2119–2124. doi: 10.1016/S0140-6736(00)02379-5

Meraviglia, V., Arendzen, C. H., Tok, M., Freund, C., Maione, A. S., Sommariva, E., et al. (2020). Generation of human induced pluripotent stem cell line LUMCi027-A and its isogenic gene-corrected line from an arrhythmogenic cardiomyopathy patient carrying the c.2013delC PKP2 mutation. *Stem Cell Res.* 46:101835. doi: 10.1016/j.scr.2020.101835

Merner, N. D., Hodgkinson, K. A., Haywood, A. F. M., Connors, S., French, V. M., Drenckhahn, J.-D., et al. (2008). Arrhythmogenic right ventricular cardiomyopathy type 5 is a fully penetrant, lethal arrhythmic disorder caused by a missense mutation in the TMEM43 gene. *Am. J. Hum. Genet.* 82, 809–821. doi: 10.1016/j.ajhg.2008.01.010

Mestroni, L., and Sbaizero, O. (2018). Arrhythmogenic cardiomyopathy. *Circulation* 137, 1611–1613. doi: 10.1161/CIRCULATIONAHA.118.033558

Meurs, K. M., Mauceli, E., Lahmers, S., Acland, G. M., White, S. N., and Lindblad-Toh, K. (2010). Genome-wide association identifies a deletion in the 3' untranslated region of striatin in a canine model of arrhythmogenic right ventricular cardiomyopathy. *Hum. Genet.* 128, 315–324. doi: 10.1007/s00439-010-0855-y

Miragoli, M., Gaudesius, G., and Rohr, S. (2006). Electrotonic modulation of cardiac impulse conduction by myofibroblasts. *Circ. Res.* 98, 801–810. doi: 10.1161/01.RES.0000214537.44195.a3

Moccia, F., Lodola, F., Stadiotti, I., Pilato, C. A., Bellin, M., Carugo, S., et al. (2019). Calcium as a key player in arrhythmogenic cardiomyopathy: adhesion disorder or intracellular alteration? *IJMS* 20:3986. doi: 10.3390/ijms20163986

Mont, L., Pelliccia, A., Sharma, S., Biffi, A., Borjesson, M., Brugada Terradellas, J., et al. (2017). Pre-participation cardiovascular evaluation for athletic participants to prevent sudden death: position paper from the EHRA and the EACPR, branches of the ESC. Endorsed by APHRS, HRS, and SOLAECE. *Eur. J. Prev. Cardiol.* 24, 41–69. doi: 10.1177/2047487316676042

Montnach, J., Agullo-Pascual, E., Tadros, R., Bezzina, C. R., and Delmar, M. (2018). Bioinformatic analysis of a plakophilin-2-dependent transcription network: implications for the mechanisms of arrhythmogenic right ventricular cardiomyopathy in humans and in boxer dogs. *Europace* 20, iii125–iii132. doi: 10.1093/europace/euy238

Moriarty, M. A., Ryan, R., Lalor, P., Dockery, P., Byrnes, L., and Grealy, M. (2012). Loss of plakophilin 2 disrupts heart development in zebrafish. *Int. J. Dev. Biol.* 56, 711–718. doi: 10.1387/ijdb.113390mm

Norgett, E. E., Hatsell, S. J., Carvajal-Huerta, L., Cabezas, J. C., Common, J., Purkis, P. E., et al. (2000). Recessive mutation in desmoplakin disrupts desmoplakin-intermediate filament interactions and causes dilated cardiomyopathy, woolly hair and keratoderma. *Hum. Mol. Genet.* 9, 2761–2766. doi: 10.1093/hmg/9.18.2761

Ongstad, E., and Kohl, P. (2016). Fibroblast–myocyte coupling in the heart: potential relevance for therapeutic interventions. *J. Mol. Cell. Cardiol.* 91, 238–246. doi: 10.1016/j.yjmcc.2016.01.010

Oxford, E. M., Danko, C. G., Fox, P. R., Kornreich, B. G., and Moïse, N. S. (2014). Change in β-catenin localization suggests involvement of the canonical Wnt pathway in Boxer dogs with arrhythmogenic right ventricular cardiomyopathy. *J. Vet. Intern. Med.* 28, 92–101. doi: 10.1111/jvim.12238

Padrón-Barthe, L., Dominguez, F., Garcia-Pavia, P., and Lara-Pezzi, E. (2017). Animal models of arrhythmogenic right ventricular cardiomyopathy: what have we learned and where do we go? Insight for therapeutics. *Basic Res. Cardiol.* 112:50. doi: 10.1007/s00395-017-0640-3

Padrón-Barthe, L., Villalba-Orero, M., Gómez-Salinero, J. M., Dominguez, F., Román, M., Larrasa-Alonso, J., et al. (2019). Severe cardiac dysfunction and death caused by arrhythmogenic right ventricular cardiomyopathy type 5 are improved by inhibition of glycogen synthase kinase-3β. *Circulation* 140, 1188–1204. doi: 10.1161/CIRCULATIONAHA.119.040366

Paller, A. S., Czarnowicki, T., Renert-Yuval, Y., Holland, K., Huynh, T., Sadlier, M., et al. (2018). The spectrum of manifestations in desmoplakin gene (DSP) spectrin repeat 6 domain mutations: immunophenotyping and response to ustekinumab. *J. Am. Acad. Dermatol.* 78, 498–505e2. doi: 10.1016/j.jaad.2017.10.026

Pannekoek, W.-J., de Rooij, J., and Gloerich, M. (2019). Force transduction by cadherin adhesions in morphogenesis. *F1000Res* 8:1044. doi: 10.12688/f1000research.18779.1

Park, S.-J., Zhang, D., Qi, Y., Li, Y., Lee, K. Y., Bezzerides, V. J., et al. (2019). Insights into the pathogenesis of catecholaminergic polymorphic ventricular tachycardia from engineered human heart tissue. *Circulation* 140, 390–404. doi: 10.1161/CIRCULATIONAHA.119.039711

Perrin, M. J., Angaran, P., Laksman, Z., Zhang, H., Porepa, L. F., Rutberg, J., et al. (2013). Exercise testing in asymptomatic gene carriers exposes a latent electrical substrate of arrhythmogenic right ventricular cardiomyopathy. *J. Am. Coll. Cardiol.* 62, 1772–1779. doi: 10.1016/j.jacc.2013.04.084

Pilato, C. A., Stadiotti, I., Maione, A. S., Saverio, V., Catto, V., Tundo, F., et al. (2018). Isolation and characterization of cardiac mesenchymal stromal cells from endomyocardial bioptic samples of arrhythmogenic cardiomyopathy patients. *J. Vis. Exp.* 132, 57263. doi: 10.3791/57263

Pilichou, K., Bezzina, C. R., Thiene, G., and Basso, C. (2011). Arrhythmogenic cardiomyopathy. *Circ. Cardiovasc. Genet.* 4, 318–326. doi: 10.1161/CIRCGENETICS.110.959031

Pilichou, K., Nava, A., Basso, C., Beffagna, G., Bauce, B., Lorenzon, A., et al. (2006). Mutations in desmoglein-2 gene are associated with arrhythmogenic right ventricular cardiomyopathy. *Circulation* 113, 1171−1179. doi: 10.1161/CIRCULATIONAHA.105.583674

Pilichou, K., Thiene, G., Bauce, B., Rigato, I., Lazzarini, E., Migliore, F., et al. (2016). Arrhythmogenic cardiomyopathy. *Orphanet J. Rare Dis.* 11:33. doi: 10.1186/s13023-016-0407-1

Ponikowski, P., Voors, A. A., Anker, S. D., Bueno, H., Cleland, J. G. F., Coats, A. J. S., et al. (2016). 2016 ESC guidelines for the diagnosis and treatment of acute and chronic heart failure. *Rev. Esp. Cardiol.* 69:1167. doi: 10.1016/j.rec.2016.11.005

Port, J. D., and Bristow, M. R. (2001). Altered beta-adrenergic receptor gene regulation and signaling in chronic heart failure. *J. Mol. Cell. Cardiol.* 33, 887–905. doi: 10.1006/jmcc.2001.1358

Prior, D., and La Gerche, A. (2020). Exercise and arrhythmogenic right ventricular cardiomyopathy. *Heart Lung Circ.* 29, 547–555. doi: 10.1016/j.hlc.2019.12.007

Puzzi, L., Borin, D., Gurha, P., Lombardi, R., Martinelli, V., Weiss, M., et al. (2019). Knock down of plakophillin 2 dysregulates adhesion pathway through upregulation of miR200b and alters the mechanical properties in cardiac cells. *Cells* 8:1639. doi: 10.3390/cells8121639

Puzzi, L., Borin, D., Martinelli, V., Mestroni, L., Kelsell, D. P., and Sbaizero, O. (2018). Cellular biomechanics impairment in keratinocytes is associated with a C-terminal truncated desmoplakin: an atomic force microscopy investigation. *Micron* 106, 27–33. doi: 10.1016/j.micron.2017.12.005

Quarta, G., Syrris, P., Ashworth, M., Jenkins, S., Zuborne Alapi, K., Morgan, J., et al. (2012). Mutations in the Lamin A/C gene mimic arrhythmogenic right ventricular cardiomyopathy. *Eur. Heart J.* 33, 1128–1136. doi: 10.1093/eurheartj/ehr451

Rampazzo, A., Nava, A., Malacrida, S., Beffagna, G., Bauce, B., Rossi, V., et al. (2002). Mutation in human desmoplakin domain binding to plakoglobin causes a dominant form of arrhythmogenic right ventricular cardiomyopathy. *Am. J. Hum. Genet.* 71, 1200−1206. doi: 10.1086/344208

Rizzo, S., Lodder, E. M., Verkerk, A. O., Wolswinkel, R., Beekman, L., Pilichou, K., et al. (2012). Intercalated disc abnormalities, reduced Na(+) current density, and conduction slowing in desmoglein-2 mutant mice prior to cardiomyopathic changes. *Cardiovasc. Res.* 95, 409–418. doi: 10.1093/cvr/cvs219

Ronaldson-Bouchard, K., Ma, S. P., Yeager, K., Chen, T., Song, L., Sirabella, D., et al. (2018). Advanced maturation of human cardiac tissue grown from pluripotent stem cells. *Nature* 556, 239–243. doi: 10.1038/s41586-018-0016-3

Ruwald, M. H., Abu-Zeitone, A., Jons, C., Ruwald, A. C., McNitt, S., Kutyifa, V., et al. (2013). Impact of carvedilol and metoprolol on inappropriate implantable cardioverter-defibrillator therapy: the MADIT-CRT trial (multicenter automatic defibrillator implantation with cardiac resynchronization therapy). *J. Am. Coll. Cardiol.* 62, 1343–1350. doi: 10.1016/j.jacc.2013.03.087

Sala, L., Bellin, M., and Mummery, C. L. (2017). Integrating cardiomyocytes from human pluripotent stem cells in safety pharmacology: has the time come? *Br. J. Pharmacol.* 174, 3749–3765. doi: 10.1111/bph.13577

Sato, P. Y., Coombs, W., Lin, X., Nekrasova, O., Green, K. J., Isom, L. L., et al. (2011). Interactions between ankyrin-G, Plakophilin-2, and Connexin43 at the cardiac intercalated disc. *Circ. Res.* 109, 193–201. doi: 10.1161/CIRCRESAHA.111.247023

Schlipp, A., Schinner, C., Spindler, V., Vielmuth, F., Gehmlich, K., Syrris, P., et al. (2014). Desmoglein-2 interaction is crucial for cardiomyocyte cohesion and function. *Cardiovasc. Res.* 104, 245–257. doi: 10.1093/cvr/cvu206

Schwartz, P. J. (2014). Cardiac sympathetic denervation to prevent life-threatening arrhythmias. *Nat. Rev. Cardiol.* 11, 346–353. doi: 10.1038/nrcardio.2014.19

Schwartz, P. J., Priori, S. G., Cerrone, M., Spazzolini, C., Odero, A., Napolitano, C., et al. (2004). Left cardiac sympathetic denervation in the management of high-risk patients affected by the long-QT syndrome. *Circulation* 109, 1826–1833. doi: 10.1161/01.CIR.0000125523.14403.1E

Sen-Chowdhry, S., Syrris, P., Ward, D., Asimaki, A., Sevdalis, E., and McKenna, W. J. (2007). Clinical and genetic characterization of families with arrhythmogenic right ventricular dysplasia/cardiomyopathy provides novel insights into patterns of disease expression. *Circulation* 115, 1710–1720. doi: 10.1161/CIRCULATIONAHA.106.660241

Shen, M. J., and Zipes, D. P. (2014). Role of the autonomic nervous system in modulating cardiac arrhythmias. *Circ. Res.* 114, 1004–1021. doi: 10.1161/CIRCRESAHA.113.302549

Silvani, A., Calandra-Buonaura, G., Dampney, R. A. L., and Cortelli, P. (2016). Brain–heart interactions: physiology and clinical implications. *Proc. R. Soc. A* 374:20150181. doi: 10.1098/rsta.2015.0181

Sommariva, E., Brambilla, S., Carbucicchio, C., Gambini, E., Meraviglia, V., Russo, D. A., et al. (2016). Cardiac mesenchymal stromal cells are a source of adipocytes in arrhythmogenic cardiomyopathy. *Eur. Heart J.* 37, 1835–1846. doi: 10.1093/eurheartj/ehv579

Sommariva, E., Stadiotti, I., Perrucci, G. L., Tondo, C., and Pompilio, G. (2017). Cell models of arrhythmogenic cardiomyopathy: advances and opportunities. *Dis. Model. Mech.* 10, 823–835. doi: 10.1242/dmm.029363

Stadiotti, I., Pompilio, G., Maione, A. S., Pilato, C. A., D'Alessandra, Y., and Sommariva, E. (2019). Arrhythmogenic cardiomyopathy: what blood can reveal? *Heart Rhythm* 16, 470–477. doi: 10.1016/j.hrthm.2018.09.023

Stokes, D. L. (2007). Desmosomes from a structural perspective. *Curr. Opin. Cell Biol.* 19, 565–571. doi: 10.1016/j.ceb.2007.09.003

Syrris, P., Ward, D., Evans, A., Asimaki, A., Gandjbakhch, E., Sen-Chowdhry, S., et al. (2006). Arrhythmogenic right ventricular dysplasia/cardiomyopathy associated with mutations in the desmosomal gene desmocollin-2. *Am. J. Hum. Genet.* 79, 978−984. doi: 10.1086/509122

Szentmiklosi, A. J., Szentandrássy, N., Hegyi, B., Horvath, B., Magyar, J., Banyasz, T., et al. (2015). Chemistry, physiology, and pharmacology of β-adrenergic mechanisms in the heart. Why are β-blocker antiarrhythmics superior? *Curr. Pharm. Des.* 21, 1030–1041. doi: 10.2174/1381612820666141029111240

Taylor, M., Graw, S., Sinagra, G., Barnes, C., Slavov, D., Brun, F., et al. (2011). Genetic variation in titin in arrhythmogenic right ventricular cardiomyopathy-overlap syndromes. *Circulation* 124, 876–885. doi: 10.1161/CIRCULATIONAHA.110.005405

Te Riele, A. S. J. M., Agullo-Pascual, E., James, C. A., Leo-Macias, A., Cerrone, M., Zhang, M., et al. (2017). Multilevel analyses of SCN5A mutations in arrhythmogenic right ventricular dysplasia/cardiomyopathy suggest non-canonical mechanisms for disease pathogenesis. *Cardiovasc. Res.* 113, 102–111. doi: 10.1093/cvr/cvw234

Thiene, G. (2015). The research venture in arrhythmogenic right ventricular cardiomyopathy: a paradigm of translational medicine. *Eur. Heart J.* 36, 837−846. doi: 10.1093/eurheartj/ehu493

Thiene, G., and Basso, C. (2001). Arrhythmogenic right ventricular cardiomyopathy: an update. *Cardiovasc. Pathol.* 10, 109–117. doi: 10.1016/s1054-8807(01)00067-9

Thiene, G., Corrado, D., and Basso, C. (2016). *Sudden Cardiac Death in the Young and Athletes*. Milano: Springer Milan, doi: 10.1007/978-88-470-5776-0

Thiene, G., and Marcus, F. (2013). Arrhythmogenic cardiomyopathy: a biventricular disease in search of a cure. *Heart Rhythm* 10, 290–291. doi: 10.1016/j.hrthm.2012.11.009

Thiene, G., Nava, A., Corrado, D., Rossi, L., and Pennelli, N. (1988). Right ventricular cardiomyopathy and sudden death in young people. *N. Engl. J. Med.* 318, 129–133. doi: 10.1056/NEJM198801213180301

Tiburcy, M., Hudson, J. E., Balfanz, P., Schlick, S., Meyer, T., Chang Liao, M.-L., et al. (2017). Defined engineered human myocardium with advanced maturation for applications in heart failure modeling and repair. *Circulation* 135, 1832–1847. doi: 10.1161/CIRCULATIONAHA.116.024145

Tiso, N., Stephan, D. A., Nava, A., Bagattin, A., Devaney, J. M., Stanchi, F., et al. (2001). Identification of mutations in the cardiac ryanodine receptor gene in families affected with arrhythmogenic right ventricular cardiomyopathy type 2 (ARVD2). *Hum. Mol. Genet.* 10, 189–194. doi: 10.1093/hmg/10.3.189

Towbin, J. A., McKenna, W. J., Abrams, D. J., Ackerman, M. J., Calkins, H., Darrieux, F. C. C., et al. (2019). 2019 HRS expert consensus statement on evaluation, risk stratification, and management of arrhythmogenic cardiomyopathy. *Heart Rhythm* 16, e301–e372. doi: 10.1016/j.hrthm.2019.05.007

Tsai, W.-C., Lee, T.-I., Chen, Y.-C., Kao, Y.-H., Lu, Y.-Y., Lin, Y.-K., et al. (2014). Testosterone replacement increases aged pulmonary vein and left atrium arrhythmogenesis with enhanced adrenergic activity. *Int. J. Cardiol.* 176, 110–118. doi: 10.1016/j.ijcard.2014.06.054

Turkowski, K. L., Tester, D. J., Bos, J. M., Haugaa, K. H., and Ackerman, M. J. (2017). Whole exome sequencing with genomic triangulation implicates CDH2-encoded N-cadherin as a novel pathogenic substrate for arrhythmogenic cardiomyopathy. *Congenit Heart Dis.* 12, 226—235. doi: 10.1111/chd.12462

Valiente-Alandi, I., Schafer, A. E., and Blaxall, B. C. (2016). Extracellular matrix-mediated cellular communication in the heart. *J. Mol. Cell. Cardiol.* 91, 228–237. doi: 10.1016/j.yjmcc.2016.01.011

van der Zwaag, P. A., van Rijsingen, I. A. W., Asimaki, A., Jongbloed, J. D. H., van Veldhuisen, D. J., Wiesfeld, A. C. P., et al. (2012). Phospholamban R14del mutation in patients diagnosed with dilated cardiomyopathy or arrhythmogenic right ventricular cardiomyopathy: evidence supporting the concept of arrhythmogenic cardiomyopathy. *Eur. J. Heart Fail.* 14, 1199–1207. doi: 10.1093/eurjhf/hfs119

van Hengel, J., Calore, M., Bauce, B., Dazzo, E., Mazzotti, E., De Bortoli, M., et al. (2013). Mutations in the area composita protein αT-catenin are associated with arrhythmogenic right ventricular cardiomyopathy. *Eur. Heart J.* 34, 201–210. doi: 10.1093/eurheartj/ehs373

van Opbergen, C. J. M., Noorman, M., Pfenniger, A., Copier, J. S., Vermij, S. H., Li, Z., et al. (2019). Plakophilin-2 haploinsufficiency causes calcium handling deficits and modulates the cardiac response towards stress. *Int. J. Mol. Sci.* 20:4076. doi: 10.3390/ijms20174076

Veerman, C. C., Kosmidis, G., Mummery, C. L., Casini, S., Verkerk, A. O., and Bellin, M. (2015). Immaturity of human stem-cell-derived cardiomyocytes in culture: fatal flaw or soluble problem? *Stem Cells Dev.* 24, 1035–1052. doi: 10.1089/scd.2014.0533

Veldhuis, J. D., Keenan, D. M., Liu, P. Y., Iranmanesh, A., Takahashi, P. Y., and Nehra, A. X. (2009). The aging male hypothalamic-pituitary-gonadal axis: pulsatility and feedback. *Mol. Cell. Endocrinol.* 299, 14–22. doi: 10.1016/j.mce.2008.09.005

Vischer, A. S., Connolly, D. J., Coats, C. J., Fuentes, V. L., McKenna, W. J., Castelletti, S., et al. (2017). Arrhythmogenic right ventricular cardiomyopathy in Boxer dogs: the diagnosis as a link to the human disease. *Acta Myol.* 36, 135–150.

Volpato, V., and Webber, C. (2020). Addressing variability in iPSC-derived models of human disease: guidelines to promote reproducibility. *Dis. Model. Mech.* 13:dmm42317. doi: 10.1242/dmm.042317

Waagstein, F. (1993). Beta blockers in heart failure. *Cardiology* 82(Suppl. 3), 13–18. doi: 10.1159/000175929

Wang, L., Liu, S., Zhang, H., Hu, S., and Wei, Y. (2015). RhoA activity increased in myocardium of arrhythmogenic cardiomyopathy patients and affected connexin 43 protein expression in HL-1 cells. *Int. J. Clin. Exp. Med.* 8, 12906–12913.

Warboys, C. M. (2018). Mechanoactivation of Wnt/β-catenin pathways in health and disease. *Emerg. Top. Life Sci.* 2, 701–712. doi: 10.1042/ETLS20180042

Wen, J.-Y., Wei, C.-Y., Shah, K., Wong, J., Wang, C., and Chen, H.-S. V. (2015). Maturation-based model of arrhythmogenic right ventricular dysplasia using patient-specific induced pluripotent stem cells. *Circ. J.* 79, 1402–1408. doi: 10.1253/circj.CJ-15-0363

Wichter, T., Schäfers, M., Rhodes, C. G., Borggrefe, M., Lerch, H., Lammertsma, A. A., et al. (2000). Abnormalities of cardiac sympathetic innervation in arrhythmogenic right ventricular cardiomyopathy : quantitative assessment of presynaptic norepinephrine reuptake and postsynaptic beta-adrenergic receptor density with positron emission tomography. *Circulation* 101, 1552–1558. doi: 10.1161/01.cir.101.13.1552

Yang, Z., Bowles, N. E., Scherer, S. E., Taylor, M. D., Kearney, D. L., Ge, S., et al. (2006). Desmosomal dysfunction due to mutations in desmoplakin causes arrhythmogenic right ventricular dysplasia/cardiomyopathy. *Circ. Res.* 99, 646–655. doi: 10.1161/01.RES.0000241482.19382.c6

Yu, J., Hu, J., Dai, X., Cao, Q., Xiong, Q., Liu, X., et al. (2014). SCN5A mutation in Chinese patients with arrhythmogenic right ventricular dysplasia. *Herz* 39, 271—275. doi: 10.1007/s00059-013-3998-5

Zaglia, T., and Mongillo, M. (2017). Cardiac sympathetic innervation, from a different point of (re)view. *J. Physiol.* 595, 3919–3930. doi: 10.1113/JP273120

Zhang, J., Vincent, K. P., Peter, A. K., Klos, M., Cheng, H., Huang, S. M., et al. (2020). Cardiomyocyte expression of ZO-1 is essential for normal atrioventricular conduction but does not alter ventricular function. *Circ. Res.* 127, 284–297. doi: 10.1161/CIRCRESAHA.119.315539

Zhang, Q., Deng, C., Rao, F., Modi, R. M., Zhu, J., Liu, X., et al. (2013). Silencing of desmoplakin decreases connexin43/Nav1.5 expression and sodium current in HL-1 cardiomyocytes. *Mol. Med. Rep.* 8, 780–786. doi: 10.3892/mmr.2013.1594

Zhang, Z., Stroud, M. J., Zhang, J., Fang, X., Ouyang, K., Kimura, K., et al. (2015). Normalization of Naxos plakoglobin levels restores cardiac function in mice. *J. Clin. Invest.* 125, 1708–1712. doi: 10.1172/JCI80335

Zhou, J., Lal, H., Chen, X., Shang, X., Song, J., Li, Y., et al. (2010). GSK-3alpha directly regulates beta-adrenergic signaling and the response of the heart to hemodynamic stress in mice. *J. Clin. Invest.* 120, 2280–2291. doi: 10.1172/JCI41407

Conflict of Interest: The authors declare that the research was conducted in the absence of any commercial or financial relationships that could be construed as a potential conflict of interest.

The handling editor declared a past co-authorship with one of the authors GB.

frontiers in Physiology

ORIGINAL RESEARCH
published: 25 January 2021
doi: 10.3389/fphys.2020.597638

A Longitudinal Study of T2 Mapping Combined With Diffusion Tensor Imaging to Quantitatively Evaluate Tissue Repair of Rat Skeletal Muscle After Frostbite

*Yue Gao[1], Zhao Lu[1], Xiaohong Lyu[2], Qiang Liu[1] and Shinong Pan[1]**

[1]Department of Radiology, Shengjing Hospital of China Medical University, Shenyang, China, [2]Department of Radiology, The First Affiliated Hospital of Jinzhou Medical University, Jinzhou, China

Purpose: T2 mapping and diffusion tensor imaging (DTI) enable the detection of changes in the skeletal muscle microenvironment. We assessed T2 relaxation times, DTI metrics, performed histological characterization of frostbite-induced skeletal muscle injury and repair, and provided diagnostic imaging biomarkers.

Design and Methods: Thirty-six Sprague Dawley rats (200 ± 10 g) were obtained. Thirty rats were used for establishing a skeletal muscle frostbite model, and six were untreated controls. Functional MR sequences were performed on rats on days 0, 3, 5, 10, and 14 ($n = 6$ per time point). Rats were then sacrificed to obtain the quadriceps muscles. Tensor eigenvalues ($\lambda 1$, $\lambda 2$, and $\lambda 3$), mean diffusivity (MD), fractional anisotropy (FA), and T2 values were compared between the frostbite model and control rats. ImageJ was used to measure the extracellular area fraction (EAF), muscle fiber cross-sectional area (fCSA), and skeletal muscle tumor necrosis factor α (TNF-α), and Myod1 expression. The correlation between the histological and imaging parameters of the frostbitten skeletal muscle was evaluated. Kolmogorov–Smirnoff test, Leven's test, one-way ANOVA, and Spearman coefficient were used for analysis.

Results: T2 relaxation time of frostbitten skeletal muscle was higher at all time points ($p < 0.01$). T2 relaxation time correlated with EAF, and TNF-α and Myod1 expression ($r = 0.42$, $p < 0.05$; $r = 0.86$, $p < 0.01$; $r = 0.84$, $p < 0.01$). The average tensor metrics (MD, $\lambda 1$, $\lambda 2$, and $\lambda 3$) of skeletal muscle at 3 and 5 days of frostbite increased ($p < 0.05$), and fCSA correlated with $\lambda 1$, $\lambda 2$, and $\lambda 3$, and MD ($r = 0.65$, $p < 0.01$; $r = 0.48$, $p < 0.01$; $r = 0.52$, $p < 0.01$; $r = 0.62$, $p < 0.01$).

Conclusion: T2 mapping and DTI imaging detect frostbite-induced skeletal muscle injury early. This combined approach can quantitatively assess skeletal muscle repair and regeneration within 2 weeks of frostbite. Imaging biomarkers for the diagnosis of frostbite were suggested.

Keywords: T2 mapping, diffusion tensor imaging, skeletal muscle, frostbite, histological characterization

OPEN ACCESS

Edited by:
Marcella Canton, University of Padua, Italy

Reviewed by:
Michelle S. Parvatiyar, Florida State University, United States
Giorgos K. Sakkas, Cardiff Metropolitan University, United Kingdom

***Correspondence:**
Shinong Pan
cjr.panshinong@vip.163.com

Specialty section:
This article was submitted to Striated Muscle Physiology, a section of the journal Frontiers in Physiology

Received: *21 August 2020*
Accepted: *30 December 2020*
Published: *25 January 2021*

Citation:
Gao Y, Lu Z, Lyu X, Liu Q and Pan S (2021) A Longitudinal Study of T2 Mapping Combined With Diffusion Tensor Imaging to Quantitatively Evaluate Tissue Repair of Rat Skeletal Muscle After Frostbite. Front. Physiol. 11:597638. doi: 10.3389/fphys.2020.597638

INTRODUCTION

The classification of cold-exposure injuries is based on the depth of tissue involved in the injury, which is divided into four levels. Skeletal muscle frostbite belongs to grade 4 frostbite, which is the most serious form of frostbite (Ingram and Raymond, 2013). Frostbite-induced pathological changes, such as cellular edema, microcirculation disorders, and inflammation in skeletal muscle tissue can cause severe sensory dysfunction, amputation, or death. Although muscle frostbite can lead to lifelong disability and even death, it does not attract as much academic interest as other muscle injuries. Clinicians lack precise diagnostic criteria for the extent and degree of frostbite in patients (Petrone et al., 2014). Surgeons may need weeks or months to wait for a clear boundary between living tissue and necrotic tissue to form before performing amputation (Woo et al., 2013).

Assessing the extent of frostbite through imaging increases the possibility of early surgical removal of necrotic tissue (Murphy et al., 2000). At present, multi-phase bone scans constitute the main diagnostic imaging method for the evaluation of frostbitten soft tissue and skeletal muscle viability (Millet et al., 2016). As multi-phase bone scanning requires injection of pertechnetate, contrast media metabolism and resulting side effects may increase the patient's burden. Another limitation of multiphase bone scans is the poor anatomical resolution of images (Manganaro et al., 2019). MRI is a non-invasive technique, which does not employ ionizing radiation. Functional MRI not only reveals anatomical abnormalities, but also reflects the physiological state of the soft tissue. T2 mapping can be used for the quantitative evaluation of the degree of muscle activation and inflammatory edema under normal physiological and pathological conditions (Meyer and Prior, 2000; Kuo and Carrino, 2007). The transverse relaxation time is represented by the T2 value, which is reflected by the change in signal intensity of the MRI. Acute activity or inflammation will cause the T2 value to rise. In clinical trials, T2 mapping can quantitatively evaluate skeletal muscle injury and myocardial infarction (Zhang et al., 2011; Radunski et al., 2017; Fu et al., 2019). Diffusion tensor imaging (DTI) parameters include three eigenvalues ($\lambda 1$, $\lambda 2$, and $\lambda 3$), fractional anisotropy (FA), and mean diffusivity (MD). The three eigenvalues indicate the direction of water diffusion, while FA describes the anisotropy of diffusion. DTI parameters have been used to quantitatively evaluate skeletal muscle injury in runners as well as microenvironmental changes in the skeletal muscle of athletes (Froeling et al., 2015; Keller et al., 2020). In addition, DTI can be used to evaluate the changes in muscle and extracellular matrix microstructure through modeling (Sinha et al., 2020). Overall, functional MRI has good potential for the evaluation of skeletal injury.

The current study aimed to explore the value of T2 mapping and DTI parameters for the noninvasive evaluation of skeletal muscle in a rat model of frostbite and to provide imaging biomarkers for the clinical diagnosis and treatment of patients with severe frostbite.

MATERIALS AND METHODS

Experiments were performed under a project license (NO.2019PS468K) granted by Ethics Committee of the institute and was conducted according to the recommendations of the "Guidelines for the Care and Use of Laboratory Animals."

Animal Model

The experimental animals were 36 Sprague Dawley (SD) rats weighing 200 ± 10 g (age: 6 weeks). After the SD rats were numbered, they were randomly divided into two groups, namely the control group (n = 6) and the experimental group (n = 30). The 30 rats in the experimental group were then randomly divided into five subgroups (six rats/subgroup). Rats in each group underwent frostbite induction followed by functional MRI sequence scans at different time points (0, 3, 5, 10, and 14 days). Immediately afterwards, the quadriceps femoris was taken and fixed with 4% paraformaldehyde solution. The experimental procedure is indicated in **Figure 1**.

Before the experiment, rats received analgesia and anesthesia. Intraperitoneal injection of the analgesic ibuprofen solution (60 mg/kg) was followed by an intraperitoneal injection of pentobarbital sodium (50 mg/kg). After anesthesia, both lower limbs of rats were shaved, exposing the skin of both lower limbs. Rats were then fixed. A 3 cm long and 1 cm thick dry ice stick (−78.5°C) was taken with an iron clip to tightly touch the bare skin of the rat's lower limb for 2.5 min to induce frostbite. After the treatment, rats were put back into the cage, and their physiological state was observed. After induction of frostbite, rats were injected with 60 mg/kg of ibuprofen twice a day until the third day after injury. The six rats of the control group did not undergo frostbite treatment.

MRI Scan

MRI scans were acquired on a 3 Tesla scanner (Ingenia, Philips, software). The elbow joint coil was used to obtain the image. Prior to the MRI scan, rats received injection of the analgesic ibuprofen solution (60 mg/kg) and pentobarbital sodium (50 mg/kg). Rats were placed in the coil in the prone position so that the femur was located in the center of the coil. The imaging sequence included conventional axial T1, sagittal, and coronal images, and the scan range included the entire femur. T2 mapping and DTI sequences were acquired using the same field-of-view (FOV) and geometry. Scan sequence parameters are shown in **Table 1**. After the MRI scan, rats were sacrificed by intraperitoneal injection of pentobarbital sodium (200 mg/kg).

Image Data Analysis

Two observers with experience in MR image analysis (Y. Gao and XH. Lyu, with 6 and 10 years of MR diagnosis experience, respectively) assessed the MR images with an assessment interval of 4 weeks. They were blind to image information when analyzing the images. To evaluate the validity of MRI measurements, test-retest reliability was analyzed. Interobserver and intra-observer reliabilities for the imaging parameters were analyzed using the intraclass correlation coefficient (ICC).

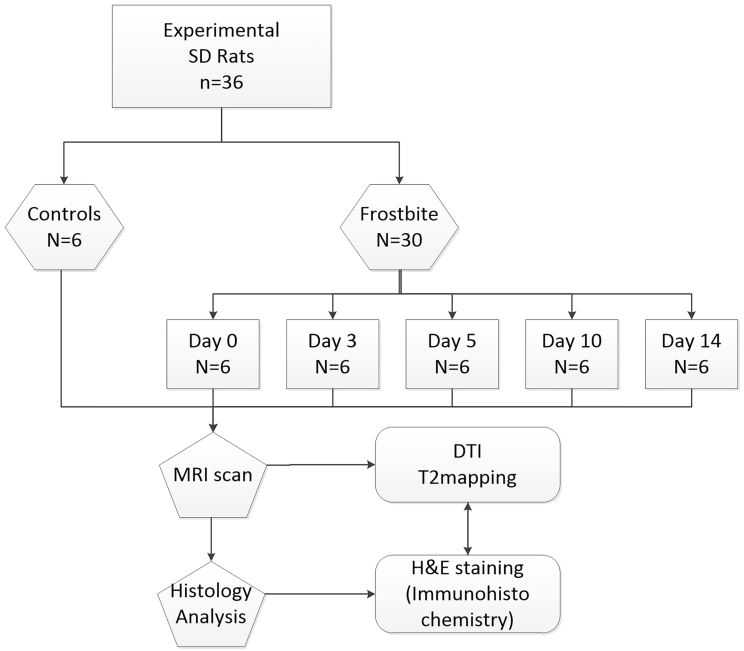

FIGURE 1 | Flowchart demonstrating the study design.

TABLE 1 | Sequence parameters for T1, diffusion tensor imaging (DTI), and T2 mapping.

Sequence	Plane	FOV	Voxel size	Flip angle (°)	TR (ms)	TE (ΔTE; ms)
T1	Axial	100 × 120 × 60	0.33 × 0.37 × 3	90	500	10
DTI	Axial	120 × 90 × 60	1.88 × 2.25 × 2.50	90	2,500	62
T2 mapping	Axial	90 × 121 × 39	0.55 × 0.76 × 3	90	1,500	9–81(9)

DTI, diffusion tensor imaging; T1, Longitudinal relaxation time; T2, transverse relaxation times; FOV, Field of view; TE, echo time; TR, repetition time.

The original images were imported into the Philips post-processing workstation and analyzed by the workstation function tool software. T2 mapping pseudo color images were automatically generated after scanning. Fiber track was implemented by workstation post-processing. The areas of interest were recognized by the observers and drawn manually (**Figure 2**).

Histological Examination

Hematoxylin-Eosin Staining

After the MRI scan, animals were euthanized using 100% carbon dioxide. Skin was cut off the rat's lower limbs, and the quadriceps muscle was separated, removed, soaked in 4% paraformaldehyde solution, and then fixed at room temperature for 1 week. After fixing, the sample was dehydrated, permeated with gradient alcohol and xylene, and embedded in paraffin. The paraffin block was cut into horizontal tissue sections (3 μm), and slices were heated at 70°C for 4 h. Paraffin sections were hematoxylin-eosin (HE) stained with an automatic cylinder passing machine.

Immunohistochemistry

The tissue sections were dewaxed, and Tris-EDTA repair solution was used to repair them. Sections were then immersed in endogenous peroxidase blocker for 30 min, followed by a wash with PBS. Sections were incubated with serum for 30 min at room temperature, followed by incubation with primary antibodies against TNF-α (1:200) and Myod1 (1:200) overnight at 4°C, or overnight incubation with PBS as a negative control. Sections were then rewarmed at room temperature for 1 h, washed with PBS, and incubated with the appropriate secondary antibody at room temperature for 25 min. After the secondary antibody was washed away, sections were incubated with peroxidase at room temperature for 25 min, and the DAB kit was used to carry out the color reaction.

Slices were sealed with gum, followed by observation and image collection under a microscope.

The Image J software was used to analyze the extracellular matrix area fraction (EAF) and fiber cross-sectional area (fCSA) of HE images as well as the expression levels of targeted proteins in histochemical images. We use Image J software to open the HE image of skeletal muscle tissue and adjust the image mode to RGB stack mode. Use the "threshold" function in the "Adjust" module to automatically identify muscle fibers, and use the "Measure" function to measure the percentage of muscle fiber area (fCSA%). EAF = 100% − fCSA%. fCSA is

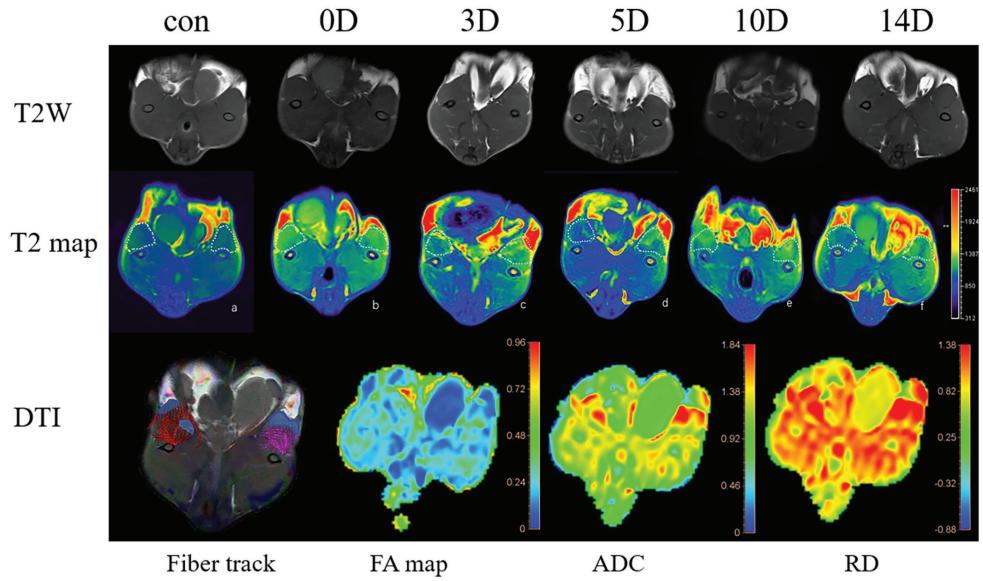

FIGURE 2 | T2WI, T2map axial sequence images in the **(a-f)** control group and frostbite group (0, 3, 5, 10, 14 days). The muscles in the ROI were manually drawn on the T2 map: the muscle in the control ROI is blue. The color of the ROI area changed significantly after frostbite. The diffusion tensor imaging (DTI) sequence: the schematic diagram of the fiber track of the DTI and the corresponding fractional anisotropy (FA) map, mean diffusivity (MD) map, and RD map. The area with fewer muscle fibers in the fiber track diagram is consistent with the high-signal area in the MD picture.

to measure the cross-sectional area of a single muscle fiber by manually contouring and measuring after the image J software identifies the muscle fiber. Six images were collected for each subgroup, and 10 muscle fCSA were collected for each image, and the average value was taken to obtain the fCSA of each subgroup.

Western Blot

Western blotting was performed using standard protocols. Extract total protein from skeletal muscle tissue and mix it with 5× loading buffer at a ratio of 4:1. Equal amounts of protein were separated by 10% sodium dodecyl sulfate-polyacrylamide gel electrophoresis (SDS-PAGE) and transferred to polyacrylamide difluoride (PVDF) membranes. After blocking with 5% skimmed milk for 2 h at room temperature, the membrane was combined with anti-Myod1 (dilution 1:1,000, catalog number 18943-1-AP, Proteintech), anti-TNF-α (dilution 1: 1,000, product catalog number 17950-1-AP, Proteintech), and anti-GAPDH (dilution 1:5,000, catalog number 60004-1-Ig, Proteintech), and then gently shake at 4°C overnight. On the second day, the Myod1 membrane and TNF-α membrane were incubated with horseradish peroxidase-conjugated goat anti-rabbit IgG antibody (dilution 1:5,000; catalog number SA00001-2, Proteintech) for 2 h at room temperature. GAPDH membrane and horseradish peroxidase-conjugated goat anti-mouse IgG antibody (dilution 1:5,000; catalog number SA00001-1, Proteintech) were incubated for 2 h at room temperature, and then washed PVDF membranes in TBST buffer (10 mM Tris/HCl, 150 mM NaCl, and 0.05% Tween-20, pH 7.5) three times, and developed using enhanced chemiluminescence reagents (NCM Biotech). The Image J software was used to analyze densitometry values and standardized to GAPDH.

Statistical Analysis

The normality of distributions was tested using the Kolmogorov–Smirnov test and normal Q-Q plots. For quantitative variables that were normally distributed, the data are expressed as mean ± SD. Leven's test was used to check the homogeneity of variance. One-way ANOVA was used to compare differences in DTI and T2 mapping parameters between groups, and the Bonferroni correction was employed to adjust the p-value for multiple comparisons. The Spearman correlation coefficient was used to analyze the correlation between TNF-α and Myod1 expression, EAF, and T2 values. The Spearman correlation coefficient was also used to analyze the correlation between fCSA, λ1, λ2, λ3, MD, and FA. Histological parameters (TNF-α, Myod1, EAF, and fCSA) were treated as independent variables, while imaging parameters (T2 value, λ1, λ2, λ3, MD, and FA) were treated as dependent variables. Statistical significance was established at $p < 0.05$. Statistical analyses were performed using SPSS (Version 22.0; SPSS Inc., Chicago, IL).

RESULTS

Morphological Changes of Skeletal Muscle Tissue Within 2 Weeks of Frostbite

At day 0 after frostbite, skeletal muscle cells exhibited edema, the intercellular space expanded, and interstitial components increased. Subsequently, inflammatory cell infiltration increased,

clearing necrotic muscle cells. Inflammatory infiltration persisted until about the tenth day. Ten days after frostbite, there were more new muscle fibers in the remodeled skeletal muscle tissue, and these were irregular in shape. At day 14 after frostbite, skeletal muscle tissue still exhibited blood cell deposition and expression of inflammatory factors (**Figure 3A**).

The schematic diagram of measuring fCSA and EAF is shown in (**Figure 3B**). The skeletal muscle cells of control group rats were closely arranged with less interstitial components. The fCSA values of the frostbite group skeletal muscle at days 3, 5, and 14 were significantly different from those of the control group skeletal muscle (all $p < 0.01$; **Table 2**; **Figures 3C,D**). Further, fCSA was correlated with λ1, λ2, λ3, and MD ($r = 0.65$, $p < 0.01$, $r = 0.48$, $p < 0.01$, $r = 0.52$, $p < 0.01$, and $r = 0.62$, $p < 0.01$, respectively). EAF decreased 10 days after frostbite and was significantly different from the EAF at 5 days after frostbite ($p = 0.01$). At 14 days after frostbite, EAF was significantly different from that of the control group ($p = 0.01$). The EAF of skeletal muscle within 5 days of frostbite was strongly positively correlated with the T2 value ($r = 0.80$, $p < 0.01$), while EAF within 2 weeks of frostbite was only moderately correlated with the T2 value ($r = 0.42$, $p < 0.05$; **Figure 3C**).

Changes in the Relative Expression Levels of TNF-α and Myod1 in Frostbitten Skeletal Muscle

The TNF-α and Myod1 values of each group followed a normal distribution. For the expression levels of TNF-α and Myod1, the results of immunohistochemistry and western blot are in good agreement (Myod1, $r = 0.72$, $p < 0.01$, TNF-α, $r = 0.66$, $p < 0.01$). Within 2 weeks of frostbite, there were two peaks in skeletal muscle TNF-α expression. These peak values were observed at day 3 and day 10 (**Figure 4**). On the 14th day after frostbite, the relative expression of TNF-α was still significantly higher than that in the control group ($p < 0.01$). The relative expression of TNF-α was positively correlated with the T2 value ($r = 0.86$, $p < 0.01$). Myod1 expression in day 10 of frostbite was significantly higher than in the control group ($p < 0.01$). Further, Myod1 expression remained higher than in the control group at 14 days of frostbite ($p < 0.01$). The relative expression of Myod1 was positively correlated with the T2 value ($r = 0.84$, $p < 0.01$).

Dynamic Changes in MR Imaging of Frostbitten Skeletal Muscle

Intraclass correlation coefficient findings revealed that the reliability of MR imaging was substantial or excellent (from 0.87 to 0.96), except for FA (0.61–0.76; **Table 3**). The T2 values and DTI parameters of the control group and the experimental group are shown in **Table 4**. The T2 value of each group conformed to normal distribution. The T2 value of frostbitten skeletal muscle was higher than that of the control group at all time points. The first peak of the T2 value was observed on the third day after frostbite. Thereafter, the T2 value decreased, and there was no significant difference between the T2 value on the fifth day and that on the third day ($p > 0.05$). The second peak was observed on the tenth day after frostbite. The skeletal muscle T2 value on day 14 after frostbite remained higher

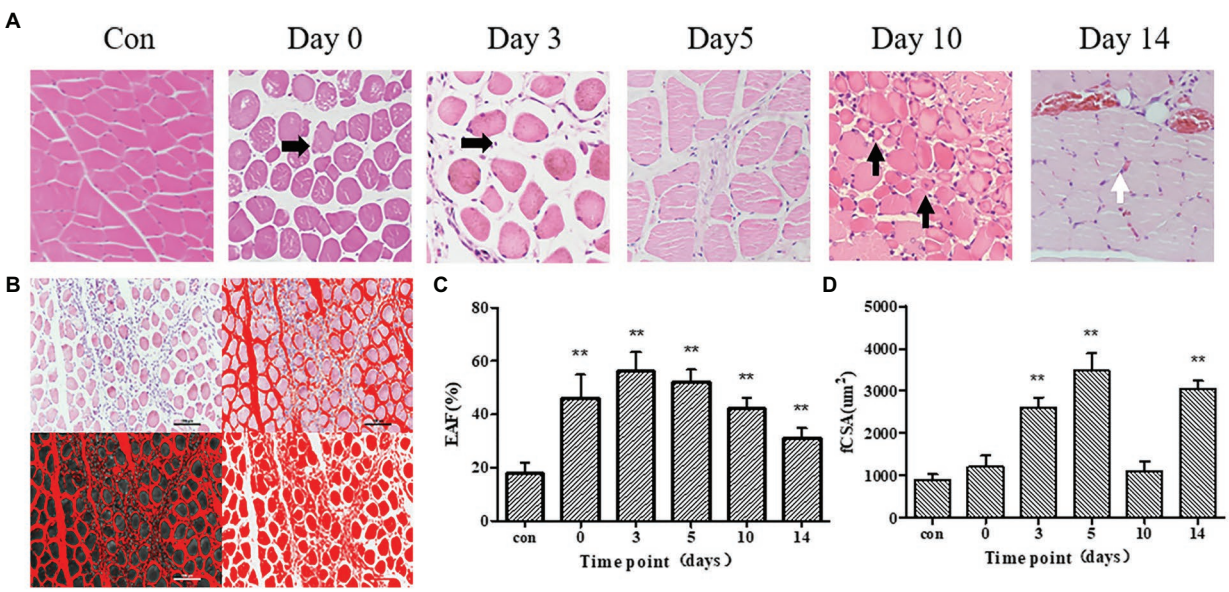

FIGURE 3 | (A) Hematoxylin-eosin (HE) stained images in control group, 0, 3, 5, 10, and 14 days after frostbite. Damaged skeletal muscle tissue exhibits diffuse swelling of muscle cells or inflammatory cells infiltration (Horizontal black arrow). On day 10, regenerated skeletal muscle (Vertical black arrow) was observed. On day 14, red blood cells (white arrows) can be observed in muscle tissue. **(B)** This example shows how to measure the fiber cross-sectional area (fCSA) and extracellular area fraction (EAF). **(C,D)**: EAF and fCSA of control group and frostbite groups. Scale bar, 200 μm. EAF, extracellular matrix area fraction; fCSA, fiber cross-sectional area. $^{**}p < 0.01$.

TABLE 2 | EAF and fCSA in frostbite and control.

Parameter	control (*N* = 6)	frostbite				
		0D (*N* = 6)	3D (*N* = 6)	5D (*N* = 6)	10D (*N* = 6)	14D (*N* = 6)
EAF(%)	18(3.85)	46(8.93)**	56(7.31)**	52(4.79)**	42(4.26)**	31(3.88)**
fCSA(um2)	895(131)	1,202(266)	2,593(248)**	3,473(409)**	1,103(218)	3,035(197)**

Data are given as mean (SD).
***p < 0.01.*
EAF, extracellular matrix area fraction; fCSA, fiber cross-sectional area.

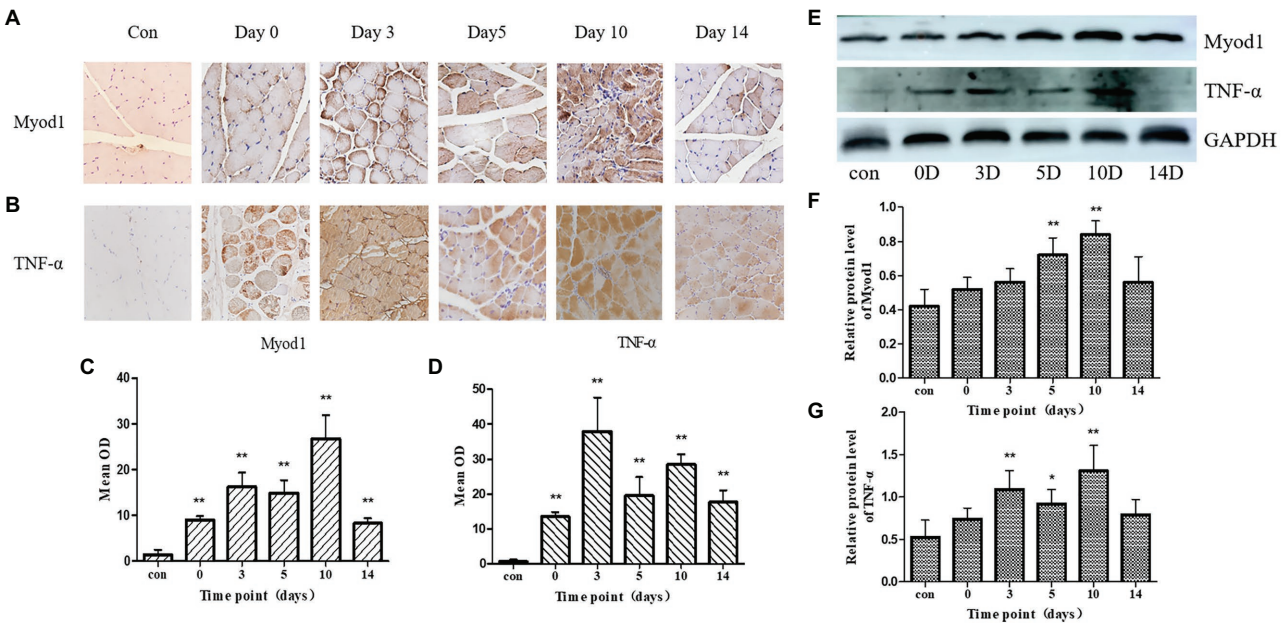

FIGURE 4 | **(A,B)**: immunohistochemical pictures of Myod1 and TNF-α at control and frostbite (0, 3, 5, 10, and 14 days). **(C,D)**: mean optical density (OD) of Myod1 and TNF-α in control group and frostbite groups. **(E)** Western blot pictures of Myod1 and TNF-α. **(F,G)**: protein expression of Myod1 and TNF-α in control group and frostbite groups. Scale bar, 200 μm. OD, optical density. $^{*}p < 0.05$, $^{**}p < 0.01$.

than that of the control group ($p < 0.01$). Further, the T2 value of the frostbitten skeletal muscle exhibited a "bimodal" change (**Figure 5**).

The MD, FA, and three eigenvalues of the control group and frostbite model were measured on the DTI sequence (**Table 4**). Three days after frostbite, MD and eigenvalues were higher ($p < 0.01$, $p < 0.01$, $p < 0.05$, $p < 0.05$), while FA was lower ($p < 0.01$). The peak of MD and the three eigenvalues was observed at 3–5 days after frostbite. Five days after frostbite, MD, FA, and eigenvalues returned to normal levels ($p > 0.05$). On day 14 after frostbite, FA appeared elevated ($p < 0.01$).

DISCUSSION

In the current study, we quantitatively described the dynamic changes occurring in the skeletal muscle microenvironment over a critical 2-week period after frostbite. The current study confirmed the use of DTI combined with T2 mapping for the quantitative evaluation of muscle tissue repair after frostbite. The main findings were as follows: (1) The T2 value reflected muscle damage and its extent after frostbite and showed a bimodal change; (2) The eigenvalues λ1–λ3 and MD of the frostbitten skeletal muscle tissue were higher, reaching peak values around 3–5 days after frostbite, accompanied by an increase in λ1, λ2, λ3, and MD, as well as a decrease in FA; and (3) The T2 value and DTI parameters were correlated with pathological changes in the frostbitten skeletal muscle.

T2 Value as an Indicator of Skeletal Muscle Damage and Repair

Skeletal muscle frostbite is characterized by the direct or indirect cell damage mediated by low temperature conditions, causing secondary vascular microcirculation disorders and inflammation in skeletal muscle tissue (Dana et al., 1969; Quinn, 1985; Imray et al., 2009; Macmillan and Sinclair, 2011). The dynamic balance between inflammation and muscle regeneration affects the prognosis of skeletal muscle frostbite. Skeletal muscle injury

TABLE 3 | Interobserver reliability and intra-observer reliability of T2 value and DTI parameters.

	Interobserver reliability	Intra-observer reliability	
		Observer 1	Observer 2
T2 value	0.95	0.92	0.90
λ1–3	0.96	0.95	0.90
FA	0.76	0.71	0.61
MD	0.96	0.90	0.87

Interobserver and intra-observer reliabilities for T2 value and DTI parameters calculated using intraclass correlation coefficient. λ1–3, three tensor eigenvalues; FA, fractional anisotropy; MD, mean diffusivity.

mainly goes through three stages, namely damage, repair, and remodeling (Hurme et al., 1991). Repair following skeletal muscle injury follows a relatively constant pattern (Filippin et al., 2009). In our study, it took approximately 2 weeks for skeletal muscle to enter the remodeling stage after frostbite. The T2 value of skeletal muscle increased immediately after frostbite and showed a bimodal change. This change was similar to the observations of Fernández and colleagues in myocardial infarction (Fernandez-Jimenez et al., 2015). They reported that the first peak was caused by myocardial ischemia-reperfusion, and the second peak represented the process of myocardial tissue repair. In our study, the two peaks in the T2 value of the skeletal muscle following frostbite appeared later than those of myocardial infarction. The peak T2 value of the skeletal muscle following frostbite was higher than the T2 values following skeletal muscle strain and contusion (Zhang et al., 2011; Fu et al., 2019). While frostbite is similar to other skeletal muscle injury, the degree of injury and the inflammatory response are more severe. Based on the current observations, the T2 value can sensitively detect muscle damage after frostbite.

During skeletal muscle frostbite, the interstitial composition of skeletal muscle tissue changes greatly. In this study, the T2 value strongly correlated with the EAF of the skeletal muscle tissue up to 5 days after frostbite. The increase in the free water in the interstitial space of the skeletal muscle cells prolongs the T2 relaxation time, resulting in an increased T2 value (Patten et al., 2003). The T2 value during the early frostbite period can accurately reflect the interstitial inflammatory edema, and inflammation of muscle tissue is the main pathological process at this stage. Five days after frostbite, the correlation between the EAF and the T2 value was poor. This phenomenon indicates that during the later period of repair following skeletal muscle frostbite, interstitial edema is not the main pathological change, and changes in muscle cells are predominant. A reason for the decrease in EAF and the increase in the T2 value 5 days after frostbite may be: (1) the accumulation of metabolites in muscle cells causing an increase in the osmotic pressure in cells and changing the mobility of water in myofibrils (Fleckenstein et al., 1991); (2) the T2 value is affected not only by the interstitial, but also by the intracellular composition, for example, through changes in protein concentration.

DTI Parameters as Indicators of the State of the Frostbitten Skeletal Muscle

Compared to T2-weighted imaging, DTI parameters can more sensitively detect changes in the muscle microenvironment (Giraudo et al., 2018). The increase in MD and decrease in FA after muscle injury represent a reduction in the limitation of water diffusion (Zaraiskaya et al., 2006; Yanagisawa et al., 2011). Further, the increase in MD and decrease in FA are associated with pathological changes, such as damaged cell swelling, interstitial edema, or destruction of the diffusion barrier (Froeling et al., 2015). In our study, MD and the three eigenvalues increased after frostbite, while FA decreased. The current results are similar to those reported by Zaraiskaya et al. (2006). This phenomenon mainly occurs within 3–5 days of frostbite, indicating that the barrier of frostbitten skeletal muscle tissue is extensively damaged, the cells are swollen, and interstitial edema is severe. In our study, λ1, λ2, λ3, and MD were sensitive to changes in the skeletal muscle microenvironment and were closely related to the fCSA. This is similar to observations by Berry et al. (2018). λ1 corresponds to the water diffusion state parallel to the long axis of the muscle fibers (Damon et al., 2002). The increase of eigenvalues λ1–3 indicates that water molecules in the muscle are easily spread in all directions as a result of the extensive swelling and rupture of skeletal muscle fibers following frostbite. Ten days after frostbite, λ2, λ3, and MD decreased to normal levels, while λ1 remained elevated, indicating that the sarcolemma of the newly formed muscle fibers was intact, but their long axes were still broken. At this point, skeletal muscle is at the stage of remodeling and regeneration. DTI parameters reflect water diffusion within frostbitten skeletal muscle but are not sensitive indicators of inflammation and skeletal muscle regeneration. This is consistent with the findings of Froeling lab (Froeling et al., 2015). The combination of T2 value and DTI parameters can comprehensively determine the survival status of frostbitten skeletal muscle and provide good imaging evidence for assessing the degree and extent of frostbite.

The Relationship Between the T2 Value, Inflammation, and Regeneration

In this study, the peak of the inflammatory factor TNF-α expression in the frostbitten skeletal muscle tissue was basically in parallel with the peak of the T2 value (**Figure 4**). Research has shown that on the third day after skeletal muscle injury, satellite cells are activated, and muscle tissue begins to regenerate (Jarvinen et al., 2005). The strong inflammatory response and initial muscle regeneration produced the first peak T2 value following frostbite. Myod1 plays an important role in the myogenic differentiation of skeletal muscle (Sabourin et al., 1999). On day 10 after frostbite, a large number of regenerate muscle fibers appeared, which was the result of the activity of Myod1 and other myogenic factors. There are many central nuclei in the regenerated muscle fiber, which is consistent with the characteristics of the regenerated muscle in other studies (Zhao et al., 2019; Mosele et al., 2020). Myod1 can regulate the transformation of muscle fiber types, which is accompanied

TABLE 4 | Mean diffusion tensor parameters and T2 values in frostbite and control.

Parameter	control (*N* = 6)	frostbite				
		0D (*N* = 6)	3D (*N* = 6)	5D (*N* = 6)	10D (*N* = 6)	14D (*N* = 6)
λ1(mm^2/s)	1.57(0.10)	1.53(0.06)	1.92(0.10)*	1.94(0.20)*	1.52(0.17)	1.78(0.13)*
λ2(mm^2/s)	1.14(0.07)	1.08(0.11)	1.46(0.22)*	1.62(0.25)*	1.10(0.06)	1.15(0.14)
λ3(mm^2/s)	0.98(0.02)	0.97(0.12)	1.33(0.21)*	1.45(0.28)*	0.87(0.08)	0.96(0.07)
MD(mm^2/s)	1.06(0.06)	1.14(0.03)	1.50(0.19)*	1.43(0.05)*	1.22(0.02)*	1.20(0.05)
FA	0.23(0.01)	0.27(0.02)*	0.25(0.02)*	0.25(0.02)	0.30(0.00)*	0.33(0.02)*
T2 (ms)	37.6(0.9)	55.5(1.4)*	87.1(3.6)*	80.4(8.1)*	106.1(4.5)*	80.4(5.2)*

Data are given as mean (SD).
$^*p < 0.05$.
λ1–3, three tensor eigenvalues.

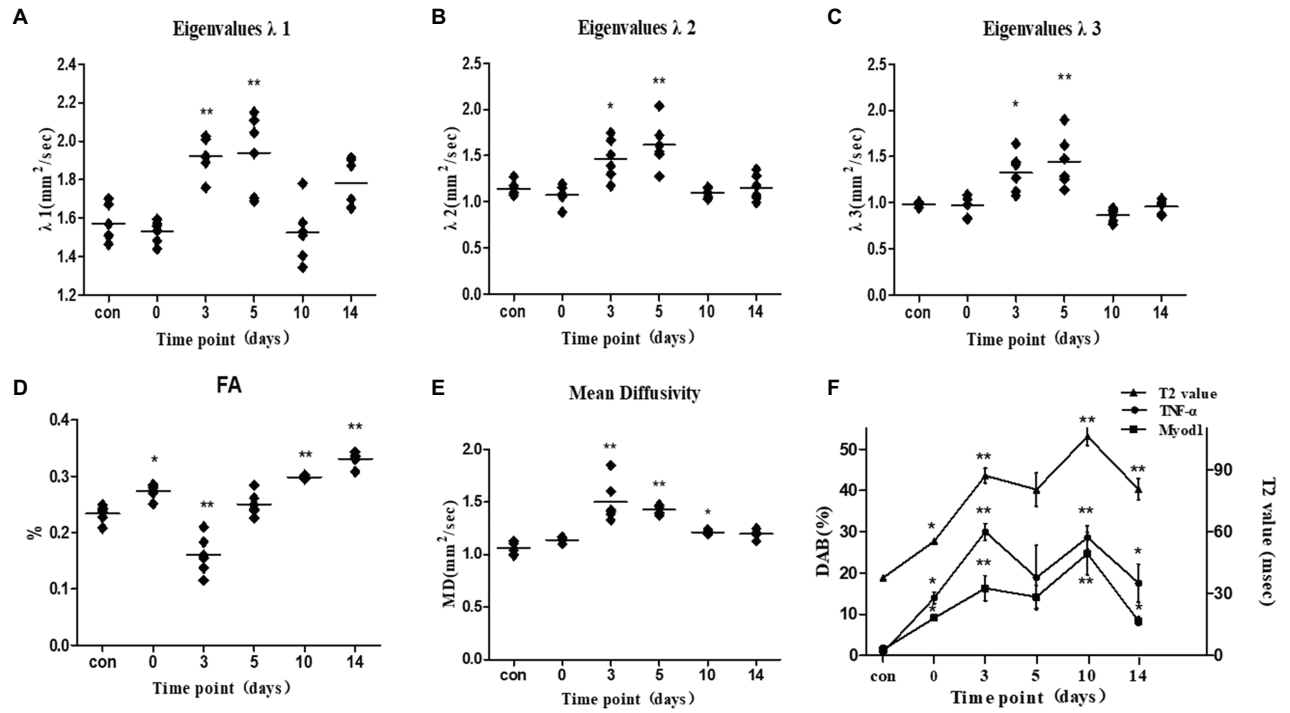

FIGURE 5 | (A–F) Frostbite skeletal muscle eigenvalues λ1, λ2, λ3, FA, MD, and T2 at different time points. Compared with the control group, the frostbite muscle MD and λ1, λ2, and λ3 increased from 3 to 5 days, and FA decreased. The last picture is a schematic diagram of the T2 value, TNF-α, and Myod1. The three curves represent relative expression levels of T2 values, TNF-α, and Myod1. The T2 values show a bimodal change. $^*p < 0.05$, $^{**}p < 0.01$.

by metabolic changes (Hughes et al., 1997; Maves et al., 2007). Thus, the increased expression of Myod1 is associated with the fiber type transformation of the regenerating muscle tissue (Talbot and Maves, 2016). The peak of Myod1 indicates that the regenerated muscle enters the remodeling stage. At the same time on day 10 of frostbite, the expression level of TNF-α in skeletal muscle reached a second peak. Muscle regeneration occurs in an environment with high levels of inflammation. Further, inflammation is considered to be a critical response required for muscle regeneration after muscle injury (Tidball, 1995, 2005), and TNF-α is a key cytokine involved in the inflammatory response during skeletal muscle regeneration. Studies have suggested that, to a certain extent, the inflammatory response promotes skeletal muscle regeneration (Cantini et al., 2002; Tidball and Wehling-Henricks, 2007). Interestingly, TNF-α is a key mediator of myogenic differentiation and plays an important role in the regulation of cell cycle exit and the initiation of myogenic differentiation in satellite cells (Li et al., 2014). Thus, as expected, the second peak of Myod1 and TNF-α expression promoted the differentiation and remodeling of the skeletal muscle after frostbite. This is consistent with previous research results (Warren et al., 2002). The regeneration, remodeling, and inflammation of frostbitten skeletal muscle also resulted in a second peak in the T2 value. The decrease in the T2 value after 10 days of frostbite indicated that skeletal muscle had entered the remodeling stage. The balance between

inflammation and regeneration determines the time required for the T2 value to return to normal levels, as well as the time for skeletal muscle repair (Tidball, 2005). Fourteen days after frostbite, the T2 value and TNF-α expression in rat skeletal muscle were still higher than normal, meaning that inflammation was still ongoing in the skeletal muscle. Of note, excessive inflammation depletes muscle satellite cells and hinders muscle regeneration. T2 values in frostbitten muscle remained high, indicating poor prognosis.

LIMITATIONS

At present, pathological indicators reflect the state of the inflammatory response in frostbitten skeletal muscle. However, the detection of pathological indicators is relatively simple, and the activity of inflammatory cells during skeletal muscle repair needs to be further explored in order to provide an effective target for the treatment of frostbite. In addition, there is little discussion about the correlation between DTI parameters and pathological status, and the relationship between the cross-sectional area of muscle fibers and the DTI parameters should be further studied. Studies have found that different tracking parameter ranges have different effects on muscle diffusion parameters (Forsting et al., 2020). To reduce bias, all experimental images were measured using the same fiber tracking stop criterion. DTI parameters are known to be affected by muscle contraction and stretching, resulting in changes in λ2, λ3, MD, and FA (Schwenzer et al., 2009), compromising the diagnostic performance of DTI with regard to the degree of muscle damage. In this study, we scanned the DTI sequence after anesthetizing rats and performed uniform positioning. Muscle contraction and extension have little effect on the results of DTI parameter measurement in our study. In our study, no conventional imaging methods were used to assess skeletal muscle frostbite. The comparative study of conventional imaging and functional imaging can more comprehensively reflect the pathological state of skeletal muscle frostbite and improve the accuracy of diagnosis, which should be further studied.

CONCLUSION

This study assessed the imaging and pathological features of frostbite-induced skeletal muscle injury, repair, and regeneration, and verified the correlation between imaging parameters and pathological indicators. The T2 value can reflect skeletal muscle frostbite from the early stage, and distinguish between the different stages of frostbite repair (inflammation and regeneration), indicating the clinical outcome of frostbite skeletal muscle. DTI reflected the muscle fiber diameter and the state of water diffusion in frostbitten skeletal muscle, but was not sensitive to skeletal muscle inflammation. The T2 value and DTI parameters can be used together as imaging biomarkers to assess the prognosis of frostbite and provide a basis for the clinical treatment of severe frostbite at different stages. Functional MRI longitudinal quantitative evaluation of skeletal muscle frostbite provides new insights for the clinical treatment of severe frostbite.

DATA AVAILABILITY STATEMENT

The original contributions presented in the study are included in the article/**Supplementary Material**, further inquiries can be directed to the corresponding author.

ETHICS STATEMENT

The animal study was reviewed and approved by Ethics Committee of Shengjing Hospital of China Medical University.

AUTHOR CONTRIBUTIONS

YG and SP conceived and designed the study. YG and XL carried out the experiments. YG and ZL analyzed the data and prepared the figures. YG, ZL, and QL interpreted the results of the experiments. YG drafted the manuscript. ZL and SP edited and revised the manuscript. All authors contributed to the article and approved the submitted version.

FUNDING

This work was supported by the National Natural Science Foundation of China (grant number 81271538), 345 Talent Project and Natural Science Foundation of Liaoning Province (grant numbers 20180530051, 2019-ZD-0794).

SUPPLEMENTARY MATERIAL

The Supplementary Material for this article can be found online at: https://www.frontiersin.org/articles/10.3389/fphys.2020.597638/full#supplementary-material

REFERENCES

Berry, D. B., Regner, B., Galinsky, V., Ward, S. R., and Frank, L. R. (2018). Relationships between tissue microstructure and the diffusion tensor in simulated skeletal muscle. *Magn. Reson. Med.* 80, 317–329. doi: 10.1002/mrm.26993

Cantini, M., Giurisato, E., Radu, C., Tiozzo, S., Pampinella, F., Senigaglia, D., et al. (2002). Macrophage-secreted myogenic factors: a promising tool for greatly enhancing the proliferative capacity of myoblasts in vitro and in vivo. *Neurol. Sci.* 23, 189–194. doi: 10.1007/s100720200060

Damon, B. M., Ding, Z., Anderson, A. W., Freyer, A. S., and Gore, J. C. (2002). Validation of diffusion tensor MRI-based muscle fiber tracking. *Magn. Reson. Med.* 48, 97–104. doi: 10.1002/mrm.10198

Dana, A. S. Jr., Rex, I. H. Jr., and Samitz, M. H. (1969). The hunting reaction. *Arch. Dermatol.* 99, 441–450.

Fernandez-Jimenez, R., Sanchez-Gonzalez, J., Aguero, J., Garcia-Prieto, J., Lopez-Martin, G. J., Garcia-Ruiz, J. M., et al. (2015). Myocardial edema after ischemia/reperfusion is not stable and follows a bimodal pattern: imaging and histological tissue characterization. *J. Am. Coll. Cardiol.* 65, 315–323. doi: 10.1016/j.jacc.2014.11.004

Filippin, L. I., Moreira, A. J., Marroni, N. P., and Xavier, R. M. (2009). Nitric oxide and repair of skeletal muscle injury. *Nitric Oxide* 21, 157–163. doi: 10.1016/j.niox.2009.08.002

Fleckenstein, J. L., Haller, R. G., Lewis, S. F., Archer, B. T., Barker, B. R., Payne, J., et al. (1991). Absence of exercise-induced MRI enhancement of skeletal muscle in McArdle's disease. *J. Appl. Physiol.* 71, 961–969. doi: 10.1152/jappl.1991.71.3.961

Forsting, J., Rehmann, R., Froeling, M., Vorgerd, M., Tegenthoff, M., and Schlaffke, L. (2020). Diffusion tensor imaging of the human thigh: consideration of DTI-based fiber tracking stop criteria. *MAGMA* 33, 343–355. doi: 10.1007/s10334-019-00791-x

Froeling, M., Oudeman, J., Strijkers, G. J., Maas, M., Drost, M. R., Nicolay, K., et al. (2015). Muscle changes detected with diffusion-tensor imaging after long-distance running. *Radiology* 274, 548–562. doi: 10.1148/radiol.14140702

Fu, C., Xia, Y., Meng, F., Li, F., Liu, Q., Zhao, H., et al. (2019). MRI quantitative analysis of eccentric exercise-induced skeletal muscle injury in rats. *Acad. Radiol.* 27, e72–e79. doi: 10.1016/j.acra.2019.05.011

Giraudo, C., Motyka, S., Weber, M., Karner, M., Resinger, C., Feiweier, T., et al. (2018). Normalized STEAM-based diffusion tensor imaging provides a robust assessment of muscle tears in football players: preliminary results of a new approach to evaluate muscle injuries. *Eur. Radiol.* 28, 2882–2889. doi: 10.1007/s00330-017-5218-9

Hughes, S. M., Koishi, K., Rudnicki, M., and Maggs, A. M. (1997). MyoD protein is differentially accumulated in fast and slow skeletal muscle fibres and required for normal fibre type balance in rodents. *Mech. Dev.* 61, 151–163. doi: 10.1016/s0925-4773(96)00631-4

Hurme, T., Kalimo, H., Lehto, M., and Jarvinen, M. (1991). Healing of skeletal muscle injury: an ultrastructural and immunohistochemical study. *Med. Sci. Sports Exerc.* 23, 801–810.

Imray, C., Grieve, A., Dhillon, S., and The Caudwell Xtreme Everest Research Group (2009). Cold damage to the extremities: frostbite and non-freezing cold injuries. *Postgrad. Med. J.* 85, 481–488. doi: 10.1136/pgmj.2008.068635

Ingram, B. J., and Raymond, T. J. (2013). Recognition and treatment of freezing and nonfreezing cold injuries. *Curr. Sports Med. Rep.* 12, 125–130. doi: 10.1249/JSR.0b013e3182877454

Jarvinen, T. A., Jarvinen, T. L., Kaariainen, M., Kalimo, H., and Jarvinen, M. (2005). Muscle injuries: biology and treatment. *Am. J. Sports Med.* 33, 745–764. doi: 10.1177/0363546505274714

Keller, S., Yamamura, J., Sedlacik, J., Wang, Z. J., Gebert, P., Starekova, J., et al. (2020). Diffusion tensor imaging combined with T2 mapping to quantify changes in the skeletal muscle associated with training and endurance exercise in competitive triathletes. *Eur. Radiol.* 30, 2830–2842. doi: 10.1007/s00330-019-06576-z

Kuo, G. P., and Carrino, J. A. (2007). Skeletal muscle imaging and inflammatory myopathies. *Curr. Opin. Rheumatol.* 19, 530–535. doi: 10.1097/BOR.0b013e3282efdc66

Li, Y. P., Niu, A., and Wen, Y. (2014). Regulation of myogenic activation of p38 MAPK by TACE-mediated TNFalpha release. *Front. Cell Dev. Biol.* 2:21. doi: 10.3389/fcell.2014.00021

Macmillan, H. A., and Sinclair, B. J. (2011). Mechanisms underlying insect chill-coma. *J. Insect Physiol.* 57, 12–20. doi: 10.1016/j.jinsphys.2010.10.004

Manganaro, M. S., Millet, J. D., Brown, R. K., Viglianti, B. L., Wale, D. J., and Wong, K. K. (2019). The utility of bone scintigraphy with SPECT/CT in the evaluation and management of frostbite injuries. *Br. J. Radiol.* 92:20180545. doi: 10.1259/bjr.20180545

Maves, L., Waskiewicz, A. J., Paul, B., Cao, Y., Tyler, A., Moens, C. B., et al. (2007). Pbx homeodomain proteins direct Myod activity to promote fast-muscle differentiation. *Development* 134, 3371–3382. doi: 10.1242/dev.003905

Meyer, R. A., and Prior, B. M. (2000). Functional magnetic resonance imaging of muscle. *Exerc. Sport Sci. Rev.* 28, 89–92.

Millet, J. D., Brown, R. K., Levi, B., Kraft, C. T., Jacobson, J. A., Gross, M. D., et al. (2016). Frostbite: spectrum of imaging findings and guidelines for management. *Radiographics* 36, 2154–2169. doi: 10.1148/rg.2016160045

Mosele, F. C., Bissi Ricci, R., Abreu, P., and Rosa Neto, J. C. (2020). Muscle regeneration in adiponectin knockout mice showed early activation of anti-inflammatory response with perturbations in myogenesis. *J. Cell. Physiol.* 235, 6183–6193. doi: 10.1002/jcp.29547

Murphy, J. V., Banwell, P. E., Roberts, A. H., and McGrouther, D. A. (2000). Frostbite: pathogenesis and treatment. *J. Trauma* 48, 171–178. doi: 10.1097/00005373-200001000-00036

Patten, C., Meyer, R. A., and Fleckenstein, J. L. (2003). T2 mapping of muscle. *Semin. Musculoskelet. Radiol.* 7, 297–305. doi: 10.1055/s-2004-815677

Petrone, P., Asensio, J. A., and Marini, C. P. (2014). Management of accidental hypothermia and cold injury. *Curr. Probl. Surg.* 51, 417–431. doi: 10.1067/j.cpsurg.2014.07.004

Quinn, P. J. (1985). A lipid-phase separation model of low-temperature damage to biological membranes. *Cryobiology* 22, 128–146. doi: 10.1016/0011-2240(85)90167-1

Radunski, U. K., Lund, G. K., Saring, D., Bohnen, S., Stehning, C., Schnackenburg, B., et al. (2017). T1 and T2 mapping cardiovascular magnetic resonance imaging techniques reveal unapparent myocardial injury in patients with myocarditis. *Clin. Res. Cardiol.* 106, 10–17. doi: 10.1007/s00392-016-1018-5

Sabourin, L. A., Girgis-Gabardo, A., Seale, P., Asakura, A., and Rudnicki, M. A. (1999). Reduced differentiation potential of primary MyoD−/− myogenic cells derived from adult skeletal muscle. *J. Cell Biol.* 144, 631–643. doi: 10.1083/jcb.144.4.631

Schwenzer, N. F., Steidle, G., Martirosian, P., Schraml, C., Springer, F., Claussen, C. D., et al. (2009). Diffusion tensor imaging of the human calf muscle: distinct changes in fractional anisotropy and mean diffusion due to passive muscle shortening and stretching. *NMR Biomed.* 22, 1047–1053. doi: 10.1002/nbm.1409

Sinha, U., Malis, V., Chen, J. S., Csapo, R., Kinugasa, R., Narici, M. V., et al. (2020). Role of the extracellular matrix in loss of muscle force with age and unloading using magnetic resonance imaging, biochemical analysis and computational models. *Front. Physiol.* 11:626. doi: 10.3389/fphys.2020.00626

Talbot, J., and Maves, L. (2016). Skeletal muscle fiber type: using insights from muscle developmental biology to dissect targets for susceptibility and resistance to muscle disease. *Wiley Interdiscip. Rev. Dev. Biol.* 5, 518–534. doi: 10.1002/wdev.230

Tidball, J. G. (1995). Inflammatory cell response to acute muscle injury. *Med. Sci. Sports Exerc.* 27, 1022–1032. doi: 10.1249/00005768-199507000-00011

Tidball, J. G. (2005). Inflammatory processes in muscle injury and repair. *Am. J. Phys. Regul. Integr. Comp. Phys.* 288, R345–R353. doi: 10.1152/ajpregu.00454.2004

Tidball, J. G., and Wehling-Henricks, M. (2007). Macrophages promote muscle membrane repair and muscle fibre growth and regeneration during modified muscle loading in mice in vivo. *J. Physiol.* 578, 327–336. doi: 10.1113/jphysiol.2006.118265

Warren, G. L., Hulderman, T., Jensen, N., McKinstry, M., Mishra, M., Luster, M. I., et al. (2002). Physiological role of tumor necrosis factor alpha in traumatic muscle injury. *FASEB J.* 16, 1630–1632. doi: 10.1096/fj.02-0187fje

Woo, E. K., Lee, J. W., Hur, G. Y., Koh, J. H., Seo, D. K., Choi, J. K., et al. (2013). Proposed treatment protocol for frostbite: a retrospective analysis of 17 cases based on a 3-year single-institution experience. *Arch. Plast. Surg.* 40, 510–516. doi: 10.5999/aps.2013.40.5.510

Yanagisawa, O., Kurihara, T., Kobayashi, N., and Fukubayashi, T. (2011). Strenuous resistance exercise effects on magnetic resonance diffusion parameters and muscle-tendon function in human skeletal muscle. *J. Magn. Reson. Imaging* 34, 887–894. doi: 10.1002/jmri.22668

Zaraiskaya, T., Kumbhare, D., and Noseworthy, M. D. (2006). Diffusion tensor imaging in evaluation of human skeletal muscle injury. *J. Magn. Reson. Imaging* 24, 402–408. doi: 10.1002/jmri.20651

Zhang, L. Y., Ding, J. T., Wang, Y., Zhang, W. G., Deng, X. J., and Chen, J. H. (2011). MRI quantitative study and pathologic analysis of crush injury in rabbit hind limb muscles. *J. Surg. Res.* 167, e357–e363. doi: 10.1016/j.jss.2010.09.014

Zhao, D. M., Zhu, S. Q., Wang, F. R., and Huang, S. S. (2019). Role of mutant TBP in regulation of myogenesis on muscle satellite cells. *Curr. Med. Sci.* 39, 734–740. doi: 10.1007/s11596-019-2099-y

Conflict of Interest: The authors declare that the research was conducted in the absence of any commercial or financial relationships that could be construed as a potential conflict of interest.

Advantages of publishing in Frontiers

OPEN ACCESS
Articles are free to read for greatest visibility and readership

FAST PUBLICATION
Around 90 days from submission to decision

HIGH QUALITY PEER-REVIEW
Rigorous, collaborative, and constructive peer-review

TRANSPARENT PEER-REVIEW
Editors and reviewers acknowledged by name on published articles

Frontiers
Avenue du Tribunal-Fédéral 34
1005 Lausanne | Switzerland

Visit us: www.frontiersin.org
Contact us: frontiersin.org/about/contact

REPRODUCIBILITY OF RESEARCH
Support open data and methods to enhance research reproducibility

DIGITAL PUBLISHING
Articles designed for optimal readership across devices

FOLLOW US
@frontiersin

IMPACT METRICS
Advanced article metrics track visibility across digital media

EXTENSIVE PROMOTION
Marketing and promotion of impactful research

LOOP RESEARCH NETWORK
Our network increases your article's readership